DOT/FAA/AR-08/21

Air Traffic Organization
Operations Planning
Office of Aviation Research
and Development
Washington, DC 20591

Analysis of Fatigue Crack Growth From Countersunk Fastener Holes

August 2008

Final Report

This document is available to the U.S. public through the National Technical Information Service (NTIS), Springfield, Virginia 22161.

U.S. Department of Transportation
Federal Aviation Administration

NOTICE

This document is disseminated under the sponsorship of the U.S. Department of Transportation in the interest of information exchange. The United States Government assumes no liability for the contents or use thereof. The United States Government does not endorse products or manufacturers. Trade or manufacturer's names appear herein solely because they are considered essential to the objective of this report. This document does not constitute FAA certification policy. Consult your local FAA aircraft certification office as to its use.

This report is available at the Federal Aviation Administration William J. Hughes Technical Center's Full-Text Technical Reports page: actlibrary.tc.faa.gov in Adobe Acrobat portable document format (PDF).

Technical Report Documentation Page

1. Report No.	2. Government Accession No.	3. Recipient's Catalog No.
DOT/FAA/AR-08/21		

4. Title and Subtitle	5. Report Date
ANALYSIS OF FATIGUE CRACK GROWTH FROM COUNTERSUNK FASTENER HOLES	August 2008
	6. Performing Organization Code
7. Author(s)	8. Performing Organization Report No.
A. F. Grandt, Jr.	
9. Performing Organization Name and Address	10. Work Unit No. (TRAIS)
School of Aeronautics and Astronautics Purdue University 315 North Grant Street West Lafayette, IN 47907-2023	
	11. Contract or Grant No.
	Cooperative Agreement No: 01-C-AW-PU
12. Sponsoring Agency Name and Address	13. Type of Report and Period Covered
U.S. Department of Transportation Federal Aviation Administration Air Traffic Organization Operations Planning Office of Aviation Research Washington, DC 20591	Final Report
	14. Sponsoring Agency Code
	ANM-115

15. Supplementary Notes

The Federal Aviation Administration Airport and Aircraft Safety R&D Division COTR was Dr. Felix Abali.

16. Abstract

This report provides experimental measurements of stress-intensity factors for cracks that develop at countersunk fastener holes. Two configurations were considered: cracks that form at open holes in plates subjected to remote tension and cracks that occur at a pin-loaded hole. In both cases, fatigue crack growth tests were conducted with transparent polymer specimens that allowed in situ photographs of the cracks as they progressed through the specimen thickness. The well-known James and Anderson backcalculation technique was then used to convert the measured fatigue crack growth rates to cyclic stress-intensity factors with the fatigue crack growth rate law established for the test material. The stress-intensity factors are presented in dimensionless form as a function of position along the crack tip perimeter for 112 different open-hole cracks and for 76 pin-loaded hole crack configurations. Some results are compared with numerical solutions obtained here and from the literature. The results of all the experiments are recorded in the appendices of this report and are proposed as benchmark solutions to compare with future analysis results.

17. Key Words	18. Distribution Statement
Countersunk holes, Stress-intensity factors, Fatigue crack growth tests, Fracture mechanics	This document is available to the U.S. public through the National Technical Information Service (NTIS) Springfield, Virginia 22161.

19. Security Classif. (of this report)	20. Security Classif. (of this page)	21. No. of Pages	22. Price
Unclassified	Unclassified	486	

Form DOT F1700.7 (8-72) Reproduction of completed page authorized

TABLE OF CONTENTS

		Page
EXECUTIVE SUMMARY		xi
1.	BACKGROUND	1-1
1.1	Objective	1-1
1.2	Overview of Experimental Approach	1-2
1.3	Overview of Numerical Approach	1-4
2.	OPEN-HOLE EXPERIMENTS	2-1
2.1	General Test Procedures	2-1
2.2	Crack Photographs and Data Analysis	2-3
2.3	Finite Element Analysis Procedures	2-5
3.	OPEN-HOLE RESULTS	3-1
3.1	Single Crack Fatigue Tests	3-1
3.2	Nonsymmetric Crack Pair Fatigue Tests	3-2
3.3	Comparisons With StressCheck	3-4
4.	PIN-LOADED EXPERIMENTS	4-1
4.1	Loading Apparatus	4-1
4.2	Fatigue Testing	4-2
4.3	Data Analysis	4-3
4.4	Discussion of Results	4-4
5.	CONCLUDING REMARKS	5-1
6.	REFERENCES	6-1
APPENDICES		
	A—Open-Hole Tension Data	
	B—Open-Hole Bending Data	
	C—Pin-Loaded Hole Data	

LIST OF FIGURES

Figure		Page
1-1	Schematic Representation of the Two Types of Loading Considered	1-2
1-2	Schematic View of the Corner, Knee, and Through-the-Thickness Cracks Located Along the Bore of a Countersunk Fastener Hole	1-2
1-3	Schematic Representation of the Backcalculation Technique Where Measured Fatigue Crack Growth Rates are Converted to Stress-Intensity Factors	1-3
2-1	Countersunk Hole Test Specimen Used for all Experiments	2-1
2-2	Photograph and Schematic Representation of Test Apparatus Showing Open-Hole Tension Specimen Mounted in Test Grips and Camera Used to Record Fatigue Crack Growth	2-2
2-3	Sequence of Crack Plane Photographs Showing Growth of Initial Corner Crack Into Through-the-Thickness Crack	2-5
2-4	Sequence of Crack Plane Photographs Showing Growth of Initial Knee Crack Into Through-the-Thickness Crack	2-6
2-5	Record of Crack Profiles Obtained From Processed Sequence of Photographs Showing Shapes of Initial Corner and Knee Cracks at Various Cyclic Intervals	2-7
2-6	Schematic Representation of Smoothed Section of an Ellipse Used to fit Digital Photograph of Crack Front	2-8
2-7	Schematic Representation of how Fatigue Crack Growth Rate was Computed at Various Locations Along With Average Crack Front Obtained From Two Successive Photographs	2-8
2-8	Definition of Physical Angle ϕ Used to Define Positions Along Crack Perimeter	2-9
2-9	Baseline Fatigue Crack Growth Data for PMMA Test Material Obtained From Edge-Cracked Bend Specimens at $R = 0.3$, Cyclic Frequency = 3 Hz With Segmented Paris Law Fit	2-9
2-10	Dimensionless Stress-Intensity Factors Versus Normalized Angle Position ϕ for Corner Crack (Specimen FAA-17)	2-10
2-11	Dimensionless Stress-Intensity Factors Versus Normalized Angle Position ϕ for Corner Crack During Transition to Through-the-Thickness Crack (Specimen FAA-17)	2-11
2-12	Dimensionless Stress-Intensity Factors Versus Normalized Angle Position ϕ for Knee Crack (Specimen FAA-18)	2-12

2-13	Dimensionless Stress-Intensity Factors Versus Normalized Angle Position ϕ for Knee Crack During Transition to Through-the-Thickness Crack (Specimen FAA-18)	2-13
3-1	Comparison of Results for Specimens FAA-18 and FAA-4	3-6
3-2	Comparison of Results for Specimens FAA-17 and FAA-4	3-7
3-3	Higher Crack Growth Rate Region	3-8
3-4	Crack Fronts at 70,000 Cycles (FAA-19)	3-9
3-5	Crack Fronts at 69,000 Cycles (FAA-20)	3-10
3-6	Geometric Factors for FAA-19 and FAA-20	3-11
3-7	Geometric Factors for FAA-19	3-12
3-8	Geometric Factors for FAA-20	3-13
3-9	Crack Fronts at 89,000 Cycles (FAA-21)	3-14
3-10	Crack Fronts at 108,000 Cycles (FAA-22)	3-15
3-11	Geometric Factors for FAA-21 and FAA-22	3-16
3-12	Geometric Factors for FAA-22	3-17
3-13	Comparison of Geometric Factors Between FAA-17 and FAA-19	3-18
3-14	Comparison Crack 1	3-19
3-15	Comparison Crack 2	3-20
3-16	Comparison Crack 3	3-21
3-17	Comparison Crack 4	3-22
3-18	Comparison Crack 5 (Right Crack)	3-23
3-19	Comparison Crack 5 (Left Crack)	3-24
3-20	Comparison Crack 6 (Right Crack)	3-25
3-21	Comparison Crack 6 (Left Crack)	3-26
3-22	Comparison Crack 7 (Right Crack)	3-27
3-23	Comparison Crack 7 (Left Crack)	3-28
3-24	Comparison Crack 8 (Right Crack)	3-29

3-25	Comparison Crack 8 (Left Crack)	3-30
3-26	Comparison Crack 9 (Right Crack)	3-31
3-27	Comparison Crack 9 (Left Crack)	3-32
3-28	Comparison Crack 10 (Right Crack)	3-33
3-29	Comparison Crack 10 (Left Crack)	3-34
3-30	Comparison Crack 11 (Right Crack)	3-35
3-31	Comparison Crack 11 (Left Ccrack)	3-36
3-32	Effect of Left Crack on Right Crack (Small Crack)	3-37
3-33	Effect of Right Crack on Left Crack (Large Crack)	3-38
4-1	Experimental Apparatus Used for the Pin-Loaded Experiments	4-11
4-2	Front and Side View Schematics of the Pin-Loaded Countersunk Hole Experiment	4-11
4-3	Schematic of Pin-Loaded Specimen Configuration Showing Remote Load Applied Reacted by Neat-Fit Pin in Countersunk Hole	4-12
4-4	Locking Rings to Prevent the PMMA Pin From Sliding During Testing	4-12
4-5	Initial Knee and Corner Crack Locations for the Countersunk Hole	4-13
4-6	Digital Image of a Type I Crack Shape From FAA-009 (Initial Corner Crack) Taken at 27,500 Cycles	4-13
4-7	Digital Image of a Type II Crack Shape From FAA-009 (Initial Corner Crack) Taken at 47,000 Cycles	4-14
4-8	Digital Image of a Type III Crack Shape From FAA-009 (Initial Corner Crack) Taken at 63,000 Cycles	4-14
4-9	Digital Image of a Type I Crack Shape From FAA-012 (Initial Knee Crack) Taken at 35,500 Cycles	4-15
4-10	Digital Image of a Type II Crack Shape From FAA-012 (Initial Knee Crack) Taken at 40,050 Cycles	4-15
4-11	Digital Image of a Type III Crack Shape From FAA-012 (Initial Knee Crack) Taken at 47,000 Cycles	4-16
4-12	Digital Images of FAA-012 Showing Fast Crack Growth, Which Coincide With the Transition From Type II to Type III Crack Profile	4-16
4-13	Digital Image of a Crack Front From FAA-009 Captured at 57,800 Cycles	4-17

4-14 Extracted Crack Front From Digital Image in Figure 4-13 4-17

4-15 Crack Front in its Actual Dimensions 4-18

4-16 A Sample of 26 Extracted Crack Fronts for Specimen FAA-009 4-18

4-17 Fitting of Ellipse to Smooth Out Discontinuities in Crack Front From FAA-009 at 57,800 Cycles 4-19

4-18 Average Crack Front (Heavier Line) Determined From Ellipse-Fitted Crack Fronts at 47,800 and 49,100 Cycles 4-19

4-19 Crack Length *a* Used to Nondimensionalize the Boundary Correction Factors is the Horizontal Distance From the Center Point 4-20

4-20 Graphical Representation of Dimensionless Stress-Intensity Factor Data for Type I Crack Reported in Table 4-2 for Specimen FAA-009 4-21

4-21 Definition of Parametric Angle Used to Locate Positions Along Crack Front (a) Type I, II, III for Initial Corner Crack and Type II, and III for Initial Knee Crack and (b) Type I for Initial Knee Crack 4-22

4-22 Thirty-Eight Average Crack Fronts Used to Determine Dimensionless Stress-Intensity Factors for Initial Corner Cracked Specimen FAA-009 4-23

4-23 Thirty-Eight Average Crack Fronts Used to Determine Dimensionless Stress-Intensity Factors for Initial Knee Cracked Specimen FAA-012 4-23

4-24 Graphical Representation of Dimensionless Stress-Intensity Factor Data for Type II Crack Reported in Table 4-3 for Specimen FAA-009 4-24

4-25 Graphical Representation of Dimensionless Stress-Intensity Factor Data for Type III Crack Reported in Table 4-4 for Specimen FAA-009 4-25

4-26 Crack Aspect Ratio B/A Ratio Plot for Specimen FAA-009 Showing B/A>1 for Non-Through-the-Thickness Cracks 4-26

4-27 Comparison of Similar Through-the-Thickness Crack Shapes for Specimens FAA-009 and FAA-012 4-27

4-28 Comparison of Dimensionless Stress-Intensity Factors for Similar Shaped Cracks in Specimens FAA-009 and FAA-012 4-27

4-29 Lug With Single Through-the-Thickness Crack Studied by Child 4-28

4-30 Comparison of $f(g)$ for Two Through-the-Thickness Cracks With Similar Shapes With StressCheck Results Available From Child 4-29

4-31 Comparison of Dimensionless Stress-Intensity Factor $f(g)$ for a Through-the-Thickness Crack in FAA-012 With StressCheck Results Reported by Child 4-30

LIST OF TABLES

Table		Page
3-1	Summary of Open-Hole Specimens Discussed in Current Report	3-5
4-1	Countersunk Hole PMMA Specimens With Successful Fatigue Tests	4-7
4-2	Typical Stress-Intensity Factor Results for Type I Crack in Specimen FAA-009	4-8
4-3	Typical Stress-Intensity Factor Results for Type II Crack in Specimen FAA-009	4-9
4-4	Typical Stress-Intensity Factor Results for Type III Crack in Specimen FAA-009	4-10

LIST OF SYMBOLS AND ACRONYMS

ϕ	Physical angle
ΔK	Cyclic stress-intensity factor
σ	Remotely applies tensile stress
da/dN	Fatigue crack growth rate
$f(g)$	Dimensionless stress-intensity factor/geometric factor
ASTM	American Society for Testing and Materials
FAA	Federal Aviation Administration
FEA	Finite element analysis
FRANC3D	Three-dimensional fracture analysis code
K	Stress-intensity factor
LEFM	Linear elastic fracture mechanics
PMMA	Polymethylmethacrylate (transparent polymer, trade name plexiglass)
t	Thickness

EXECUTIVE SUMMARY

This report summarizes research directed at determining stress-intensity factors for fatigue cracks that originate at countersunk holes in plates. Two loading configurations were considered: open holes loaded in remote tension and remote tension reacted by a pin placed in the countersunk hole. Both experimental and computational studies were conducted for single knee cracks, single corner cracks, and nonsymmetric knee and/or corner crack pairs. The experimental approach employed the James and Anderson method, where measured fatigue crack growth rates are used to backcalculate cyclic stress-intensity factors from the baseline da/dN-ΔK properties of the test material. Following this approach, fatigue tests were conducted with transparent polymer specimens that allow in situ photographs of crack growth that provide details of both crack shape and size changes. The digital photographs were analyzed to determine the fatigue crack growth rate distribution, and thus, the cyclic stress-intensity factor at various positions along the crack front. The normalized stress-intensity factors were then compared with new results obtained by the finite element method. Results for nonsymmetric crack configurations were compared with corresponding single and symmetric crack pair solutions to determine the effect of the nonsymmetry on the results. The goal of these latter comparisons is to determine how well single and/or symmetric solutions estimate the nonsymmetric case.

1. BACKGROUND.

Fracture mechanics analyses of fatigue crack growth require accurate determination of the crack tip stress-intensity factor, K. While solutions are well established for many through-the-thickness crack geometries, surface and corner cracks that develop along the bore of countersunk fastener holes have a complex three-dimensional nature that complicates development of general solutions. The stress-intensity factor usually varies along the crack front, so that there is not a single value for a given crack configuration. This variation in K leads to different fatigue crack growth rates along the crack perimeter and to changes in shape. Thus, three-dimensional crack geometries are difficult to study analytically or numerically, and, since crack shapes change as the crack grows, each case will be different, precluding development of general solutions. Due to these complexities, an experimental approach was employed here to determine the natural crack shapes that should be modeled and to establish a database of stress-intensity factors for evaluating future numerical approaches.

This report summarizes a 3-year research program conducted by the Purdue University School of Aeronautics and Astronautics for the Federal Aviation Administration (FAA) William J. Hughes Technical Center. Additional details of this work are reported in the Ph.D. theses of C. Y. Park [1] and J. Suh [2], in the M.S. thesis by L. K. Chiew [3], and in other papers referenced in this report. Since it is not practical to include all the individual results reported in references 1-3, emphasis is given here to a summary of the most complete and generic interest sets of data.

1.1 OBJECTIVE.

The primary objective of this effort was to obtain experimental measurements of stress-intensity factors for natural fatigue cracks that form at countersunk holes in a plate. As shown in figure 1-1, the particular loading configurations studied include open holes in plates subjected to remote tension and pin-loaded holes.

Both the open-hole and pin-loaded hole configurations considered initial corner, knee, and through-the-thickness cracks that emanated from the bore of the countersunk hole, as shown in figure 1-2. Both single cracks and double cracks located on opposite sides of the hole (symmetric or nonsymmetric) were considered. The general goal was to determine experimentally the variation in stress-intensity factor around the crack perimeter and then to compare the experimental results with numerical solutions obtained for particular crack geometries. It was suggested that the experimental results could be used by future investigators to establish confidence in various numerical approaches before embarking on a large numerical study to develop parametric solutions for natural types of cracks.

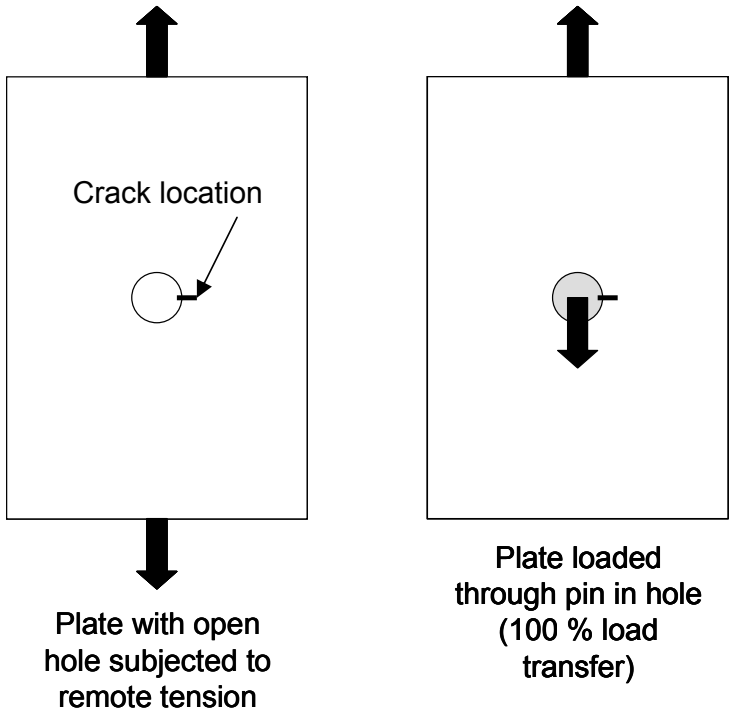

Figure 1-1. Schematic Representation of the Two Types of Loading Considered

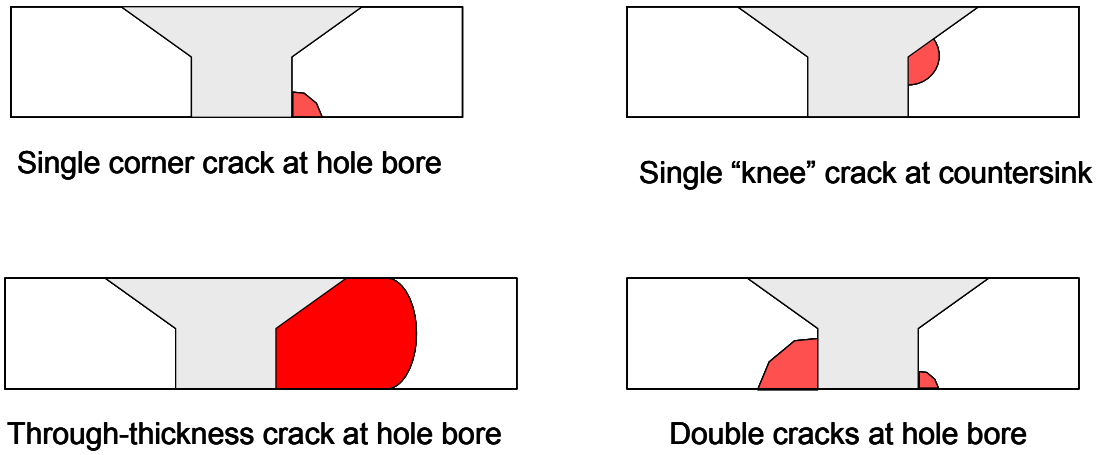

Figure 1-2. Schematic View of the Corner, Knee, and Through-the-Thickness Cracks Located Along the Bore of a Countersunk Fastener Hole

1.2 OVERVIEW OF EXPERIMENTAL APPROACH.

One goal of this effort was to obtain fatigue crack growth data that can be used to evaluate stress-intensity factor solutions for cracks that form at countersunk fastener holes. Direct observation of crack sizes and shapes is impossible in metal specimens, since much of the crack perimeter is hidden from the free surface. Although indirect measurements of crack growth can be obtained

from fracture surface measurements by marker band techniques, these procedures are quite tedious and time consuming.

In light of the difficulty in measuring internal cracks in metal specimens, experiments were conducted with transparent polymer specimens. These tests employed the transparent polymer polymethylmethacrylate (PMMA) (or plexiglass). PMMA is an excellent model material for the current tests in that it may be readily characterized with fracture mechanics concept. In the past, employing transparent model materials for fracture mechanics research dealing with complex three-dimensional crack shapes has been successful. Both stress-intensity factor evaluations [4-13] and fatigue crack closure investigations [14-19] have successfully employed transparent model materials. The transparent nature of PMMA allows direct observation of internal cracks, such as those of interest here.

Time lapse photographs of crack growth in the transparent specimens were analyzed to determine local measurements of the fatigue crack growth rate at various positions along the crack fronts. These crack growth rate data were then used with the James and Anderson technique [20] to backcalculate the cyclic stress-intensity factor using the fatigue crack growth rate data established for the test material with baseline experiments conducted with standard specimen configurations. This technique is shown in figure 1-3.

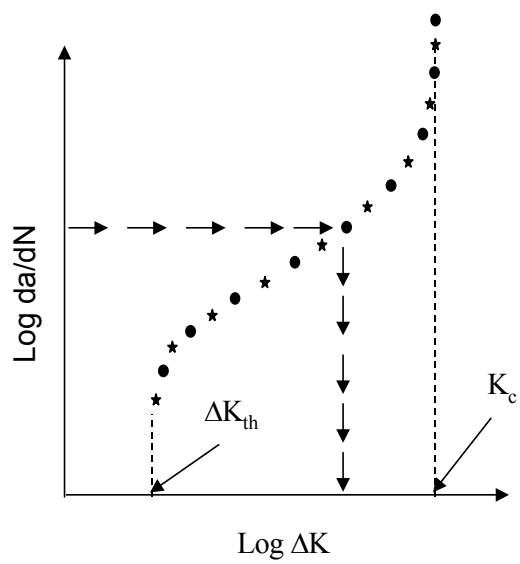

Figure 1-3. Schematic Representation of the Backcalculation Technique Where Measured Fatigue Crack Growth Rates are Converted to Stress-Intensity Factors

Application of the polymer model results to metal structures is possible provided that a mechanics-based analysis to describe the results is developed. If the mechanics model is shown to describe the polymer behavior, then one merely needs to input the appropriate metal material properties to apply the analysis to conventional structural materials. Examples of how linear elastic fracture mechanics life prediction models have been verified with transparent polymer specimens are described in references 6, 8, and 9. Subsequent application of these polymer-verified models to structural metal specimens constructed from titanium, waspalloy, and aluminum are reported in references 8, 21, and 22.

1.3 OVERVIEW OF NUMERICAL APPROACH.

Earlier research on the countersunk hole problem involved numerical studies described in references 23-27. While the primary emphasis of this project was experimental, certain crack configurations were also studied numerically for comparison. Some of the early experiments were compared with results from reference 24 and with calculations made by the three-dimensional fracture analysis code (FRANC3D), version 1.15, developed by Cornell University. Those comparisons are reported in references 1 and 28, while more recent work [2] that employed the StressCheck™ finite element software [29] are discussed later in this report. As described in section 3.1, three-dimensional crack closure effects complicate interpretation of some of the initial experimental results given in references 1 and 28, so emphasis in this report is given to the more recent work that employed StressCheck analyses.

2. OPEN-HOLE EXPERIMENTS.

This section summarizes the general approach for the experiments conducted with the open hole specimens. Additional details are given in references 1 and 2. The pin-loaded tests followed a similar test procedure and are summarized in section 4.

2.1 GENERAL TEST PROCEDURES.

All the specimens studied employed the specimen configuration shown in figure 2-1. The particular geometry shown was chosen to match that employed in prior numerical studies of the countersink problem [23-25] and was scaled so that the specimen thickness, t, matched the 3/8-inch-thick sheet of PMMA purchased for the experiments. All the specimens were machined from the same PMMA sheet (taking care to maintain the same crack orientation relative to the sheet), and then annealed to relieve potential residual stresses. The specimens were bonded to steel grips designed to provide optical access to the crack plane while the specimens were loaded in remote tension, as shown in figure 2-2.

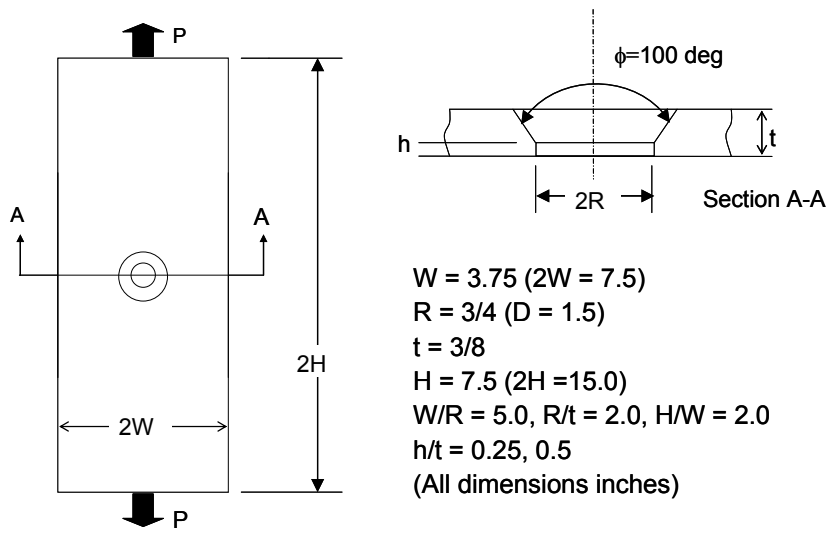

Figure 2-1. Countersunk Hole Test Specimen Used for all Experiments

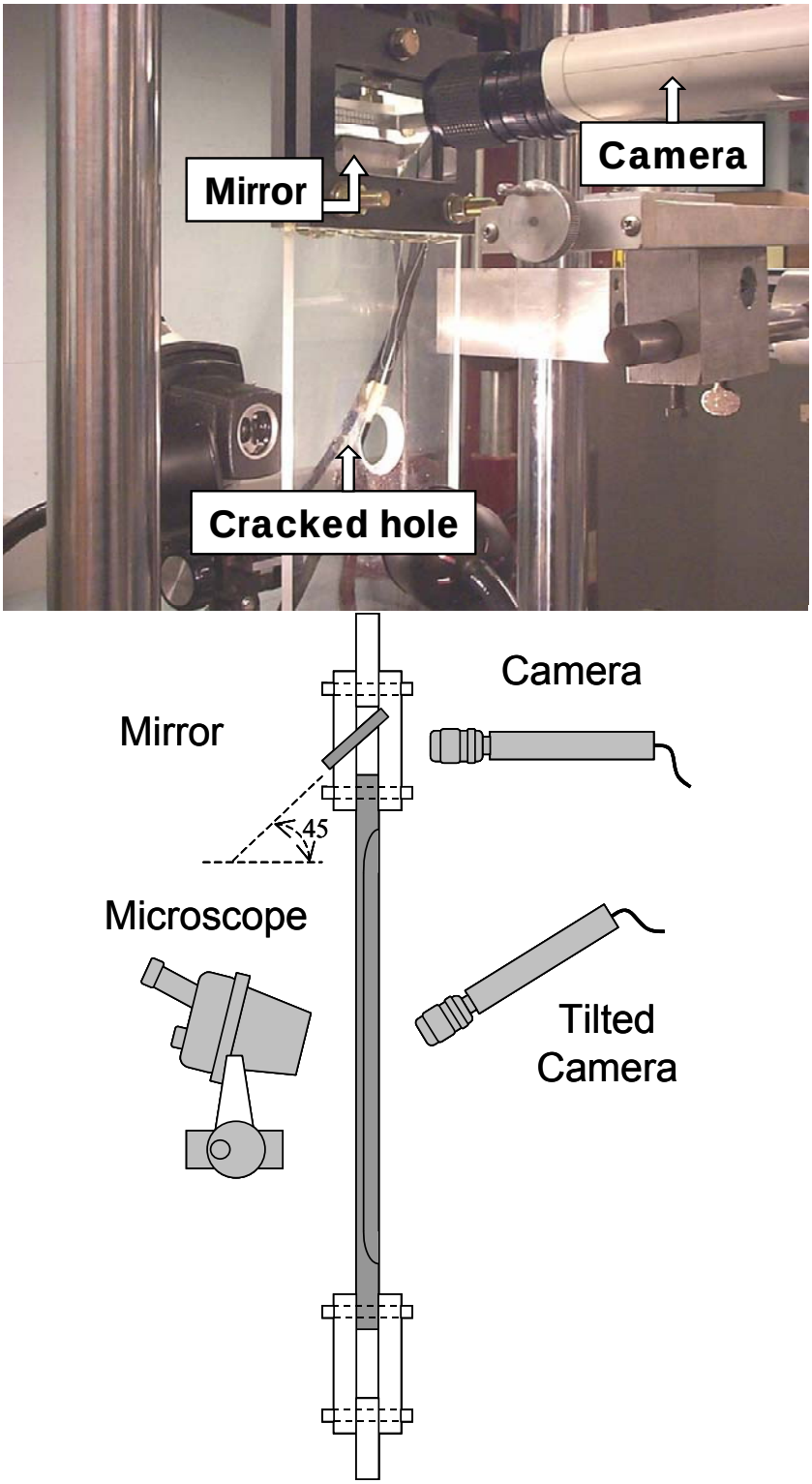

Figure 2-2. Photograph and Schematic Representation of Test Apparatus Showing Open-Hole Tension Specimen Mounted in Test Grips and Camera Used to Record Fatigue Crack Growth

All specimens were subjected to cyclic loading using either a 10- or 20-kip electro-hydraulic fatigue machine located in the Purdue School of Aeronautics and Astronautics Fatigue and Fracture Laboratory. All fatigue tests were conducted at a cyclic frequency of 3 Hz to avoid potential time-dependent effects in the polymer specimens. Initially, the stress ratio R was set at 0.1, but changed in later experiments to $R = 0.3$ to avoid potential differences in fatigue crack closure at the specimen surface and specimen interior as discussed in references 1 and 14–19. All of the results presented in this report employed $R = 0.3$ cycling.

2.2 CRACK PHOTOGRAPHS AND DATA ANALYSIS.

Crack lengths were measured as a function of applied cycles by the three methods described below. The primary method of data acquisition was to photograph the crack plane through the polished end of the specimen. As indicated in figure 2-2, a mirror located at 45° to the specimen end allowed the digital camera to photograph a perpendicular view of the crack plane. With the second crack length measurement method the camera was moved down to the crack plane and placed at an angle that allowed observation of front, back, and interior locations on the crack front. Since this skewed view of the crack plane does not give a true measurement of crack dimensions, data processing techniques were used to transform the skewed view to a perpendicular view of the crack plane (see references 1-3 for details). The third measurement method used a traveling microscope to measure the free surface crack length on one side of the specimen, as shown in figure 2-2. These surface measurements also helped calibrate the photographs obtained by methods 1 and 2.

Figures 2-3 and 2-4 present typical crack plane photographs showing the growth and transition of a single corner or knee cracks into through-the-thickness cracks (only the right-hand side of the hole bore is shown for clarity). Also, note that the Types I, II, and III crack geometries definitions are used to designate the crack shape relative to its countersink position. Photographs were taken at periodic cyclic intervals to record changes in crack size and dimension. (Only a small sample of the many photographs taken for a given experiment is shown here.) As described in references 1-3, individual photographs were digitized and then smoothed and processed to give a complete record of the crack progression. Figure 2-5, for example, shows the final sets of smoothed and scaled crack profiles determined for corner crack specimen FAA-009 and knee crack specimen FAA-012 (these two particular pin-loaded specimens are discussed in section 4). Although the specific cyclic intervals represented for each crack profile are not given on these particular figures, they are known and recorded in appendix C (note that the cyclic intervals were not uniform in the figure 2-5 examples.) The actual crack front from individual photographs was digitized and fitted with a section of an ellipse, as shown in figure 2-6. Here, the horizontal position of the ellipse center was required to lie along the hole bore, while the vertical location was allowed to vary for the best fit. The actual parameters used to define each ellipse are recorded in appendix A of this report.

Fatigue crack growth rates then were determined at various locations along the crack front, as shown schematically in figure 2-7. The crack growth rate was found at various points along the crack perimeter, defined by the physical angle ϕ, shown in figure 2-8, for individual crack fronts (such as those represented by the dotted lines in figure 2-5). This particular procedure was to determine the perpendicular distance at various ϕ locations between two successive cracks and to divide by the cyclic interval. The crack growth rates defined in this manner were then associated

with the average crack shape defined by the two original cracks, as shown schematically in figure 2-7. This procedure is a modification of the secant method for obtaining growth rates described in American Society for Testing and Materials (ASTM) E 647 [30]. Note that, in general, since the crack shape changes as it grows, the fatigue crack growth rate *da*/*dN* will vary with location ϕ along the crack front.

This local variation in *da*/*dN* is directly related to the cyclic stress-intensity factor at those locations through the baseline fatigue crack growth properties of the test material, and forms the basis for determining the cyclic stress-intensity factor ΔK from the measured *da*/*dN* by the James and Anderson [20] technique (recall figure 1-3). The baseline *da*/*dN*-ΔK behavior for the PMMA sheet was established with a series of separate fatigue tests conducted with edge-cracked specimens loaded in cyclic bending. (The edge-cracked specimens have a well established K solution.) Again, care was taken to orient the crack planes in the same sheet direction and to employ the same annealing procedure, cyclic frequency, and *R* used for the countersunk hole tests. The baseline fatigue crack growth data obtained are shown in figure 2-9 for $R = 0.3$, along with a segmented Paris law used to fit that data.

The measured cyclic stress-intensity factors were normalized with stress and crack length to obtain the dimensionless factor *f(g)* at various positions along the crack front. The normalizing factor *f(g)* used for the open-hole tension specimens is defined by equation 2-1.

$$f(g) = \frac{K}{\sigma\sqrt{\pi a}} \tag{2-1}$$

Here, *K* is the stress-intensity factor at the crack front position of interest (located by the physical angle ϕ defined in figure 2-8), σ is the remotely applied tensile stress, and *a* is the maximum horizontal distance from the edge of the hole to the crack front, as shown in figure 2-6. In the current instance, the cyclic values of ΔK and $\Delta\sigma$ are used to define *f*(*g*). Now, ΔK is obtained from the segmented Paris law ($da/dN = C\,\Delta K^m$) used to fit the baseline data, as shown in figure 2-9. In terms of the experimental parameters, *f*(*g*) is given by equation 2-2.

$$f(g) = \frac{\left(\frac{\frac{da}{dN}}{C}\right)^{\frac{1}{m}}}{\Delta\sigma\sqrt{\pi a}} \tag{2-2}$$

Here, *da*/*dN* is the measured fatigue rack growth rate at position ϕ as discussed above, *C* and *m* are the appropriate Paris constants for the given range of *da*/*dN* (see figure 2-9), $\Delta\sigma$ is the remotely applied cyclic stress, and *a* is the crack dimension defined in figure 2-6.

Some typical values of the dimensionless stress-intensity factors found in this manner are given in figures 2-10 and 2-11 for corner crack specimen FAA-18 and in figures 2-12 and 2-13 for knee crack specimen FAA-17. (The circles around a particular data point correspond to the crack perimeter location shown on the accompanying sketch.) Additional results are described in section 3-1.

2.3 FINITE ELEMENT ANALYSIS PROCEDURES.

The finite element analysis (FEA) software StressCheck [29], developed by Engineering Software Research and Development, was used to compare numerical and experimental results. StressCheck is a finite element software package that automatically extracts stress-intensity factors in linear elastic fracture mechanics [29].

StressCheck is based on the p-version of the finite element method. In p-version FEA, unlike the h version, the mesh is not refined as the number of degrees of freedom is increased, but the number of elements is kept fixed, and convergence is obtained by increasing the order of the polynomial within each element. The p-version method has substantial advantages in calculating stress-intensity factors since the mesh design does not need to be overly refined at the crack tip. For problems in which the materials are isotropic, as in the present case, StressCheck uses the contour integral method to compute stress-intensity factors in two dimensions and three dimensions.

To validate the results of StressCheck, several comparisons were made with benchmark solutions for standard crack configurations. As described in reference 2, solutions were obtained for the standard compact tension specimen and for plates loaded in remote tension that contained embedded elliptical cracks, surface cracks, corner cracks, and corner cracks located at open holes. All the baseline calculations gave stress-intensity factor solutions that agreed well with prior published results, providing confidence that the software was being applied correctly. Section 3.3 compares numerical and experimental solutions for the stress-intensity factors.

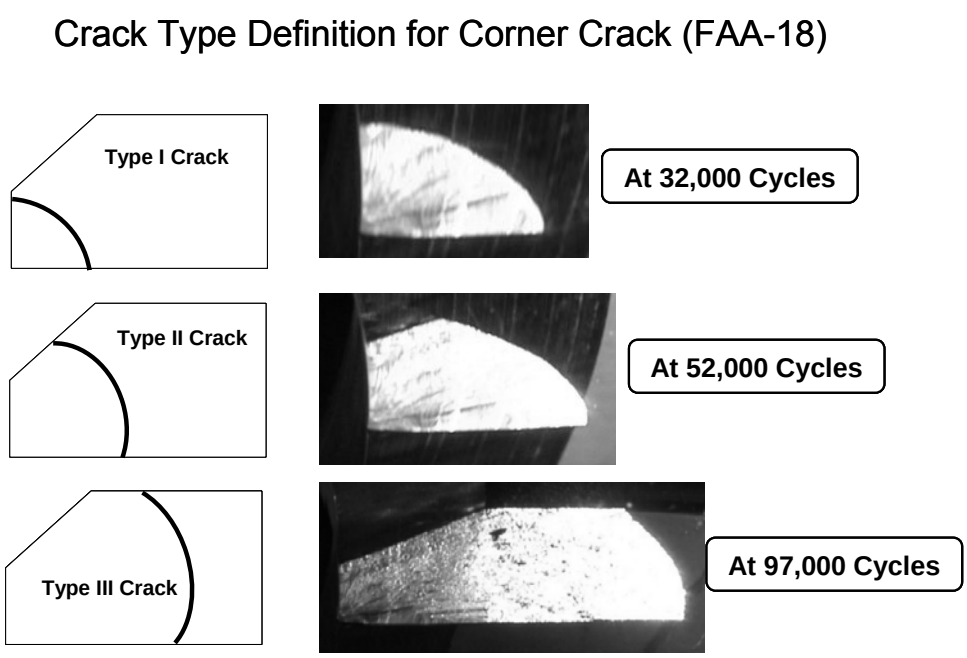

Figure 2-3. Sequence of Crack Plane Photographs Showing Growth of Initial Corner Crack Into Through-the-Thickness Crack

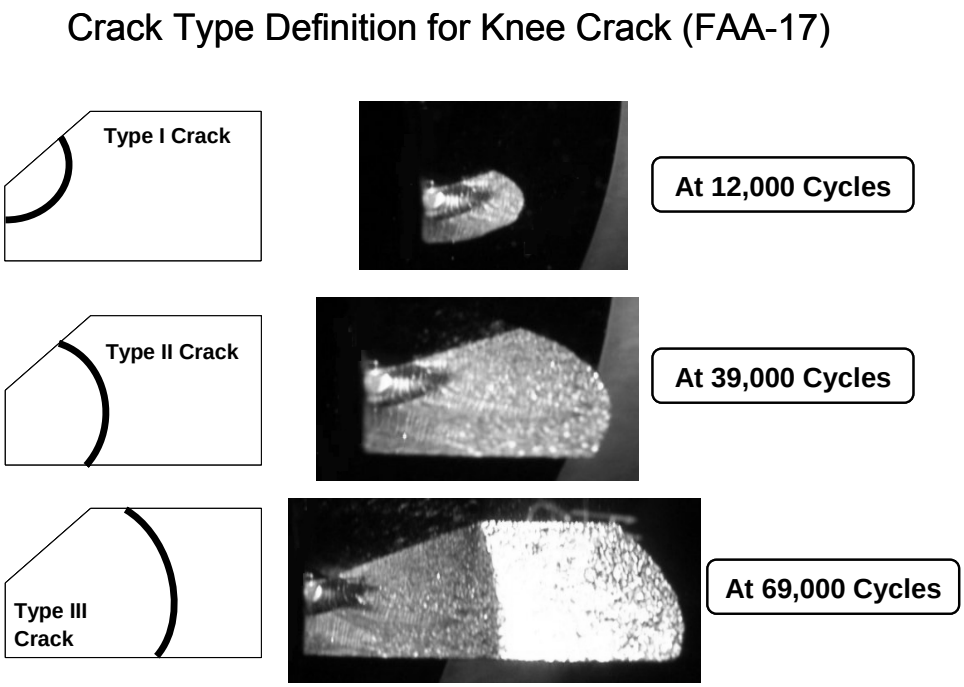

Figure 2-4. Sequence of Crack Plane Photographs Showing Growth of Initial Knee Crack Into Through-the-Thickness Crack

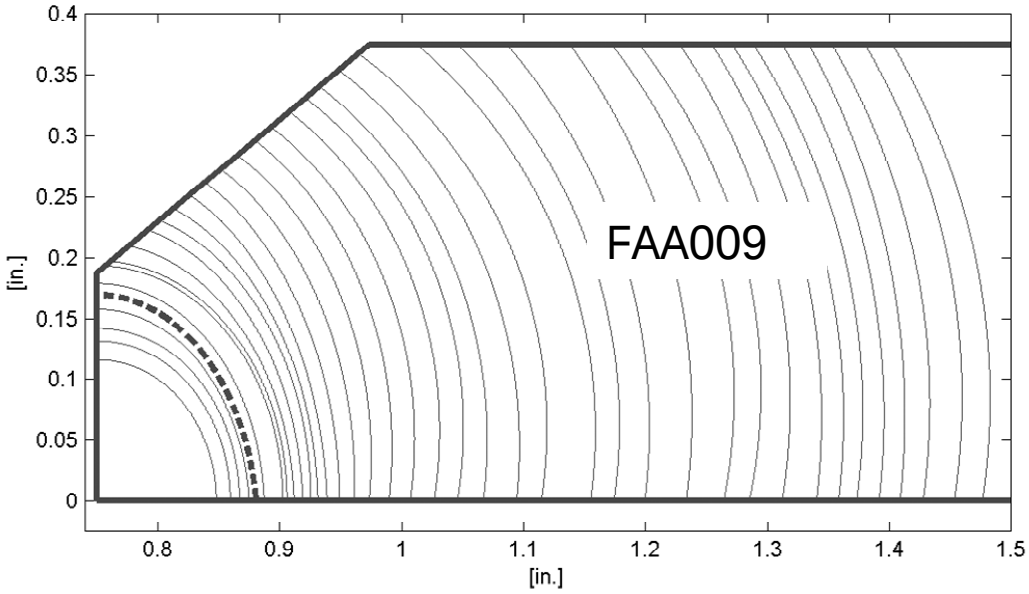

corner crack profiles

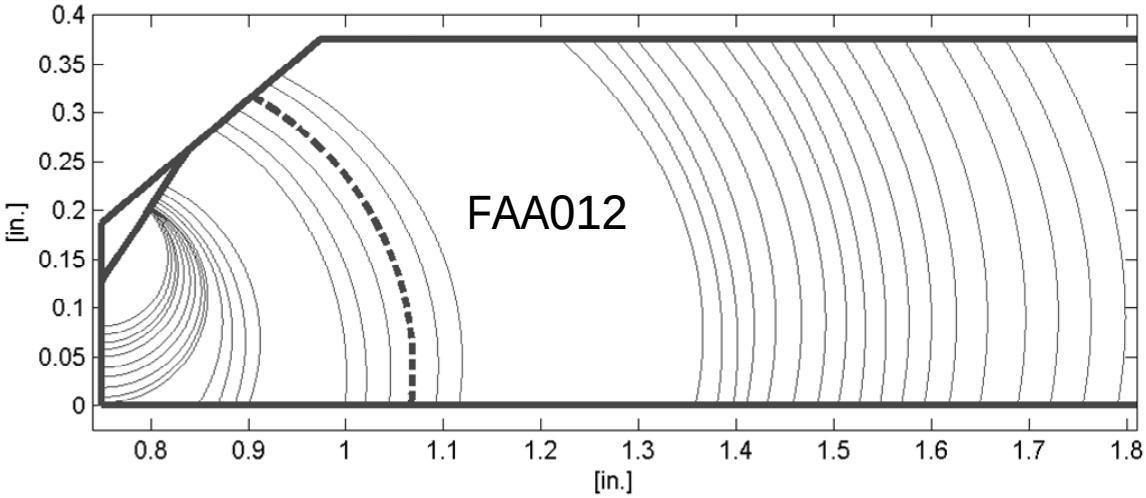

knee crack profiles

Figure 2-5. Record of Crack Profiles Obtained From Processed Sequence of Photographs Showing Shapes of Initial Corner and Knee Cracks at Various Cyclic Intervals

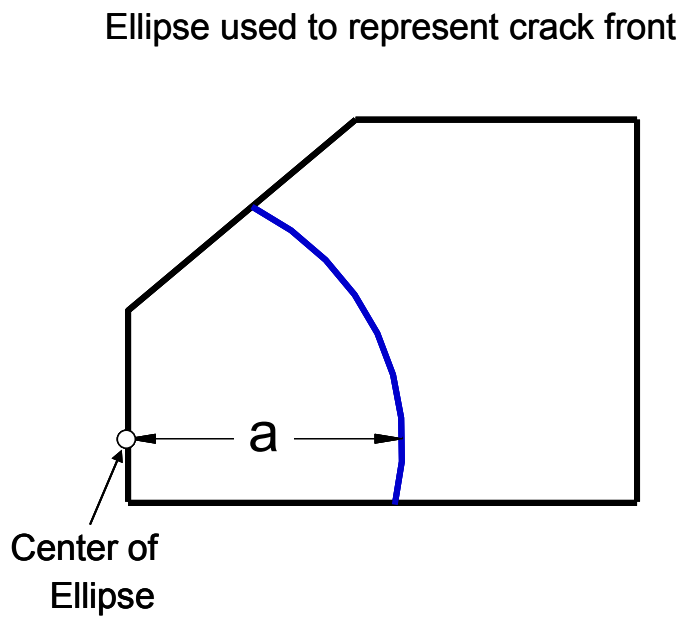

Figure 2-6. Schematic Representation of Smoothed Section of an Ellipse Used to fit Digital Photograph of Crack Front (Note location of ellipse center and definition of dimension *a*.)

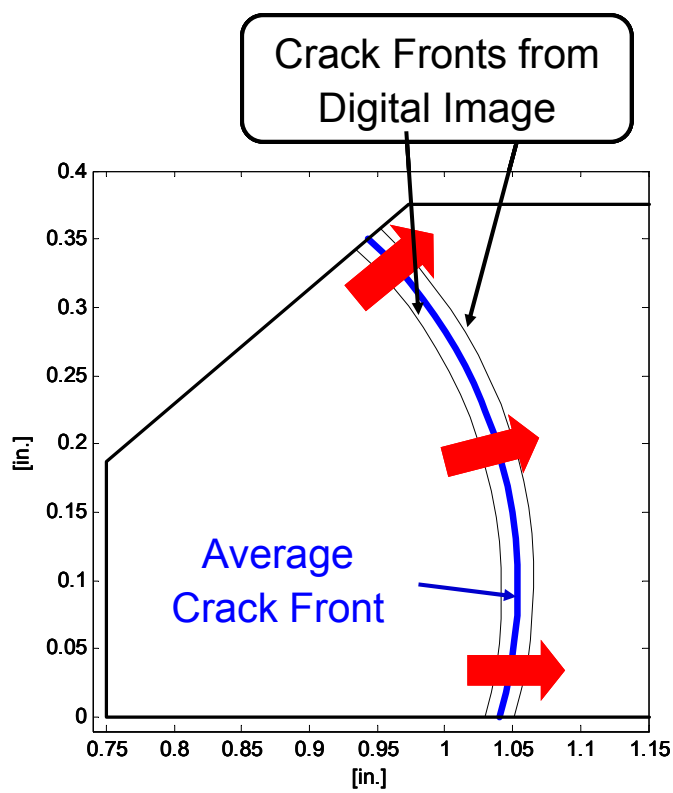

Figure 2-7. Schematic Representation of how Fatigue Crack Growth Rate was Computed at Various Locations Along With Average Crack Front Obtained From Two Successive Photographs

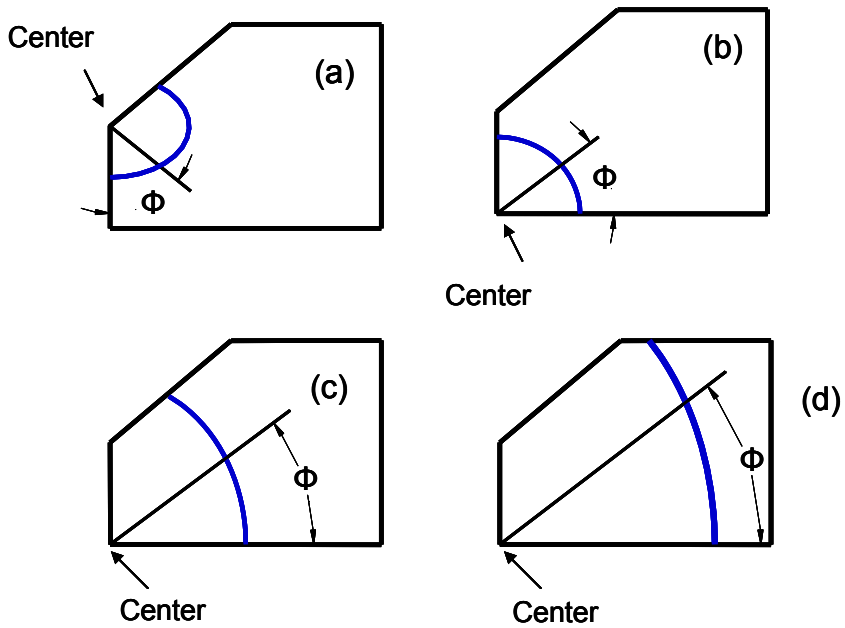

Figure 2-8. Definition of Physical Angle ϕ Used to Define Positions Along Crack Perimeter

da/dN = 7.3965e-58 x $\Delta K^{19.548}$	$350 < \Delta K \leq 428 \quad psi\sqrt{in}$
da/dN = 8.0430e-21 x $\Delta K^{5.474}$	$428 \leq \Delta K \leq 660 \quad psi\sqrt{in}$
da/dN = 1.3743e-39 x $\Delta K^{12.103}$	$660 \leq \Delta K < 880 \quad psi\sqrt{in}$

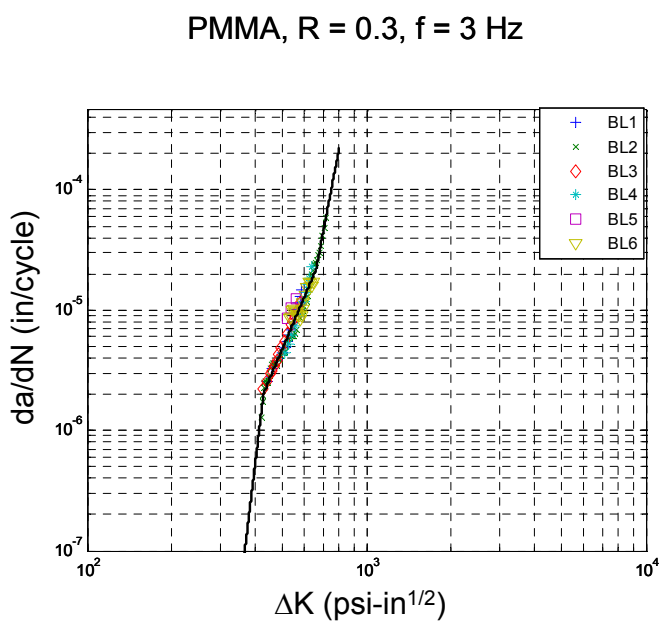

Figure 2-9. Baseline Fatigue Crack Growth Data for PMMA Test Material Obtained From Edge-Cracked Bend Specimens at R = 0.3, Cyclic Frequency = 3 Hz With Segmented Paris Law Fit

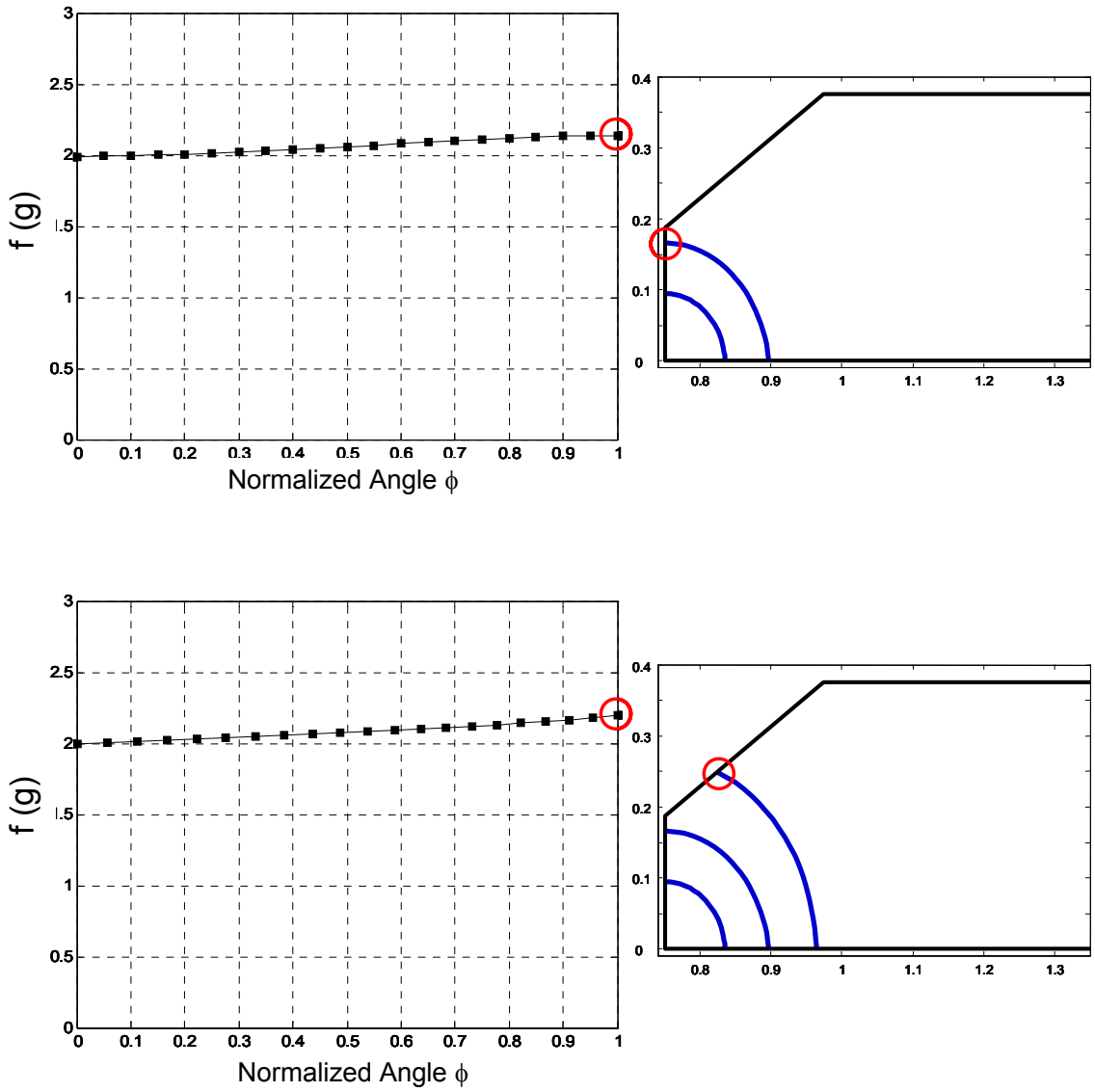

Figure 2-10. Dimensionless Stress-Intensity Factors Versus Normalized Angle Position ϕ for Corner Crack (Specimen FAA-17)

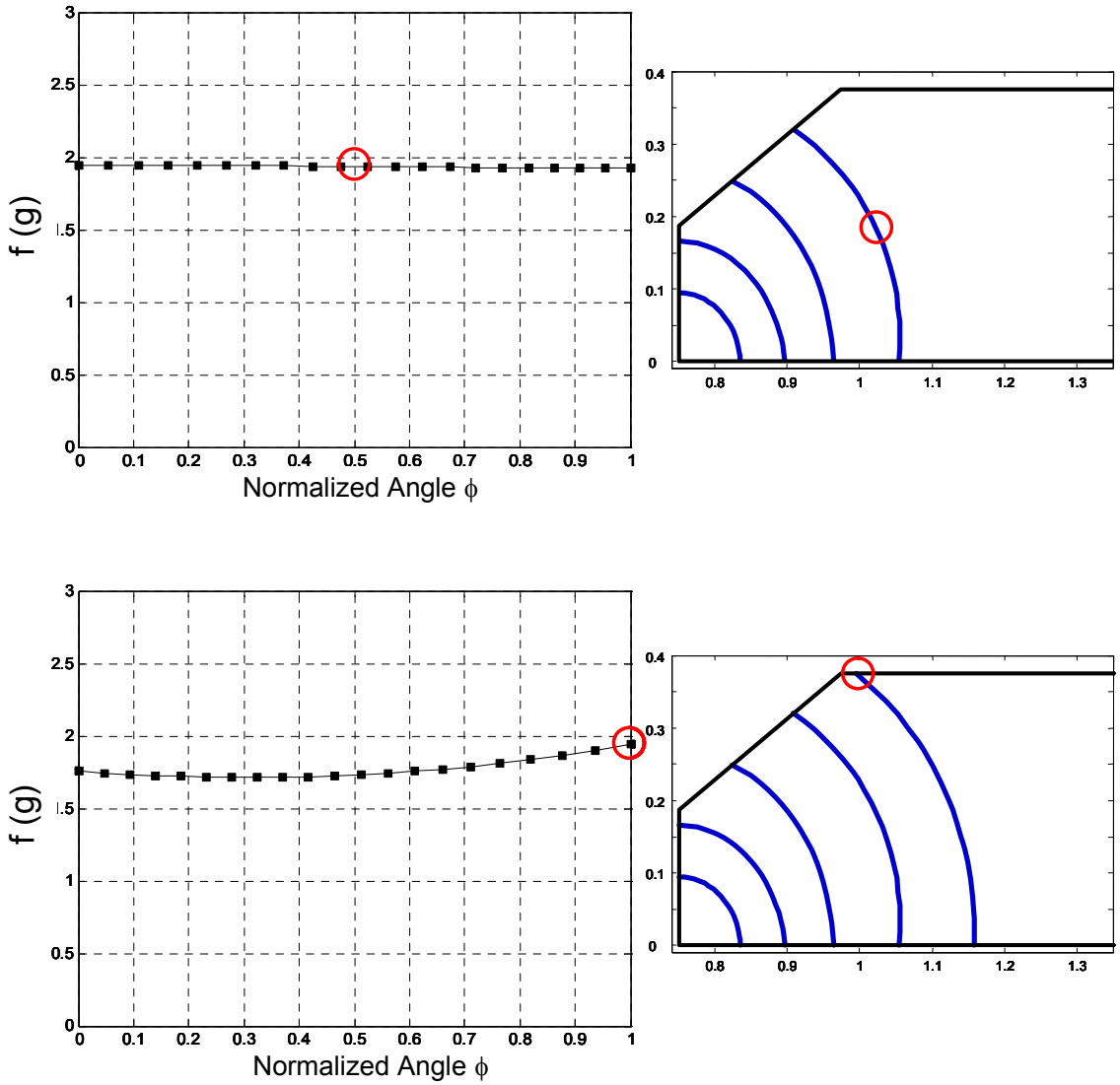

Figure 2-11. Dimensionless Stress-Intensity Factors Versus Normalized Angle Position ϕ for Corner Crack During Transition to Through-the-Thickness Crack (Specimen FAA-17)

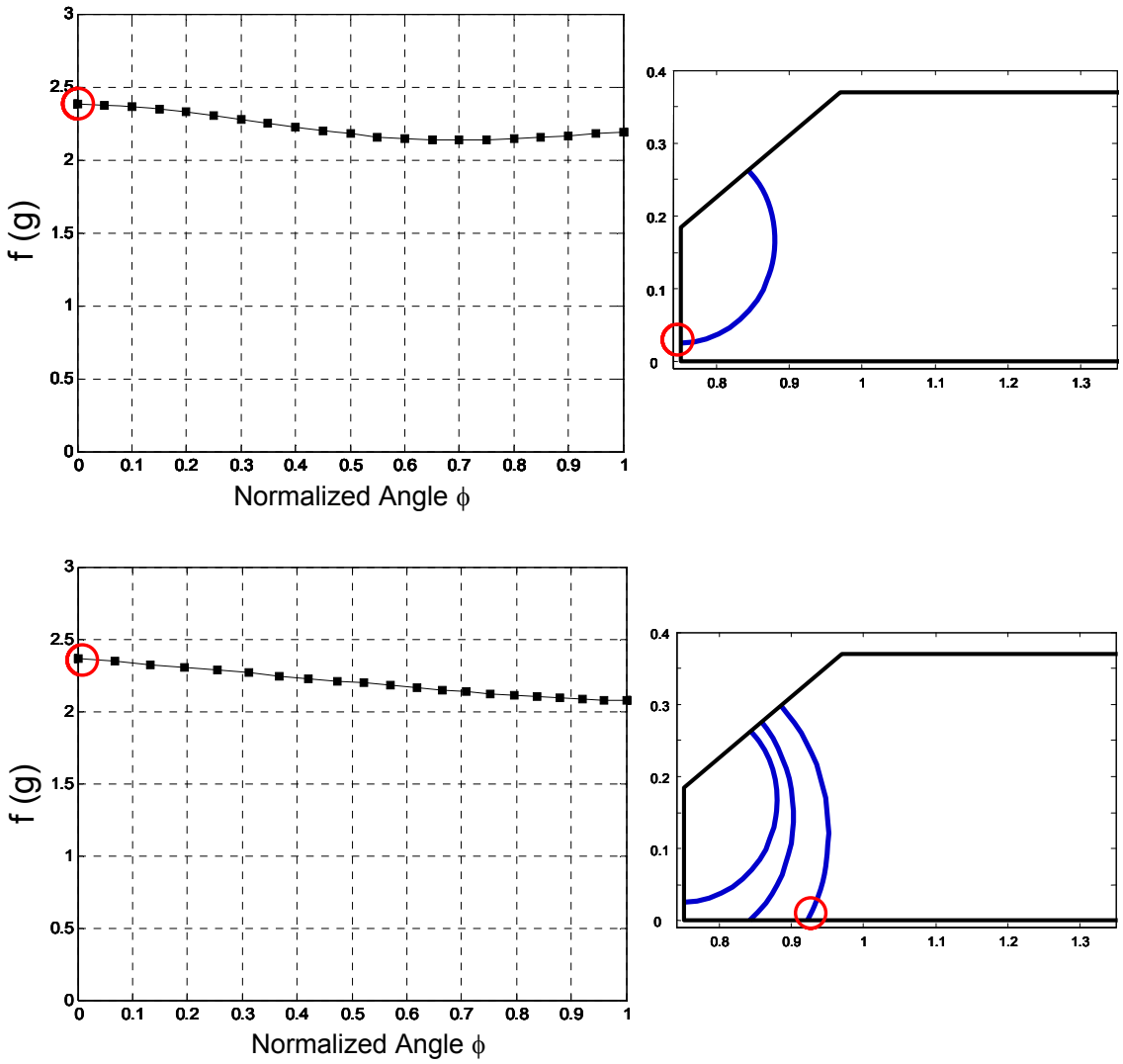

Figure 2-12. Dimensionless Stress-Intensity Factors Versus Normalized Angle Position ϕ for Knee Crack (Specimen FAA-18)

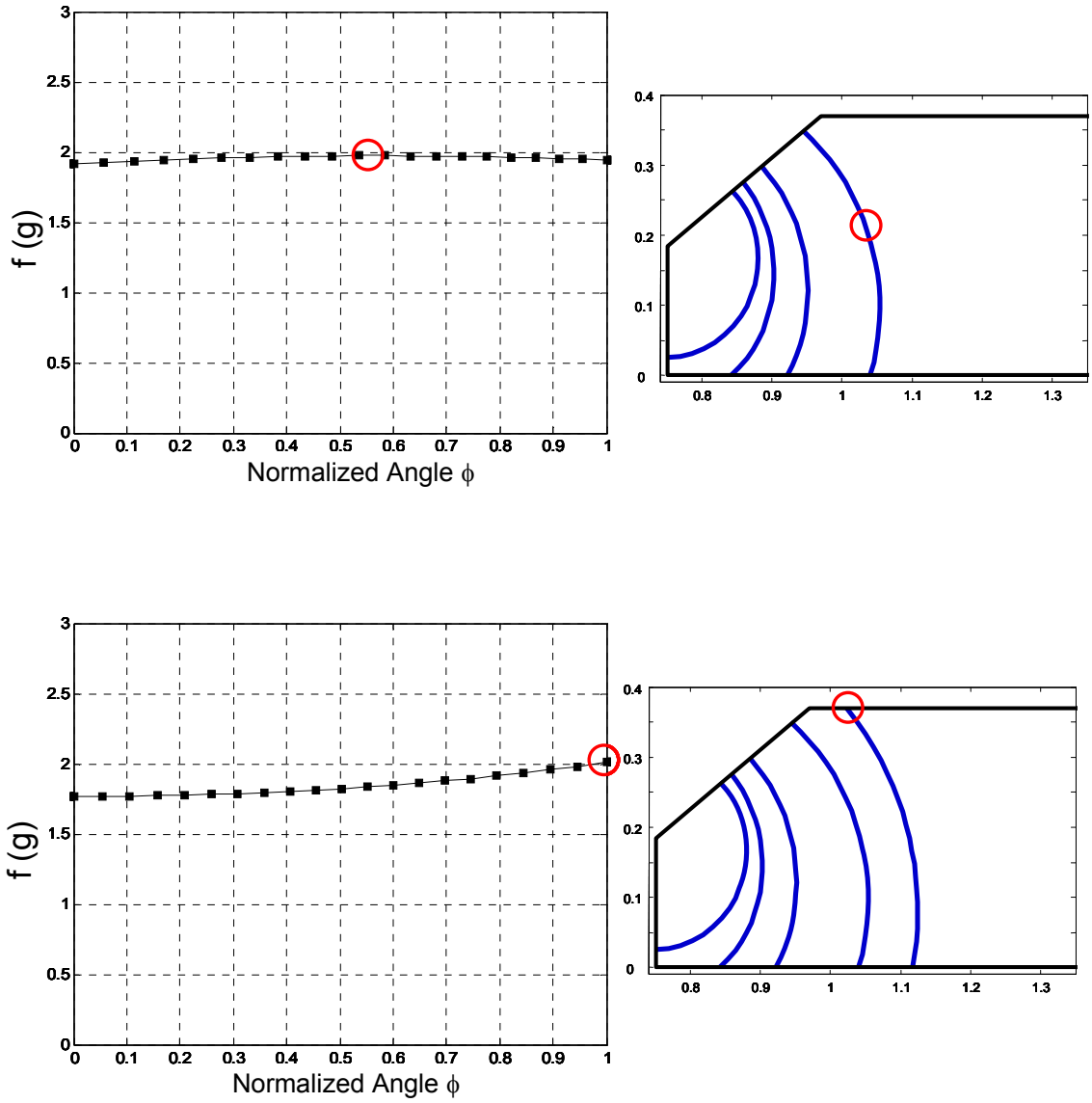

Figure 2-13. Dimensionless Stress-Intensity Factors Versus Normalized Angle Position ϕ for Knee Crack During Transition to Through-the-Thickness Crack (Specimen FAA-18)

3. OPEN-HOLE RESULTS.

This section and its subsections describe results obtained from remote tensile loading of the countersunk hole specimens. Results from seven fatigue tests with three single crack and four nonsymmetric crack geometries obtained by the procedures described in section 2.1 are explained. Additional results with open-hole specimens are also reported in references 1 and 28. However, those tests employed $R = 0.1$ test conditions, rather than the $R = 0.3$ loading reported here and are further complicated by three-dimensional aspects of fatigue crack closure described in section 3.1. In particular, it has been observed [15] that fatigue crack closure is much more pronounced at free surface locations (i.e., normalized $\phi \sim 0$ or 1) than at internal crack locations. By conducting the fatigue tests at $R = 0.3$, the crack surfaces are open for all ϕ, and the effects of fatigue crack closure on the da/dN-ΔK material behavior are minimized. Thus, it was decided to only present the $R = 0.3$ results in this final report.

The test matrix is shown in table 3-1. In these experiments, cracks nucleated at two different initial locations—knee cracks at the intersection between the countersunk and straight shank portion of the hole and corner cracks at the bottom of the hole, as shown in table 3-1. The precrack was made by introducing a small flaw at the hole bore with a razor blade and then applying a remote cyclic load. Once a fatigue precrack was formed, cyclic tensile loading continued to be applied throughout the experiment. Additional details of the precracking procedure are described in references 1 and 2.

3.1 SINGLE CRACK FATIGUE TESTS.

For the single knee crack specimens (FAA-17 and FAA-17A), the crack shapes observed throughout the test were divided into three categories: Types I, II, and III, as depicted earlier in figure 2-4. This figure shows a Type I crack front at 12,000 cycles for specimen FAA-17 and Types II and III crack front at 39,000 and 69,000 cycles, respectively. The transition from Type I to Type II occurs at approximately 18,300 cycles into the test. At 60,000 cycles, the crack front has taken a through-the-thickness Type III crack.

For the corner crack specimens, the crack shapes observed throughout the tests were divided into the three major categories shown previously in figure 2-3: Types I, II, and III. Figure 2-3 shows a Type I crack front at 32,000 cycles for the single corner crack specimen FAA-18 and Types II and III crack fronts at 52,000 and 97000 cycles, respectively. The transition from Type I to Type II occurred between 35,000 and 38,000 into the test. It was observed at 85,000 cycles that the crack front has taken a through-the-thickness Type III crack. Fracture of specimen FAA-18 occurred at 106,159 cycles.

Dimensionless stress-intensity factors $f(g)$, defined earlier by equation 2-1, are given in figures 2-10 and 2-11 for specimen FAA-17 and in figures 2-12 and 2-13 for specimen FAA-18. More complete details for these two tests, and for all seven of the experiments summarized in table 3-1, are given in appendices A and B. The appendix data includes both tabular and graphical presentations of $f(g)$ versus 21 crack perimeter positions defined by the normalized angle ϕ for each of the 112 different cracks examined, along with details of the crack shape, location, elapsed cycles, and applied load.

In an effort to determine the repeatability of the experimental results, the crack photographs were compared to find cracks with the same size and shape. This was a difficult task, however, since the fatigue cracks developed naturally, and were usually not identical from specimen to specimen. Nevertheless, two similar crack sizes and shapes were found among the many open-hole photographs, and the stress-intensity factors were compared. Figure 3-1 compares the dimensionless stress-intensity factors with Park's [1] earlier results for specimen FAA-4 with the results for specimen FAA-18, and figure 3-2 compares the results of specimens FAA-17 and FAA-4. It should be noted that specimen FAA-4 was tested at $R = 0.1$ rather than the $R = 0.3$ stress ratio used for FAA-17 and FAA-18 [2]. Figure 3-1 compares the dimensionless geometric factors and the corresponding type I corner crack shapes for specimens FAA-18 and FAA-4. Outlines of the crack shapes for these two tests are also shown and indicate that these two cracks were nearly identical in size and shape. Note that the dimensionless stress-intensity factor coefficient $f(g)$ is nearly constant along the crack perimeter (as defined by the normalized angle ϕ) and the results from the two experiments are fairly close to each other.

Figure 3-2 compares geometric factors and the corresponding crack shapes for larger type III cracks in specimens FAA-17 and FAA-4. Note that although these two cracks have the same size and shape, their initial crack locations were different (initial knee crack for specimen FAA-17 and initial corner crack geometry for FAA-4). These comparisons show similar stress-intensity factor trends in the specimen interior but there are differences near the free surfaces for the cracks outside of the countersunk hole (i.e., normalized $\phi = 0$ or 1). It is believed that these differences are associated with the difference in closure effects at the surface and interior locations and the fact that Park's research used a stress ratio of $R = 0.1$ rather the $R = 0.3$ value used for FAA-17. The crack closure phenomena in PMMA, was extensively studied by Ray [15], who showed that differences in plane stress conditions at the specimen surface compared to plane strain conditions in the specimen interior, resulted in different crack opening loads at these two locations. This difference in crack closure load complicates the choice of the da/dN-ΔK law used to backcalculate the cyclic stress-intensity factors. Although Park attempted to account for crack closure [1 and 28] when presenting the results for specimen FAA-4, the differences shown in figure 3-2 for normalized $\phi = 0$ or 1 may be associated with the three-dimensional closure phenomena.

When comparing single knee and corner cracks, it was generally observed that the knee crack tends to grow faster around the bottom corner of the countersunk hole and along the top free surface just after the crack becomes a Type II crack profile, as shown in figure 3-3(a). The corner crack tends to grow faster around the knee of the countersunk hole and along the top free surface of the countersunk hole just after the crack becomes a Type III crack profile, as shown in figure 3-3(b). Similar trends were observed for the two nonsymmetric knee and corner cracks.

3.2 NONSYMMETRIC CRACK PAIR FATIGUE TESTS.

Four specimens were tested with nonsymmetric crack pairs, including two knee crack specimens (FAA-19 and FAA-20) and two corner crack specimens (FAA-21 and FAA-22). The goal of these experiments was to determine stress-intensity factors for nonsymmetric crack pairs located on opposite sides of the countersunk specimen.

Figure 3-4 shows photographs of two knee crack fronts at 70,000 cycles for specimen FAA-19. These photographs, along with others reported in this section, were taken at an angle to the transparent specimen; while they give a skewed view of the crack plane, they show the relative crack sizes and shapes. Perpendicular views of the crack plane made by digitizing and processing the crack, as shown in figure 3-5, and detailed information about these crack shapes are presented in appendix A (e.g., tables A-33 through A-34 and figures A-33 through A-34). The right crack of specimen FAA-19 became a Type II crack at 75,000 cycles and a Type III crack at 100,000 cycles. The left crack of specimen FAA-19 became a Type II crack at 25,000 cycles and a Type III crack at 64,000 cycles.

The crack fronts at 69,000 elapsed cycles for specimen FAA-20 are shown in figure 3-5. The starter notch made for the left crack is clearly seen in this figure. The right crack of specimen FAA-20 became a Type II crack between 53,000 and 56,000 cycles, while the left crack became a Type II crack earlier in life between 10,000 and 11,000 cycles. The transition from Type II and Type III of the left crack occurred between 35,000 and 38,000 cycles.

For the two nonsymmetric knee crack specimens, it was observed that if one crack was bigger than the other at the knee, the larger crack tended to grow much faster than the smaller crack due to the higher stress concentration. Comparisons of dimensionless stress-intensity factors $f(g)$ for similar crack pairs found in specimens FAA-19 and FAA-20 are given in figure 3-6. The designations "R" and "L" in the legend of that figure refer to the right and left cracks, respectively. Although the crack shapes are slightly different, the stress-intensity factors show similar trends for the corresponding cracks. Figures 3-7 and 3-8 compare $f(g)$ for the right and left cracks of specimen FAA-19 and FAA-20, respectively. As expected, the geometric factor for the bigger crack in each pair is larger than for the smaller crack.

Figure 3-9 shows photographs of the crack fronts at 89,000 cycles for corner crack specimen FAA-21. The right and left cracks of specimen FAA-21 grew at approximately the same rate. The right and left cracks of specimen FAA-21 took the Type II shape at 51,000 cycles and the Type III shape at 98,000 cycles. Fracture of specimen FAA-21 occurred at 107,216 cycles.

Photographs of crack fronts at 108,000 cycles for specimen FAA-22 are shown in figure 3-10. The right crack of specimen FAA-22 transitioned to a Type II crack between 42,000 and 45,000 cycles, and from Type II to Type III between 99,000 and 102,000 cycles. The left crack became a Type II later than the right crack at 57,000 cycles. Fracture of specimen FAA-22 occurred at 114,709 cycles before the left crack developed into a Type III crack.

A comparison of geometric factors was made between FAA-21 and FAA-22 in figure 3-11. The left crack of specimen FAA-21 is slightly smaller than in FAA-22, and its $f(g)$ factors are slightly smaller than those of the other three cracks. However, the geometric factors for these cracks do not differ significantly, and show similar trends. Figure 3-12 compares $f(g)$ for the right and left cracks in specimen FAA-22. Note that the geometric factor for the bigger crack is larger than for the smaller crack.

The geometric factors for a single crack were compared with results for a nonsymmetric crack pair to evaluate the effect of the larger crack on the smaller crack. Figure 3-13 compares $f(g)$ for the corresponding cracks. Note that the right crack of double-crack specimen FAA-19 is slightly

smaller than the single crack in specimen FAA-17, since exactly matching crack fronts could not be found. Although the right crack of specimen FAA-19 is smaller than the single crack in specimen FAA-17, the geometric factors for the FAA-19 right-hand crack are larger than those for single crack specimen FAA-17. Thus, the presence of the left-hand crack on the opposite side of the hole does elevate the stress-intensity factor.

3.3 COMPARISONS WITH StressCheck.

A total of 11 comparisons were made between the experimentally determined stress-intensity factors and those obtained numerically by the StressCheck finite element software. These comparisons are shown below for single crack specimens (FAA-17 and FAA-18) and for the two nonsymmetric crack pair specimens (FAA-19, FAA-20, FAA-21, and FAA-22). Details of the finite element model and convergence studies used for these results are described in reference 2.

Figures 3-14 through 3-31 show the comparisons between experimental and StressCheck FEA results. Two comparisons are given for single knee crack specimens, two for single corner crack specimens, three for nonsymmetric knee crack pair specimens, and four comparisons for nonsymmetric corner crack pair specimens. In general, the StressCheck and experimental results agree reasonably well except at crack locations given by normalized ϕ near 0 and 1 (i.e., at the plate surface where $\phi = 0$ and at the hole bore where normalized $\phi = 1$). It is well known that such free surface locations are notorious for causing problems with FEA calculations for stress-intensity factors due to changes in the crack tip singularity at those positions. The average percent differences in the dimensionless stress-intensity factor are within 9.1% compared to the experimental results. Among the cracks compared, the right crack of comparison crack 5 and the right and left cracks of comparison crack 8 exhibit differences in geometric factor, as shown in figures 3-18, 3-24, and 3-25. StressCheck results tend to underestimate geometric factors for the smaller Type I crack profiles.

A numerical study was conducted to evaluate the influence of a second crack located on the opposite side of the hole to comparison crack 6. Single crack, symmetric crack, and nonsymmetric crack cases were considered. Figures 3-32 and 3-33 show the comparison of the FEA geometric factors for three cases with the experimental results. For the right crack (small crack) in FAA-20, the geometric factors for the symmetric case increase by 1.7% on average, and the geometric factors in the nonsymmetric case increase by 10.6% on average, due to the second crack (large crack) when compared to those in the single crack case. For the left crack (large crack) of FAA-20, the geometric factors in the symmetric case increase by 10% on average, and the geometric factors in the nonsymmetric case increase by 1.6% on average due, to the second crack (small crack) when compared to those in the single crack case. Therefore, the large crack has a great effect of geometric factors on the small crack, while the small crack does not have much effect on the large crack.

Table 3-1. Summary of Open-Hole Specimens Discussed in Current Report

Specimen ID	Crack Shapes Studied	Remarks
FAA-17 FAA-17A		Single Knee Crack
FAA-18		Single Corner Crack
FAA-19		Nonsymmetric Knee Crack
FAA-20		
FAA-21		Nonsymmetric Corner Crack
FAA-22		

Specimen ID	Number of Crack Shapes Examined	Appendix A Tables
FAA-17	15	A-1-A-15
FAA-17A	8	A-105-A-112
FAA-18	13	A-16-A-28
FAA-19	18	A-29-A-46
FAA-20	16	A-47-A-62
FAA-21	22	A-63-A-84
FAA-20	20	A-85-A-104

Note: Tabulated stress-intensity factor results are reported for 112 total cracks in appendix A.

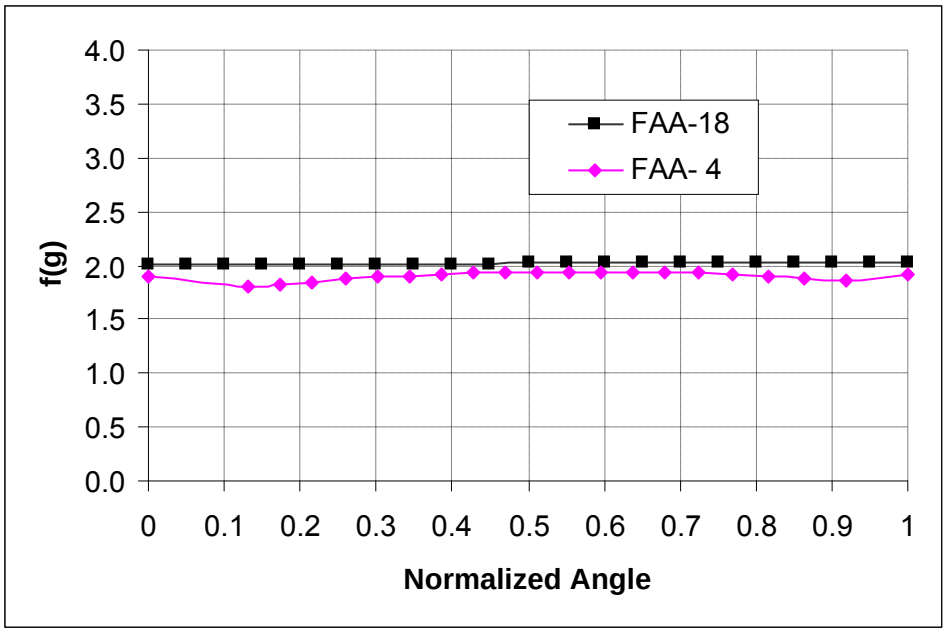

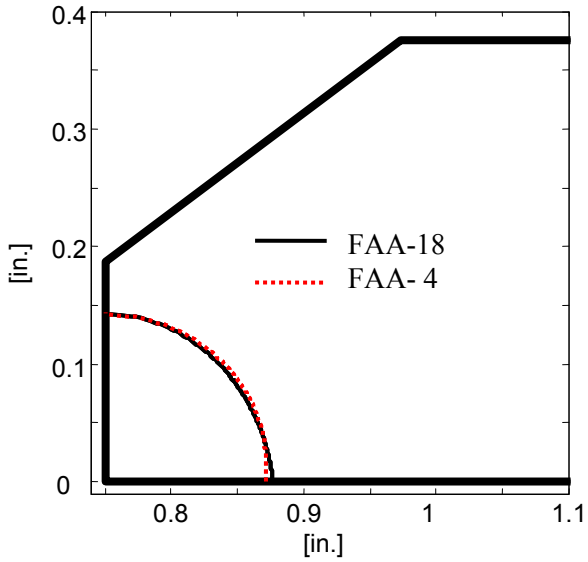

Figure 3-1. Comparison of Results for Specimens FAA-18 and FAA-4

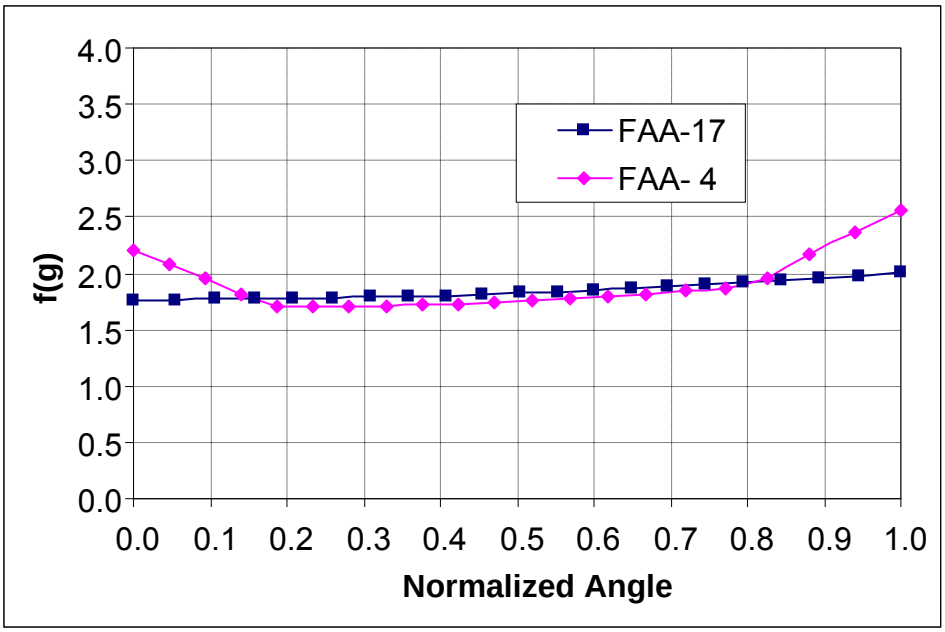

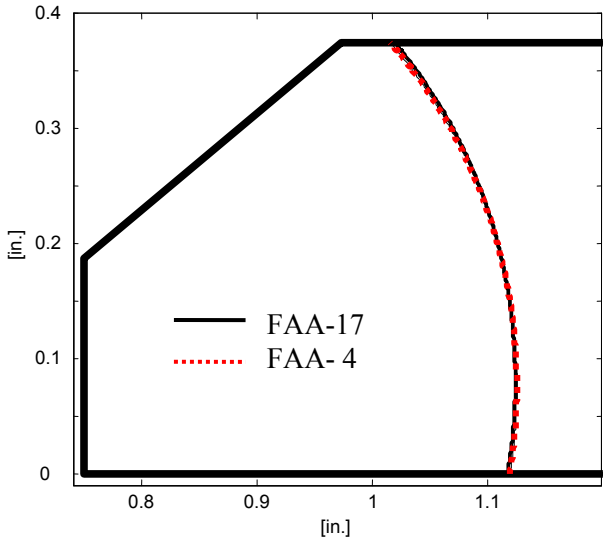

Figure 3-2. Comparison of Results for Specimens FAA-17 and FAA-4

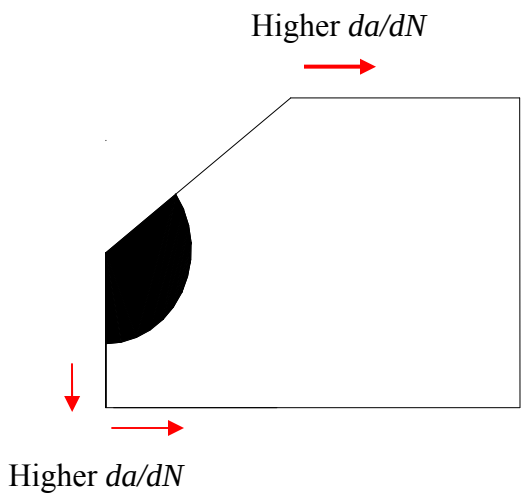

(a) Knee Crack

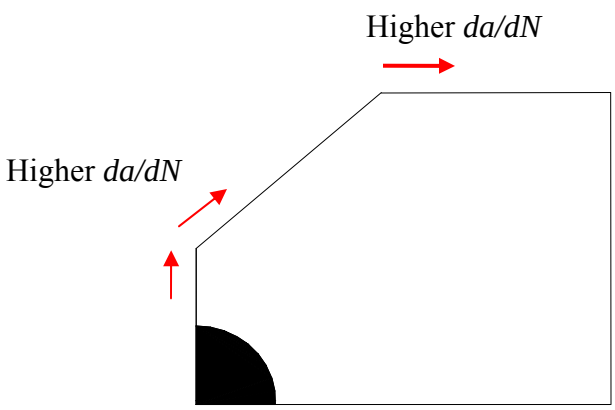

(b) Corner Crack

Figure 3-3. Higher Crack Growth Rate Region

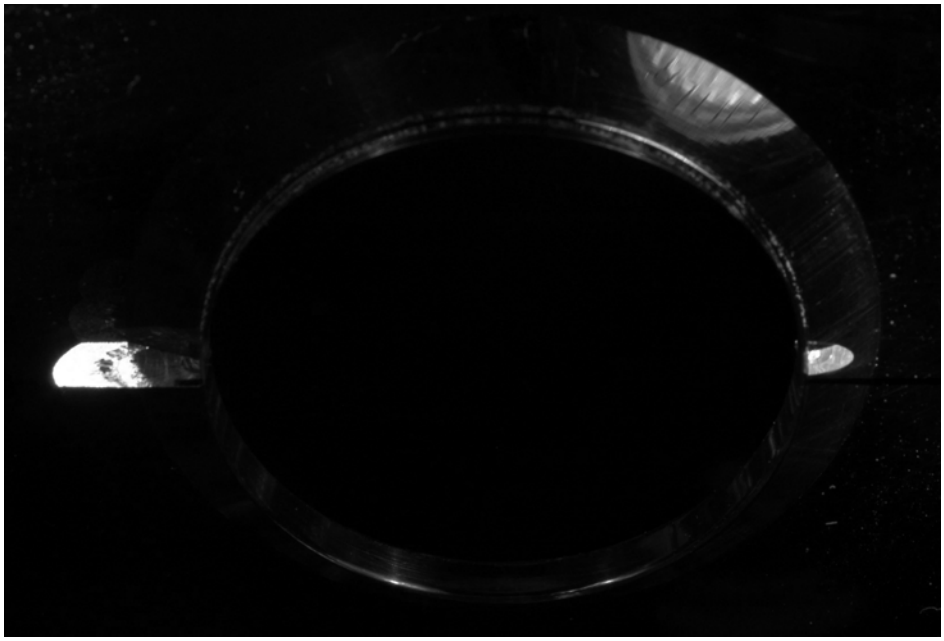

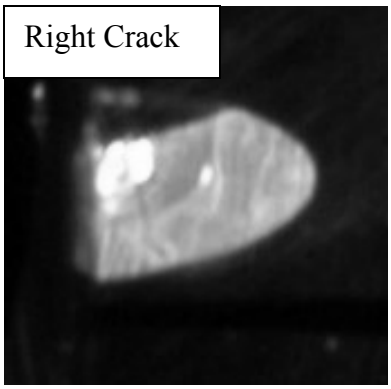

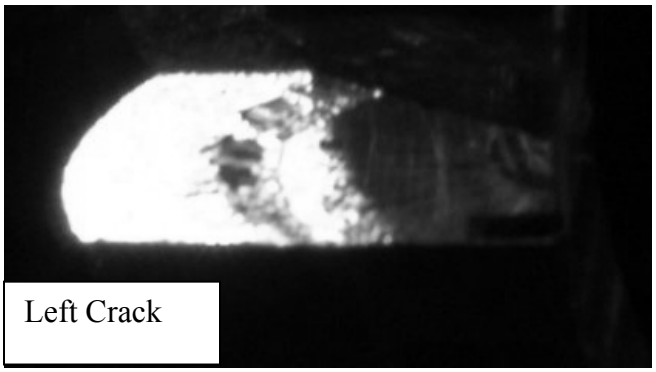

Figure 3-4. Crack Fronts at 70,000 Cycles (FAA-19)

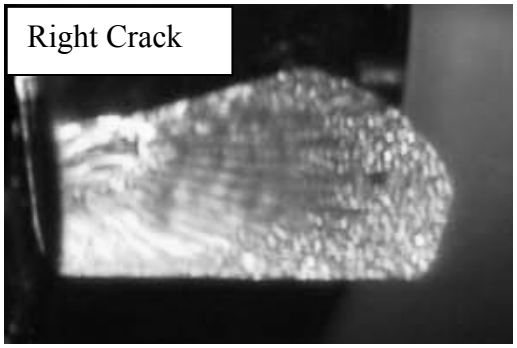

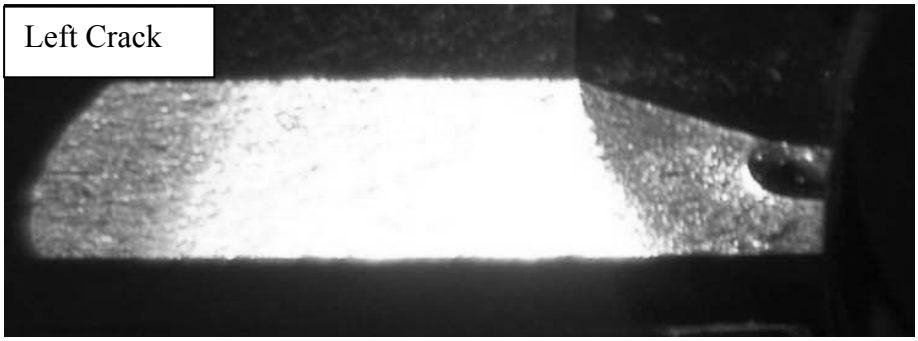

Figure 3-5. Crack Fronts at 69,000 Cycles (FAA-20)

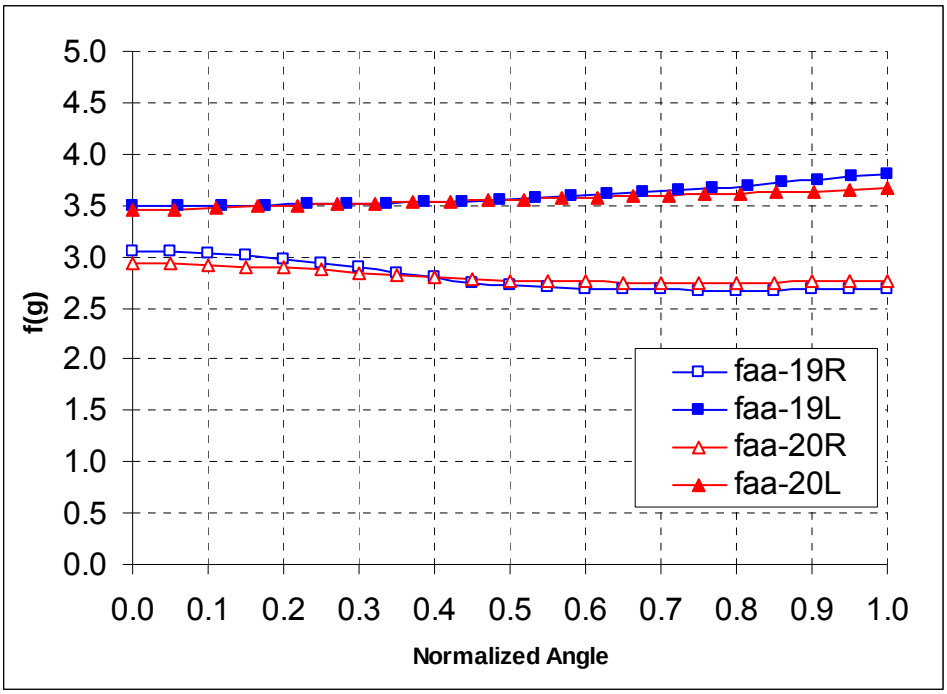

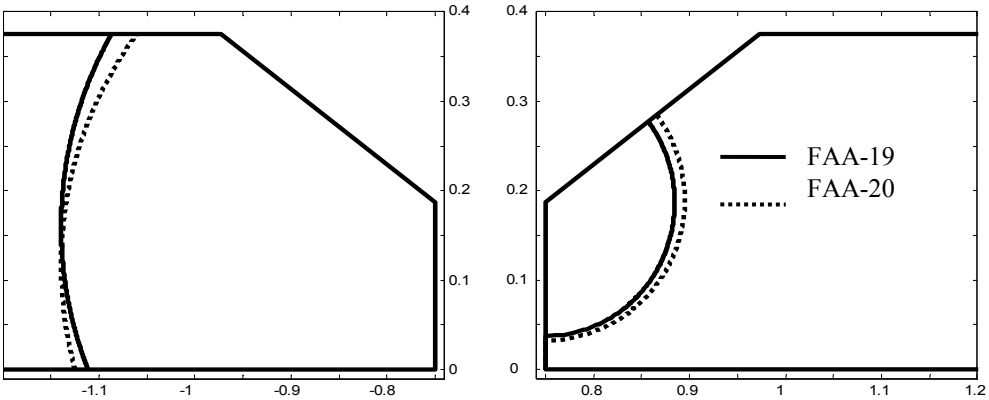

Figure 3-6. Geometric Factors for FAA-19 and FAA-20

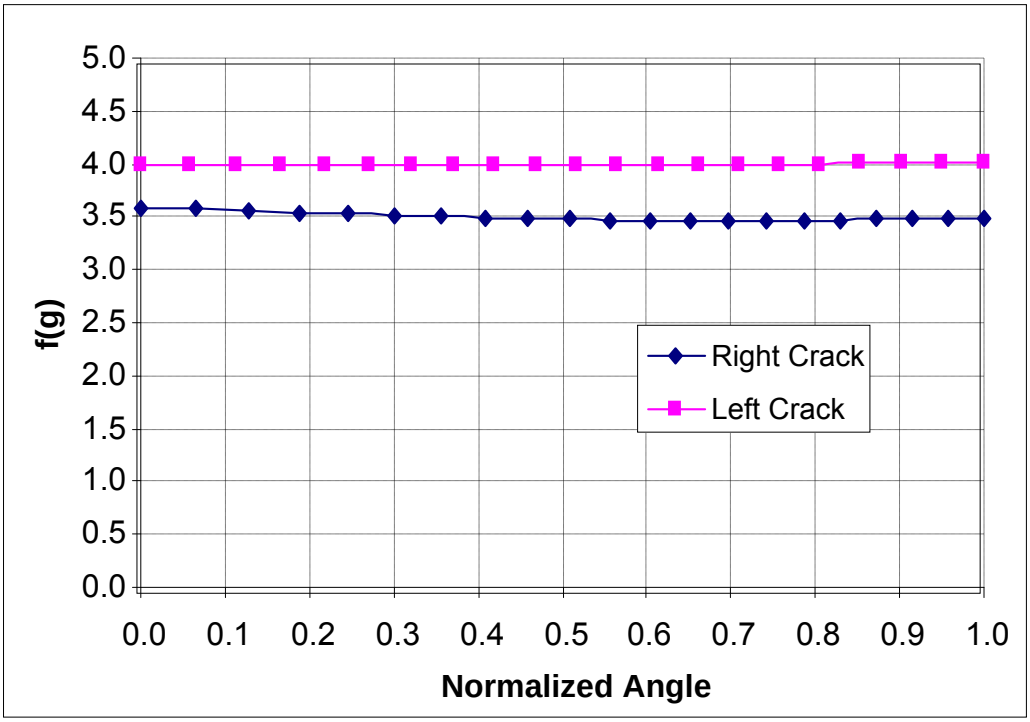

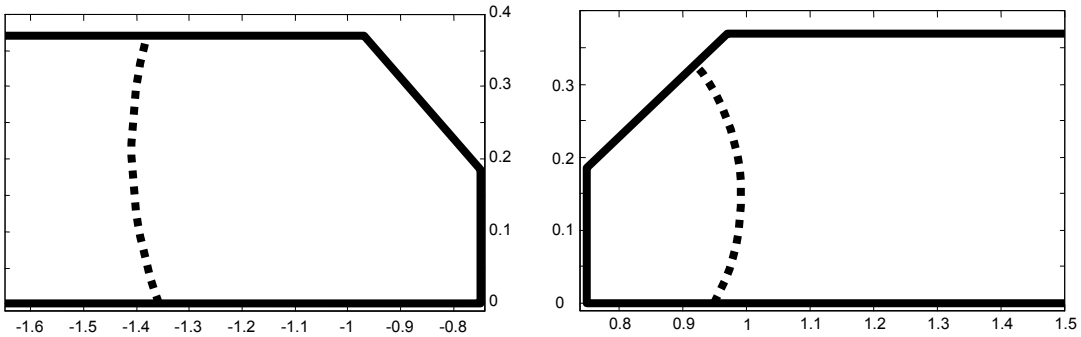

Figure 3-7. Geometric Factors for FAA-19

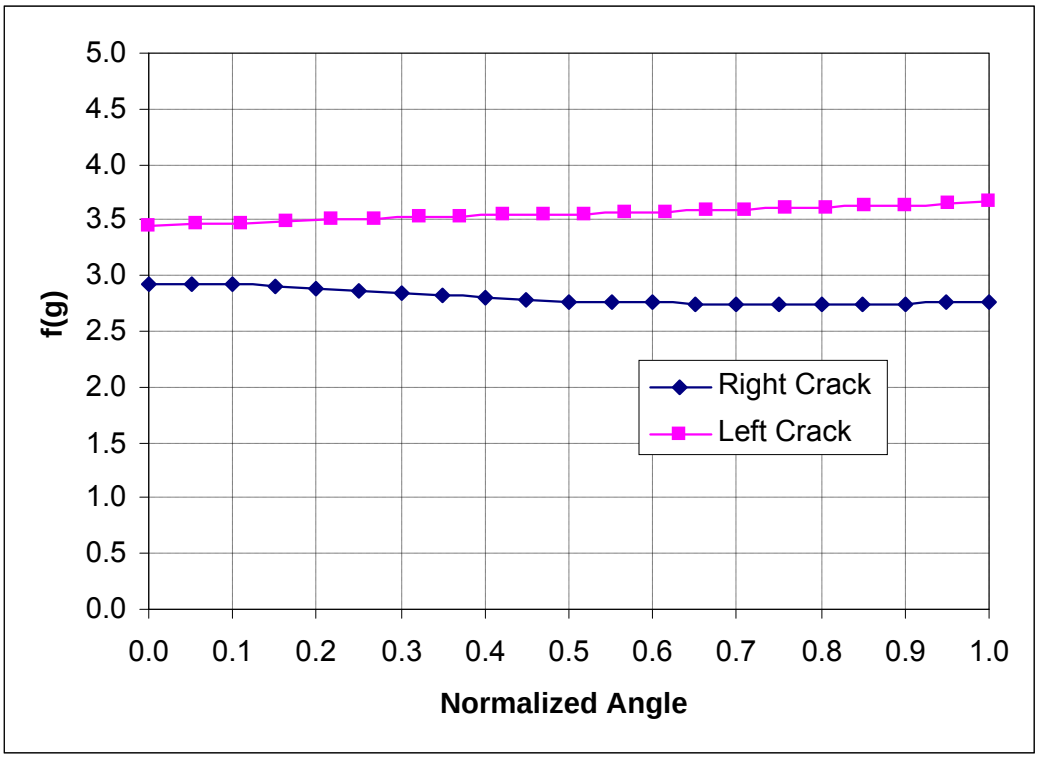

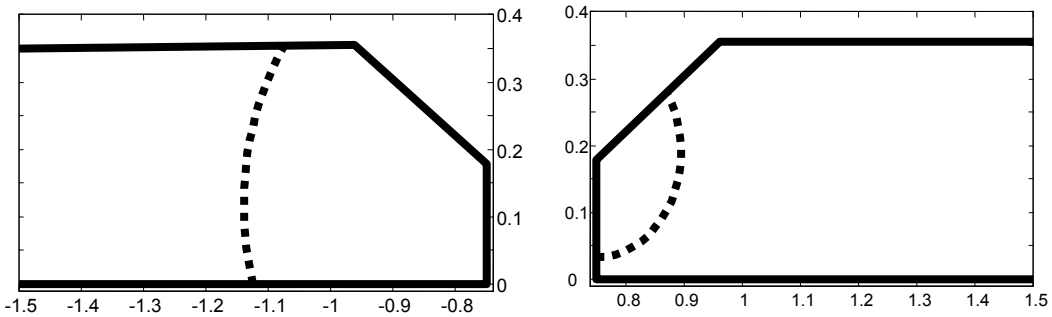

Figure 3-8. Geometric Factors for FAA-20

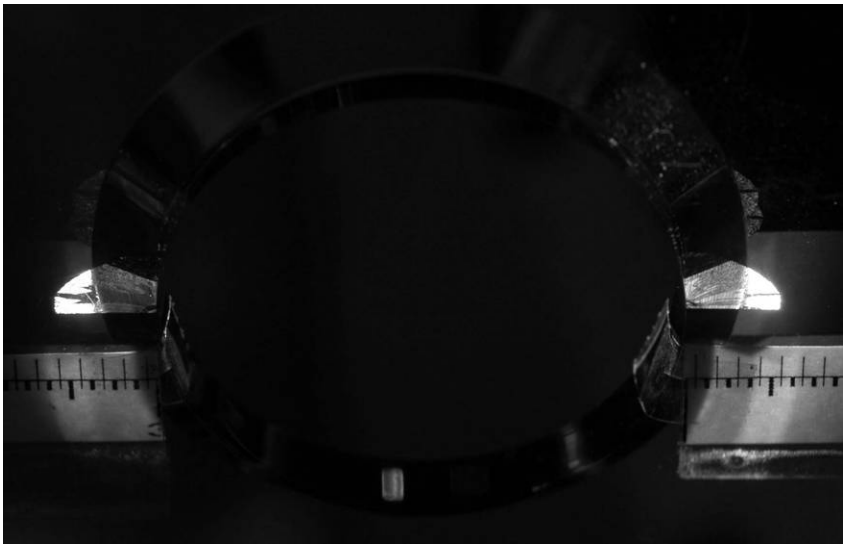

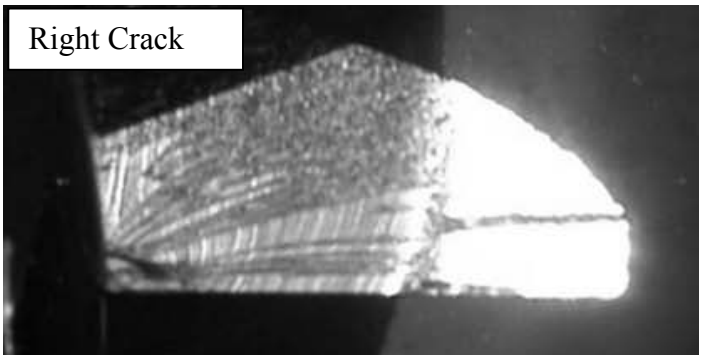

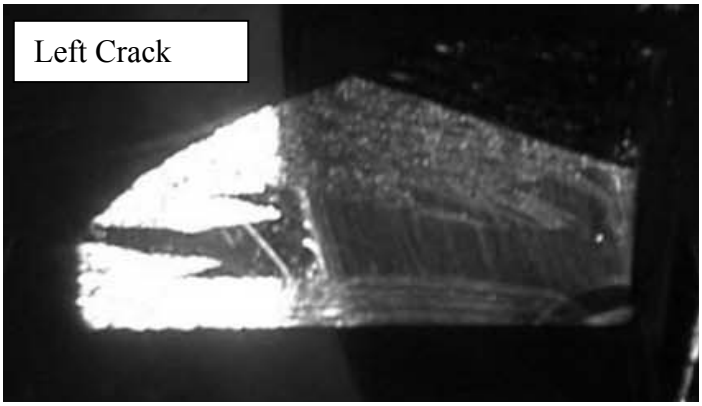

Figure 3-9. Crack Fronts at 89,000 Cycles (FAA-21)

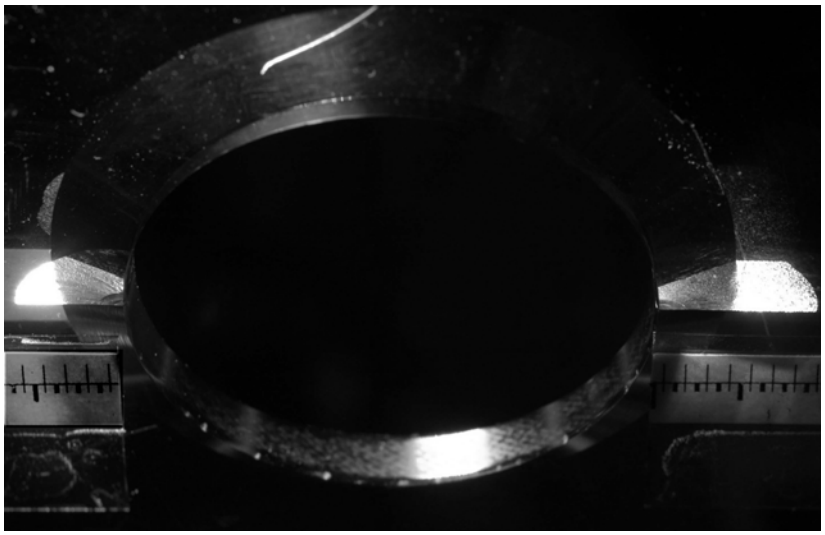

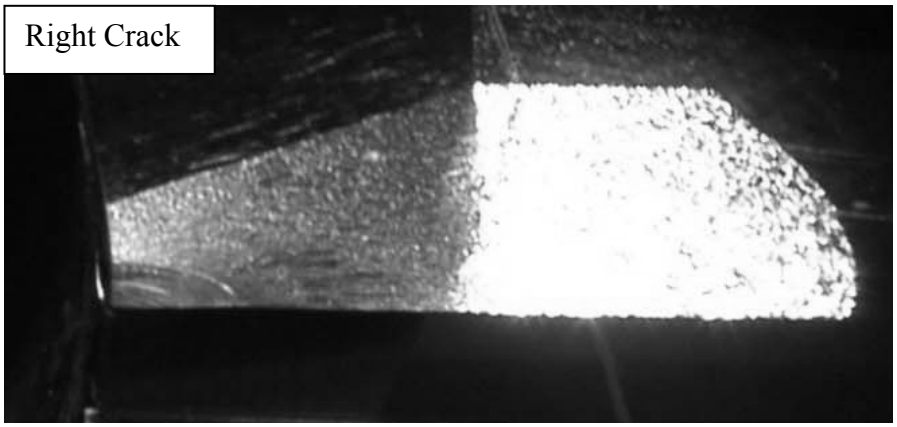

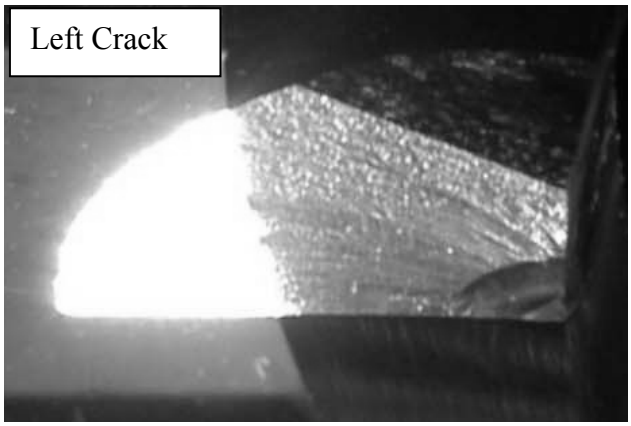

Figure 3-10. Crack Fronts at 108,000 Cycles (FAA-22)

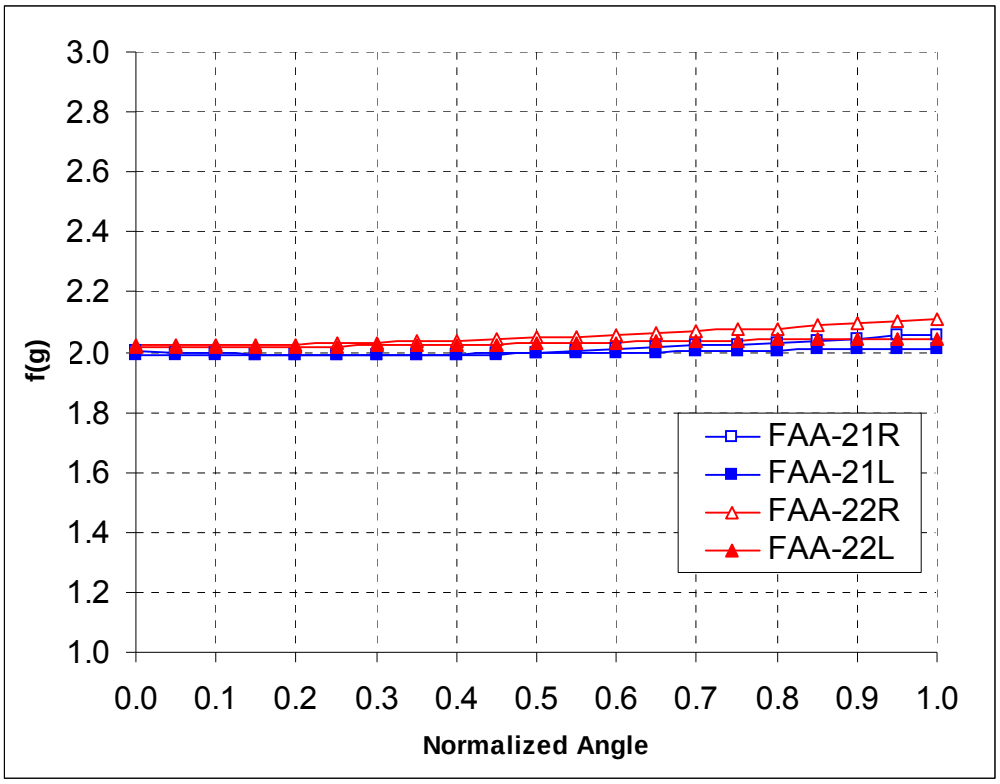

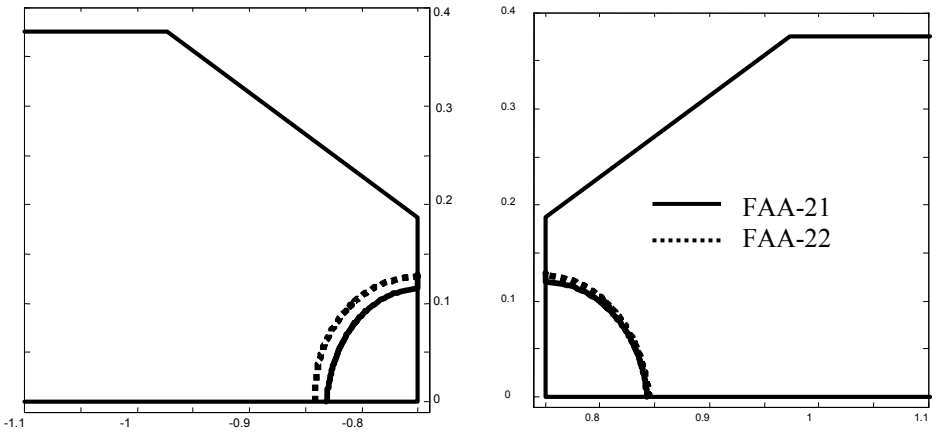

Figure 3-11. Geometric Factors for FAA-21 and FAA-22

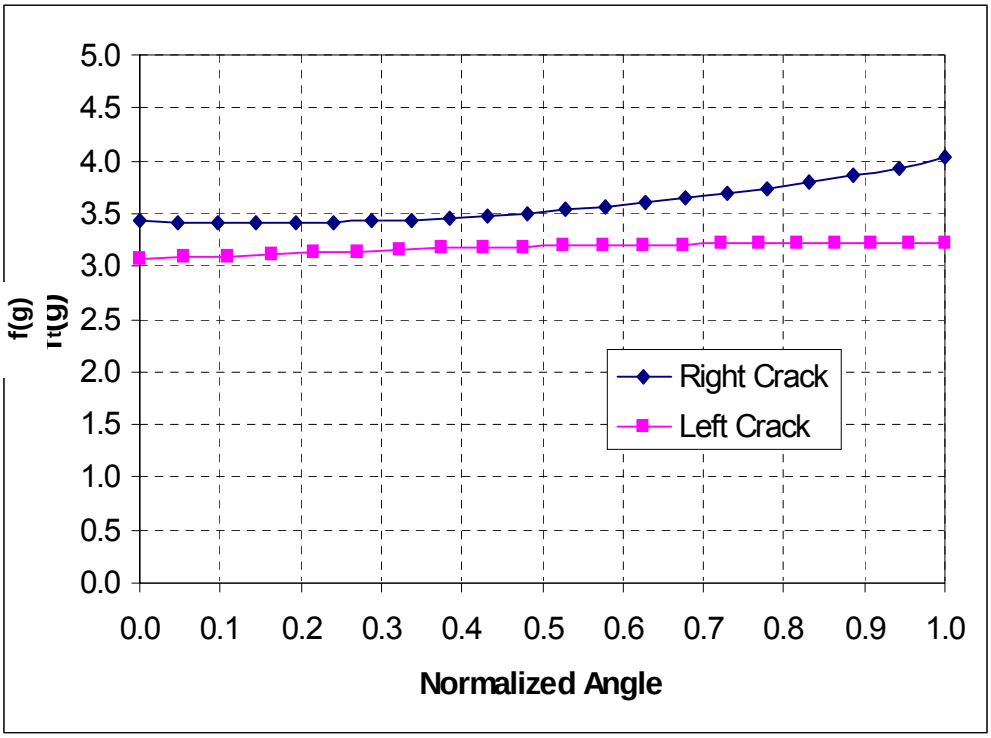

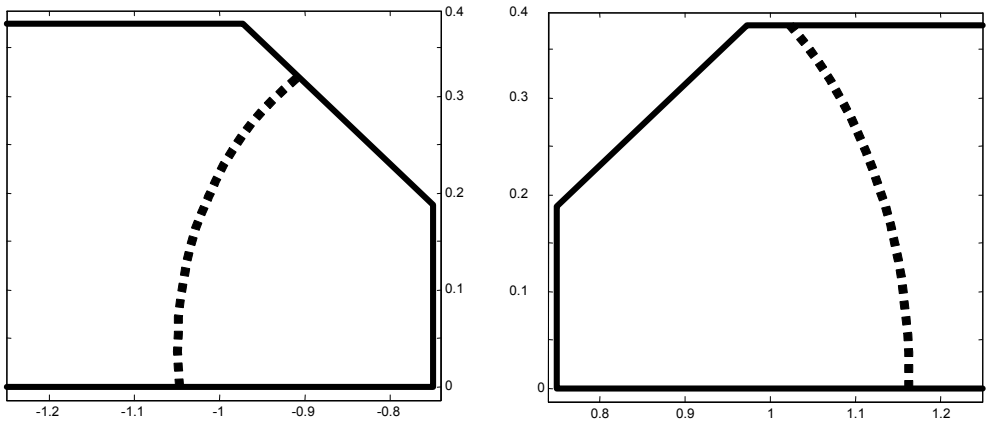

Figure 3-12. Geometric Factors for FAA-22

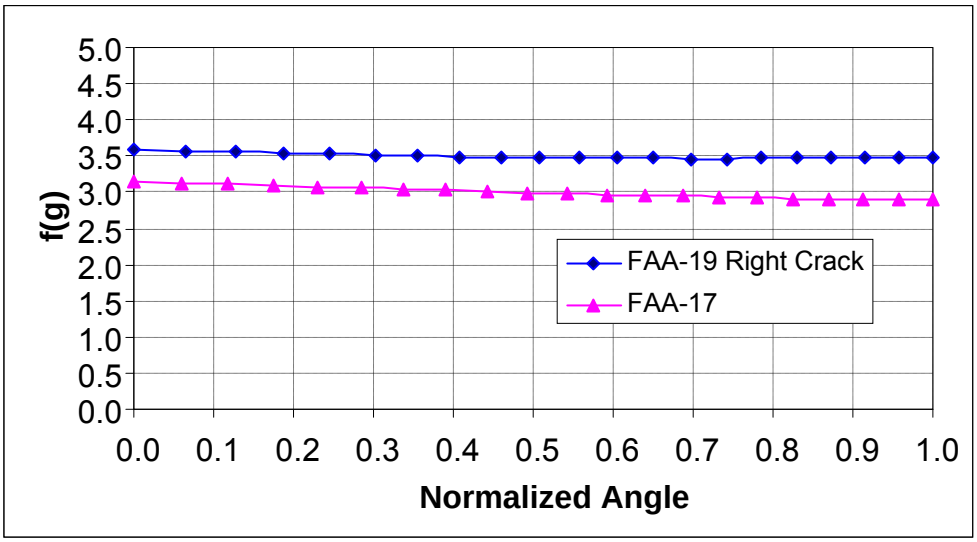

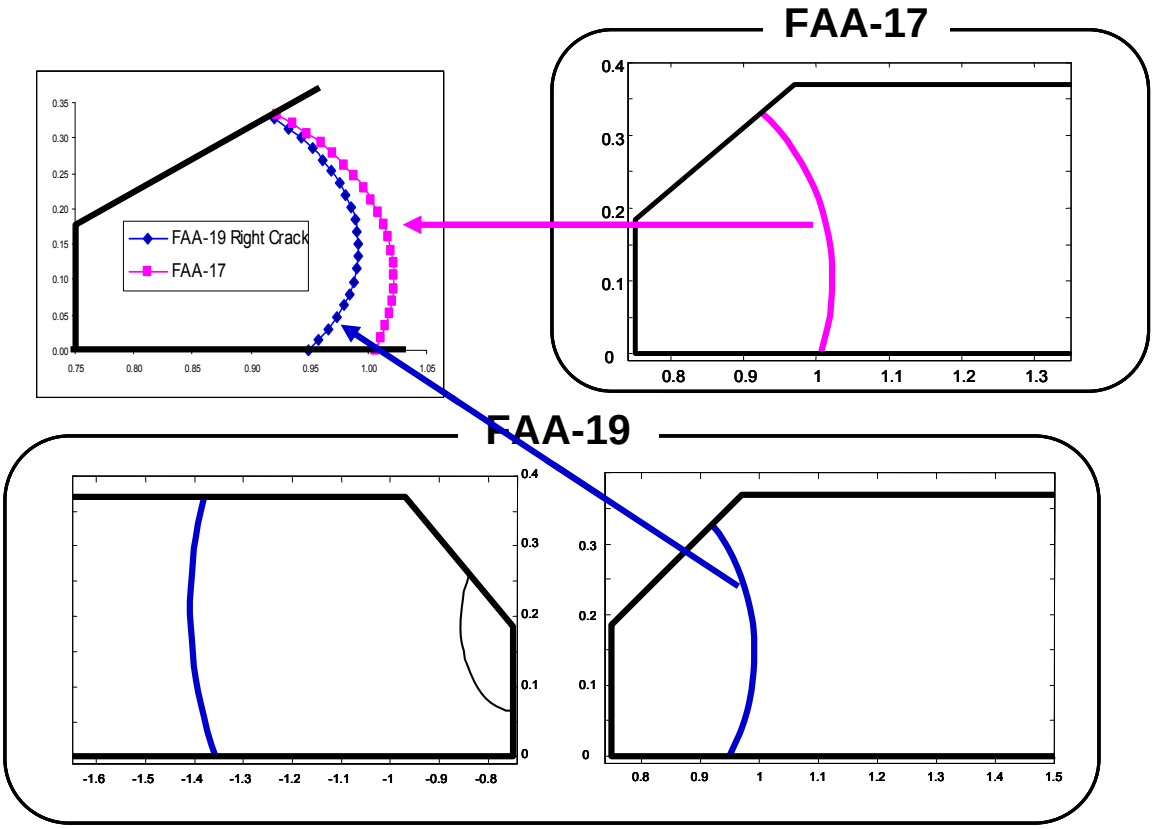

Figure 3-13. Comparison of Geometric Factors Between FAA-17 and FAA-19

Crack Length, a	**0.0950 in**
Crack Depth, c	**0.0980 in**
Center of Ellipse	**0.1780 in**

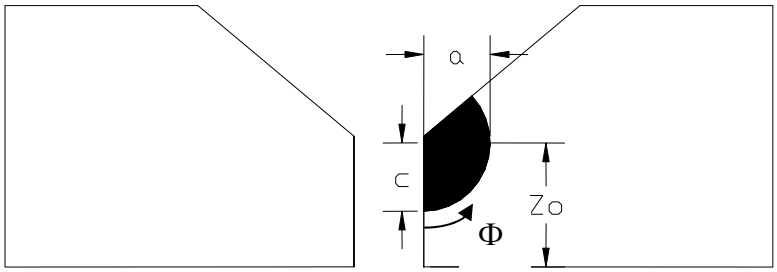

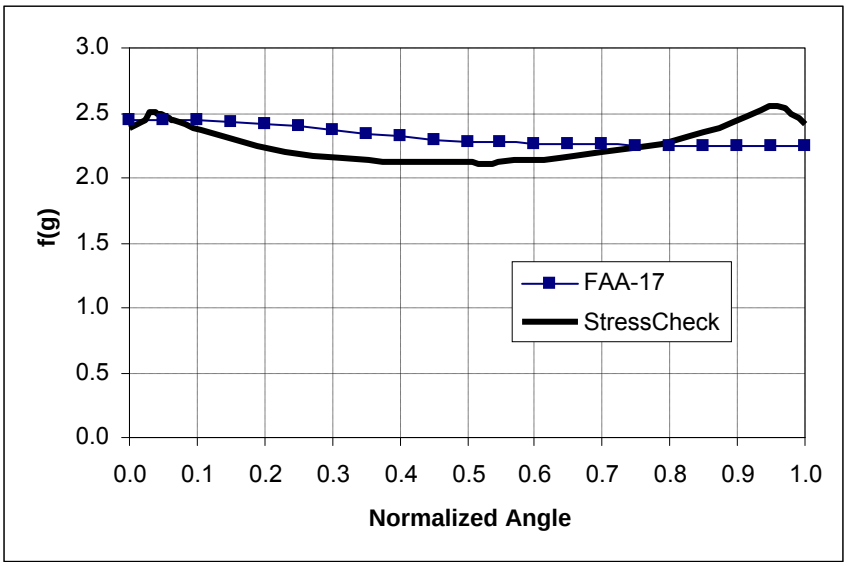

Figure 3-14. Comparison Crack 1

Crack Length, a	**0.1745 in**
Crack Depth, c	**0.2080 in**
Center	**0.1355 in**

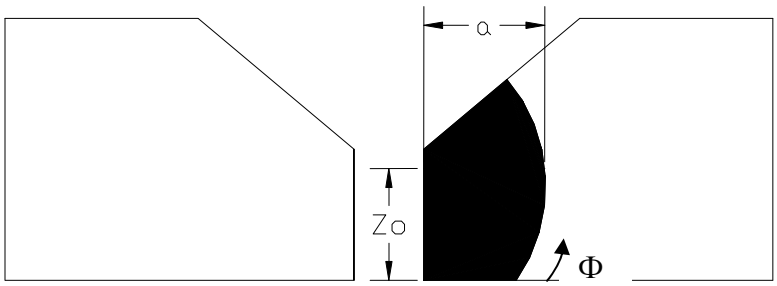

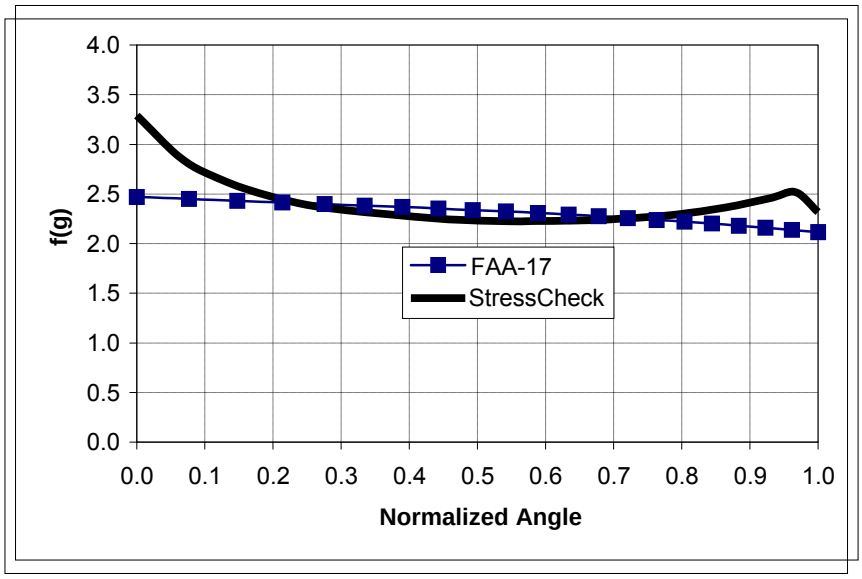

Figure 3-15. Comparison Crack 2

Crack Length, a	**0.1279 in**
Crack Depth, c	**0.1630 in**
Center of Ellipse	**-0.0202 in**

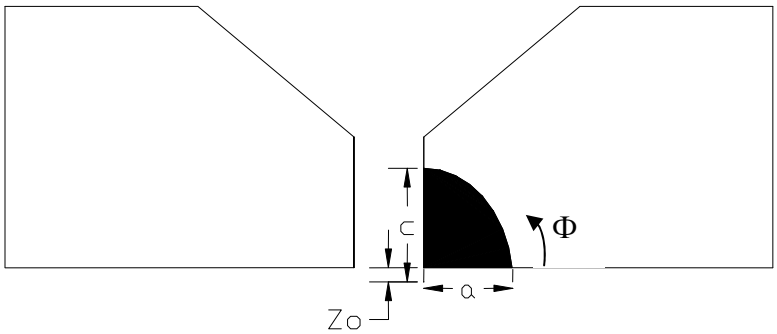

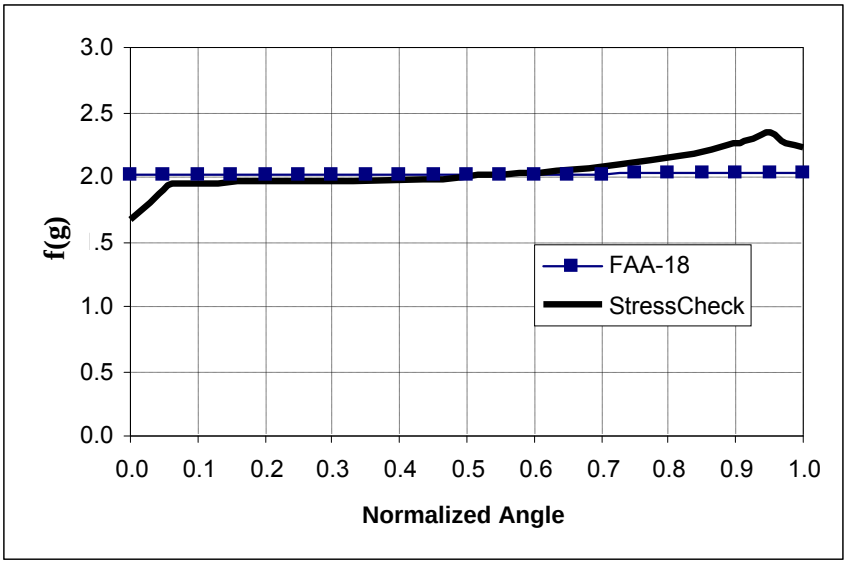

Figure 3-16. Comparison Crack 3

Crack Length, a	**0.3060 in**
Crack Depth, c	**0.3397 in**
Center of Ellipse	**0.0306 in**

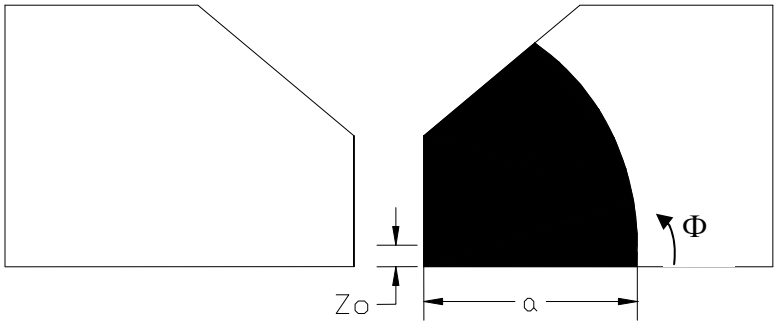

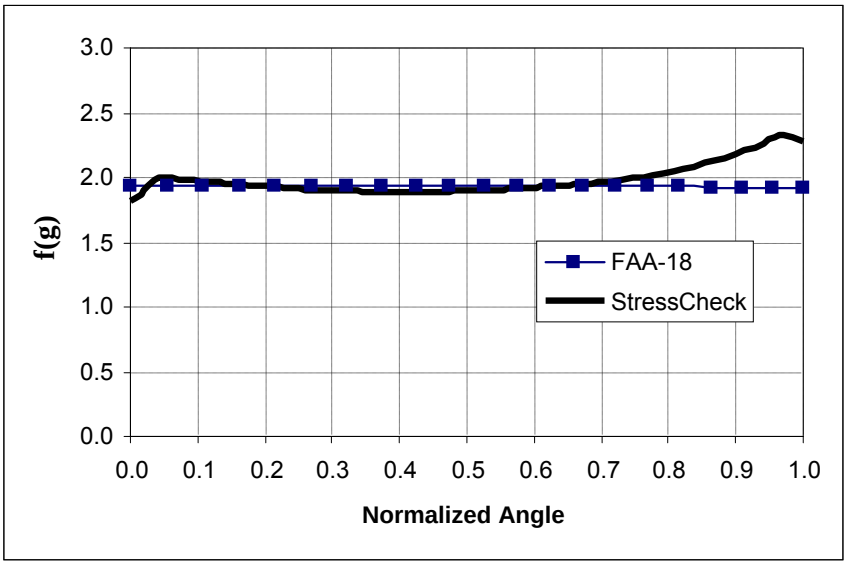

Figure 3-17. Comparison Crack 4

Right Crack		Left Crack	
Crack Length, a	0.0895 in	Crack Length, a	0.1385 in
Crack Depth, c	0.0948 in	Crack Depth, c	0.1485 in
Center of Ellipse	0.2035 in	Center of Ellipse	0.1925 in

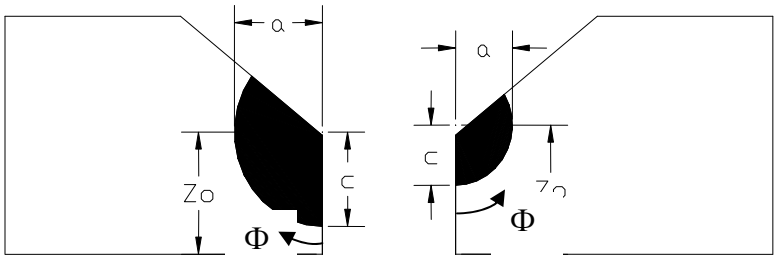

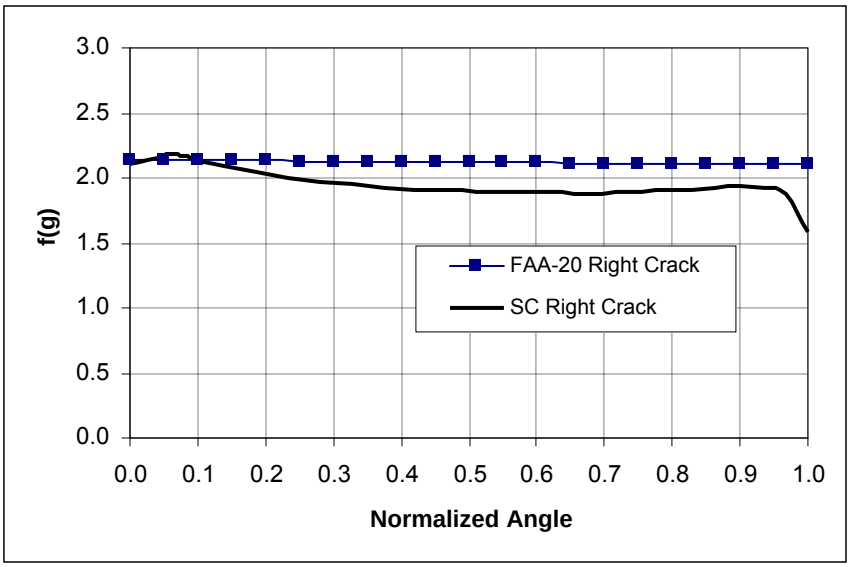

Figure 3-18. Comparison Crack 5 (Right Crack)

Right Crack		Left Crack	
Crack Length, a	0.0895 in	Crack Length, a	0.1385 in
Crack Depth, c	0.0948 in	Crack Depth, c	0.1485 in
Center of Ellipse	0.2035 in	Center of Ellipse	0.1925 in

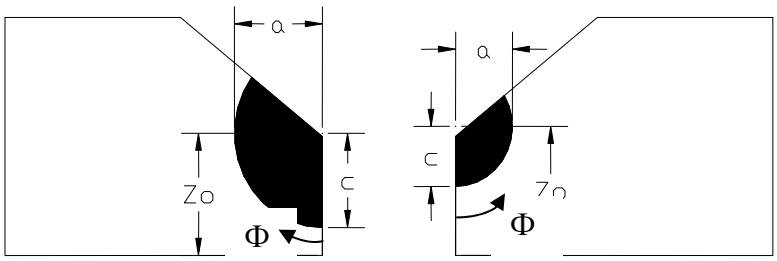

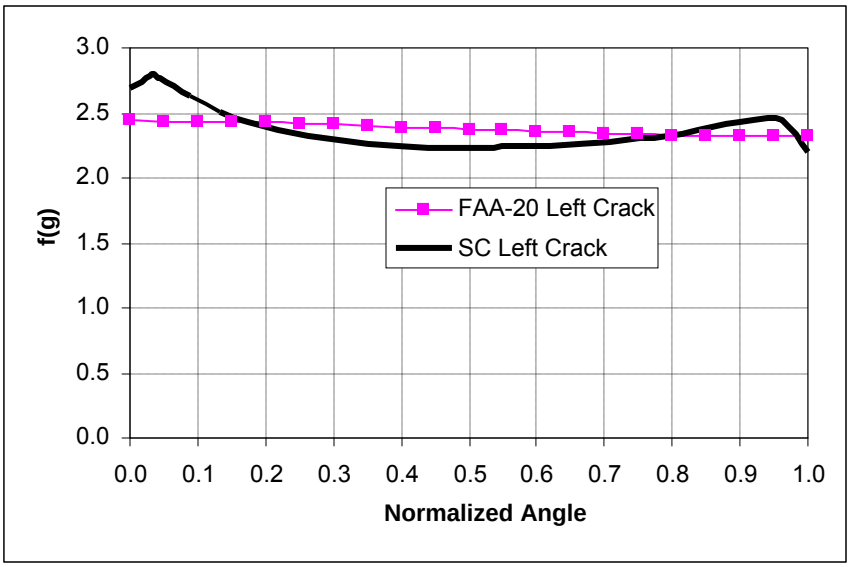

Figure 3-19. Comparison Crack 5 (Left Crack)

Right Crack		Left Crack	
Crack Length, a	0.1900 in	Crack Length, a	0.5290 in
Crack Depth, c	0.2225 in	Crack Depth, c	0.6100 in
Center of Ellipse	0.1615 in	Center of Ellipse	0.1510 in

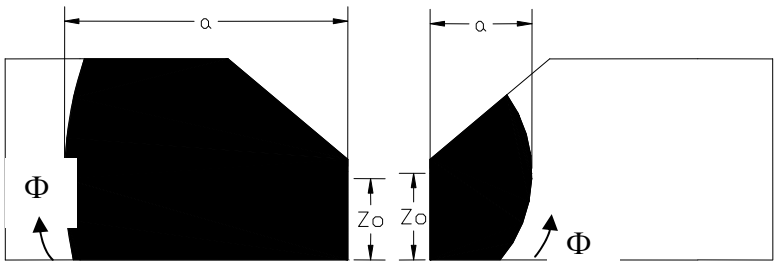

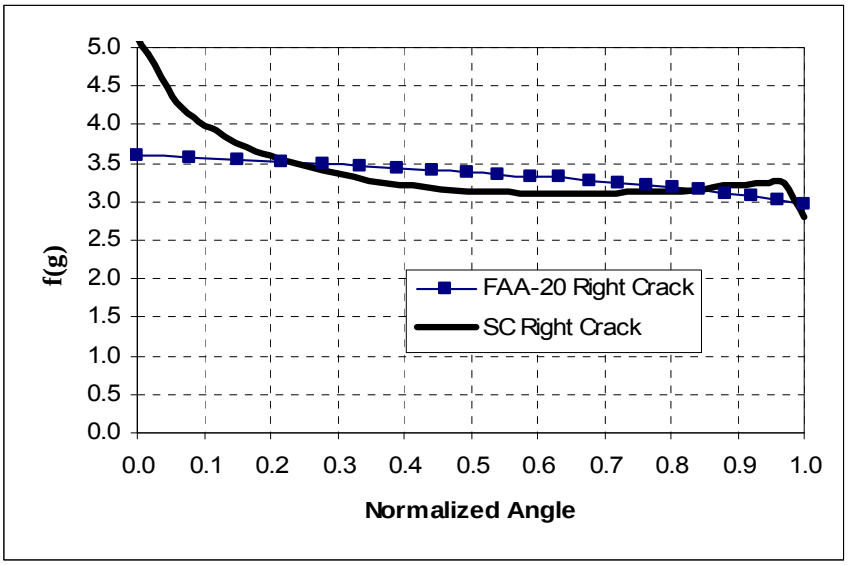

Figure 3-20. Comparison Crack 6 (Right Crack)

Right Crack		Left Crack	
Crack Length, a	0.1900 in	Crack Length, a	0.5290 in
Crack Depth, c	0.2225 in	Crack Depth, c	0.6100 in
Center of Ellipse	0.1615 in	Center of Ellipse	0.1510 in

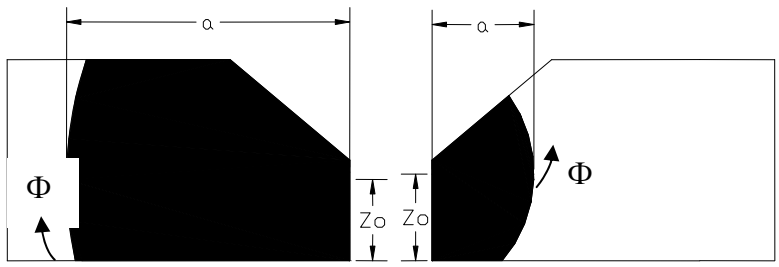

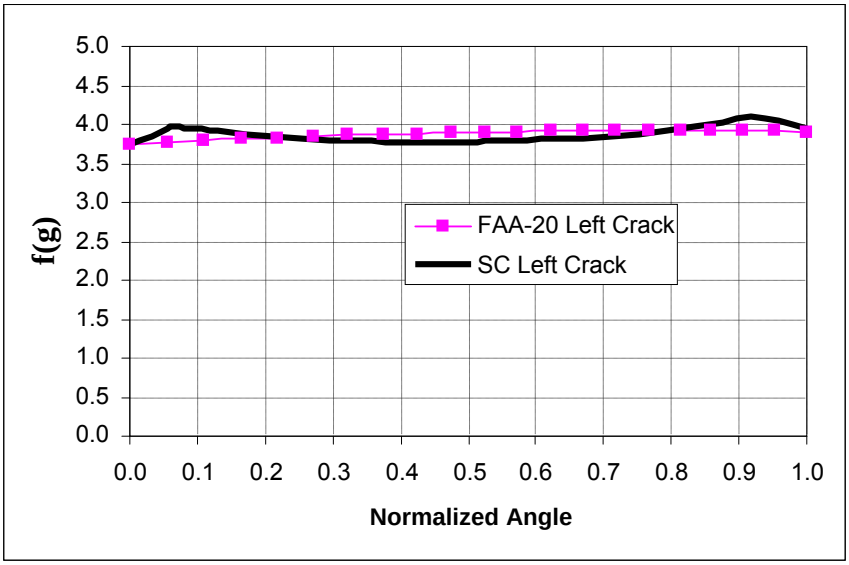

Figure 3-21. Comparison Crack 6 (Left Crack)

Right Crack		Left Crack	
Crack Length, a	0.2420 in	Crack Length, a	0.6590 in
Crack Depth, c	0.2560 in	Crack Depth, c	0.5475 in
Center of Ellipse	0.1450 in	Center of Ellipse	0.2125 in

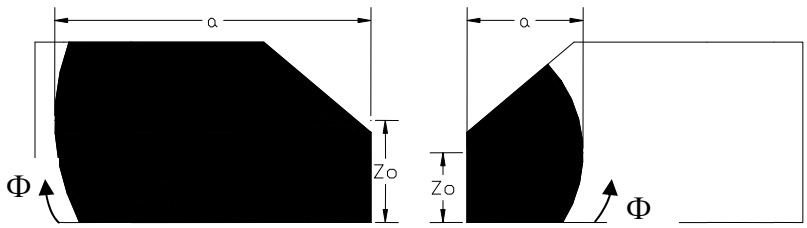

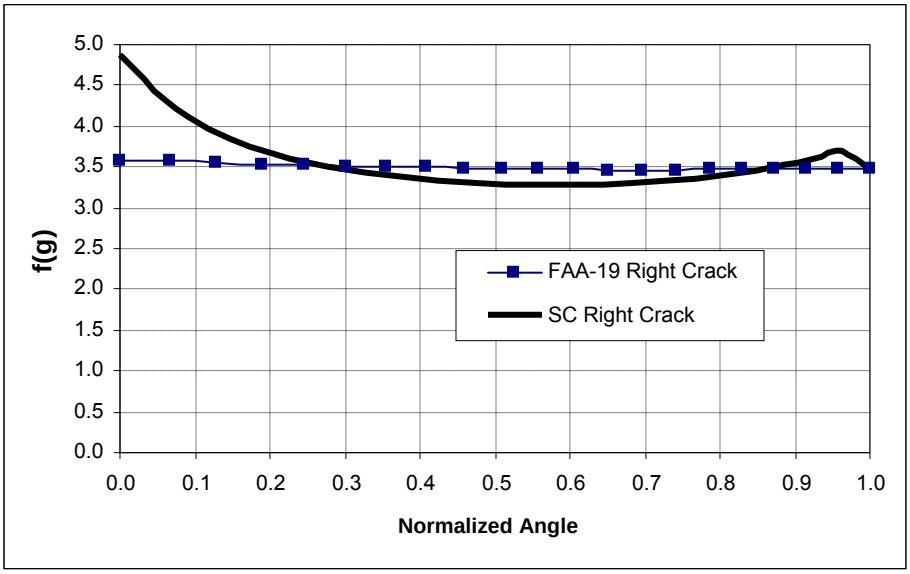

Figure 3-22. Comparison Crack 7 (Right Crack)

Right Crack		Left Crack	
Crack Length, a	0.2420 in	Crack Length, a	0.6590 in
Crack Depth, c	0.2560 in	Crack Depth, c	0.5475 in
Center of Ellipse	0.1450 in	Center of Ellipse	0.2125 in

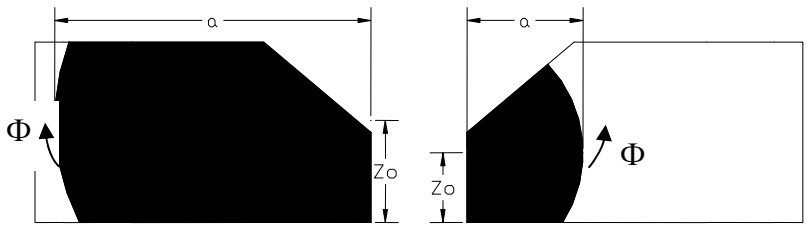

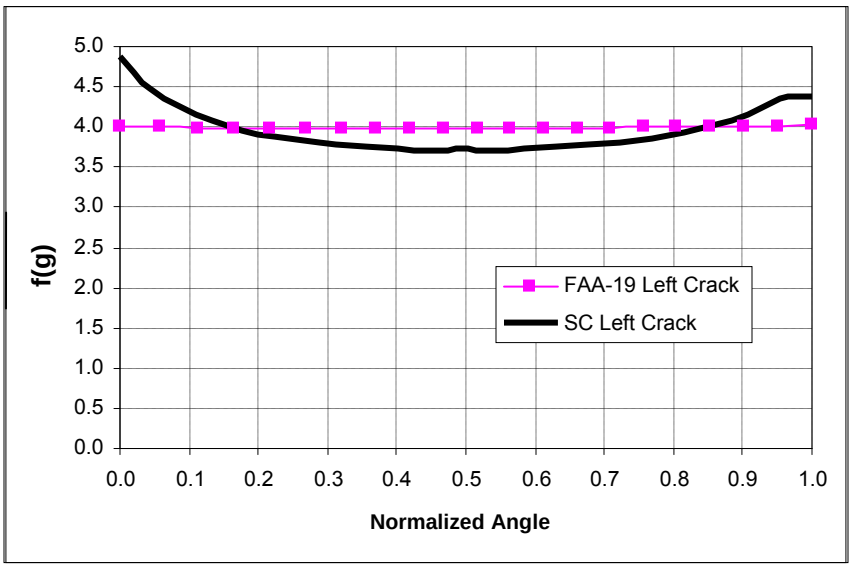

Figure 3-23. Comparison Crack 7 (Left Crack)

Right Crack		Left Crack	
Crack Length, a	**0.0822 in**	**Crack Length, a**	**0.0713 in**
Crack Depth, c	**0.1091 in**	**Crack Depth, c**	**0.1052 in**
Center of Ellipse	**-0.0035 in**	**Center of Ellipse**	**-0.0027 in**

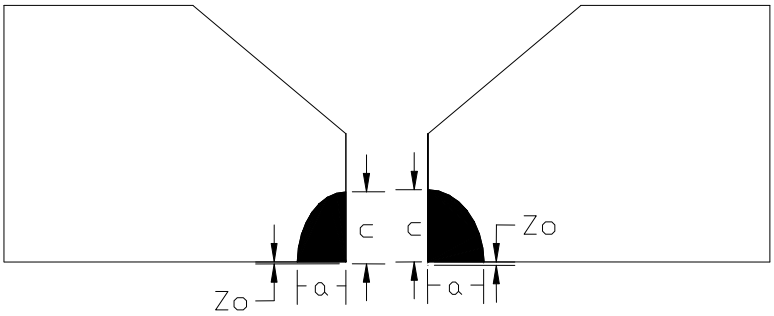

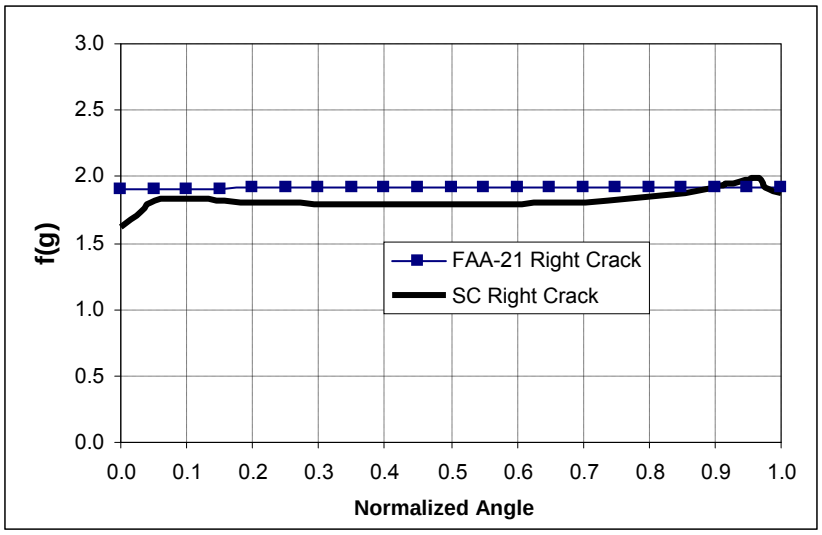

Figure 3-24. Comparison Crack 8 (Right Crack)

Right Crack		Left Crack	
Crack Length, a	0.0822 in	Crack Length, a	0.0713 in
Crack Depth, c	0.1091 in	Crack Depth, c	0.1052 in
Center of Ellipse	-0.0035 in	Center of Ellipse	-0.0027 in

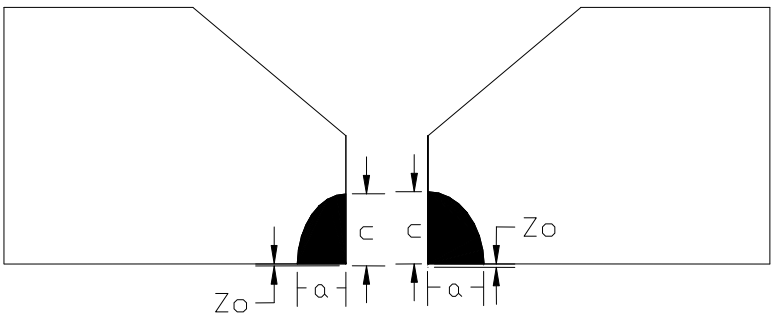

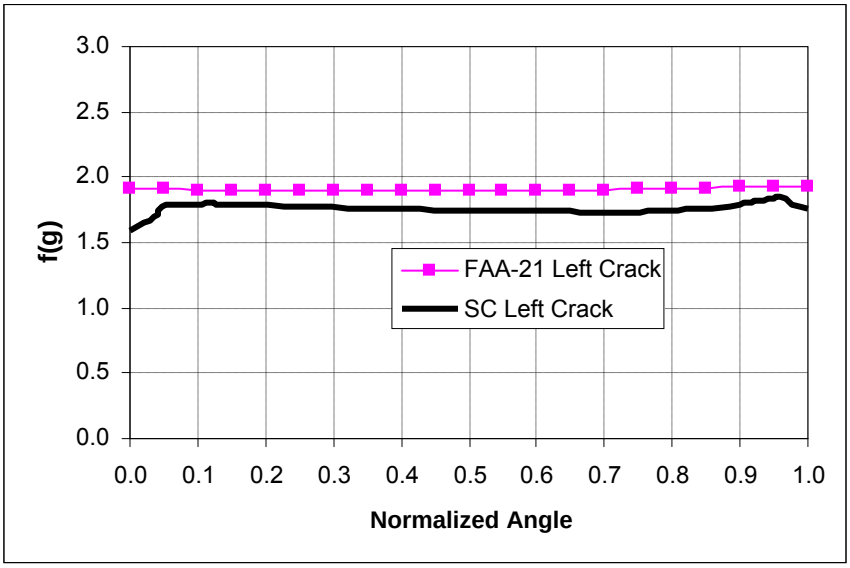

Figure 3-25. Comparison Crack 8 (Left Crack)

Right Crack		Left Crack	
Crack Length, a	0.1095 in	Crack Length, a	0.0960 in
Crack Depth, c	0.1653 in	Crack Depth, c	0.1438 in
Center of Ellipse	-0.0186 in	Center of Ellipse	-0.0089 in

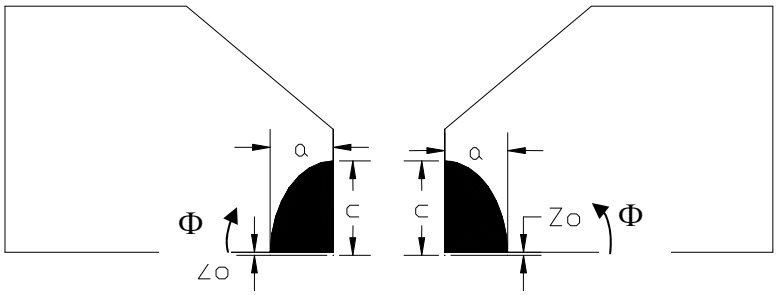

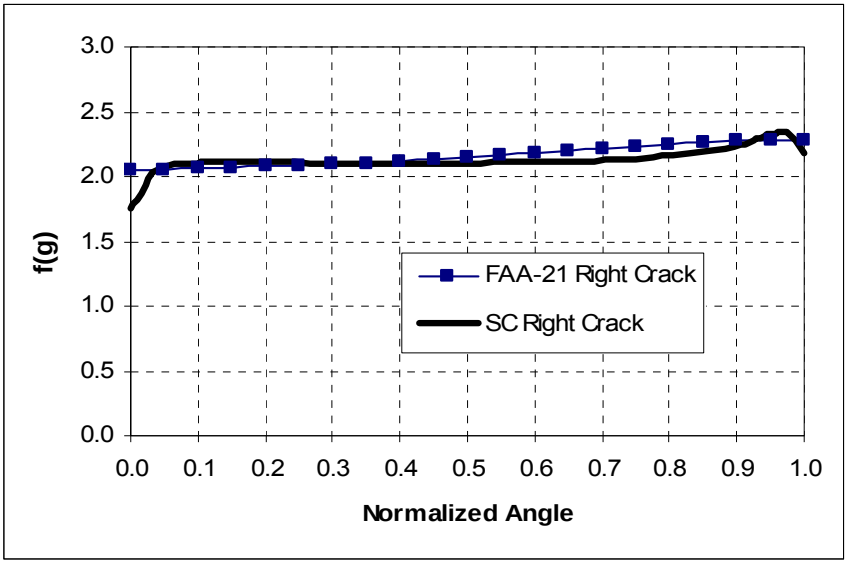

Figure 3-26. Comparison Crack 9 (Right Crack)

Right Crack		Left Crack	
Crack Length, a	0.1095 in	Crack Length, a	0.0960 in
Crack Depth, c	0.1653 in	Crack Depth, c	0.1438 in
Center of Ellipse	-0.0186 in	Center of Ellipse	-0.0089 in

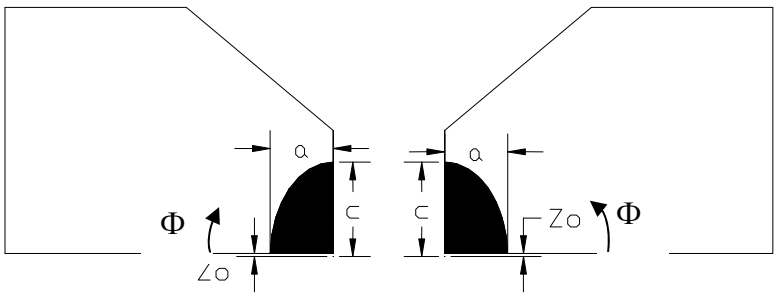

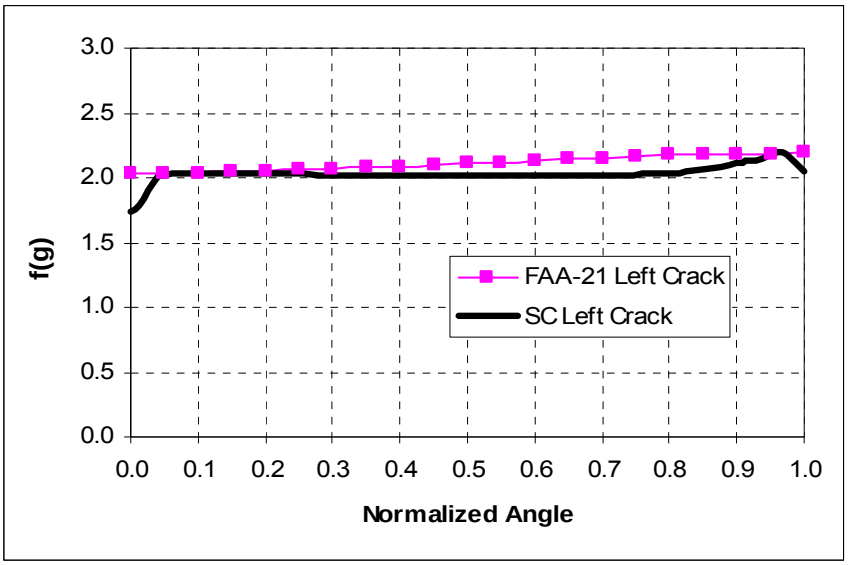

Figure 3-27. Comparison Crack 9 (Left Crack)

Right Crack		Left Crack	
Crack Length, a	0.2003 in	Crack Length, a	0.1626 in
Crack Depth, c	0.2647 in	Crack Depth, c	0.2271 in
Center of Ellipse	0.0158 in	Center of Ellipse	0.0066 in

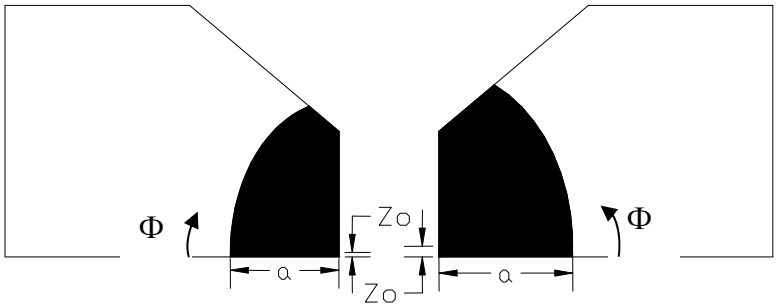

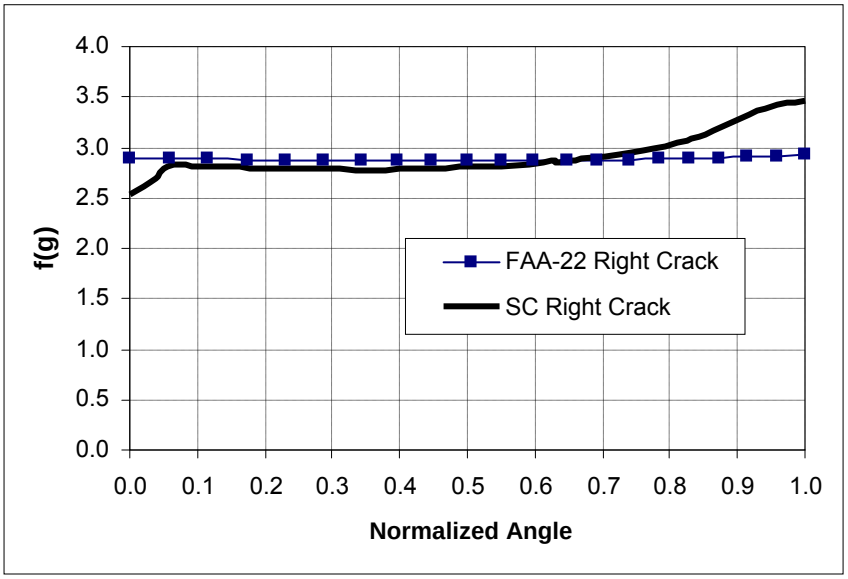

Figure 3-28. Comparison Crack 10 (Right Crack)

Right Crack		Left Crack	
Crack Length, a	0.2003 in	Crack Length, a	0.1626 in
Crack Depth, c	0.2647 in	Crack Depth, c	0.2271 in
Center of Ellipse	0.0158 in	Center of Ellipse	0.0066 in

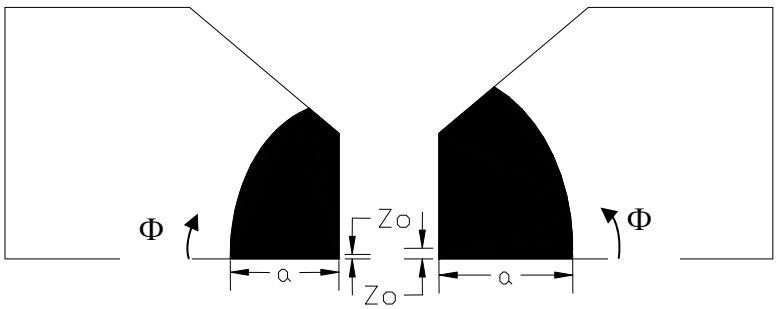

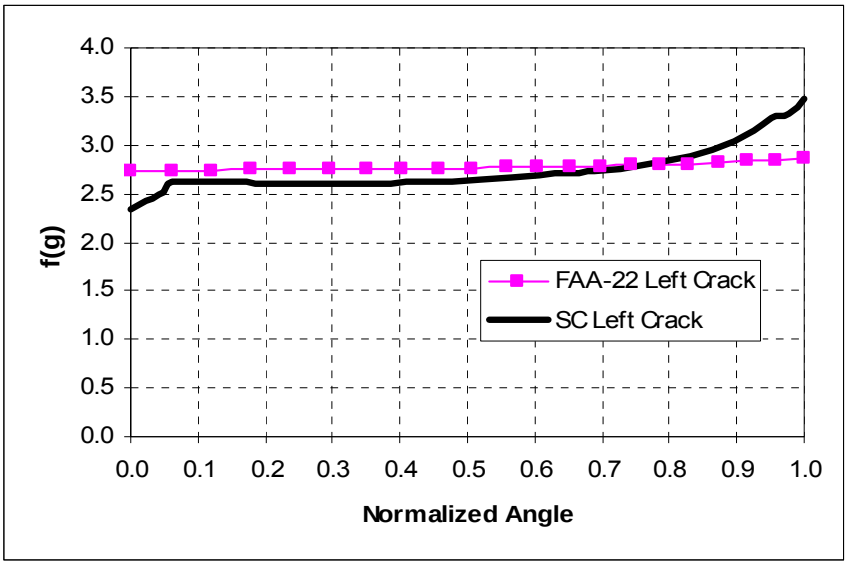

Figure 3-29. Comparison Crack 10 (Left Crack)

Right Crack		Left Crack	
Crack Length, a	0.4445 in	Crack Length, a	0.3176 in
Crack Depth, c	0.5355 in	Crack Depth, c	0.3462 in
Center of Ellipse	0.0299 in	Center of Ellipse	0.0472 in

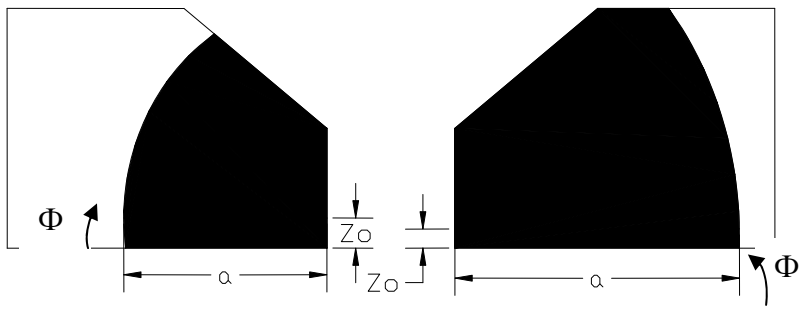

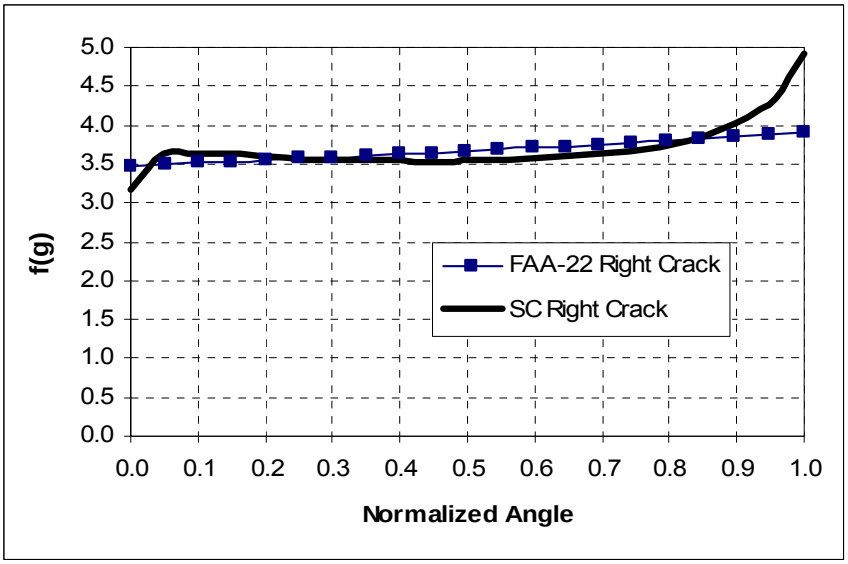

Figure 3-30. Comparison Crack 11 (Right Crack)

Right Crack		Left Crack	
Crack Length, a	0.4445 in	Crack Length, a	0.3176 in
Crack Depth, c	0.5355 in	Crack Depth, c	0.3462 in
Center of Ellipse	0.0299 in	Center of Ellipse	0.0472 in

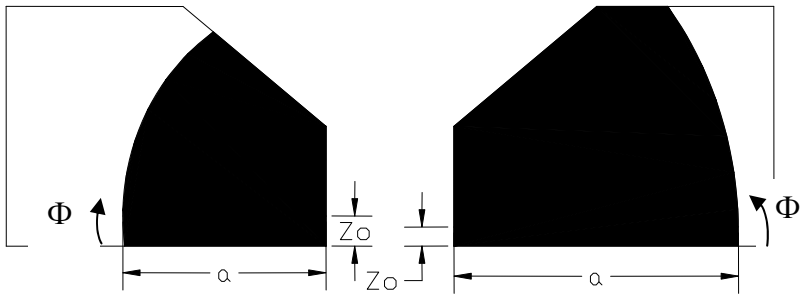

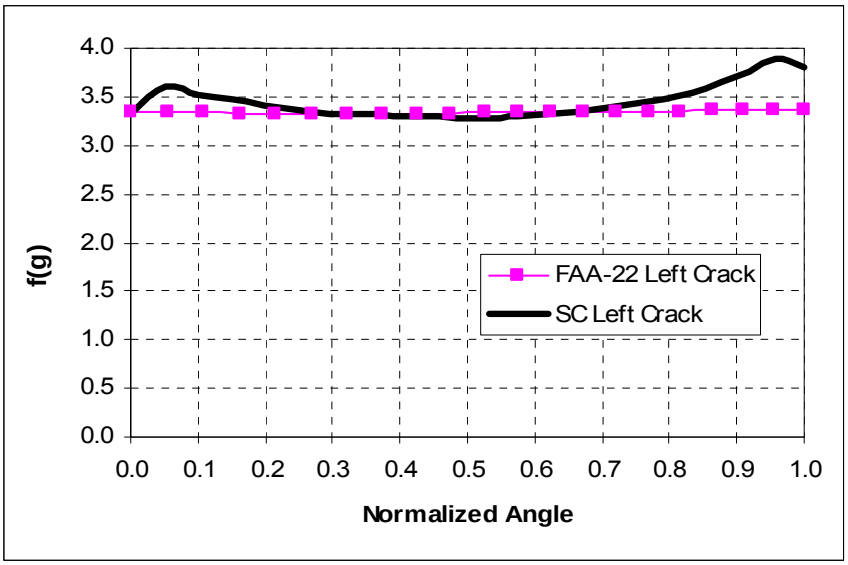

Figure 3-31. Comparison Crack 11 (Left Crack)

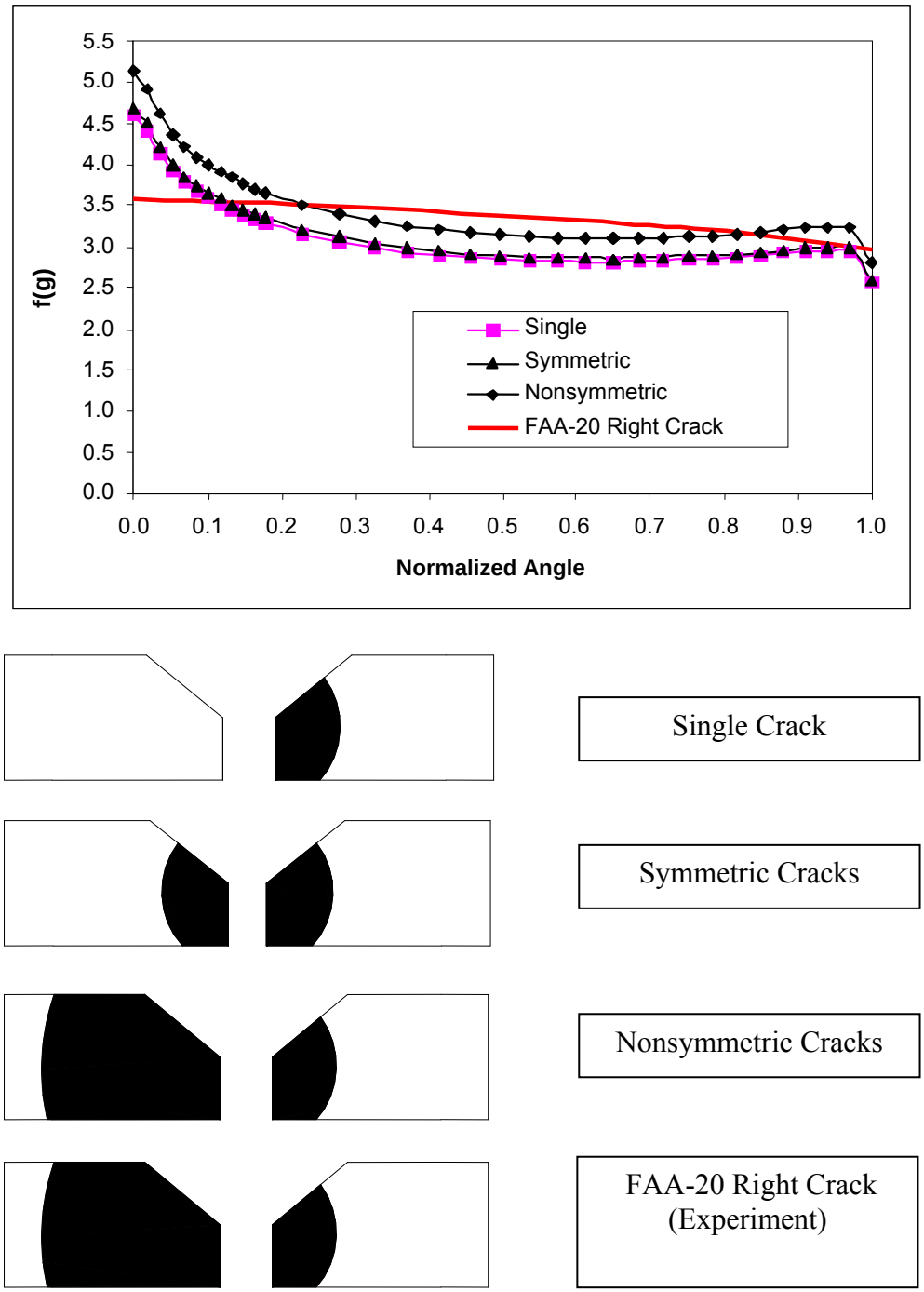

Figure 3-32. Effect of Left Crack on Right Crack (Small Crack)

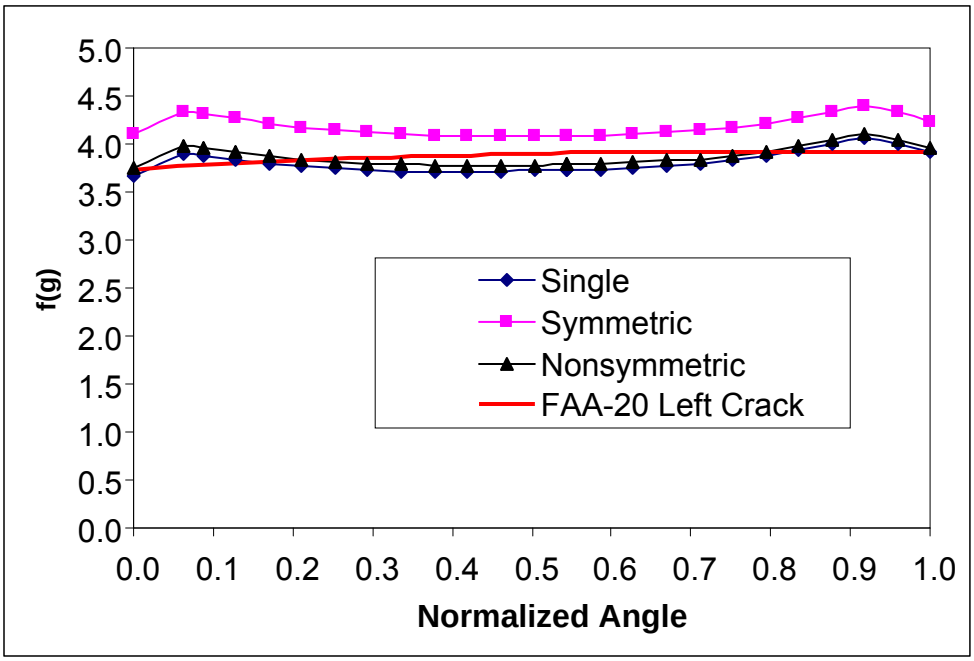

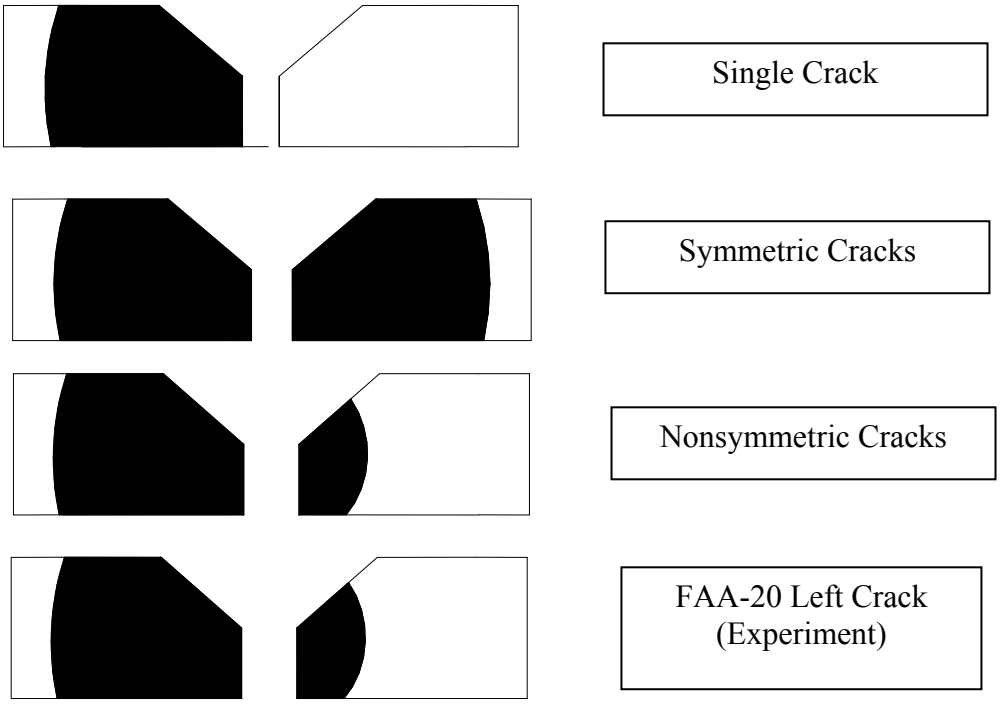

Figure 3-33. Effect of Right Crack on Left Crack (Large Crack)

4. PIN-LOADED EXPERIMENTS.

This section documents the results of fatigue tests involving cracks at countersunk holes under the pin-loading conditions shown in figure 1-1. The countersunk hole specimens were made from the same sheet of PMMA as before, and had the same dimensions as the open-hole specimens shown in figure 2-1. Again, the transparent specimens allowed in situ crack measurements during fatigue testing, and the measured fatigue crack growth rates were used to obtain dimensionless stress-intensity factors by the James and Anderson backcalculation method. The loading apparatus shown in figures 4-1 and 4-2 is a modification to that used for the open-hole tension tests; the modification involved attaching steel grips to one end of the specimen and applying a force through a neat-fit pin placed in the countersunk hole. Visual access was again provided through the polished specimen end by means of a mirror, while a microscope was again used to record free surface crack dimensions. The same $R = 0.3$ constant-amplitude cycling at 3 Hz was used for both the pin-loaded and the open-hole experiments. Some additional features of the experiments are described in the following section, while complete details are given in reference 3.

4.1 LOADING APPARATUS.

The goal here was to obtain test data for the 100% load transfer case where all load in the joint is transferred through a fastener placed in the countersunk hole. In this case, one end of the plate was subjected to a uniform tensile stress that was then reacted through a pin placed in the countersunk hole, as shown in figure 4-3. Since the degree of fit between the pin and hole influence the stress distribution at that location, it was decided to model the neat fit condition as close as possible (i.e., interference fit fasteners were not considered in this case).

Care was given to the choice of pin material to use with the transparent polymer plates, since the stress distribution depends on both the pin and plate materials. Although steel pins were desired to carry the large loads transferred by the pins, there was concern that the difference in elastic modulus between metal pins and polymer plates could provide results that would not be typical of practical applications, where both plate and fastener would be metal. The approximate elastic moduli E of interest, for example, are 10,000 ksi for aluminum, 30,000 ksi for steel, and 375 ksi for PMMA.

The results of an FEA study [3] conducted to determine the contact stresses for steel or PMMA pins placed in the PMMA sheet are summarized below. One end of the PMMA countersunk hole specimen was fixed while uniform pressure was applied at the other end. The pin was also held fixed. The FEA results of that study showed that the maximum principal stresses around the vicinity of the countersunk hole in a PMMA plate that is loaded with either a steel or PMMA pin have similar stress distributions, although the maximum principal stress at the hole for the steel pin case is 10% larger than for the PMMA pin. The larger contact stresses caused by the steel pin are due to the much larger elastic modulus of steel compared to PMMA (the ratio of steel/PMMA elastic modulus = 30,000/375 = 80). Thus, it was concluded that a PMMA loading pin should be used to obtain experimental results that would more closely match the practical situation where the pin and parent structure have similar E.

However, since PMMA is quite brittle, there was concern that a PMMA loading pin could fracture during the fatigue test if the load was transferred directly through it. To minimize this problem, a 0.5-inch-diameter straight shank hole was drilled through the center of the 1.5-inch-diameter PMMA pin to fit a steel pin. The load was transferred from the steel pin through the PMMA sleeve, and finally, to the PMMA plate. This design proved successful since no PMMA pins broke or cracked during fatigue testing, and the desired boundary condition of having similar materials at the pin/plate interface was achieved. To prevent the pin from sliding out of the countersunk hole during testing, locking rings were employed, as shown in figure 4-4. In addition, to delay the onset of fretting, a small layer of Dow Corning Molykote® G-n paste was applied to the contact surface of the countersunk hole prior to the insertion of the PMMA pin.

Figure 4-2 shows the front and side view schematics of the experimental setup. One end of the PMMA specimen was bolted and glued to steel plates using 3M™ Scotch-Weld™ DP-100 Plus epoxy adhesive to transfer load from the test machine. The 45° angled mirror allows the crack front at various cycles to be captured using a digital camera. The digital camera employed here was a Polaroid Digital Microscope Camera Model 1 with a RMC Tokina 35-105-mm close focus lens. Figure 4-1 gives photographs of the experimental setup. Note that the photograph on the right shows the arrangement when a through-the-thickness crack has grown beyond the view of the 45° angled mirror and has taken on a stable through-the-thickness crack shape. The crack size on both front and back surfaces was recorded with Bausch and Lomb's Stereo Zoom 5 model microscopes mounted on traversing slides, and the through-the-thickness crack shape was reconstructed using data from the digital camera.

4.2 FATIGUE TESTING.

Figure 4-5 shows the two different initial crack configurations that were studied: corner cracks where the straight section of the hole bore intersects the free surface and knee cracks located at the intersection of the countersink with the hole bore. To initiate the crack, a notch was created at the desired location using a cutting blade. Although precracks were introduced perpendicular to the direction of loading, the natural fatigue cracks tended to propagate at a slight angle to this plane, differing by a maximum observed angle of 5° relative to the perpendicular of the loading direction.

Precracking employed the same apparatus as the actual fatigue test, and followed the procedures and recommendations outlined in ASTM E 647 where appropriate [30]. A total of nine specimens were tested. From these nine specimens, five gave successful results, while four specimens fractured during precracking. From the five successful tests, two were conducted with initial corner crack locations and three were conducted with initial knee crack locations. Table 4-1 summarizes these tests, the corresponding initial crack location, and the number of precracking and test cycles. Results from specimens FAA-009 (initial corner crack) and FAA-012 (initial knee crack) are reported here, while results for specimens FAA-014 and FAA-015 are presented in reference 3. (However, these latter two specimens did not yield as much useful information as specimens FAA-009 and FAA-012, and are not included in this summary.)

The crack shapes observed throughout the fatigue test were divided into the same three major categories (Type I, Type II, and Type III) shown in figures 2-3 (corner crack) and 2-4 (knee

crack) for the open-hole specimens. Figure 4-6 shows a photograph of a Type I crack shape at 27,500 cycles for specimen FAA-009, while figures 4-7 and 4-8 show photographs of Type II and Type III crack shapes taken at 47,000 and 63,000 cycles, respectively. Note that the reflections seen in the photographs were removed during subsequent processing of the digital image. The transition from Type I to Type II occurred at approximately 34,250 cycles into the test, and by 57,300 cycles, the crack front has taken a through-the-thickness Type III profile. Fracture of specimen FAA-009 occurred at 245,839 cycles.

Three specimens with initial knee crack locations were also tested. The crack shapes observed throughout the fatigue test were again divided into the three major Type I, Type II, and Type III categories, as shown in figure 2-4. Figure 4-9 shows a Type I crack front photograph taken at 35,500 cycles for specimen FAA-012, while figures 4-10 and 4-11 are photographs of Type II and Type III crack fronts at 40,050 and 47,000 cycles, respectively. Again, note the reflections of the crack fronts in the photographs.

The transition from Type I to Type II crack shape occurred at approximately 37,600 cycles into this test. There was a period of fast crack growth between 41,340 and 41,400 cycles, which was the transition from the Type II to Type III crack profile. Figure 4-12 shows this fast crack growth period. A reduction of the maximum load was necessary at the end of this growth period to prevent the specimen from fracturing and to allow for more crack fronts to be captured digitally. Fracture of the specimen occurred at 220,856 cycles.

4.3 DATA ANALYSIS.

Crack photographs for the pin-loaded specimens were analyzed in a manner similar to the open-hole tests described in section 2.2. A MATLAB® code was written to process the digital images captured at various cycles during the fatigue test. Again, the raw photographs were digitized, each crack front was smoothed with a section of an ellipse, and fatigue crack growth rates were determined at various locations along the crack front by the secant method. As described in section 2.2, in connection with figure 2-7, the secant method for computing fatigue crack growth rate simply involves dividing the crack growth increment in a particular direction by the cyclic interval between the two observations [30].

Figure 4-13 is a photograph of specimen FAA-009 taken after 57,800 elapsed cycles, and figure 4-14 shows the extracted crack front obtained from the digital photograph. This image was scaled and processed to eliminate reflections, as shown in figure 4-15. Figure 4-16 shows a sample of 26 sets of raw crack profiles obtained for specimen FAA-009. Note how the initial corner crack transitions into the Type II and III shapes.

To obtain fatigue crack growth rates along the crack perimeter, the individual images were fit with a section of an ellipse to smooth the scraggly crack fronts associated with the digitizing process, as shown in figure 4-17. The horizontal positions of the center of the fitted ellipse was fixed at the straight shank of the countersunk hole ($x = 0.75$ inch), while the vertical position was not constrained. Two successive smoothed crack fronts were then averaged, as shown in figure 4-18, and the crack growth rates along this average crack front were then obtained by the secant method, which simply involved taking the difference between the two original crack fronts and dividing by the cyclic interval. The fatigue crack growth rates were then used to compute the

cyclic stress-intensity factor ΔK from the baseline fatigue crack growth properties obtained previously for the PMMA test material, as shown in figure 2-9. These cyclic stress-intensity factors were then expressed in dimensionless form to give the boundary correction factor $f(g)$ defined in equation 4-1.

$$\textit{Boundary correction factor}, \quad f(g) = \frac{\Delta K}{\Delta\sigma\sqrt{\pi a}} \tag{4-1}$$

Here, ΔK is the cyclic stress-intensity factor, $\Delta\sigma$ is the stress range, and a is the reference crack length shown in figure 4-19. Note that in this case, a is defined as the maximum horizontal distance from the center of the hole to far edge of the fatigue crack. Note that this is a different definition for crack than used previously for the open-hole specimens, where a was measured from the edge of the hole, as shown in figure 2-6.

In terms of the measured fatigue crack growth rates and the baseline fatigue crack growth properties, $f(g)$ is given by equation 4-2.

$$f(g) = \frac{\left(\frac{da}{dN}/C\right)^{\frac{1}{m}}}{\Delta\sigma\sqrt{\pi a}} \tag{4-2}$$

where da/dN is the crack growth rate measured at various location along the crack front in the countersunk hole specimens

C and m are the Paris constants from the baseline da/dN-ΔK curve (figure 2-9)

$\Delta\sigma$ is the remote cyclic stress at the end of the countersunk hole specimen, which is the crack length a, used to nondimensionalize $f(g)$ (see figure 20) is the horizontal distance from the center of the countersunk hole.

The parametric angle ϕ used to represent the different points along the crack front is defined in figure 4-21, and differs from that used for the open-hole tests. Here, ϕ defines points along a circle, which is circumscribed about the elliptical crack. Projections from the circle to the ellipse then specify points on the elliptical crack front. Although this is a conventional way for defining points on part-elliptical cracks, it should be emphasized again that this is a different procedure than the open-hole results described in sections 2 and 3 (i.e., the angle ϕ defined in figures 2-8 and 4-21 are different).

As described above, the dimensionless stress-intensity factor $f(g)$ was obtained for several pin-loaded specimens and presented as a function of parametric angle ϕ. Detailed results for two specimens, including a total of 76 different crack fronts, are reported in appendix C. Some aspects of those results are discussed in the following section.

4.4 DISCUSSION OF RESULTS.

A total of 38 average crack fronts were obtained from 41 digitally processed crack photographs for corner crack specimen FAA-009, as shown in figure 4-22. An additional 38 cracks, as shown

in figure 4-23, were also characterized for knee crack specimen FAA-012. For each of the average crack shapes, 25 point locations were selected to tabulate the boundary correction factors, $f(g)$. Typical results are reported in tables 4-2 to 4-4 and figures 4-20, 4-24, and 4-25 for Types I, II, and III cracks for this specimen. Note that for each analyzed crack, there is a table that summarizes the type of crack, the parameters that define its elliptical shape, and the cycles corresponding to the particular crack under consideration (recall that each analyzed crack is actually the average obtained from two sequential crack photographs). The dimensionless stress-intensity factors are given in tabular form as a function of the parametric angle ϕ, and for reference, the coordinates of the point along the crack front defined by ϕ are also given. Each set of tabular data is accompanied by a scale drawing of the given crack and a plot of $f(g)$ plotted versus parametric angle ϕ. Table 4-2, for example, gives the tabular data for a typical Type I crack averaged from photographs taken at 25,500 and 28,500 elapsed cycles for specimen FAA-009, while figure 4-20 contains the corresponding graphical presentation of data for this particular crack.

Similar data for all 38 of the cracks analyzed for corner crack specimen FAA-009 and for the 38 cracks studied for knee crack specimen FAA-0012 are given in appendix C. It should be noted that the original reporting of these results, given in reference 3, contained an error in the baseline fatigue crack growth rate data used to backcalculate $f(g)$ from the measured growth rates. The original baseline data used in reference 3 were obtained for a different stress ratio than for the pin-loaded tests, and the wrong Paris law constants C and m were used in equation 4-2. That error has been corrected here, and all the pin-loaded $f(g)$ results reported here and in appendix C for specimens FAA-009 and FAA-012 have been recomputed using the correct $R = 0.3$ fatigue crack growth properties reported in figure 2-9.

Note in figure 4-23 that the Type I cracks, and some of the Type II cracks, for specimen FAA-012 do not intersect the original countersunk angle, but intersect the starter notch that were used to introduce the knee crack. The location of the starter notch was approximated from the digital images and is included in all crack front images for FAA-012.

As discussed in section 2.2, a section of an ellipse was used to represent each photographed crack front. Growth of the part-through (Types I and II) cracks in specimen FAA-009 was such that the length of the horizontal axis was always smaller than the length of the vertical axis. Thus, as shown in figure 4-26, the ratio B/A is greater than 1, where B and A are the vertical and horizontal axis, respectively, of the fitted ellipse (see figure 4-20). The through-the-thickness Type III crack shape becomes more consistent as the crack grows away from the countersunk hole.

In general, it was noted that $f(g)$ increases as the parametric angle ϕ increases for the Type I and II corner crack shapes in this corner crack specimen. The trend for Type III cracks varies, with some exhibiting increasing $f(g)$ as ϕ increases and some with decreasing $f(g)$ as ϕ increases. However, as the through-the-thickness crack becomes larger, the dimensionless stress-intensity factors take on a more constant value along the crack front, leading to a stable shape, as expected.

The same section of an ellipse was also used to represent the knee crack fronts for specimen FAA-012. Until the small Type I knee crack penetrates the front face, the growth rate along the

straight bore is faster than the growth along the countersunk. Upon penetrating the bottom free surface, the crack begins to take on a similar shape as a Type II corner crack. The shape of the through-the-thickness cracks became more consistent as the crack grows away from the countersunk hole.

In general, the $f(g)$ for Type I knee cracks decreases as ϕ increases. As the Type II crack increases in size, $f(g)$ increases as ϕ increases, as observed previously for the Types I and II corner cracks. Again, when a Type III through-the-thickness crack shape is reached, the stress-intensity factor takes on a more constant value as the crack becomes large and approaches a stable shape.

To determine the repeatability of the experimental measurements for $f(g)$, attention focused on finding similar cracks in specimens FAA-009 and FAA-012. Although 78 cracks were examined in these two specimens, they had different initial shapes (corner versus knee), so it was not possible to compare results until well after development of a through-the-thickness crack. Figure 4-27 compares two large type III through-the-thickness cracks that have nearly the same shape in these two specimens, and figure 4-28 compares the resulting dimensionless stress-intensity factors for these two cases. Note that the experimentally determined $f(g)$ values agree quite closely in these two specimens. However, since the crack shapes are slightly different, a parametric angle comparison cannot be performed. Instead, the $f(g)$ values are compared using the vertical coordinate of the points along the crack perimeter. Although the initial crack locations were different for these two specimens (corner crack for FAA-009 and knee crack for FAA-012), the $f(g)$ values compare quite closely for these two cracks. The average difference in the stress-intensity factors measured along the two crack fronts is 3.8%.

Although it was beyond the scope of the current effort to obtain numerical solutions for the pin-loaded cracks, and the authors are unaware of published results for the particular countersunk configuration studied, it was decided to compare the current results with a two-dimensional lug solution for a uniform through-the-thickness crack. Child [31] reports finite element results obtained by the StressCheck software for the two-dimensional lug configuration, as shown in figure 4-29. Note that in this case, the lug had a finite radius at the free end, rather than the long rectangular end studied, and a uniform diameter pin was placed in a straight shank hole. Although these two geometries are different, it was decided to examine how well the two-dimensional lug solutions would estimate the three-dimensional stress-intensity factors for large through-the-thickness cracks. (Clearly the configurations would be expected to give different results for small cracks where the countersunk dimension is important.)

Figure 4-30 compares the three-dimensional results shown earlier in figure 4-28 for two similar cracks in specimens FAA-009 and FAA-012 with the two-dimensional StressCheck lug solution. Figure 4-31 gives a similar comparison between the FEA and experimental results for a larger crack in FAA-012. Note that in both of these cases, the experimental data indicated a stable crack configuration, and $f(g)$ is nearly constant along the crack perimeter. (The two-dimensional StressCheck solution assumes a uniform through-the-thickness crack, so by definition, the stress-intensity factor is constant through the thickness for this case.) Also, when comparing the FEA and experimental results, the countersink was ignored in the lug solution, and a constant hole diameter was assumed, leading to a lug width W to hole diameter D ratio W/D = 7.5/1.5 = 5. Also, the average through-the-thickness crack length observed in the experiments was used for

comparison purposes. Note in figure 4-30 that the maximum difference in $f(g)$ between the two experiments and the StressCheck solution is 9.4%, and in figure 4-31 the experimental and FEA results differ by 7.3%. Thus, although the two-dimensional and three-dimensional problems are different, the simple straight shank lug results provided a reasonable estimate for the countersunk hole problem in these cases. However, the countersunk hole results gave larger stress-intensity factors in this case, so the two-dimensional lug estimate would be nonconservative.

Table 4-1. Countersunk Hole PMMA Specimens With Successful Fatigue Tests

Specimen ID	Initial Crack Location	Precracking Cycles	Test Cycles
FAA-009 (corner)	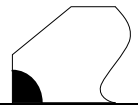	270,000	245,839
FAA-012 (knee)	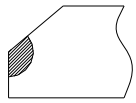	314,000	220,856
FAA-014 (knee)	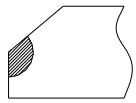	130,000	182,040
FAA-015 (knee)	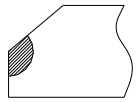	161,000	196,390
FAA-016 (corner)	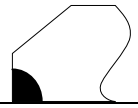	170,000	329,339

Table 4-2. Typical Stress-Intensity Factor Results for Type I Crack in Specimen FAA-009 (Also see figure 4-23)

Initial Crack Location	Corner
Type	I
Center of Ellipse	(0.75, 0)
Horizontal Axis	0.11700
Vertical Axis	0.14225
Cycle	25500-28500

ϕ [degree]	x [inch]	y [inch]	$f(g)$
0	0.867	0	1.5635
4.54	0.86663	0.01123	1.5659
6.5	0.86625	0.01607	1.5686
10.43	0.86507	0.02571	1.5767
14.43	0.86331	0.0354	1.5883
18.51	0.86095	0.04508	1.6040
22.71	0.85793	0.05481	1.6234
28.54	0.85278	0.06785	1.6560
31.6	0.84966	0.07441	1.6752
36.44	0.84413	0.08436	1.7081
39.84	0.83983	0.09101	1.7304
43.48	0.8349	0.09775	1.7400
47.37	0.82924	0.10453	1.7508
49.45	0.82606	0.10797	1.7566
53.94	0.81887	0.11488	1.7693
56.42	0.81471	0.11841	1.7798
59.08	0.81012	0.12193	1.7938
61.99	0.80494	0.1255	1.8088
65.3	0.7989	0.12916	1.8252
69.08	0.79178	0.13282	1.8431
71.27	0.78757	0.13467	1.8529
73.74	0.78277	0.13652	1.8634
76.71	0.77689	0.13841	1.8752
80.56	0.76918	0.14031	1.8892
90	0.75	0.14225	1.9155

Table 4-3. Typical Stress-Intensity Factor Results for Type II Crack in Specimen FAA-009 (Also see figure 4-24)

Initial Crack Location	Corner
Type	II
Center of Ellipse	(0.75, 0.0575)
Horizontal Axis	0.28100
Vertical Axis	0.31700
Cycle	50500-52000

ϕ [degree]	x [inch]	y [inch]	*f*(*g*)
-10.45	1.02634	0	1.9934
-8.95	1.02758	0.00827	1.9874
-6.84	1.029	0.01985	1.9863
-4.98	1.02994	0.03015	1.9860
-2.89	1.03064	0.04176	1.9867
-0.89	1.03097	0.05334	1.9885
-0.5	1.03099	0.05852	1.9895
0.62	1.03098	0.0598	1.9895
2.33	1.03077	0.07014	1.9923
8.15	1.02816	0.10242	2.0058
10.04	1.0267	0.11275	2.0119
15.8	1.02039	0.14378	2.0351
17.99	1.01725	0.15543	2.0459
20.23	1.01367	0.16711	2.0581
24.53	1.00564	0.18912	2.0854
28.72	0.99642	0.20985	2.1407
31.16	0.99046	0.22153	2.1498
34.23	0.98232	0.23583	2.1623
36.53	0.9758	0.2462	2.1725
39.21	0.96772	0.25791	2.1850
42.31	0.9578	0.2709	2.2006
45.24	0.94785	0.28261	2.2164
48.33	0.93683	0.29429	2.2343
51.25	0.92589	0.30472	2.2522
55.85	0.90772	0.31985	2.2875

Table 4-4. Typical Stress-Intensity Factor Results for Type III Crack in Specimen FAA-009 (Also see figure 4-25)

Initial Crack Location	Corner
Type	III
Center of Ellipse	(0.75, 0.06875)
Horizontal Axis	0.61225
Vertical Axis	0.58250
Cycle	73500-74750

ϕ [degree]	x [inch]	y [inch]	$f(g)$
-6.87	1.35785	0	1.6426
-5.5	1.35943	0.01422	1.6520
-4.22	1.36059	0.02741	1.6618
-3.17	1.36132	0.03837	1.6694
-2.14	1.36182	0.04939	1.6766
-1.09	1.36214	0.06257	1.6845
-0.87	1.36218	0.06919	1.6883
0.9	1.36217	0.07142	1.6894
2.14	1.36182	0.08906	1.7000
4.22	1.36059	0.11109	1.7119
6.59	1.35821	0.13541	1.7246
8.55	1.35545	0.15527	1.7352
10.31	1.35237	0.17296	1.7448
12.3	1.34821	0.19283	1.7558
14.31	1.34326	0.21275	1.7672
16.33	1.33754	0.23261	1.7787
18.38	1.33102	0.25247	1.7910
20.45	1.32368	0.27228	1.8037
22.31	1.31642	0.28992	1.8157
24.43	1.30742	0.30973	1.8296
26.34	1.29867	0.32726	1.8632
28.29	1.28915	0.34479	1.8694
31.01	1.27472	0.36889	1.8787
31.21	1.27366	0.37057	1.8806
31.7	1.27092	0.3749	1.9078

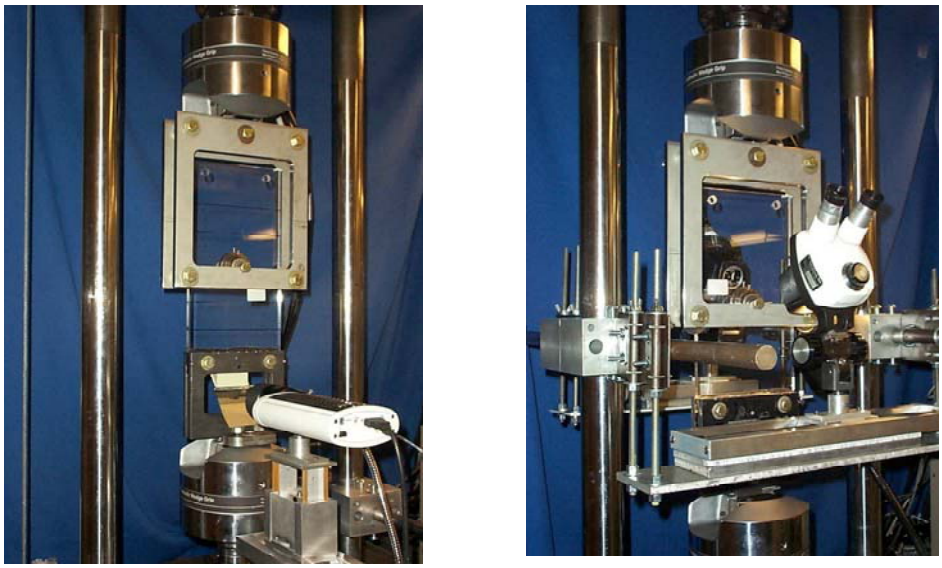

Figure 4-1. Experimental Apparatus Used for the Pin-Loaded Experiments [3]

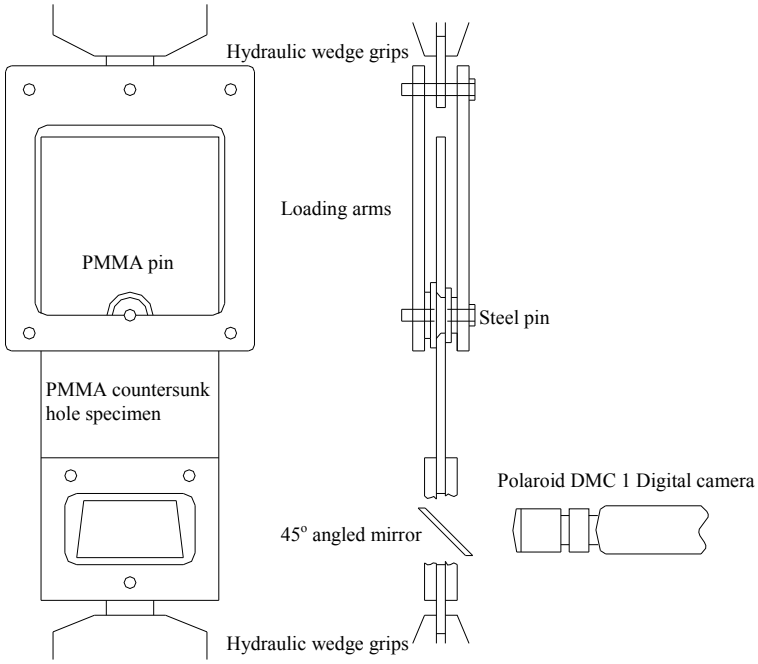

Figure 4-2. Front and Side View Schematics of the Pin-Loaded Countersunk Hole Experiment

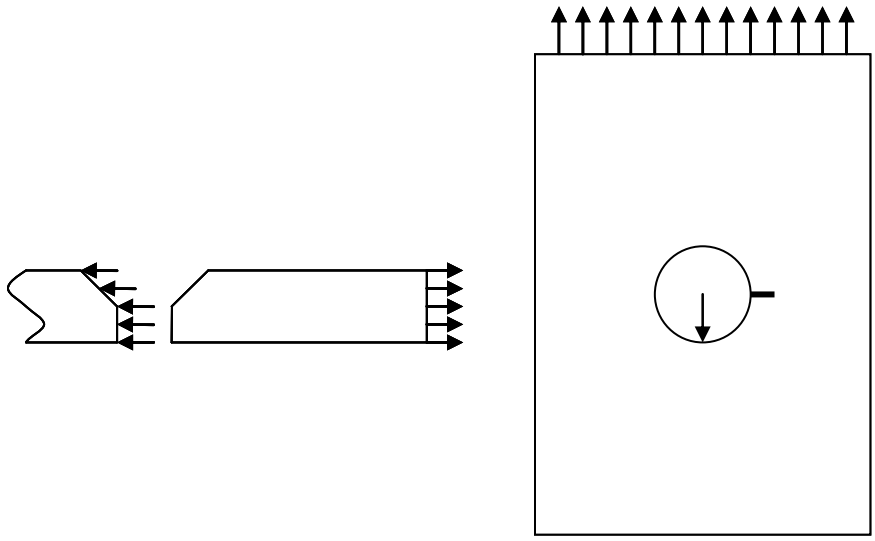

Figure 4-3. Schematic of Pin-Loaded Specimen Configuration Showing Remote Load Applied Reacted by Neat-Fit Pin in Countersunk Hole

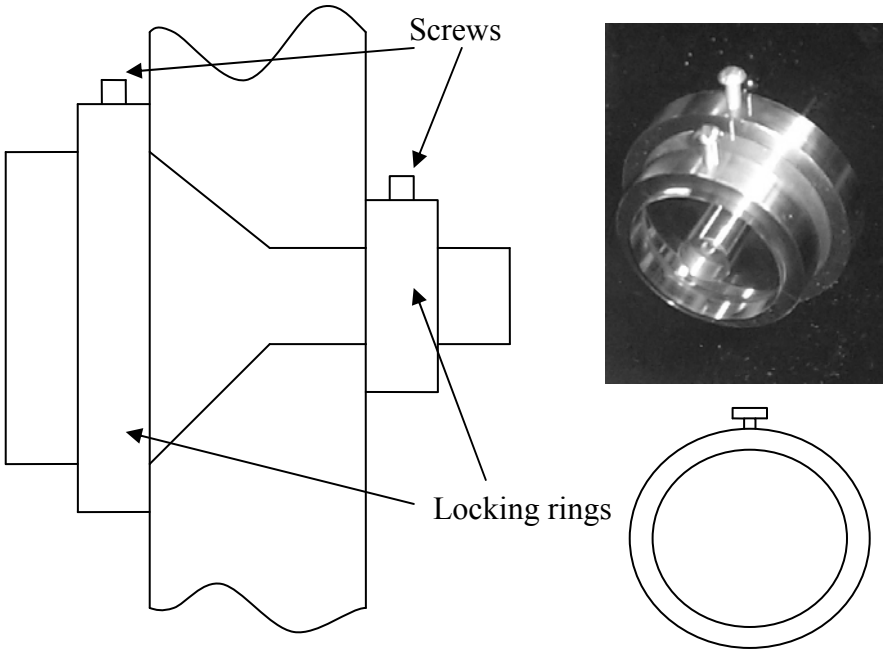

Figure 4-4. Locking Rings to Prevent the PMMA Pin From Sliding During Testing

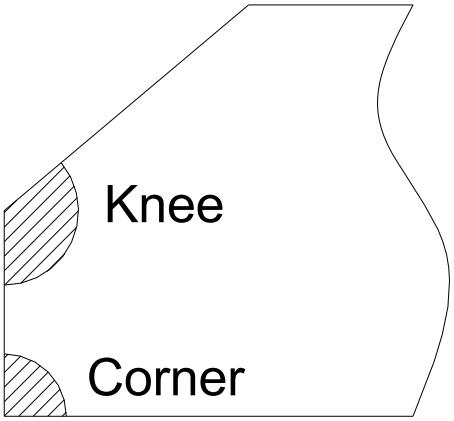

Figure 4-5. Initial Knee and Corner Crack Locations for the Countersunk Hole

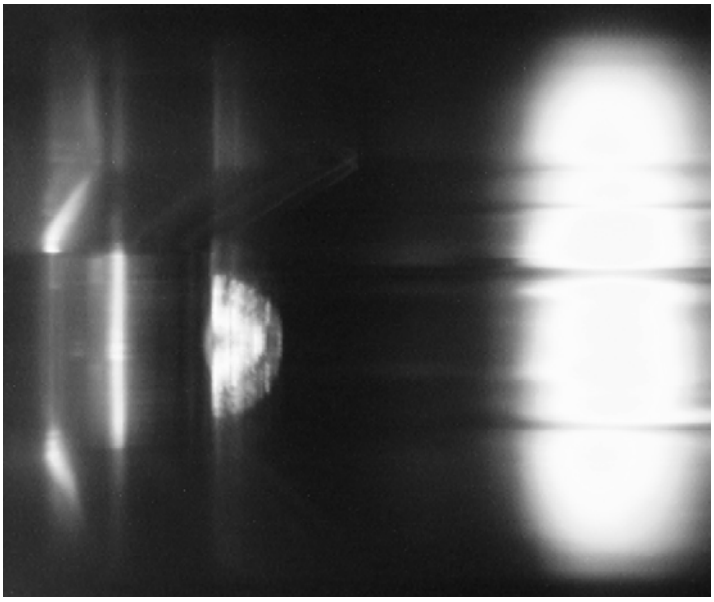

Figure 4-6. Digital Image of a Type I Crack Shape From FAA-009 (Initial Corner Crack) Taken at 27,500 Cycles

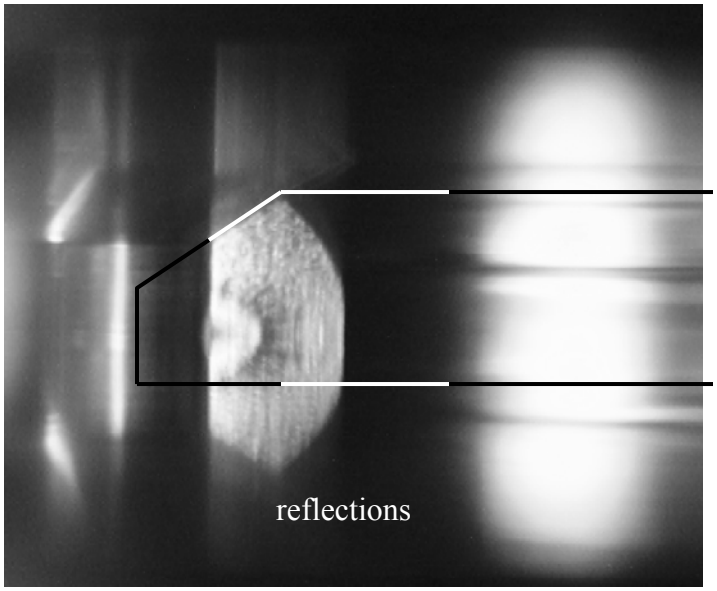

Figure 4-7. Digital Image of a Type II Crack Shape From FAA-009 (Initial Corner Crack) Taken at 47,000 Cycles

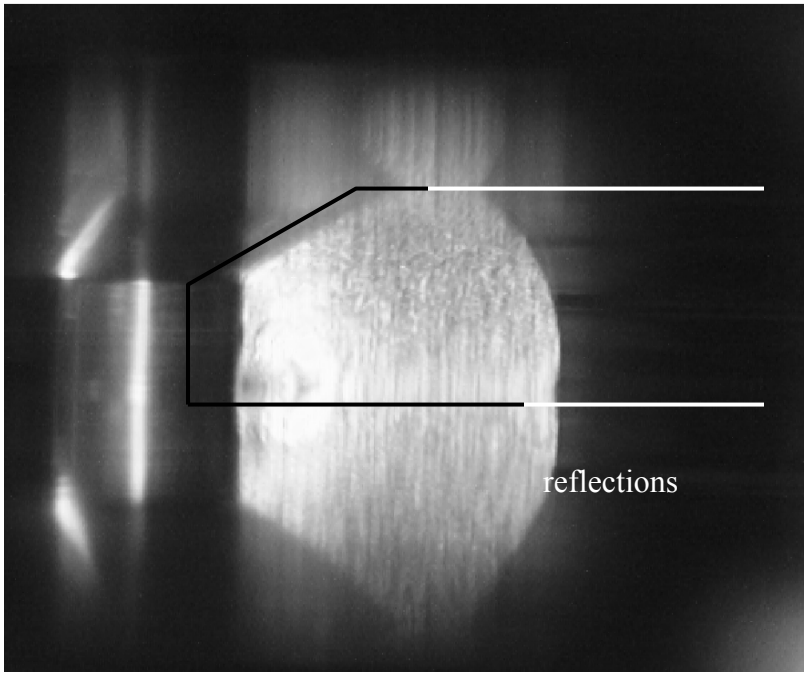

Figure 4-8. Digital Image of a Type III Crack Shape From FAA-009 (Initial Corner Crack) Taken at 63,000 Cycles

Figure 4-9. Digital Image of a Type I Crack Shape From FAA-012 (Initial Knee Crack) Taken at 35,500 Cycles

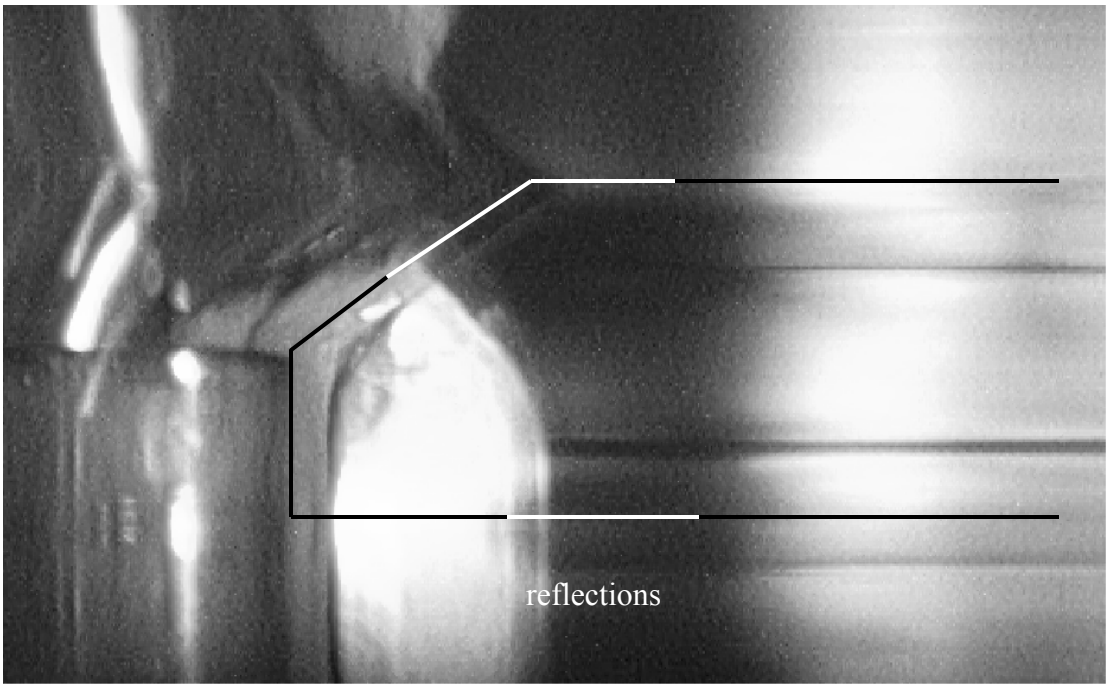

Figure 4-10. Digital Image of a Type II Crack Shape From FAA-012 (Initial Knee Crack) Taken at 40,050 Cycles

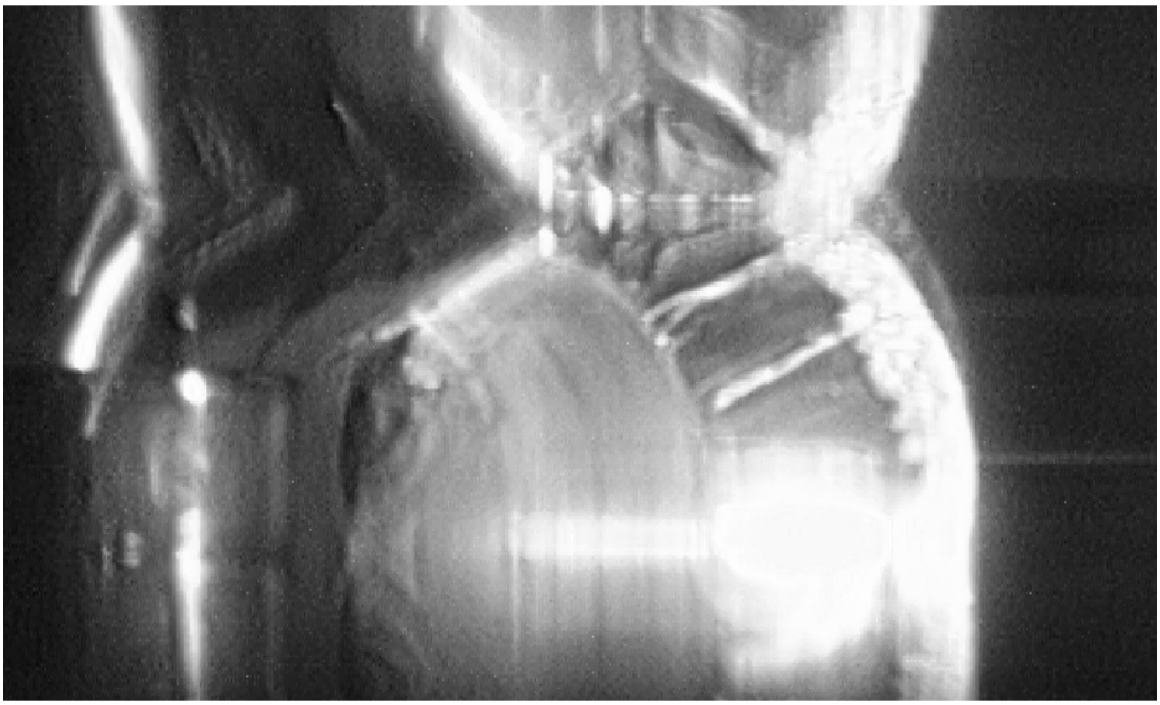

Figure 4-11. Digital Image of a Type III Crack Shape From FAA-012 (Initial Knee Crack) Taken at 47,000 Cycles

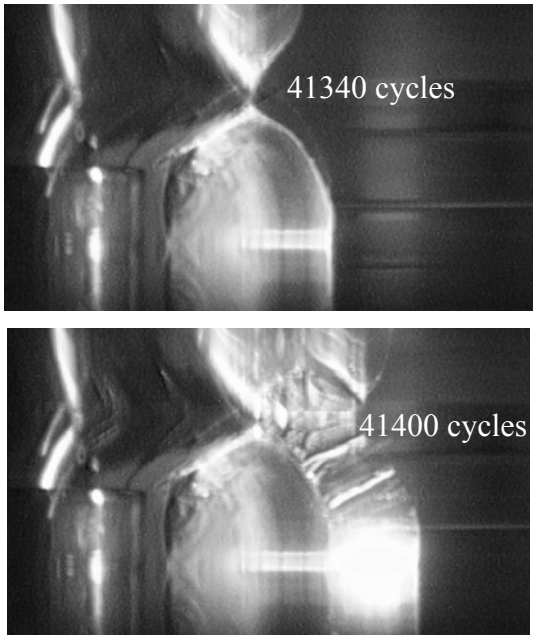

Figure 4-12. Digital Images of FAA-012 Showing Fast Crack Growth, Which Coincide With the Transition From Type II to Type III Crack Profile

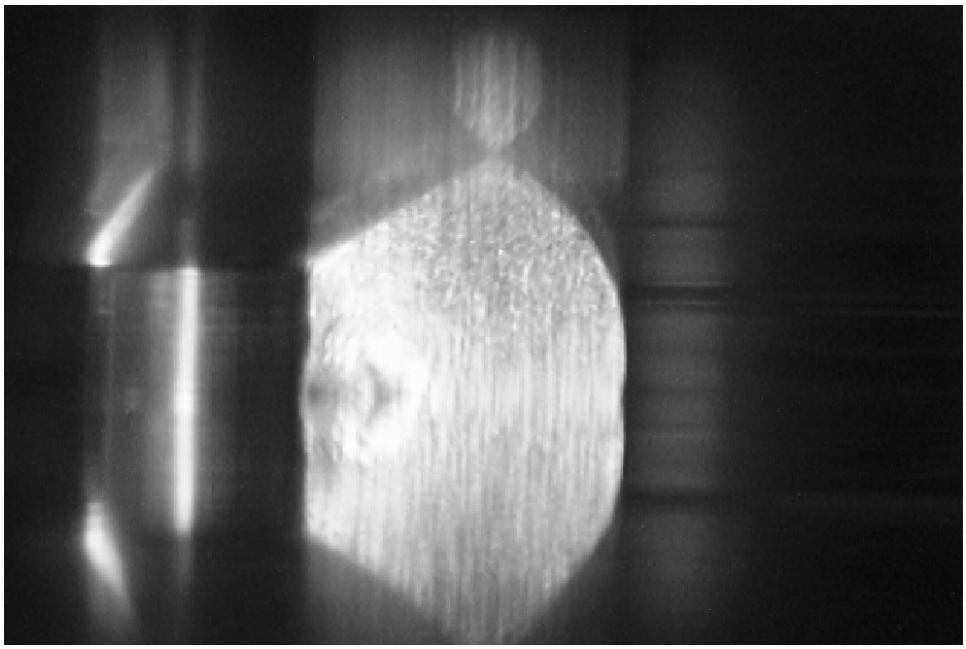

Figure 4-13. Digital Image of a Crack Front From FAA-009 Captured at 57,800 Cycles

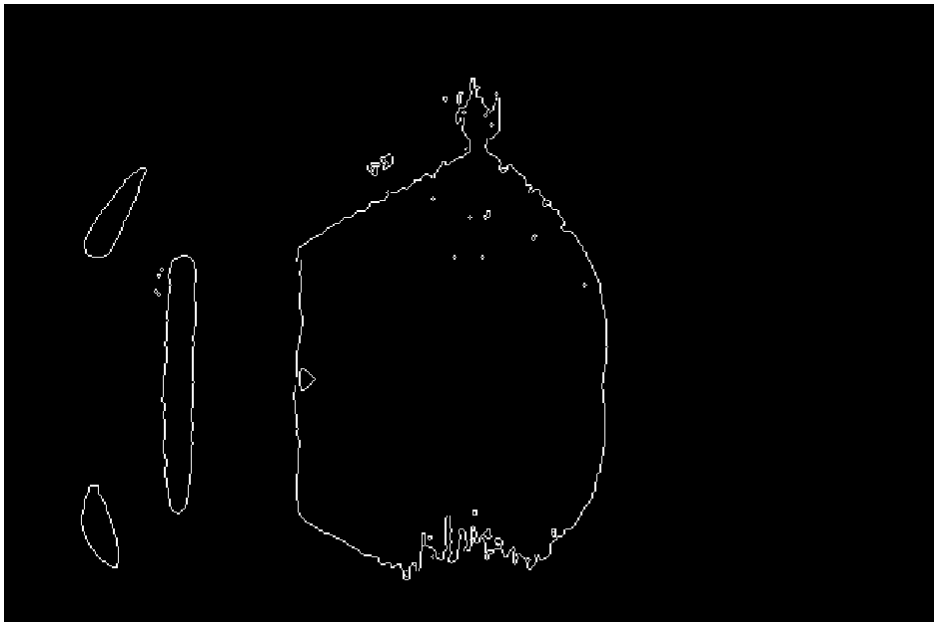

Figure 4-14. Extracted Crack Front From Digital Image in Figure 4-13

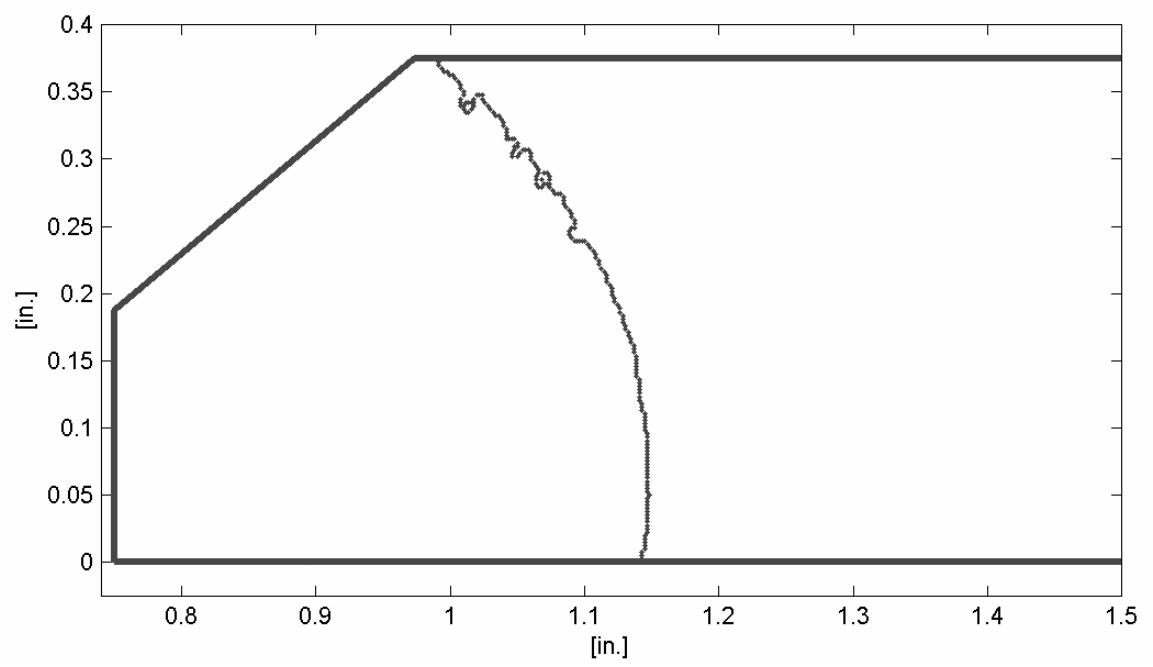

Figure 4-15. Crack Front in its Actual Dimensions

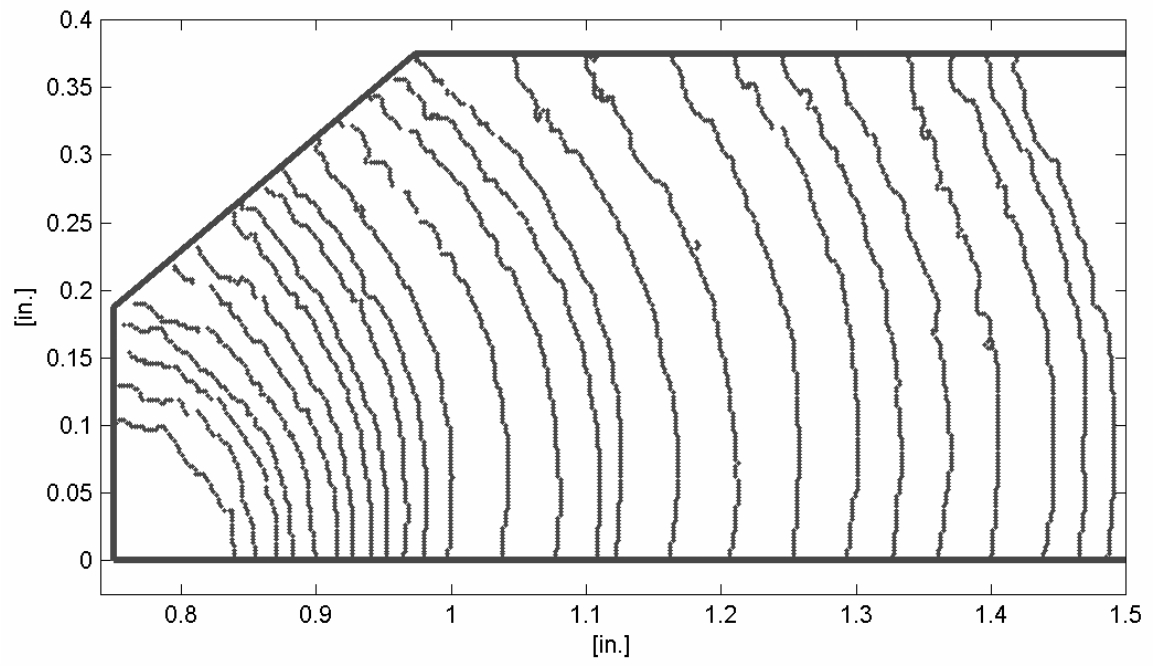

Figure 4-16. A Sample of 26 Extracted Crack Fronts for Specimen FAA-009

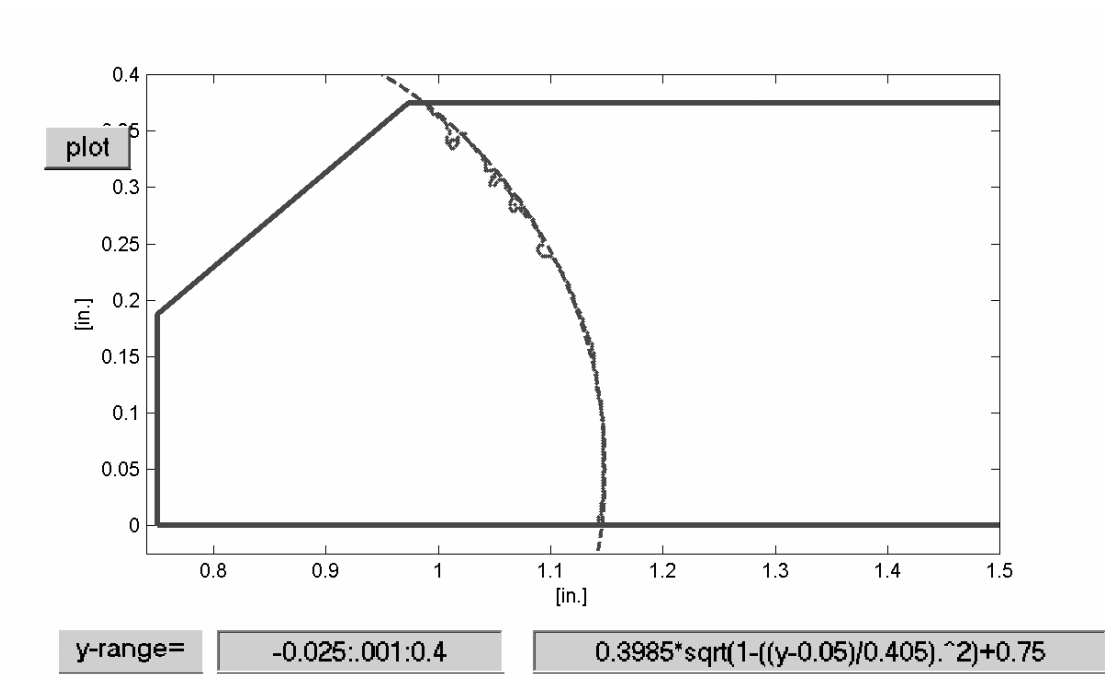

Figure 4-17. Fitting of Ellipse to Smooth Out Discontinuities in Crack Front From FAA-009 at 57,800 Cycles (The horizontal position of the elliptic center of the ellipse was fixed at the straight shank of the countersunk hole (X = 0.75 inch), while the vertical position was not constrained.)

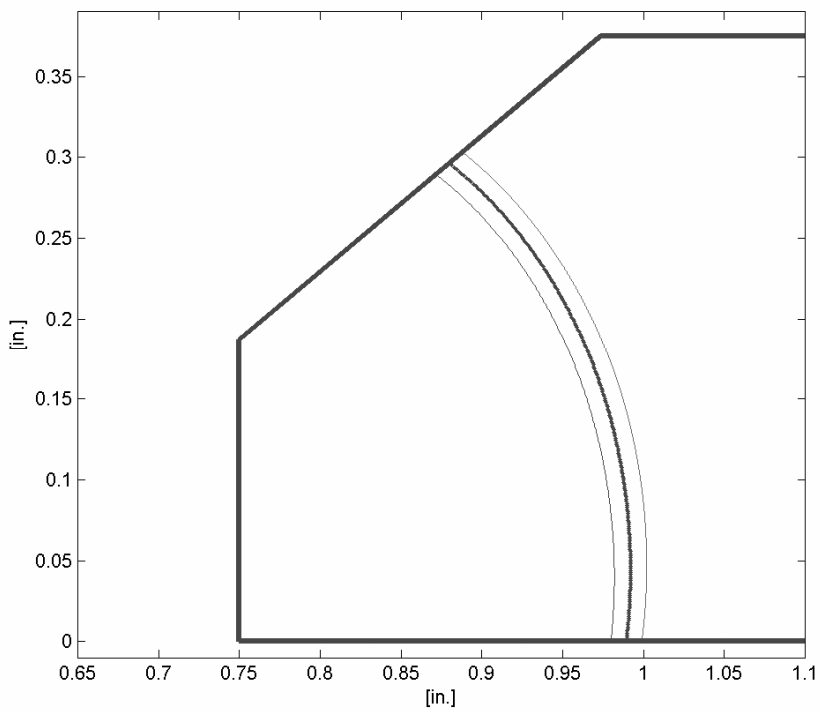

Figure 4-18. Average Crack Front (Heavier Line) Determined From Ellipse-Fitted Crack Fronts at 47,800 and 49,100 Cycles

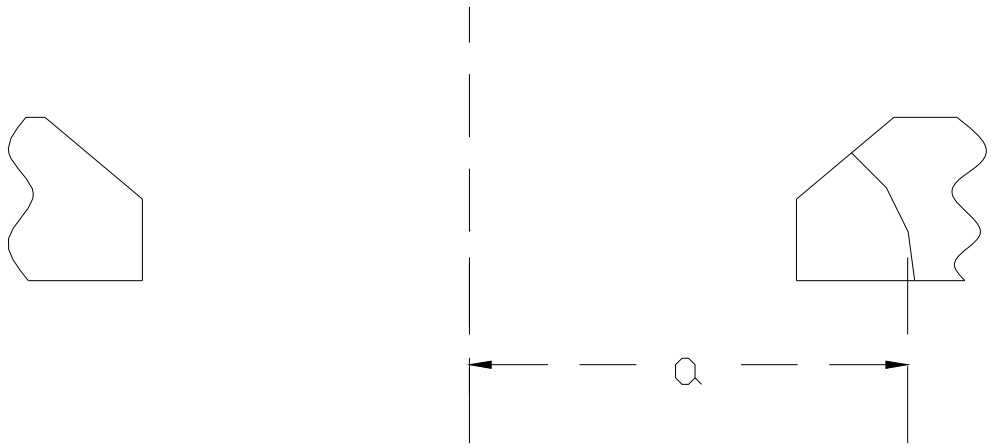

Figure 4-19. Crack Length *a* Used to Nondimensionalize the Boundary Correction Factors is the Horizontal Distance From the Center Point

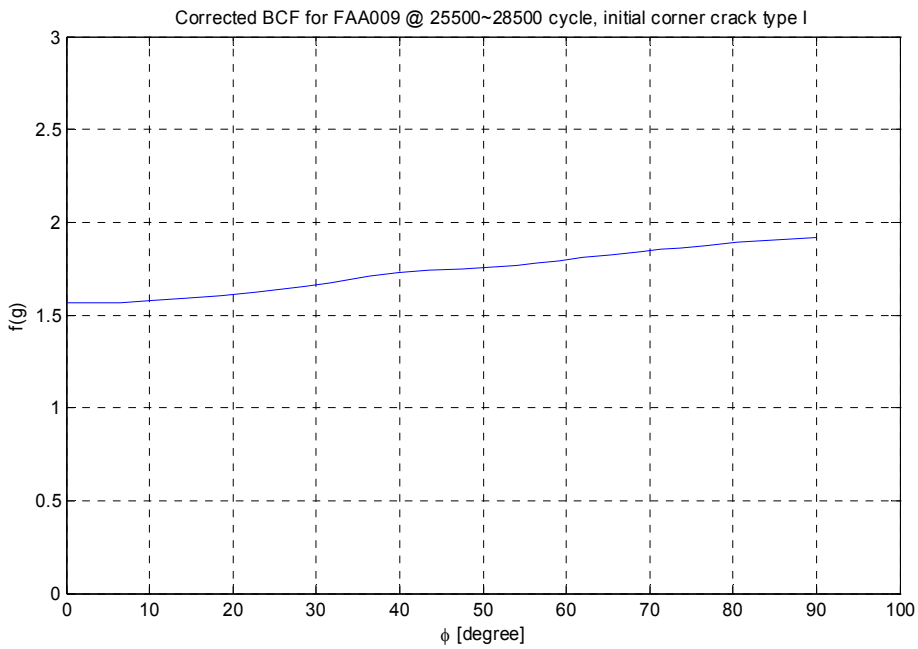

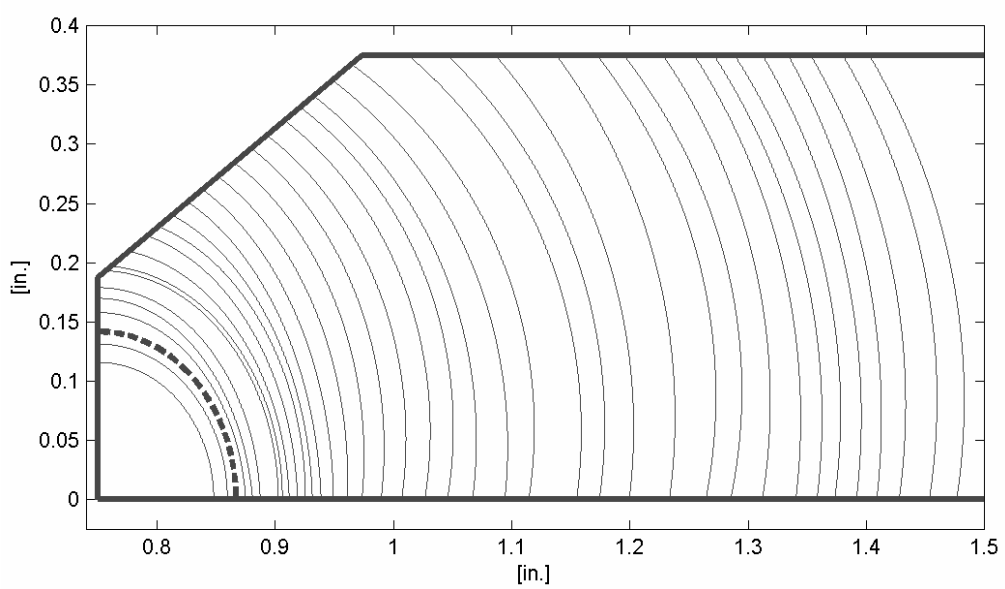

Figure 4-20. Graphical Representation of Dimensionless Stress-Intensity Factor Data for Type I Crack Reported in Table 4-2 for Specimen FAA-009

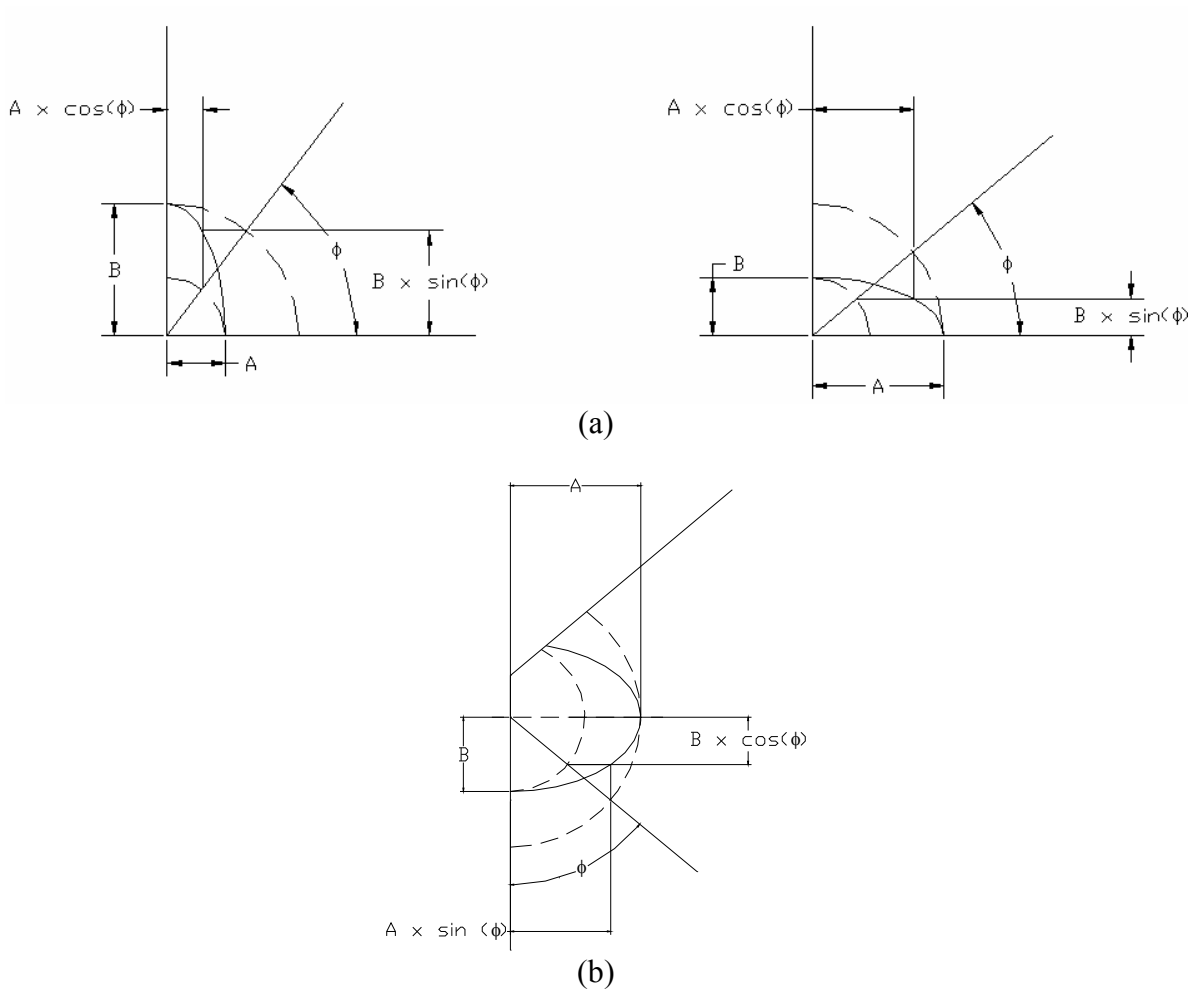

Figure 4-21. Definition of Parametric Angle Used to Locate Positions Along Crack Front (a) Type I, II, III for Initial Corner Crack and Type II, and III for Initial Knee Crack and (b) Type I for Initial Knee Crack

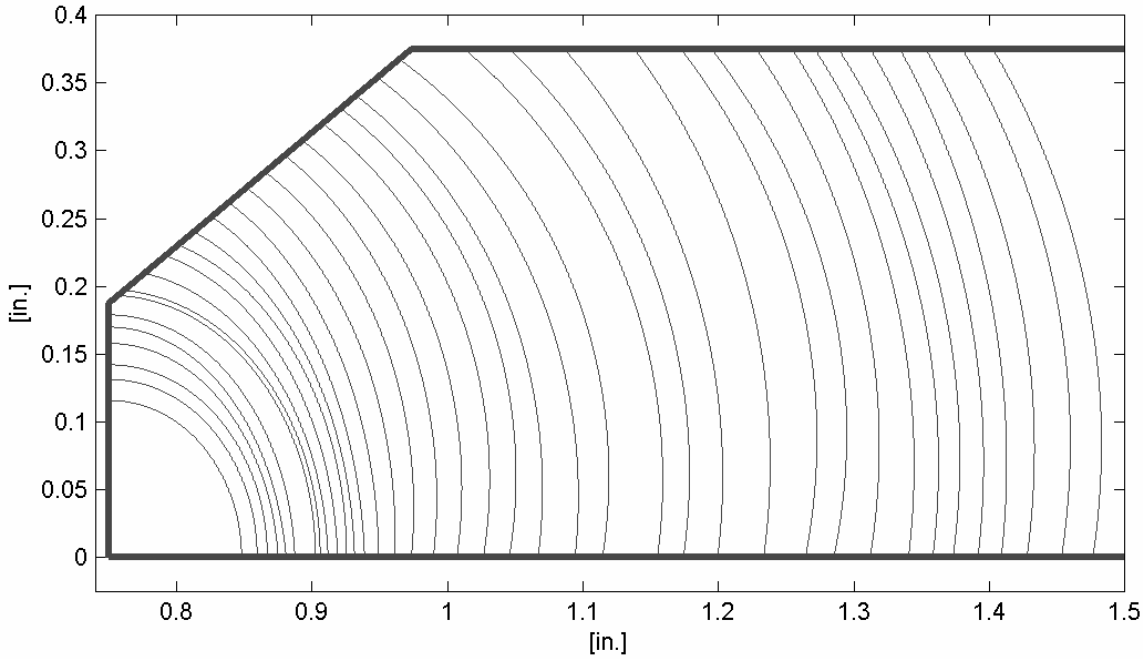

Figure 4-22. Thirty-Eight Average Crack Fronts Used to Determine Dimensionless Stress-Intensity Factors for Initial Corner Cracked Specimen FAA-009

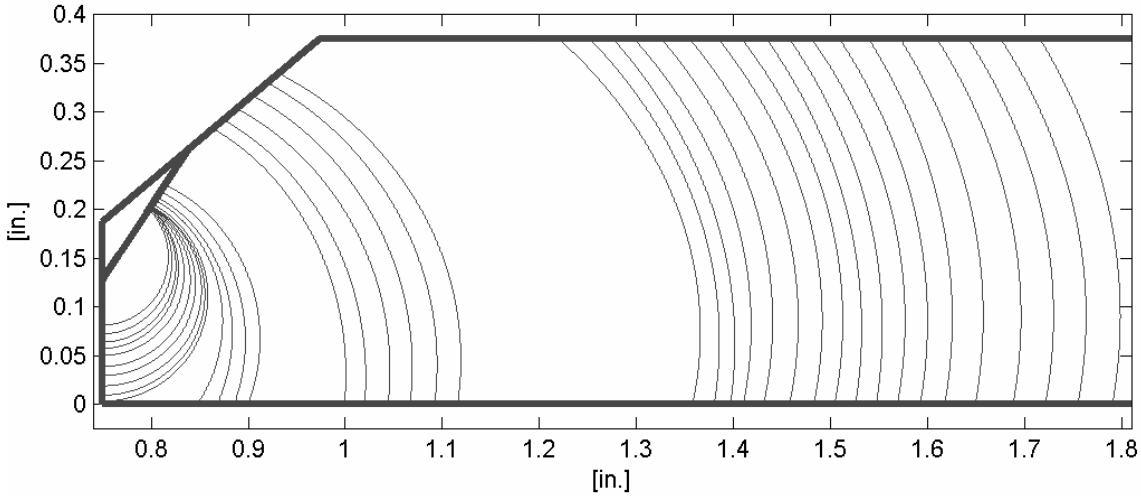

Figure 4-23. Thirty-Eight Average Crack Fronts Used to Determine Dimensionless Stress-Intensity Factors for Initial Knee Cracked Specimen FAA-012

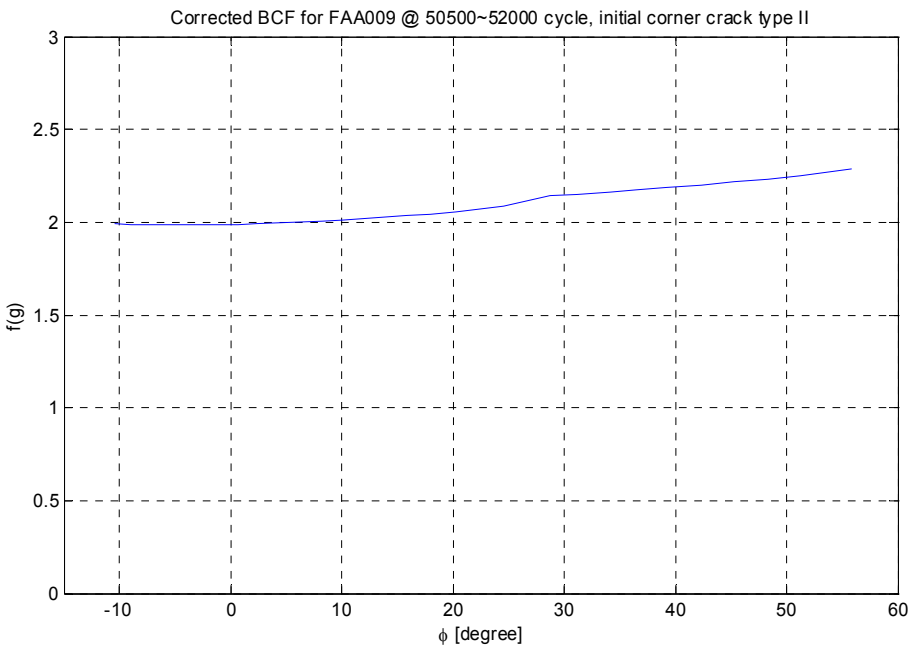

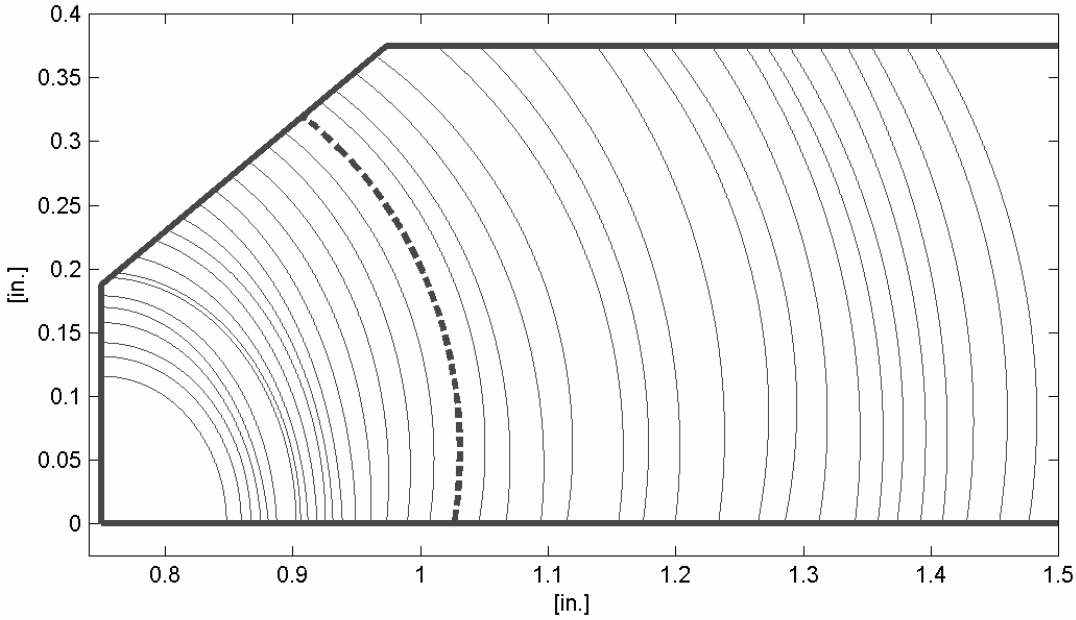

Figure 4-24. Graphical Representation of Dimensionless Stress-Intensity Factor Data for Type II Crack Reported in Table 4-3 for Specimen FAA-009

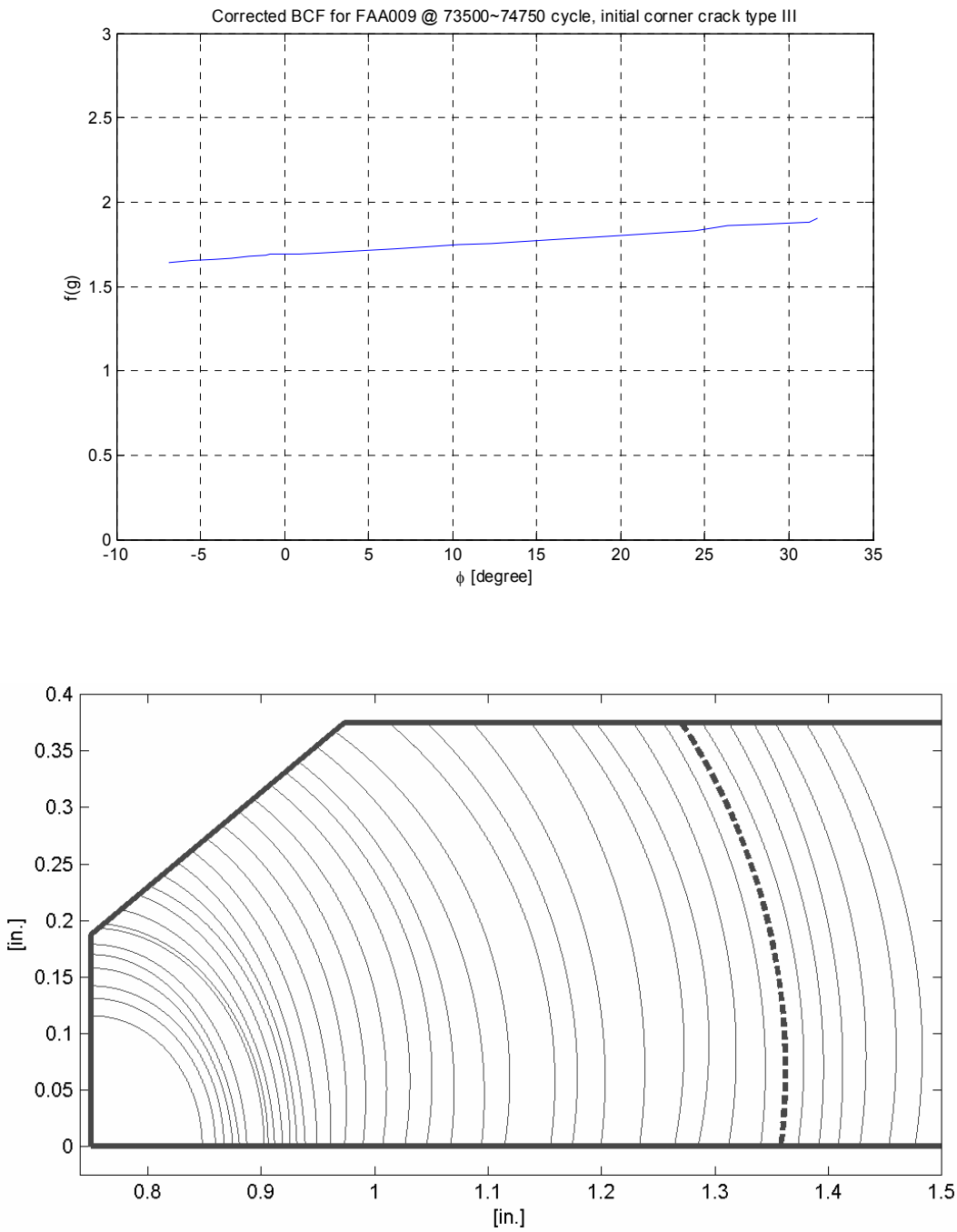

Figure 4-25. Graphical Representation of Dimensionless Stress-Intensity Factor Data for Type III Crack Reported in Table 4-4 for Specimen FAA-009

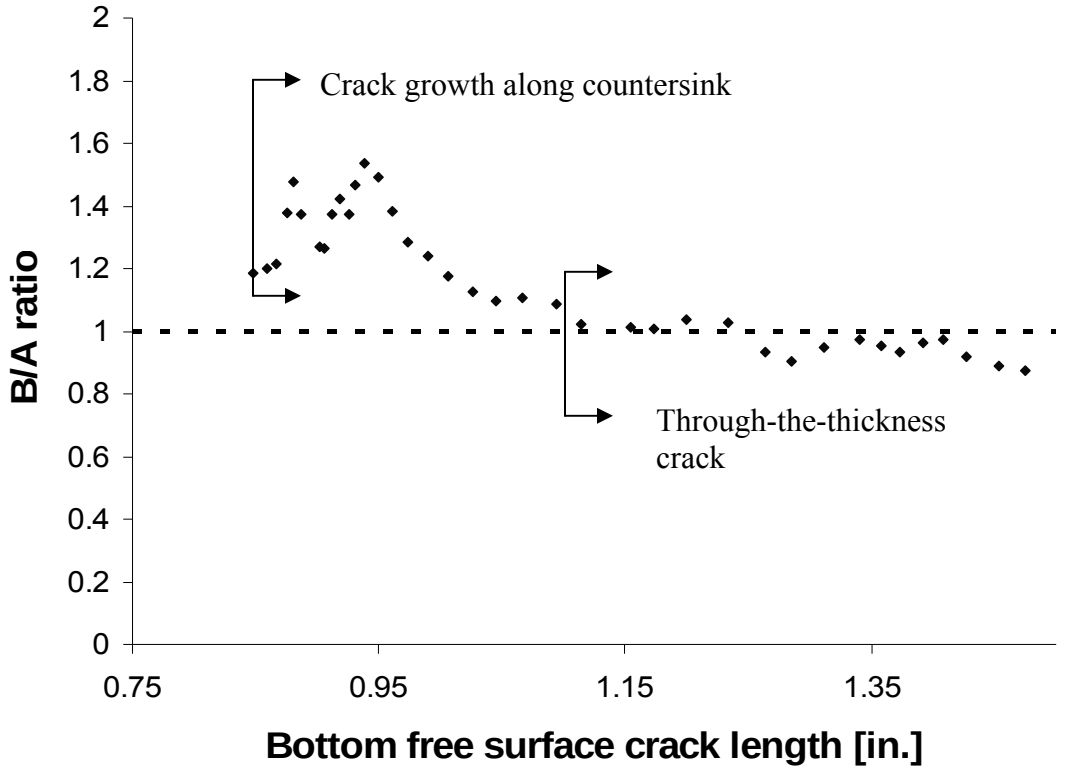

Figure 4-26. Crack Aspect Ratio B/A Ratio Plot for Specimen FAA-009 Showing B/A>1 for Non-Through-the-Thickness Cracks

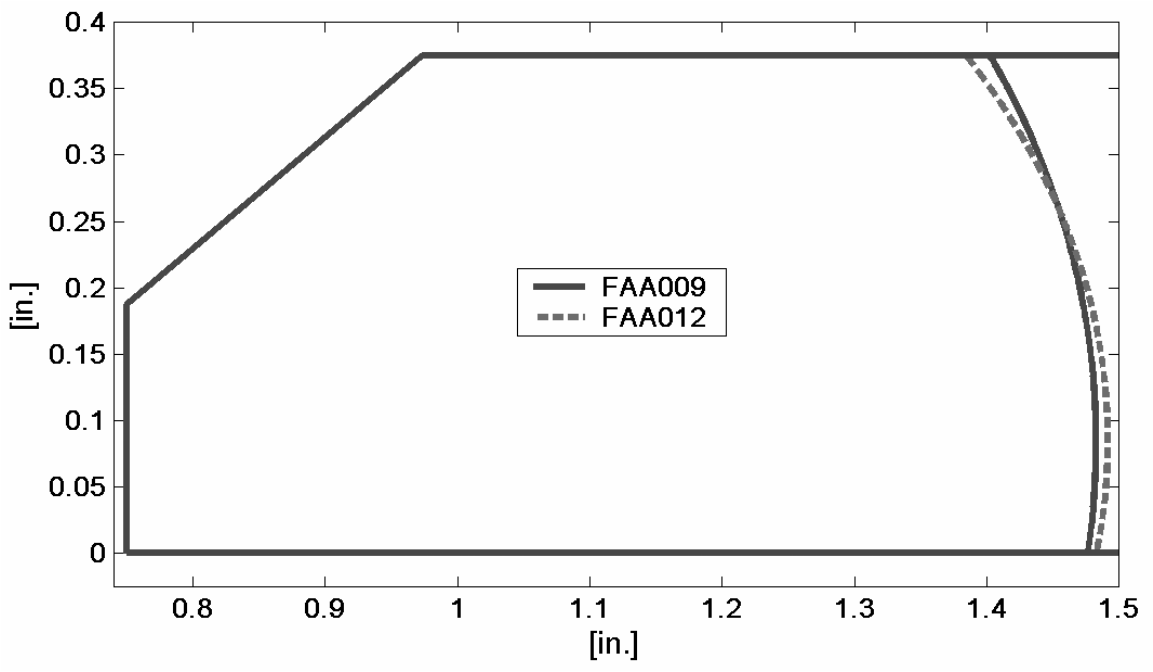

Figure 4-27. Comparison of Similar Through-the-Thickness Crack Shapes for Specimens FAA-009 and FAA-012

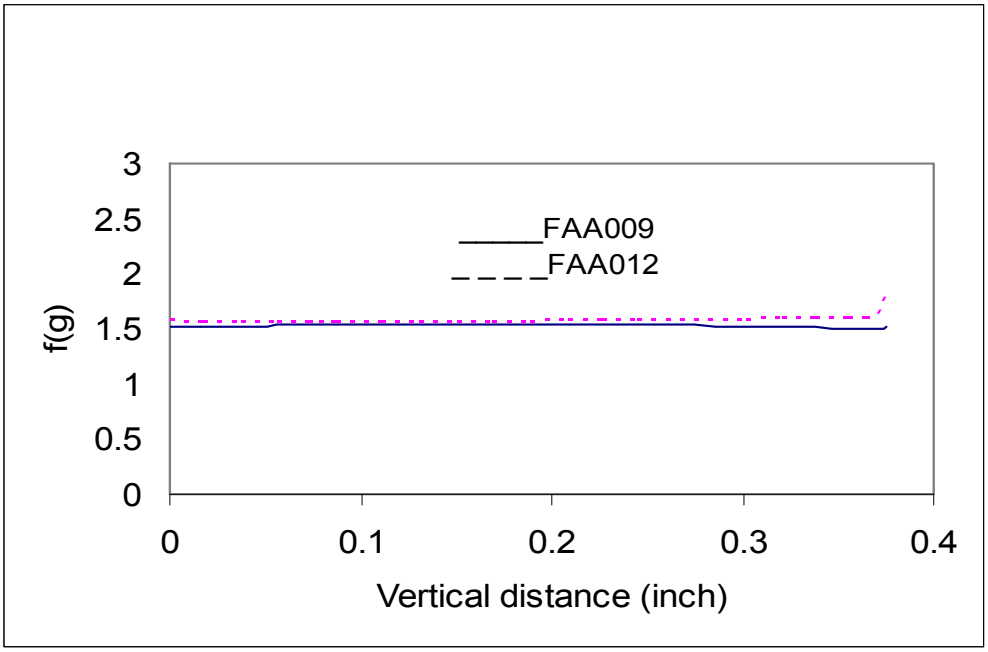

Figure 4-28. Comparison of Dimensionless Stress-Intensity Factors for Similar Shaped Cracks in Specimens FAA-009 and FAA-012

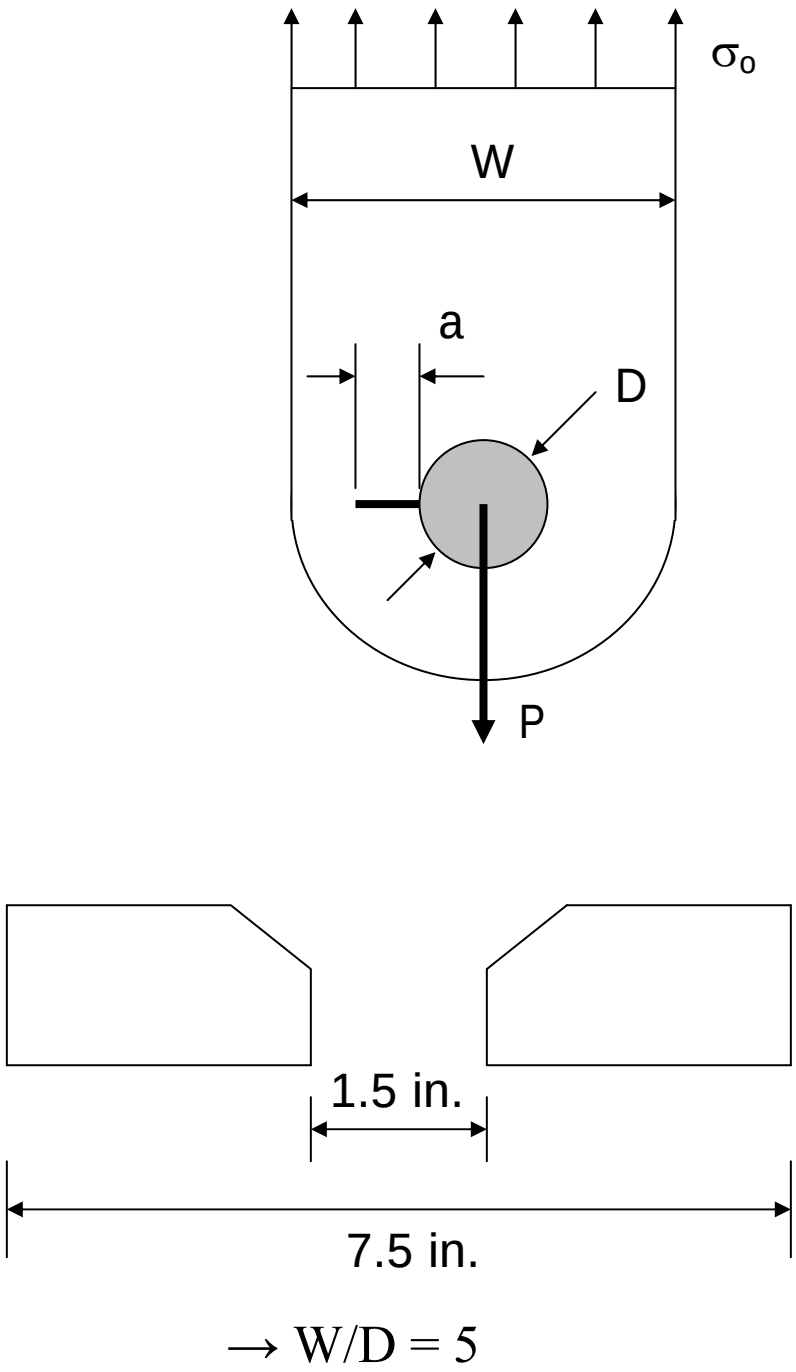

Figure 4-29. Lug With Single Through-the-Thickness Crack Studied by Child

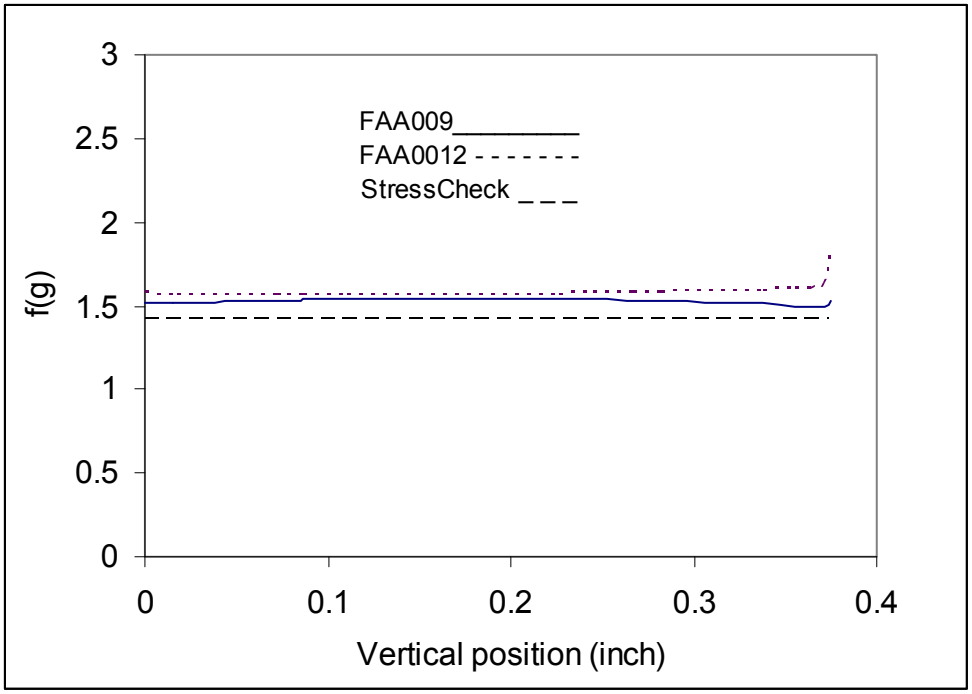

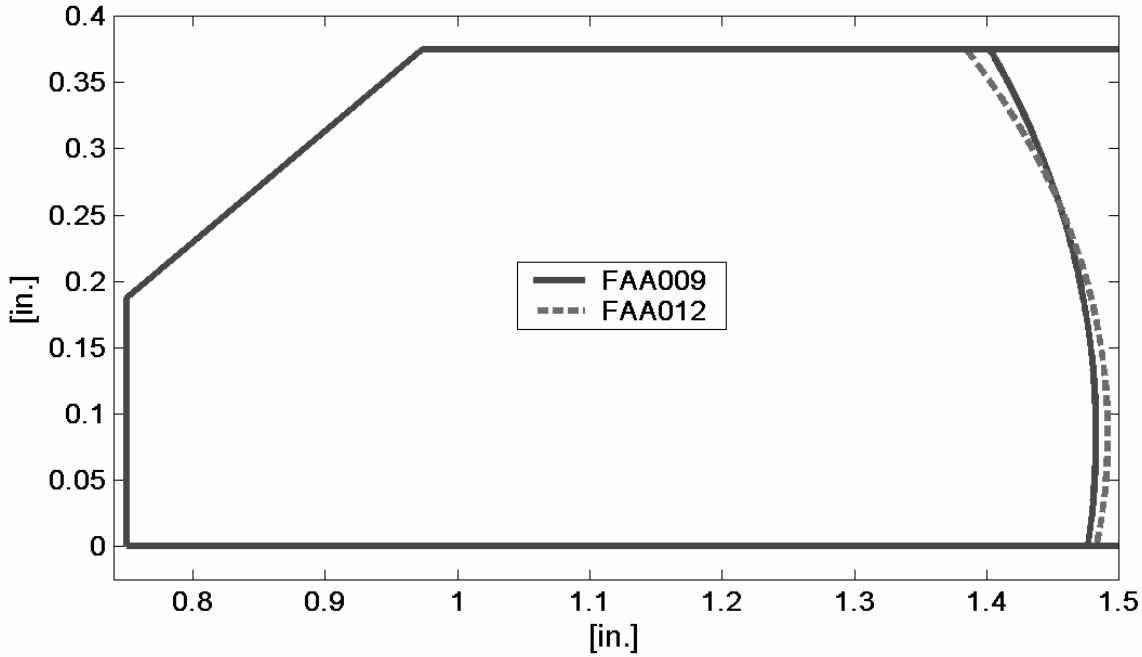

Figure 4-30. Comparison of *f*(*g*) for Two Through-the-Thickness Cracks With Similar Shapes With StressCheck Results Available From Child

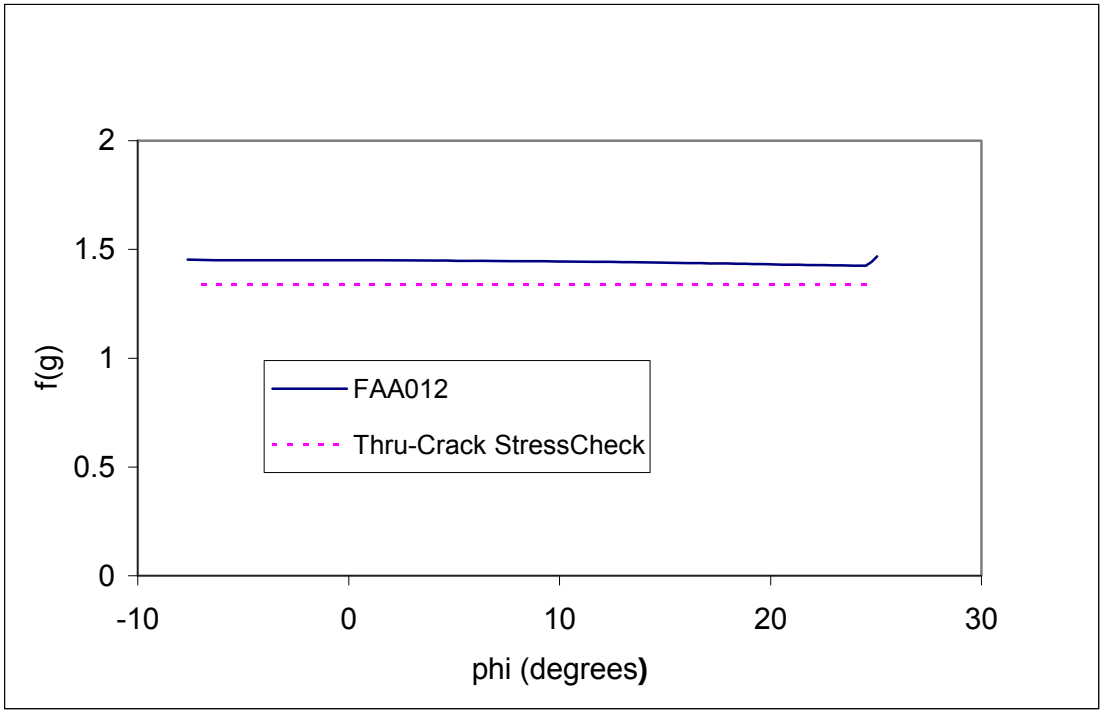

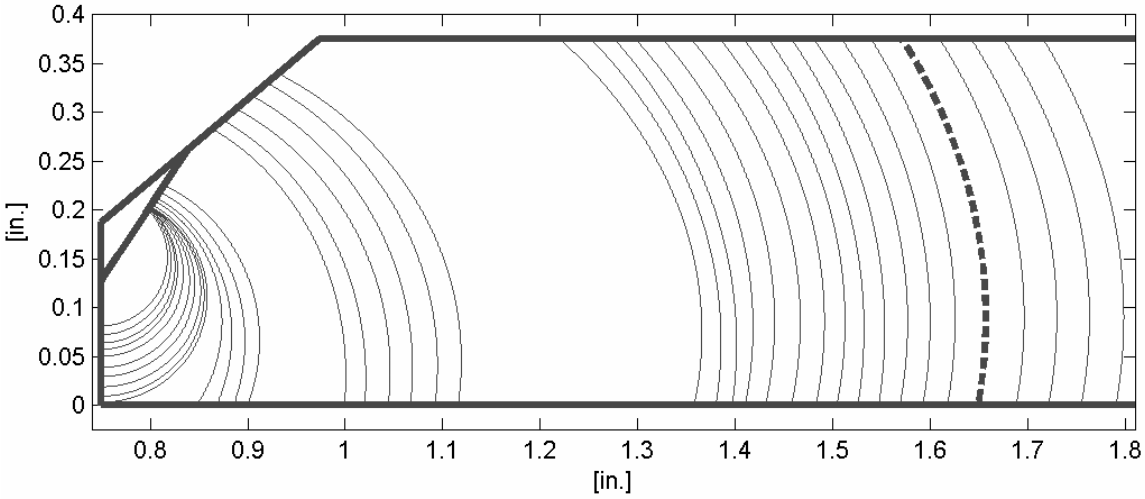

Figure 4-31. Comparison of Dimensionless Stress-Intensity Factor *f*(*g*) for a Through-the-Thickness Crack in FAA-012 With StressCheck Results Reported by Child [31]

5. CONCLUDING REMARKS.

This report presents the results of fatigue tests conducted with transparent polymer specimens intended to characterize the growth of fatigue cracks located at countersunk holes. Two configurations were examined: open holes subjected to remote tensile loading, and pin-loaded holes subjected to 100% load transfer through the pin. Digital photographs of crack growth in the transparent specimens were used to determine the local variation of fatigue crack growth rate along the crack perimeters. The measured crack growth rates were then converted to cyclic stress-intensity factors by using the baseline fatigue crack growth model for the test material. Dimensionless forms of the stress-intensity factors are given in the appendices for 112 different open-hole cracks and for 76 different pin-loaded hole cracks. In addition, a few of these cracks were modeled with the StressCheck finite element software, and generally good agreement was found between the experimental and finite element solutions (except at the specimen surface locations). It is suggested that the data reported here may be used by future investigators to evaluate K solutions for these crack configurations.

Additional details of all of the experiments and analyses conducted for this project are given in the graduate theses of Park [1], Suh [2], and Chiew [3]. Other publications and presentations resulting from this work are given in references 32-37.

6. REFERENCES.

1. Park, C.Y., "Durability of Countersunk Fastener Holes," Ph.D. Thesis, Purdue University, 2003.

2. Suh, J., "Analysis of Fatigue Crack Growth From Countersunk Fastener Holes," Ph.D. Thesis, Purdue University, 2005.

3. Chiew, L.K., "Stress-Intensity Factor Solutions for Countersunk Holes Under Pin-Loading," M.S. Thesis, Purdue University, 2004.

4. Grandt, A.F., Jr. and Sinclair, G.M., "Stress-Intensity Factors for Surface Cracks in Bending," *Stress Analysis and Growth of Cracks*, ASTM, Special Technical Publication 513, American Society for Testing and Materials, 1972, pp. 37-58.

5. Grandt, A.F., Jr. and Macha, D.E., "Digitized Measurements of the Shape of Corner Cracks at Fastener Holes," *Engineering Fracture Mechanics*, Vol. 17, No. 1, 1983, pp. 63-73.

6. Grandt, A.F., Jr., Harter, J.A., and Heath, B.J., "The Transition of Part-Through Cracks at Holes into Through-The-Thickness Flaws," *Fracture Mechanics, Fifteenth Symposium*, ASTM Special Technical Publication 833, American Society for Testing and Materials 1984, pp. 7-23.

7. Grandt, A.F., Jr., Harter, J.A., and Myers, T.F., "Digitized Measurements of Surface Crack Shapes Originating at an Open Hole," *Engineering Fracture Mechanics*, Vol. 20, No. 1, 1984, pp. 187-189.

8. Grandt, A.F., Jr., Thakker, A.B., and Tritsch, D.E., "An Experimental and Numerical Investigation of the Growth and Coalescence of Multiple Fatigue Cracks at Notches," *Fracture Mechanics: Seventeenth Symposium*, ASTM Special Technical Publication, 905, American Society for Testing and Materials, 1986, pp. 239-252.

9. McComb, T.H., Pope, J.E., and Grandt, A.F., Jr., "Growth and Coalescence of Multiple Fatigue Cracks in Polycarbonate Test Specimens," *Engineering Fracture Mechanics*, Vol. 24, No. 4, 1986, pp. 601-608.

10. Perez, R., Tritsch, D.E., and Grandt, A.F., Jr., "Interpolative Estimates of Stress-Intensity Factors for Fatigue Crack Growth Predictions," *Engineering Fracture Mechanics*, Vol. 24, No. 4, 1986, pp. 629-633.

11. Perez, R., Ray, S.K., and Grandt, A.F., Jr., "Application of a Weight Function to Predict the Fatigue Life of Corner Cracked Holes Loaded in Bending," *Engineering Fracture Mechanics*, Vol. 28, No. 3, 1987, pp. 283-291.

12. Heinimann, M.B., Doerfler, M.T., and Grandt, A.F., Jr., "Analysis of Cracks at Deep Notches," *Engineering Fracture Mechanics,* Vol. 55, No. 4, 1996, pp. 605-616.

13. Rifani, A.I. and Grandt, A.F., Jr., "A Fracture Mechanics Analysis of Fatigue Crack Growth in a Complex Cross Section," *Engineering Failure Analysis*, Vol. 3, No. 4, 1996, pp. 249-265.

14. Pitoniak, F.J., Grandt, A.F., Jr., Montulli, L.T., and Packman, P.F., "Fatigue Crack Retardation and Closure in Polymethylmethacrylate," *Engineering Fracture Mechanics,* Vol. 6, No. 4, 1974, pp. 663-670.

15. Ray, S.K., Perez, R., and Grandt, A.F., Jr., "Fatigue Crack Closure of Corner Cracks Located at Holes Loaded in Tension or Bending," *Fatigue & Fracture of Engineering Materials & Structures, an International Journal*, Vol. 10, No. 3, 1987, pp. 239-250.

16. Grandt, A.F., Jr., Ray, S., and Andrew, S., "Three-Dimensional Measurements of Fatigue Crack Closure and Opening," *Basic Questions in Fatigue*, Vol. II, ASTM Special Technical Publication 924, 1988, pp. 275-293.

17. Troha, W.A., Nicholas, T., and Grandt, A.F., Jr., "Three-Dimensional Aspects of Fatigue Crack Closure in Surface Flaws in Polymethylmethacrylate," *Mechanics of Fatigue Crack Closure*, ASTM Special Technical Publication 982, 1988, pp. 598-616.

18. Ray, S.K. and Grandt, A.F., Jr., "Fatigue Crack Closure of Surface Flaws Loaded in Pure Bending," *Experimental Mechanics*, Vol. 28, No. 3, September 1988, pp. 273-280.

19. Troha, W.A., Nicholas, T., and Grandt, A.F., Jr., "Observations of Three-Dimensional Surface Flaw Geometries During Fatigue Crack Growth in PMMA," *Surface Crack Growth*: *Models, Experiments and Structures*, ASTM Special Technical Publication 1060, 1990, pp. 260-285.

20. James, L.A. and Anderson, W.E., "A Simple Procedure for Stress-Intensity Factor Calibration," *Journal of Engineering Fracture Mechanics,* Vol. 1, April 1969, pp. 565-568.

21. Grandt, A.F., Jr., Hinkle, A.J., Scheumann, T.D., and Todd, R.E., "Modeling the Influence of Initial Material Inhomogeneities on the Fatigue Life of Notched Components," *Fatigue & Fracture of Engineering Materials and Structures*, Vol. 16, No. 2, 1993, pp. 199-213.

22. Grandt, A.F., Jr. and Hinkle, A.J., "Predicting the Influence of Initial Material Quality on Fatigue Life," *Durability and Structural Integrity of Airframes*, Vol. I, Proceedings of 17th Symposium of the International Committee on Aeronautical Fatigue," A.F. Blom, ed., Stockholm, Sweden, June 9-11, 1993, pp. 305-319.

23. Gosz, M. and Moran, B., FAA report, "Stress-Intensity Factors for Elliptical Cracks Emanating from Countersunk Rivet Holes," FAA report DOT/FAA/AR-95/111, April 1998.

24. Bakuckas, J.G., "Comparison of Boundary Correction Factor Solutions for Two Symmetric Cracks in a Straight-Shank Hole," FAA report DOT/FAA/AR-98/36, April 1999.

25. Rahman, A., Bakuckas, J., Bigelow, C., and Tan, P., "Boundary Correction Factors for Elliptic Surface Cracks Emanating from Countersunk Rivet Holes under Tension, Bending and Wedge Loading Conditions," FAA report DOT/FAA/AR-98/37, March 1999.

26. De Rijck, J.J.M. and Fawaz, S.A., "Stress-Intensity Factor Solutions for Countersunk Holes Subjected to Tension, Bending and Pin Loading," *Sixth Joint DoD/FAA/NASA Conference on Aging Aircraft*.

27. Fawaz, S.A. and Anderson, Borje, "Accurate Stress-Intensity Factor Solutions for Corner Cracks at a Hole," *Engineering Fracture Mechanics*, Vol. 71, 2004, pp. 1235-1254.

28. Park, C.Y., Grandt, A.F., Jr., and Suh, J.J., "Stress-Intensity Factors for Surface Cracks at Countersunk Holes," *Journal of Engineering Fracture Mechanics,* Vol. 13, Issue 73, 2006, pp. 1872-1898.

29. StressCheck Master Guide, Release 7.0. Engineering Software Research and Development, Inc., 2005.

30. "Standard Test Method for Constant-Load-Amplitude Fatigue Crack Growth Rates," ASTM Standard E647, in *Annual Book of ASTM Standards, Volume 03.01*, American Society for Testing and Materials, West Conshohocken, Pennsylvania, 2000.

31. Child, D.R., "Experimental Validation of Mode I Stress-Intensity Factors for the Single-Cracked Pin-Loaded Lug," M.S. Thesis, School of Aeronautics and Astronautics, Purdue University, May 2004.

32. Park, C.Y. and Grandt, A.F., Jr., "A Proposed Test Protocol for Generic Mechanical Joints," *Journal of Engineering Failure Analysis*, Vol. 13, No. 1, January 2006, pp. 136-154.

33. Park, C.Y. and Grandt, A.F., Jr., "Effect of Load Transfer on the Fatigue Cracking Behavior at Countersunk Fastener Holes," *International Journal of Fatigue*, Vol 29, 2007, pp. 146-157.

34. Grandt, A.F., Jr. and Park, C.Y., "Analysis of Fatigue Crack Growth From Countersunk Fastener Holes," *FAA 2nd Annual Centers of Excellence Meeting*, October 21-24, 2002, Wichita, Kansas (presentation only).

35. Grandt, A.F., Jr. and Park, C.Y., "Analysis of Fatigue Crack Growth From Countersunk Fastener Holes," *FAA Materials and Structures R&D Workshop*, June 3-5, 2003, FAA William J. Hughes Technical Center, Atlantic City International Airport, NJ.

36. Grandt, A.F., Jr., Chiew, L.K., Park, C.Y., and Suh, J., "Experimental Measurements of Stress-Intensity Factors for Cracks at Countersunk Holes," 8th Joint NASA/FAA/DoD Conference on Aging Aircraft, January 31-February 3, 2005, Palm Springs, CA.

37. Grandt, A.F., Jr. and Suh, J., "Stress-Intensity Factors for Nonsymmetric Cracks at Countersunk Fastener Holes," *9th Joint FAA/DoD/NASA Conference on Aging Aircraft*, March 6-9, 2006, Atlanta, GA.

APPENDIX A—OPEN-HOLE TENSION DATA

Table A-1. Geometric Factors for FAA-17 (See figure A-1)

ϕ	x [in.]	z [in.]	f(g)
0.00	0.7500	0.0800	2.4505
0.05	0.7622	0.0808	2.4480
0.10	0.7741	0.0832	2.4407
0.15	0.7855	0.0871	2.4288
0.20	0.7964	0.0925	2.4127
0.25	0.8063	0.0991	2.3930
0.30	0.8153	0.1069	2.3704
0.35	0.8232	0.1156	2.3457
0.40	0.8299	0.1251	2.3198
0.45	0.8354	0.1352	2.2936
0.50	0.8397	0.1457	2.2799
0.55	0.8427	0.1565	2.2731
0.60	0.8444	0.1674	2.2668
0.65	0.8450	0.1784	2.2613
0.70	0.8444	0.1892	2.2568
0.75	0.8426	0.1997	2.2533
0.80	0.8398	0.2099	2.2509
0.85	0.8360	0.2197	2.2496
0.90	0.8312	0.2289	2.2492
0.95	0.8255	0.2375	2.2497
1.00	0.8190	0.2454	2.2508

Initial Crack Location	Knee
Center of Ellipse	(0.75, 0.1780)
Crack Length	0.0950
Crack Depth	0.0980
Average Crack Front	1 and 6000 cycles

Table A-2. Geometric Factors for FAA-17 (See figure A-2)

ϕ	x [in.]	z [in.]	f(g)
0.00	0.7500	0.0610	2.3484
0.05	0.7643	0.0620	2.3471
0.10	0.7783	0.0650	2.3433
0.15	0.7917	0.0699	2.3372
0.20	0.8042	0.0765	2.3290
0.25	0.8156	0.0846	2.3192
0.30	0.8257	0.0940	2.3082
0.35	0.8346	0.1044	2.2963
0.40	0.8419	0.1157	2.2841
0.45	0.8479	0.1275	2.2718
0.50	0.8523	0.1398	2.2600
0.55	0.8554	0.1522	2.2488
0.60	0.8571	0.1647	2.2385
0.65	0.8575	0.1772	2.2292
0.70	0.8566	0.1894	2.2212
0.75	0.8545	0.2013	2.2143
0.80	0.8512	0.2127	2.2088
0.85	0.8469	0.2237	2.2044
0.90	0.8415	0.2341	2.2013
0.95	0.8351	0.2438	2.1991
1.00	0.8278	0.2528	2.1979

Initial Crack Location	Knee
Center of Ellipse	(0.75, 0.1745)
Crack Length	0.1075
Crack Depth	0.1135
Average Crack Front	6,001 and 12,000 cycles

Table A-3. Geometric Factors for FAA-17 (See figure A-3)

ϕ	x [in.]	z [in.]	f(g)
0.00	0.7500	0.0430	2.4220
0.05	0.7663	0.0442	2.4205
0.10	0.7823	0.0477	2.4159
0.15	0.7975	0.0534	2.4084
0.20	0.8117	0.0611	2.3982
0.25	0.8246	0.0705	2.3853
0.30	0.8359	0.0814	2.3701
0.35	0.8457	0.0934	2.3527
0.40	0.8538	0.1064	2.3335
0.45	0.8603	0.1199	2.3125
0.50	0.8650	0.1339	2.2901
0.55	0.8682	0.1480	2.2664
0.60	0.8698	0.1621	2.2416
0.65	0.8699	0.1760	2.2158
0.70	0.8686	0.1896	2.1892
0.75	0.8659	0.2028	2.1619
0.80	0.8620	0.2154	2.1339
0.85	0.8570	0.2275	2.1055
0.90	0.8508	0.2389	2.0767
0.95	0.8436	0.2495	2.0479
1.00	0.8354	0.2592	2.0290

Initial Crack Location	Knee
Center of Ellipse	(0.75, 0.1700)
Crack Length	0.1200
Crack Depth	0.1270
Average Crack Front	12,001 and 15,000 cycles

Table A-4. Geometric Factors for FAA-17 (See figure A-4)

ϕ	x [in.]	z [in.]	f(g)
0.00	0.7500	0.0260	2.3776
0.05	0.7682	0.0274	2.3743
0.10	0.7860	0.0315	2.3644
0.15	0.8029	0.0381	2.3488
0.20	0.8185	0.0470	2.3282
0.25	0.8326	0.0579	2.3038
0.30	0.8449	0.0703	2.2772
0.35	0.8553	0.0840	2.2497
0.40	0.8639	0.0985	2.2227
0.45	0.8706	0.1136	2.1977
0.50	0.8754	0.1290	2.1758
0.55	0.8785	0.1445	2.1579
0.60	0.8799	0.1599	2.1447
0.65	0.8797	0.1750	2.1365
0.70	0.8781	0.1897	2.1333
0.75	0.8751	0.2040	2.1348
0.80	0.8708	0.2176	2.1406
0.85	0.8653	0.2306	2.1500
0.90	0.8586	0.2429	2.1621
0.95	0.8509	0.2543	2.1763
1.00	0.8421	0.2648	2.1916

Initial Crack Location	Knee
Center of Ellipse	(0.75, 0.1660)
Crack Length	0.1300
Crack Depth	0.1400
Average Crack Front	15,001 and 18,000 cycles

Table A-5. Geometric Factors for FAA-17 (See figure A-5)

ϕ	x [in.]	z [in.]	f(g)
0.00	0.8422	0.0000	2.6972
0.09	0.8537	0.0114	2.6450
0.17	0.8637	0.0236	2.6010
0.24	0.8724	0.0364	2.5627
0.30	0.8798	0.0497	2.5286
0.36	0.8862	0.0634	2.4978
0.42	0.8915	0.0776	2.4696
0.47	0.8957	0.0920	2.4436
0.52	0.8989	0.1068	2.4195
0.56	0.9010	0.1217	2.3972
0.61	0.9022	0.1367	2.3763
0.65	0.9023	0.1518	2.3569
0.69	0.9014	0.1669	2.3389
0.73	0.8994	0.1819	2.3222
0.77	0.8965	0.1967	2.3069
0.81	0.8925	0.2113	2.2930
0.85	0.8875	0.2256	2.2805
0.89	0.8814	0.2394	2.2695
0.93	0.8743	0.2527	2.2602
0.96	0.8662	0.2654	2.2527
1.00	0.8570	0.2773	2.2471

Initial Crack Location	Knee
Center of Ellipse	(0.75, 0.1455)
Crack Length	0.1525
Crack Depth	0.1850
Average Crack Front	20,001 and 27,000 cycles

Table A-6. Geometric Factors for FAA-17 (See figure A-6)

ϕ	x [in.]	z [in.]	f(g)
0.00	0.8818	0.0000	2.4692
0.08	0.8904	0.0127	2.4498
0.15	0.8980	0.0260	2.4321
0.21	0.9046	0.0397	2.4156
0.28	0.9102	0.0539	2.3998
0.33	0.9149	0.0685	2.3845
0.39	0.9187	0.0834	2.3695
0.44	0.9215	0.0985	2.3545
0.49	0.9233	0.1138	2.3395
0.54	0.9242	0.1292	2.3242
0.59	0.9241	0.1447	2.3085
0.63	0.9231	0.1602	2.2923
0.68	0.9211	0.1757	2.2755
0.72	0.9180	0.1910	2.2581
0.76	0.9140	0.2060	2.2399
0.80	0.9090	0.2208	2.2210
0.84	0.9030	0.2353	2.2014
0.88	0.8960	0.2492	2.1811
0.92	0.8880	0.2626	2.1602
0.96	0.8790	0.2754	2.1389
1.00	0.8691	0.2875	2.1174

Initial Crack Location	Knee
Center of Ellipse	(0.75, 0.1355)
Crack Length	0.1745
Crack Depth	0.2080
Average Crack Front	27,001 and 33,000 cycles

Table A-7. Geometric Factors for FAA-17 (See figure A-7)

ϕ	x [in.]	z [in.]	f(g)
0.00	0.9225	0.0000	2.3668
0.07	0.9291	0.0141	2.3447
0.13	0.9349	0.0286	2.3233
0.20	0.9398	0.0434	2.3027
0.26	0.9439	0.0587	2.2828
0.31	0.9471	0.0742	2.2635
0.37	0.9494	0.0899	2.2448
0.42	0.9507	0.1058	2.2269
0.47	0.9512	0.1218	2.2096
0.52	0.9507	0.1378	2.1930
0.57	0.9494	0.1539	2.1771
0.62	0.9470	0.1699	2.1620
0.66	0.9438	0.1858	2.1478
0.71	0.9395	0.2014	2.1344
0.75	0.9343	0.2169	2.1219
0.79	0.9282	0.2319	2.1105
0.84	0.9211	0.2466	2.1001
0.88	0.9131	0.2608	2.0909
0.92	0.9041	0.2743	2.0829
0.96	0.8942	0.2873	2.0763
1.00	0.8834	0.2994	2.0712

Initial Crack Location	Knee
Center of Ellipse	(0.75, 0.1210)
Crack Length	0.2015
Crack Depth	0.2380
Average Crack Front	33,001 and 39,000 cycles

Table A-8. Geometric Factors for FAA-17 (See figure A-8)

ϕ	x [in.]	z [in.]	f(g)
0.00	0.9633	0.0000	2.1345
0.06	0.9690	0.0155	2.1377
0.12	0.9738	0.0313	2.1400
0.18	0.9778	0.0474	2.1414
0.24	0.9808	0.0638	2.1419
0.30	0.9829	0.0805	2.1412
0.35	0.9842	0.0973	2.1396
0.40	0.9844	0.1142	2.1368
0.46	0.9838	0.1311	2.1329
0.51	0.9822	0.1481	2.1278
0.56	0.9796	0.1649	2.1215
0.60	0.9761	0.1816	2.1141
0.65	0.9716	0.1982	2.1054
0.70	0.9661	0.2144	2.0956
0.74	0.9597	0.2303	2.0846
0.79	0.9523	0.2458	2.0724
0.83	0.9440	0.2609	2.0592
0.87	0.9347	0.2753	2.0449
0.92	0.9245	0.2892	2.0298
0.96	0.9135	0.3023	2.0140
1.00	0.9015	0.3147	1.9978

Initial Crack Location	Knee
Center of Ellipse	(0.75, 0.1110)
Crack Length	0.2345
Crack Depth	0.2670
Average Crack Front	39,001 and 45,000 cycles

Table A-9. Geometric Factors for FAA-17 (See figure A-9)

ϕ	x [in.]	z [in.]	f(g)
0.00	1.0061	0.0000	2.0662
0.06	1.0111	0.0169	2.0540
0.12	1.0152	0.0342	2.0419
0.17	1.0184	0.0517	2.0302
0.23	1.0207	0.0695	2.0187
0.28	1.0219	0.0874	2.0076
0.34	1.0222	0.1054	1.9968
0.39	1.0215	0.1234	1.9863
0.44	1.0198	0.1415	1.9762
0.49	1.0171	0.1594	1.9666
0.54	1.0134	0.1772	1.9574
0.59	1.0087	0.1948	1.9487
0.64	1.0030	0.2122	1.9405
0.69	0.9963	0.2292	1.9328
0.73	0.9886	0.2457	1.9257
0.78	0.9800	0.2618	1.9192
0.82	0.9704	0.2774	1.9134
0.87	0.9599	0.2923	1.9082
0.91	0.9485	0.3066	1.9038
0.96	0.9362	0.3201	1.9001
1.00	0.9231	0.3327	1.8972

Initial Crack Location	Knee
Center of Ellipse	(0.75, 0.1010)
Crack Length	0.2725
Crack Depth	0.3000
Average Crack Front	45,001 and 51,000 cycles

Table A-10. Geometric Factors for FAA-17 (See figure A-10)

ϕ	x [in.]	z [in.]	f(g)
0.00	1.0406	0.0000	1.9183
0.06	1.0452	0.0181	1.9289
0.11	1.0488	0.0365	1.9382
0.17	1.0515	0.0552	1.9464
0.22	1.0532	0.0740	1.9534
0.28	1.0538	0.0930	1.9594
0.33	1.0535	0.1120	1.9643
0.38	1.0521	0.1311	1.9681
0.44	1.0497	0.1500	1.9710
0.49	1.0463	0.1689	1.9729
0.54	1.0418	0.1876	1.9738
0.59	1.0364	0.2060	1.9739
0.63	1.0299	0.2241	1.9731
0.68	1.0224	0.2419	1.9716
0.73	1.0139	0.2591	1.9694
0.77	1.0044	0.2759	1.9665
0.82	0.9940	0.2921	1.9631
0.87	0.9826	0.3077	1.9593
0.91	0.9704	0.3225	1.9551
0.96	0.9573	0.3366	1.9506
1.00	0.9434	0.3498	1.9461

Initial Crack Location	Knee
Center of Ellipse	(0.75, 0.0960)
Crack Length	0.3039
Crack Depth	0.3290
Average Crack Front	51,001 and 54,000 cycles

Table A-11. Geometric Factors for FAA-17 (See figure A-11)

ϕ	x [in.]	z [in.]	f(g)
0.00	1.1178	0.0000	1.7663
0.05	1.1206	0.0185	1.7671
0.11	1.1226	0.0370	1.7690
0.16	1.1239	0.0555	1.7720
0.21	1.1244	0.0740	1.7762
0.26	1.1243	0.0925	1.7814
0.31	1.1235	0.1110	1.7876
0.36	1.1219	0.1295	1.7949
0.41	1.1196	0.1480	1.8032
0.46	1.1165	0.1665	1.8126
0.50	1.1128	0.1850	1.8231
0.55	1.1082	0.2035	1.8348
0.60	1.1028	0.2220	1.8476
0.65	1.0965	0.2405	1.8617
0.70	1.0893	0.2590	1.8772
0.75	1.0812	0.2775	1.8942
0.79	1.0721	0.2960	1.9129
0.84	1.0618	0.3145	1.9336
0.89	1.0502	0.3330	1.9565
0.95	1.0372	0.3515	1.9821
1.00	1.0227	0.3700	2.0111

Initial Crack Location	Knee
Center of Ellipse	(0.75, 0.0800)
Crack Length	0.3745
Crack Depth	0.4251
Average Crack Front	60,001 and 63,000 cycles

Table A-12. Geometric Factors for FAA-17 (See figure A-12)

ϕ	x [in.]	z [in.]	f(g)
0.00	1.1462	0.0000	1.7985
0.05	1.1490	0.0185	1.7983
0.11	1.1511	0.0370	1.7986
0.16	1.1525	0.0555	1.7994
0.21	1.1533	0.0740	1.8006
0.26	1.1535	0.0925	1.8022
0.31	1.1530	0.1110	1.8043
0.36	1.1518	0.1295	1.8068
0.41	1.1500	0.1480	1.8098
0.46	1.1475	0.1665	1.8133
0.51	1.1444	0.1850	1.8173
0.56	1.1406	0.2035	1.8218
0.61	1.1360	0.2220	1.8269
0.66	1.1307	0.2405	1.8326
0.70	1.1246	0.2590	1.8390
0.75	1.1178	0.2775	1.8462
0.80	1.1100	0.2960	1.8543
0.85	1.1014	0.3145	1.8633
0.90	1.0918	0.3330	1.8735
0.95	1.0811	0.3515	1.8851
1.00	1.0692	0.3700	1.8983

Initial Crack Location	Knee
Center of Ellipse	(0.75, 0.0875)
Crack Length	0.4035
Crack Depth	0.4625
Average Crack Front	63,001 and 66,000 cycles

Table A-13. Geometric Factors for FAA-17 (See figure A-13)

ϕ	x [in.]	z [in.]	f(g)
0.00	1.0000	0.0000	1.7428
0.05	1.1822	0.0185	1.7389
0.11	1.1841	0.0370	1.7359
0.16	1.1855	0.0555	1.7338
0.21	1.1863	0.0740	1.7326
0.26	1.1865	0.0925	1.7323
0.31	1.1861	0.1110	1.7328
0.36	1.1852	0.1295	1.7343
0.41	1.1837	0.1480	1.7366
0.46	1.1815	0.1665	1.7399
0.51	1.1788	0.1850	1.7440
0.56	1.1755	0.2035	1.7491
0.61	1.1715	0.2220	1.7551
0.66	1.1669	0.2405	1.7621
0.71	1.1617	0.2590	1.7701
0.76	1.1557	0.2775	1.7791
0.80	1.1490	0.2960	1.7892
0.85	1.1416	0.3145	1.8005
0.90	1.1334	0.3330	1.8130
0.95	1.1243	0.3515	1.8268
1.00	1.1142	0.3700	1.8422

Initial Crack Location	Knee
Center of Ellipse	(0.75, 0.0900)
Crack Length	0.4365
Crack Depth	0.5100
Average Crack Front	66,001 and 69,000 cycles

Table A-14. Geometric Factors for FAA-17 (See figure A-14)

ϕ	x [in.]	z [in.]	f(g)
0.00	1.2139	0.0000	1.6768
0.05	1.2169	0.0185	1.6885
0.11	1.2194	0.0370	1.6991
0.16	1.2212	0.0555	1.7087
0.21	1.2225	0.0740	1.7174
0.26	1.2232	0.0925	1.7254
0.31	1.2233	0.1110	1.7326
0.36	1.2229	0.1295	1.7391
0.42	1.2218	0.1480	1.7451
0.46	1.2203	0.1665	1.7505
0.51	1.2181	0.1850	1.7554
0.56	1.2154	0.2035	1.7598
0.61	1.2120	0.2220	1.7638
0.66	1.2081	0.2405	1.7673
0.71	1.2035	0.2590	1.7705
0.76	1.1982	0.2775	1.7733
0.81	1.1924	0.2960	1.7758
0.85	1.1858	0.3145	1.7779
0.90	1.1784	0.3330	1.7798
0.95	1.1704	0.3515	1.7813
1.00	1.1615	0.3700	1.7827

Initial Crack Location	Knee
Center of Ellipse	(0.75, 0.1050)
Crack Length	0.4735
Crack Depth	0.5350
Average Crack Front	69,001 and 72,000 cycles

Table A-15. Geometric Factors for FAA-17 (See figure A-15)

ϕ	x [in.]	z [in.]	f(g)
0.00	1.2553	0.0000	1.7023
0.05	1.2593	0.0185	1.7057
0.11	1.2626	0.0370	1.7087
0.16	1.2652	0.0555	1.7115
0.21	1.2672	0.0740	1.7139
0.26	1.2686	0.0925	1.7161
0.31	1.2693	0.1110	1.7181
0.36	1.2695	0.1295	1.7198
0.41	1.2690	0.1480	1.7213
0.46	1.2679	0.1665	1.7225
0.51	1.2661	0.1850	1.7235
0.56	1.2637	0.2035	1.7243
0.61	1.2607	0.2220	1.7249
0.66	1.2571	0.2405	1.7253
0.70	1.2527	0.2590	1.7255
0.75	1.2477	0.2775	1.7255
0.80	1.2420	0.2960	1.7253
0.85	1.2355	0.3145	1.7250
0.90	1.2283	0.3330	1.7245
0.95	1.2203	0.3515	1.7239
1.00	1.2114	0.3700	1.7231

Initial Crack Location	Knee
Center of Ellipse	(0.75, 0.1240)
Crack Length	0.5195
Crack Depth	0.5350
Average Crack Front	72,001 and 75,000 cycles

Table A-16. Geometric Factors for FAA-18 (See figure A-16)

ϕ	x [in.]	z [in.]	f(g)
0.00	0.8354	0.0000	2.1222
0.05	0.8349	0.0067	2.1231
0.10	0.8340	0.0133	2.1241
0.15	0.8327	0.0199	2.1250
0.20	0.8311	0.0263	2.1261
0.25	0.8291	0.0327	2.1271
0.30	0.8266	0.0390	2.1282
0.35	0.8238	0.0452	2.1293
0.40	0.8205	0.0512	2.1304
0.45	0.8169	0.0571	2.1314
0.50	0.8127	0.0627	2.1324
0.55	0.8082	0.0681	2.1334
0.60	0.8031	0.0731	2.1344
0.65	0.7977	0.0778	2.1352
0.70	0.7918	0.0820	2.1360
0.75	0.7855	0.0858	2.1366
0.80	0.7789	0.0889	2.1372
0.85	0.7720	0.0915	2.1376
0.90	0.7648	0.0933	2.1379
0.95	0.7574	0.0945	2.1381
1.00	0.7500	0.0949	2.1382

Initial Crack Location	Corner
Center of Ellipse	(0.75, -0.0055)
Crack Length	0.0855
Crack Depth	0.1003
Average Crack Front	1 and 14,000 cycles

Table A-17. Geometric Factors for FAA-18 (See figure A-17)

ϕ	x [in.]	z [in.]	f(g)
0.00	0.8522	0.0000	1.9780
0.05	0.8514	0.0080	1.9746
0.10	0.8503	0.0159	1.9718
0.15	0.8487	0.0237	1.9698
0.20	0.8467	0.0314	1.9686
0.25	0.8442	0.0390	1.9681
0.30	0.8413	0.0465	1.9683
0.35	0.8380	0.0539	1.9693
0.40	0.8342	0.0612	1.9709
0.45	0.8299	0.0682	1.9731
0.50	0.8251	0.0751	1.9758
0.55	0.8197	0.0816	1.9790
0.60	0.8138	0.0879	1.9824
0.65	0.8074	0.0937	1.9860
0.70	0.8004	0.0990	1.9896
0.75	0.7930	0.1037	1.9930
0.8	0.7850	0.1077	2.0031
0.85	0.7767	0.1110	2.0124
0.90	0.7680	0.1134	2.0194
0.95	0.7590	0.1149	2.0238
1.00	0.7500	0.1154	2.0253

Initial Crack Location	Corner
Center of Ellipse	(0.75, -0.0118)
Crack Length	0.1028
Crack Depth	0.1271
Average Crack Front	14,001 and 24,000 cycles

Table A-18. Geometric Factors for FAA-18 (See figure A-18)

ϕ	x [in.]	z [in.]	f(g)
0.00	0.8769	0.0000	2.0177
0.05	0.8757	0.0099	2.0162
0.10	0.8740	0.0196	2.0151
0.15	0.8719	0.0293	2.0145
0.20	0.8693	0.0387	2.0142
0.25	0.8661	0.0481	2.0144
0.30	0.8625	0.0573	2.0149
0.35	0.8584	0.0664	2.0157
0.40	0.8537	0.0753	2.0167
0.45	0.8484	0.0840	2.0179
0.50	0.8425	0.0924	2.0192
0.55	0.8359	0.1006	2.0205
0.60	0.8287	0.1083	2.0218
0.65	0.8208	0.1155	2.0230
0.70	0.8123	0.1222	2.0241
0.75	0.8031	0.1281	2.0249
0.80	0.7933	0.1332	2.0256
0.85	0.7830	0.1373	2.0261
0.90	0.7722	0.1403	2.0264
0.95	0.7612	0.1422	2.0266
1.00	0.7500	0.1428	2.0267

Initial Crack Location	Corner
Center of Ellipse	(0.75, -0.0202)
Crack Length	0.1279
Crack Depth	0.1630
Average Crack Front	24,001 and 32,000 cycles

Table A-19. Geometric Factors for FAA-18 (See figure A-19)

ϕ	x [in.]	z [in.]	f(g)
0.00	0.8971	0.0000	1.9907
0.05	0.8956	0.0115	1.9928
0.10	0.8936	0.0227	1.9961
0.15	0.8911	0.0339	2.0005
0.20	0.8880	0.0449	2.0059
0.25	0.8844	0.0557	2.0125
0.30	0.8802	0.0664	2.0200
0.35	0.8755	0.0769	2.0285
0.40	0.8700	0.0872	2.0378
0.45	0.8639	0.0973	2.0478
0.50	0.8571	0.1071	2.0584
0.55	0.8496	0.1166	2.0694
0.60	0.8412	0.1256	2.0805
0.65	0.8321	0.1340	2.0915
0.70	0.8223	0.1418	2.1020
0.75	0.8116	0.1488	2.1118
0.80	0.8003	0.1547	2.1205
0.85	0.7883	0.1596	2.1277
0.90	0.7758	0.1631	2.1331
0.95	0.7630	0.1653	2.1364
1.00	0.7500	0.1661	2.1375

Initial Crack Location	Corner
Center of Ellipse	(0.75, -0.0231)
Crack Length	0.1483
Crack Depth	0.1889
Average Crack Front	32,001 and 35,000 cycles

Table A-20. Geometric Factors for FAA-18 (See figure A-20)

ϕ	x [in.]	z [in.]	f(g)
0.00	0.9437	0.0000	2.0849
0.06	0.9424	0.0145	2.0822
0.11	0.9404	0.0289	2.0797
0.17	0.9379	0.0432	2.0775
0.22	0.9347	0.0574	2.0756
0.28	0.9310	0.0713	2.0739
0.33	0.9266	0.0851	2.0727
0.38	0.9217	0.0985	2.0717
0.44	0.9161	0.1117	2.0712
0.49	0.9099	0.1246	2.0712
0.54	0.9031	0.1371	2.0717
0.59	0.8957	0.1491	2.0727
0.64	0.8876	0.1608	2.0745
0.68	0.8788	0.1718	2.0771
0.73	0.8695	0.1824	2.0806
0.78	0.8594	0.1922	2.0852
0.82	0.8488	0.2014	2.0910
0.87	0.8374	0.2097	2.0983
0.91	0.8254	0.2172	2.1074
0.96	0.8128	0.2237	2.1185
1.00	0.7995	0.2291	2.1319

Initial Crack Location	Corner
Center of Ellipse	(0.75, -0.0256)
Crack Length	0.1947
Crack Depth	0.2634
Average Crack Front	49,001 and 52,000 cycles

Table A-21. Geometric Factors for FAA-18 (See figure A-21)

ϕ	x [in.]	z [in.]	f(g)
0.00	0.9641	0.0000	1.9959
0.06	0.9631	0.0152	2.0049
0.11	0.9615	0.0304	2.0139
0.17	0.9592	0.0455	2.0226
0.22	0.9564	0.0604	2.0313
0.28	0.9529	0.0752	2.0399
0.33	0.9487	0.0898	2.0484
0.38	0.9440	0.1041	2.0570
0.44	0.9386	0.1182	2.0656
0.49	0.9326	0.1319	2.0743
0.54	0.9259	0.1454	2.0832
0.59	0.9186	0.1584	2.0922
0.64	0.9107	0.1710	2.1015
0.68	0.9021	0.1832	2.1110
0.73	0.8928	0.1948	2.1210
0.78	0.8829	0.2058	2.1314
0.82	0.8723	0.2161	2.1423
0.87	0.8611	0.2257	2.1538
0.91	0.8492	0.2345	2.1661
0.96	0.8367	0.2424	2.1792
1.00	0.8236	0.2493	2.1932

Initial Crack Location	Corner
Center of Ellipse	(0.75, -0.0172)
Crack Length	0.2147
Crack Depth	0.2845
Average Crack Front	52,001 and 61,000 cycles

Table A-22. Geometric Factors for FAA-18 (See figure A-22)

ϕ	x [in.]	z [in.]	f(g)
0.00	0.9996	0.0000	1.9403
0.06	0.9999	0.0165	1.9555
0.11	0.9994	0.0331	1.9689
0.17	0.9981	0.0496	1.9807
0.22	0.9961	0.0660	1.9910
0.27	0.9933	0.0823	2.0000
0.33	0.9898	0.0985	2.0077
0.38	0.9856	0.1145	2.0143
0.43	0.9806	0.1302	2.0199
0.48	0.9748	0.1457	2.0245
0.53	0.9683	0.1608	2.0282
0.58	0.9611	0.1756	2.0312
0.63	0.9531	0.1899	2.0334
0.68	0.9443	0.2038	2.0351
0.73	0.9349	0.2171	2.0362
0.77	0.9247	0.2299	2.0370
0.82	0.9138	0.2420	2.0376
0.87	0.9023	0.2535	2.0381
0.91	0.8901	0.2641	2.0387
0.96	0.8772	0.2740	2.0395
1.00	0.8637	0.2830	2.0408

Initial Crack Location	Corner
Center of Ellipse	(0.75, 0.0116)
Crack Length	0.2504
Crack Depth	0.3045
Average Crack Front	61,001 and 70,000 cycles

Table A-23. Geometric Factors for FAA-18 (See figure A-23)

ϕ	x [in.]	z [in.]	f(g)
0.00	1.0548	0.0000	1.9413
0.05	1.0558	0.0185	1.9415
0.11	1.0559	0.0370	1.9415
0.16	1.0551	0.0556	1.9414
0.22	1.0534	0.0740	1.9410
0.27	1.0507	0.0924	1.9405
0.32	1.0472	0.1107	1.9398
0.37	1.0427	0.1287	1.9389
0.42	1.0373	0.1465	1.9378
0.47	1.0311	0.1639	1.9366
0.53	1.0239	0.1811	1.9353
0.58	1.0159	0.1977	1.9340
0.62	1.0070	0.2140	1.9326
0.67	0.9973	0.2296	1.9311
0.72	0.9868	0.2448	1.9297
0.77	0.9755	0.2592	1.9284
0.82	0.9635	0.2730	1.9272
0.86	0.9507	0.2861	1.9262
0.91	0.9372	0.2984	1.9254
0.95	0.9230	0.3098	1.9249
1.00	0.9082	0.3203	1.9248

Initial Crack Location	Corner
Center of Ellipse	(0.75, 0.0306)
Crack Length	0.3060
Crack Depth	0.3397
Average Crack Front	70,001 and 79,000 cycles

Table A-24. Geometric Factors for FAA-18 (See figure A-24)

ϕ	x [in.]	z [in.]	f(g)
0.00	1.1034	0.0000	1.9592
0.05	1.1041	0.0202	1.9522
0.11	1.1039	0.0404	1.9455
0.16	1.1027	0.0606	1.9391
0.21	1.1005	0.0807	1.9329
0.26	1.0973	0.1007	1.9270
0.32	1.0932	0.1205	1.9215
0.37	1.0881	0.1400	1.9163
0.42	1.0820	0.1593	1.9114
0.47	1.0750	0.1782	1.9070
0.52	1.0671	0.1968	1.9029
0.57	1.0583	0.2149	1.8992
0.62	1.0486	0.2325	1.8959
0.67	1.0380	0.2495	1.8930
0.72	1.0266	0.2659	1.8905
0.77	1.0143	0.2817	1.8885
0.81	1.0013	0.2967	1.8869
0.86	0.9876	0.3110	1.8857
0.91	0.9731	0.3245	1.8850
0.95	0.9580	0.3371	1.8847
1.00	0.9422	0.3488	1.8848

Initial Crack Location	Corner
Center of Ellipse	(0.75, 0.0251)
Crack Length	0.3542
Crack Depth	0.3855
Average Crack Front	79,001 and 82,000 cycles

Table A-25. Geometric Factors for FAA-18 (See figure A-25)

ϕ	x [in.]	z [in.]	f(g)
0.00	1.1580	0.0000	1.7566
0.05	1.1584	0.0188	1.7453
0.09	1.1580	0.0375	1.7356
0.14	1.1570	0.0563	1.7274
0.18	1.1552	0.0750	1.7210
0.23	1.1526	0.0938	1.7164
0.28	1.1493	0.1125	1.7136
0.32	1.1453	0.1313	1.7128
0.37	1.1404	0.1500	1.7141
0.42	1.1347	0.1688	1.7175
0.46	1.1281	0.1875	1.7231
0.51	1.1207	0.2063	1.7311
0.56	1.1122	0.2250	1.7415
0.61	1.1027	0.2438	1.7545
0.66	1.0921	0.2625	1.7703
0.71	1.0803	0.2813	1.7890
0.76	1.0670	0.3000	1.8110
0.82	1.0522	0.3188	1.8367
0.88	1.0356	0.3375	1.8669
0.94	1.0168	0.3563	1.9025
1.00	0.9952	0.3750	1.9453

Initial Crack Location	Corner
Center of Ellipse	(0.75, 0.0178)
Crack Length	0.4086
Crack Depth	0.4483
Average Crack Front	85,001 and 88,000 cycles

Table A-26. Geometric Factors for FAA-18 (See figure A-26)

ϕ	x [in.]	z [in.]	f(g)
0.00	1.1897	0.0000	1.7313
0.05	1.1898	0.0188	1.7357
0.10	1.1892	0.0375	1.7404
0.14	1.1881	0.0563	1.7453
0.19	1.1863	0.0750	1.7507
0.24	1.1839	0.0938	1.7563
0.29	1.1808	0.1125	1.7623
0.33	1.1771	0.1313	1.7687
0.38	1.1727	0.1500	1.7756
0.43	1.1676	0.1688	1.7829
0.48	1.1617	0.1875	1.7907
0.53	1.1551	0.2063	1.7991
0.58	1.1477	0.2250	1.8082
0.63	1.1394	0.2438	1.8180
0.68	1.1303	0.2625	1.8287
0.73	1.1202	0.2813	1.8404
0.78	1.1090	0.3000	1.8534
0.83	1.0966	0.3188	1.8677
0.89	1.0830	0.3375	1.8839
0.94	1.0679	0.3563	1.9022
1.00	1.0511	0.3750	1.9234

Initial Crack Location	Corner
Center of Ellipse	(0.75, 0.0126)
Crack Length	0.4399
Crack Depth	0.4986
Average Crack Front	88,001 and 91,000 cycles

Table A-27. Geometric Factors for FAA-18 (See figure A-27)

ϕ	x [in.]	z [in.]	f(g)
0.00	1.2252	0.0000	1.6994
0.05	1.2254	0.0188	1.6970
0.10	1.2251	0.0375	1.6953
0.15	1.2241	0.0563	1.6945
0.19	1.2226	0.0750	1.6945
0.24	1.2206	0.0938	1.6952
0.29	1.2180	0.1125	1.6969
0.34	1.2147	0.1313	1.6993
0.39	1.2109	0.1500	1.7027
0.44	1.2065	0.1688	1.7069
0.49	1.2015	0.1875	1.7120
0.54	1.1958	0.2063	1.7181
0.59	1.1894	0.2250	1.7252
0.64	1.1823	0.2438	1.7333
0.69	1.1745	0.2625	1.7425
0.74	1.1659	0.2813	1.7529
0.79	1.1564	0.3000	1.7645
0.84	1.1461	0.3188	1.7775
0.89	1.1348	0.3375	1.7920
0.95	1.1224	0.3563	1.8082
1.00	1.1088	0.3750	1.8264

Initial Crack Location	Corner
Center of Ellipse	(0.75, 0.0153)
Crack Length	0.4755
Crack Depth	0.5503
Average Crack Front	91,001 and 94,000 cycles

Table A-28. Geometric Factors for FAA-18 (See figure A-28)

ϕ	x [in.]	z [in.]	f(g)
0.00	1.2658	0.0000	1.6756
0.05	1.2661	0.0188	1.6798
0.10	1.2659	0.0375	1.6836
0.15	1.2652	0.0563	1.6871
0.20	1.2640	0.0750	1.6904
0.24	1.2622	0.0938	1.6933
0.29	1.2598	0.1125	1.6960
0.34	1.2570	0.1313	1.6985
0.39	1.2535	0.1500	1.7008
0.44	1.2495	0.1688	1.7028
0.49	1.2449	0.1875	1.7046
0.54	1.2397	0.2063	1.7063
0.59	1.2339	0.2250	1.7078
0.64	1.2275	0.2438	1.7091
0.69	1.2204	0.2625	1.7103
0.74	1.2126	0.2813	1.7114
0.79	1.2040	0.3000	1.7125
0.84	1.1947	0.3188	1.7134
0.89	1.1845	0.3375	1.7144
0.95	1.1735	0.3563	1.7154
1.00	1.1615	0.3750	1.7165

Initial Crack Location	Corner
Center of Ellipse	(0.75, 0.0209)
Crack Length	0.5162
Crack Depth	0.5862
Average Crack Front	94,001 and 97,000 cycles

Table A-29. Geometric Factors for FAA-19 (See figure A-29)

ϕ	x [in.]	z [in.]	f(g)
0.00	0.7500	0.0883	2.1615
0.05	0.7609	0.0890	2.1620
0.10	0.7715	0.0914	2.1634
0.15	0.7817	0.0951	2.1654
0.20	0.7912	0.1001	2.1676
0.25	0.7999	0.1062	2.1696
0.30	0.8077	0.1133	2.1712
0.35	0.8146	0.1210	2.1720
0.40	0.8206	0.1293	2.1720
0.45	0.8257	0.1381	2.1711
0.50	0.8300	0.1472	2.1691
0.55	0.8333	0.1566	2.1661
0.60	0.8359	0.1663	2.1618
0.65	0.8376	0.1761	2.1560
0.70	0.8384	0.1860	2.1485
0.75	0.8385	0.1962	2.1387
0.80	0.8377	0.2064	2.1259
0.85	0.8360	0.2167	2.1087
0.90	0.8334	0.2270	2.0848
0.95	0.8297	0.2373	2.0493
1.00	0.8250	0.2474	1.9875

Initial Crack Location	Knee
Center of Ellipse	(0.75, 0.1930)
Crack Length	0.0888
Crack Depth	0.1043
Average Crack Front	1 and 12,000 cycles

Table A-30. Geometric Factors for FAA-19 (See figure A-30)

ϕ	x [in.]	z [in.]	f(g)
0.00	-0.7500	0.0655	2.2022
0.05	-0.7634	0.0665	2.2025
0.10	-0.7766	0.0695	2.2034
0.15	-0.7891	0.0742	2.2046
0.20	-0.8007	0.0806	2.2060
0.25	-0.8113	0.0883	2.2073
0.30	-0.8208	0.0971	2.2083
0.35	-0.8291	0.1068	2.2089
0.40	-0.8362	0.1171	2.2089
0.45	-0.8422	0.1280	2.2084
0.50	-0.8471	0.1392	2.2074
0.55	-0.8510	0.1507	2.2058
0.60	-0.8538	0.1624	2.2036
0.65	-0.8556	0.1743	2.2008
0.70	-0.8564	0.1864	2.1973
0.75	-0.8562	0.1985	2.1930
0.80	-0.8550	0.2107	2.1877
0.85	-0.8527	0.2229	2.1812
0.90	-0.8493	0.2351	2.1732
0.95	-0.8447	0.2472	2.1634
1.00	-0.8388	0.2590	2.1512

Initial Crack Location	Knee
Center of Ellipse	(-0.75, 0.1910)
Crack Length	0.1065
Crack Depth	0.1250
Average Crack Front	1 and 12,000 cycles

Table A-31. Geometric Factors for FAA-19 (See figure A-31)

ϕ	x [in.]	z [in.]	f(g)
0.00	0.7500	0.0660	2.4158
0.05	0.7634	0.0669	2.4157
0.10	0.7766	0.0695	2.4153
0.15	0.7892	0.0738	2.4147
0.20	0.8012	0.0796	2.4138
0.25	0.8122	0.0868	2.4125
0.30	0.8223	0.0952	2.4108
0.35	0.8313	0.1046	2.4086
0.40	0.8391	0.1149	2.4060
0.45	0.8458	0.1258	2.4028
0.50	0.8512	0.1373	2.3990
0.55	0.8554	0.1492	2.3947
0.60	0.8585	0.1614	2.3896
0.65	0.8603	0.1739	2.3838
0.70	0.8610	0.1864	2.3771
0.75	0.8604	0.1990	2.3694
0.80	0.8587	0.2116	2.3606
0.85	0.8556	0.2240	2.3503
0.90	0.8514	0.2362	2.3384
0.95	0.8459	0.2479	2.3246
1.00	0.8390	0.2592	2.3085

Initial Crack Location	Knee
Center of Ellipse	(0.75, 0.1875)
Crack Length	0.1110
Crack Depth	0.1210
Average Crack Front	46,001 and 58,000 cycles

Table A-32. Geometric Factors for FAA-19 (See figure A-32)

ϕ	x [in.]	z [in.]	f(g)
0.00	-0.8616	0.0000	3.3390
0.08	-0.8791	0.0122	3.2659
0.16	-0.8937	0.0254	3.2097
0.22	-0.9062	0.0395	3.1626
0.28	-0.9169	0.0544	3.1213
0.34	-0.9260	0.0698	3.0843
0.39	-0.9336	0.0858	3.0503
0.44	-0.9399	0.1022	3.0187
0.49	-0.9447	0.1189	2.9890
0.54	-0.9482	0.1358	2.9609
0.58	-0.9503	0.1529	2.9342
0.63	-0.9511	0.1701	2.9086
0.67	-0.9506	0.1872	2.8840
0.71	-0.9488	0.2042	2.8603
0.76	-0.9457	0.2209	2.8376
0.80	-0.9413	0.2374	2.8158
0.84	-0.9357	0.2534	2.7948
0.88	-0.9289	0.2690	2.7749
0.92	-0.9209	0.2839	2.7560
0.96	-0.9118	0.2982	2.7384
1.00	-0.9015	0.3117	2.7221

Initial Crack Location	Knee
Center of Ellipse	(-0.75, 0.17)
Crack Length	0.2020
Crack Depth	0.2145
Average Crack Front	46,001 and 58,000 cycles

Table A-33. Geometric Factors for FAA-19 (See figure A-33)

ϕ	x [in.]	z [in.]	f(g)
0.00	0.7500	0.0370	3.0522
0.05	0.7667	0.0382	3.0473
0.10	0.7830	0.0416	3.0327
0.15	0.7986	0.0472	3.0091
0.20	0.8133	0.0547	2.9777
0.25	0.8268	0.0639	2.9397
0.30	0.8390	0.0746	2.8967
0.35	0.8498	0.0864	2.8503
0.40	0.8591	0.0993	2.8021
0.45	0.8669	0.1128	2.7539
0.50	0.8733	0.1270	2.7172
0.55	0.8782	0.1416	2.7050
0.60	0.8817	0.1565	2.6941
0.65	0.8838	0.1716	2.6850
0.70	0.8845	0.1869	2.6782
0.75	0.8838	0.2021	2.6741
0.80	0.8816	0.2173	2.6729
0.85	0.8780	0.2324	2.6746
0.90	0.8729	0.2471	2.6791
0.95	0.8663	0.2615	2.6859
1.00	0.8582	0.2753	2.6945

Initial Crack Location	Knee
Center of Ellipse	(0.75, 0.1870)
Crack Length	0.1345
Crack Depth	0.1495
Average Crack Front	67,001 and 73,000 cycles

Table A-34. Geometric Factors for FAA-19 (See figure A-34)

ϕ	x [in.]	z [in.]	f(g)
0.00	-1.1115	0.0000	3.4977
0.06	-1.1178	0.0185	3.4977
0.12	-1.1232	0.0369	3.4996
0.18	-1.1278	0.0554	3.5034
0.23	-1.1316	0.0738	3.5089
0.28	-1.1346	0.0923	3.5161
0.34	-1.1368	0.1107	3.5249
0.39	-1.1384	0.1292	3.5351
0.44	-1.1392	0.1476	3.5469
0.49	-1.1392	0.1661	3.5601
0.54	-1.1386	0.1845	3.5747
0.58	-1.1372	0.2030	3.5909
0.63	-1.1351	0.2214	3.6085
0.68	-1.1322	0.2399	3.6277
0.72	-1.1286	0.2583	3.6485
0.77	-1.1241	0.2768	3.6710
0.81	-1.1189	0.2952	3.6954
0.86	--1.1127	0.3137	3.7218
0.91	-1.1057	0.3321	3.7504
0.95	-1.0977	0.3506	3.7815
1.00	-1.0886	0.3690	3.8154

Initial Crack Location	Knee
Center of Ellipse	(-0.75, 0.16)
Crack Length	0.3895
Crack Depth	0.4300
Average Crack Front	67,001 and 73,000 cycles

Table A-35. Geometric Factors for FAA-19 (See figure A-35)

ϕ	x [in.]	z [in.]	f(g)
0.00	0.8261	0.0000	3.8780
0.10	0.8436	0.0109	3.7638
0.18	0.8581	0.0229	3.6824
0.25	0.8706	0.0358	3.6183
0.31	0.8813	0.0494	3.5650
0.37	0.8905	0.0635	3.5187
0.42	0.8982	0.0782	3.4772
0.47	0.9046	0.0934	3.4392
0.51	0.9097	0.1089	3.4036
0.56	0.9135	0.1246	3.3697
0.60	0.9161	0.1405	3.3368
0.65	0.9174	0.1565	3.3046
0.69	0.9175	0.1725	3.2726
0.73	0.9163	0.1884	3.2407
0.77	0.9140	0.2041	3.2086
0.81	0.9105	0.2196	3.1762
0.85	0.9057	0.2347	3.1435
0.89	0.8999	0.2494	3.1104
0.92	0.8928	0.2635	3.0770
0.96	0.8847	0.2770	3.0435
1.00	0.8755	0.2898	3.0102

Initial Crack Location	Knee
Center of Ellipse	(0.75, 0.1653)
Crack Length	0.1678
Crack Depth	0.1876
Average Crack Front	78,501 and 82,000 cycles

Table A-36. Geometric Factors for FAA-19 (See figure A-36)

ϕ	x [in.]	z [in.]	f(g)
0.00	-1.2102	0.0000	3.6247
0.06	-1.2168	0.0185	3.6408
0.12	-1.2226	0.0369	3.6556
0.17	-1.2277	0.0554	3.6694
0.23	-1.2321	0.0738	3.6821
0.28	-1.2358	0.0923	3.6939
0.33	-1.2388	0.1107	3.7048
0.38	-1.2412	0.1292	3.7150
0.43	-1.2429	0.1476	3.7245
0.48	-1.2440	0.1661	3.7334
0.53	-1.2444	0.1845	3.7416
0.58	-1.2443	0.2030	3.7493
0.63	-1.2434	0.2214	3.7565
0.67	-1.2420	0.2399	3.7632
0.72	-1.2399	0.2583	3.7695
0.77	-1.2371	0.2768	3.7755
0.81	-1.2337	0.2952	3.7811
0.86	-1.2296	0.3137	3.7863
0.91	-1.2248	0.3321	3.7914
0.95	-1.2193	0.3506	3.7962
1.00	-1.2130	0.3690	3.8009

Initial Crack Location	Knee
Center of Ellipse	(-0.75, 0.1882)
Crack Length	0.4945
Crack Depth	0.5150
Average Crack Front	78,501 and 82,000 cycles

Table A-37. Geometric Factors for FAA-19 (See figure A-37)

ϕ	x [in.]	z [in.]	f(g)
0.00	0.8710	0.0000	3.6385
0.08	0.8832	0.0123	3.5856
0.15	0.8940	0.0254	3.5394
0.22	0.9036	0.0393	3.4984
0.28	0.9120	0.0537	3.4618
0.34	0.9191	0.0686	3.4291
0.39	0.9252	0.0840	3.3999
0.44	0.9300	0.0997	3.3739
0.49	0.9337	0.1157	3.3510
0.54	0.9363	0.1320	3.3309
0.59	0.9376	0.1483	3.3135
0.63	0.9379	0.1647	3.2989
0.68	0.9370	0.1811	3.2869
0.72	0.9349	0.1974	3.2775
0.76	0.9317	0.2135	3.2705
0.80	0.9273	0.2293	3.2660
0.84	0.9218	0.2448	3.2639
0.88	0.9152	0.2597	3.2640
0.92	0.9075	0.2742	3.2664
0.96	0.8987	0.2880	3.2708
1.00	0.8889	0.3010	3.2772

Initial Crack Location	Knee
Center of Ellipse	(0.75, 0.1595)
Crack Length	0.1880
Crack Depth	0.2100
Average Crack Front	82,001 and 86,000 cycles

Table A-38. Geometric Factors for FAA-19 (See figure A-38)

ϕ	x [in.]	z [in.]	f(g)
0.00	-1.2505	0.0000	3.7343
0.06	-1.2584	0.0185	3.7606
0.11	-1.2655	0.0369	3.7838
0.17	-1.2717	0.0554	3.8041
0.22	-1.2771	0.0738	3.8219
0.28	-1.2817	0.0923	3.8375
0.33	-1.2856	0.1107	3.8510
0.38	-1.2887	0.1292	3.8626
0.43	-1.2911	0.1476	3.8725
0.48	-1.2927	0.1661	3.8808
0.53	-1.2937	0.1845	3.8875
0.57	-1.2940	0.2030	3.8927
0.62	-1.2935	0.2214	3.8964
0.67	-1.2924	0.2399	3.8987
0.72	-1.2905	0.2583	3.8997
0.76	-1.2879	0.2768	3.8992
0.81	-1.2846	0.2952	3.8973
0.86	-1.2805	0.3137	3.8940
0.90	-1.2757	0.3321	3.8892
0.95	-1.2701	0.3506	3.8829
1.00	-1.2636	0.3690	3.8750

Initial Crack Location	Knee
Center of Ellipse	(-0.75, 0.2000)
Crack Length	0.5440
Crack Depth	0.5125
Average Crack Front	82,001 and 86,000 cycles

Table A-39. Geometric Factors for FAA-19 (See figure A-39)

ϕ	x [in.]	z [in.]	f(g)
0.00	0.9108	0.0000	3.6264
0.07	0.9209	0.0136	3.6099
0.14	0.9299	0.0280	3.5940
0.20	0.9379	0.0429	3.5782
0.26	0.9448	0.0583	3.5619
0.32	0.9505	0.0741	3.5446
0.37	0.9552	0.0904	3.5262
0.42	0.9588	0.1069	3.5062
0.47	0.9612	0.1236	3.4843
0.52	0.9625	0.1405	3.4603
0.57	0.9627	0.1574	3.4338
0.62	0.9617	0.1744	3.4047
0.66	0.9596	0.1912	3.3726
0.71	0.9563	0.2079	3.3373
0.75	0.9519	0.2243	3.2985
0.79	0.9464	0.2403	3.2559
0.84	0.9398	0.2560	3.2093
0.88	0.9320	0.2711	3.1582
0.92	0.9233	0.2856	3.1022
0.96	0.9135	0.2995	3.0411
1.00	0.9027	0.3126	2.9744

Initial Crack Location	Knee
Center of Ellipse	(0.75, 0.1515)
Crack Length	0.2130
Crack Depth	0.2315
Average Crack Front	86,001 and 90,000 cycles

Table A-40. Geometric Factors for FAA-19 (See figure A-40)

ϕ	x [in.]	z [in.]	f(g)
0.00	-1.2987	0.0000	3.7889
0.06	-1.3077	0.0185	3.7931
0.11	-1.3157	0.0369	3.7971
0.17	-1.3227	0.0554	3.8011
0.22	-1.3289	0.0738	3.8049
0.27	-1.3343	0.0923	3.8086
0.32	-1.3388	0.1107	3.8121
0.37	-1.3425	0.1292	3.8155
0.42	-1.3454	0.1476	3.8188
0.47	-1.3475	0.1661	3.8219
0.52	-1.3489	0.1845	3.8249
0.57	-1.3495	0.2030	3.8277
0.62	-1.3493	0.2214	3.8304
0.66	-1.3483	0.2399	3.8331
0.71	-1.3466	0.2583	3.8356
0.76	-1.3441	0.2768	3.8380
0.81	-1.3407	0.2952	3.8404
0.85	-1.3366	0.3137	3.8428
0.90	-1.3317	0.3321	3.8451
0.95	-1.3259	0.3506	3.8475
1.00	-1.3193	0.3690	3.8500

Initial Crack Location	Knee
Center of Ellipse	(-0.75, 0.2075)
Crack Length	0.5995
Crack Depth	0.5150
Average Crack Front	86,001 and 90,000 cycles

Table A-41. Geometric Factors for FAA-19 (See figure A-41)

ϕ	x [in.]	z [in.]	f(g)
0.00	0.9491	0.0000	3.5905
0.07	0.9582	0.0149	3.5717
0.13	0.9662	0.0305	3.5547
0.19	0.9732	0.0466	3.5392
0.25	0.9791	0.0631	3.5254
0.30	0.9840	0.0800	3.5130
0.36	0.9877	0.0973	3.5022
0.41	0.9902	0.1147	3.4929
0.46	0.9917	0.1323	3.4850
0.51	0.9919	0.1501	3.4786
0.56	0.9910	0.1678	3.4735
0.60	0.9890	0.1854	3.4699
0.65	0.9857	0.2029	3.4675
0.70	0.9814	0.2201	3.4665
0.74	0.9758	0.2370	3.4667
0.79	0.9692	0.2535	3.4682
0.83	0.9614	0.2695	3.4708
0.87	0.9526	0.2850	3.4745
0.92	0.9427	0.2998	3.4793
0.96	0.9319	0.3139	3.4851
1.00	0.9200	0.3272	3.4919

Initial Crack Location	Knee
Center of Ellipse	(0.75, 0.1450)
Crack Length	0.2420
Crack Depth	0.2560
Average Crack Front	90,001 and 94,000 cycles

Table A-42. Geometric Factors for FAA-19 (See figure A-42)

ϕ	x [in.]	z [in.]	f(g)
0.00	-1.3573	0.0000	3.9975
0.06	-1.3662	0.0185	3.9928
0.11	-1.3742	0.0369	3.9889
0.17	-1.3813	0.0554	3.9858
0.22	-1.3875	0.0738	3.9834
0.27	-1.3929	0.0923	3.9818
0.32	-1.3975	0.1107	3.9807
0.37	-1.4013	0.1292	3.9802
0.42	-1.4044	0.1476	3.9803
0.47	-1.4066	0.1661	3.9810
0.52	-1.4081	0.1845	3.9822
0.56	-1.4089	0.2030	3.9839
0.61	-1.4089	0.2214	3.9861
0.66	-1.4082	0.2399	3.9888
0.71	-1.4067	0.2583	3.9921
0.76	-1.4044	0.2768	3.9960
0.80	-1.4014	0.2952	4.0004
0.85	-1.3976	0.3137	4.0054
0.90	-1.3930	0.3321	4.0111
0.95	-1.3876	0.3506	4.0174
1.00	-1.3814	0.3690	4.0245

Initial Crack Location	Knee
Center of Ellipse	(-0.75, 0.2125)
Crack Length	0.6590
Crack Depth	0.5475
Average Crack Front	90,001 and 94,000 cycles

Table A-43. Geometric Factors for FAA-19 (See figure A-43)

ϕ	x [in.]	z [in.]	f(g)
0.00	0.9867	0.0000	3.6010
0.06	0.9952	0.0162	3.5997
0.12	1.0027	0.0330	3.5987
0.18	1.0091	0.0503	3.5980
0.24	1.0145	0.0681	3.5974
0.29	1.0188	0.0862	3.5969
0.35	1.0220	0.1046	3.5964
0.40	1.0240	0.1232	3.5958
0.45	1.0249	0.1419	3.5951
0.50	1.0247	0.1607	3.5944
0.55	1.0232	0.1795	3.5934
0.60	1.0206	0.1982	3.5924
0.64	1.0169	0.2167	3.5912
0.69	1.0119	0.2350	3.5900
0.74	1.0058	0.2530	3.5887
0.78	0.9986	0.2705	3.5873
0.83	0.9903	0.2876	3.5860
0.87	0.9809	0.3040	3.5848
0.91	0.9704	0.3199	3.5838
0.96	0.9589	0.3350	3.5830
1.00	0.9464	0.3493	3.5826

Initial Crack Location	Knee
Center of Ellipse	(0.75, 0.1470)
Crack Length	0.2750
Crack Depth	0.2890
Average Crack Front	94,001 and 98,000 cycles

Table A-44. Geometric Factors for FAA-19 (See figure A-44)

ϕ	x [in.]	z [in.]	f(g)
0.00	-1.4323	0.0000	4.1533
0.06	-1.4407	0.0185	4.1487
0.11	-1.4483	0.0369	4.1444
0.16	-1.4550	0.0554	4.1402
0.21	-1.4609	0.0738	4.1362
0.27	-1.4660	0.0923	4.1324
0.32	-1.4704	0.1107	4.1286
0.37	-1.4740	0.1292	4.1248
0.41	-1.4768	0.1476	4.1211
0.46	-1.4789	0.1661	4.1174
0.51	-1.4803	0.1845	4.1136
0.56	-1.4809	0.2030	4.1099
0.61	-1.4808	0.2214	4.1061
0.66	-1.4800	0.2399	4.1022
0.71	-1.4785	0.2583	4.0983
0.75	-1.4762	0.2768	4.0943
0.80	-1.4732	0.2952	4.0903
0.85	-1.4694	0.3137	4.0862
0.90	-1.4649	0.3321	4.0819
0.95	-1.4596	0.3506	4.0776
1.00	-1.4535	0.3690	4.0732

Initial Crack Location	Knee
Center of Ellipse	(-0.75, 0.2100)
Crack Length	0.7310
Crack Depth	0.5850
Average Crack Front	94,001 and 98,000 cycles

Table A-45. Geometric Factors for FAA-19 (See figure A-45)

ϕ	x [in.]	z [in.]	f(g)
0.00	1.0533	0.0000	4.1346
0.06	1.0607	0.0185	4.0939
0.12	1.0670	0.0369	4.0590
0.18	1.0722	0.0554	4.0297
0.23	1.0765	0.0738	4.0058
0.29	1.0797	0.0923	3.9872
0.34	1.0821	0.1107	3.9738
0.39	1.0835	0.1292	3.9656
0.44	1.0840	0.1476	3.9626
0.48	1.0836	0.1661	3.9648
0.53	1.0823	0.1845	3.9722
0.58	1.0801	0.2030	3.9848
0.62	1.0770	0.2214	4.0026
0.67	1.0729	0.2399	4.0257
0.72	1.0678	0.2583	4.0542
0.76	1.0617	0.2768	4.0882
0.81	1.0545	0.2952	4.1280
0.85	1.0460	0.3137	4.1740
0.90	1.0363	0.3321	4.2711
0.95	1.0250	0.3506	4.2985
1.00	1.0121	0.3690	4.3297

Initial Crack Location	Knee
Center of Ellipse	(0.75, 0.149)
Crack Length	0.3340
Crack Depth	0.3585
Average Crack Front	100,001 and 102,000 cycles

Table A-46. Geometric Factors for FAA-19 (See figure A-46)

ϕ	x [in.]	z [in.]	f(g)
0.00	-1.5506	0.0000	4.3542
0.05	-1.5581	0.0185	4.3555
0.11	-1.5648	0.0369	4.3567
0.16	-1.5707	0.0554	4.3576
0.21	-1.5759	0.0738	4.3583
0.26	-1.5803	0.0923	4.3588
0.31	-1.5840	0.1107	4.3590
0.36	-1.5870	0.1292	4.3591
0.41	-1.5893	0.1476	4.3589
0.46	-1.5909	0.1661	4.3585
0.51	-1.5918	0.1845	4.3578
0.55	-1.5920	0.2030	4.3570
0.60	-1.5915	0.2214	4.3559
0.65	-1.5903	0.2399	4.3545
0.70	-1.5884	0.2583	4.3529
0.75	-1.5858	0.2768	4.3511
0.80	-1.5825	0.2952	4.3490
0.85	-1.5785	0.3137	4.3467
0.90	-1.5737	0.3321	4.3440
0.95	-1.5682	0.3506	4.3411
1.00	-1.5620	0.3690	4.3379

Initial Crack Location	Knee
Center of Ellipse	(-0.75, 0.1990)
Crack Length	0.8420
Crack Depth	0.6425
Average Crack Front	100,001 and 102,000 cycles

Table A-47. Geometric Factors for FAA-20 (See figure A-47)

ϕ	x [in.]	z [in.]	f(g)
0.00	0.7500	0.1088	2.1333
0.05	0.7578	0.1091	2.1331
0.10	0.7655	0.1102	2.1326
0.15	0.7732	0.1120	2.1319
0.20	0.7807	0.1145	2.1308
0.25	0.7881	0.1178	2.1295
0.30	0.7952	0.1218	2.1280
0.35	0.8020	0.1264	2.1262
0.40	0.8085	0.1318	2.1242
0.45	0.8145	0.1380	2.1222
0.50	0.8202	0.1448	2.1200
0.55	0.8252	0.1523	2.1179
0.60	0.8297	0.1606	2.1158
0.65	0.8335	0.1695	2.1138
0.70	0.8364	0.1790	2.1121
0.75	0.8384	0.1891	2.1106
0.80	0.8394	0.1998	2.1095
0.85	0.8392	0.2109	2.1089
0.90	0.8377	0.2222	2.1088
0.95	0.8348	0.2337	2.1093
1.00	0.8305	0.2450	2.1103

Initial Crack Location	Knee
Center of Ellipse	(0.75, 0.2035)
Crack Length	0.0895
Crack Depth	0.0948
Average Crack Front	1 and 10,000 cycles

Table A-48. Geometric Factors for FAA-20 (See figure A-48)

ϕ	x [in.]	z [in.]	f(g)
0.00	-0.7500	0.0440	2.4391
0.05	-0.7651	0.0449	2.4382
0.10	-0.7800	0.0475	2.4355
0.15	-0.7945	0.0519	2.4311
0.20	-0.8084	0.0579	2.4253
0.25	-0.8215	0.0653	2.4182
0.30	-0.8337	0.0742	2.4102
0.35	-0.8448	0.0843	2.4014
0.40	-0.8549	0.0956	2.3922
0.45	-0.8637	0.1078	2.3829
0.50	-0.8713	0.1209	2.3737
0.55	-0.8776	0.1348	2.3648
0.60	-0.8825	0.1494	2.3563
0.65	-0.8859	0.1644	2.3486
0.70	-0.8879	0.1799	2.3416
0.75	-0.8884	0.1957	2.3355
0.80	-0.8873	0.2117	2.3303
0.85	-0.8845	0.2278	2.3261
0.90	-0.8800	0.2437	2.3228
0.95	-0.8737	0.2593	2.3205
1.00	-0.8655	0.2744	2.3190

Initial Crack Location	Knee
Center of Ellipse	(-0.75, 0.1925)
Crack Length	0.1385
Crack Depth	0.1485
Average Crack Front	1 and 10,000 cycles

Table A-49. Geometric Factors for FAA-20 (See figure A-49)

ϕ	x [in.]	z [in.]	f(g)
0.00	0.7500	0.0860	2.4857
0.05	0.7604	0.0865	2.4852
0.10	0.7706	0.0881	2.4838
0.15	0.7807	0.0908	2.4814
0.20	0.7905	0.0945	2.4782
0.25	0.7999	0.0991	2.4740
0.30	0.8089	0.1048	2.4691
0.35	0.8173	0.1114	2.4634
0.40	0.8251	0.1188	2.4571
0.45	0.8323	0.1271	2.4501
0.50	0.8386	0.1362	2.4427
0.55	0.8441	0.1460	2.4350
0.60	0.8486	0.1565	2.4270
0.65	0.8522	0.1677	2.4191
0.70	0.8546	0.1793	2.4114
0.75	0.8558	0.1914	2.4042
0.80	0.8558	0.2039	2.3978
0.85	0.8543	0.2165	2.3925
0.90	0.8514	0.2292	2.3886
0.95	0.8470	0.2417	2.3862
1.00	0.8410	0.2539	2.3853

Initial Crack Location	Knee
Center of Ellipse	(0.75, 0.1970)
Crack Length	0.1060
Crack Depth	0.1110
Average Crack Front	14,001 and 23,000 cycles

Table A-50. Geometric Factors for FAA-20 (See figure A-50)

ϕ	x [in.]	z [in.]	f(g)
0.00	-0.8786	0.0000	3.3951
0.08	-0.8894	0.0123	3.3514
0.15	-0.8989	0.0252	3.3122
0.22	-0.9074	0.0388	3.2760
0.28	-0.9147	0.0529	3.2419
0.34	-0.9211	0.0675	3.2092
0.39	-0.9264	0.0825	3.1774
0.44	-0.9308	0.0978	3.1462
0.49	-0.9342	0.1135	3.1152
0.54	-0.9366	0.1294	3.0841
0.59	-0.9380	0.1454	3.0528
0.64	-0.9385	0.1616	3.0208
0.68	-0.9379	0.1779	2.9881
0.72	-0.9364	0.1941	2.9543
0.76	-0.9338	0.2102	2.9194
0.80	-0.9303	0.2262	2.8831
0.84	-0.9257	0.2420	2.8452
0.88	-0.9201	0.2574	2.8056
0.92	-0.9135	0.2725	2.7640
0.96	-0.9058	0.2870	2.7204
1.00	-0.8972	0.3010	2.6747

Initial Crack Location	Knee
Center of Ellipse	(-0.75, 0.1590)
Crack Length	0.1900
Crack Depth	0.2265
Average Crack Front	14,001 and 23,000 cycles

Table A-51. Geometric Factors for FAA-20 (See figure A-51)

ϕ	x [in.]	z [in.]	f(g)
0.00	0.7500	0.0680	2.4775
0.05	0.7624	0.0687	2.4775
0.10	0.7747	0.0707	2.4775
0.15	0.7866	0.0741	2.4775
0.20	0.7982	0.0787	2.4774
0.25	0.8092	0.0846	2.4773
0.30	0.8196	0.0916	2.4772
0.35	0.8292	0.0997	2.4770
0.40	0.8380	0.1088	2.4768
0.45	0.8459	0.1188	2.4765
0.50	0.8527	0.1296	2.4761
0.55	0.8585	0.1412	2.4757
0.60	0.8631	0.1535	2.4751
0.65	0.8666	0.1663	2.4743
0.70	0.8687	0.1796	2.4734
0.75	0.8695	0.1932	2.4723
0.80	0.8688	0.2071	2.4710
0.85	0.8667	0.2211	2.4694
0.90	0.8630	0.2351	2.4677
0.95	0.8576	0.2487	2.4656
1.00	0.8506	0.2619	2.4634

Initial Crack Location	Knee
Center of Ellipse	(0.75, 0.194)
Crack Length	0.1195
Crack Depth	0.1260
Average Crack Front	23,001 and 35,000 cycles

Table A-52. Geometric Factors for FAA-20 (See figure A-52)

ϕ	x [in.]	z [in.]	f(g)
0.00	-0.9846	0.0000	3.3180
0.06	-0.9908	0.0158	3.3045
0.12	-0.9961	0.0320	3.2913
0.18	-1.0006	0.0486	3.2782
0.24	-1.0042	0.0655	3.2653
0.29	-1.0069	0.0826	3.2526
0.35	-1.0088	0.1000	3.2398
0.40	-1.0097	0.1175	3.2272
0.45	-1.0098	0.1351	3.2145
0.50	-1.0089	0.1528	3.2019
0.55	-1.0070	0.1705	3.1893
0.60	-1.0042	0.1882	3.1767
0.65	-1.0004	0.2057	3.1641
0.69	-0.9957	0.2230	3.1515
0.74	-0.9900	0.2401	3.1389
0.78	-0.9834	0.2569	3.1265
0.83	-0.9758	0.2733	3.1142
0.87	-0.9672	0.2892	3.1022
0.92	-0.9577	0.3046	3.0905
0.96	-0.9473	0.3194	3.0792
1.00	-0.9359	0.3335	3.0685

Initial Crack Location	Knee
Center of Ellipse	(0.75, 0.194)
Crack Length	0.1195
Crack Depth	0.1260
Average Crack Front	23,001 and 35,000 cycles

Table A-53. Geometric Factors for FAA-20 (See figure A-53)

ϕ	x [in.]	z [in.]	f(g)
0.00	0.7500	0.0325	2.9286
0.05	0.7664	0.0335	2.9259
0.10	0.7825	0.0365	2.9179
0.15	0.7982	0.0415	2.9050
0.20	0.8131	0.0482	2.8877
0.25	0.8270	0.0566	2.8669
0.30	0.8399	0.0665	2.8434
0.35	0.8515	0.0777	2.8183
0.40	0.8619	0.0900	2.7925
0.45	0.8710	0.1034	2.7722
0.50	0.8786	0.1175	2.7654
0.55	0.8849	0.1324	2.7592
0.60	0.8897	0.1478	2.7539
0.65	0.8929	0.1637	2.7497
0.70	0.8947	0.1800	2.7469
0.75	0.8949	0.1966	2.7455
0.80	0.8934	0.2133	2.7458
0.85	0.8903	0.2299	2.7476
0.90	0.8854	0.2465	2.7510
0.95	0.8787	0.2627	2.7557
1.00	0.8701	0.2783	2.7614

Initial Crack Location	Knee
Center of Ellipse	(0.75, 0.1900)
Crack Length	0.1450
Crack Depth	0.1575
Average Crack Front	41,001 and 53,000 cycles

Table A-54. Geometric Factors for FAA-20 (See figure A-54)

ϕ	x [in.]	z [in.]	f(g)
0.00	-1.1245	0.0000	3.4506
0.06	-1.1286	0.0178	3.4635
0.11	-1.1321	0.0355	3.4758
0.17	-1.1348	0.0533	3.4874
0.22	-1.1369	0.0710	3.4985
0.27	-1.1383	0.0888	3.5090
0.32	-1.1390	0.1065	3.5192
0.37	-1.1391	0.1243	3.5290
0.42	-1.1385	0.1420	3.5385
0.47	-1.1372	0.1598	3.5478
0.52	-1.1352	0.1775	3.5569
0.57	-1.1326	0.1953	3.5659
0.62	-1.1293	0.2130	3.5749
0.66	-1.1252	0.2308	3.5839
0.71	-1.1204	0.2485	3.5931
0.76	-1.1148	0.2663	3.6026
0.81	-1.1084	0.2840	3.6125
0.85	-1.1012	0.3018	3.6230
0.90	-1.0930	0.3195	3.6343
0.95	-1.0838	0.3373	3.6466
1.00	-1.0735	0.3550	3.6603

Initial Crack Location	Knee
Center of Ellipse	(-0.75, 0.1165)
Crack Length	0.3895
Crack Depth	0.4295
Average Crack Front	41,001 and 53,000 cycles

Table A-55. Geometric Factors for FAA-20 (See figure A-55)

ϕ	x [in.]	z [in.]	f(g)
0.00	0.8253	0.0000	4.0041
0.10	0.8436	0.0107	3.8552
0.18	0.8581	0.0223	3.7490
0.25	0.8703	0.0349	3.6619
0.31	0.8809	0.0481	3.5864
0.37	0.8901	0.0620	3.5186
0.42	0.8979	0.0764	3.4568
0.47	0.9045	0.0913	3.3997
0.52	0.9099	0.1065	3.3467
0.56	0.9142	0.1221	3.2973
0.61	0.9173	0.1379	3.2515
0.65	0.9193	0.1539	3.2091
0.69	0.9202	0.1700	3.1701
0.73	0.9200	0.1861	3.1348
0.77	0.9186	0.2021	3.1031
0.81	0.9161	0.2180	3.0754
0.85	0.9125	0.2337	3.0516
0.89	0.9078	0.2491	3.0320
0.93	0.9020	0.2641	3.0167
0.96	0.8951	0.2786	3.0055
1.00	0.8870	0.2925	2.9986

Initial Crack Location	Knee
Center of Ellipse	(0.75, 0.1735)
Crack Length	0.1705
Crack Depth	0.2000
Average Crack Front	56,001 and 61,000 cycles

Table A-56. Geometric Factors for FAA-20 (See figure A-56)

ϕ	x [in.]	z [in.]	f(g)
0.00	-1.2139	0.0000	3.7616
0.06	-1.2174	0.0178	3.7478
0.11	-1.2204	0.0355	3.7360
0.17	-1.2228	0.0533	3.7262
0.22	-1.2248	0.0710	3.7185
0.27	-1.2263	0.0888	3.7128
0.32	-1.2274	0.1065	3.7092
0.37	-1.2279	0.1243	3.7076
0.43	-1.2280	0.1420	3.7079
0.48	-1.2276	0.1598	3.7104
0.53	-1.2267	0.1775	3.7148
0.57	-1.2253	0.1953	3.7213
0.62	-1.2235	0.2130	3.7297
0.67	-1.2212	0.2308	3.7402
0.72	-1.2183	0.2485	3.7527
0.77	-1.2150	0.2663	3.7672
0.81	-1.2112	0.2840	3.7837
0.86	-1.2068	0.3018	3.8022
0.91	-1.2019	0.3195	3.8228
0.95	-1.1964	0.3373	3.8454
1.00	-1.1903	0.3550	3.8702

Initial Crack Location	Knee
Center of Ellipse	(-0.75, 0.1360)
Crack Length	0.4780
Crack Depth	0.5700
Average Crack Front	56,001 and 61,000 cycles

Table A-57. Geometric Factors for FAA-20 (See figure A-57)

ϕ	x [in.]	z [in.]	f(g)
0.00	0.8802	0.0000	3.5913
0.08	0.8905	0.0123	3.5606
0.15	0.8999	0.0253	3.5327
0.22	0.9082	0.0389	3.5069
0.28	0.9156	0.0530	3.4823
0.34	0.9220	0.0676	3.4586
0.39	0.9275	0.0827	3.4352
0.44	0.9319	0.0981	3.4117
0.49	0.9354	0.1138	3.3878
0.54	0.9379	0.1298	3.3632
0.59	0.9394	0.1459	3.3376
0.63	0.9398	0.1622	3.3107
0.68	0.9393	0.1785	3.2824
0.72	0.9377	0.1947	3.2522
0.76	0.9351	0.2109	3.2201
0.80	0.9314	0.2269	3.1858
0.84	0.9268	0.2426	3.1490
0.88	0.9210	0.2580	3.1097
0.92	0.9143	0.2730	3.0674
0.96	0.9065	0.2875	3.0222
1.00	0.8976	0.3014	2.9739

Initial Crack Location	Knee
Center of Ellipse	(0.75, 0.1615)
Crack Length	0.1900
Crack Depth	0.2225
Average Crack Front	61,001 and 65,000 cycles

Table A-58. Geometric Factors for FAA-20 (See figure A-58)

ϕ	x [in.]	z [in.]	f(g)
0.00	-1.2619	0.0000	3.7390
0.06	-1.2657	0.0178	3.7653
0.11	-1.2689	0.0355	3.7888
0.16	-1.2717	0.0533	3.8098
0.22	-1.2741	0.0710	3.8285
0.27	-1.2759	0.0888	3.8451
0.32	-1.2773	0.1065	3.8598
0.37	-1.2783	0.1243	3.8727
0.42	-1.2788	0.1420	3.8840
0.47	-1.2788	0.1598	3.8938
0.52	-1.2784	0.1775	3.9020
0.57	-1.2776	0.1953	3.9089
0.62	-1.2762	0.2130	3.9143
0.67	-1.2745	0.2308	3.9184
0.72	-1.2722	0.2485	3.9212
0.77	-1.2695	0.2663	3.9227
0.81	-1.2664	0.2840	3.9228
0.86	-1.2627	0.3018	3.9217
0.91	-1.2585	0.3195	3.9192
0.95	-1.2539	0.3373	3.9153
1.00	-1.2487	0.3550	3.9100

Initial Crack Location	Knee
Center of Ellipse	(-0.75, 0.1510)
Crack Length	0.5290
Crack Depth	0.6100
Average Crack Front	61,001 and 65,000 cycles

Table A-59. Geometric Factors for FAA-20 (See figure A-59)

ϕ	x [in.]	z [in.]	f(g)
0.00	0.9172	0.0000	3.7147
0.07	0.9255	0.0135	3.6703
0.14	0.9329	0.0276	3.6280
0.20	0.9395	0.0422	3.5880
0.26	0.9453	0.0572	3.5503
0.32	0.9502	0.0726	3.5153
0.37	0.9543	0.0884	3.4830
0.43	0.9574	0.1045	3.4538
0.48	0.9597	0.1208	3.4280
0.53	0.9610	0.1373	3.4057
0.58	0.9614	0.1539	3.3873
0.62	0.9609	0.1707	3.3728
0.67	0.9594	0.1874	3.3626
0.71	0.9569	0.2041	3.3565
0.76	0.9535	0.2207	3.3547
0.80	0.9491	0.2371	3.3570
0.84	0.9436	0.2532	3.3633
0.88	0.9372	0.2690	3.3733
0.92	0.9298	0.2844	3.3867
0.96	0.9215	0.2992	3.4032
1.00	0.9121	0.3135	3.4223

Initial Crack Location	Knee
Center of Ellipse	(0.75, 0.1520)
Crack Length	0.2115
Crack Depth	0.2515
Average Crack Front	65,001 and 69,000 cycles

Table A-60. Geometric Factors for FAA-20 (See figure A-60)

ϕ	x [in.]	z [in.]	f(g)
0.00	-1.3104	0.0000	3.9304
0.05	-1.3150	0.0178	3.9319
0.11	-1.3191	0.0355	3.9330
0.16	-1.3226	0.0533	3.9338
0.21	-1.3256	0.0710	3.9341
0.27	-1.3280	0.0888	3.9341
0.32	-1.3299	0.1065	3.9336
0.37	-1.3313	0.1243	3.9328
0.42	-1.3322	0.1420	3.9316
0.47	-1.3325	0.1598	3.9300
0.52	-1.3323	0.1775	3.9279
0.57	-1.3316	0.1953	3.9254
0.61	-1.3304	0.2130	3.9225
0.66	-1.3286	0.2308	3.9192
0.71	-1.3264	0.2485	3.9154
0.76	-1.3236	0.2663	3.9111
0.81	-1.3202	0.2840	3.9064
0.86	-1.3163	0.3018	3.9011
0.90	-1.3118	0.3195	3.8953
0.95	-1.3068	0.3373	3.8890
1.00	-1.3012	0.3550	3.8821

Initial Crack Location	Knee
Center of Ellipse	(-0.75, 0.1625)
Crack Length	0.5825
Crack Depth	0.5975
Average Crack Front	65,001 and 69,000 cycles

Table A-61. Geometric Factors for FAA-20 (See figure A-61)

ϕ	x [in.]	z [in.]	f(g)
0.00	0.9619	0.0000	3.7431
0.06	0.9686	0.0150	3.7352
0.13	0.9745	0.0305	3.7269
0.19	0.9796	0.0464	3.7182
0.25	0.9840	0.0626	3.7089
0.30	0.9875	0.0792	3.6989
0.36	0.9902	0.0960	3.6880
0.41	0.9921	0.1131	3.6762
0.46	0.9931	0.1304	3.6634
0.51	0.9932	0.1478	3.6494
0.56	0.9924	0.1652	3.6341
0.61	0.9907	0.1827	3.6175
0.66	0.9881	0.2002	3.5995
0.70	0.9846	0.2176	3.5800
0.75	0.9801	0.2348	3.5590
0.79	0.9746	0.2518	3.5363
0.83	0.9682	0.2686	3.5120
0.88	0.9609	0.2849	3.4862
0.92	0.9526	0.3009	3.4587
0.96	0.9433	0.3163	3.4297
1.00	0.9330	0.3311	3.3993

Initial Crack Location	Knee
Center of Ellipse	(0.75, 0.1415)
Crack Length	0.2435
Crack Depth	0.2880
Average Crack Front	69,001 and 73,000 cycles

Table A-62. Geometric Factors for FAA-20 (See figure A-62)

ϕ	x [in.]	z [in.]	f(g)
0.00	-1.3742	0.0000	4.1334
0.05	-1.3787	0.0178	4.1304
0.11	-1.3827	0.0355	4.1273
0.16	-1.3861	0.0533	4.1243
0.21	-1.3889	0.0710	4.1213
0.26	-1.3912	0.0888	4.1183
0.31	-1.3930	0.1065	4.1153
0.36	-1.3942	0.1243	4.1122
0.41	-1.3948	0.1420	4.1090
0.46	-1.3950	0.1598	4.1058
0.51	-1.3945	0.1775	4.1025
0.56	-1.3936	0.1953	4.0991
0.61	-1.3921	0.2130	4.0956
0.66	-1.3901	0.2308	4.0920
0.71	-1.3875	0.2485	4.0884
0.75	-1.3843	0.2663	4.0846
0.80	-1.3806	0.2840	4.0807
0.85	-1.3764	0.3018	4.0767
0.90	-1.3715	0.3195	4.0725
0.95	-1.3660	0.3373	4.0683
1.00	-1.3599	0.3550	4.0640

Initial Crack Location	Knee
Center of Ellipse	(-0.75, 0.1550)
Crack Length	0.6450
Crack Depth	0.6175
Average Crack Front	69,001 and 73,000 cycles

Table A-63. Geometric Factors for FAA-21 (See figure A-63)

ϕ	x [in.]	z [in.]	f(g)
0.00	0.8322	0.0000	1.9065
0.05	0.8319	0.0064	1.9081
0.10	0.8313	0.0129	1.9096
0.15	0.8304	0.0193	1.9110
0.20	0.8292	0.0257	1.9124
0.25	0.8277	0.0322	1.9138
0.30	0.8258	0.0386	1.9151
0.35	0.8236	0.0451	1.9163
0.40	0.8209	0.0515	1.9175
0.45	0.8179	0.0580	1.9185
0.50	0.8143	0.0643	1.9193
0.55	0.8103	0.0706	1.9200
0.60	0.8057	0.0767	1.9204
0.65	0.8005	0.0825	1.9206
0.70	0.7948	0.0879	1.9207
0.75	0.7885	0.0928	1.9205
0.80	0.7816	0.0971	1.9201
0.85	0.7742	0.1007	1.9197
0.90	0.7664	0.1033	1.9193
0.95	0.7583	0.1050	1.9190
1.00	0.7500	0.1055	1.9189

Initial Crack Location	Corner
Center of Ellipse	(0.75,-0.0035)
Crack Length	0.0822
Crack Depth	0.1091
Average Crack Front	1 and 15,000 cycles

Table A-64. Geometric Factors for FAA-21 (See figure A-64)

ϕ	x [in.]	z [in.]	f(g)
0.00	-0.8211	0.0000	1.9138
0.05	-0.8209	0.0056	1.9091
0.10	-0.8206	0.0112	1.9049
0.15	-0.8200	0.0168	1.9012
0.20	-0.8191	0.0225	1.8981
0.25	-0.8181	0.0282	1.8955
0.30	-0.8168	0.0340	1.8936
0.35	-0.8152	0.0399	1.8924
0.40	-0.8132	0.0459	1.8919
0.45	-0.8109	0.0520	1.8922
0.50	-0.8082	0.0582	1.8932
0.55	-0.8050	0.0643	1.8952
0.60	-0.8012	0.0705	1.8979
0.65	-0.7969	0.0766	1.9014
0.70	-0.7920	0.0824	1.9054
0.75	-0.7864	0.0878	1.9097
0.80	-0.7801	0.0927	1.9141
0.85	-0.7732	0.0968	1.9180
0.90	-0.7658	0.0999	1.9212
0.95	-0.7580	0.1019	1.9233
1.00	-0.7500	0.1026	1.9240

Initial Crack Location	Corner
Center of Ellipse	(-0.75, -0.0027)
Crack Length	0.0713
Crack Depth	0.1052
Average Crack Front	1 and 15,000 cycles

Table A-65. Geometric Factors for FAA-21 (See figure A-65)

ϕ	x [in.]	z [in.]	f(g)
0.00	0.8427	0.0000	2.0020
0.05	0.8422	0.0073	1.9975
0.10	0.8414	0.0145	1.9938
0.15	0.8402	0.0217	1.9910
0.20	0.8388	0.0288	1.9891
0.25	0.8370	0.0360	1.9882
0.30	0.8349	0.0432	1.9882
0.35	0.8323	0.0505	1.9892
0.40	0.8294	0.0577	1.9913
0.45	0.8260	0.0649	1.9943
0.50	0.8221	0.0721	1.9982
0.55	0.8176	0.0792	2.0030
0.60	0.8125	0.0861	2.0084
0.65	0.8068	0.0927	2.0143
0.70	0.8005	0.0990	2.0204
0.75	0.7934	0.1048	2.0264
0.80	0.7857	0.1099	2.0320
0.85	0.7774	0.1141	2.0368
0.90	0.7686	0.1172	2.0453
0.95	0.7594	0.1192	2.0536
1.00	0.7500	0.1199	2.0565

Initial Crack Location	Corner
Center of Ellipse	(0.75, -0.0110)
Crack Length	0.0932
Crack Depth	0.1308
Average Crack Front	15,001 and 24,000 cycles

Table A-66. Geometric Factors for FAA-21 (See figure A-66)

ϕ	x [in.]	z [in.]	f(g)
0.00	-0.8312	0.0000	1.9887
0.05	-0.8308	0.0064	1.9878
0.10	-0.8301	0.0127	1.9873
0.15	-0.8292	0.0190	1.9870
0.20	-0.8281	0.0254	1.9872
0.25	-0.8267	0.0318	1.9876
0.30	-0.8250	0.0382	1.9883
0.35	-0.8231	0.0448	1.9894
0.40	-0.8208	0.0514	1.9907
0.45	-0.8181	0.0581	1.9922
0.50	-0.8149	0.0649	1.9939
0.55	-0.8113	0.0718	1.9959
0.60	-0.8071	0.0786	1.9979
0.65	-0.8023	0.0853	2.0000
0.70	-0.7968	0.0918	2.0021
0.75	-0.7905	0.0979	2.0041
0.80	-0.7836	0.1033	2.0059
0.85	-0.7759	0.1080	2.0074
0.90	-0.7677	0.1115	2.0086
0.95	-0.7590	0.1137	2.0093
1.00	-0.7500	0.1145	2.0096

Initial Crack Location	Corner
Center of Ellipse	(-0.75, -0.0109)
Crack Length	0.0816
Crack Depth	0.1253
Average Crack Front	15,001 and 24,000 cycles

Table A-67. Geometric Factors for FAA-21 (See figure A-67)

ϕ	x [in.]	z [in.]	f(g)
0.00	0.8588	0.0000	2.0538
0.05	0.8580	0.0085	2.0569
0.10	0.8569	0.0169	2.0615
0.15	0.8555	0.0253	2.0675
0.20	0.8538	0.0337	2.0750
0.25	0.8518	0.0422	2.0840
0.30	0.8494	0.0506	2.0945
0.35	0.8466	0.0592	2.1064
0.40	0.8433	0.0678	2.1196
0.45	0.8395	0.0765	2.1342
0.50	0.8352	0.0852	2.1500
0.55	0.8302	0.0939	2.1667
0.60	0.8245	0.1025	2.1842
0.65	0.8180	0.1109	2.2021
0.70	0.8106	0.1190	2.2198
0.75	0.8024	0.1265	2.2367
0.80	0.7933	0.1332	2.2522
0.85	0.7833	0.1388	2.2655
0.90	0.7727	0.1431	2.2757
0.95	0.7615	0.1457	2.2821
1.00	0.7500	0.1467	2.2843

Initial Crack Location	Corner
Center of Ellipse	(0.75, -0.0186)
Crack Length	0.1095
Crack Depth	0.1653
Average Crack Front	24,001 and 33,000 cycles

Table A-68. Geometric Factors for FAA-21 (See figure A-68)

ϕ	x [in.]	z [in.]	f(g)
0.00	0.8458	0.0000	2.0348
0.05	0.8453	0.0075	2.0363
0.10	0.8446	0.0150	2.0380
0.15	0.8437	0.0225	2.0433
0.20	0.8424	0.0300	2.0509
0.25	0.8408	0.0376	2.0593
0.30	0.8389	0.0453	2.0684
0.35	0.8366	0.0531	2.0782
0.40	0.8339	0.0610	2.0886
0.45	0.8308	0.0690	2.0996
0.50	0.8270	0.0770	2.1109
0.55	0.8227	0.0851	2.1224
0.60	0.8177	0.0932	2.1339
0.65	0.8119	0.1011	2.1451
0.70	0.8054	0.1087	2.1556
0.75	0.7980	0.1158	2.1652
0.80	0.7897	0.1221	2.1736
0.85	0.7806	0.1275	2.1804
0.90	0.7708	0.1316	2.1854
0.95	0.7606	0.1341	2.1885
1.00	0.7500	0.1350	2.1895

Initial Crack Location	Corner
Center of Ellipse	(-0.75, -0.0089)
Crack Length	0.0960
Crack Depth	0.1438
Average Crack Front	24,001 and 33,000 cycles

Table A-69. Geometric Factors for FAA-21 (See figure A-69)

ϕ	x [in.]	z [in.]	f(g)
0.00	0.8739	0.0000	2.2792
0.05	0.8735	0.0097	2.2897
0.10	0.8728	0.0194	2.2992
0.15	0.8716	0.0292	2.3079
0.20	0.8701	0.0390	2.3160
0.25	0.8681	0.0489	2.3236
0.30	0.8656	0.0589	2.3308
0.35	0.8627	0.0690	2.3377
0.40	0.8591	0.0793	2.3443
0.45	0.8549	0.0896	2.3505
0.50	0.8500	0.1000	2.3565
0.55	0.8443	0.1104	2.3620
0.60	0.8377	0.1207	2.3671
0.65	0.8301	0.1307	2.3748
0.70	0.8215	0.1403	2.3892
0.75	0.8118	0.1491	2.4015
0.80	0.8010	0.1570	2.4115
0.85	0.7893	0.1636	2.4191
0.90	0.7767	0.1686	2.4243
0.95	0.7635	0.1717	2.4274
1.00	0.7500	0.1728	2.4284

Initial Crack Location	Corner
Center of Ellipse	(0.75, -0.0051)
Crack Length	0.1240
Crack Depth	0.1779
Average Crack Front	39,001 and 42,000 cycles

Table A-70. Geometric Factors for FAA-21 (See figure A-70)

ϕ	x [in.]	z [in.]	f(g)
0.00	-0.8607	0.0000	2.2186
0.05	-0.8608	0.0087	2.2281
0.10	-0.8606	0.0175	2.2371
0.15	-0.8600	0.0264	2.2457
0.20	-0.8590	0.0354	2.2540
0.25	-0.8576	0.0446	2.2621
0.30	-0.8558	0.0539	2.2701
0.35	-0.8535	0.0634	2.2780
0.40	-0.8506	0.0731	2.2858
0.45	-0.8471	0.0829	2.2935
0.50	-0.8428	0.0928	2.3011
0.55	-0.8378	0.1028	2.3084
0.60	-0.8319	0.1128	2.3155
0.65	-0.8251	0.1225	2.3222
0.70	-0.8172	0.1319	2.3285
0.75	-0.8082	0.1406	2.3341
0.80	-0.7982	0.1484	2.3389
0.85	-0.7872	0.1549	2.3429
0.90	-0.7753	0.1598	2.3458
0.95	-0.7628	0.1629	2.3476
1.00	-0.7500	0.1640	2.3482

Initial Crack Location	Corner
Center of Ellipse	(-0.75, 0.0073)
Crack Length	0.1108
Crack Depth	0.1567
Average Crack Front	39,001 and 42,000 cycles

Table A-71. Geometric Factors for FAA-21 (See figure A-71)

ϕ	x [in.]	z [in.]	f(g)
0.00	0.9110	0.0000	2.7591
0.06	0.9123	0.0132	2.7578
0.12	0.9131	0.0264	2.7577
0.18	0.9132	0.0397	2.7587
0.24	0.9126	0.0530	2.7608
0.30	0.9114	0.0663	2.7640
0.35	0.9096	0.0795	2.7683
0.41	0.9071	0.0927	2.7738
0.46	0.9039	0.1057	2.7804
0.51	0.9001	0.1185	2.7881
0.56	0.8956	0.1311	2.7970
0.61	0.8904	0.1434	2.8070
0.65	0.8845	0.1554	2.8183
0.70	0.8779	0.1670	2.8308
0.74	0.8706	0.1782	2.8446
0.79	0.8626	0.1888	2.8597
0.83	0.8538	0.1989	2.8763
0.87	0.8444	0.2083	2.8945
0.92	0.8342	0.2170	2.9143
0.96	0.8232	0.2248	2.9359
1.00	0.8116	0.2317	2.9596

Initial Crack Location	Corner
Center of Ellipse	(0.75, 0.0351)
Crack Length	0.1632
Crack Depth	0.2123
Average Crack Front	60,001 and 63,000 cycles

Table A-72. Geometric Factors for FAA-21 (See figure A-72)

ϕ	x [in.]	z [in.]	f(g)
0.00	-0.9028	0.0000	2.7457
0.06	-0.9049	0.0129	2.7542
0.12	-0.9062	0.0259	2.7621
0.18	-0.9068	0.0390	2.7694
0.24	-0.9066	0.0522	2.7760
0.30	-0.9058	0.0653	2.7821
0.35	-0.9042	0.0784	2.7876
0.41	-0.9019	0.0914	2.7926
0.46	-0.8989	0.1042	2.7972
0.51	-0.8951	0.1168	2.8015
0.56	-0.8906	0.1292	2.8055
0.60	-0.8853	0.1413	2.8094
0.65	-0.8793	0.1531	2.8133
0.70	-0.8725	0.1644	2.8174
0.74	-0.8650	0.1752	2.8220
0.79	-0.8567	0.1855	2.8273
0.83	-0.8477	0.1951	2.8335
0.87	-0.8379	0.2040	2.8412
0.91	-0.8273	0.2121	2.8507
0.96	-0.8161	0.2192	2.8625
1.00	-0.8041	0.2254	2.8774

Initial Crack Location	Corner
Center of Ellipse	(-0.75, 0.0433)
Crack Length	0.1568
Crack Depth	0.1940
Average Crack Front	60,001 and 63,000 cycles

Table A-73. Geometric Factors for FAA-21 (See figure A-73)

ϕ	x [in.]	z [in.]	f(g)
0.00	0.9289	0.0000	2.8164
0.06	0.9308	0.0138	2.8342
0.12	0.9319	0.0277	2.8502
0.18	0.9324	0.0417	2.8644
0.24	0.9321	0.0557	2.8769
0.29	0.9312	0.0698	2.8880
0.35	0.9295	0.0838	2.8976
0.40	0.9272	0.0977	2.9059
0.45	0.9241	0.1114	2.9129
0.50	0.9203	0.1250	2.9189
0.55	0.9157	0.1384	2.9238
0.60	0.9105	0.1515	2.9279
0.65	0.9045	0.1643	2.9312
0.70	0.8977	0.1767	2.9339
0.74	0.8902	0.1886	2.9362
0.79	0.8820	0.2001	2.9383
0.83	0.8731	0.2110	2.9404
0.87	0.8634	0.2212	2.9430
0.92	0.8530	0.2307	2.9462
0.96	0.8419	0.2394	2.9506
1.00	0.8301	0.2472	2.9566

Initial Crack Location	Corner
Center of Ellipse	(0.75, 0.0436)
Crack Length	0.1825
Crack Depth	0.2267
Average Crack Front	63,001 and 72,000 cycles

Table A-74. Geometric Factors for FAA-21 (See figure A-74)

ϕ	x [in.]	z [in.]	f(g)
0.00	-0.9216	0.0000	2.8468
0.06	-0.9249	0.0136	2.8909
0.12	-0.9274	0.0274	2.9283
0.18	-0.9290	0.0414	2.9599
0.23	-0.9298	0.0554	2.9866
0.29	-0.9296	0.0695	3.0087
0.34	-0.9286	0.0836	3.0269
0.40	-0.9267	0.0975	3.0414
0.45	-0.9238	0.1114	3.0527
0.50	-0.9201	0.1250	3.0609
0.55	-0.9156	0.1383	3.0664
0.59	-0.9101	0.1514	3.0695
0.64	-0.9038	0.1640	3.0704
0.69	-0.8966	0.1761	3.0695
0.73	-0.8886	0.1878	3.0671
0.78	-0.8798	0.1988	3.0636
0.82	-0.8702	0.2091	3.0594
0.87	-0.8598	0.2188	3.0550
0.91	-0.8487	0.2276	3.0511
0.96	-0.8369	0.2355	3.0483
1.00	-0.8244	0.2424	3.0475

Initial Crack Location	Corner
Center of Ellipse	(-0.75, 0.0587)
Crack Length	0.1801
Crack Depth	0.2016
Average Crack Front	63,001 and 72,000 cycles

Table A-75. Geometric Factors for FAA-21 (See figure A-75)

ϕ	x [in.]	z [in.]	f(g)
0.00	0.9621	0.0000	3.0571
0.06	0.9645	0.0150	3.0602
0.12	0.9661	0.0301	3.0629
0.17	0.9669	0.0453	3.0651
0.23	0.9670	0.0606	3.0669
0.28	0.9662	0.0759	3.0683
0.34	0.9646	0.0912	3.0693
0.39	0.9623	0.1064	3.0698
0.44	0.9591	0.1215	3.0700
0.49	0.9550	0.1363	3.0698
0.54	0.9502	0.1510	3.0693
0.59	0.9446	0.1653	3.0686
0.64	0.9382	0.1793	3.0677
0.69	0.9309	0.1929	3.0667
0.73	0.9229	0.2060	3.0657
0.78	0.9141	0.2186	3.0649
0.82	0.9045	0.2306	3.0643
0.87	0.8942	0.2420	3.0642
0.91	0.8832	0.2526	3.0647
0.96	0.8714	0.2625	3.0661
1.00	0.8590	0.2715	3.0685

Initial Crack Location	Corner
Center of Ellipse	(0.75, -0.0537)
Crack Length	0.2170
Crack Depth	0.2519
Average Crack Front	72,001 and 80,000 cycles

Table A-76. Geometric Factors for FAA-21 (See figure A-76)

ϕ	x [in.]	z [in.]	f(g)
0.00	-0.9587	0.0000	3.1428
0.06	-0.9635	0.0149	3.1486
0.12	-0.9673	0.0302	3.1540
0.17	-0.9701	0.0457	3.1590
0.23	-0.9717	0.0613	3.1634
0.28	-0.9723	0.0770	3.1672
0.33	-0.9717	0.0927	3.1704
0.39	-0.9701	0.1084	3.1731
0.44	-0.9673	0.1238	3.1753
0.49	-0.9636	0.1391	3.1769
0.54	-0.9587	0.1540	3.1781
0.58	-0.9528	0.1686	3.1790
0.63	-0.9459	0.1827	3.1796
0.68	-0.9381	0.1964	3.1800
0.73	-0.9293	0.2094	3.1804
0.77	-0.9196	0.2217	3.1809
0.82	-0.9090	0.2334	3.1817
0.86	-0.8977	0.2443	3.1828
0.91	-0.8856	0.2544	3.1845
0.96	-0.8728	0.2635	3.1869
1.00	-0.8594	0.2718	3.1902

Initial Crack Location	Corner
Center of Ellipse	(-0.75, 0.0771)
Crack Length	0.2223
Crack Depth	0.2238
Average Crack Front	72,001 and 80,000 cycles

Table A-77. Geometric Factors for FAA-21 (See figure A-77)

ϕ	x [in.]	z [in.]	f(g)
0.00	1.0048	0.0000	3.1020
0.06	1.0080	0.0165	3.1174
0.11	1.0102	0.0332	3.1312
0.17	1.0115	0.0500	3.1433
0.22	1.0119	0.0670	3.1540
0.28	1.0113	0.0839	3.1632
0.33	1.0098	0.1008	3.1709
0.38	1.0074	0.1177	3.1773
0.43	1.0040	0.1344	3.1824
0.48	0.9997	0.1508	3.1863
0.53	0.9944	0.1670	3.1890
0.58	0.9883	0.1829	3.1907
0.63	0.9812	0.1984	3.1914
0.68	0.9732	0.2135	3.1914
0.73	0.9644	0.2281	3.1906
0.77	0.9547	0.2420	3.1893
0.82	0.9442	0.2554	3.1875
0.87	0.9329	0.2681	3.1856
0.91	0.9209	0.2800	3.1835
0.96	0.9081	0.2911	3.1817
1.00	0.8947	0.3014	3.1802

Initial Crack Location	Corner
Center of Ellipse	(0.75, 0.0650)
Crack Length	0.2620
Crack Depth	0.2835
Average Crack Front	80,001 and 89,000 cycles

Table A-78. Geometric Factors for FAA-21 (See figure A-78)

ϕ	x [in.]	z [in.]	f(g)
0.00	-1.0134	0.0000	3.2885
0.06	-1.0183	0.0169	3.2839
0.11	-1.0219	0.0340	3.2793
0.17	-1.0244	0.0514	3.2747
0.22	-1.0258	0.0689	3.2701
0.27	-1.0259	0.0865	3.2653
0.32	-1.0249	0.1040	3.2606
0.38	-1.0227	0.1215	3.2557
0.43	-1.0194	0.1388	3.2508
0.48	-1.0148	0.1558	3.2459
0.53	-1.0092	0.1724	3.2411
0.58	-1.0024	0.1887	3.2363
0.62	-0.9946	0.2044	3.2316
0.67	-0.9858	0.2196	3.2271
0.72	-0.9760	0.2342	3.2229
0.77	-0.9652	0.2481	3.2190
0.81	-0.9536	0.2613	3.2155
0.86	-0.9412	0.2737	3.2124
0.91	-0.9280	0.2852	3.2099
0.95	-0.9141	0.2958	3.2081
1.00	-0.8996	0.3056	3.2070

Initial Crack Location	Corner
Center of Ellipse	(-0.75, 0.0799)
Crack Length	0.2761
Crack Depth	0.2686
Average Crack Front	80,001 and 89,000 cycles

Table A-79. Geometric Factors for FAA-21 (See figure A-79)

ϕ	x [in.]	z [in.]	f(g)
0.00	1.0388	0.0000	3.2678
0.06	1.0425	0.0177	3.2652
0.11	1.0452	0.0356	3.2629
0.17	1.0469	0.0537	3.2608
0.22	1.0475	0.0720	3.2589
0.27	1.0472	0.0902	3.2572
0.33	1.0457	0.1085	3.2558
0.38	1.0433	0.1266	3.2546
0.43	1.0398	0.1446	3.2536
0.48	1.0352	0.1624	3.2529
0.53	1.0297	0.1799	3.2524
0.58	1.0231	0.1970	3.2522
0.63	1.0155	0.2137	3.2522
0.67	1.0070	0.2300	3.2526
0.72	0.9976	0.2457	3.2533
0.77	0.9872	0.2608	3.2543
0.82	0.9760	0.2753	3.2557
0.86	0.9639	0.2890	3.2575
0.91	0.9511	0.3020	3.2596
0.95	0.9375	0.3141	3.2622
1.00	0.9233	0.3254	3.2653

Initial Crack Location	Corner
Center of Ellipse	(0.75, 0.0744)
Crack Length	0.2975
Crack Depth	0.3087
Average Crack Front	89,001 and 92,000 cycles

Table A-80. Geometric Factors for FAA-21 (See figure A-80)

ϕ	x [in.]	z [in.]	f(g)
0.00	-1.0565	0.0000	3.3355
0.06	-1.0608	0.0183	3.3237
0.11	-1.0640	0.0370	3.3141
0.16	-1.0660	0.0558	3.3070
0.22	-1.0669	0.0747	3.3023
0.27	-1.0665	0.0936	3.3002
0.32	-1.0650	0.1126	3.3007
0.37	-1.0624	0.1314	3.3036
0.42	-1.0585	0.1500	3.3089
0.47	-1.0535	0.1683	3.3165
0.52	-1.0473	0.1863	3.3261
0.57	-1.0401	0.2039	3.3375
0.62	-1.0318	0.2210	3.3504
0.67	-1.0225	0.2375	3.3647
0.72	-1.0121	0.2534	3.3800
0.77	-1.0008	0.2687	3.3961
0.81	-0.9887	0.2832	3.4128
0.86	-0.9757	0.2969	3.4298
0.91	-0.9619	0.3098	3.4470
0.95	-0.9474	0.3218	3.4640
1.00	-0.9323	0.3329	3.4808

Initial Crack Location	Corner
Center of Ellipse	(-0.75, 0.0789)
Crack Length	0.3169
Crack Depth	0.3107
Average Crack Front	89,001 and 92,000 cycles

Table A-81. Geometric Factors for FAA-21 (See figure A-81)

ϕ	x [in.]	z [in.]	f(g)
0.00	1.1083	0.0000	3.4540
0.05	1.1113	0.0180	3.4406
0.10	1.1136	0.0360	3.4311
0.15	1.1150	0.0540	3.4254
0.20	1.1157	0.0720	3.4237
0.25	1.1156	0.0900	3.4257
0.30	1.1148	0.1080	3.4316
0.35	1.1131	0.1260	3.4414
0.40	1.1108	0.1440	3.4549
0.45	1.1076	0.1620	3.4722
0.49	1.1036	0.1800	3.4933
0.54	1.0987	0.1980	3.5183
0.59	1.0930	0.2160	3.5471
0.64	1.0863	0.2340	3.5799
0.69	1.0786	0.2520	3.6169
0.74	1.0699	0.2700	3.6583
0.79	1.0600	0.2880	3.7045
0.84	1.0489	0.3060	3.7560
0.89	1.0363	0.3240	3.8137
0.94	1.0220	0.3420	3.8788
1.00	1.0058	0.3600	3.9532

Initial Crack Location	Corner
Center of Ellipse	(0.75, 0.0791)
Crack Length	0.3658
Crack Depth	0.3963
Average Crack Front	98,001 and 101,000 cycles

Table A-82. Geometric Factors for FAA-21 (See figure A-82)

ϕ	x [in.]	z [in.]	f(g)
0.00	-1.1205	0.0000	3.4905
0.05	-1.1239	0.0180	3.5040
0.11	-1.1267	0.0360	3.5179
0.16	-1.1287	0.0540	3.5323
0.21	-1.1300	0.0720	3.5470
0.26	-1.1306	0.0900	3.5623
0.31	-1.1305	0.1080	3.5781
0.36	-1.1297	0.1260	3.5945
0.41	-1.1282	0.1440	3.6115
0.46	-1.1259	0.1620	3.6292
0.51	-1.1230	0.1800	3.6478
0.56	-1.1193	0.1980	3.6672
0.61	-1.1148	0.2160	3.6877
0.65	-1.1095	0.2340	3.7094
0.70	-1.1034	0.2520	3.7324
0.75	-1.0964	0.2700	3.7571
0.80	-1.0885	0.2880	3.7836
0.85	-1.0796	0.3060	3.8124
0.90	-1.0696	0.3240	3.8438
0.95	-1.0583	0.3420	3.8786
1.00	-1.0457	0.3600	3.9174

Initial Crack Location	Corner
Center of Ellipse	(-0.75, 0.0967)
Crack Length	0.3808
Crack Depth	0.4200
Average Crack Front	98,001 and 101,000 cycles

Table A-83. Geometric Factors for FAA-21 (See figure A-83)

ϕ	x [in.]	z [in.]	f(g)
0.00	1.1376	0.0000	3.4986
0.05	1.1411	0.0180	3.5345
0.11	1.1440	0.0360	3.5670
0.16	1.1461	0.0540	3.5967
0.21	1.1475	0.0720	3.6239
0.26	1.1482	0.0900	3.6491
0.31	1.1481	0.1080	3.6725
0.36	1.1474	0.1260	3.6944
0.41	1.1459	0.1440	3.7150
0.46	1.1437	0.1620	3.7345
0.51	1.1408	0.1800	3.7530
0.55	1.1371	0.1980	3.7709
0.60	1.1327	0.2160	3.7881
0.65	1.1274	0.2340	3.8050
0.70	1.1213	0.2520	3.8216
0.75	1.1143	0.2700	3.8382
0.80	1.1064	0.2880	3.8551
0.85	1.0976	0.3060	3.8725
0.90	1.0876	0.3240	3.8907
0.95	1.0764	0.3420	3.9103
1.00	1.0640	0.3600	3.9317

Initial Crack Location	Corner
Center of Ellipse	(0.75, 0.0973)
Crack Length	0.3985
Crack Depth	0.4269
Average Crack Front	101,001 and 104,000 cycles

Table A-84. Geometric Factors for FAA-21 (See figure A-84)

ϕ	x [in.]	z [in.]	f(g)
0.00	-1.1492	0.0000	3.4407
0.06	-1.1540	0.0180	3.4854
0.11	-1.1581	0.0360	3.5259
0.16	-1.1614	0.0540	3.5631
0.22	-1.1639	0.0720	3.5973
0.27	-1.1658	0.0900	3.6292
0.32	-1.1669	0.1080	3.6592
0.37	-1.1674	0.1260	3.6874
0.42	-1.1672	0.1440	3.7142
0.47	-1.1662	0.1620	3.7399
0.52	-1.1646	0.1800	3.7646
0.57	-1.1623	0.1980	3.7886
0.61	-1.1592	0.2160	3.8120
0.66	-1.1554	0.2340	3.8350
0.71	-1.1508	0.2520	3.8578
0.76	-1.1455	0.2700	3.8807
0.80	-1.1393	0.2880	3.9037
0.85	-1.1323	0.3060	3.9271
0.90	-1.1243	0.3240	3.9512
0.95	-1.1154	0.3420	3.9764
1.00	-1.1055	0.3600	4.0029

Initial Crack Location	Corner
Center of Ellipse	(-0.75, 0.1285)
Crack Length	0.4179
Crack Depth	0.4422
Average Crack Front	101,001 and 104,000 cycles

Table A-85. Geometric Factors for FAA-22 (See figure A-85)

ϕ	x [in.]	z [in.]	f(g)
0.00	0.8361	0.0000	1.9105
0.05	0.8354	0.0067	1.8989
0.10	0.8345	0.0134	1.8887
0.15	0.8333	0.0200	1.8804
0.20	0.8318	0.0266	1.8744
0.25	0.8300	0.0332	1.8712
0.30	0.8280	0.0397	1.8711
0.35	0.8255	0.0463	1.8742
0.40	0.8227	0.0528	1.8805
0.45	0.8195	0.0594	1.8894
0.50	0.8159	0.0659	1.9006
0.55	0.8117	0.0722	1.9132
0.60	0.8070	0.0785	1.9268
0.65	0.8018	0.0845	1.9405
0.70	0.7959	0.0902	1.9538
0.75	0.7895	0.0954	1.9663
0.80	0.7825	0.0999	1.9772
0.85	0.7749	0.1037	1.9863
0.90	0.7669	0.1065	1.9932
0.95	0.7585	0.1083	1.9974
1.00	0.7500	0.1089	1.9988

Initial Crack Location	Corner
Center of Ellipse	(0.75, -0.0146)
Crack Length	0.0868
Crack Depth	0.1235
Average Crack Front	1 and 15,000 cycles

Table A-86. Geometric Factors for FAA-22 (See figure A-86)

ϕ	x [in.]	z [in.]	f(g)
0.00	-0.8331	0.0000	1.8786
0.05	-0.8334	0.0066	1.8819
0.10	-0.8333	0.0132	1.8860
0.15	-0.8329	0.0199	1.8909
0.20	-0.8321	0.0267	1.8965
0.25	-0.8310	0.0335	1.9027
0.30	-0.8294	0.0405	1.9095
0.35	-0.8275	0.0475	1.9168
0.40	-0.8250	0.0545	1.9245
0.45	-0.8221	0.0615	1.9325
0.50	-0.8185	0.0685	1.9407
0.55	-0.8144	0.0754	1.9490
0.60	-0.8097	0.0822	1.9571
0.65	-0.8043	0.0886	1.9650
0.70	-0.7982	0.0946	1.9724
0.75	-0.7915	0.1001	1.9791
0.80	-0.7841	0.1049	1.9850
0.85	-0.7761	0.1088	1.9898
0.90	-0.7677	0.1117	1.9934
0.95	-0.7589	0.1135	1.9956
1.00	-0.7500	0.1141	1.9964

Initial Crack Location	Corner
Center of Ellipse	(-0.75, 0.0083)
Crack Length	0.0834
Crack Depth	0.1058
Average Crack Front	1 and 15,000 cycles

Table A-87. Geometric Factors for FAA-22 (See figure A-87)

ϕ	x [in.]	z [in.]	f(g)
0.00	0.8448	0.0000	2.0219
0.05	0.8440	0.0074	2.0222
0.10	0.8429	0.0147	2.0231
0.15	0.8415	0.0220	2.0245
0.20	0.8399	0.0292	2.0264
0.25	0.8380	0.0365	2.0288
0.30	0.8358	0.0437	2.0316
0.35	0.8333	0.0511	2.0350
0.40	0.8304	0.0584	2.0388
0.45	0.8271	0.0659	2.0430
0.50	0.8233	0.0733	2.0476
0.55	0.8190	0.0808	2.0526
0.60	0.8140	0.0882	2.0579
0.65	0.8085	0.0954	2.0632
0.70	0.8021	0.1023	2.0686
0.75	0.7951	0.1088	2.0738
0.80	0.7872	0.1146	2.0786
0.85	0.7787	0.1195	2.0878
0.90	0.7695	0.1232	2.0991
0.95	0.7599	0.1255	2.1063
1.00	0.7500	0.1263	2.1087

Initial Crack Location	Corner
Center of Ellipse	(0.75, -0.0229)
Crack Length	0.0960
Crack Depth	0.1492
Average Crack Front	15,001 and 27,000 cycles

Table A-88. Geometric Factors for FAA-22 (See figure A-88)

ϕ	x [in.]	z [in.]	f(g)
0.00	-0.8412	0.0000	2.0183
0.05	-0.8414	0.0072	2.0178
0.10	-0.8413	0.0145	2.0176
0.15	-0.8408	0.0218	2.0177
0.20	-0.8400	0.0292	2.0182
0.25	-0.8388	0.0368	2.0190
0.30	-0.8371	0.0444	2.0200
0.35	-0.8350	0.0521	2.0214
0.40	-0.8324	0.0598	2.0230
0.45	-0.8292	0.0676	2.0249
0.50	-0.8254	0.0754	2.0270
0.55	-0.8210	0.0831	2.0293
0.60	-0.8159	0.0906	2.0316
0.65	-0.8100	0.0979	2.0341
0.70	-0.8033	0.1047	2.0365
0.75	-0.7959	0.1109	2.0388
0.80	-0.7878	0.1163	2.0408
0.85	-0.7790	0.1208	2.0426
0.90	-0.7697	0.1242	2.0439
0.95	-0.7599	0.1263	2.0447
1.00	-0.7500	0.1270	2.0450

Initial Crack Location	Corner
Center of Ellipse	(-0.75, 0.0085)
Crack Length	0.0914
Crack Depth	0.1185
Average Crack Front	15,001 and 27,000 cycles

Table A-89. Geometric Factors for FAA-22 (See figure A-89)

ϕ	x [in.]	z [in.]	f(g)
0.00	0.8544	0.0000	2.0615
0.05	0.8535	0.0081	2.0615
0.10	0.8524	0.0162	2.0620
0.15	0.8510	0.0243	2.0630
0.20	0.8494	0.0323	2.0644
0.25	0.8474	0.0403	2.0662
0.30	0.8451	0.0485	2.0684
0.35	0.8425	0.0567	2.0711
0.40	0.8394	0.0650	2.0742
0.45	0.8359	0.0734	2.0776
0.50	0.8318	0.0818	2.0836
0.55	0.8272	0.0904	2.0983
0.60	0.8218	0.0989	2.1139
0.65	0.8157	0.1072	2.1302
0.70	0.8088	0.1153	2.1466
0.75	0.8009	0.1229	2.1625
0.80	0.7922	0.1298	2.1773
0.85	0.7826	0.1356	2.1901
0.90	0.7722	0.1400	2.2000
0.95	0.7612	0.1428	2.2063
1.00	0.7500	0.1438	2.2085

Initial Crack Location	Corner
Center of Ellipse	(0.75, -0.0239)
Crack Length	0.1055
Crack Depth	0.1676
Average Crack Front	27,001 and 33,000 cycles

Table A-90. Geometric Factors for FAA-22 (See figure A-90)

ϕ	x [in.]	z [in.]	f(g)
0.00	-0.8505	0.0000	2.0620
0.05	-0.8507	0.0079	2.0613
0.10	-0.8504	0.0159	2.0610
0.15	-0.8498	0.0240	2.0610
0.20	-0.8488	0.0321	2.0613
0.25	-0.8474	0.0404	2.0619
0.30	-0.8455	0.0487	2.0628
0.35	-0.8432	0.0571	2.0639
0.40	-0.8403	0.0656	2.0653
0.45	-0.8367	0.0741	2.0670
0.50	-0.8326	0.0826	2.0689
0.55	-0.8277	0.0910	2.0709
0.60	-0.8221	0.0992	2.0731
0.65	-0.8156	0.1071	2.0753
0.70	-0.8084	0.1145	2.0774
0.75	-0.8003	0.1213	2.0795
0.80	-0.7914	0.1273	2.0833
0.85	-0.7817	0.1322	2.0890
0.90	-0.7715	0.1359	2.0933
0.95	-0.7609	0.1381	2.0960
1.00	-0.7500	0.1389	2.0969

Initial Crack Location	Corner
Center of Ellipse	(-0.75, 0.0073)
Crack Length	0.1007
Crack Depth	0.1316
Average Crack Front	27,001 and 33,000 cycles

Table A-91. Geometric Factors for FAA-22 (See figure A-91)

ϕ	x [in.]	z [in.]	f(g)
0.00	0.8671	0.0000	2.1833
0.05	0.8667	0.0092	2.1735
0.10	0.8660	0.0184	2.1653
0.15	0.8650	0.0276	2.1586
0.20	0.8636	0.0369	2.1534
0.25	0.8618	0.0463	2.1496
0.30	0.8596	0.0558	2.1472
0.35	0.8569	0.0655	2.1461
0.40	0.8537	0.0753	2.1463
0.45	0.8498	0.0853	2.1479
0.50	0.8453	0.0953	2.1506
0.55	0.8401	0.1054	2.1545
0.60	0.8339	0.1155	2.1594
0.65	0.8268	0.1254	2.1651
0.70	0.8187	0.1349	2.1714
0.75	0.8096	0.1438	2.1780
0.80	0.7993	0.1518	2.1844
0.85	0.7880	0.1585	2.1902
0.90	0.7759	0.1636	2.1949
0.95	0.7631	0.1668	2.1979
1.00	0.7500	0.1679	2.1989

Initial Crack Location	Corner
Center of Ellipse	(0.75, -0.0157)
Crack Length	0.1172
Crack Depth	0.1732
Average Crack Front	33,001 and 36,000 cycles

Table A-92. Geometric Factors for FAA-22 (See figure A-92)

ϕ	x [in.]	z [in.]	f(g)
0.00	-0.8624	0.0000	2.1848
0.05	-0.8630	0.0089	2.1584
0.10	-0.8631	0.0179	2.1338
0.15	-0.8627	0.0271	2.1113
0.20	-0.8619	0.0363	2.0912
0.25	-0.8605	0.0458	2.0787
0.30	-0.8586	0.0553	2.0748
0.35	-0.8561	0.0650	2.0720
0.40	-0.8529	0.0748	2.0703
0.45	-0.8491	0.0846	2.0700
0.50	-0.8444	0.0944	2.0710
0.55	-0.8389	0.1041	2.0734
0.60	-0.8325	0.1135	2.0770
0.65	-0.8251	0.1226	2.0842
0.70	-0.8168	0.1311	2.1031
0.75	-0.8075	0.1389	2.1229
0.80	-0.7973	0.1456	2.1422
0.85	-0.7863	0.1512	2.1592
0.90	-0.7746	0.1554	2.1727
0.95	-0.7624	0.1579	2.1812
1.00	-0.7500	0.1588	2.1842

Initial Crack Location	Corner
Center of Ellipse	(-0.75, 0.0151)
Crack Length	0.1132
Crack Depth	0.1437
Average Crack Front	33,001 and 36,000 cycles

Table A-93. Geometric Factors for FAA-22 (See figure A-93)

ϕ	x [in.]	z [in.]	f(g)
0.00	0.9499	0.0000	2.8913
0.06	0.9503	0.0148	2.8867
0.12	0.9500	0.0296	2.8826
0.17	0.9491	0.0444	2.8790
0.23	0.9476	0.0592	2.8759
0.29	0.9454	0.0739	2.8733
0.34	0.9426	0.0884	2.8712
0.40	0.9392	0.1029	2.8697
0.45	0.9350	0.1172	2.8688
0.50	0.9303	0.1312	2.8684
0.55	0.9248	0.1450	2.8688
0.60	0.9187	0.1585	2.8698
0.65	0.9119	0.1716	2.8716
0.69	0.9045	0.1843	2.8743
0.74	0.8963	0.1966	2.8779
0.78	0.8874	0.2084	2.8825
0.83	0.8779	0.2196	2.8883
0.87	0.8676	0.2301	2.8953
0.92	0.8566	0.2399	2.9039
0.96	0.8450	0.2488	2.9140
1.00	0.8327	0.2569	2.9261

Initial Crack Location	Corner
Center of Ellipse	(0.75, 0.0158)
Crack Length	0.2003
Crack Depth	0.2647
Average Crack Front	66,001 and 72,000 cycles

Table A-94. Geometric Factors for FAA-22 (See figure A-94)

ϕ	x [in.]	z [in.]	f(g)
0.00	-0.9125	0.0000	2.7336
0.06	-0.9125	0.0135	2.7374
0.12	-0.9119	0.0270	2.7410
0.18	-0.9108	0.0404	2.7446
0.24	-0.9091	0.0538	2.7480
0.29	-0.9067	0.0670	2.7513
0.35	-0.9038	0.0802	2.7546
0.40	-0.9003	0.0932	2.7579
0.46	-0.8962	0.1060	2.7613
0.51	-0.8915	0.1186	2.7650
0.56	-0.8861	0.1309	2.7688
0.61	-0.8801	0.1429	2.7732
0.65	-0.8734	0.1545	2.7780
0.70	-0.8661	0.1656	2.7837
0.74	-0.8580	0.1763	2.7903
0.79	-0.8493	0.1864	2.7983
0.83	-0.8399	0.1958	2.8079
0.87	-0.8297	0.2045	2.8196
0.91	-0.8188	0.2123	2.8340
0.96	-0.8071	0.2192	2.8518
1.00	-0.7946	0.2249	2.8740

Initial Crack Location	Corner
Center of Ellipse	(-0.75, 0.0066)
Crack Length	0.1626
Crack Depth	0.2271
Average Crack Front	66,001 and 72,000 cycles

Table A-95. Geometric Factors for FAA-22 (See figure A-95)

ϕ	x [in.]	z [in.]	f(g)
0.00	0.9880	0.0000	3.0133
0.06	0.9892	0.0162	3.0259
0.11	0.9897	0.0324	3.0370
0.17	0.9894	0.0487	3.0468
0.23	0.9884	0.0649	3.0553
0.28	0.9867	0.0811	3.0626
0.33	0.9842	0.0973	3.0686
0.39	0.9809	0.1133	3.0736
0.44	0.9769	0.1291	3.0775
0.49	0.9721	0.1448	3.0803
0.54	0.9665	0.1602	3.0823
0.59	0.9602	0.1752	3.0834
0.64	0.9531	0.1899	3.0838
0.69	0.9453	0.2043	3.0835
0.73	0.9367	0.2181	3.0827
0.78	0.9273	0.2314	3.0815
0.82	0.9172	0.2441	3.0802
0.87	0.9064	0.2562	3.0788
0.91	0.8948	0.2676	3.0776
0.96	0.8826	0.2782	3.0768
1.00	0.8697	0.2880	3.0768

Initial Crack Location	Corner
Center of Ellipse	(0.75, 0.0348)
Crack Length	0.2397
Crack Depth	0.2922
Average Crack Front	72,001 and 81,000 cycles

Table A-96. Geometric Factors for FAA-22 (See figure A-96)

ϕ	x [in.]	z [in.]	f(g)
0.00	-0.9388	0.0000	2.7125
0.06	-0.9397	0.0144	2.7398
0.12	-0.9399	0.0289	2.7637
0.17	-0.9394	0.0434	2.7847
0.23	-0.9382	0.0579	2.8029
0.29	-0.9363	0.0722	2.8186
0.34	-0.9336	0.0865	2.8322
0.39	-0.9303	0.1007	2.8437
0.45	-0.9263	0.1146	2.8535
0.50	-0.9215	0.1283	2.8615
0.55	-0.9160	0.1418	2.8682
0.60	-0.9098	0.1549	2.8735
0.64	-0.9028	0.1676	2.8778
0.69	-0.8952	0.1798	2.8812
0.74	-0.8868	0.1916	2.8840
0.78	-0.8776	0.2027	2.8865
0.83	-0.8678	0.2132	2.8890
0.87	-0.8572	0.2230	2.8918
0.91	-0.8459	0.2320	2.8955
0.96	-0.8339	0.2402	2.9006
1.00	-0.8212	0.2473	2.9077

Initial Crack Location	Corner
Center of Ellipse	(-0.75, 0.0257)
Crack Length	0.1899
Crack Depth	0.2391
Average Crack Front	72,001 and 81,000 cycles

Table A-97. Geometric Factors for FAA-22 (See figure A-97)

ϕ	x [in.]	z [in.]	f(g)
0.00	1.0403	0.0000	3.1904
0.06	1.0412	0.0180	3.1772
0.11	1.0413	0.0360	3.1656
0.17	1.0405	0.0540	3.1555
0.22	1.0390	0.0720	3.1471
0.27	1.0367	0.0900	3.1404
0.33	1.0336	0.1078	3.1355
0.38	1.0297	0.1255	3.1323
0.43	1.0250	0.1429	3.1309
0.48	1.0194	0.1602	3.1313
0.53	1.0131	0.1771	3.1334
0.58	1.0060	0.1937	3.1373
0.63	0.9981	0.2100	3.1427
0.68	0.9894	0.2258	3.1497
0.73	0.9799	0.2411	3.1581
0.77	0.9697	0.2559	3.1679
0.82	0.9587	0.2701	3.1789
0.87	0.9469	0.2836	3.1910
0.91	0.9345	0.2964	3.2040
0.96	0.9213	0.3085	3.2179
1.00	0.9075	0.3197	3.2324

Initial Crack Location	Corner
Center of Ellipse	(0.75, 0.0285)
Crack Length	0.2914
Crack Depth	0.3463
Average Crack Front	81,001 and 90,000 cycles

Table A-98. Geometric Factors for FAA-22 (See figure A-98)

ϕ	x [in.]	z [in.]	f(g)
0.00	-0.9705	0.0000	2.9160
0.06	-0.9724	0.0156	2.9302
0.11	-0.9735	0.0313	2.9431
0.17	-0.9737	0.0470	2.9547
0.23	-0.9731	0.0628	2.9652
0.28	-0.9716	0.0785	2.9745
0.33	-0.9693	0.0941	2.9827
0.39	-0.9661	0.1096	2.9899
0.44	-0.9621	0.1249	2.9962
0.49	-0.9572	0.1399	3.0017
0.54	-0.9515	0.1547	3.0064
0.59	-0.9449	0.1690	3.0105
0.64	-0.9374	0.1830	3.0141
0.68	-0.9292	0.1964	3.0173
0.73	-0.9202	0.2093	3.0202
0.78	-0.9103	0.2216	3.0231
0.82	-0.8997	0.2332	3.0261
0.87	-0.8884	0.2441	3.0294
0.91	-0.8764	0.2542	3.0332
0.96	-0.8637	0.2634	3.0378
1.00	-0.8503	0.2717	3.0433

Initial Crack Location	Corner
Center of Ellipse	(-0.75, 0.0436)
Crack Length	0.2238
Crack Depth	0.2552
Average Crack Front	81,001 and 90,000 cycles

Table A-99. Geometric Factors for FAA-22 (See figure A-99)

ϕ	x [in.]	z [in.]	f(g)
0.00	1.1068	0.0000	3.3150
0.05	1.1078	0.0203	3.3206
0.11	1.1078	0.0407	3.3251
0.16	1.1069	0.0610	3.3284
0.21	1.1050	0.0813	3.3306
0.27	1.1022	0.1015	3.3317
0.32	1.0984	0.1216	3.3317
0.37	1.0936	0.1414	3.3307
0.42	1.0879	0.1610	3.3287
0.47	1.0812	0.1802	3.3258
0.52	1.0737	0.1992	3.3219
0.57	1.0652	0.2176	3.3172
0.62	1.0558	0.2357	3.3117
0.67	1.0455	0.2531	3.3056
0.72	1.0344	0.2700	3.2988
0.77	1.0224	0.2863	3.2916
0.81	1.0097	0.3019	3.2839
0.86	0.9961	0.3168	3.2760
0.91	0.9819	0.3309	3.2680
0.95	0.9669	0.3441	3.2601
1.00	0.9513	0.3565	3.2523

Initial Crack Location	Corner
Center of Ellipse	(0.75, 0.0311)
Crack Length	0.3580
Crack Depth	0.3935
Average Crack Front	90,001 and 99,000 cycles

Table A-100. Geometric Factors for FAA-22 (See figure A-100)

ϕ	x [in.]	z [in.]	f(g)
0.00	-1.0130	0.0000	3.0608
0.06	-1.0148	0.0171	3.0650
0.11	-1.0156	0.0342	3.0688
0.17	-1.0156	0.0514	3.0720
0.22	-1.0147	0.0686	3.0747
0.27	-1.0129	0.0858	3.0769
0.33	-1.0102	0.1028	3.0787
0.38	-1.0065	0.1197	3.0800
0.43	-1.0020	0.1364	3.0808
0.48	-0.9966	0.1527	3.0813
0.53	-0.9903	0.1688	3.0815
0.58	-0.9831	0.1845	3.0814
0.63	-0.9751	0.1997	3.0810
0.68	-0.9662	0.2144	3.0806
0.73	-0.9565	0.2286	3.0801
0.77	-0.9460	0.2422	3.0797
0.82	-0.9347	0.2551	3.0794
0.86	-0.9226	0.2672	3.0795
0.91	-0.9099	0.2786	3.0800
0.96	-0.8965	0.2891	3.0810
1.00	-0.8825	0.2987	3.0828

Initial Crack Location	Corner
Center of Ellipse	(-0.75, 0.0426)
Crack Length	0.2658
Crack Depth	0.2955
Average Crack Front	90,001 and 99,000 cycles

Table A-101. Geometric Factors for FAA-22 (See figure A-101)

ϕ	x [in.]	z [in.]	f(g)
0.00	1.1622	0.0000	3.4284
0.05	1.1624	0.0188	3.4196
0.10	1.1621	0.0375	3.4143
0.14	1.1611	0.0563	3.4127
0.19	1.1594	0.0750	3.4148
0.24	1.1572	0.0938	3.4206
0.29	1.1542	0.1125	3.4301
0.34	1.1506	0.1313	3.4433
0.38	1.1463	0.1500	3.4603
0.43	1.1413	0.1688	3.4811
0.48	1.1355	0.1875	3.5057
0.53	1.1290	0.2063	3.5340
0.58	1.1217	0.2250	3.5662
0.63	1.1135	0.2438	3.6024
0.68	1.1043	0.2625	3.6427
0.73	1.0941	0.2813	3.6873
0.78	1.0829	0.3000	3.7367
0.83	1.0703	0.3188	3.7913
0.89	1.0564	0.3375	3.8520
0.94	1.0409	0.3563	3.9200
1.00	1.0234	0.3750	4.0283

Initial Crack Location	Corner
Center of Ellipse	(0.75, 0.0166)
Crack Length	0.4125
Crack Depth	0.4834
Average Crack Front	102,001 and 105,000 cycles

Table A-102. Geometric Factors for FAA-22 (See figure A-102)

ϕ	x [in.]	z [in.]	f(g)
0.00	-1.0468	0.0000	3.0598
0.05	-1.0485	0.0182	3.0799
0.11	-1.0493	0.0366	3.0981
0.16	-1.0491	0.0549	3.1146
0.22	-1.0480	0.0733	3.1296
0.27	-1.0459	0.0916	3.1430
0.32	-1.0429	0.1098	3.1549
0.37	-1.0389	0.1278	3.1655
0.43	-1.0340	0.1455	3.1749
0.48	-1.0282	0.1630	3.1832
0.53	-1.0214	0.1801	3.1904
0.58	-1.0138	0.1969	3.1966
0.63	-1.0052	0.2132	3.2020
0.67	-0.9958	0.2289	3.2067
0.72	-0.9856	0.2441	3.2107
0.77	-0.9745	0.2587	3.2142
0.82	-0.9627	0.2725	3.2173
0.86	-0.9500	0.2857	3.2202
0.91	-0.9367	0.2980	3.2229
0.95	-0.9227	0.3095	3.2257
1.00	-0.9080	0.3202	3.2287

Initial Crack Location	Corner
Center of Ellipse	(-0.75, 0.0421)
Crack Length	0.2994
Crack Depth	0.3274
Average Crack Front	102,001 and 105,000 cycles

Table A-103. Geometric Factors for FAA-22 (See figure A-103)

ϕ	x [in.]	z [in.]	f(g)
0.00	1.1935	0.0000	3.4703
0.05	1.1941	0.0188	3.4912
0.10	1.1941	0.0375	3.5116
0.15	1.1936	0.0563	3.5314
0.20	1.1926	0.0750	3.5509
0.25	1.1910	0.0938	3.5700
0.30	1.1889	0.1125	3.5889
0.35	1.1861	0.1313	3.6077
0.40	1.1828	0.1500	3.6265
0.45	1.1790	0.1688	3.6454
0.50	1.1745	0.1875	3.6644
0.55	1.1693	0.2063	3.6837
0.60	1.1636	0.2250	3.7034
0.65	1.1571	0.2438	3.7237
0.70	1.1500	0.2625	3.7446
0.74	1.1420	0.2813	3.7665
0.79	1.1333	0.3000	3.7894
0.85	1.1238	0.3188	3.8138
0.90	1.1132	0.3375	3.8398
0.95	1.1017	0.3563	3.8678
1.00	1.0891	0.3750	3.8985

Initial Crack Location	Corner
Center of Ellipse	(0.75, 0.0299)
Crack Length	0.4445
Crack Depth	0.5355
Average Crack Front	105,001 and 108,000 cycles

Table A-104. Geometric Factors for FAA-22 (See figure A-104)

ϕ	x [in.]	z [in.]	f(g)
0.00	-1.0680	0.0000	3.3385
0.05	-1.0700	0.0190	3.3364
0.11	-1.0709	0.0381	3.3347
0.16	-1.0709	0.0572	3.3333
0.22	-1.0699	0.0764	3.3324
0.27	-1.0679	0.0955	3.3318
0.32	-1.0649	0.1145	3.3316
0.37	-1.0610	0.1333	3.3318
0.42	-1.0560	0.1518	3.3323
0.47	-1.0501	0.1701	3.3333
0.53	-1.0433	0.1881	3.3347
0.57	-1.0355	0.2056	3.3364
0.62	-1.0267	0.2227	3.3386
0.67	-1.0171	0.2393	3.3411
0.72	-1.0066	0.2553	3.3441
0.77	-0.9952	0.2706	3.3475
0.82	-0.9831	0.2853	3.3512
0.86	-0.9701	0.2992	3.3554
0.91	-0.9564	0.3123	3.3601
0.95	-0.9420	0.3246	3.3651
1.00	-0.9270	0.3360	3.3706

Initial Crack Location	Corner
Center of Ellipse	(-0.75, 0.0472)
Crack Length	0.3176
Crack Depth	0.3462
Average Crack Front	105,001 and 108,000 cycles

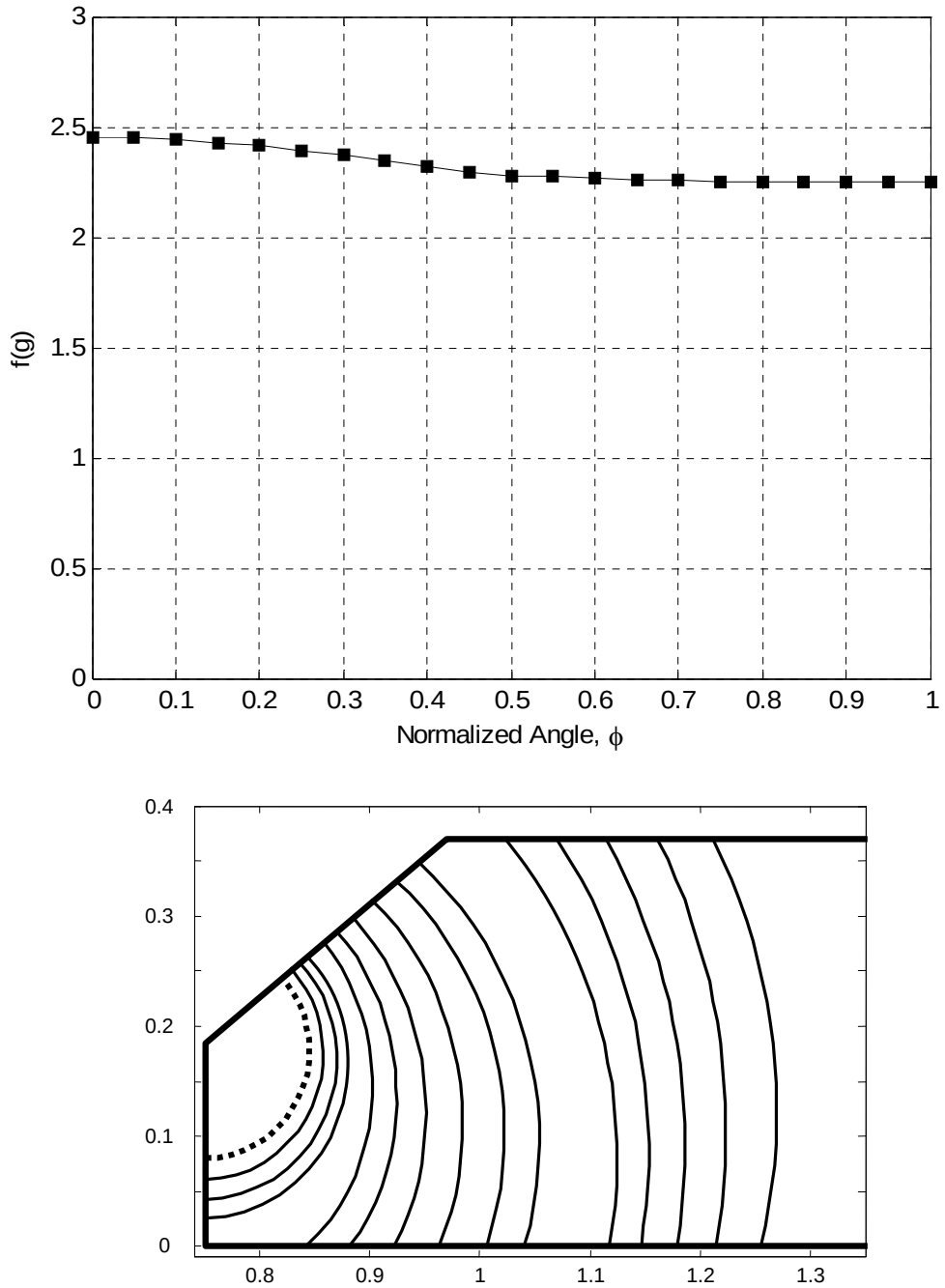

Figure A-1. Geometric Factors for FAA-17 (See table A-1)

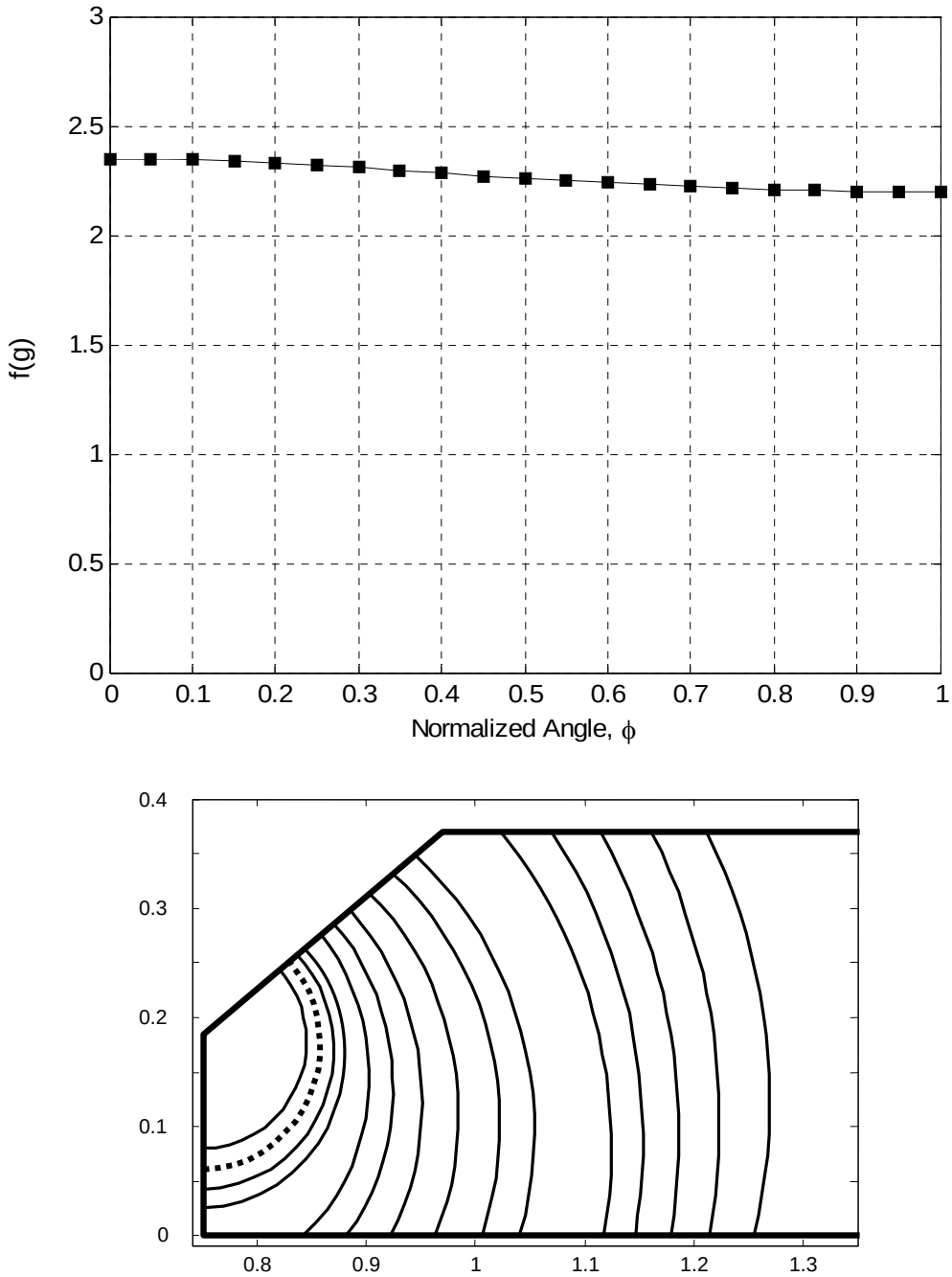

Figure A-2. Geometric Factors for FAA-17 (See table A-2)

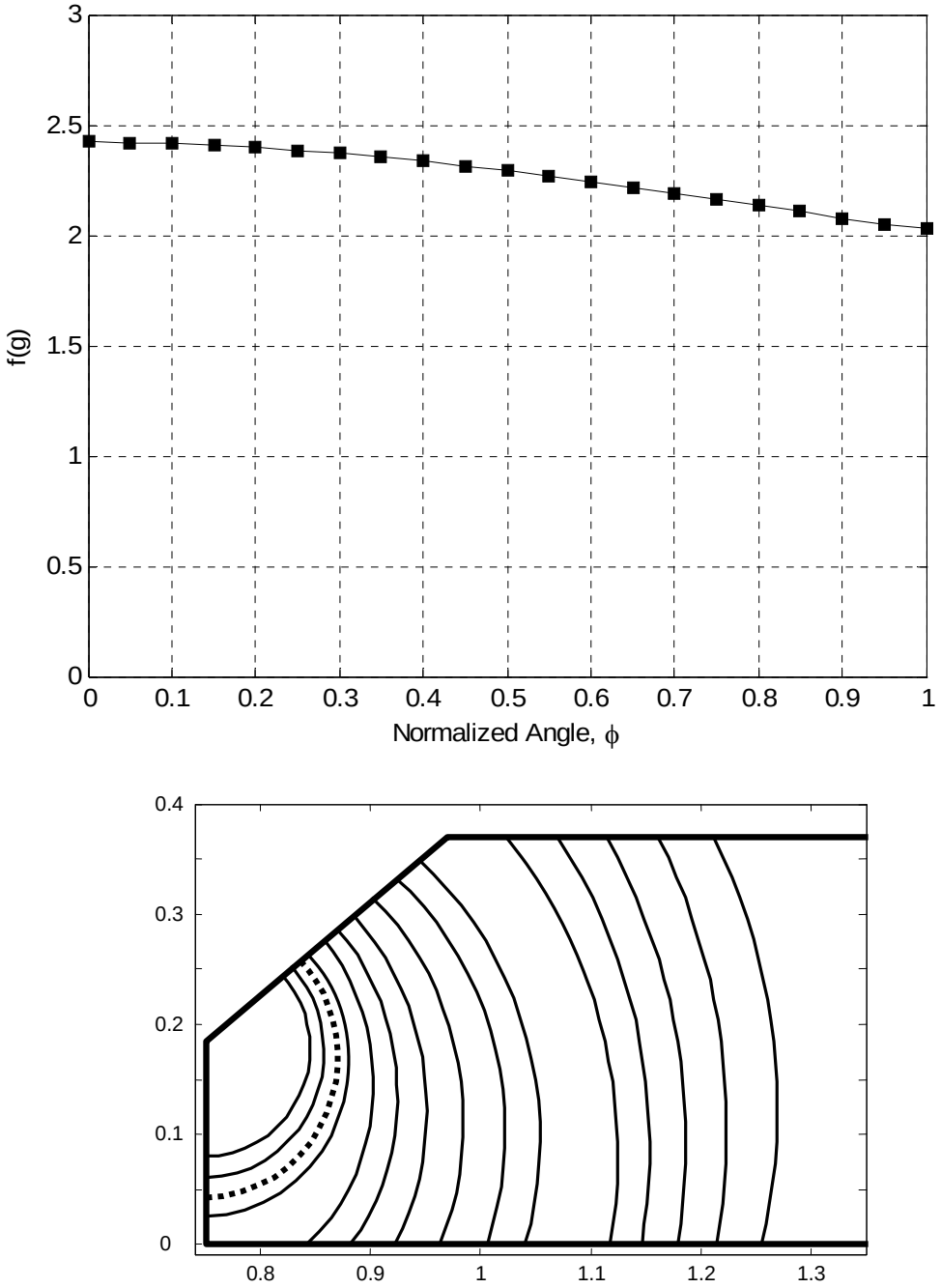

Figure A-3. Geometric Factors for FAA-17 (See table A-3)

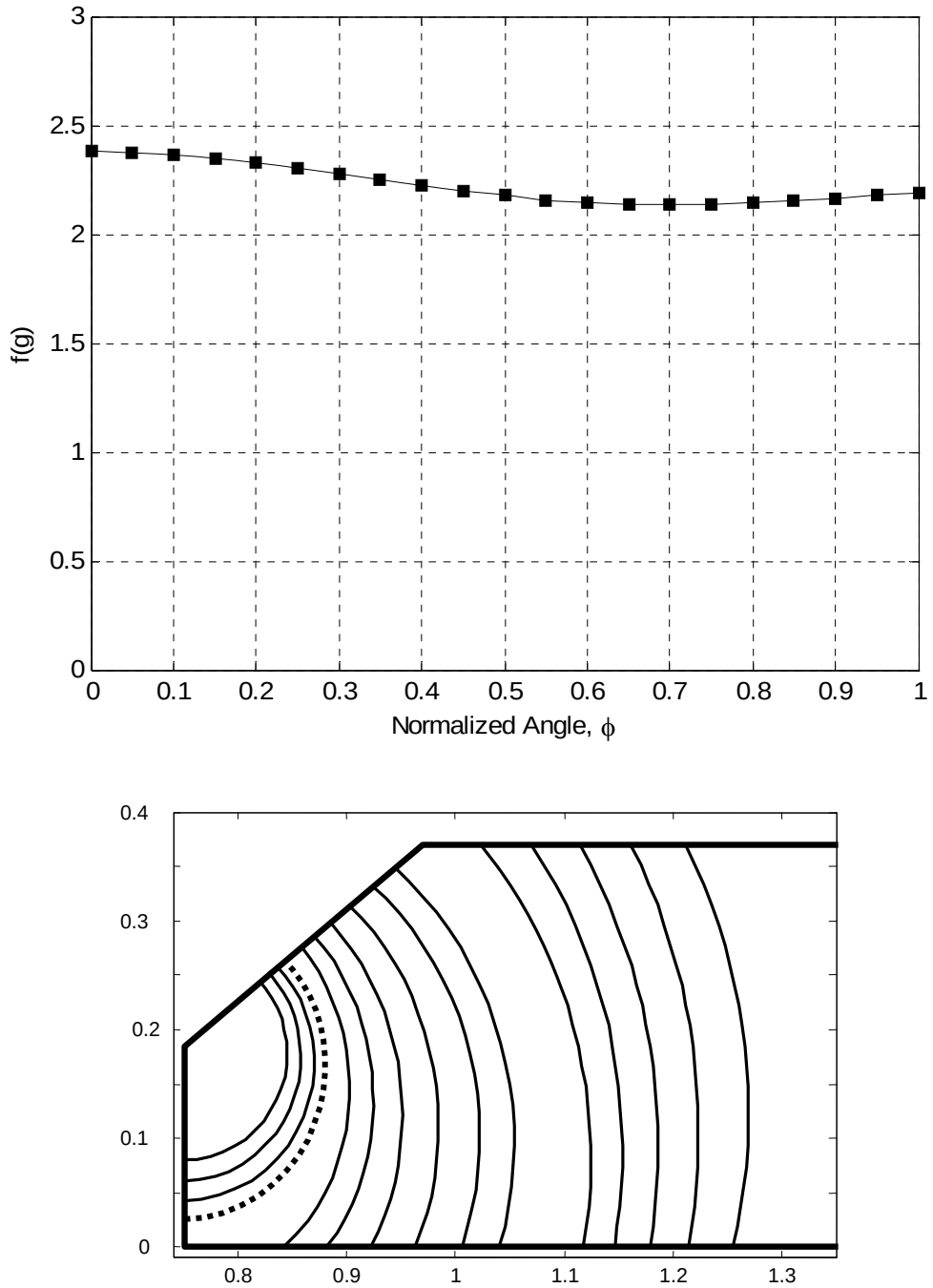

Figure A-4. Geometric Factors for FAA-17 (See table A-4)

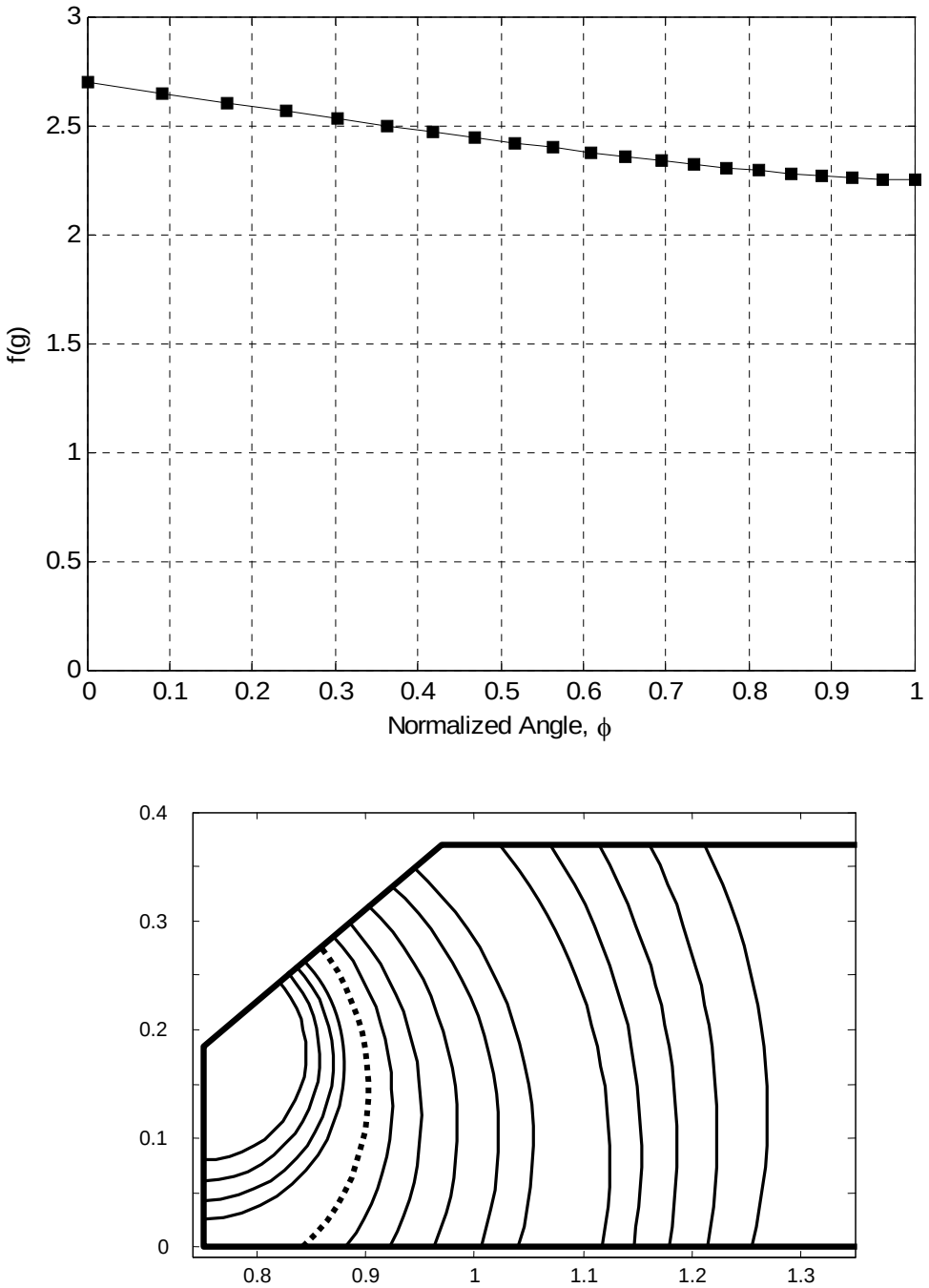

Figure A-5. Geometric Factors for FAA-17 (See table A-5)

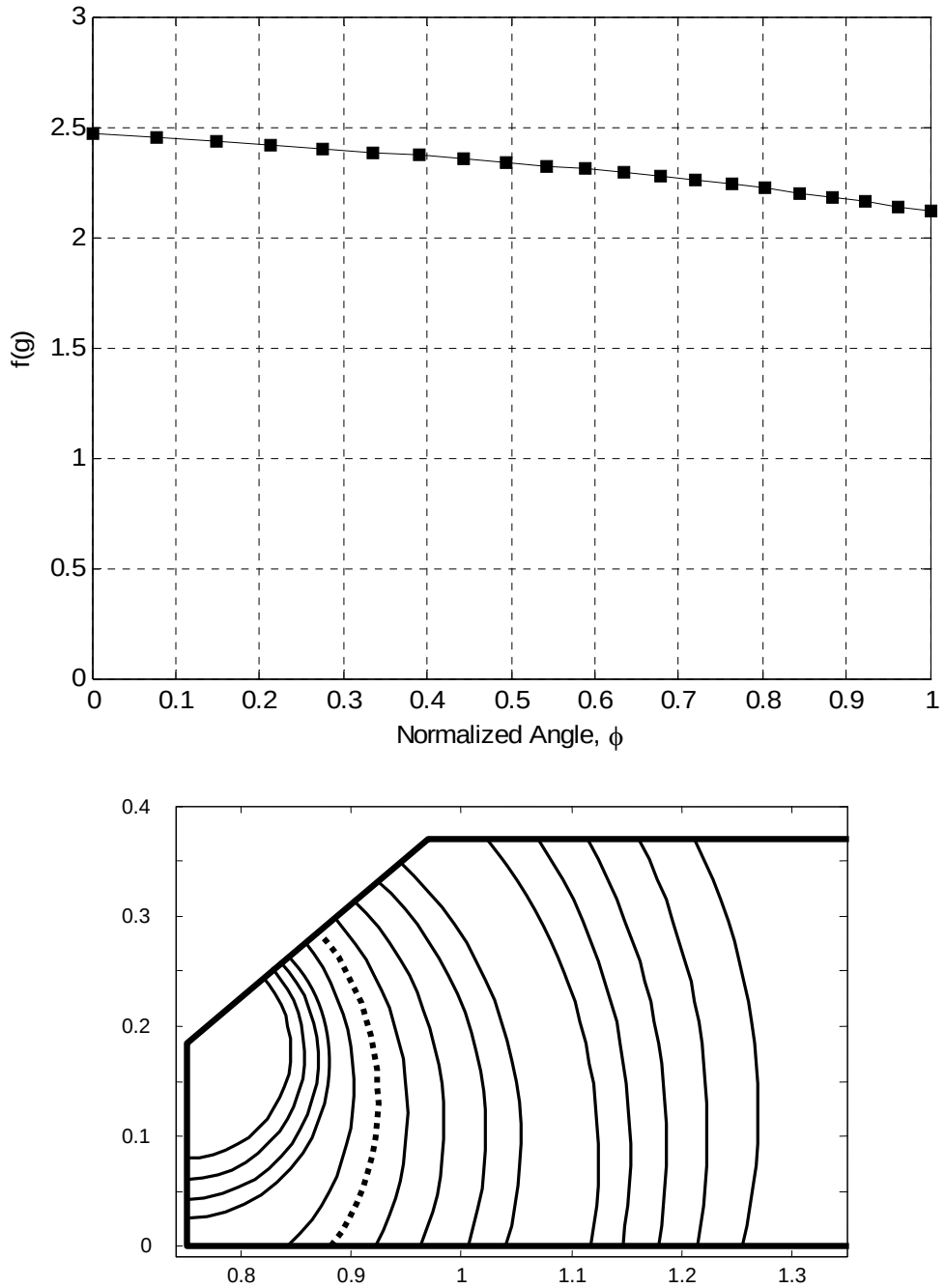

Figure A-6. Geometric Factors for FAA-17 (See table A-6)

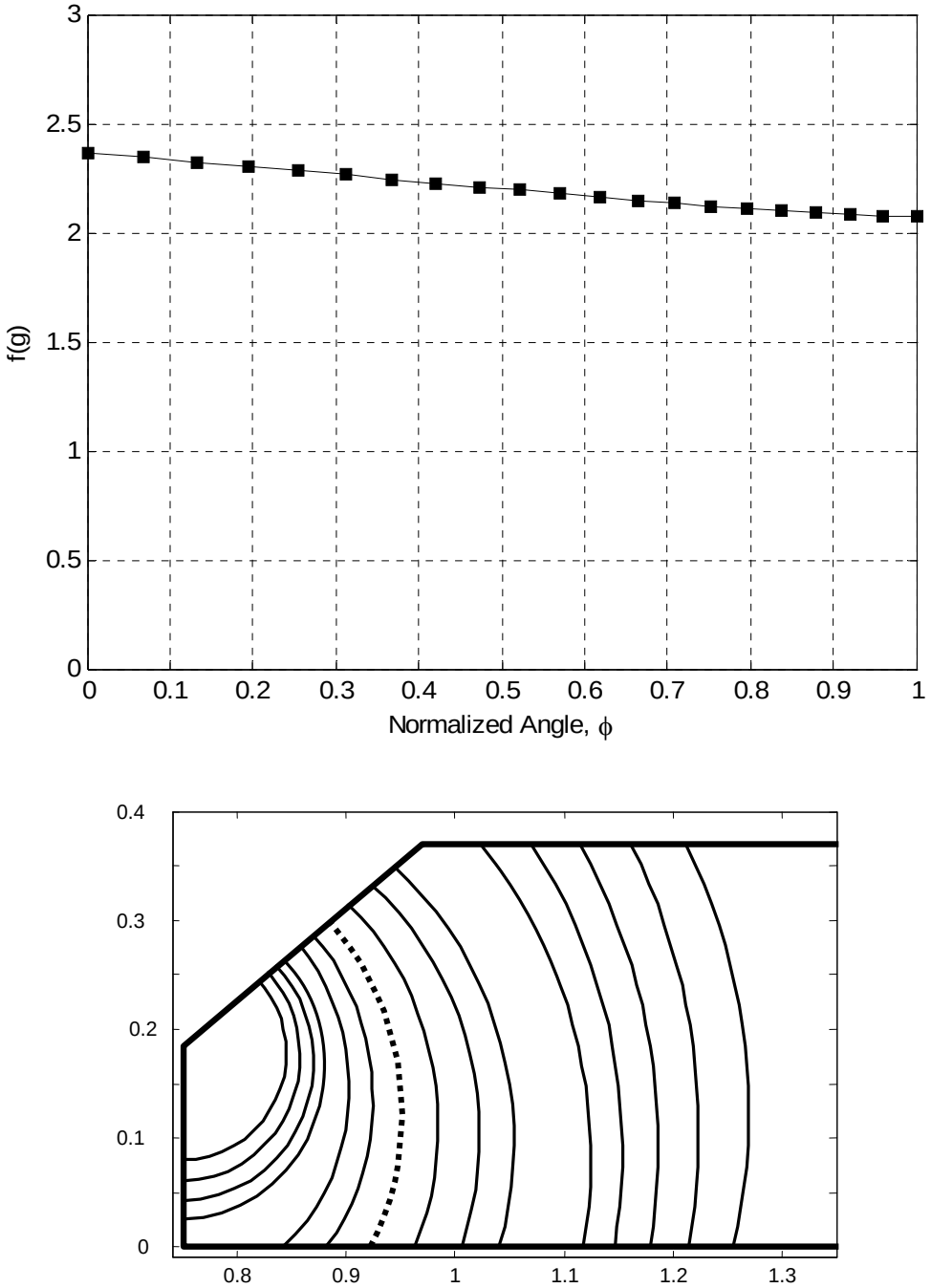

Figure A-7. Geometric Factors for FAA-17 (See table A-7)

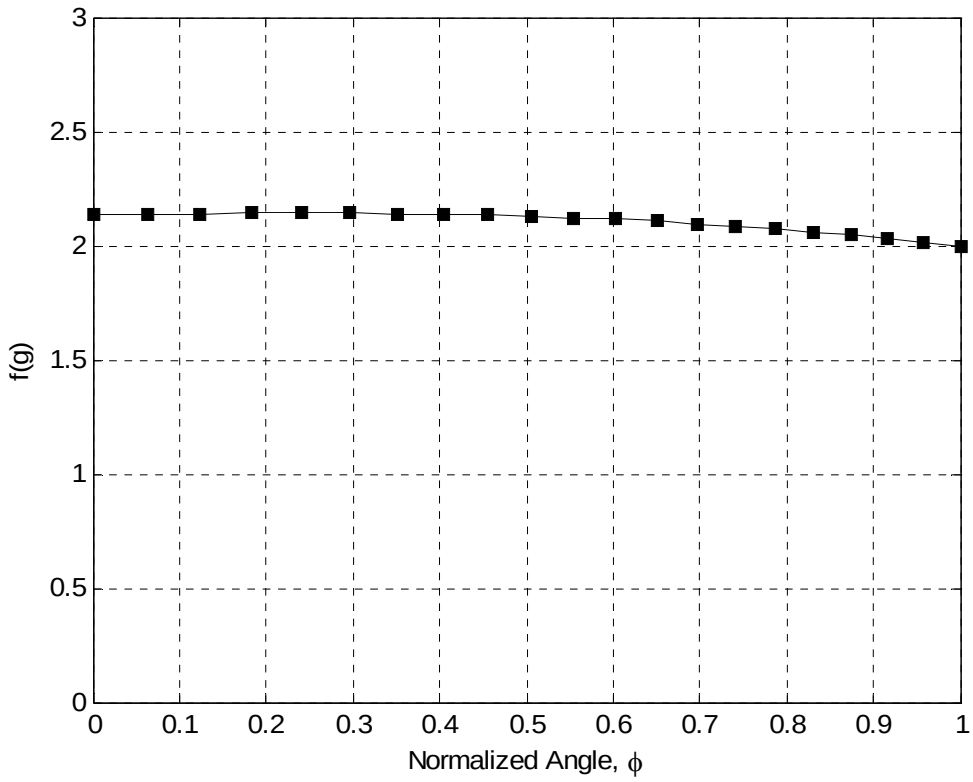

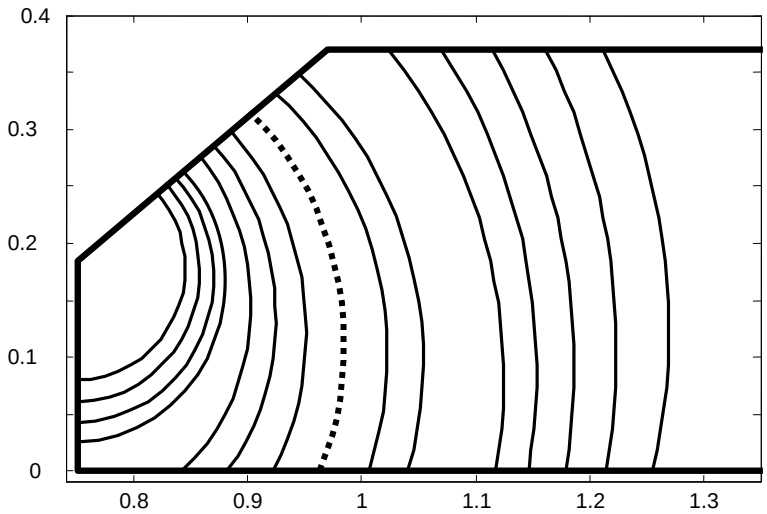

Figure A-8. Geometric Factors for FAA-17 (See table A-8)

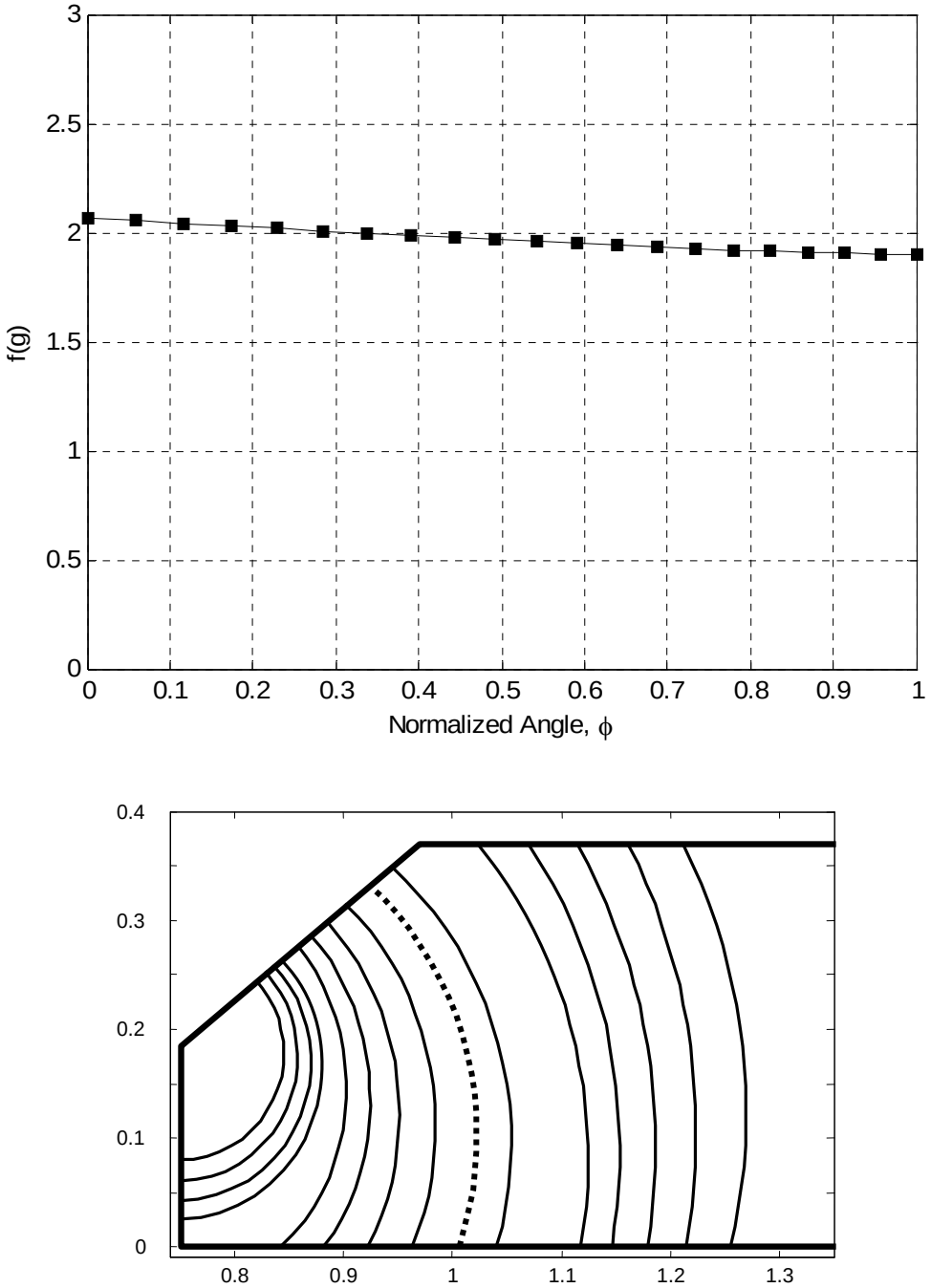

Figure A-9. Geometric Factors for FAA-17 (See table A-9)

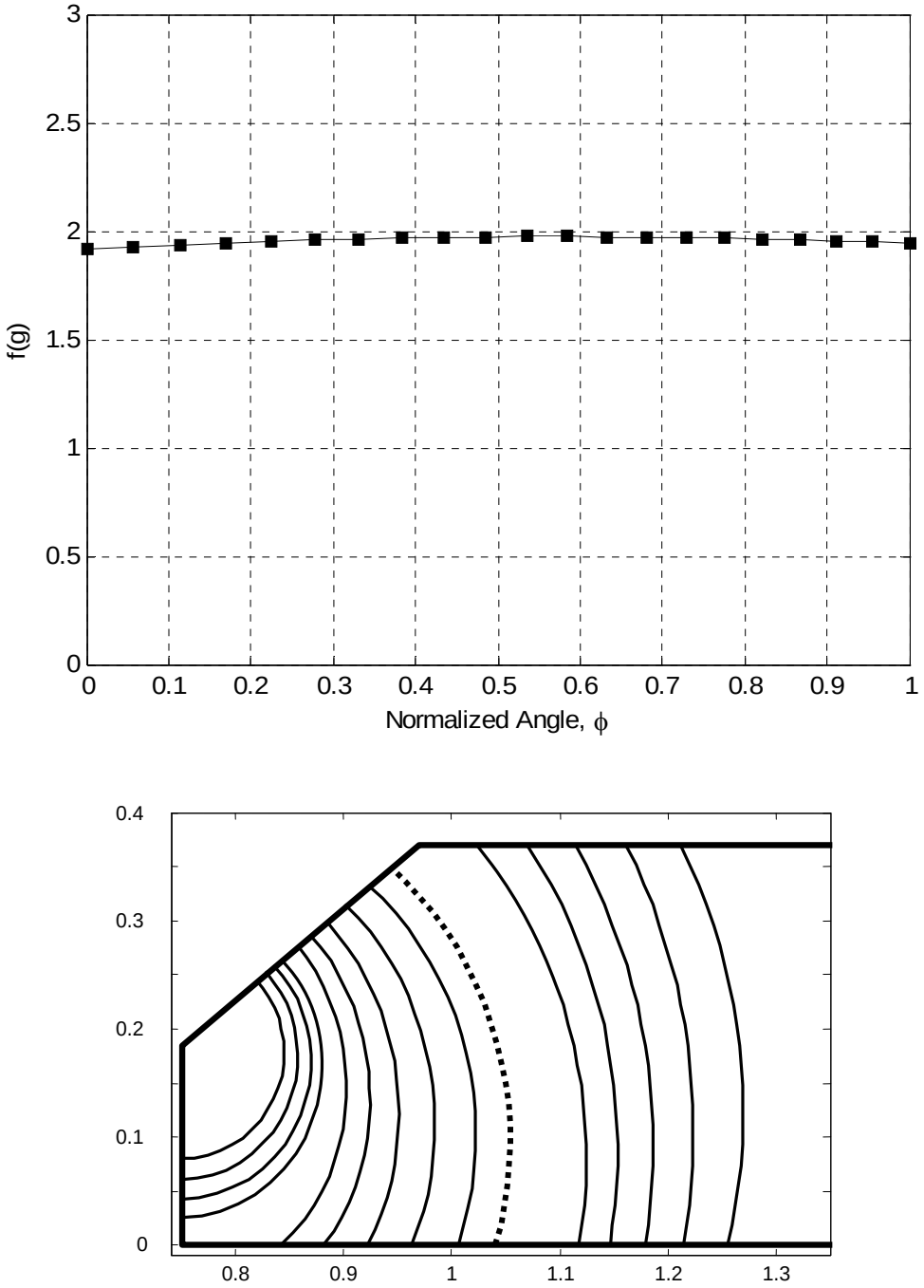

Figure A-10. Geometric Factors for FAA-17 (See table A-10)

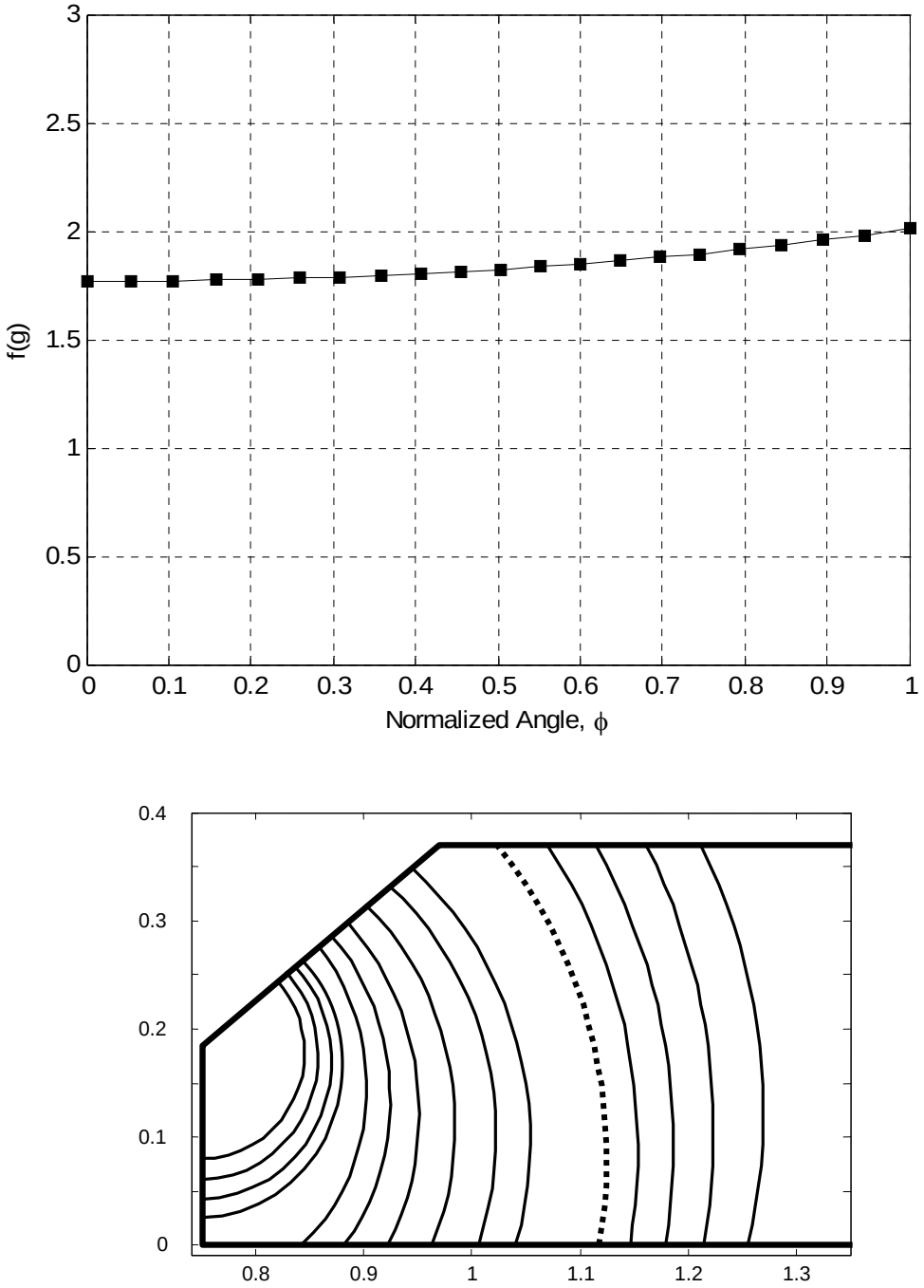

Figure A-11. Geometric Factors for FAA-17 (See table A-11)

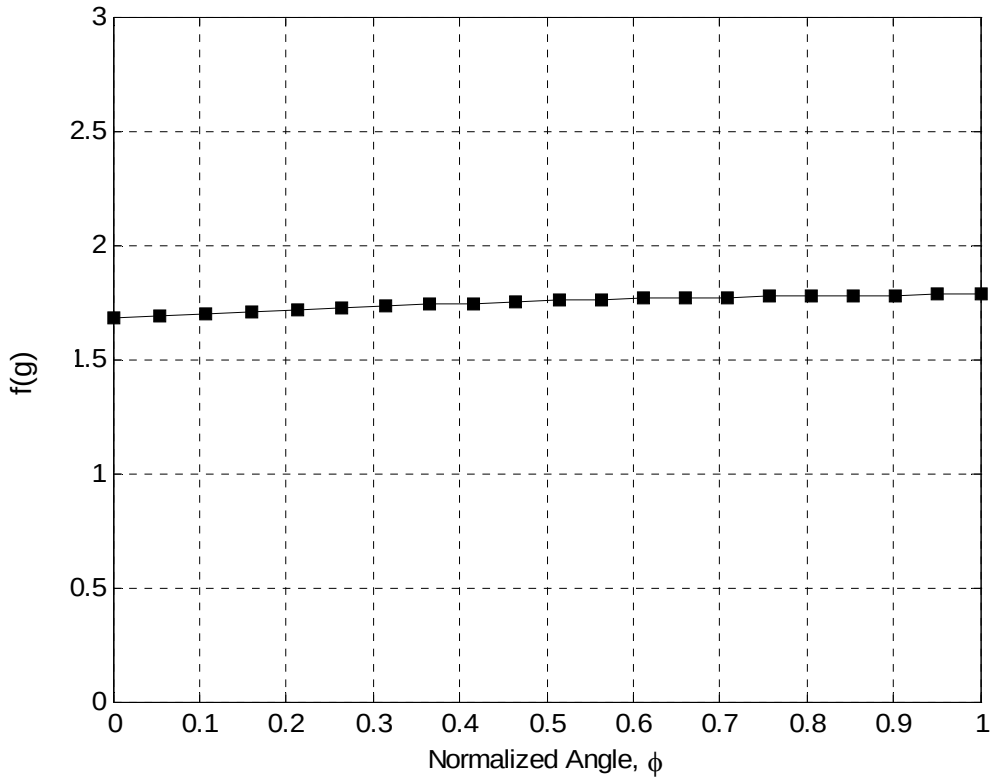

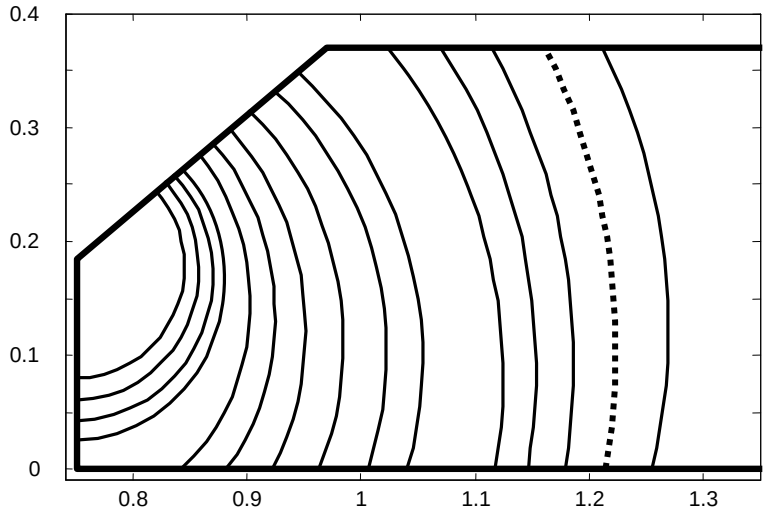

Figure A-12. Geometric Factors for FAA-17 (See table A-12)

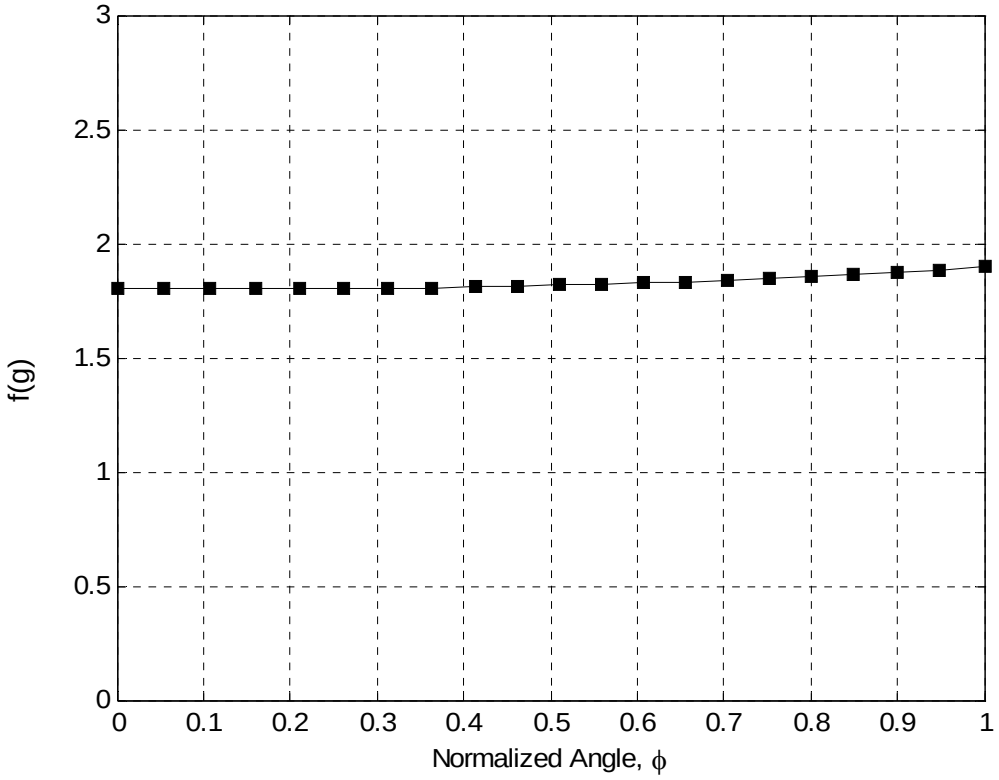

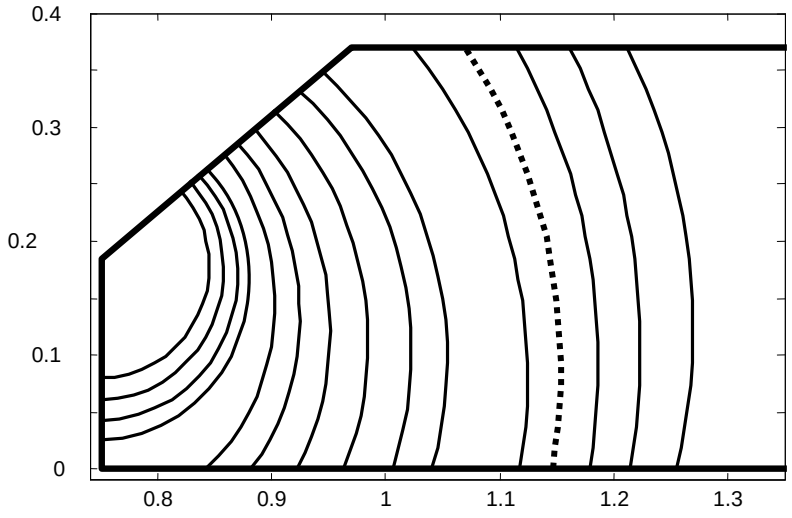

Figure A-13. Geometric Factors for FAA-17 (See table A-13)

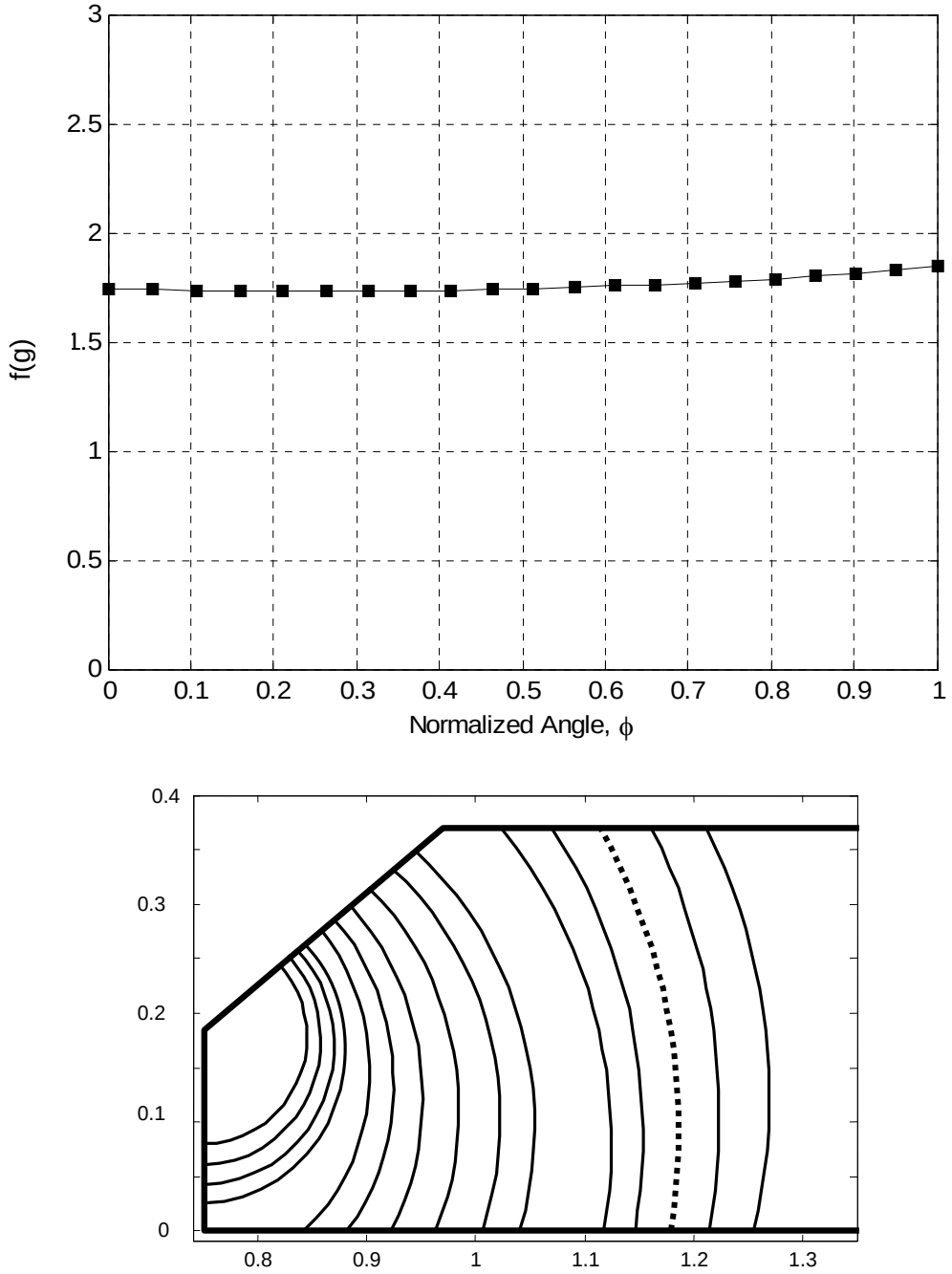

Figure A-14. Geometric Factors for FAA-17 (See table A-14)

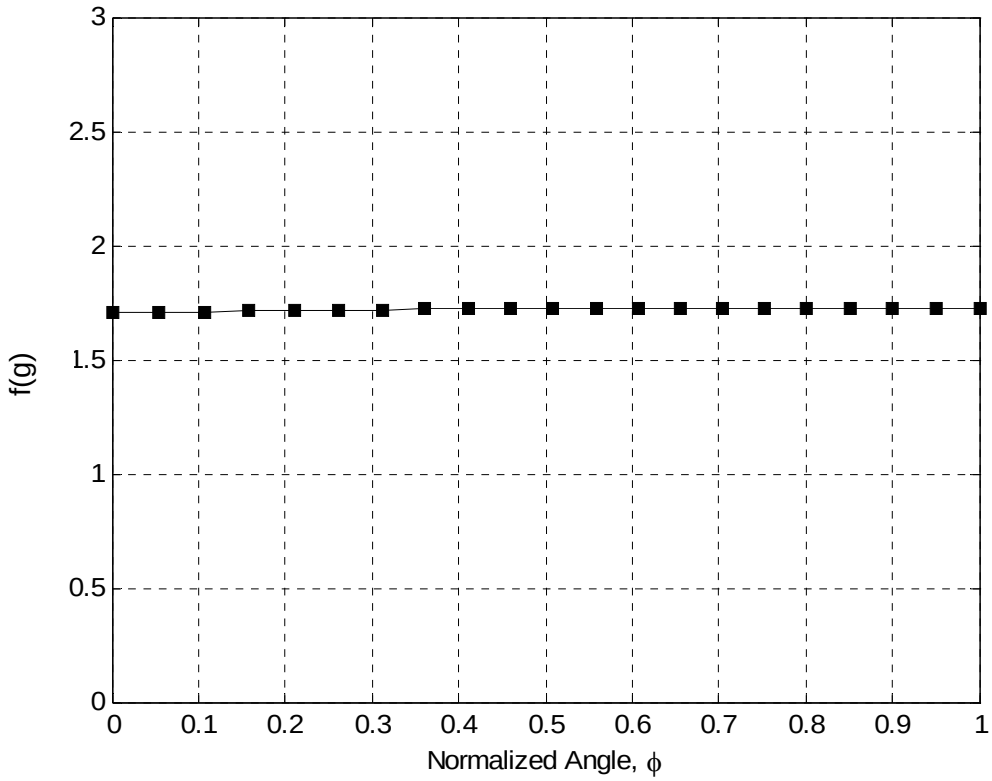

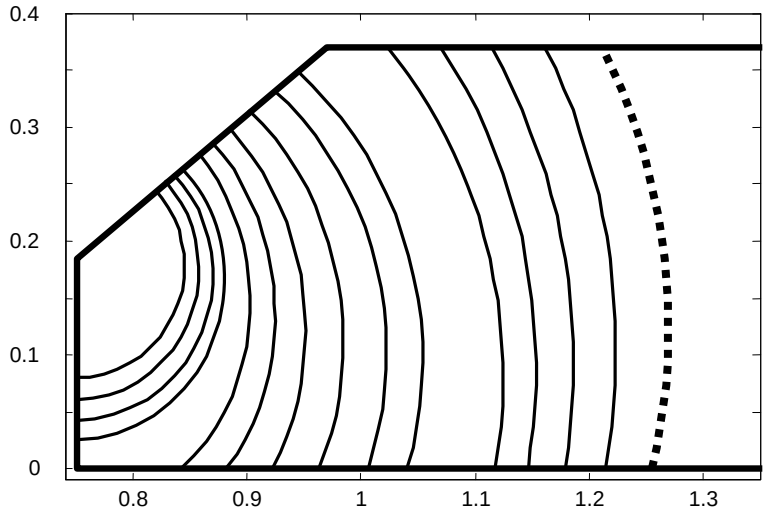

Figure A-15. Geometric Factors for FAA-17 (See table A-15)

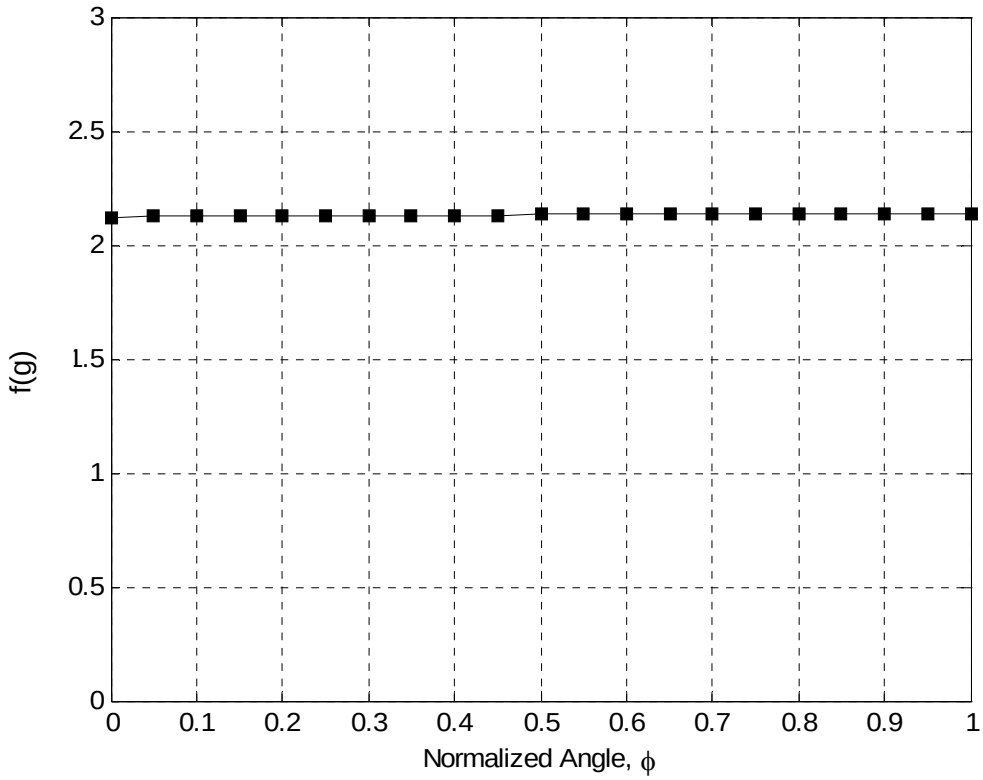

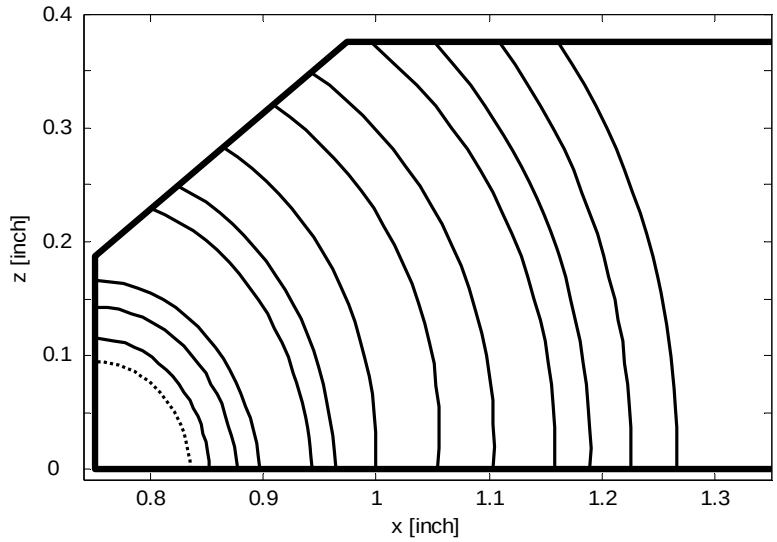

Figure A-16. Geometric Factors for FAA-18 (See table A-16)

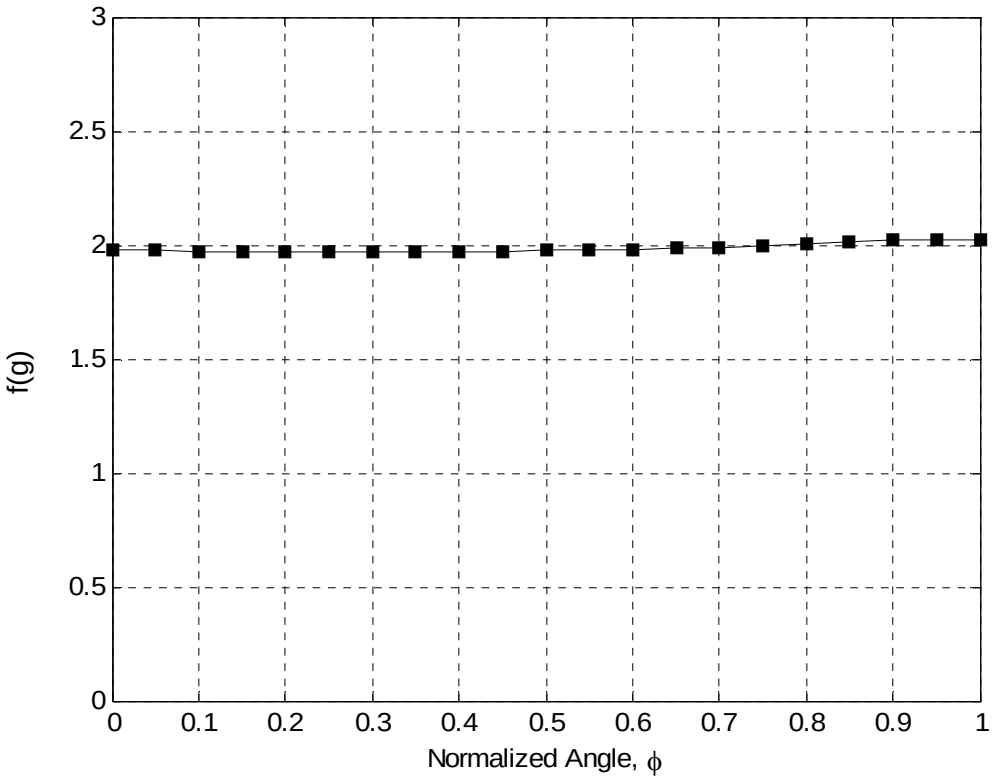

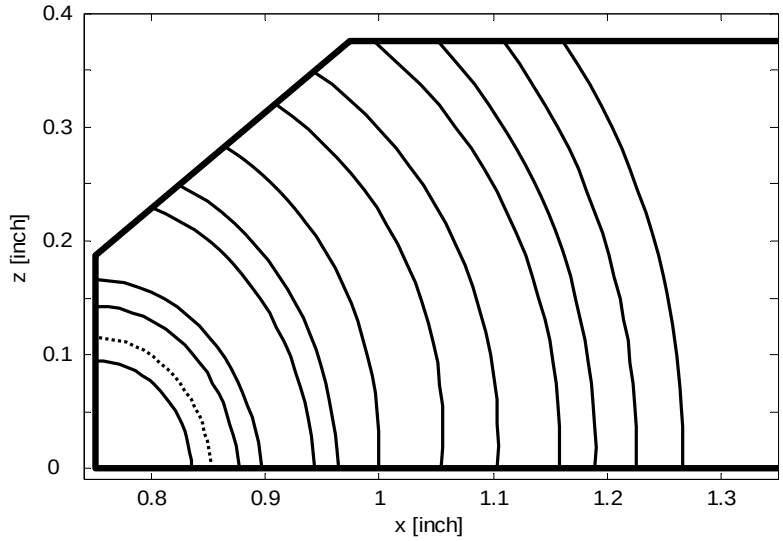

Figure A-17. Geometric Factors for FAA-18 (See table A-17)

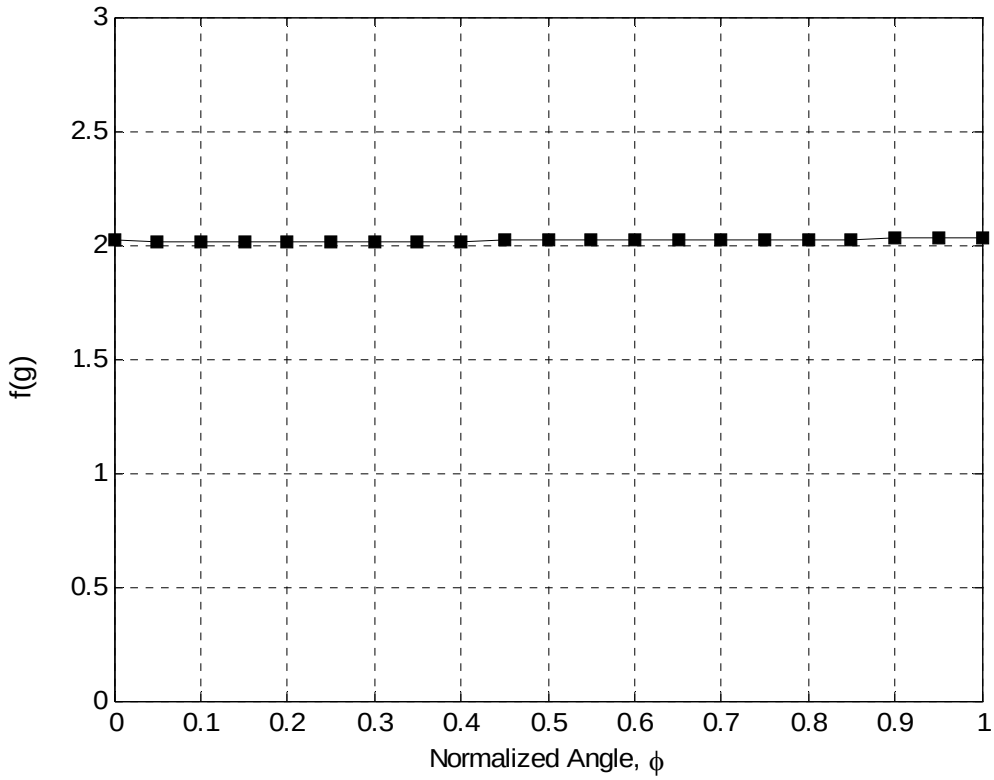

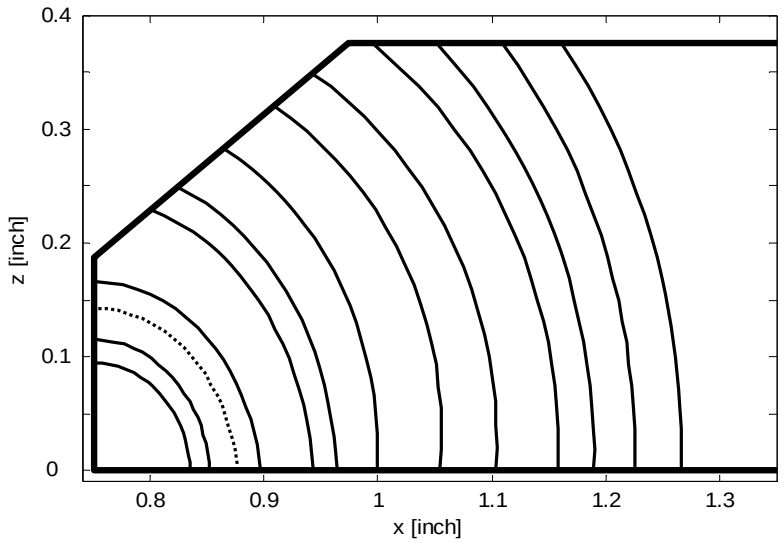

Figure A-18. Geometric Factors for FAA-18 (See table A-18)

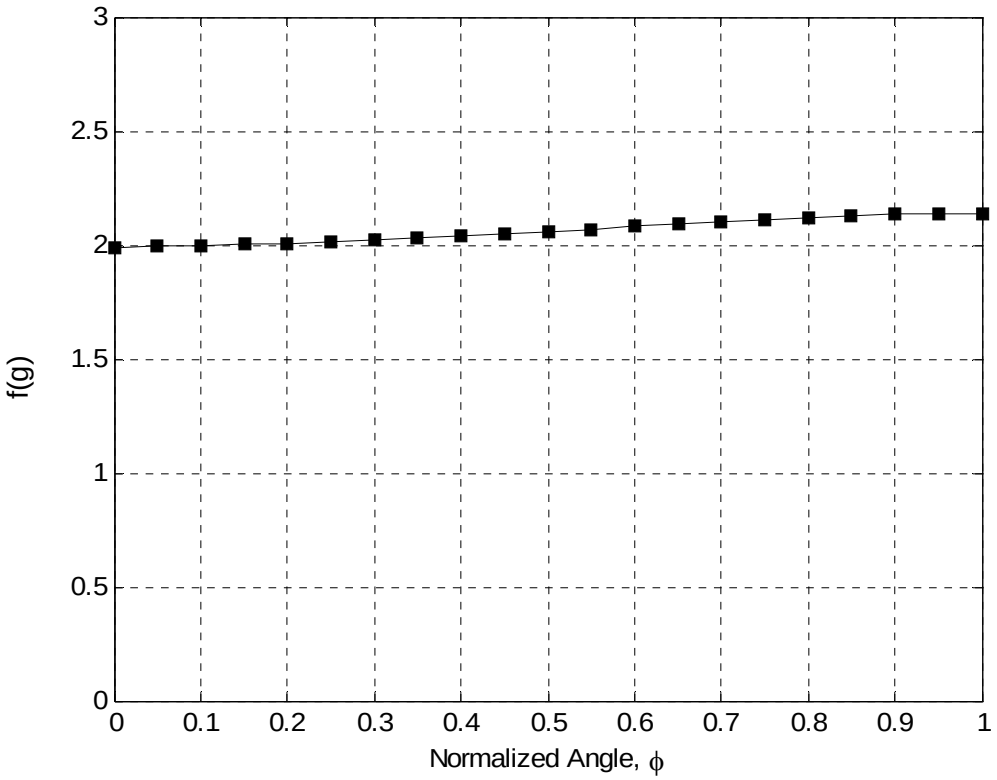

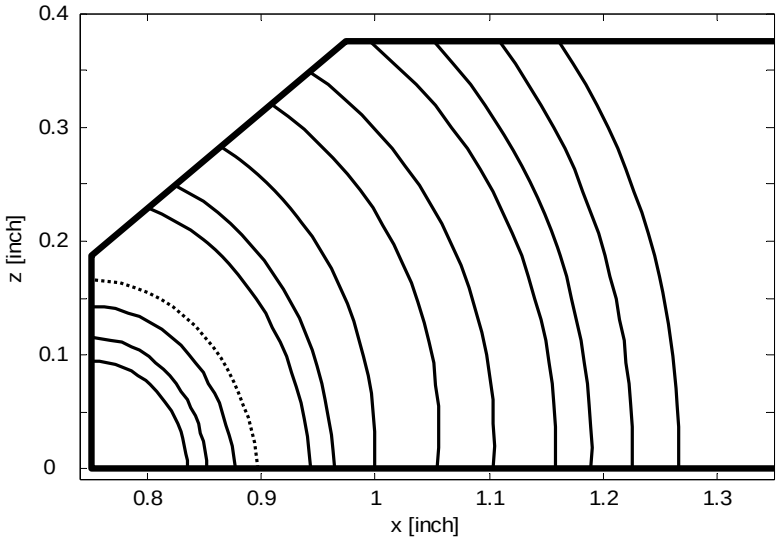

Figure A-19. Geometric Factors for FAA-18 (See table A-19)

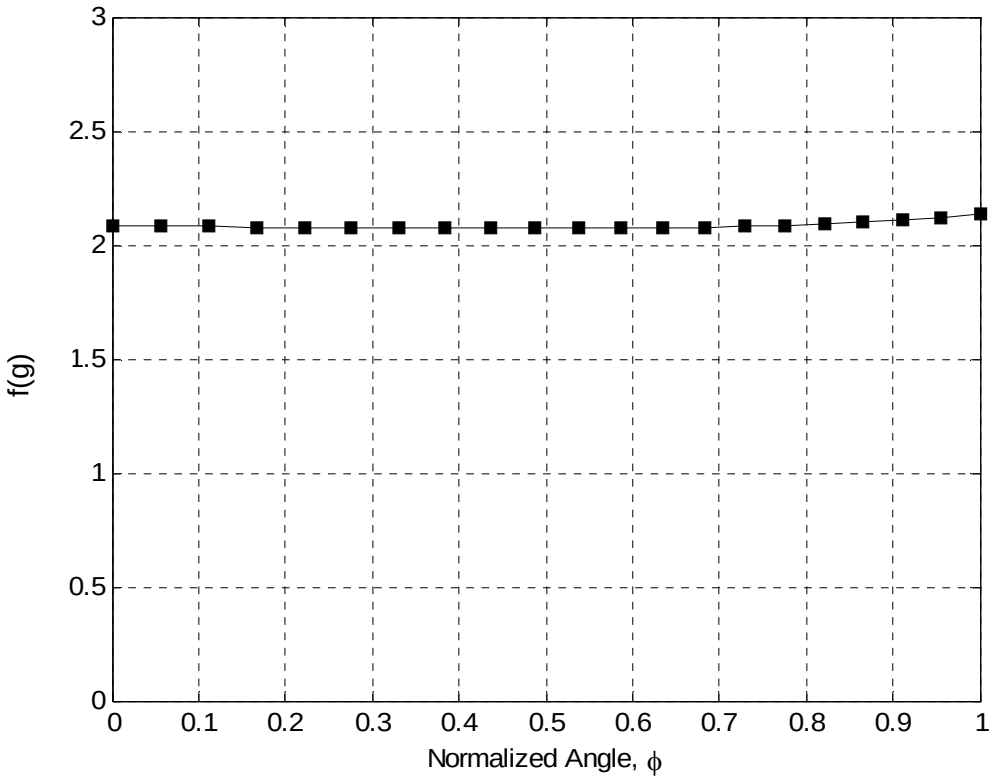

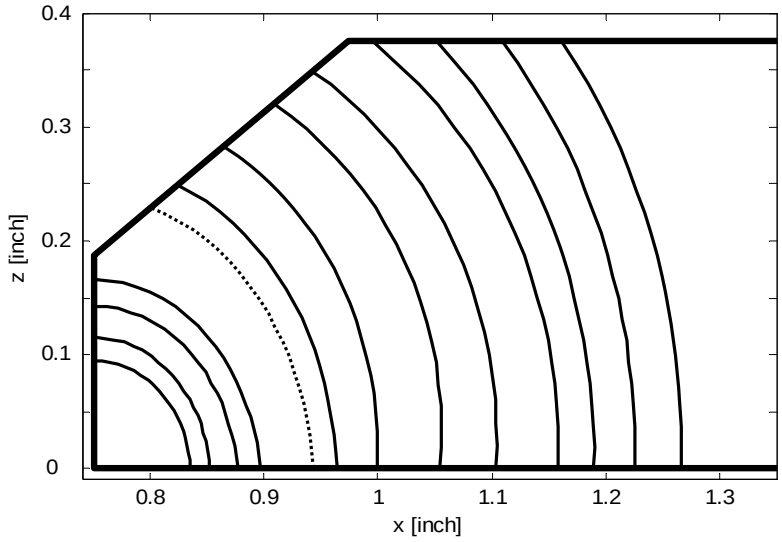

Figure A-20. Geometric Factors for FAA-18 (See table A-20)

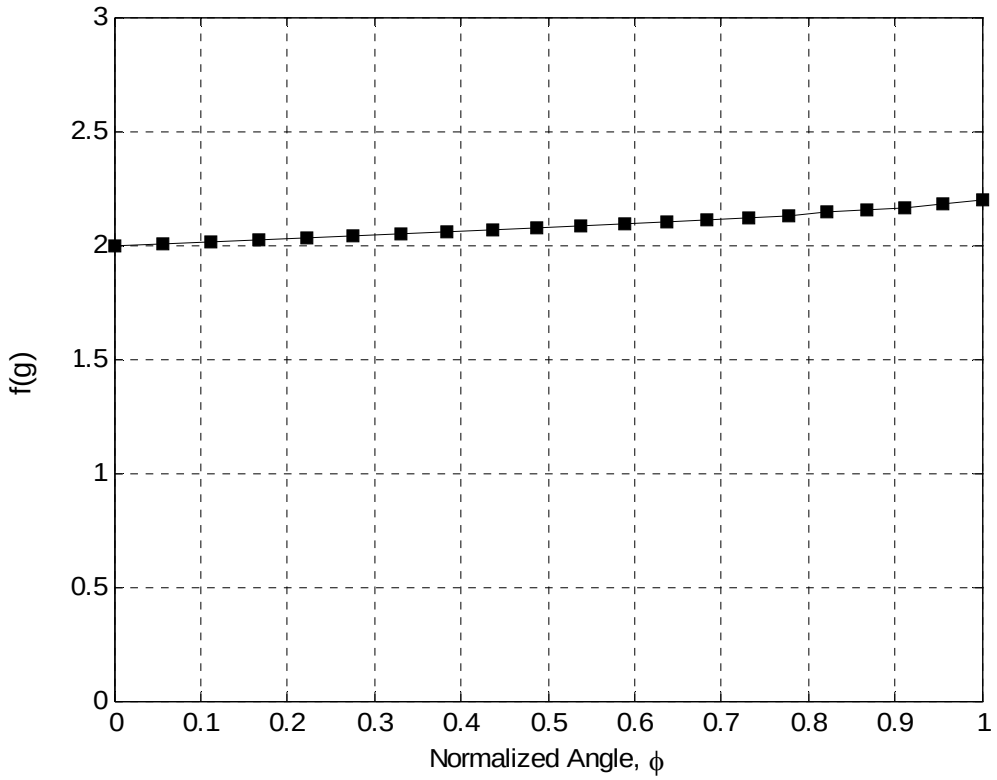

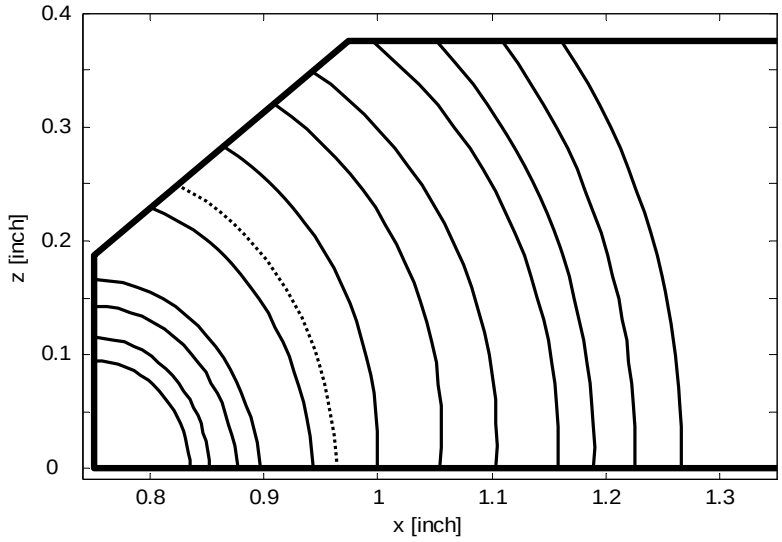

Figure A-21. Geometric Factors for FAA-18 (See table A-21)

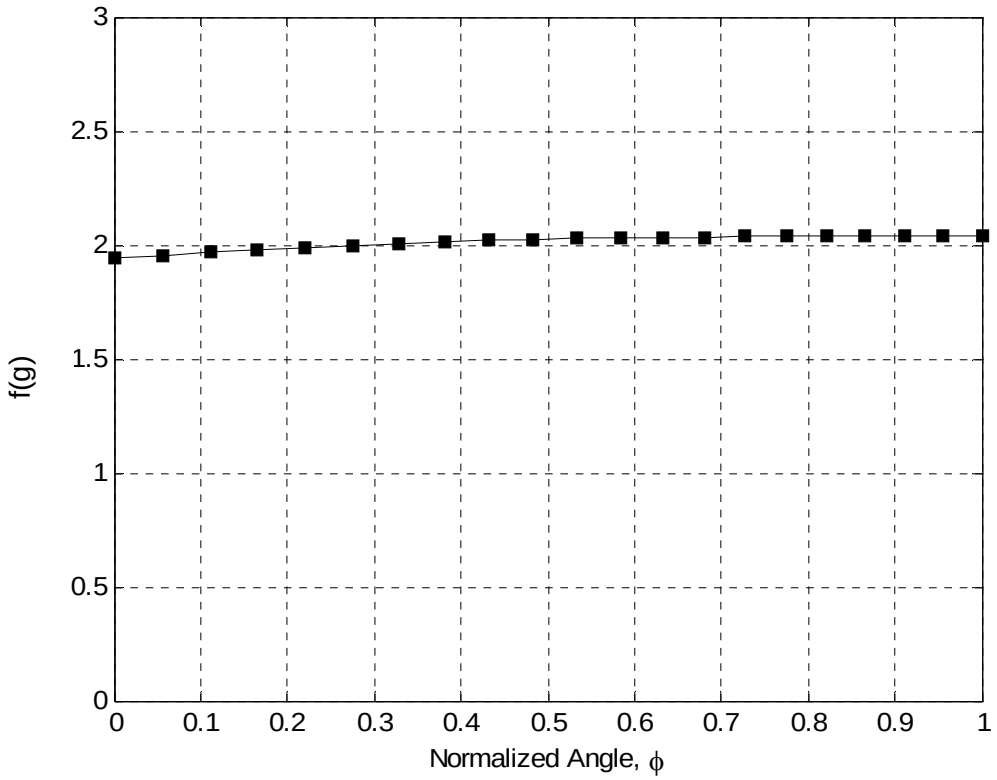

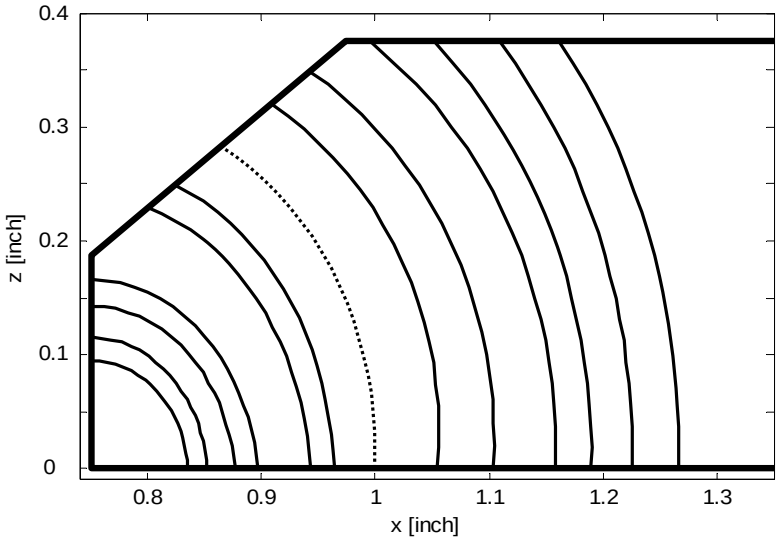

Figure A-22. Geometric Factors for FAA-18 (See table A-22)

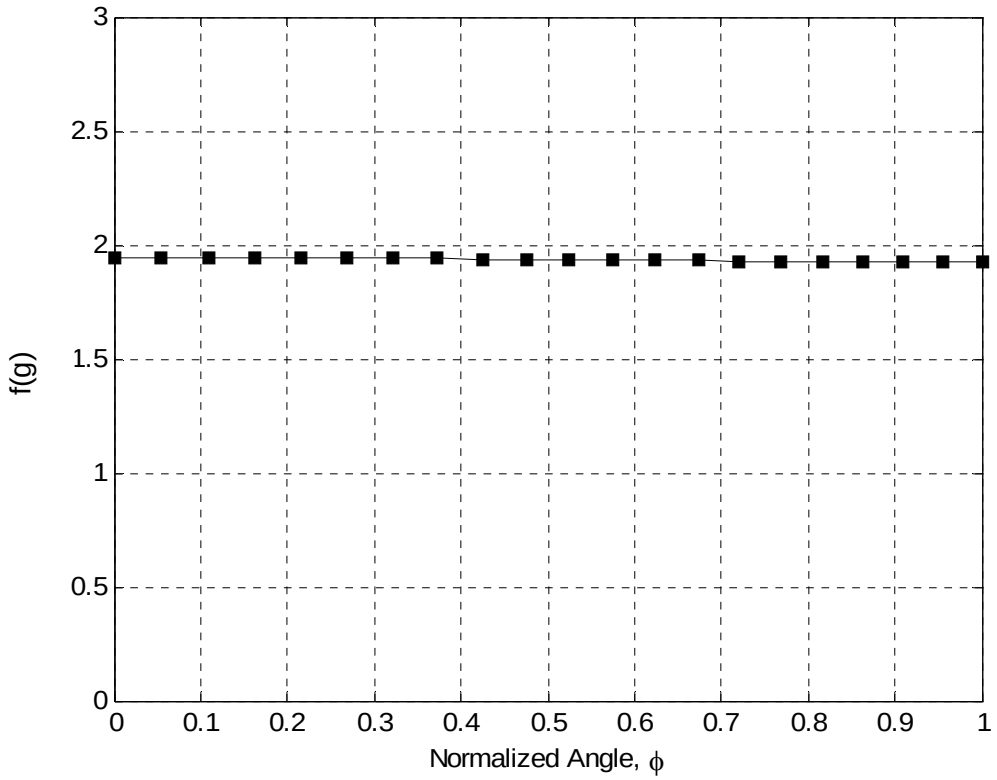

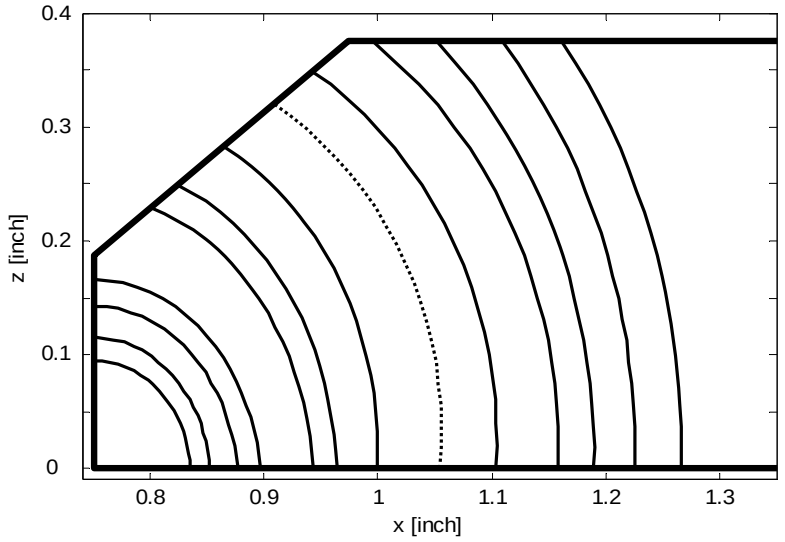

Figure A-23. Geometric Factors for FAA-18 (See table A-23)

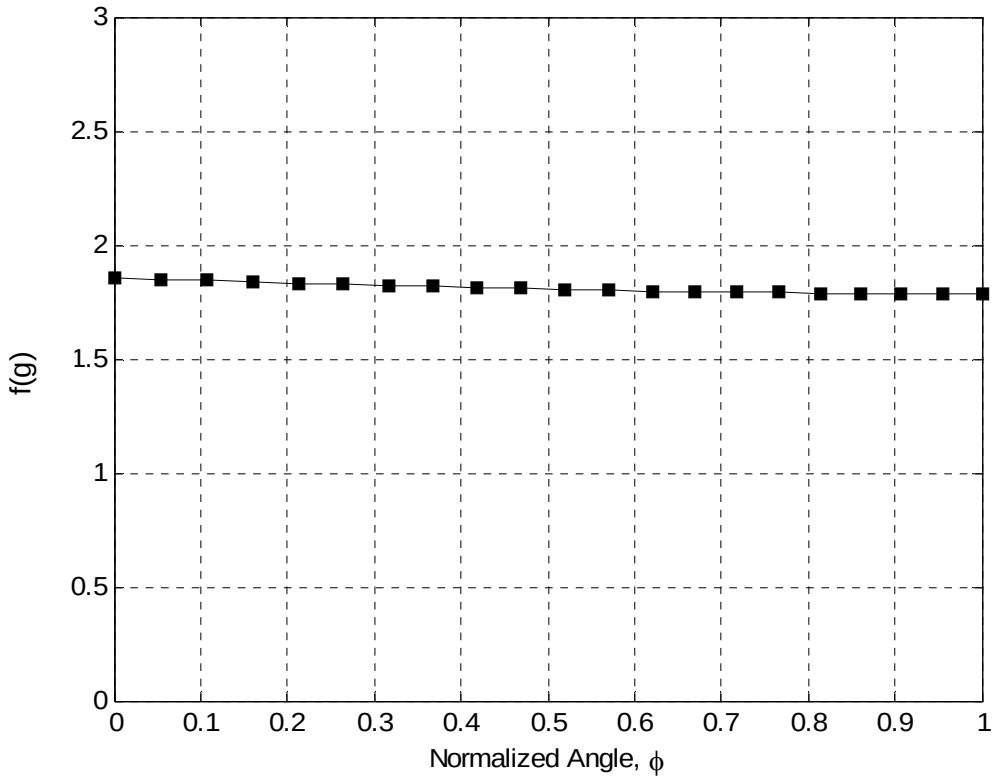

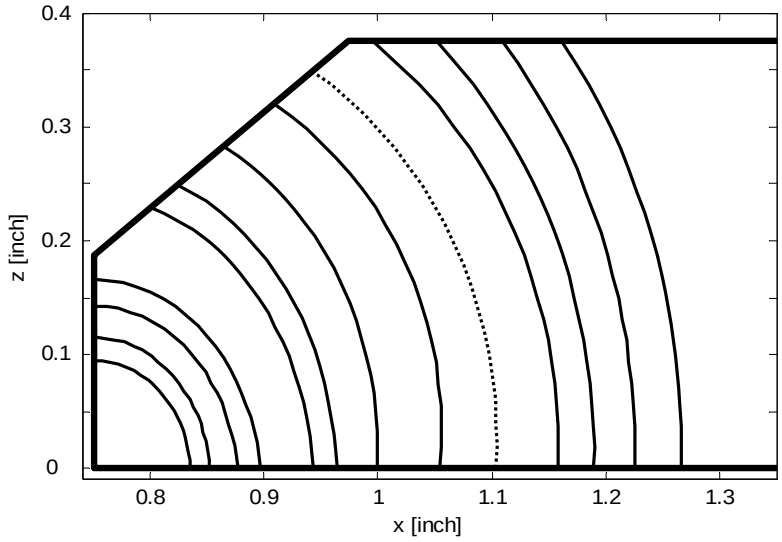

Figure A-24. Geometric Factors for FAA-18 (See table A-24)

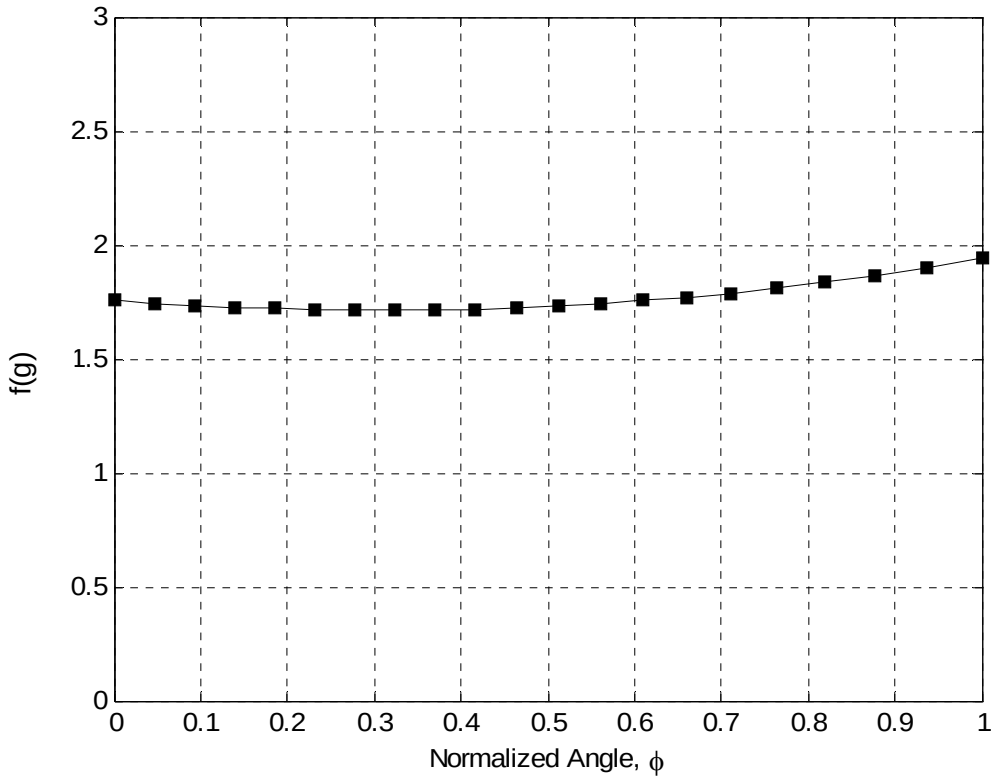

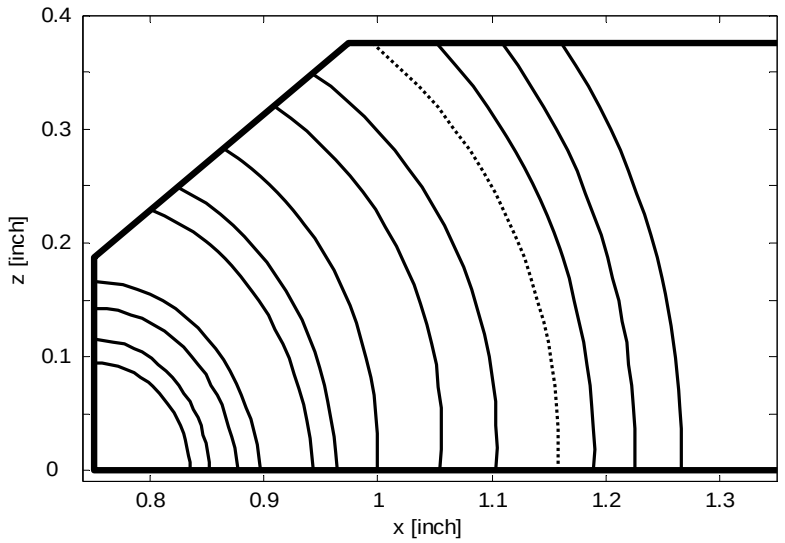

Figure A-25. Geometric Factors for FAA-18 (See table A-25)

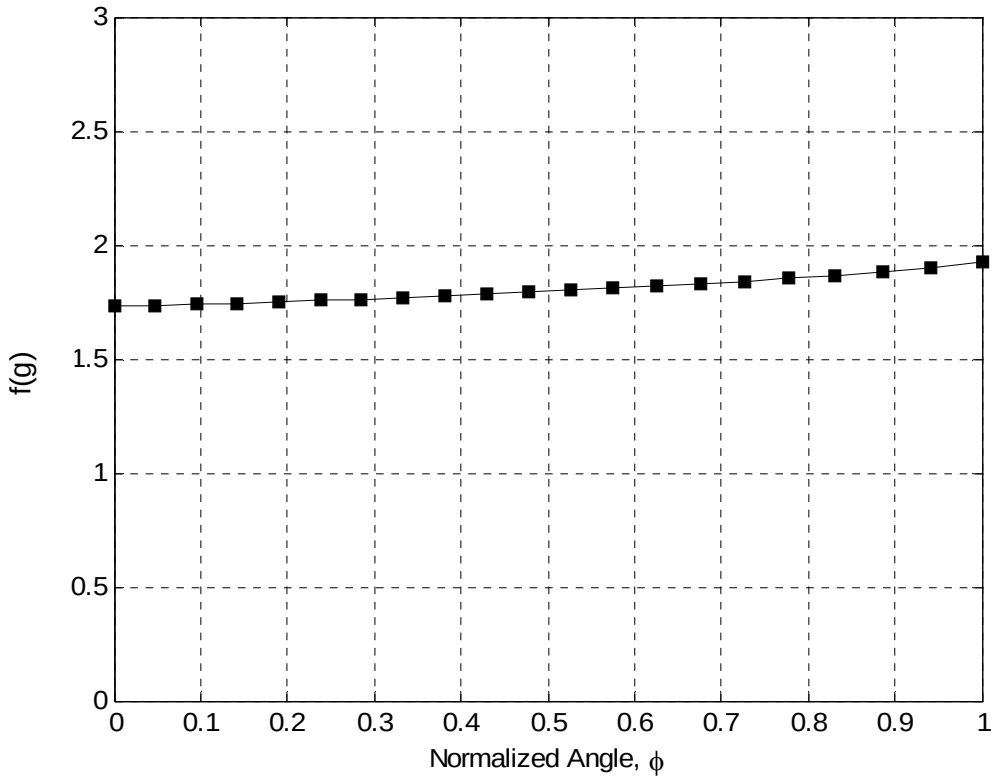

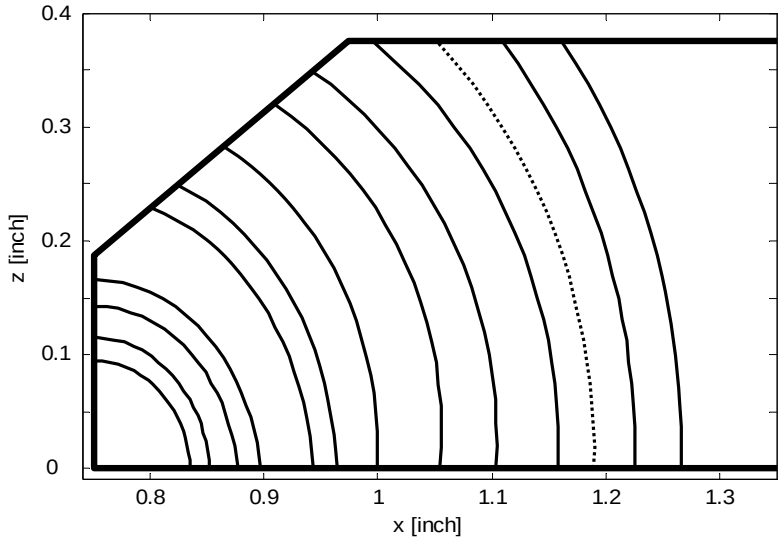

Figure A-26. Geometric Factors for FAA-18 (See table A-26)

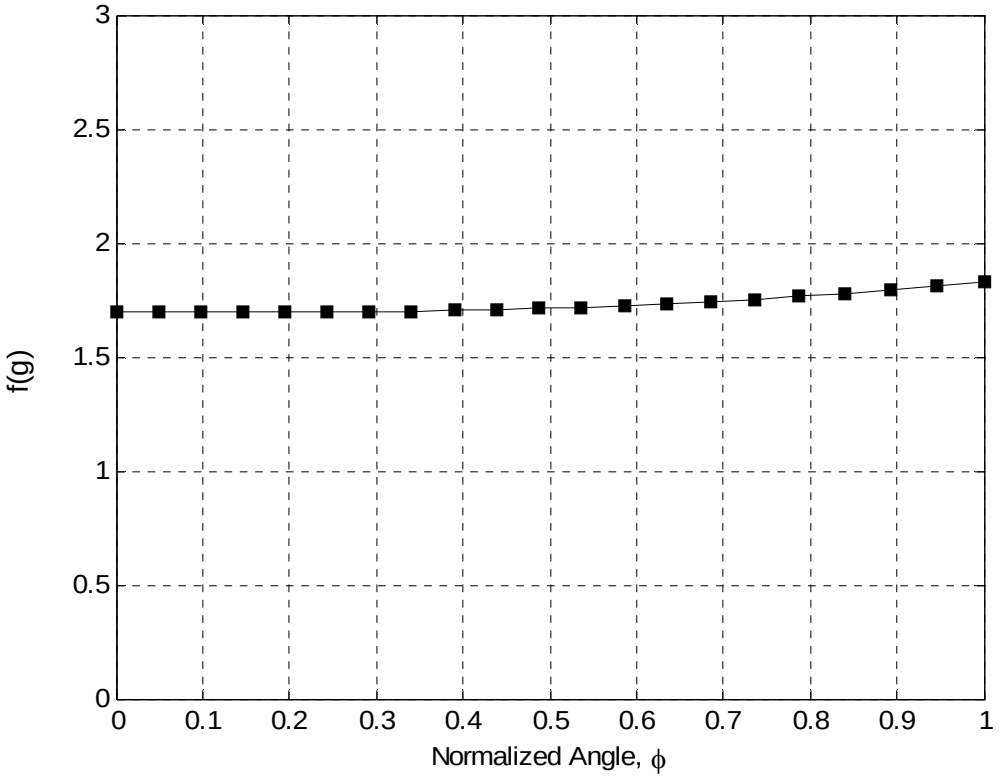

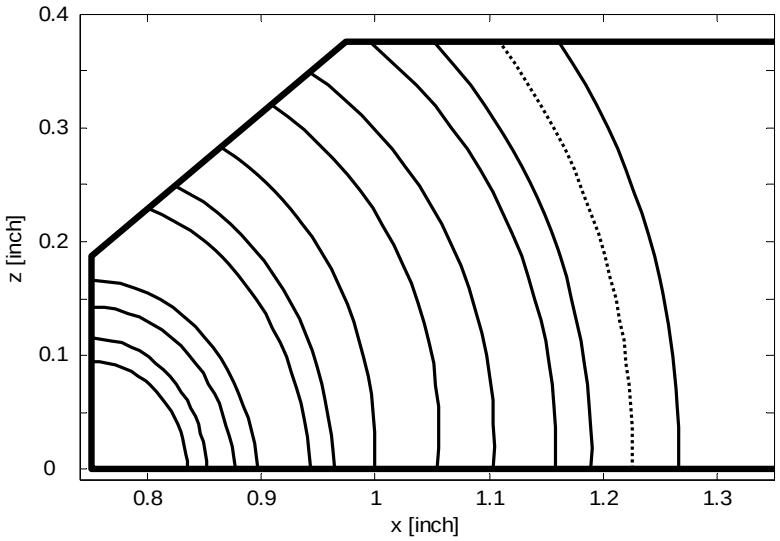

Figure A-27. Geometric Factors for FAA-18 (See table A-27)

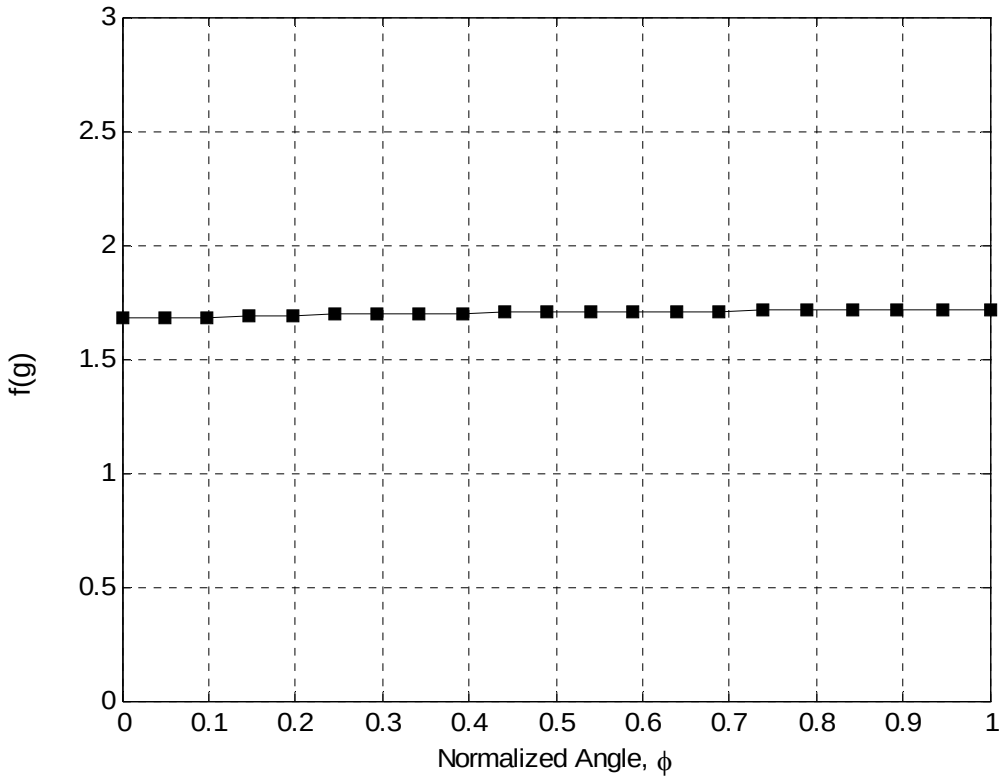

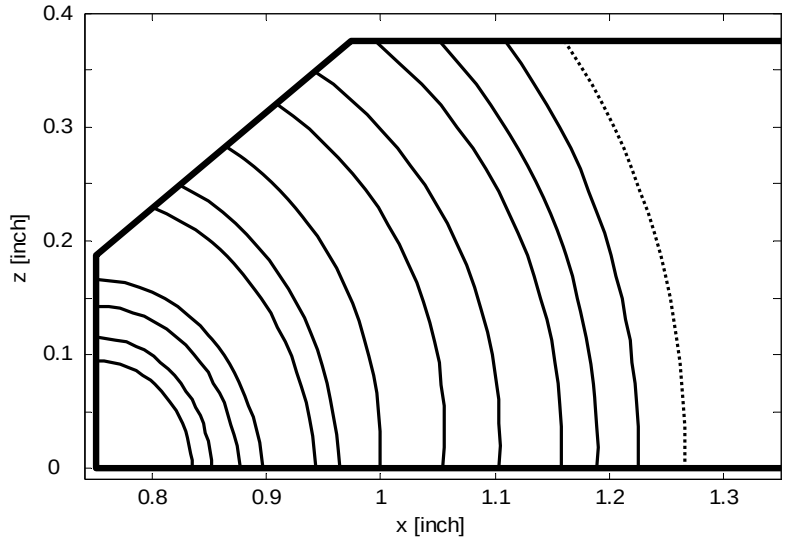

Figure A-28. Geometric Factors for FAA-18 (See table A-28)

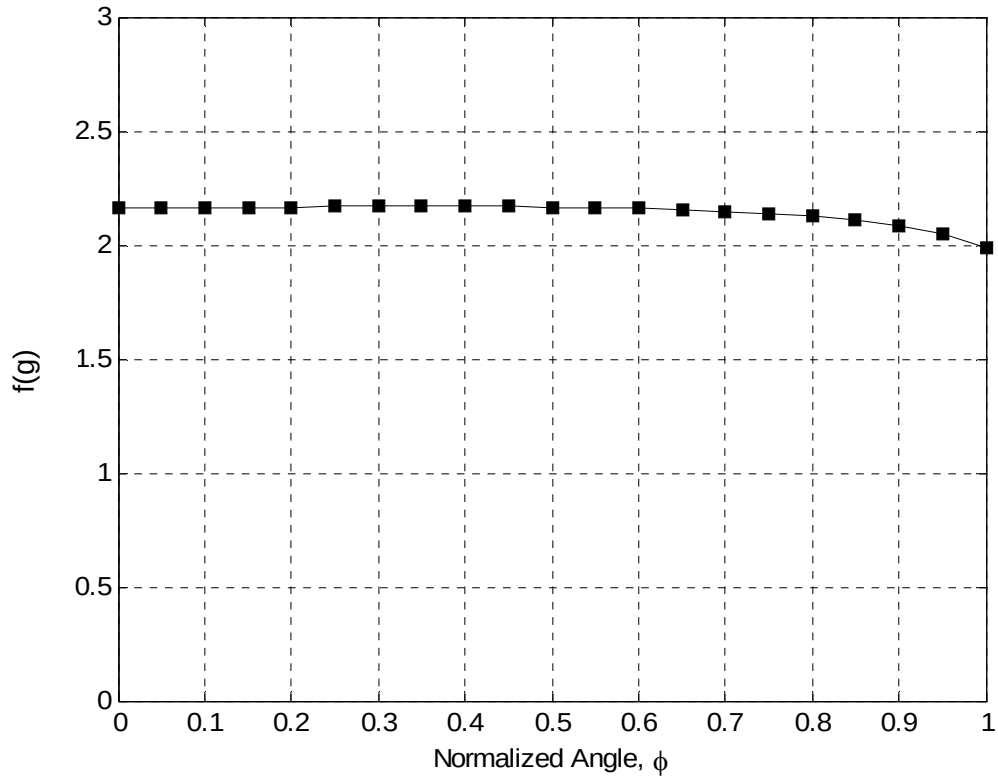

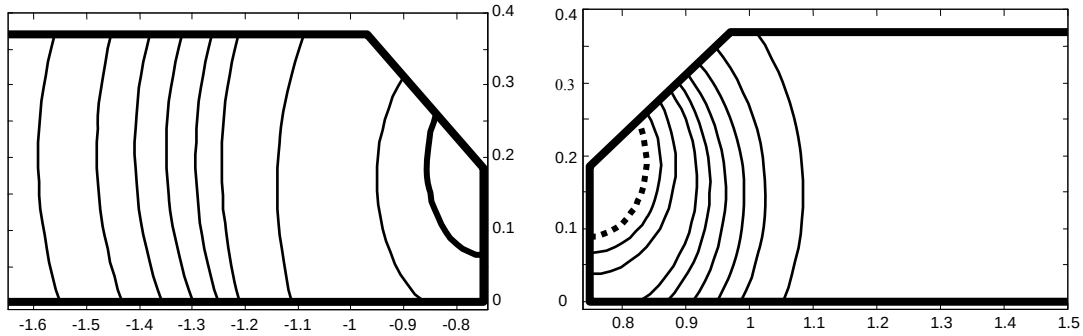

Figure A-29. Geometric Factors for FAA-19 (See table A-29)

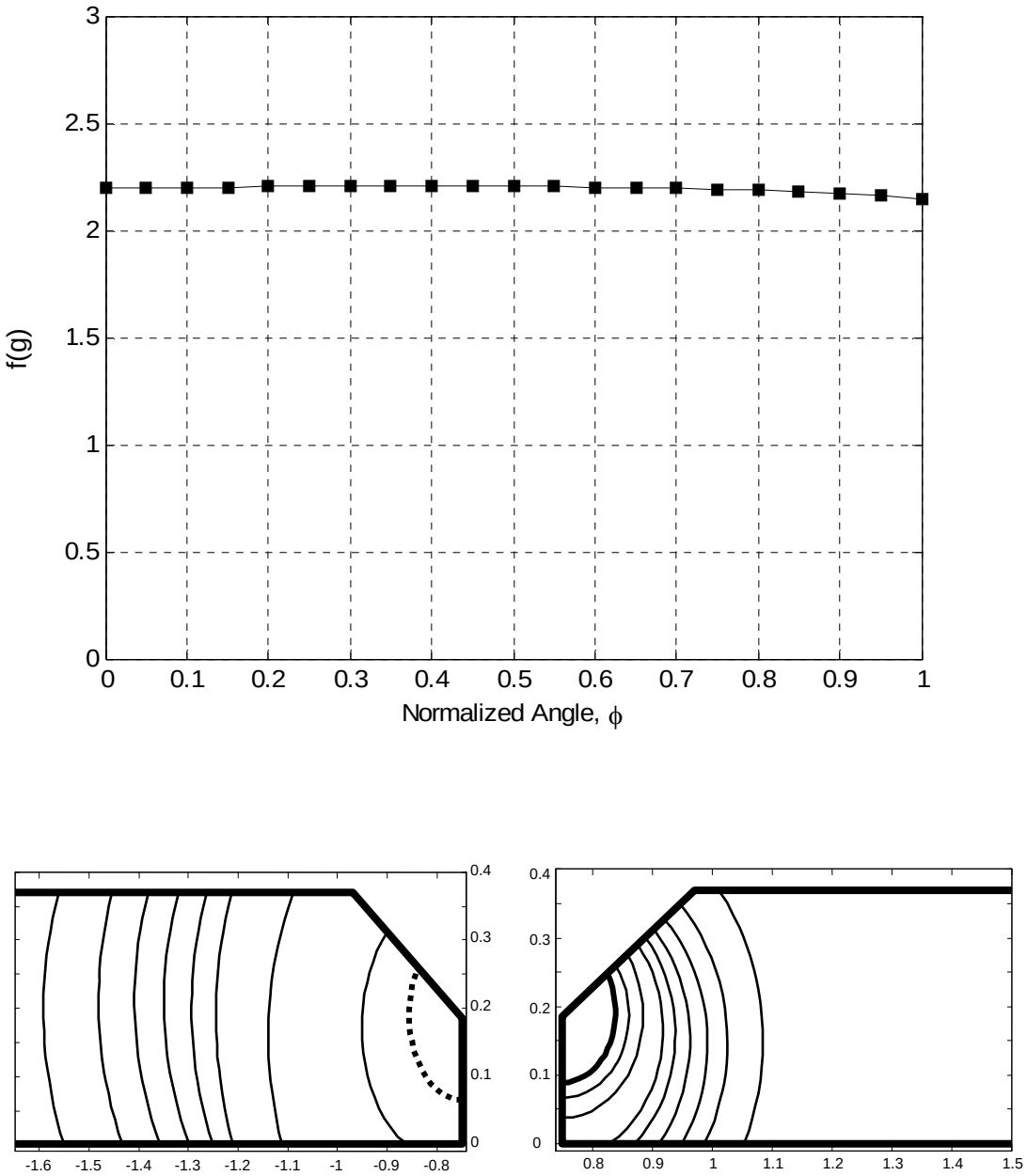

Figure A-30. Geometric Factors for FAA-19 (See table A-30)

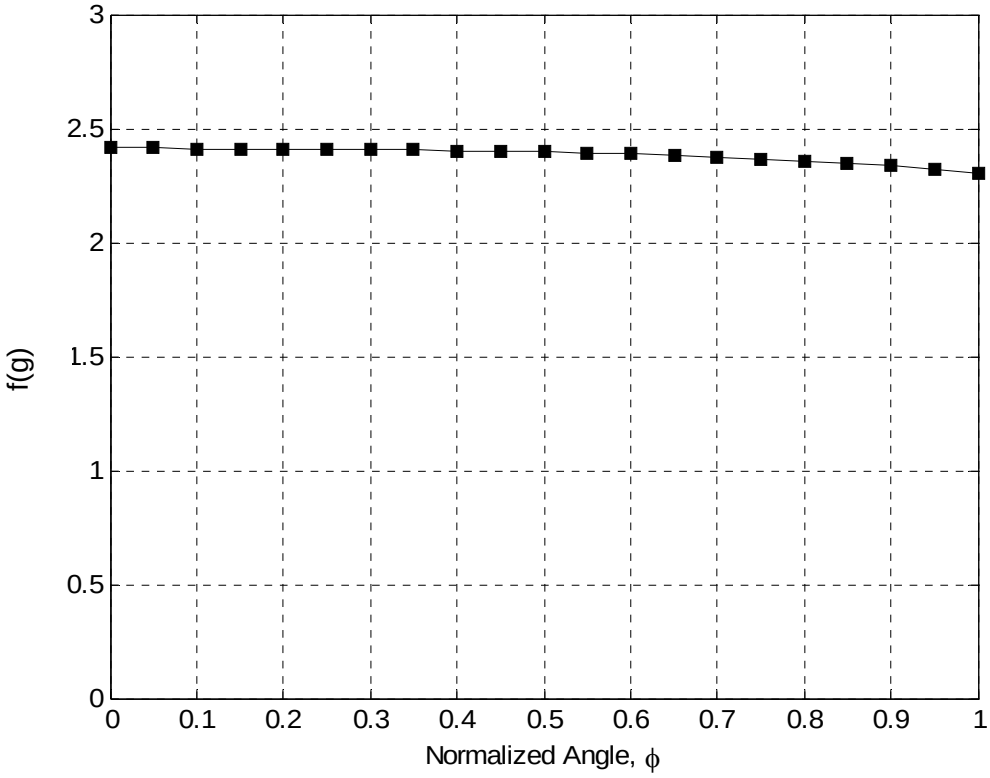

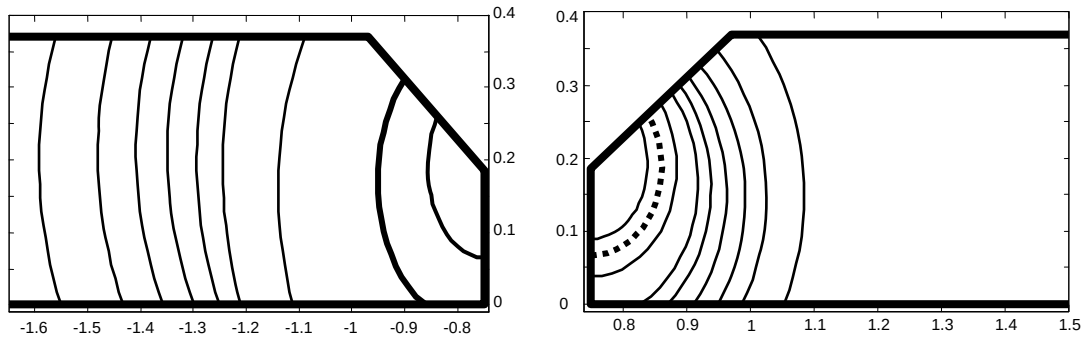

Figure A-31. Geometric Factors for FAA-19 (See table A-31)

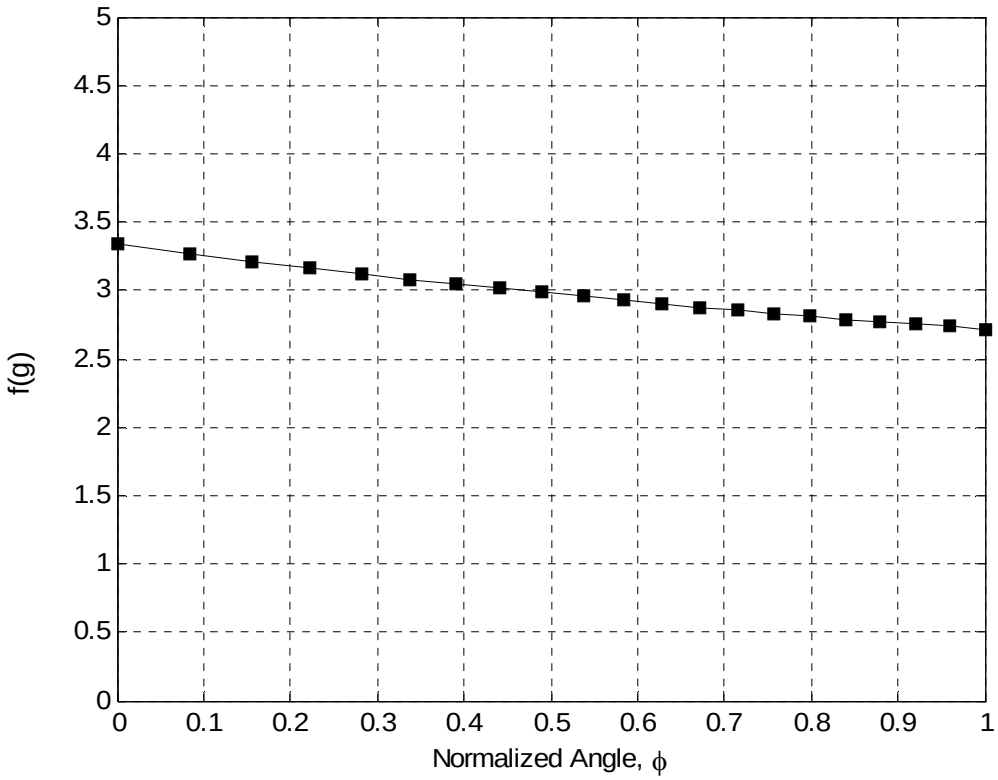

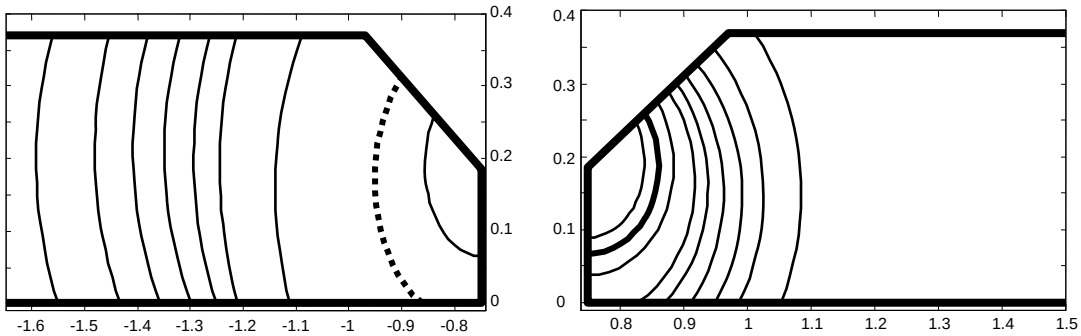

Figure A-32. Geometric Factors for FAA-19 (See table A-32)

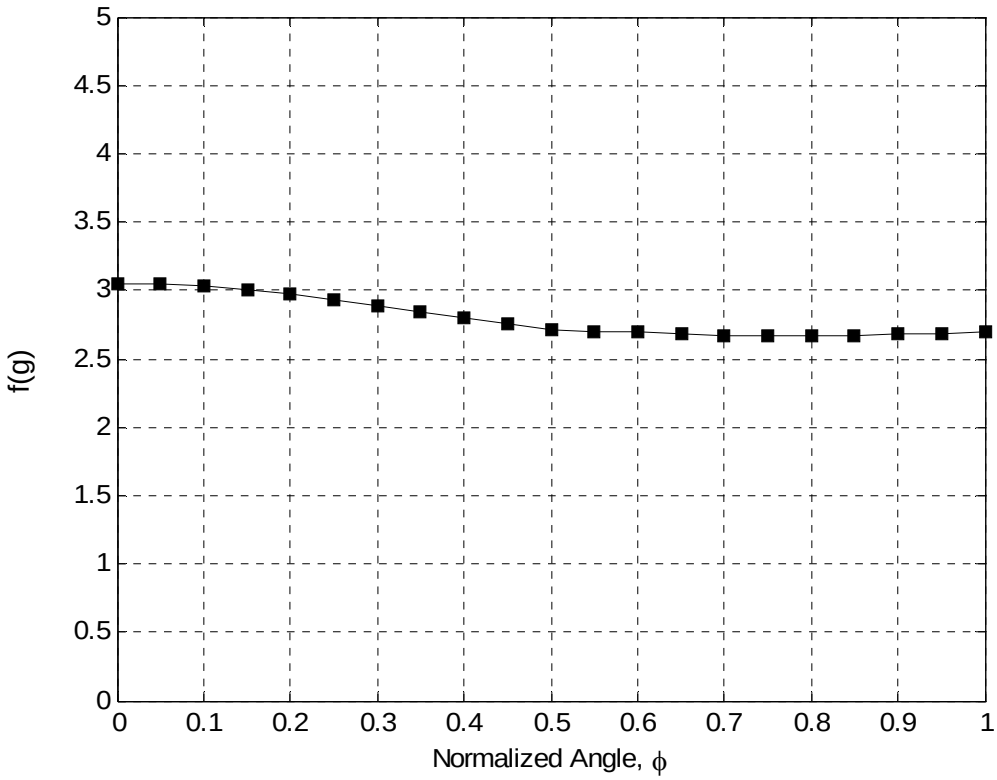

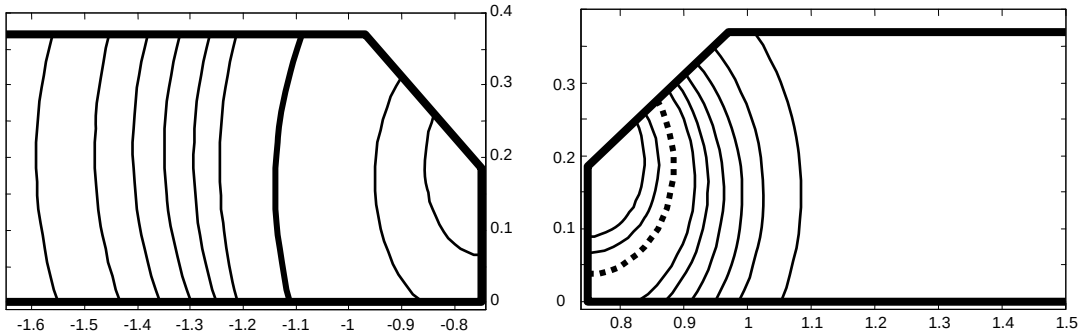

Figure A-33. Geometric Factors for FAA-19 (See table A-33)

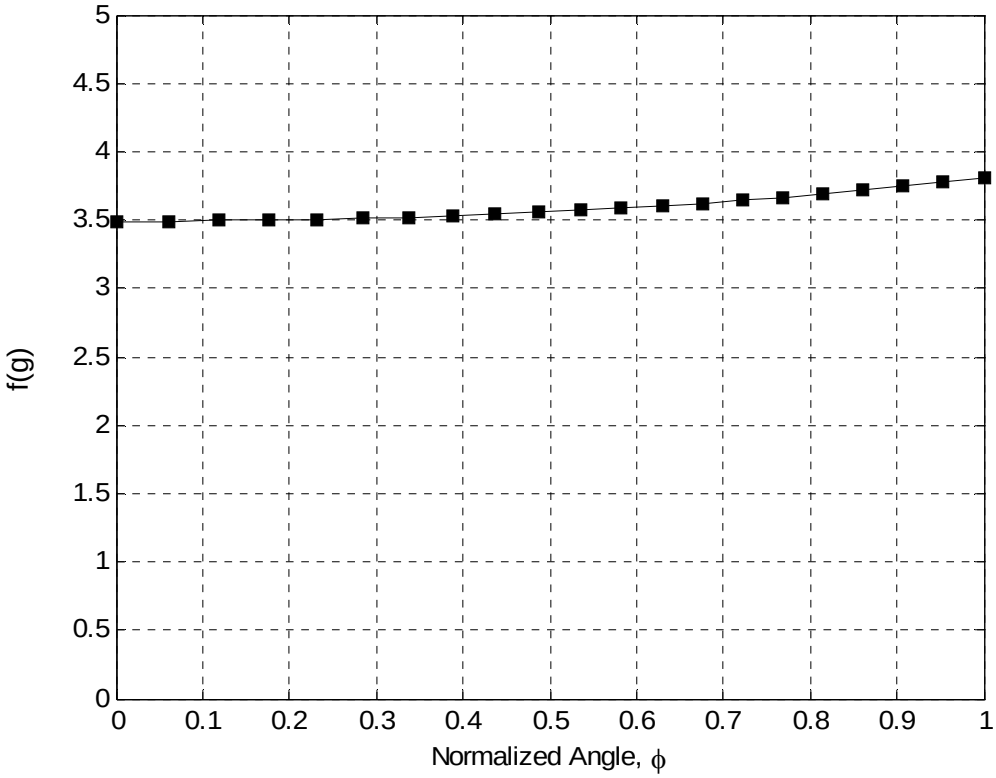

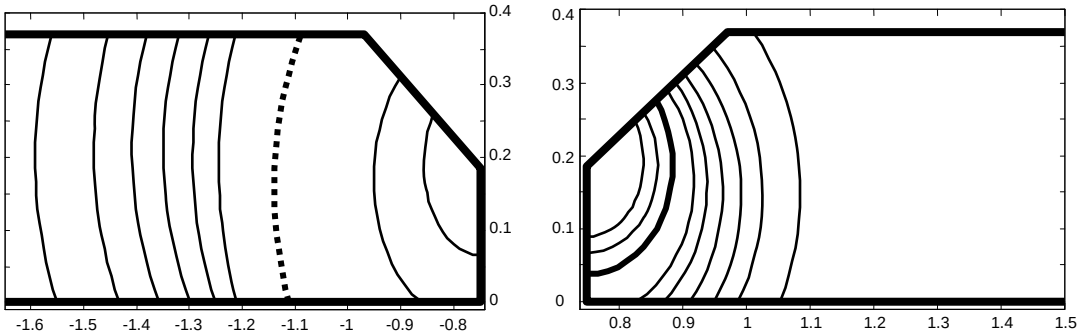

Figure A-34. Geometric Factors for FAA-19 (See table A-34)

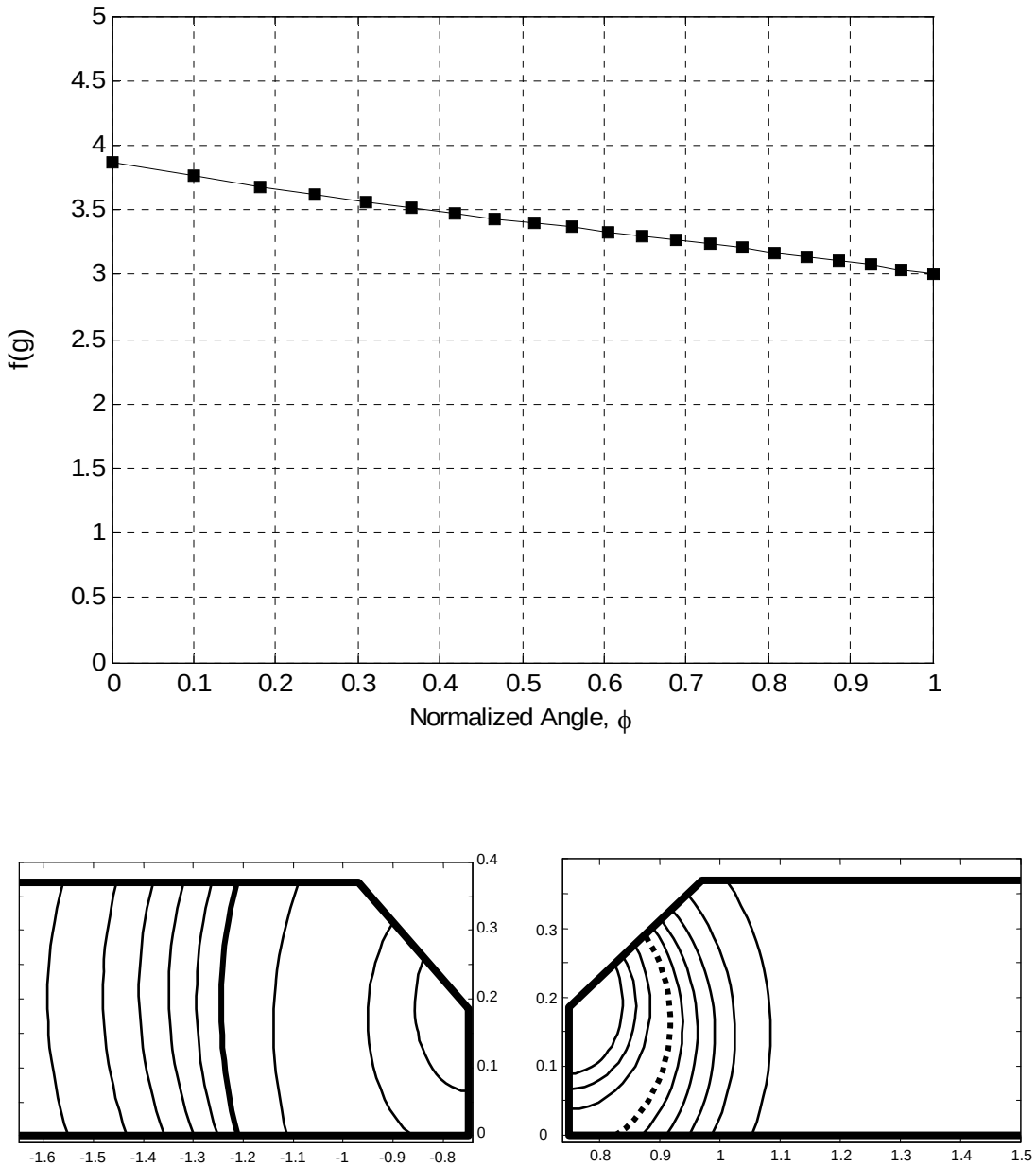

Figure A-35. Geometric Factors for FAA-19 (See table A-35)

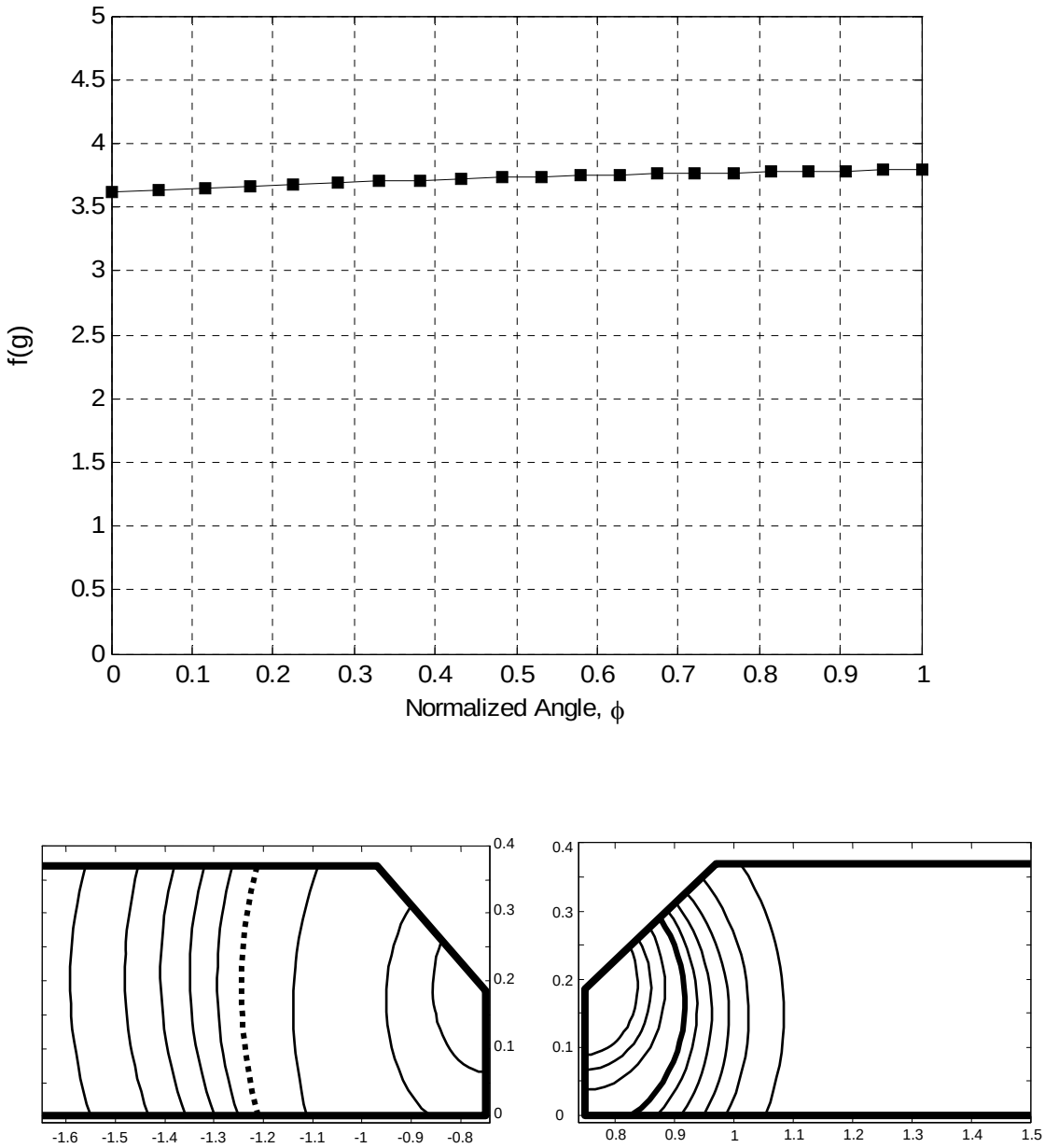

Figure A-36. Geometric Factors for FAA-19 (See table A-36)

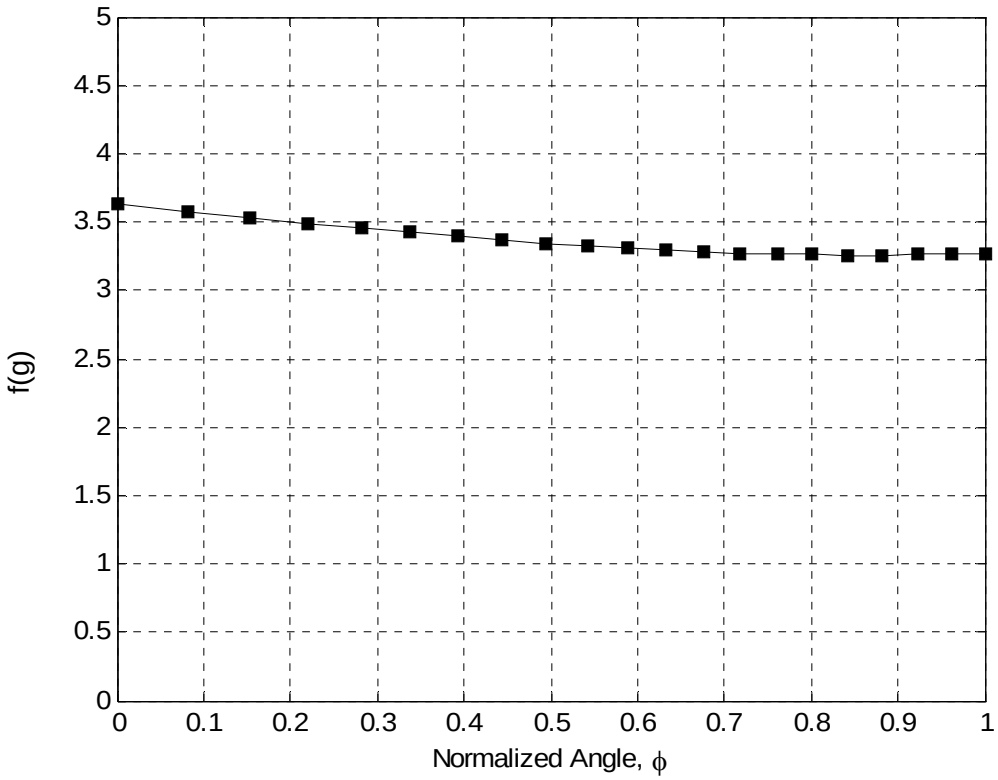

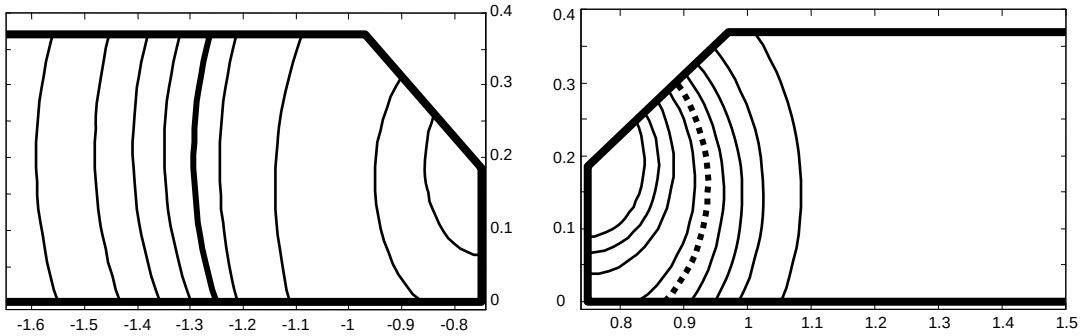

Figure A-37. Geometric Factors for FAA-19 (See table A-37)

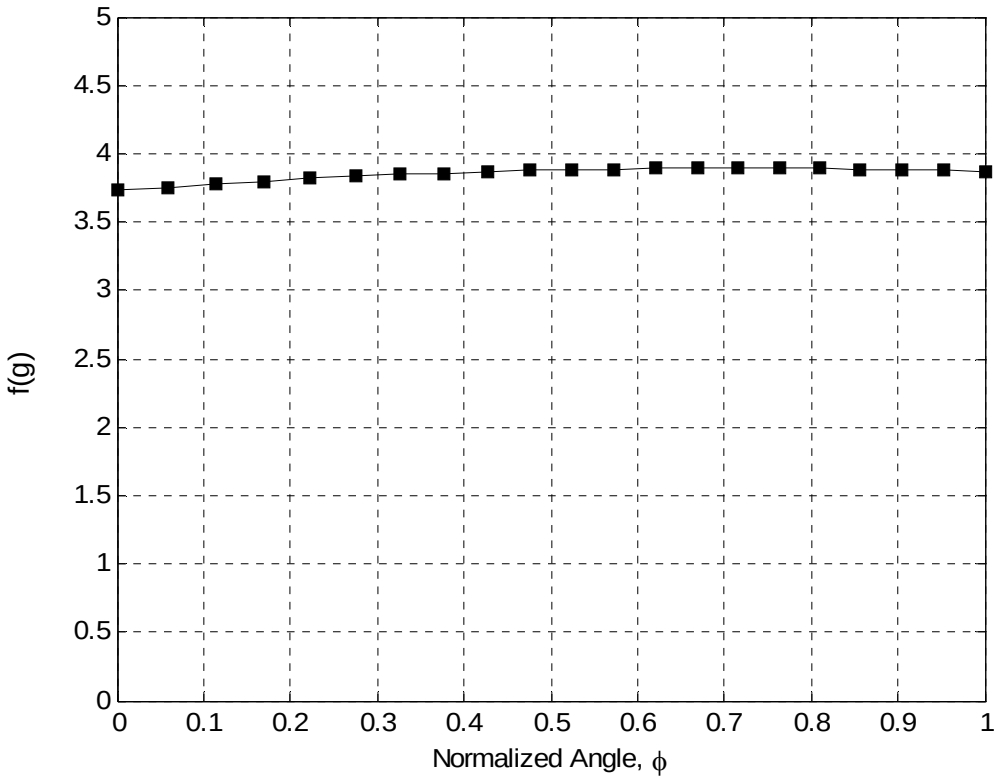

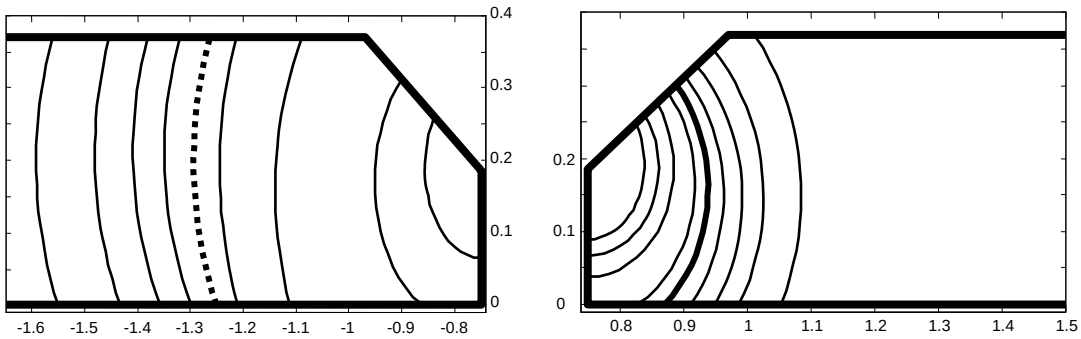

Figure A-38. Geometric Factors for FAA-19 (See table A-38)

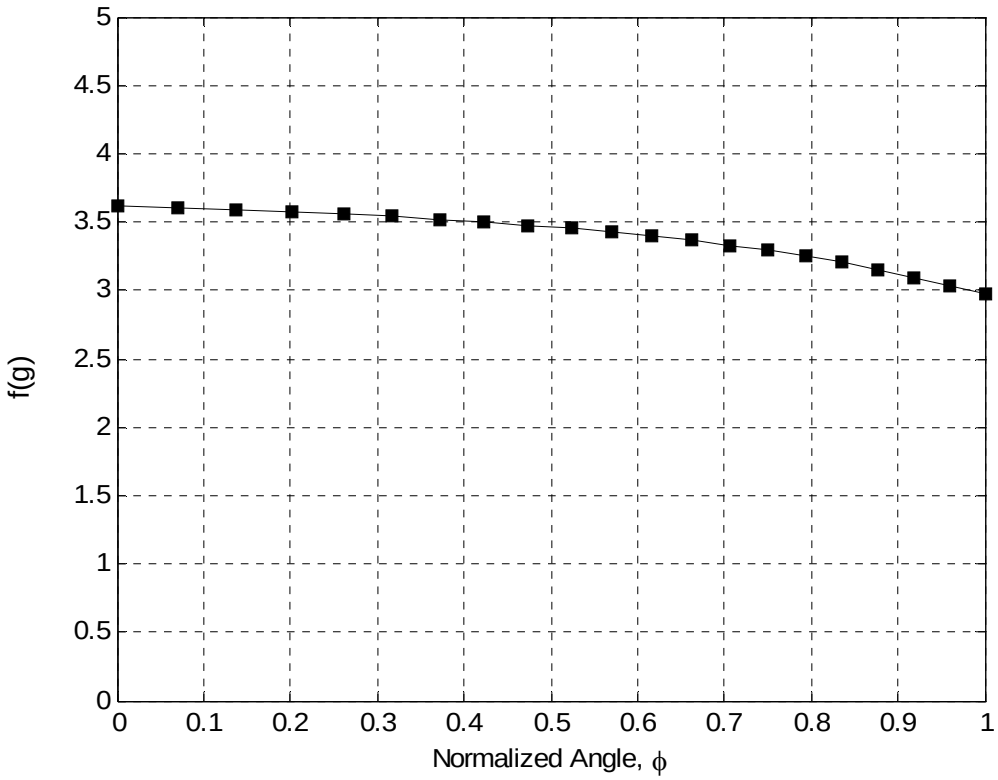

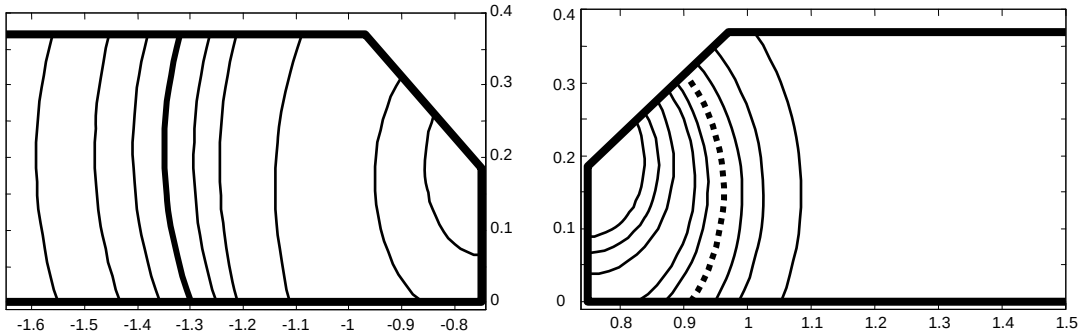

Figure A-39. Geometric Factors for FAA-19 (See table A-39)

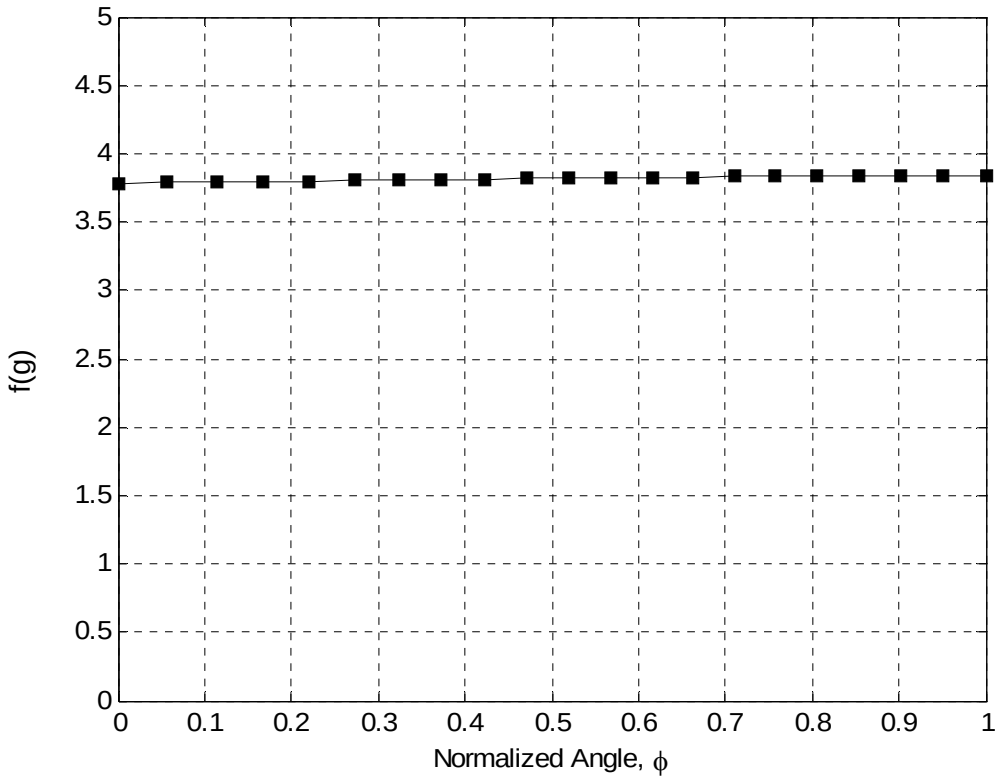

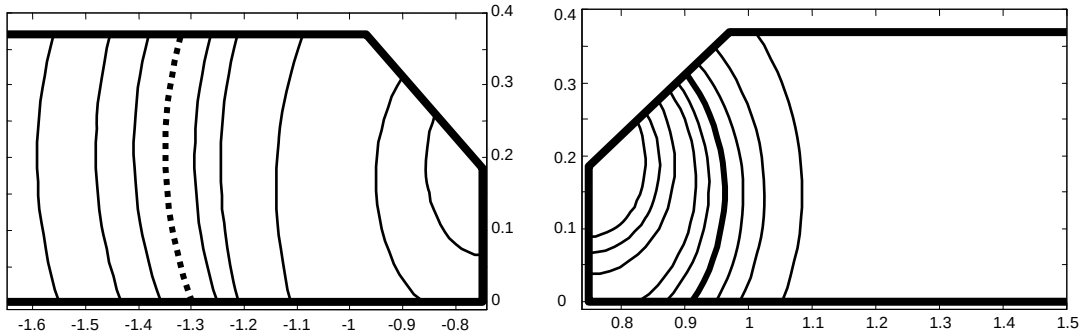

Figure A-40. Geometric Factors for FAA-19 (See table A-40)

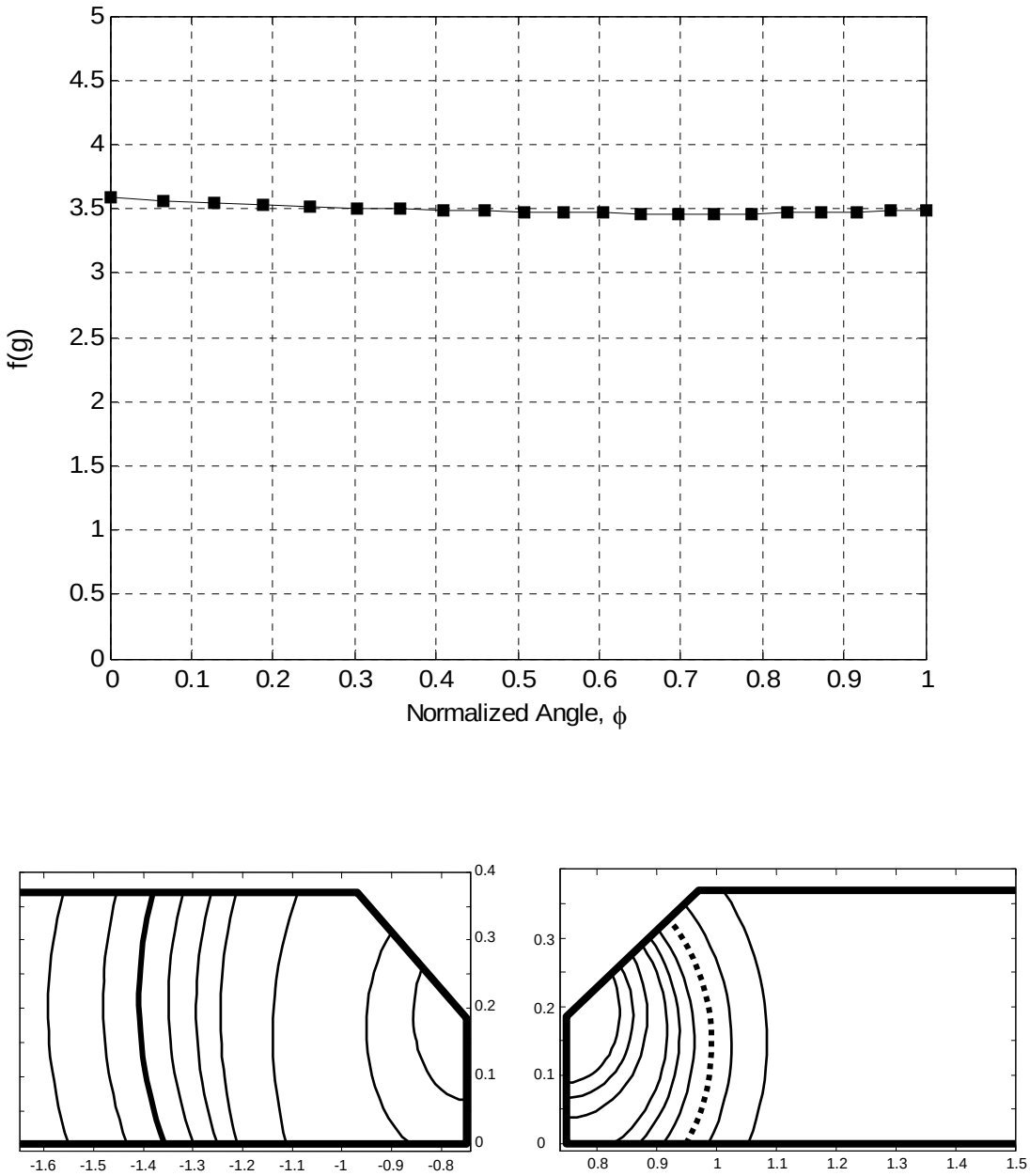

Figure A-41. Geometric Factors for FAA-19 (See table A-41)

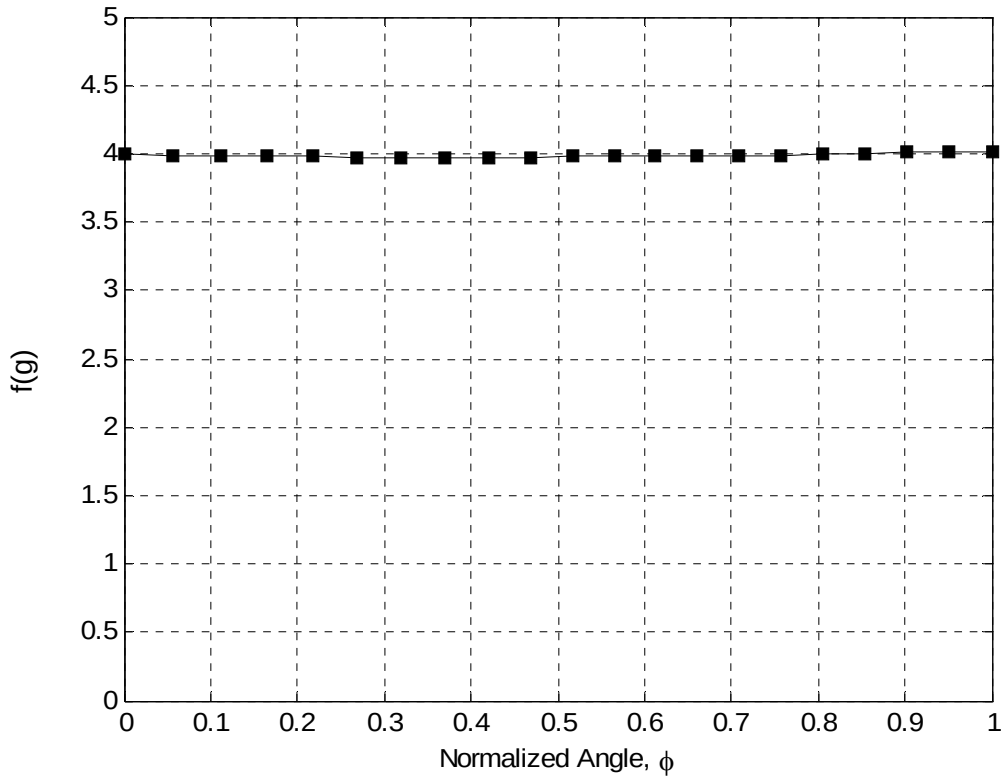

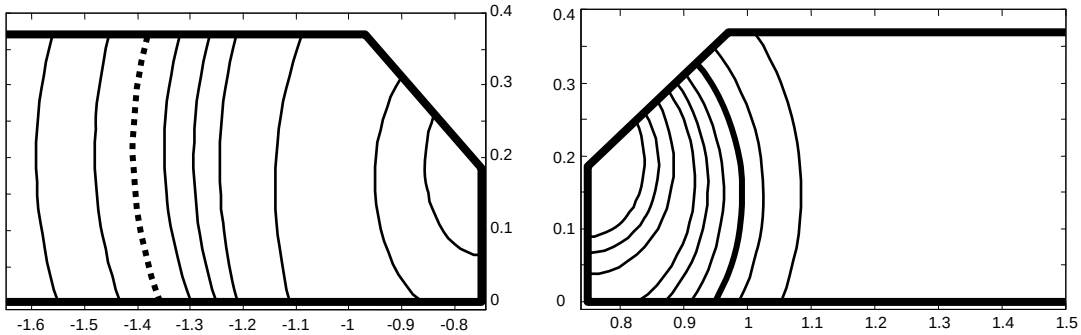

Figure A-42. Geometric Factors for FAA-19 (See table A-42)

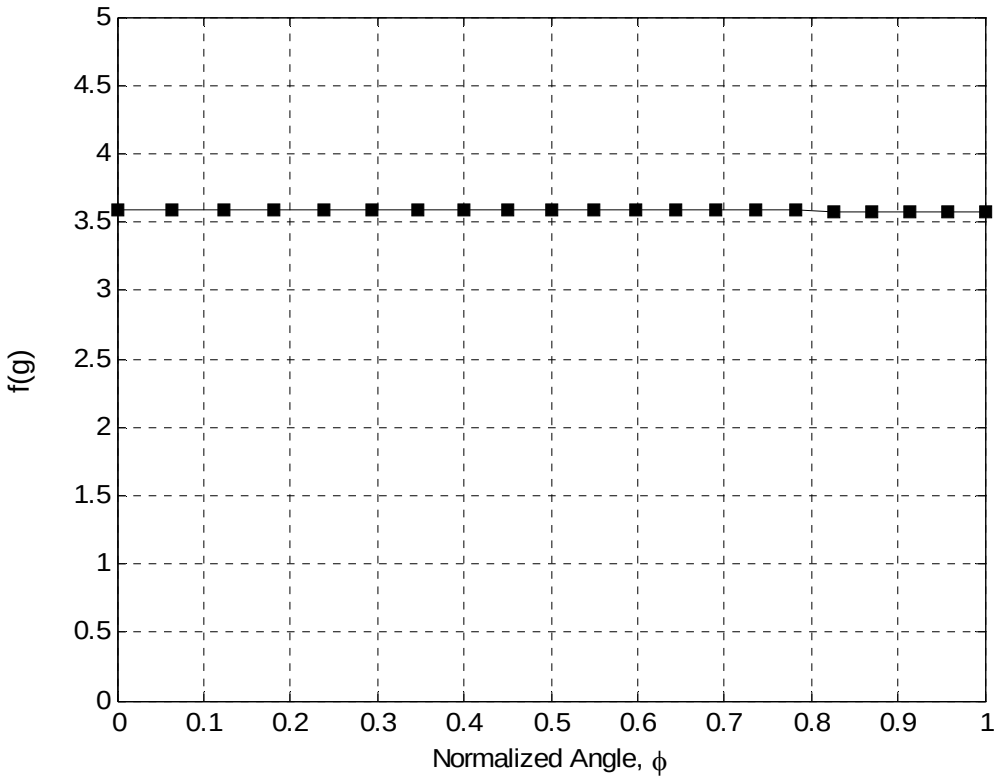

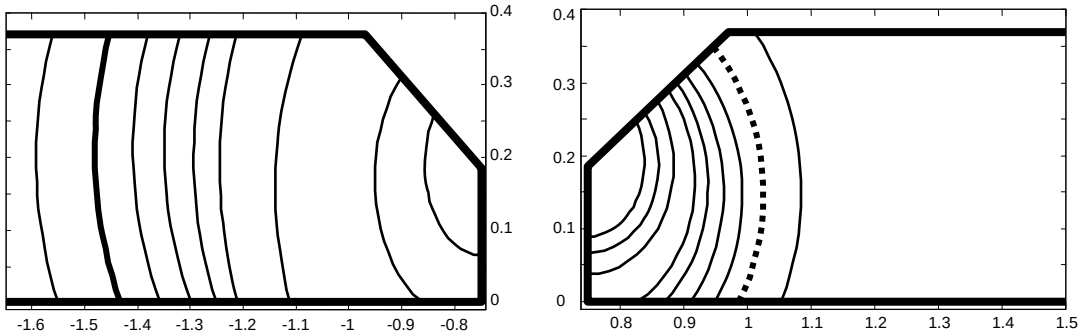

Figure A-43. Geometric Factors for FAA-19 (See table A-43)

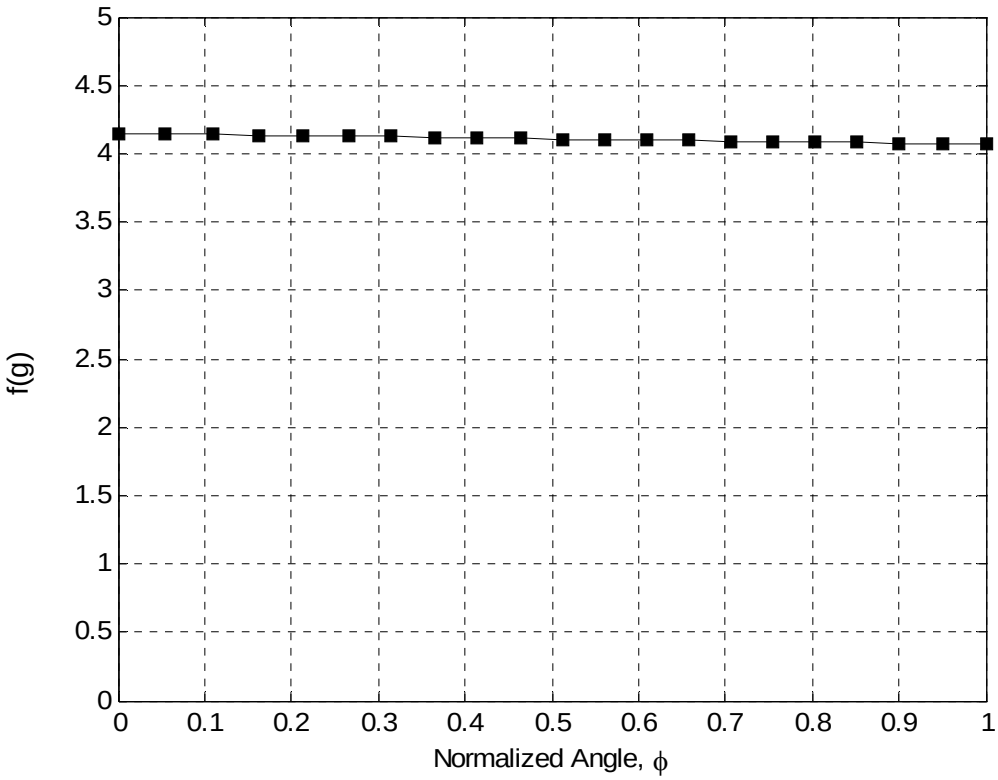

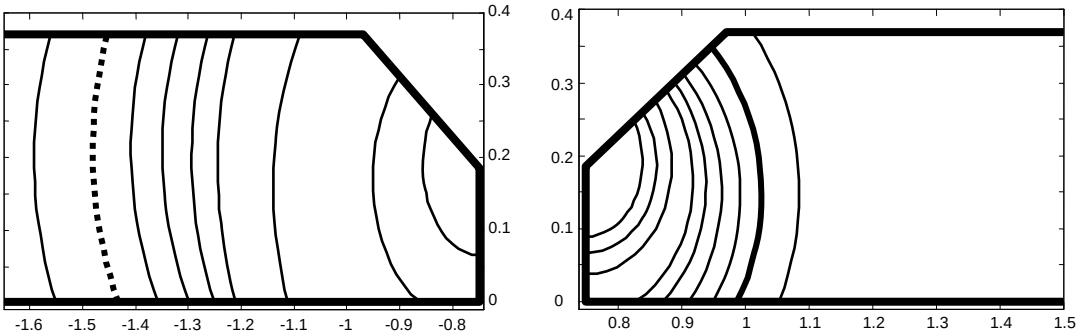

Figure A-44. Geometric Factors for FAA-19 (See table A-44)

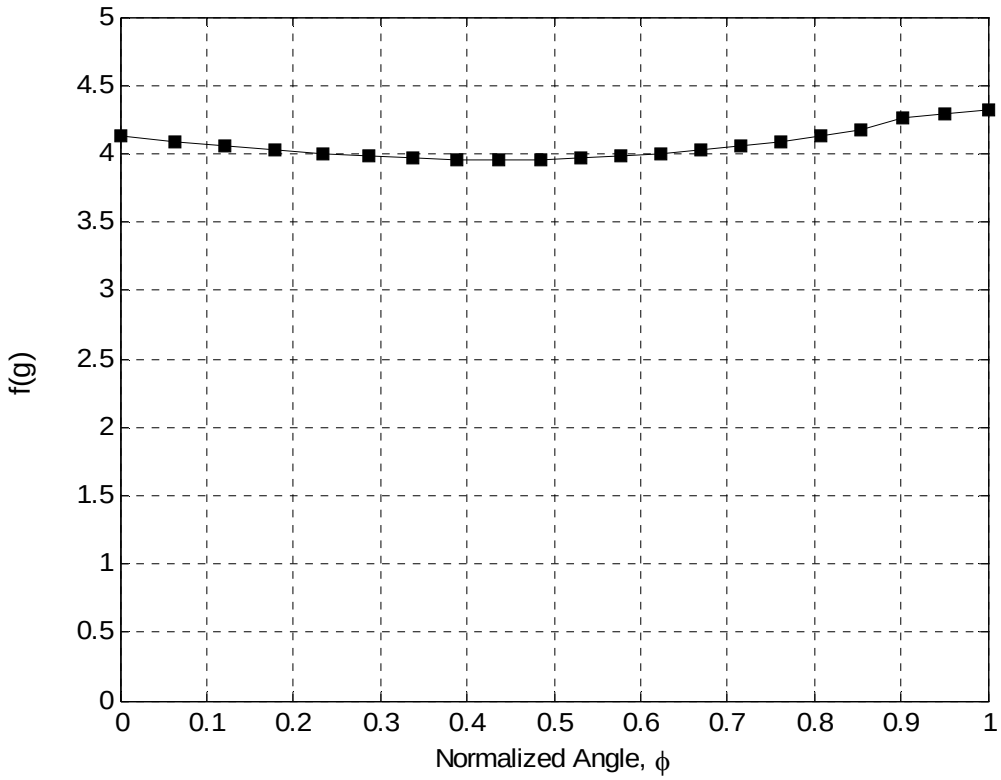

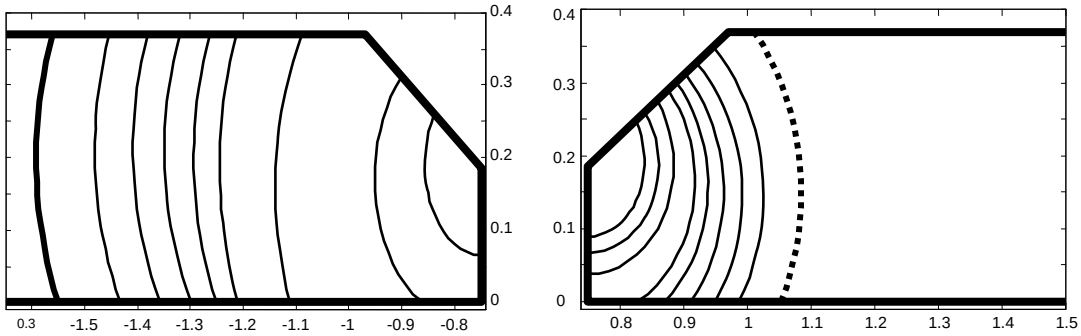

Figure A-45. Geometric Factors for FAA-19 (See table A-45)

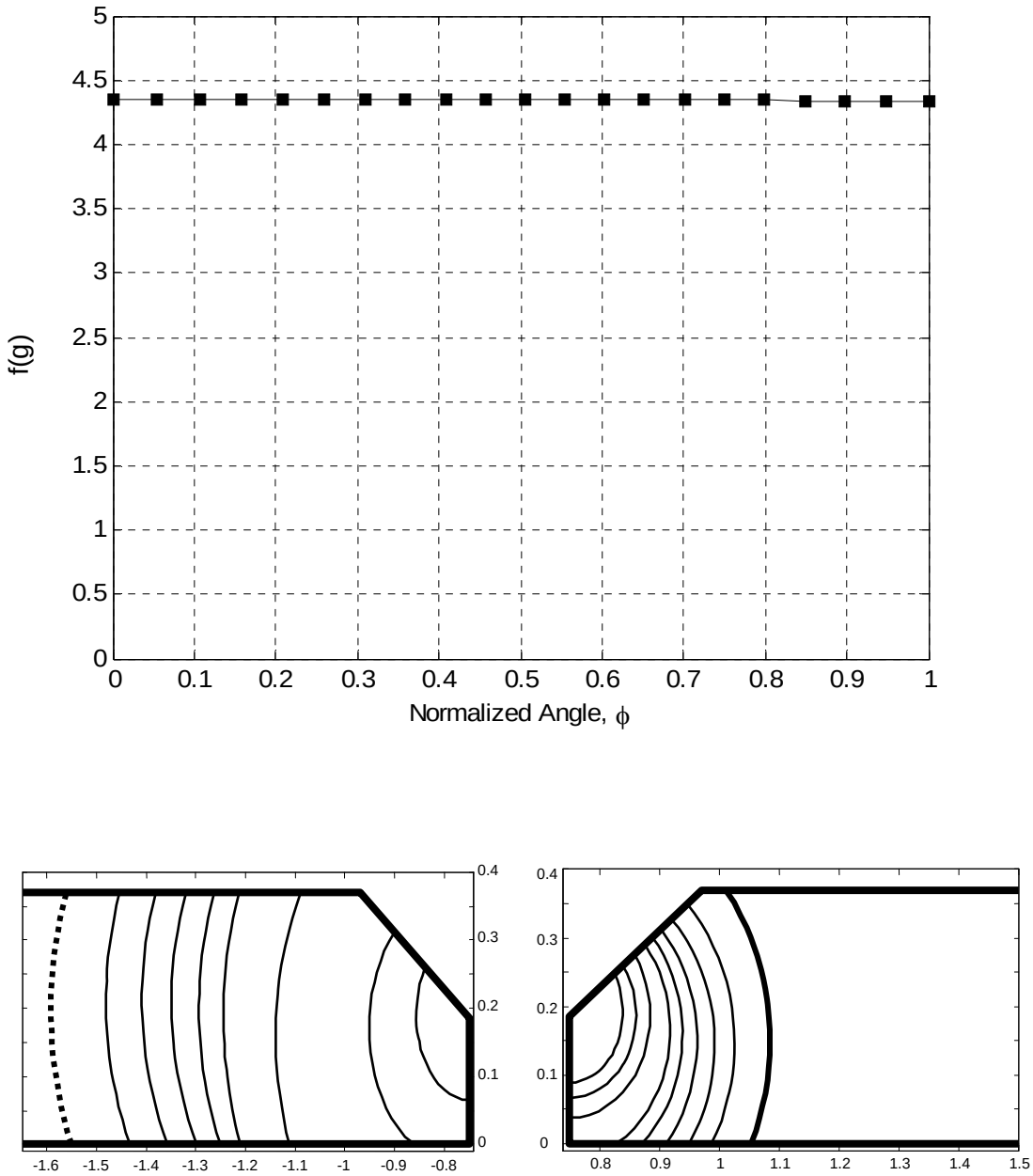

Figure A-46. Geometric Factors for FAA-19 (See table A-46)

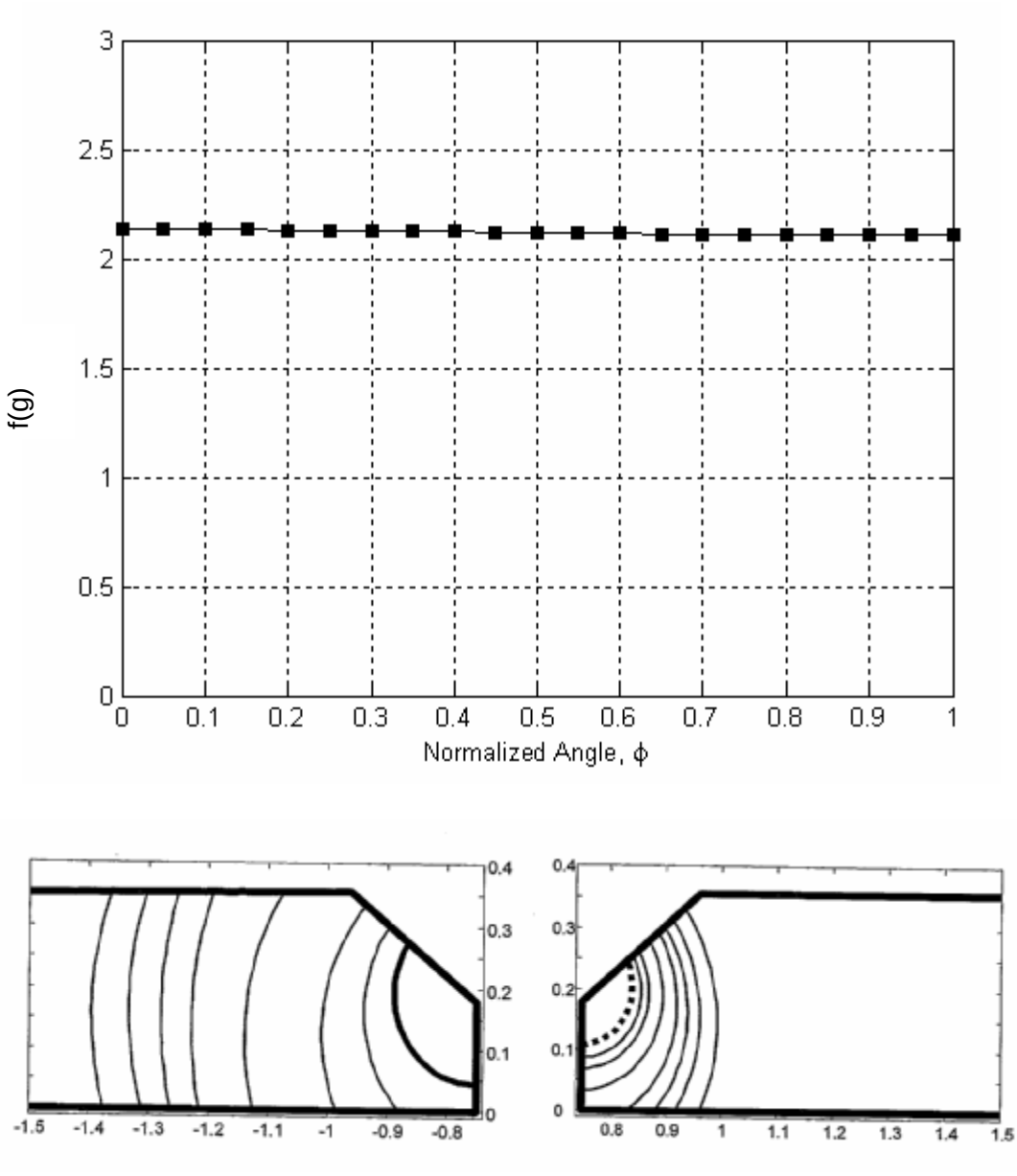

Figure A-47. Geometric Factors for FAA-20 (See table A-47)

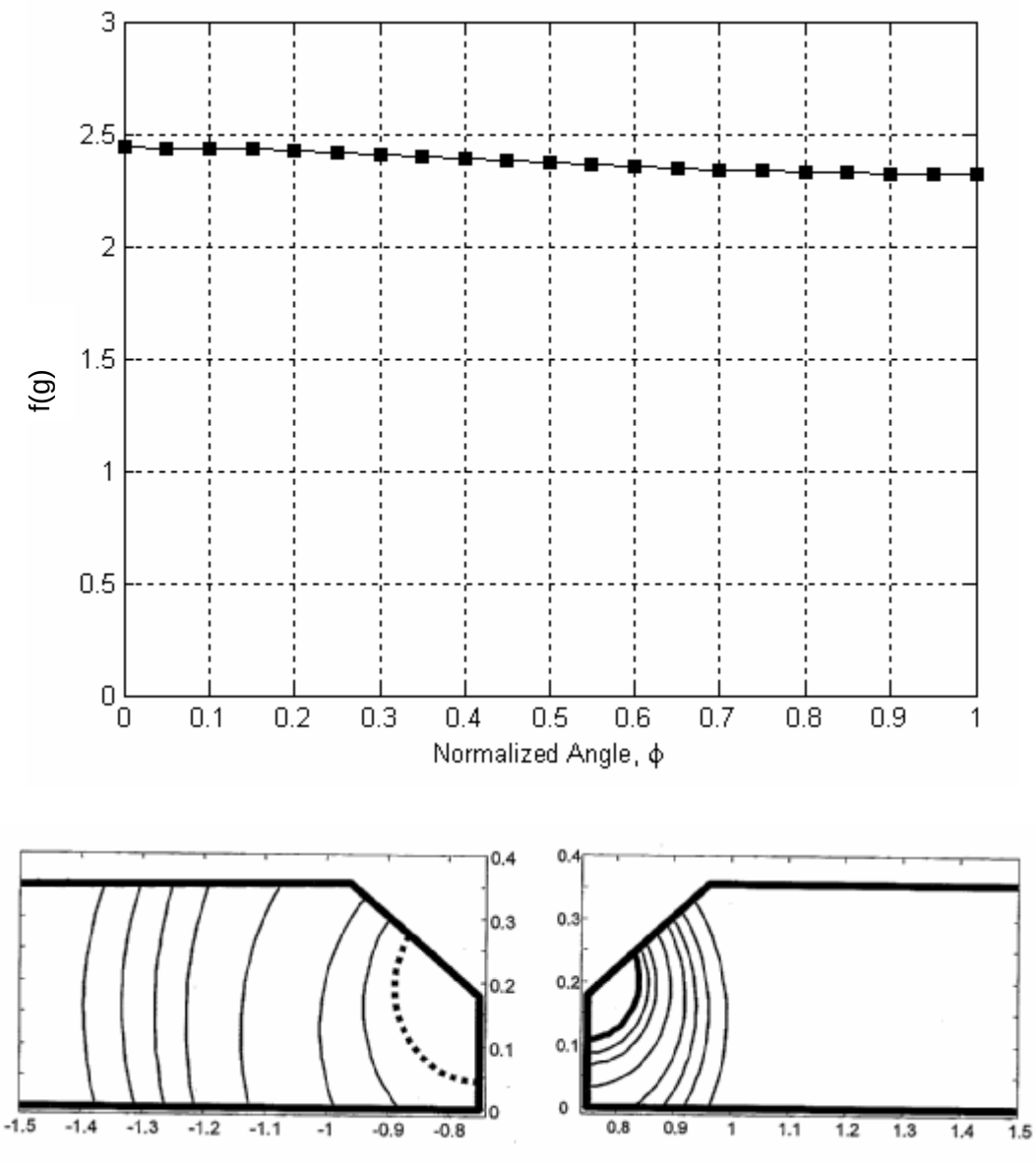

Figure A-48. Geometric Factors for FAA-20 (See table A-48)

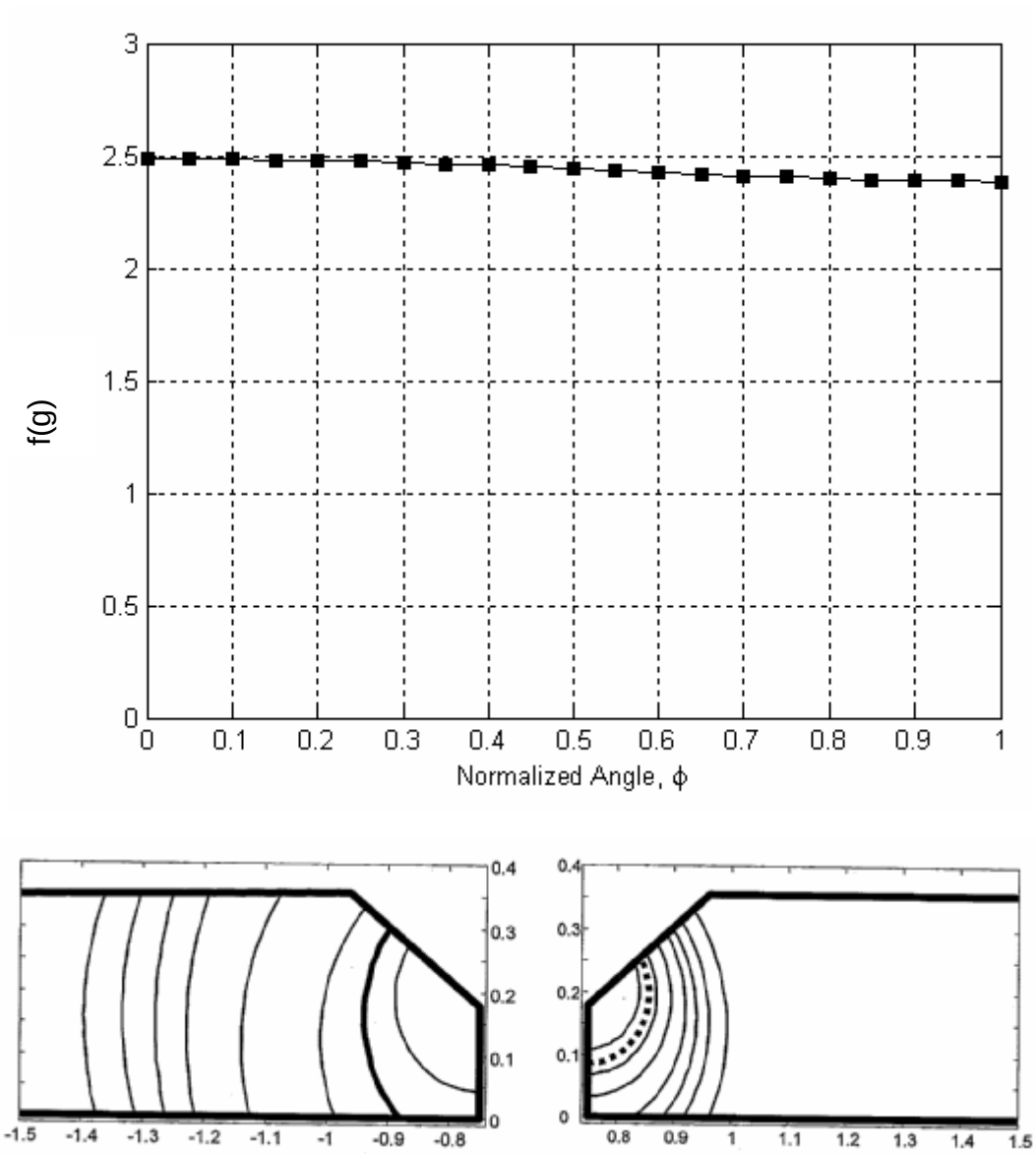

Figure A-49. Geometric Factors for FAA-20 (See table A-49)

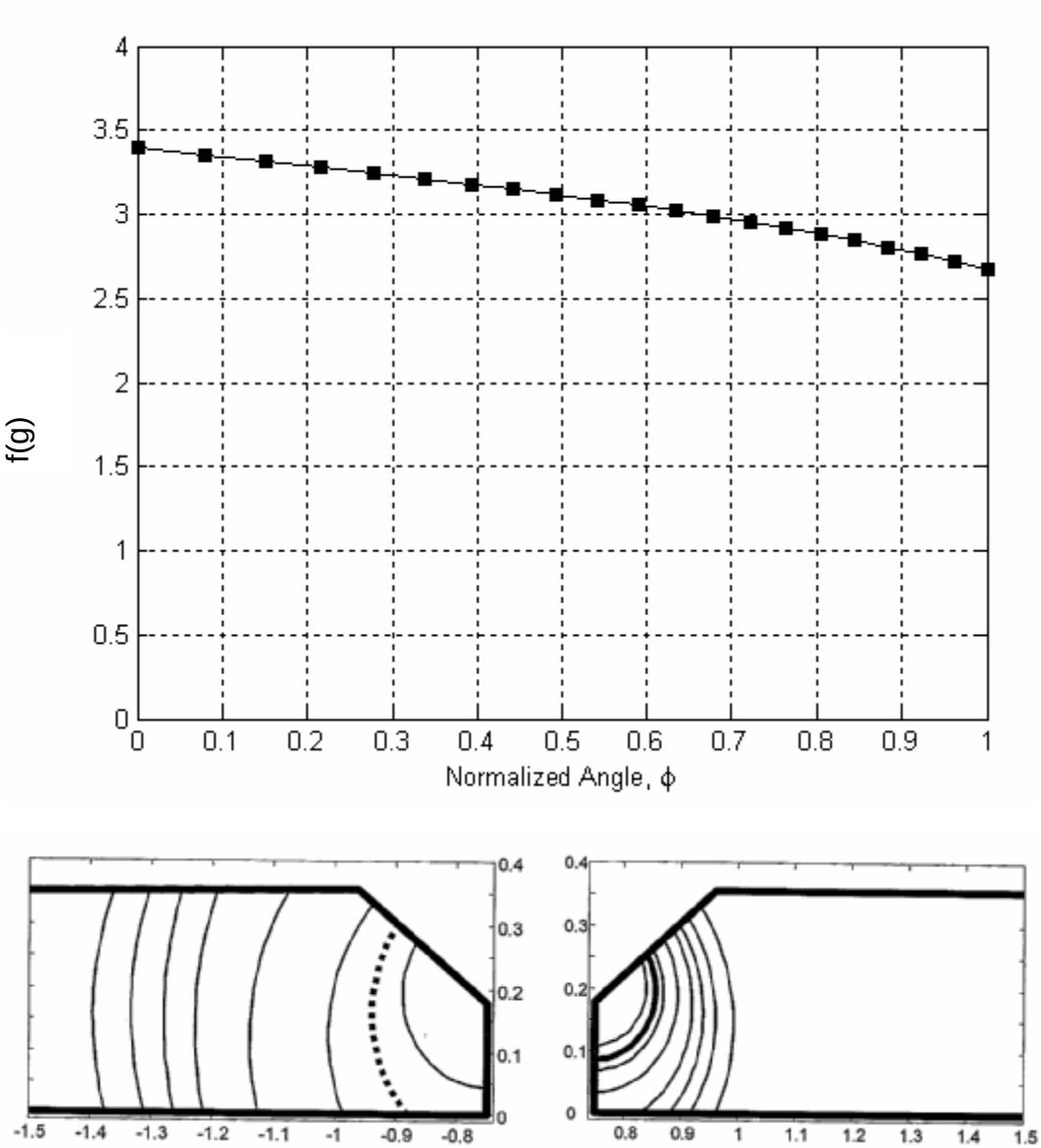

Figure A-50. Geometric Factors for FAA-20 (See table A-50)

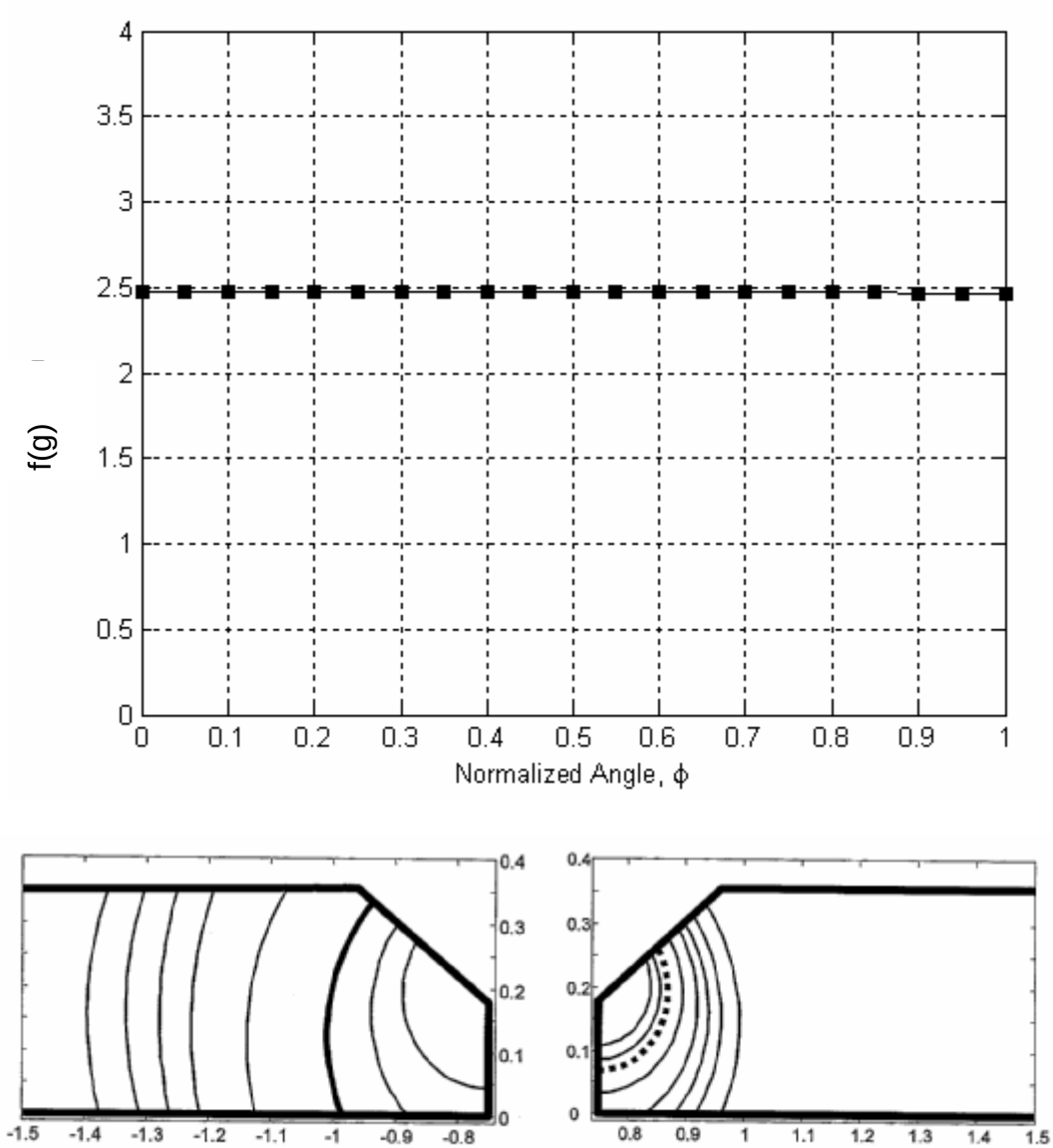

Figure A-51. Geometric Factors for FAA-20 (See table A-51)

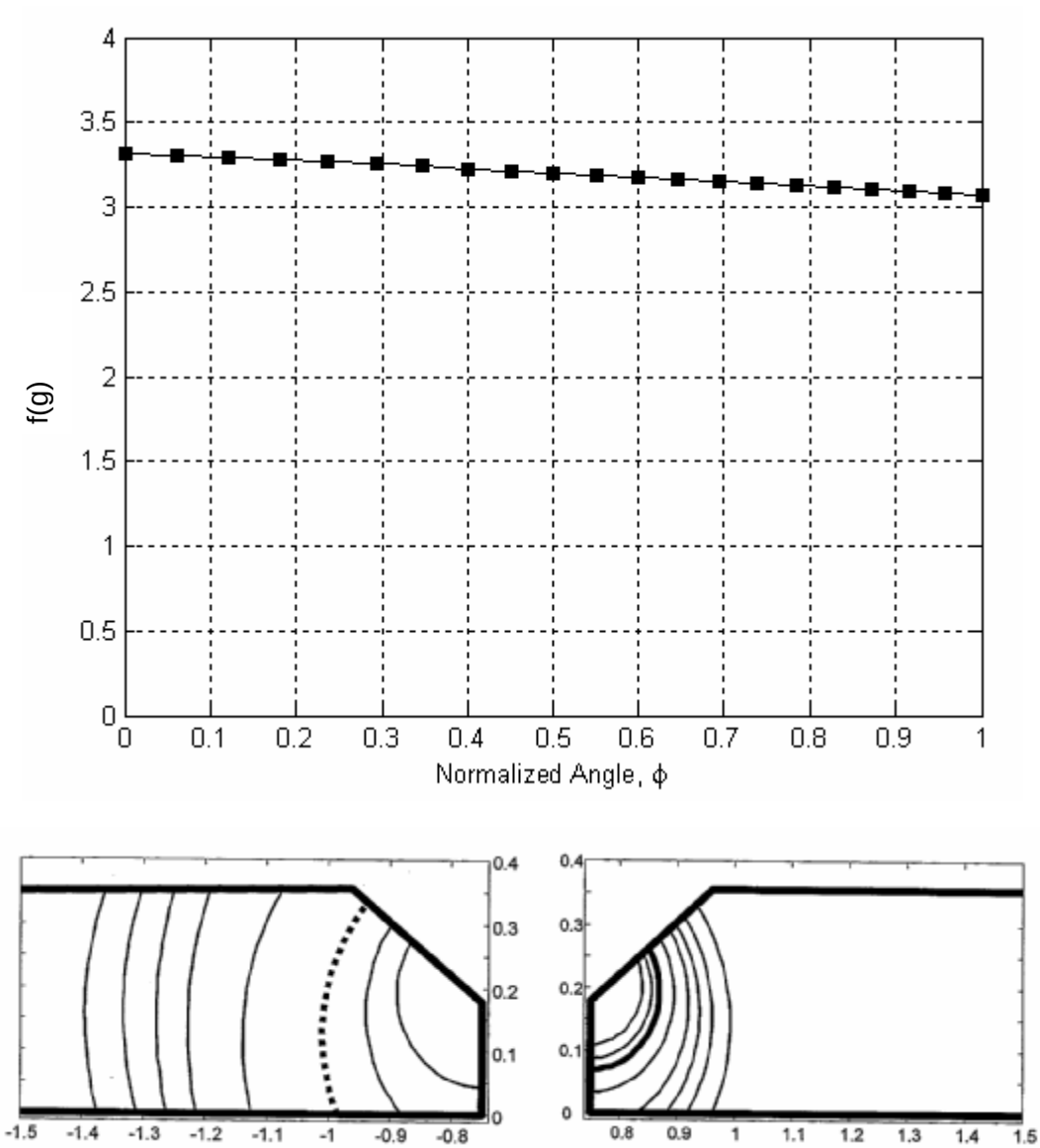

Figure A-52. Geometric Factors for FAA-20 (See table A-52)

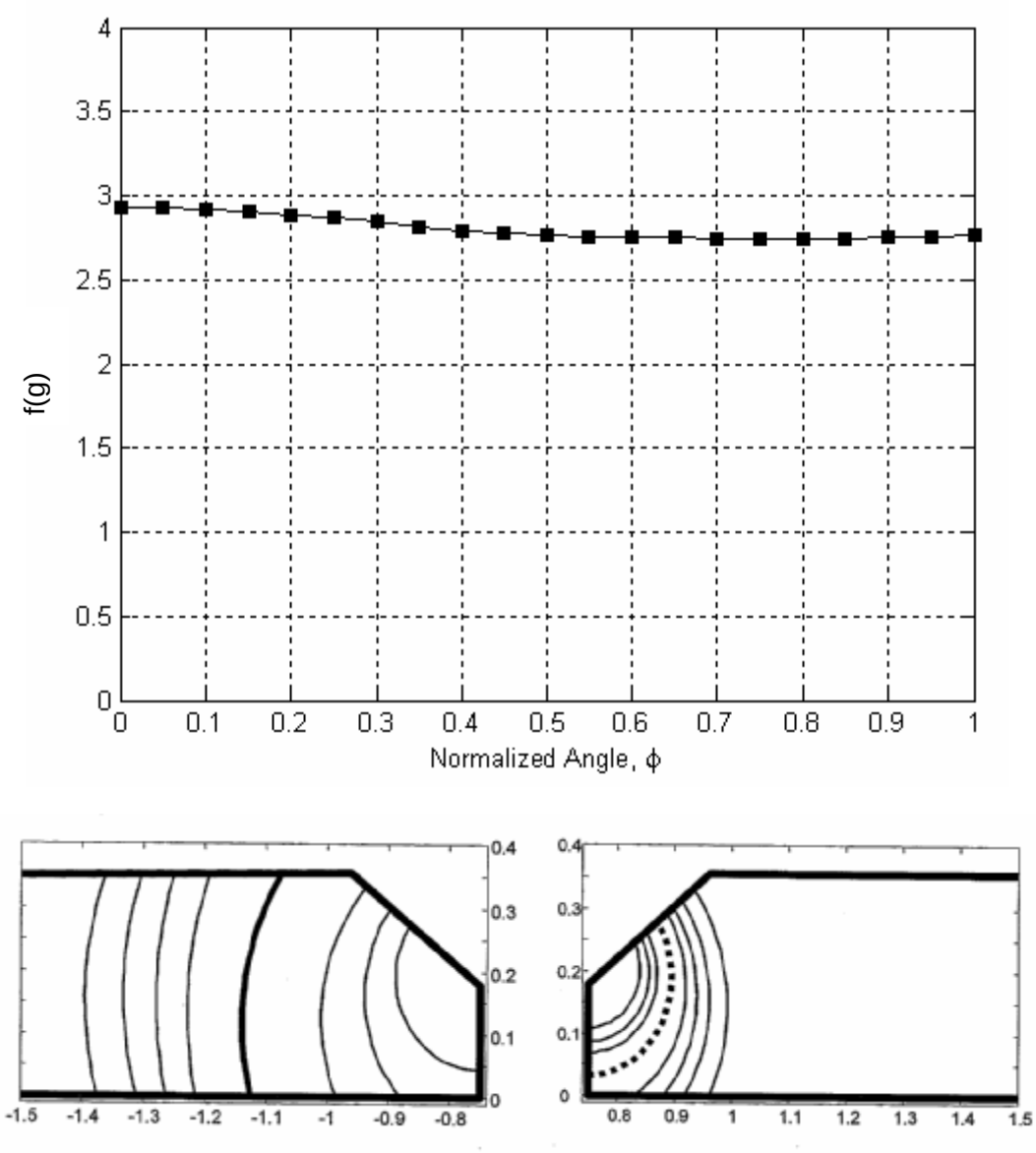

Figure A-53. Geometric Factors for FAA-20 (See table A-53)

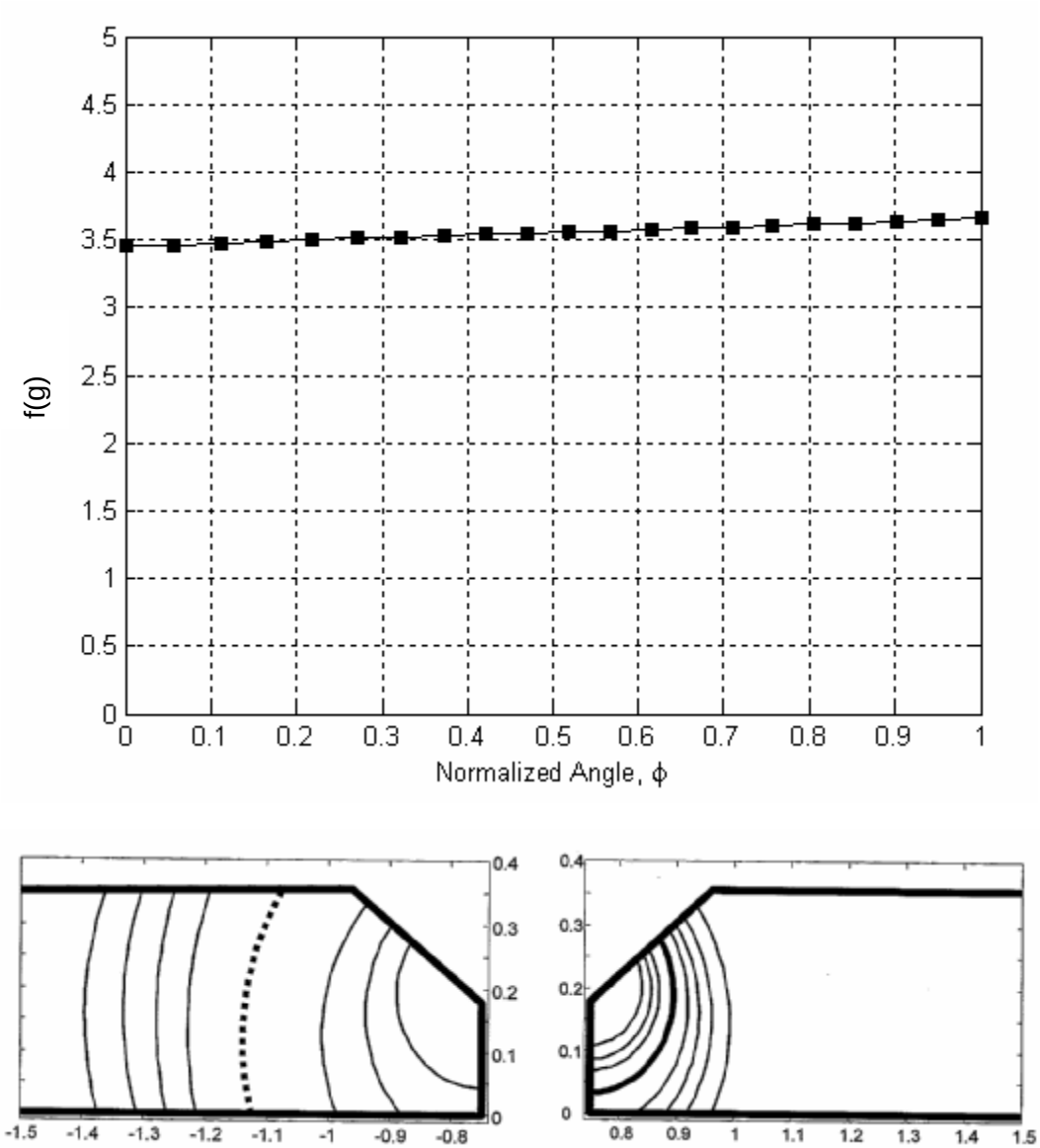

Figure A-54. Geometric Factors for FAA-20 (See table A-54)

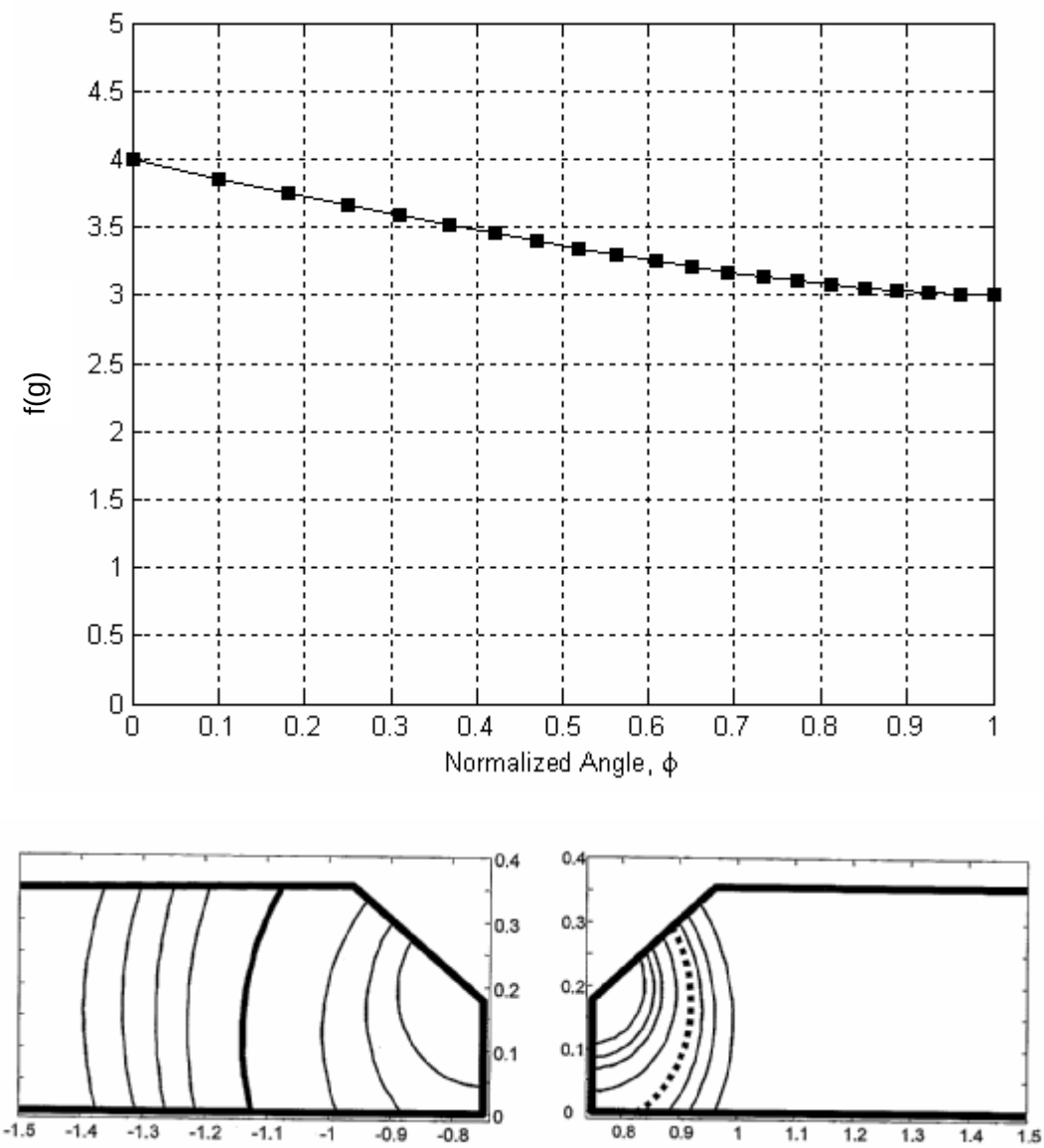

Figure A-55. Geometric Factors for FAA-20 (See table A-55)

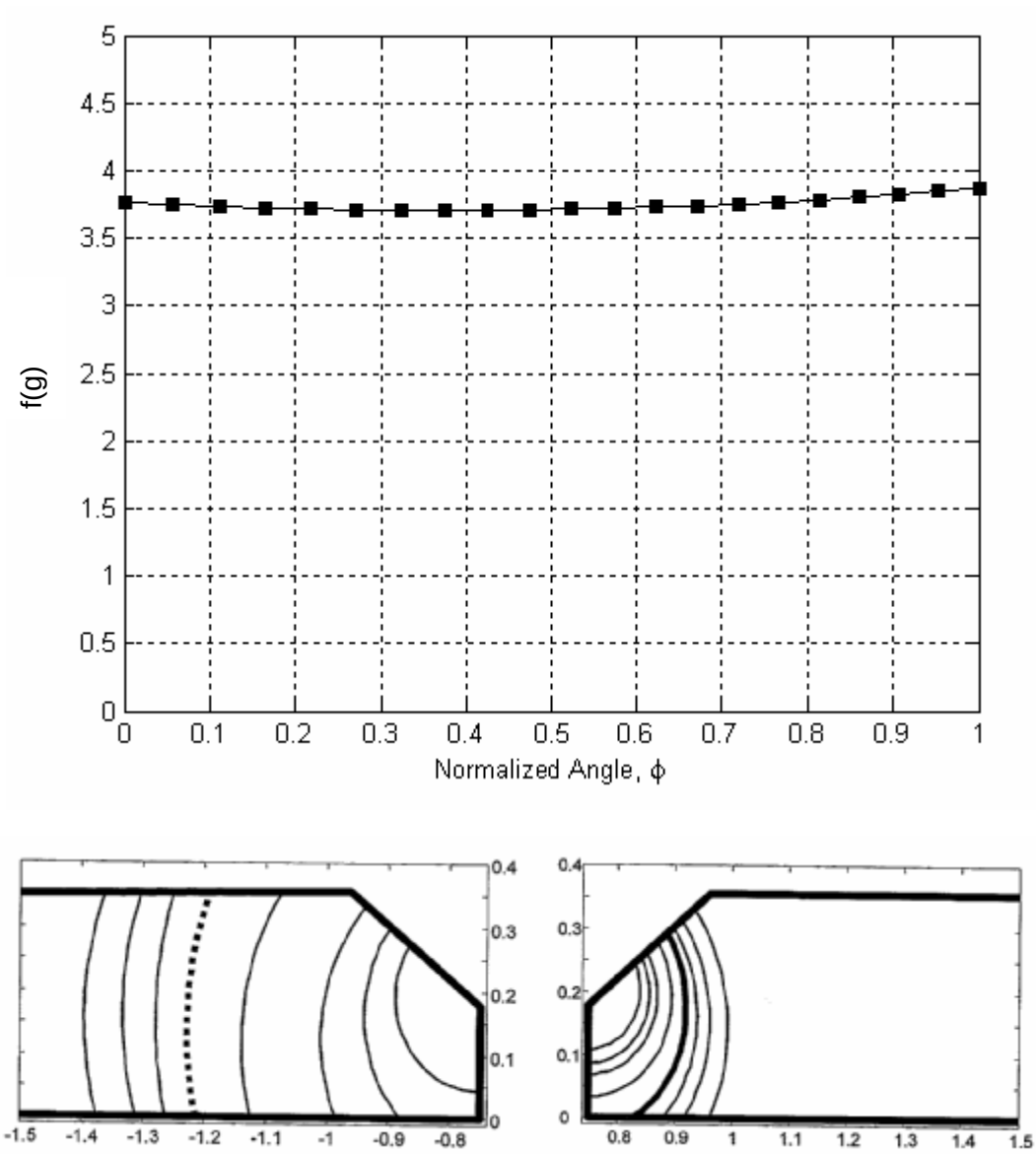

Figure A-56. Geometric Factors for FAA-20 (See table A-56)

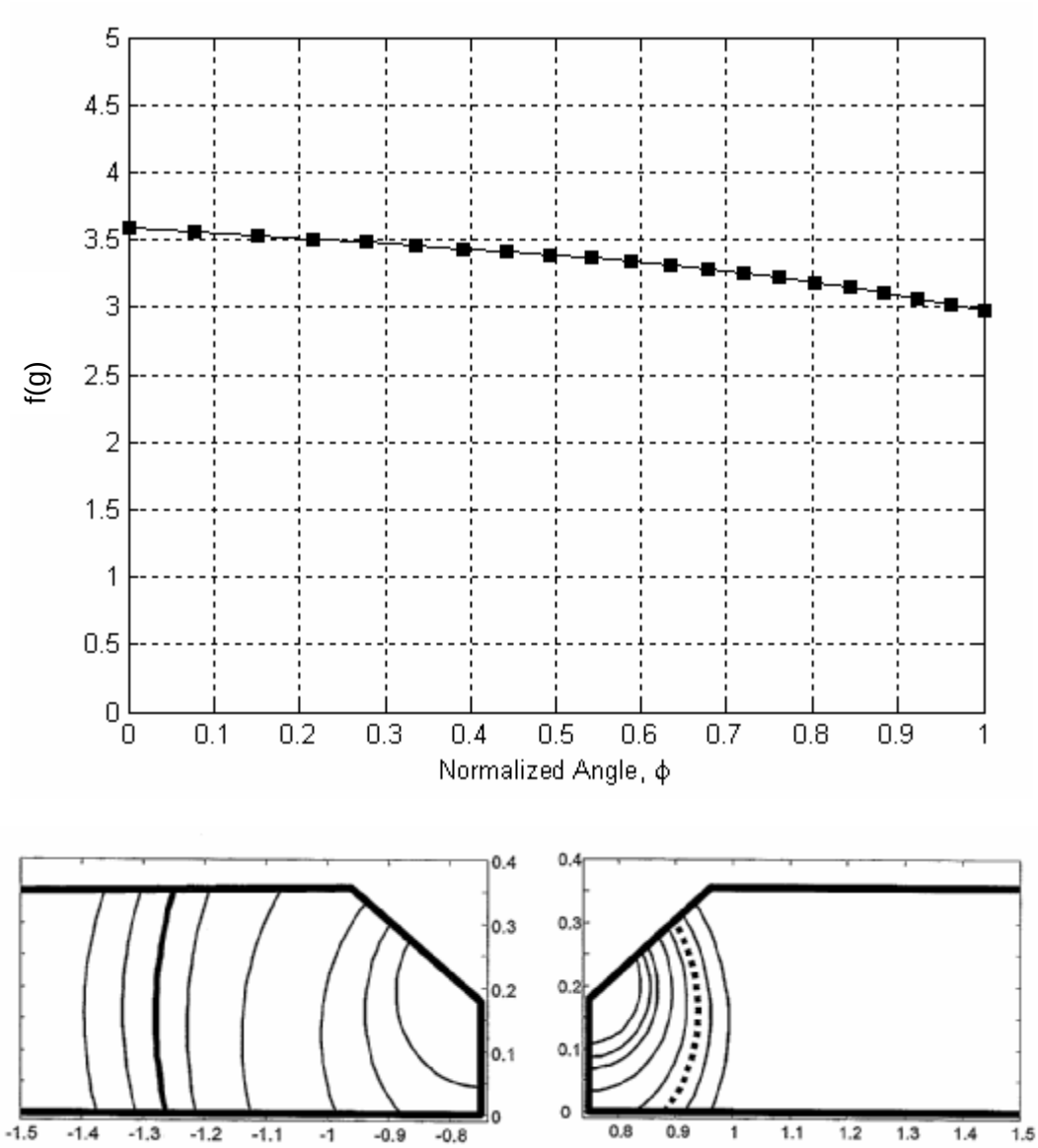

Figure A-57. Geometric Factors for FAA-20 (See table A-57)

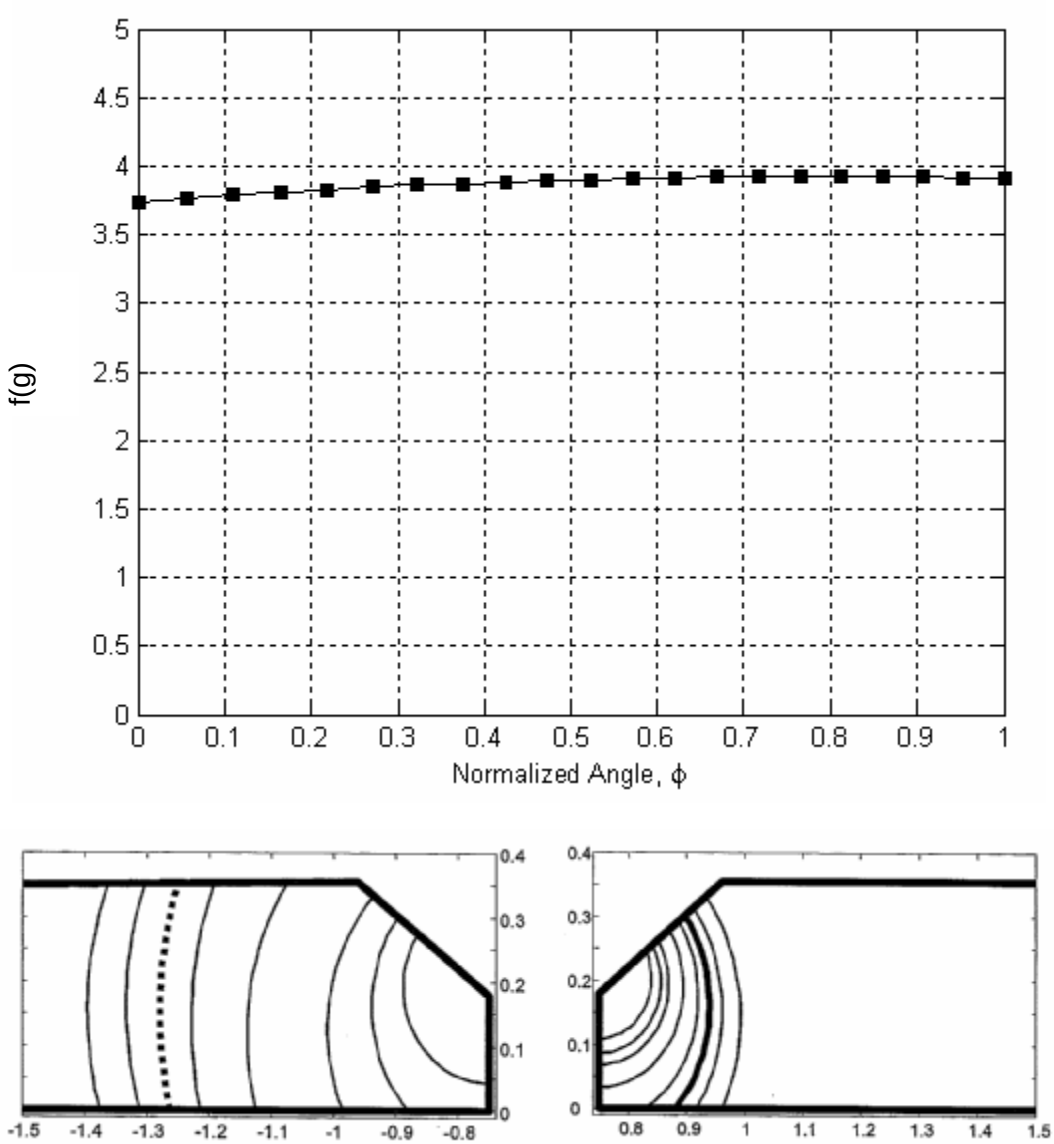

Figure A-58. Geometric Factors for FAA-20 (See table A-58)

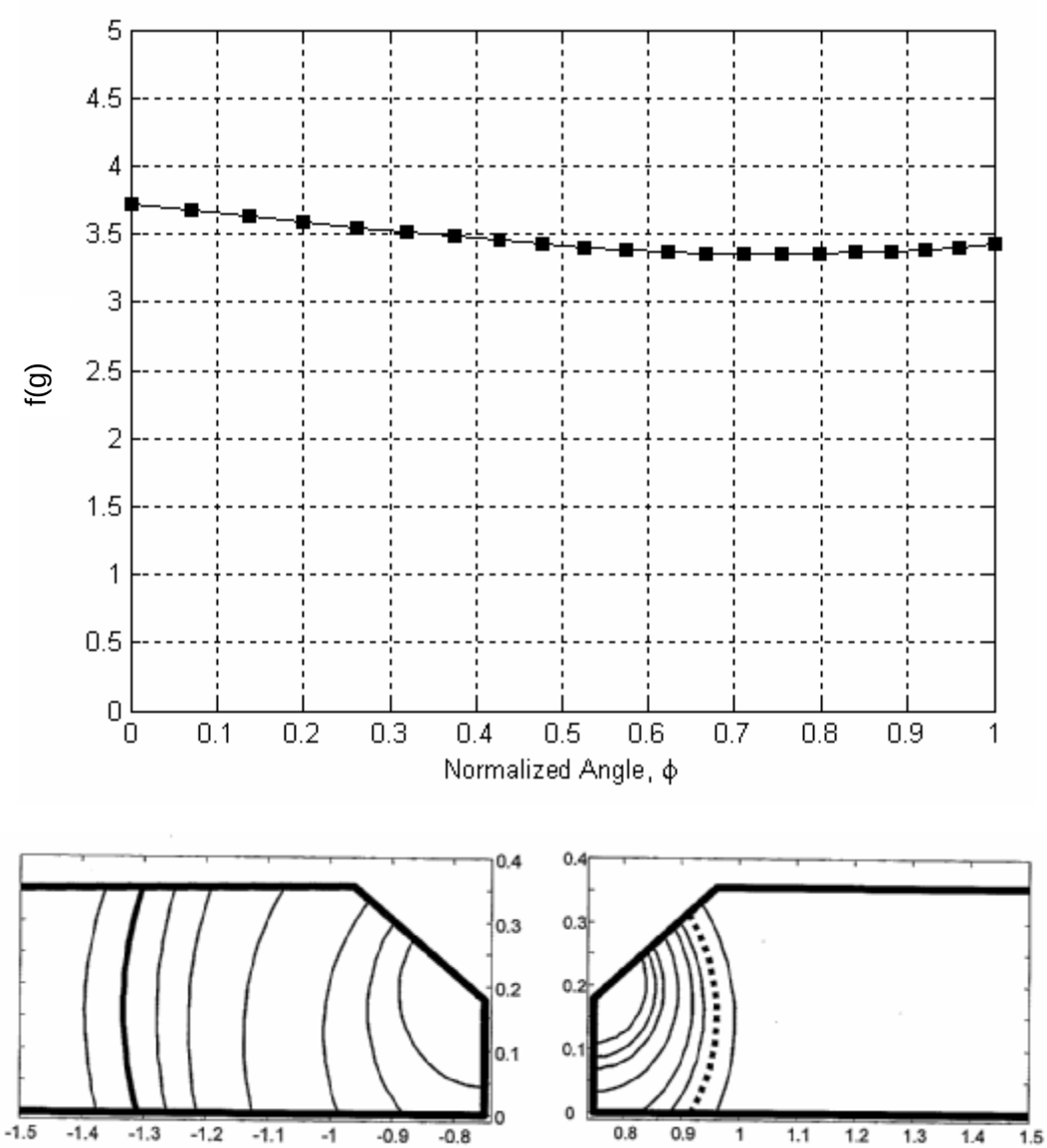

Figure A-59. Geometric Factors for FAA-20 (See table A-59)

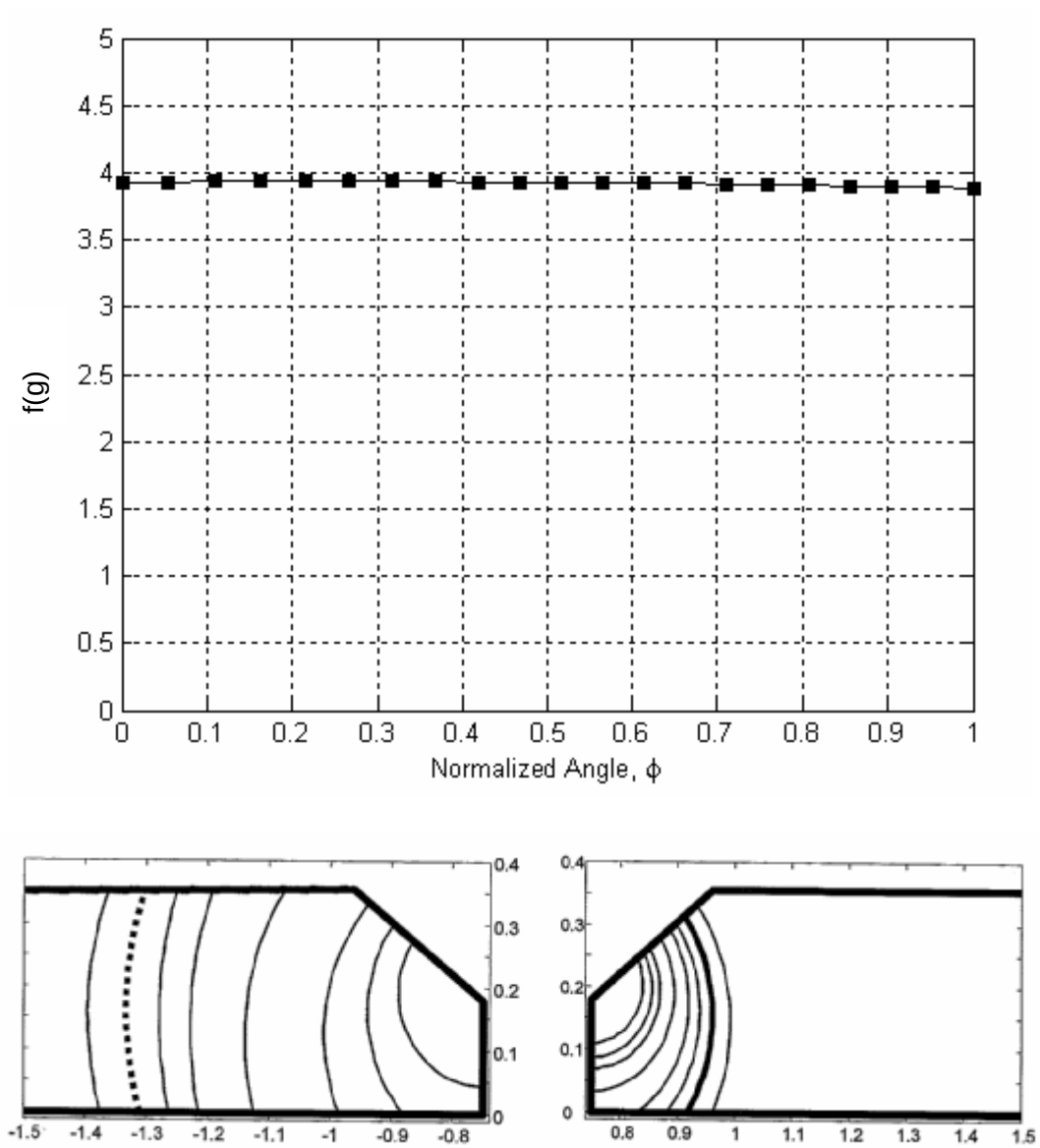

Figure A-60. Geometric Factors for FAA-20 (See table A-60)

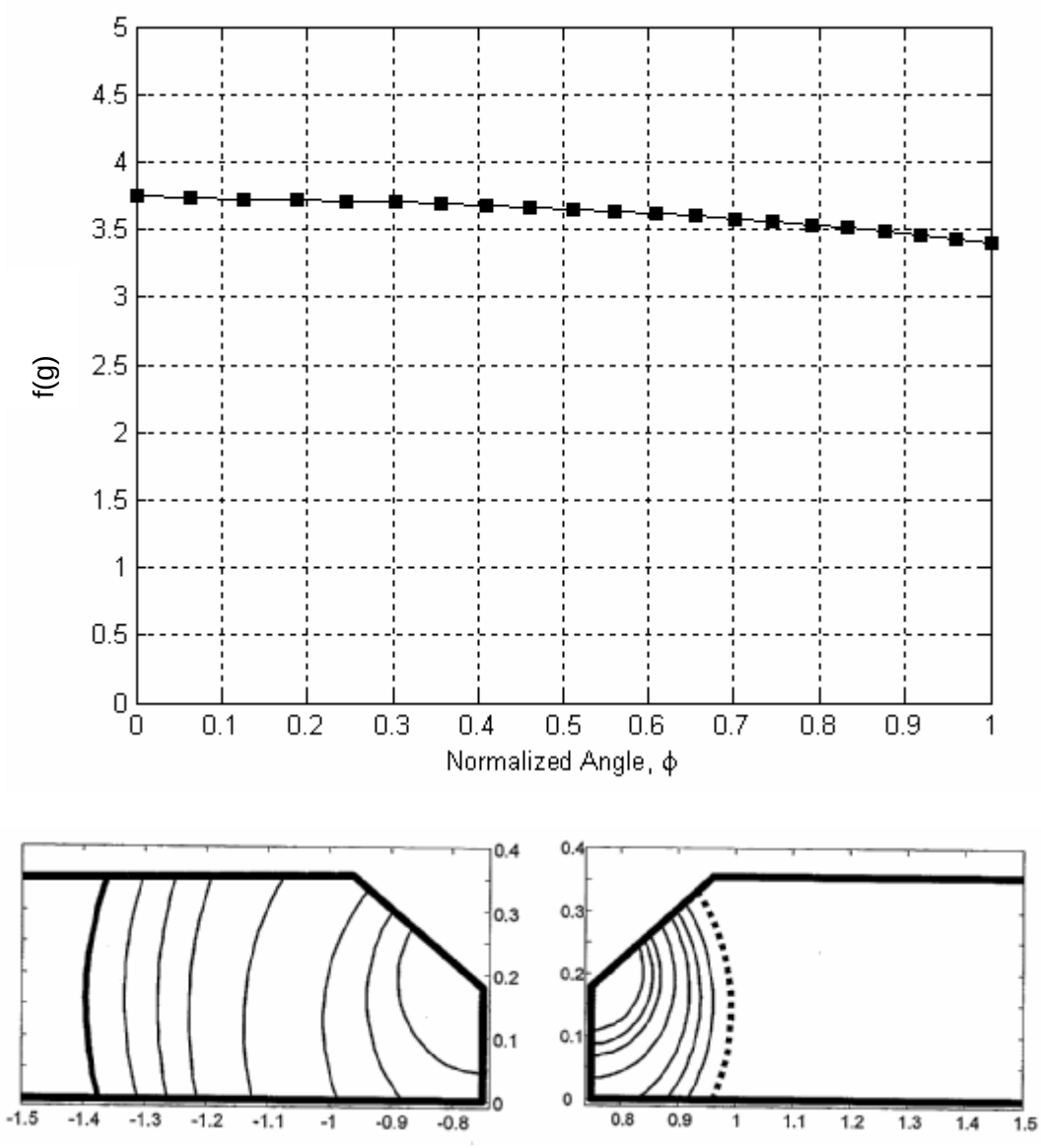

Figure A-61. Geometric Factors for FAA-20 (See table A-61)

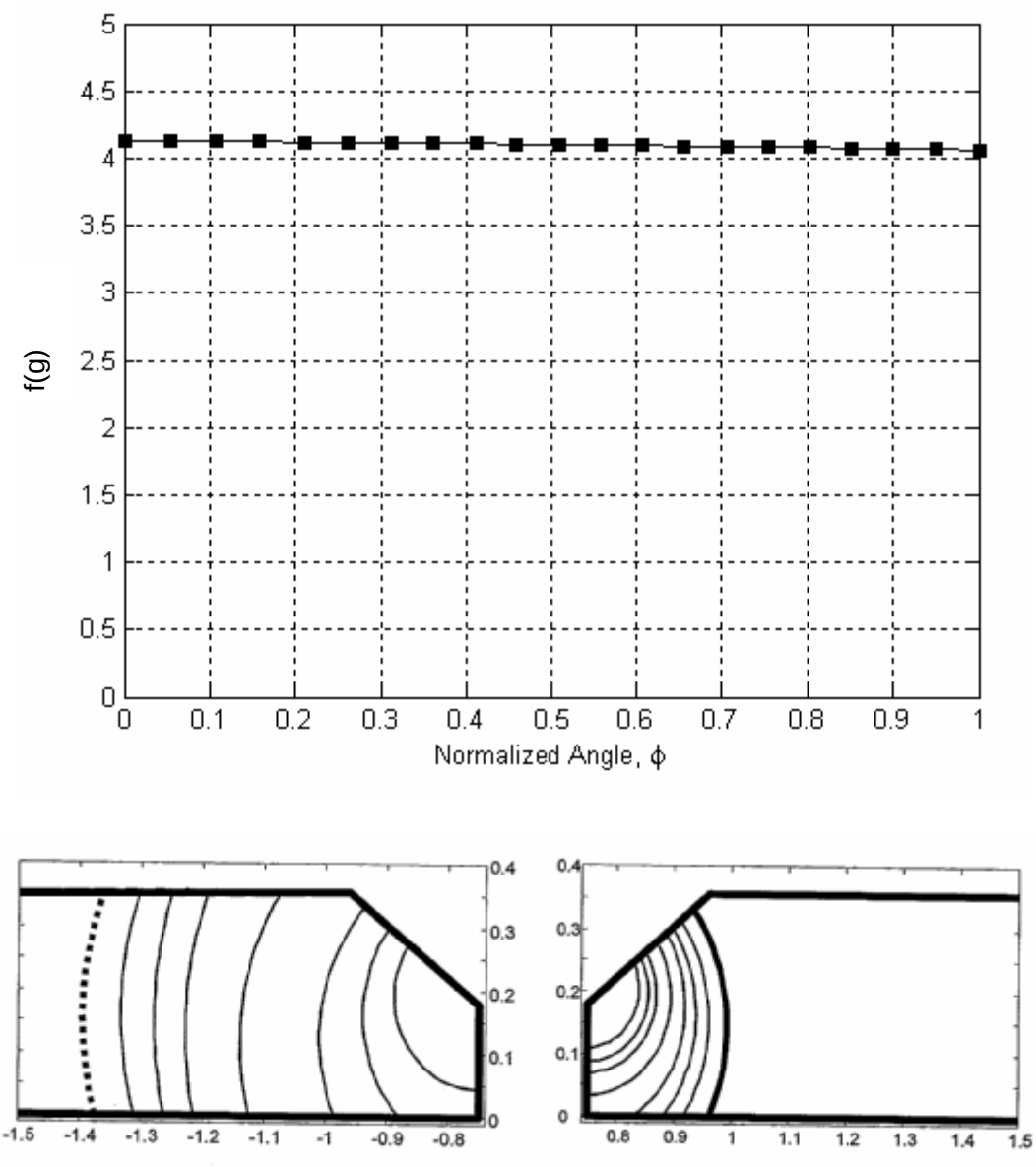

Figure A-62. Geometric Factors for FAA-20 (See table A-62)

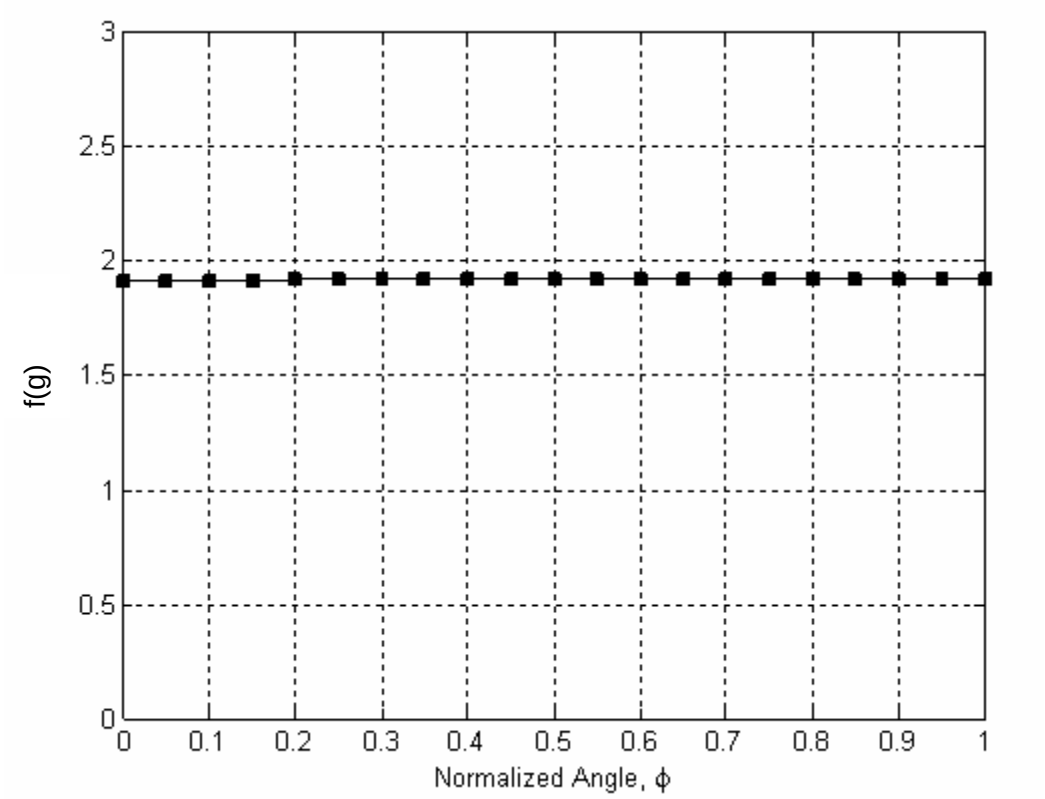

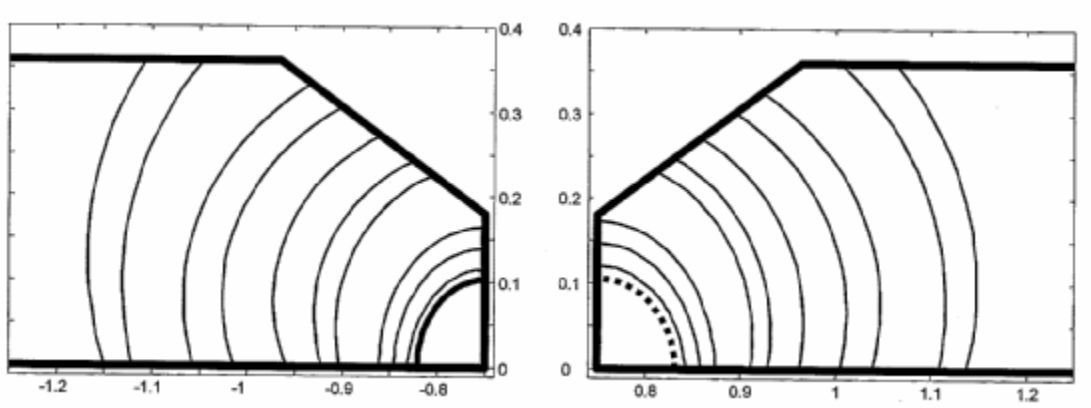

Figure A-63. Geometric Factors for FAA-21 (See table A-63)

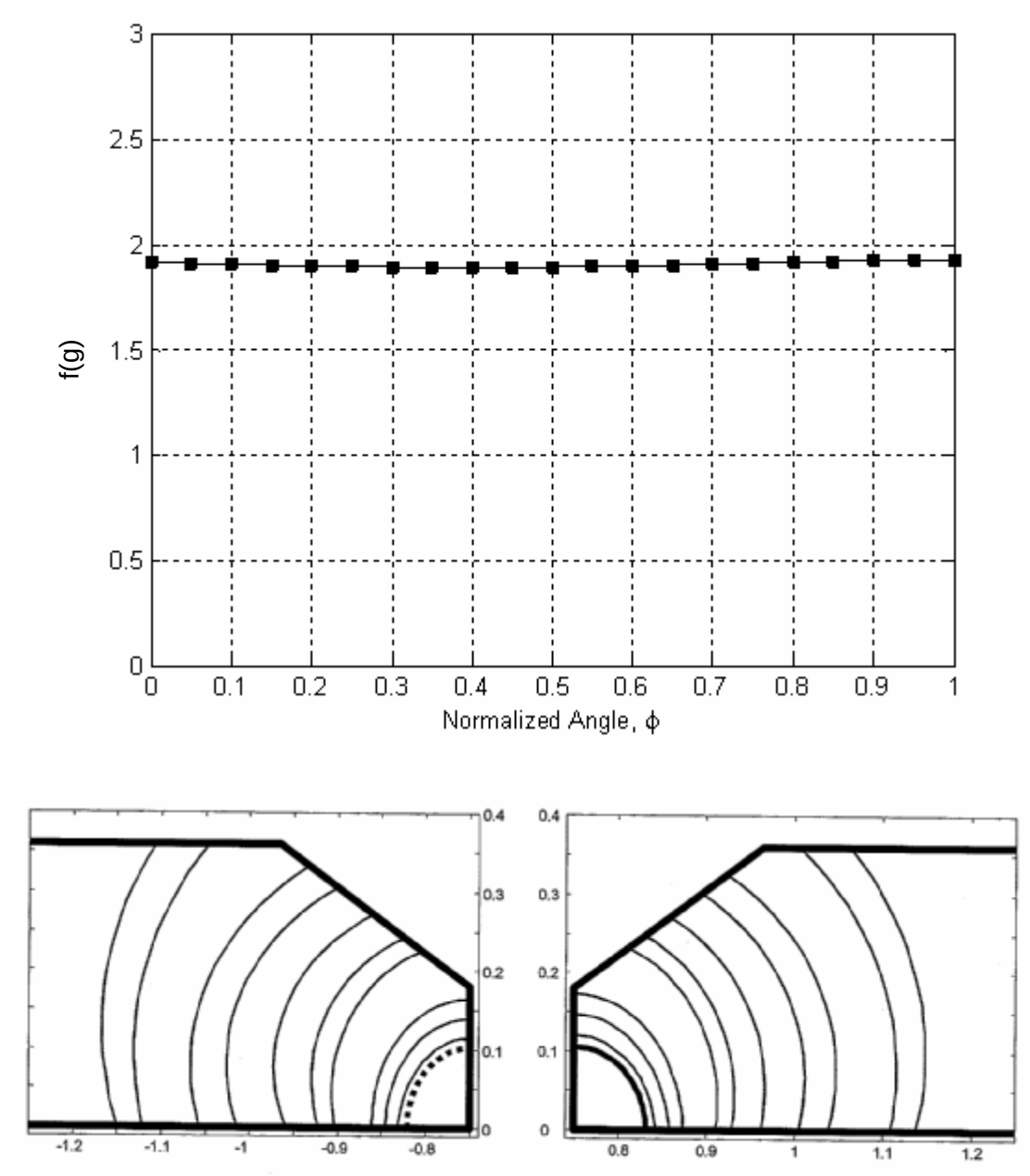

Figure A-64. Geometric Factors for FAA-21 (See table A-64)

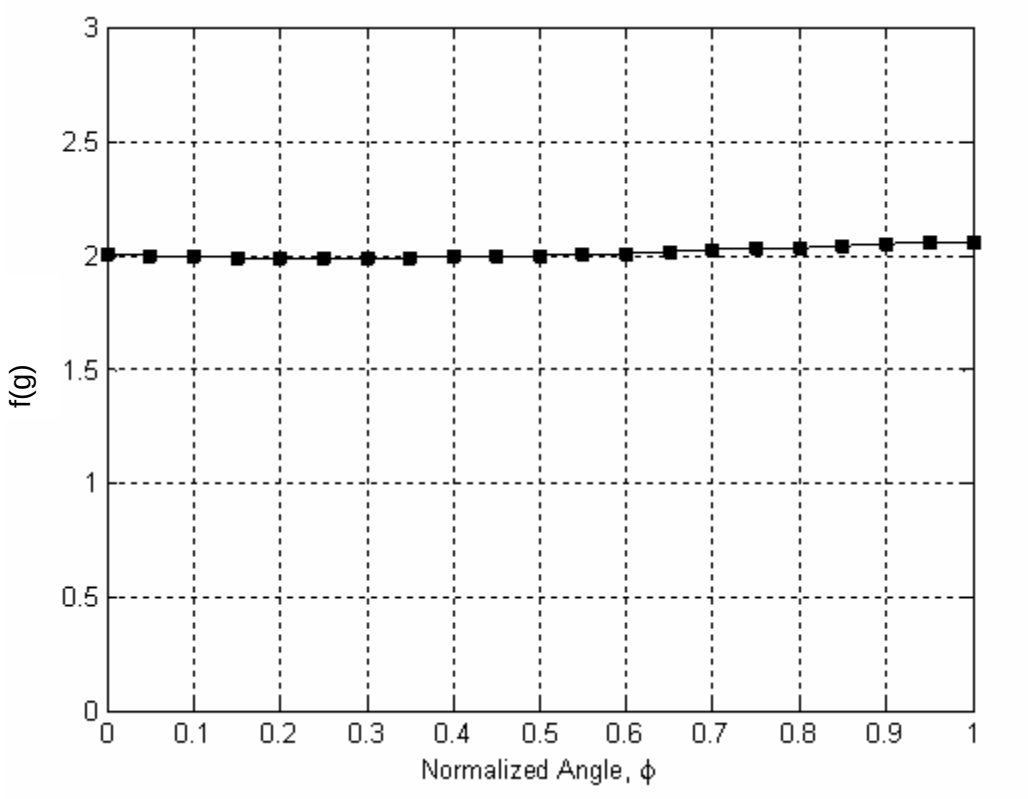

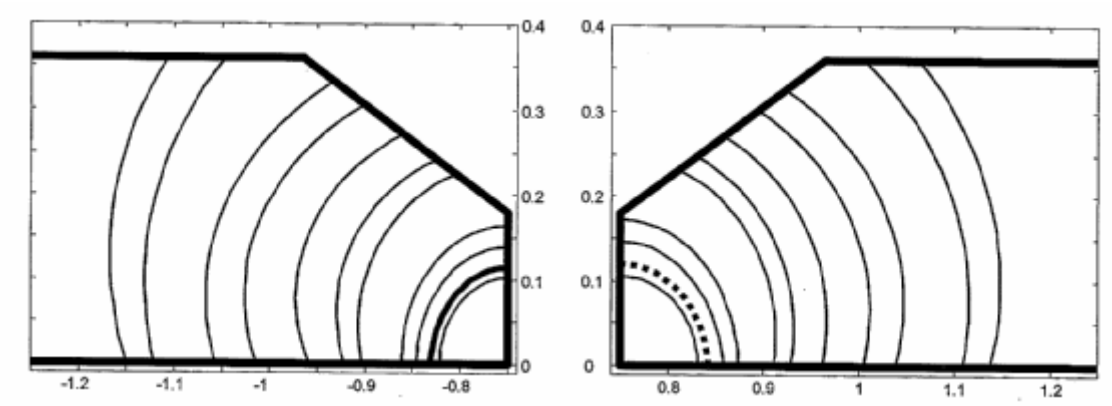

Figure A-65. Geometric Factors for FAA-21 (See table A-65)

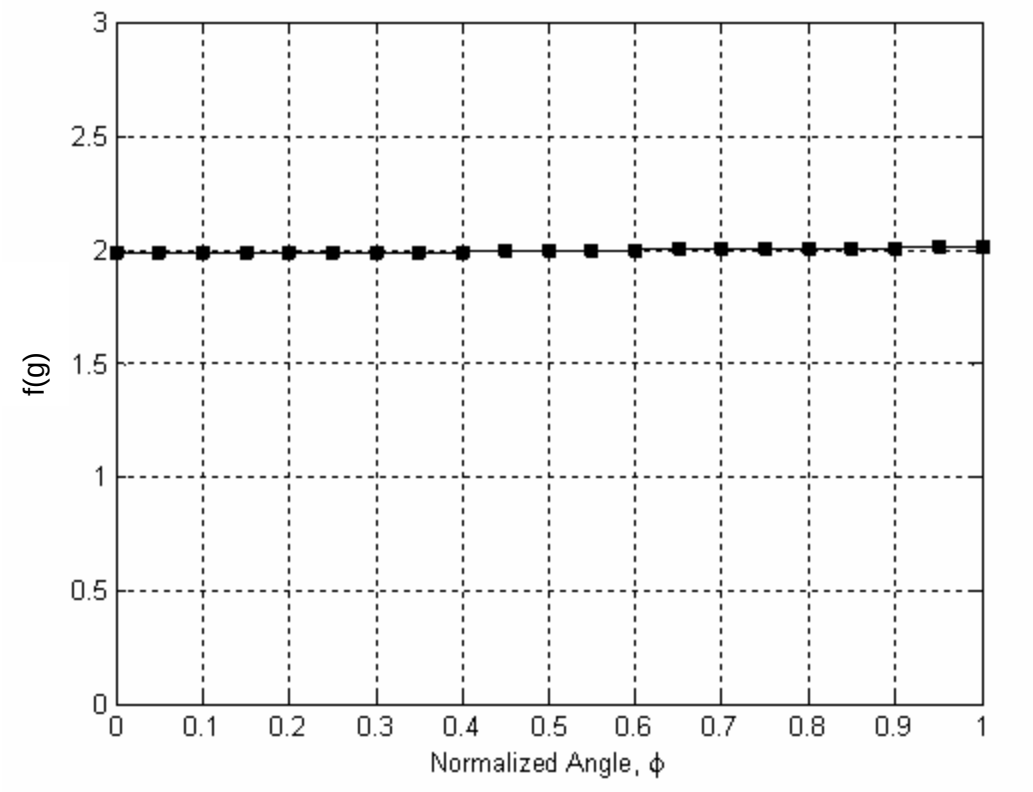

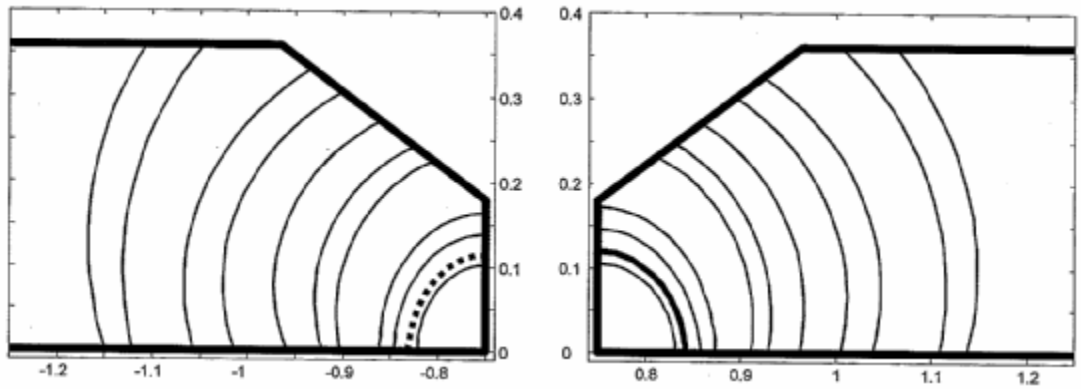

Figure A-66. Geometric Factors for FAA-21 (See table A-66)

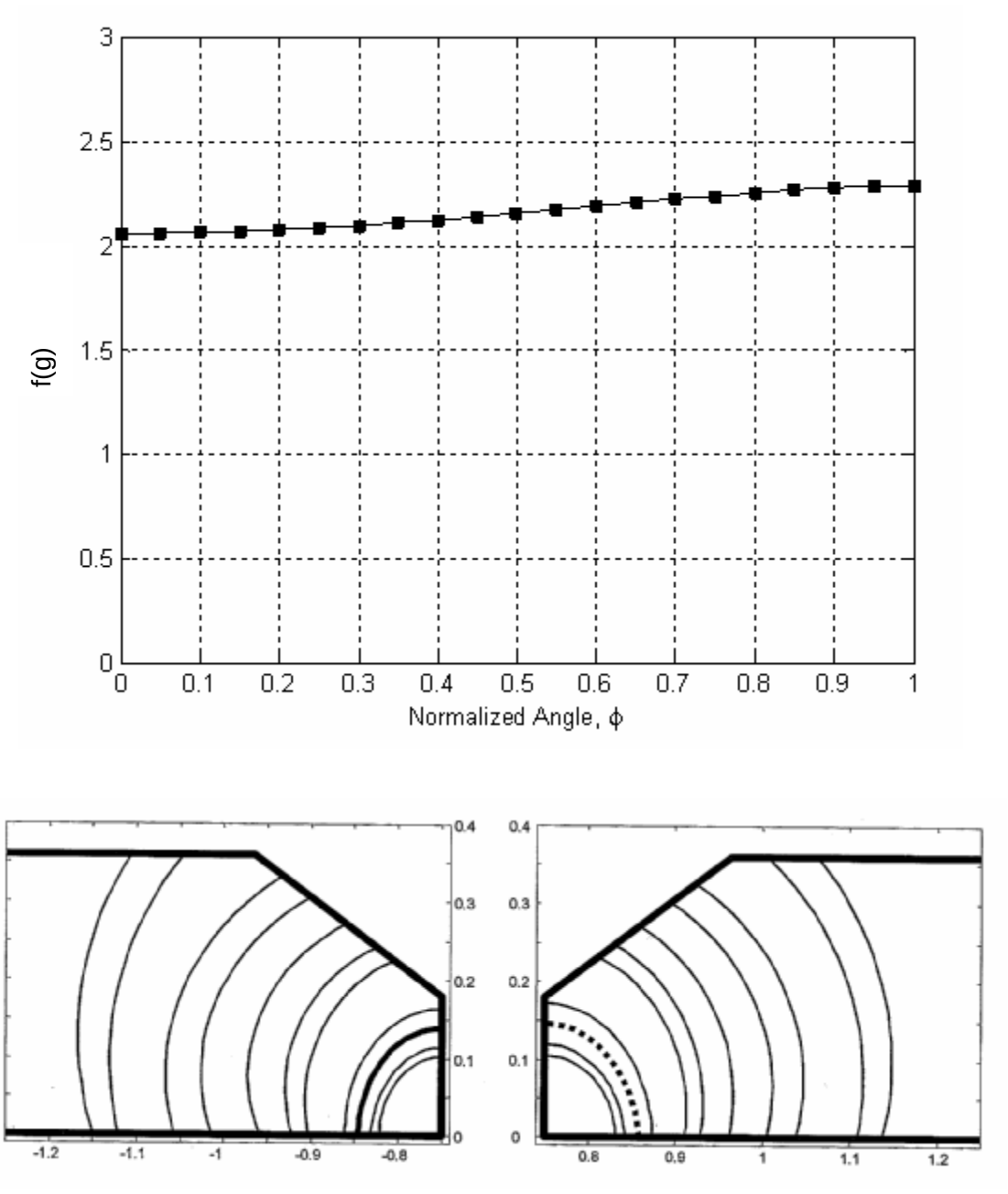

Figure A-67. Geometric Factors for FAA-21 (See table A-67)

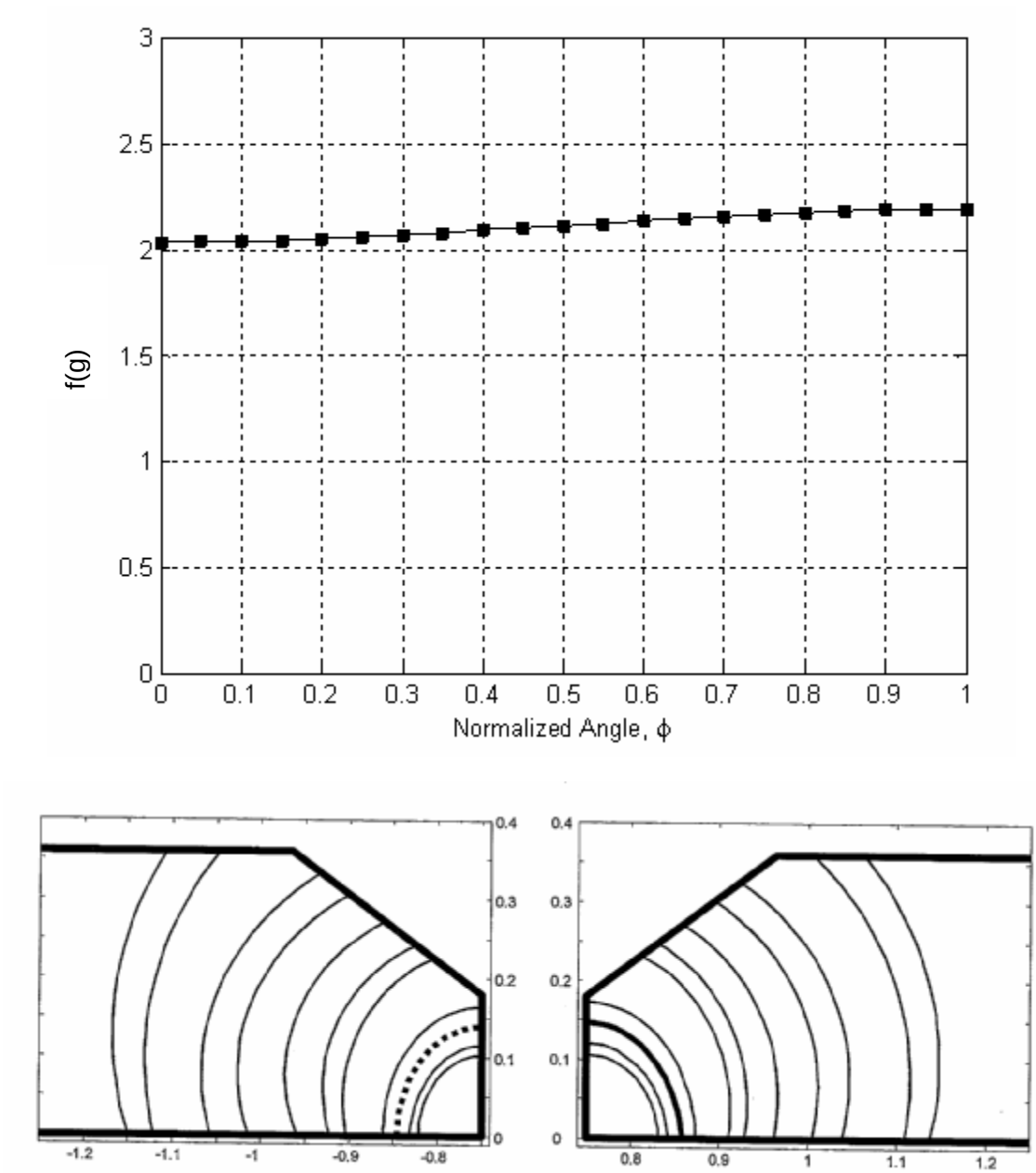

Figure A-68. Geometric Factors for FAA-21 (See table A-68)

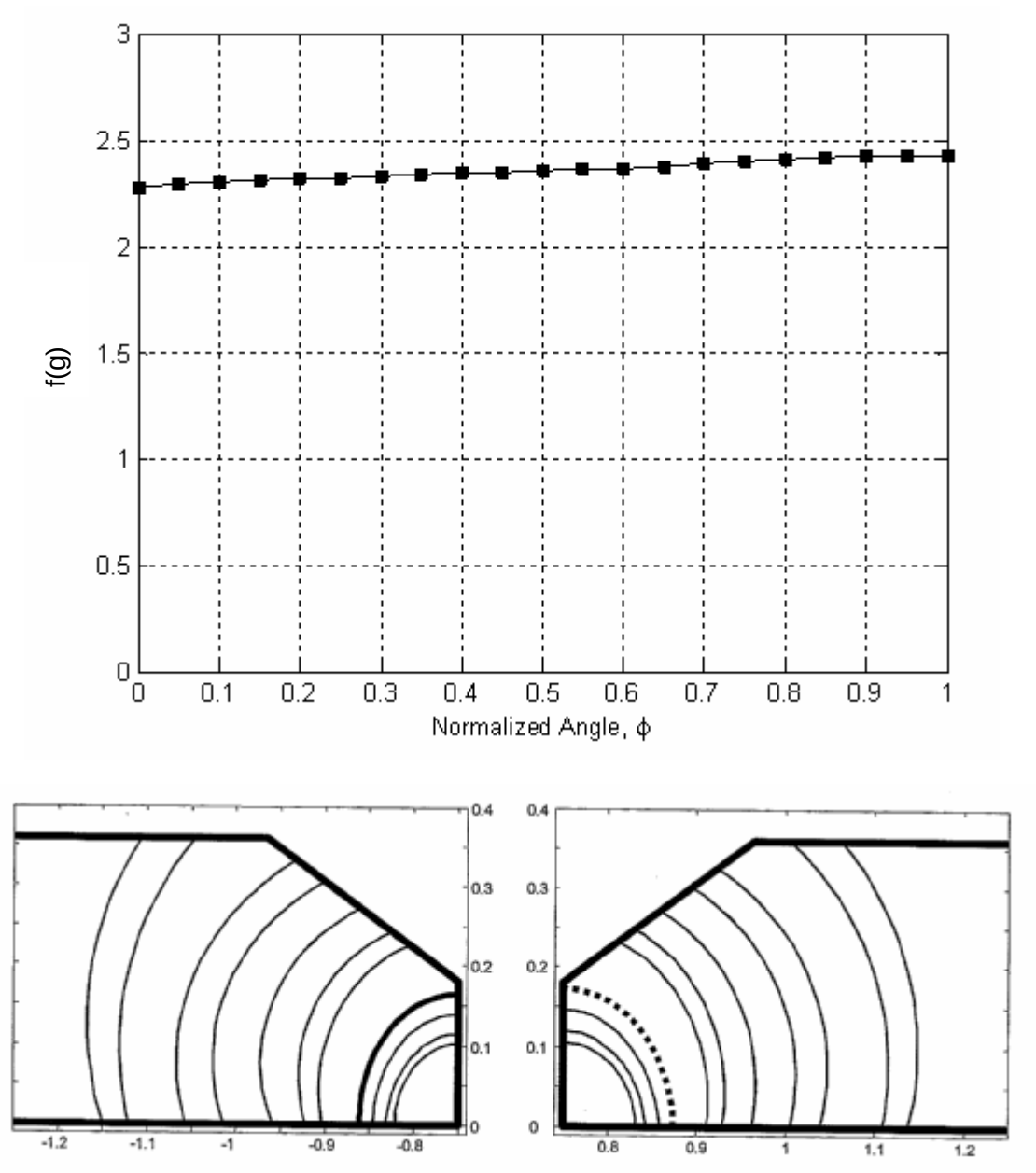

Figure A-69. Geometric Factors for FAA-21 (See table A-69)

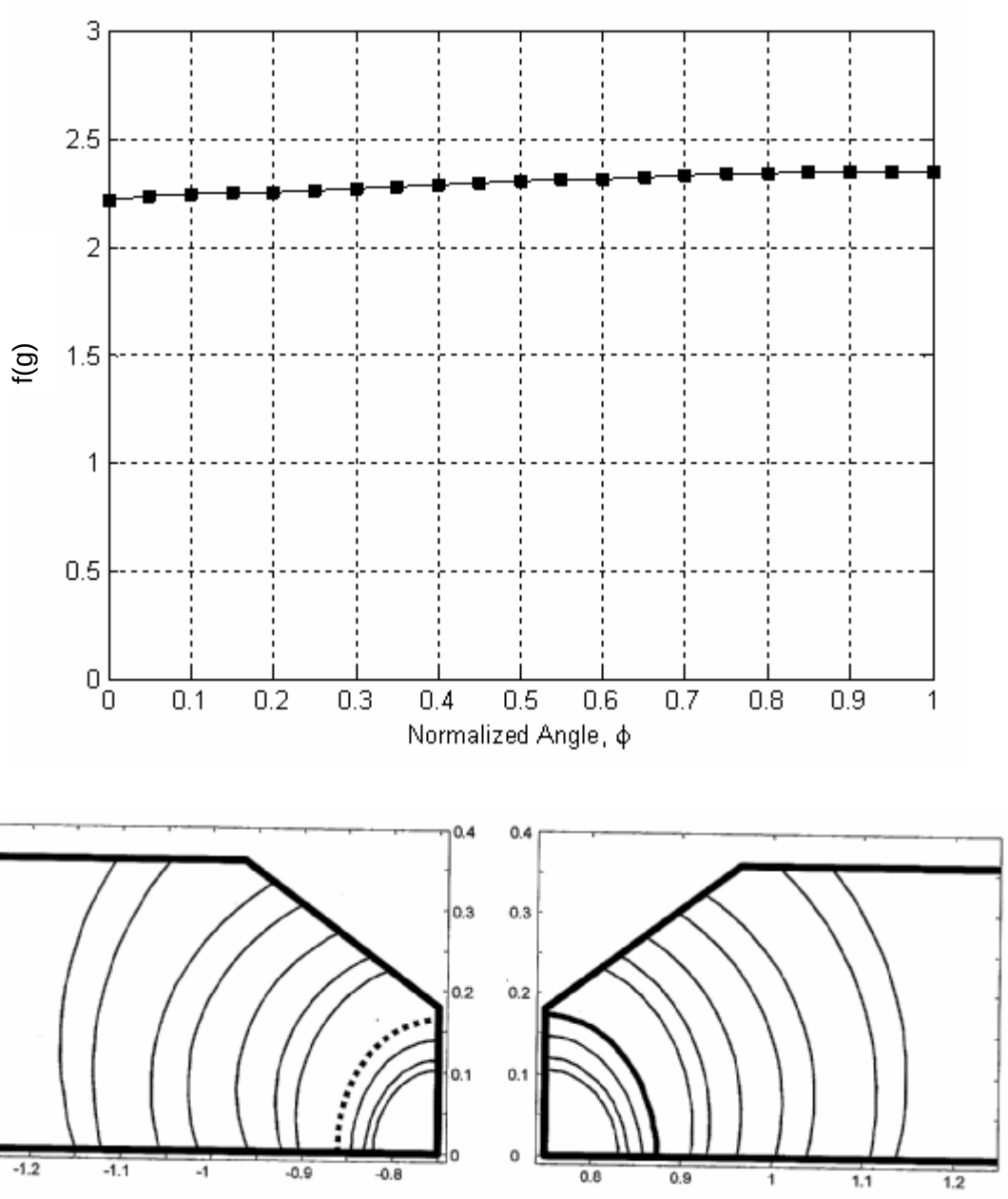

Figure A-70. Geometric Factors for FAA-21 (See table A-70)

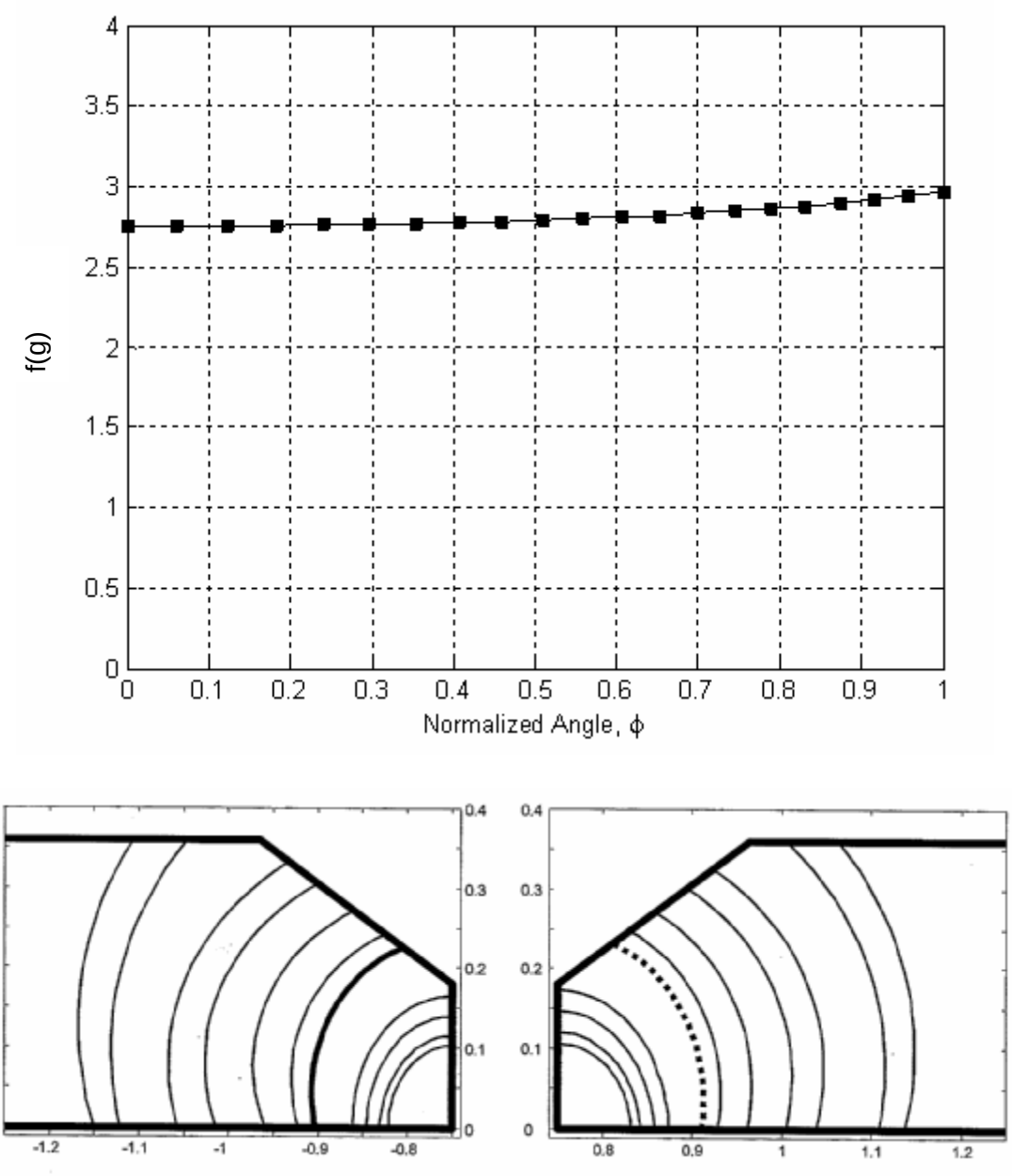

Figure A-71. Geometric Factors for FAA-21 (See table A-71)

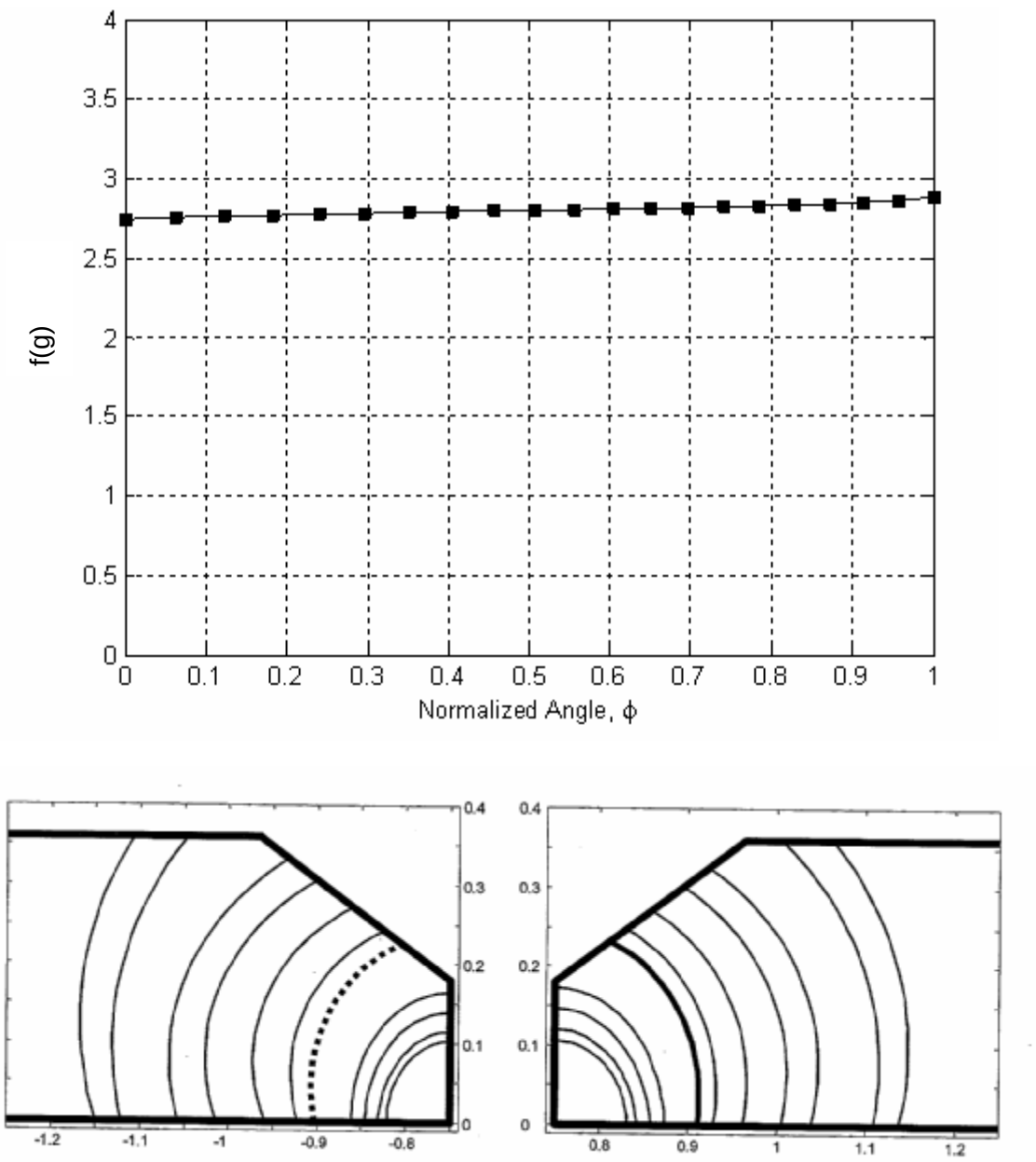

Figure A-72. Geometric Factors for FAA-21 (See table A-72)

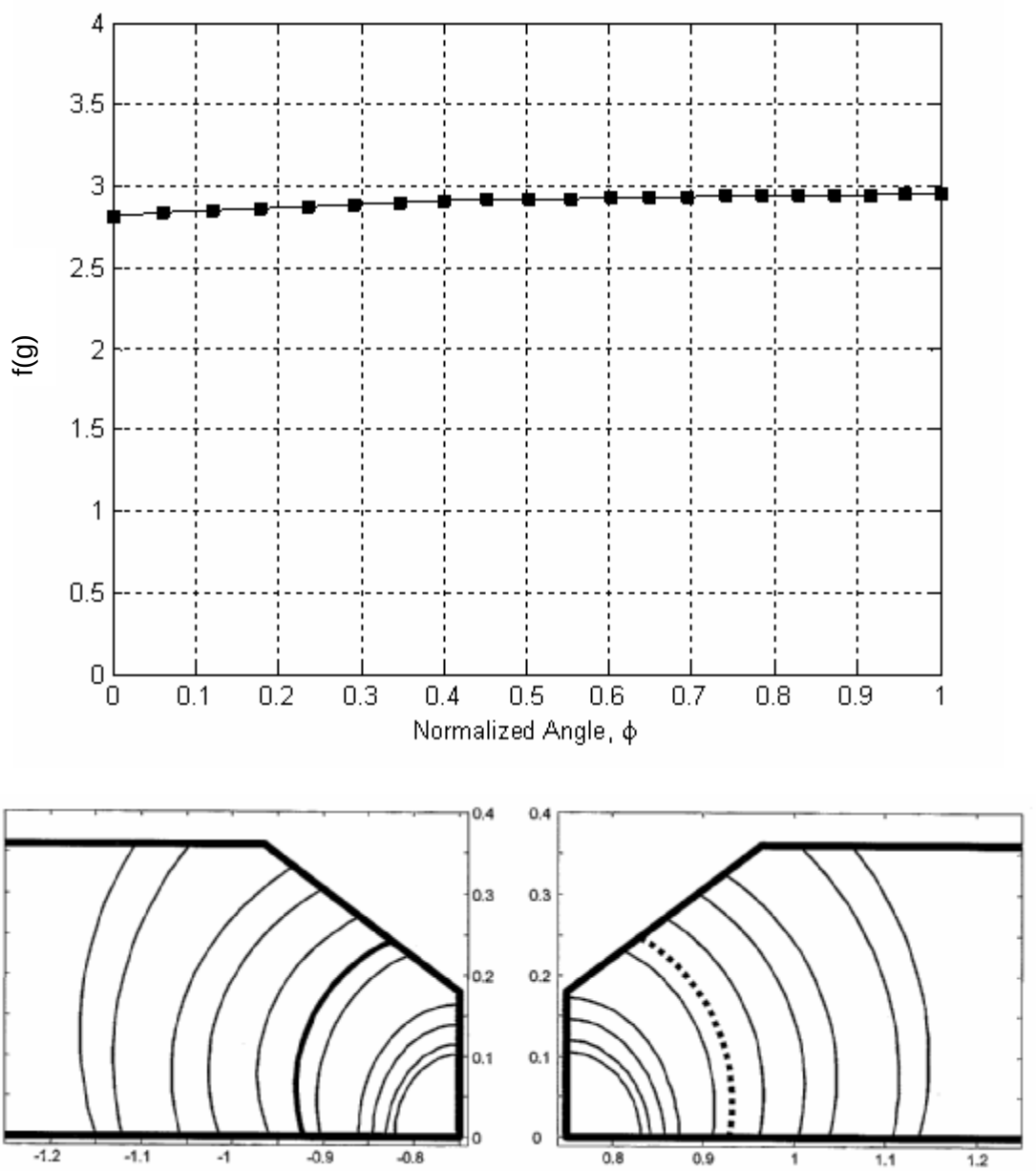

Figure A-73. Geometric Factors for FAA-21 (See table A-73)

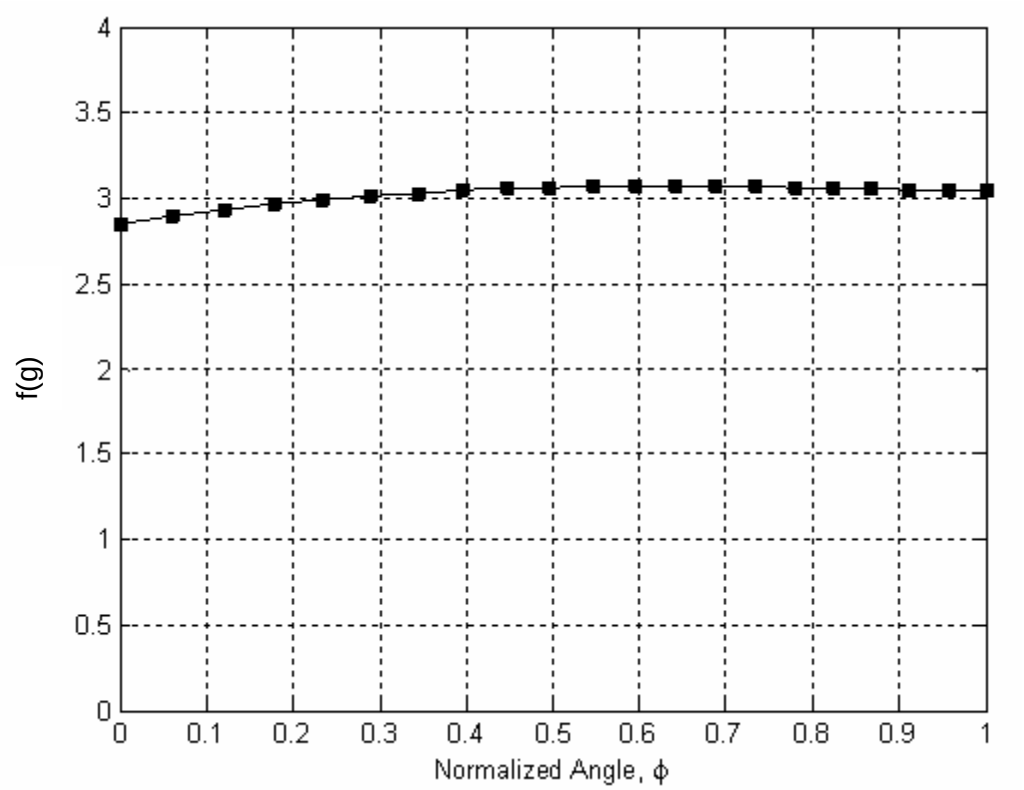

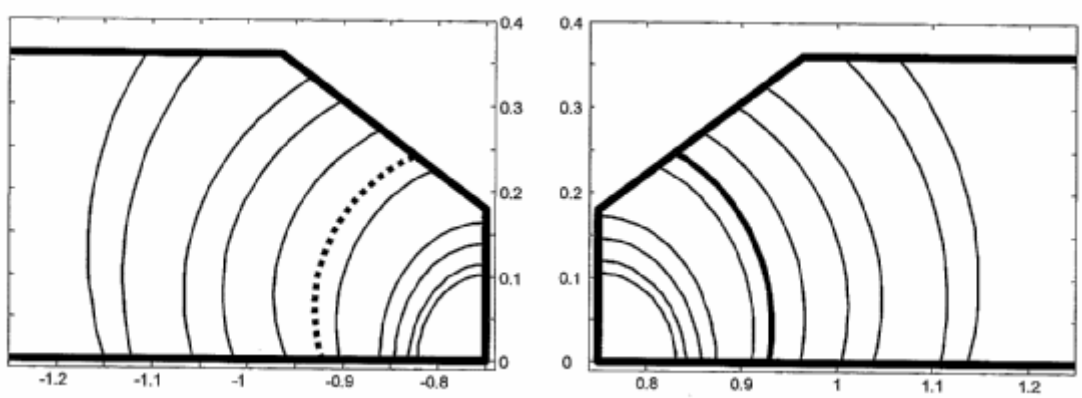

Figure A-74. Geometric Factors for FAA-21 (See table A-74)

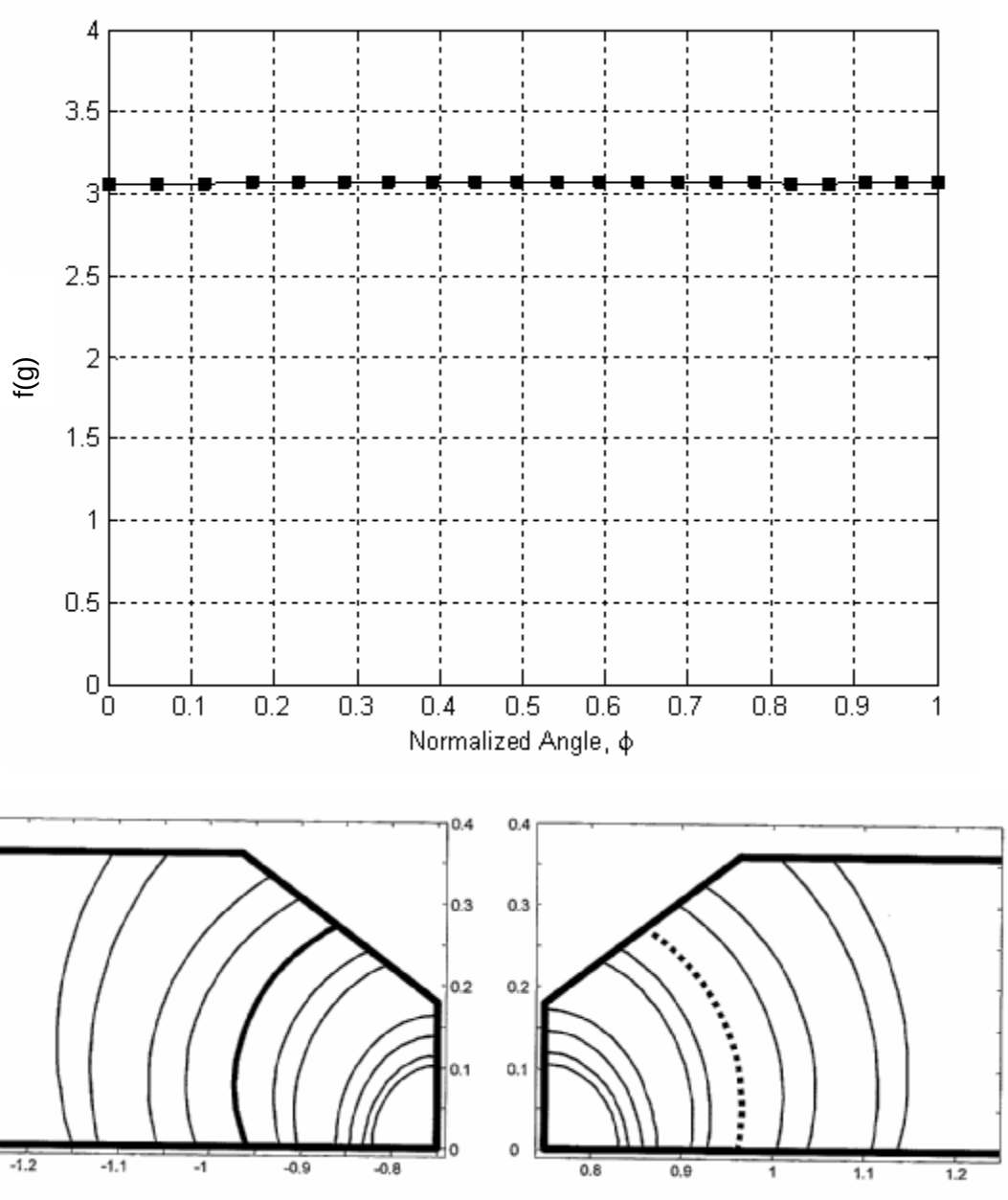

Figure A-75. Geometric Factors for FAA-21 (See table A-75)

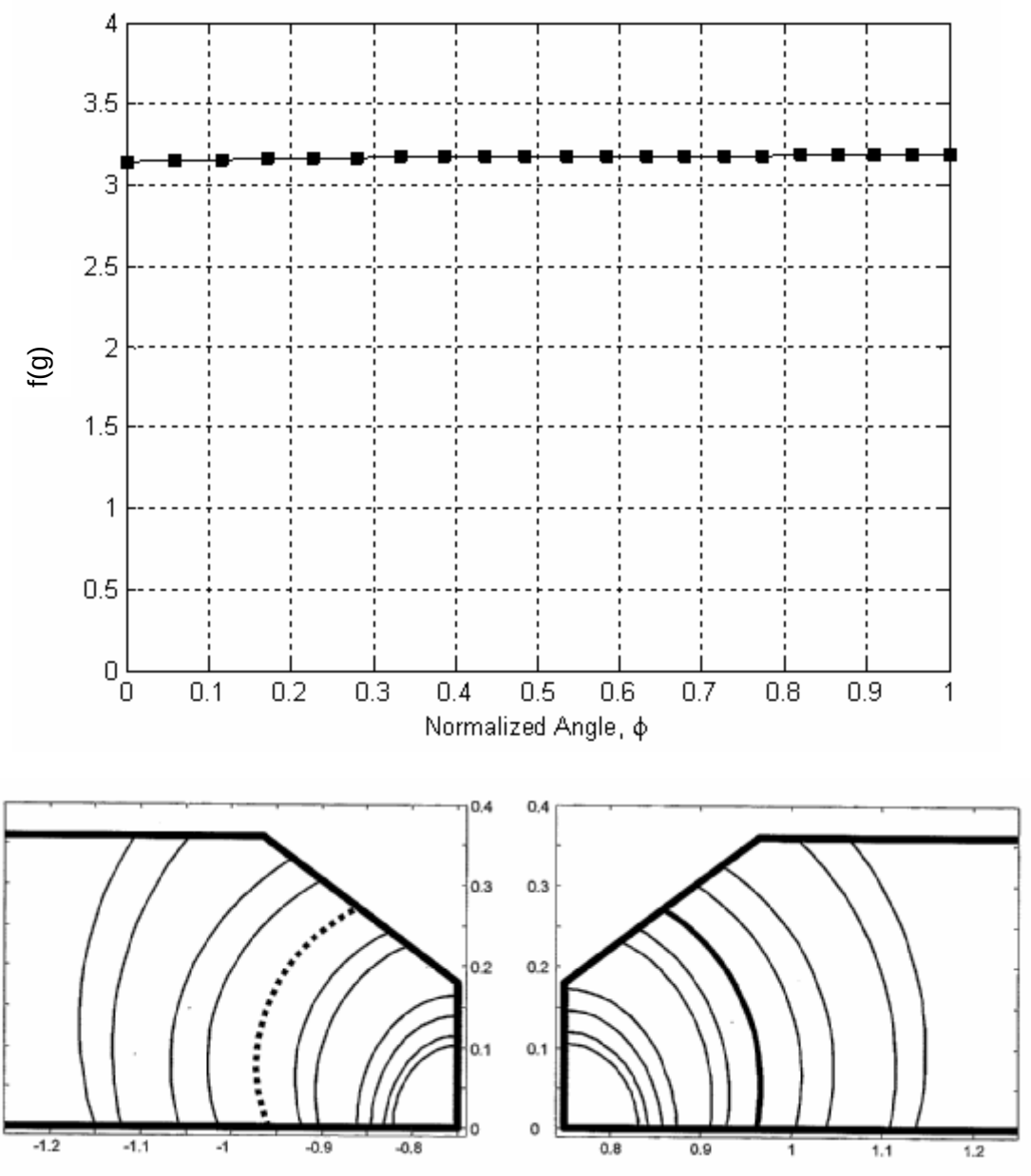

Figure A-76. Geometric Factors for FAA-21 (See table A-76)

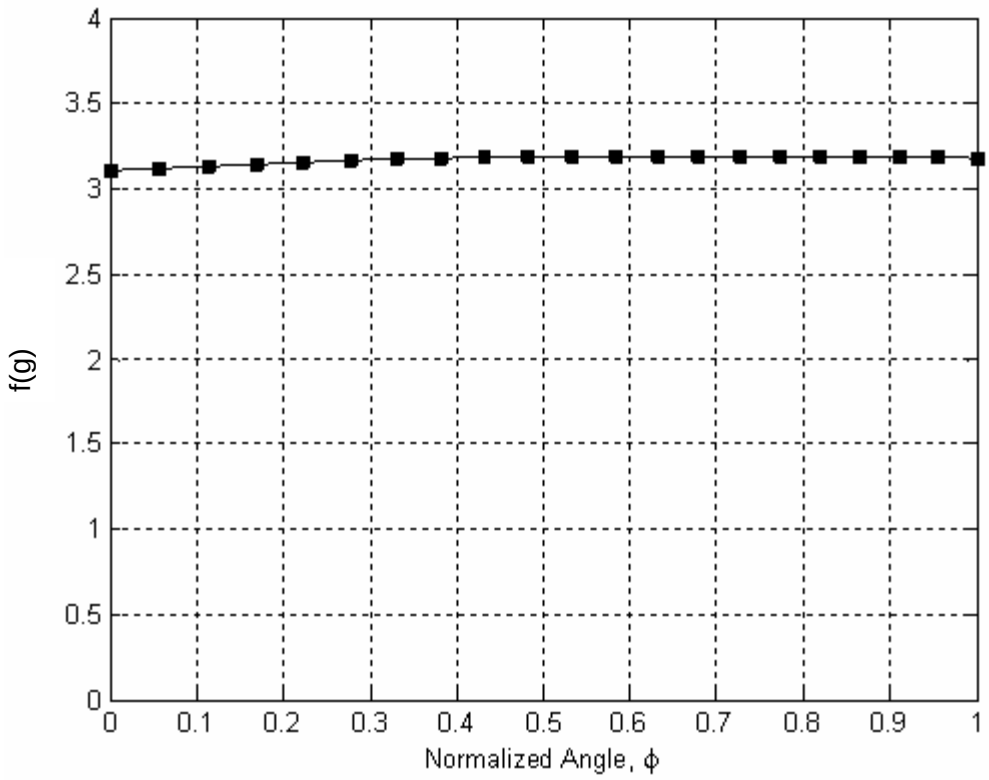

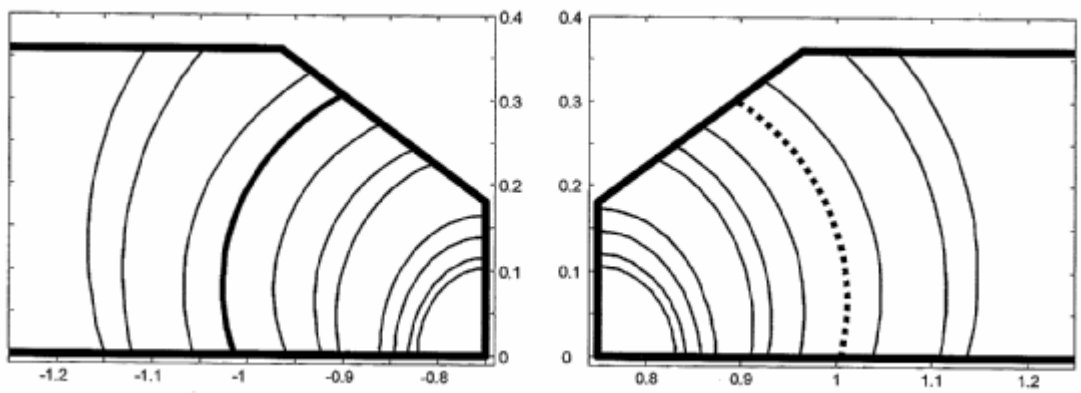

Figure A-77. Geometric Factors for FAA-21 (See table A-77)

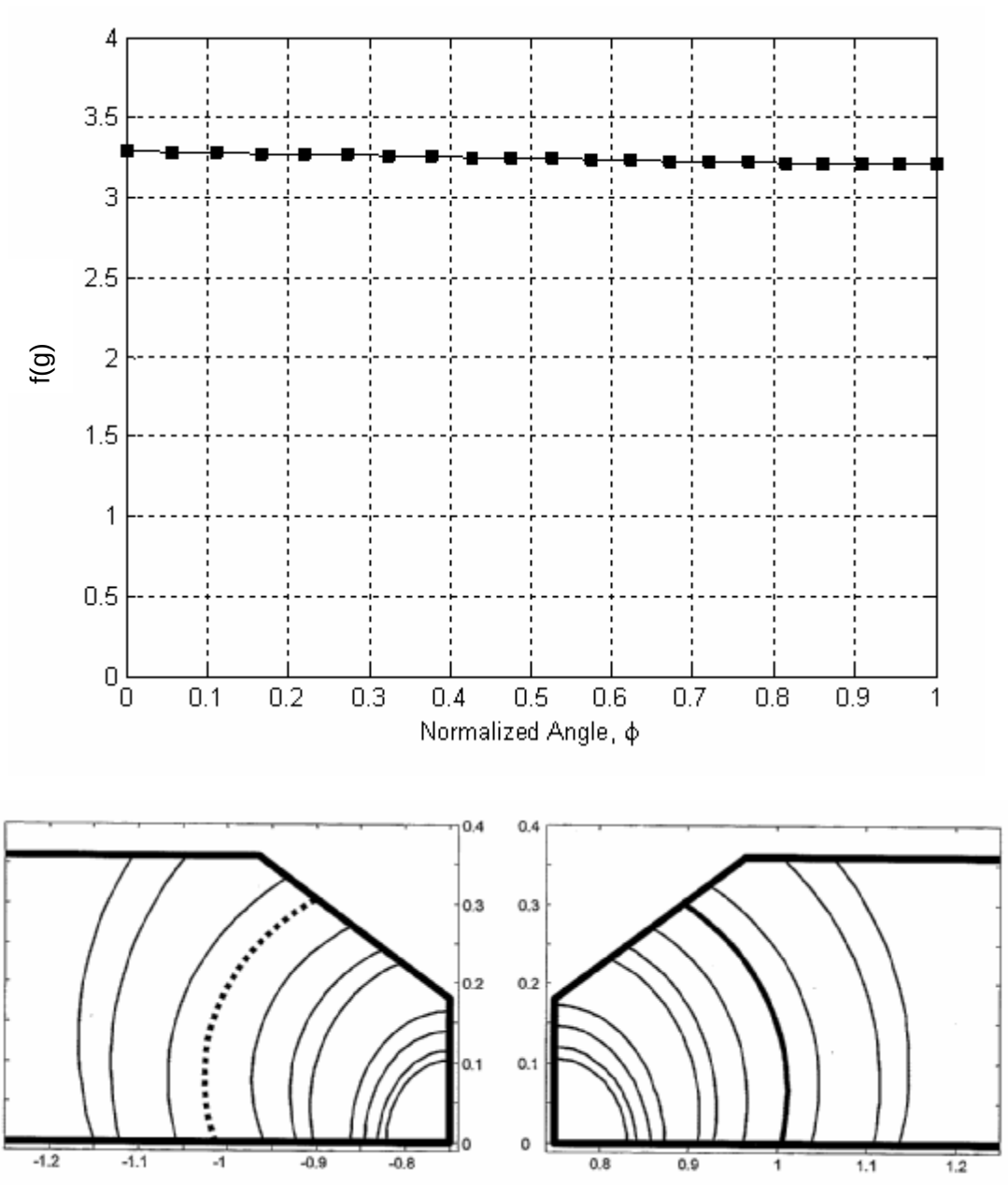

Figure A-78. Geometric Factors for FAA-21 (See table A-78)

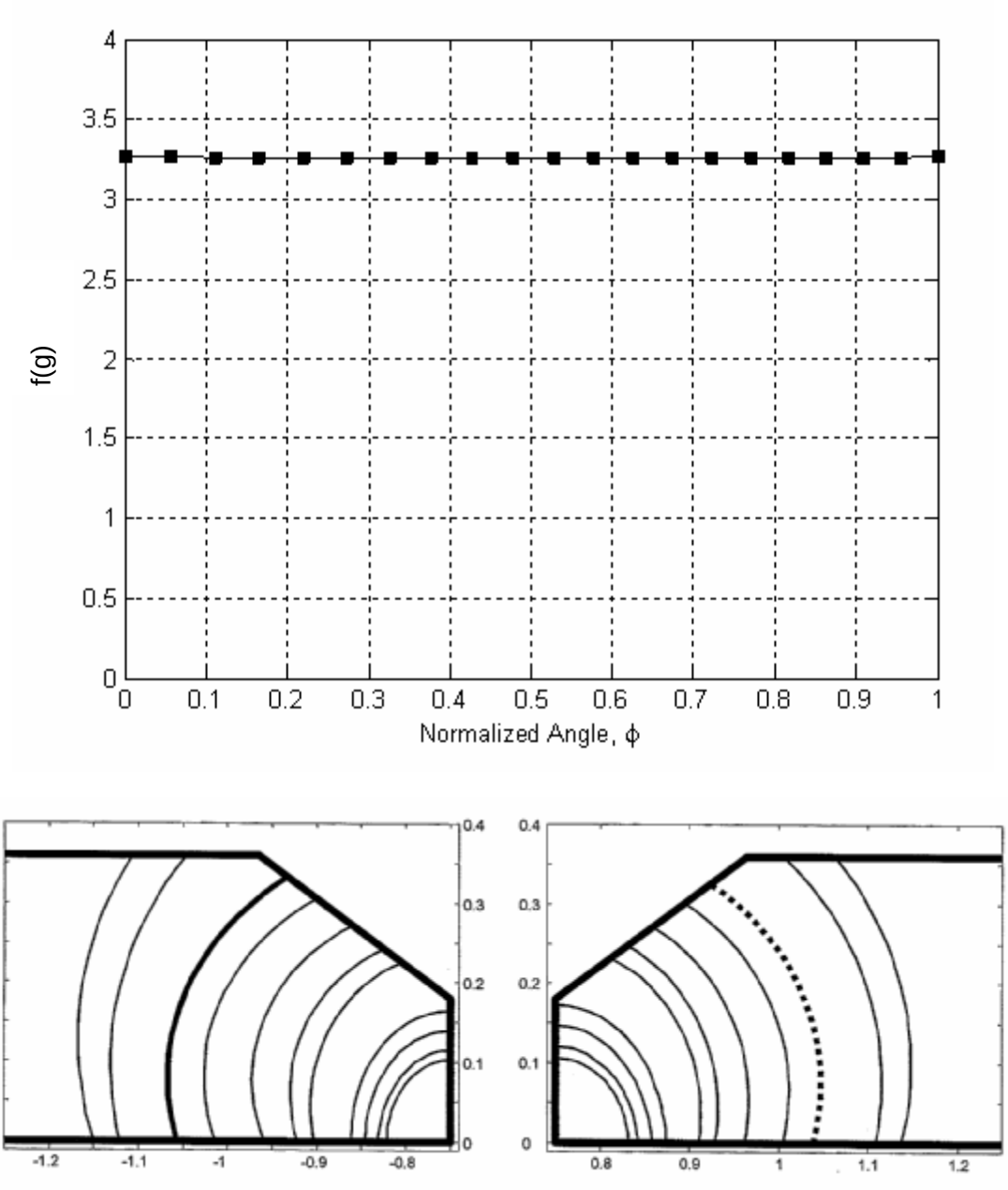

Figure A-79. Geometric Factors for FAA-21 (See table A-79)

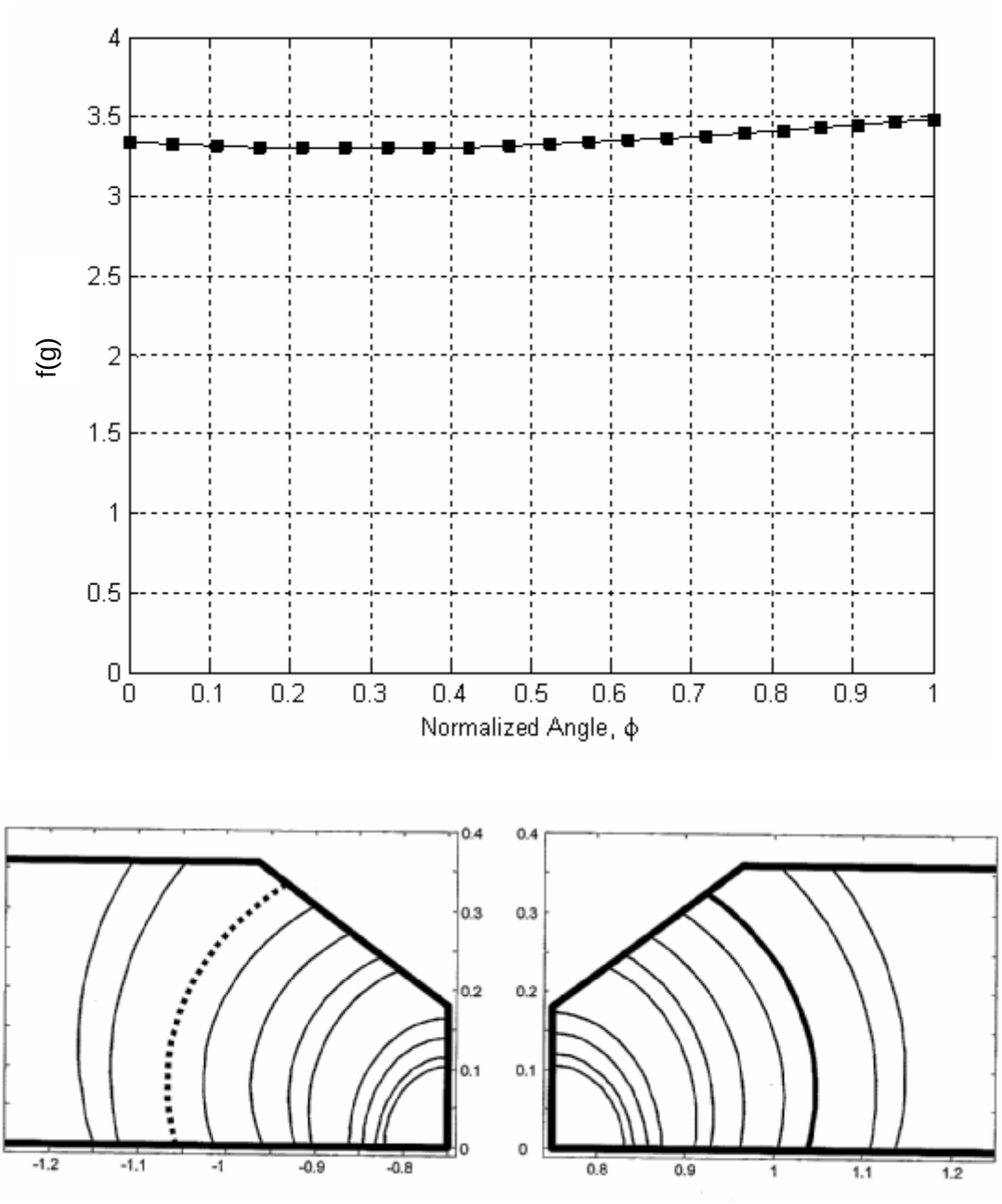

Figure A-80. Geometric Factors for FAA-21 (See table A-80)

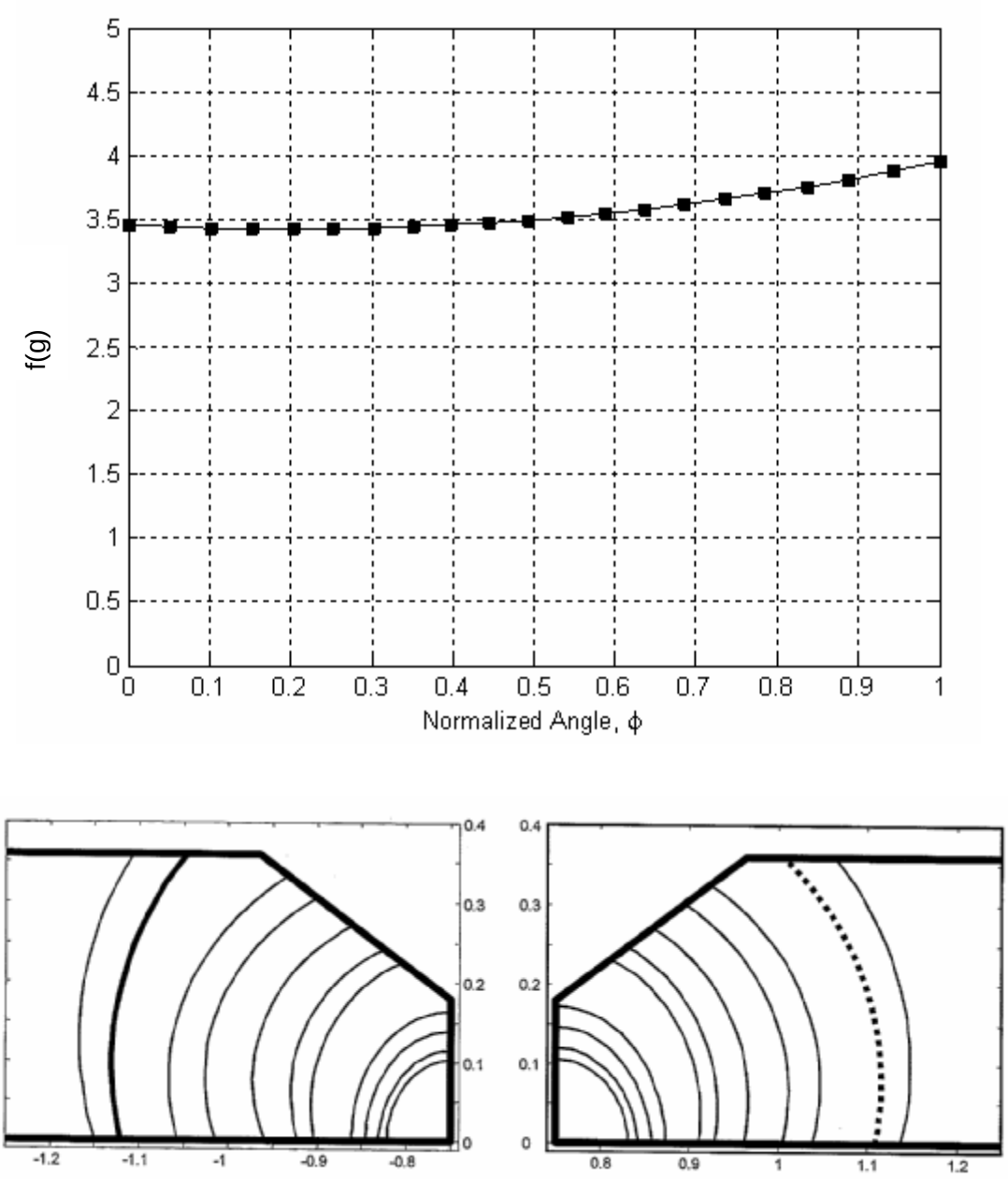

Figure A-81. Geometric Factors for FAA-21 (See table A-81)

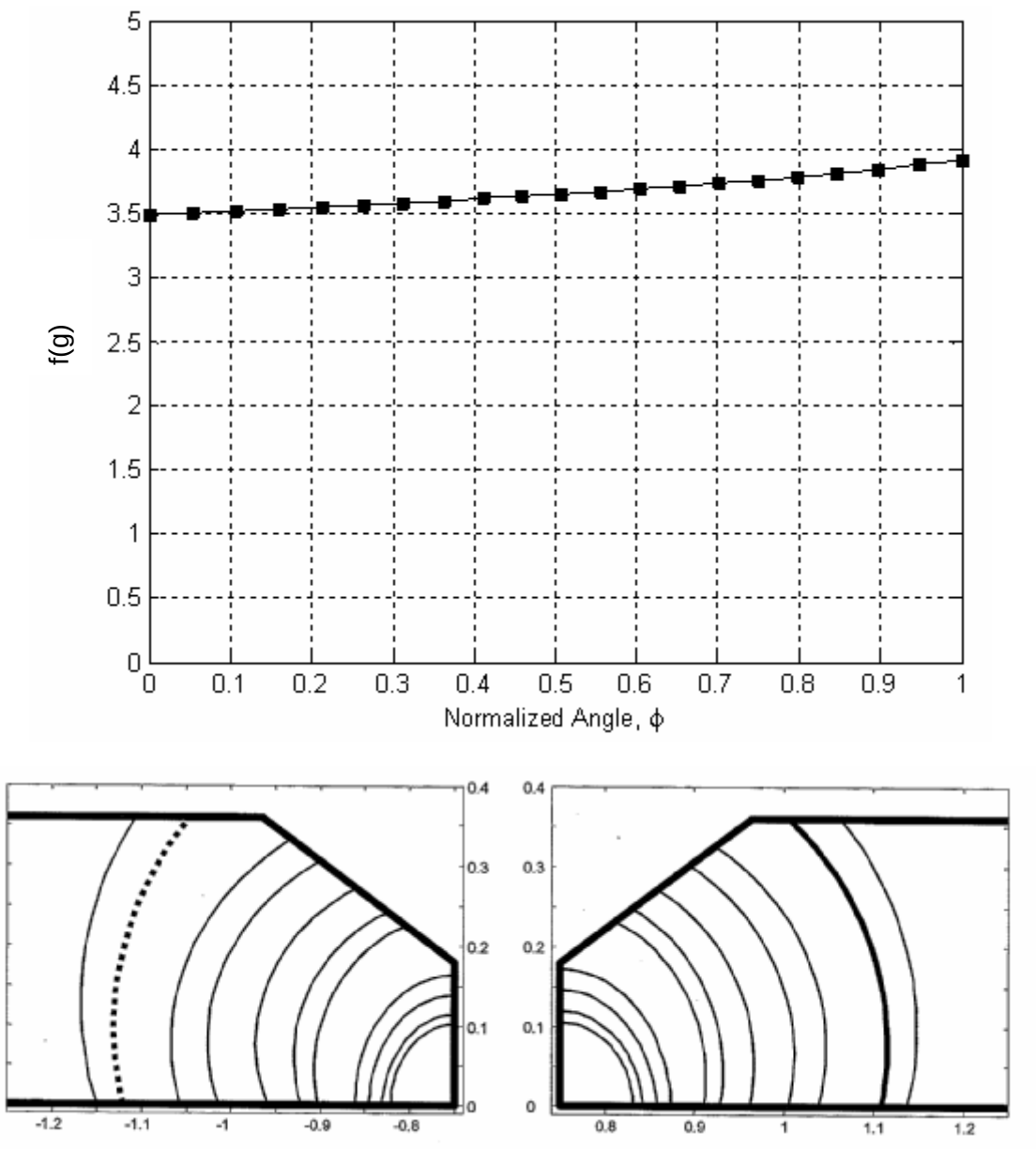

Figure A-82. Geometric Factors for FAA-21 (See table A-82)

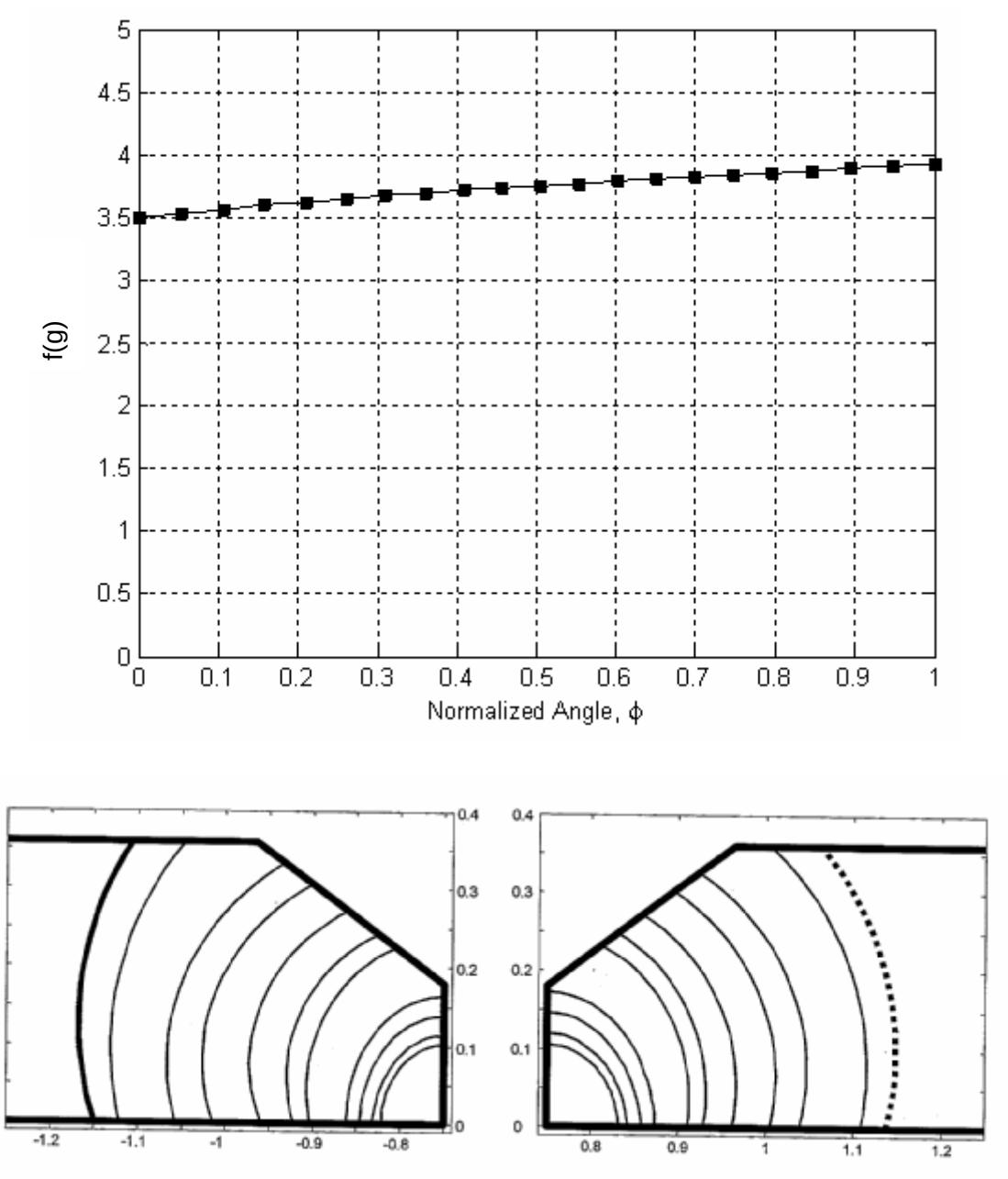

Figure A-83. Geometric Factors for FAA-21 (See table A-83)

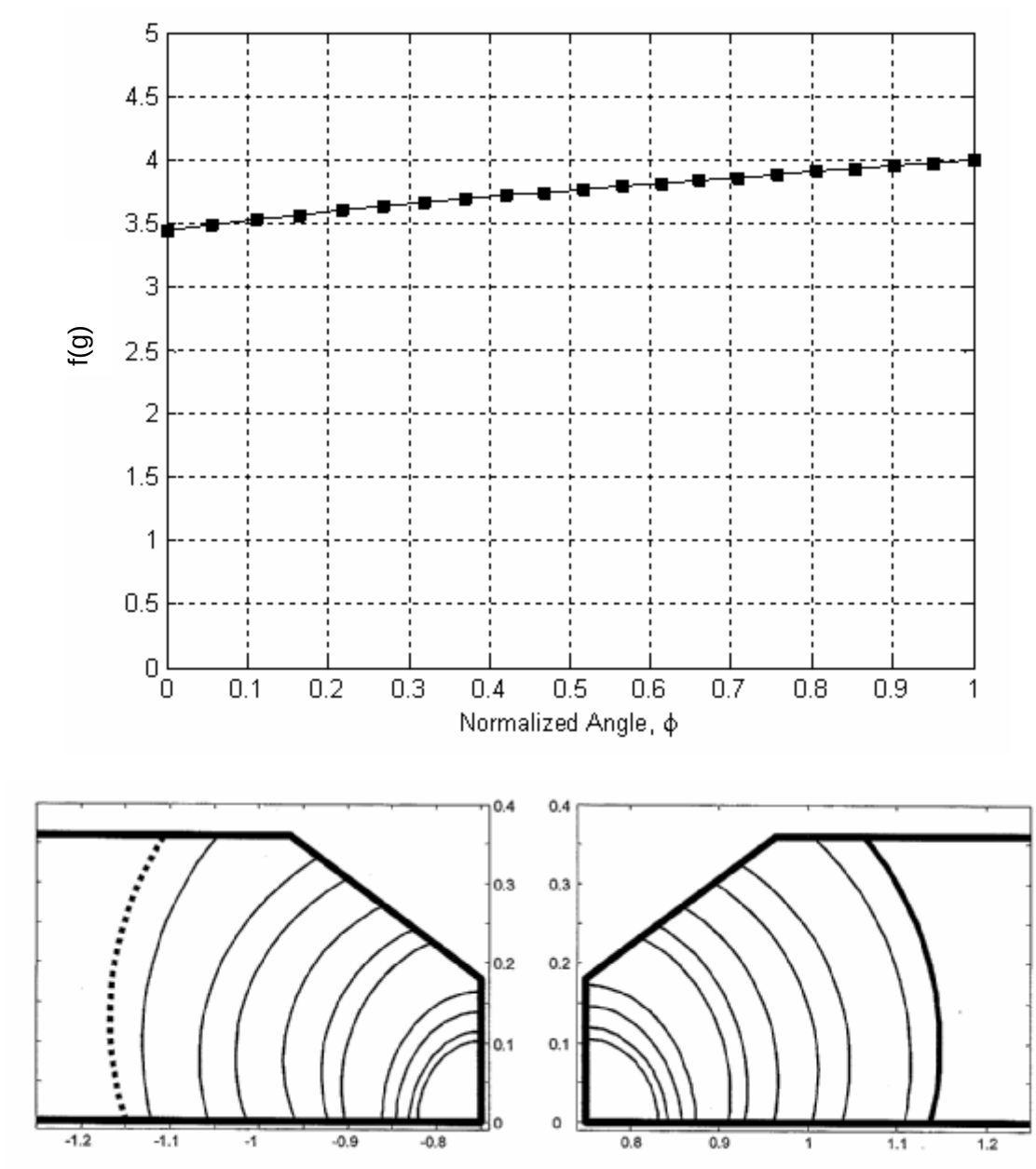

Figure A-84. Geometric Factors for FAA-21 (See table A-84)

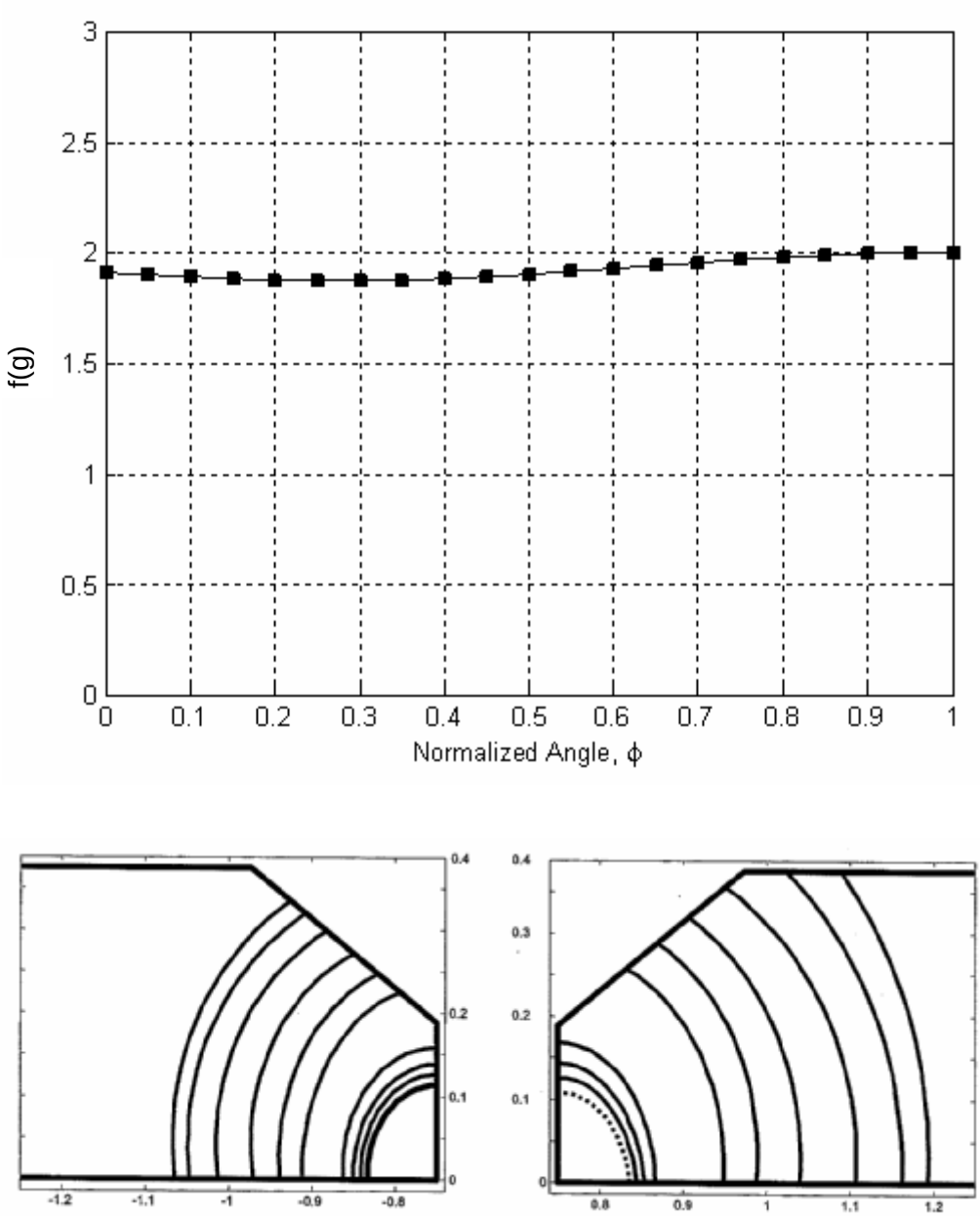

Figure A-85. Geometric Factors for FAA-22 (See table A-85)

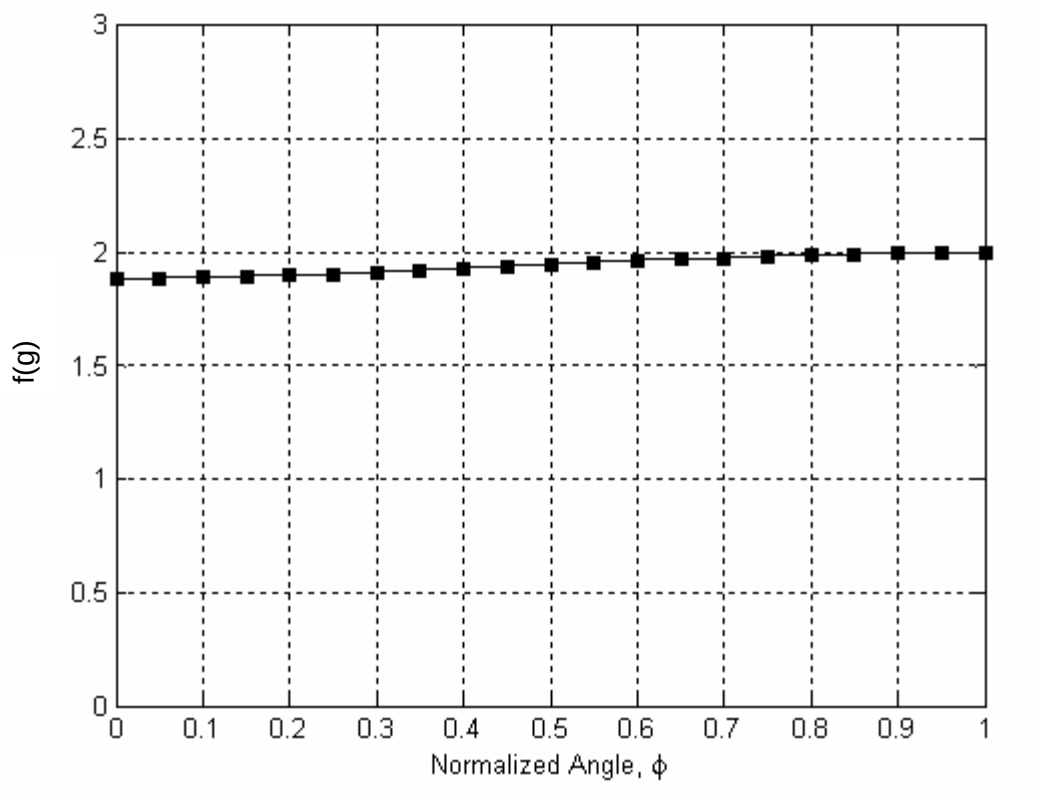

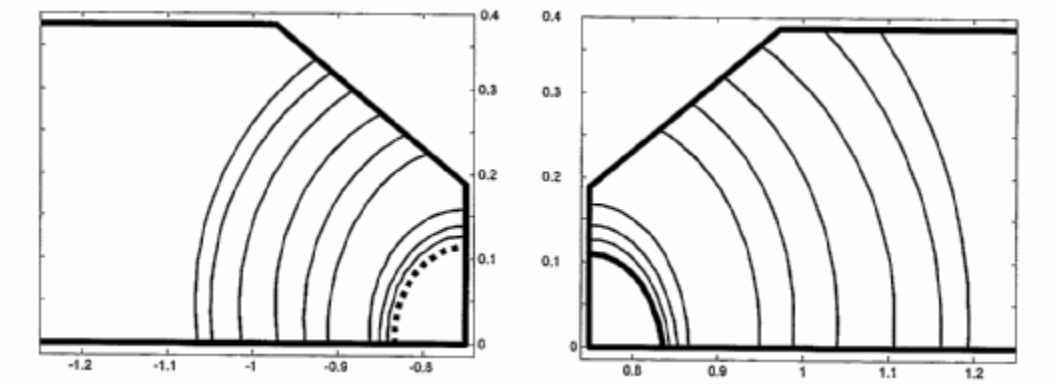

Figure A-86. Geometric Factors for FAA-22 (See table A-86)

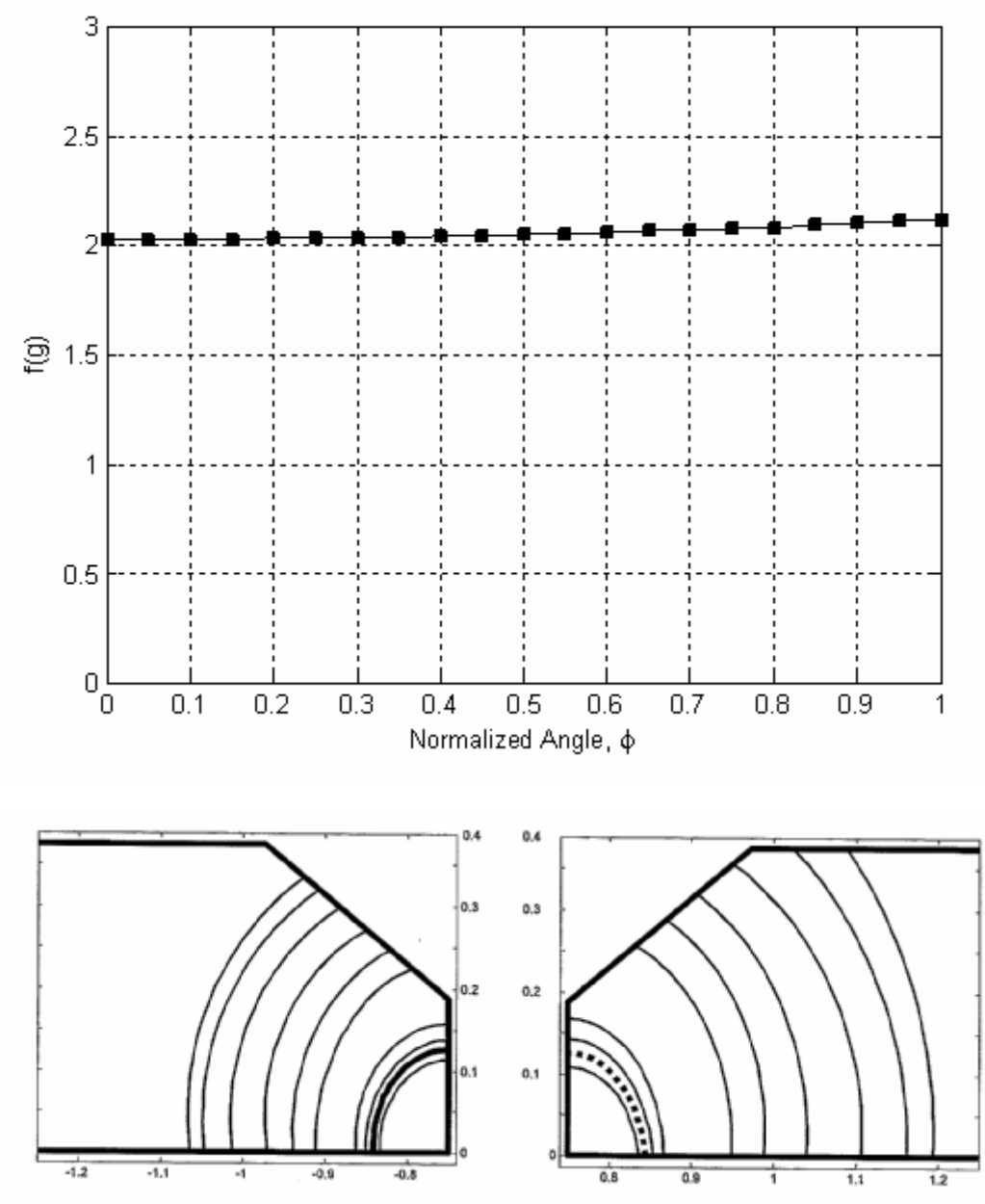

Figure A-87. Geometric Factors for FAA-22 (See table A-87)

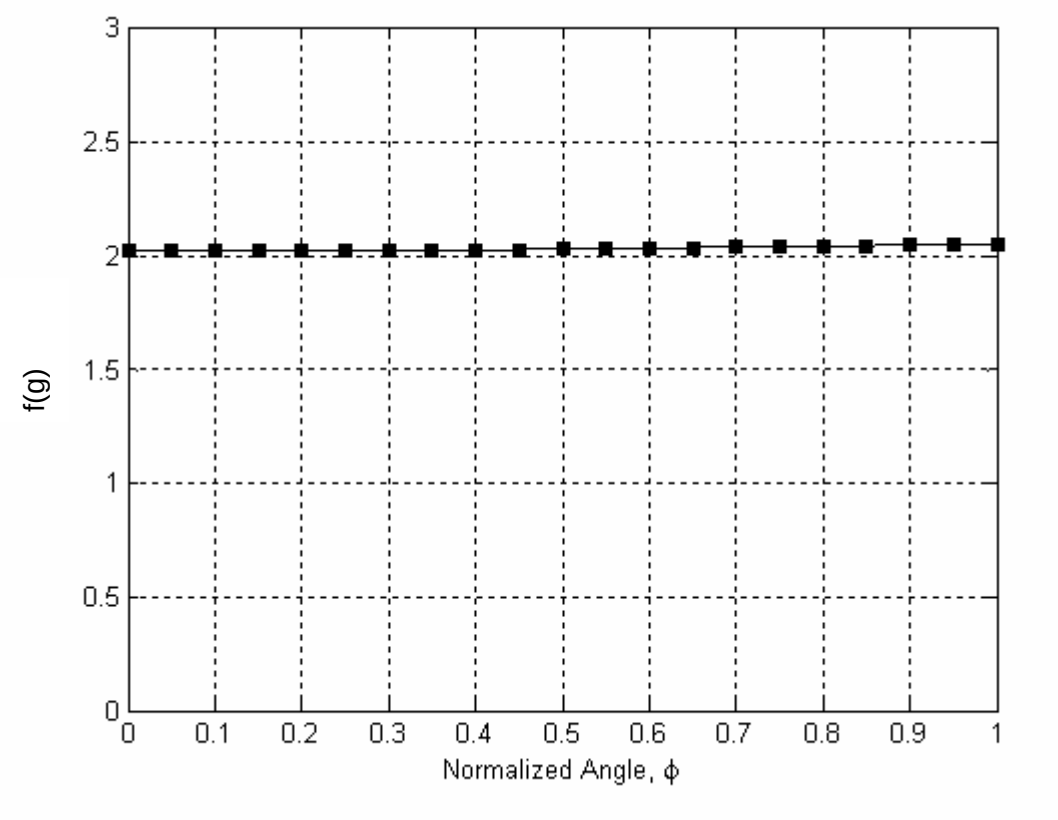

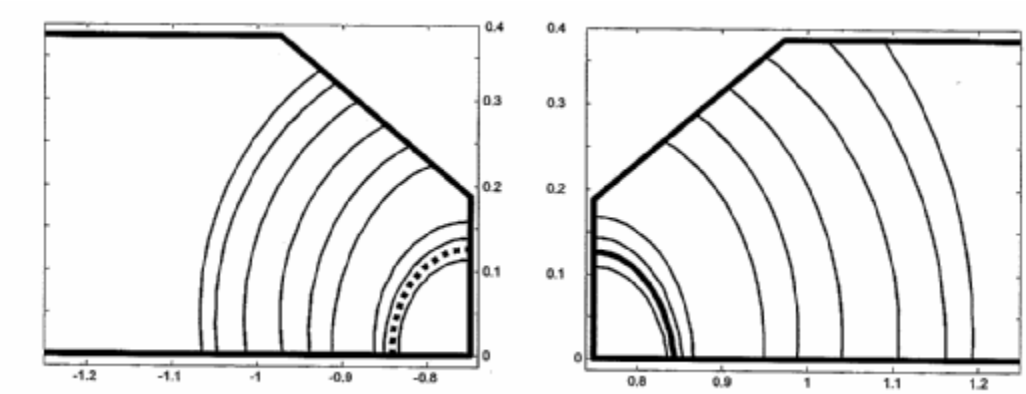

Figure A-88. Geometric Factors for FAA-22 (See table A-88)

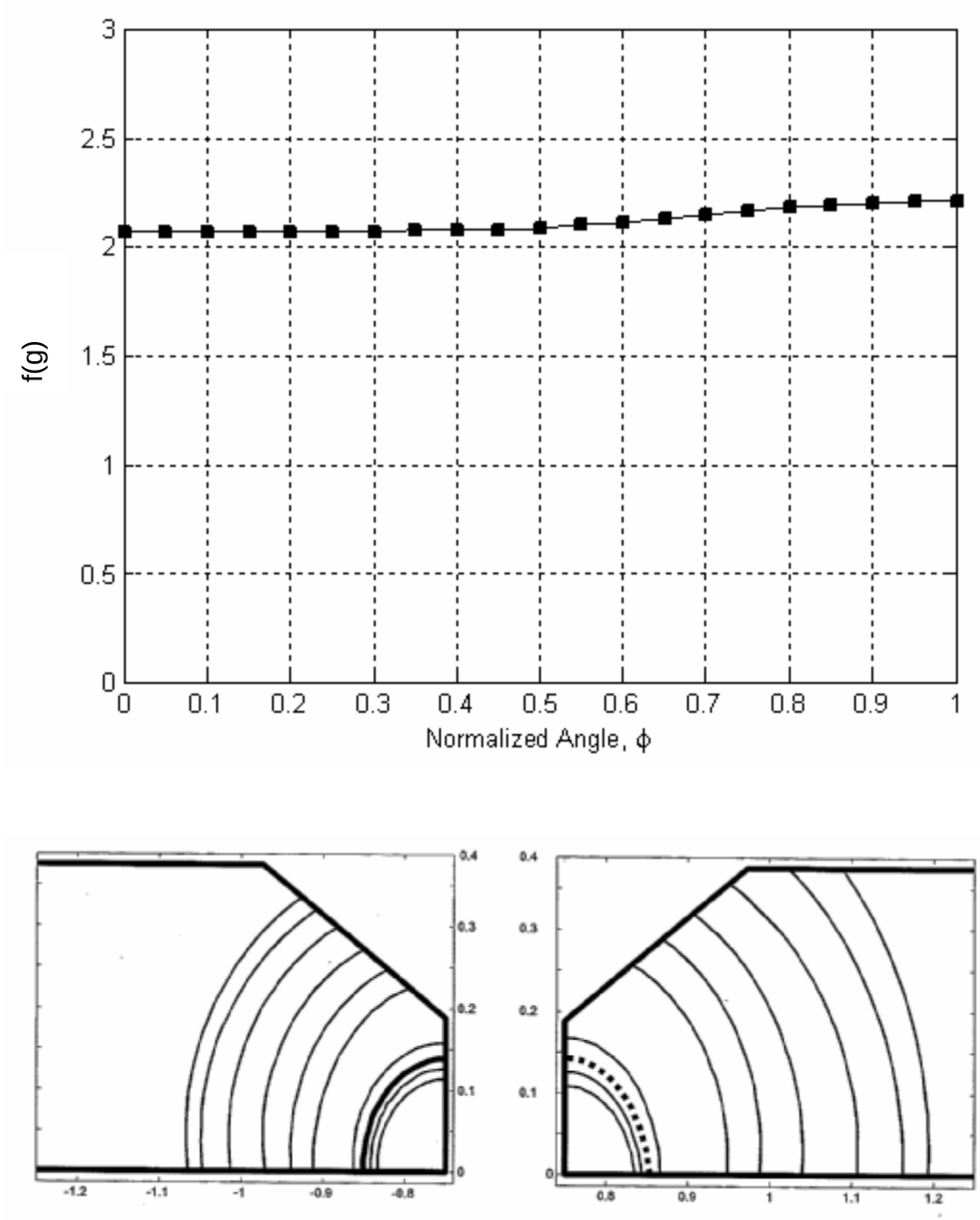

Figure A-89. Geometric Factors for FAA-22 (See table A-89)

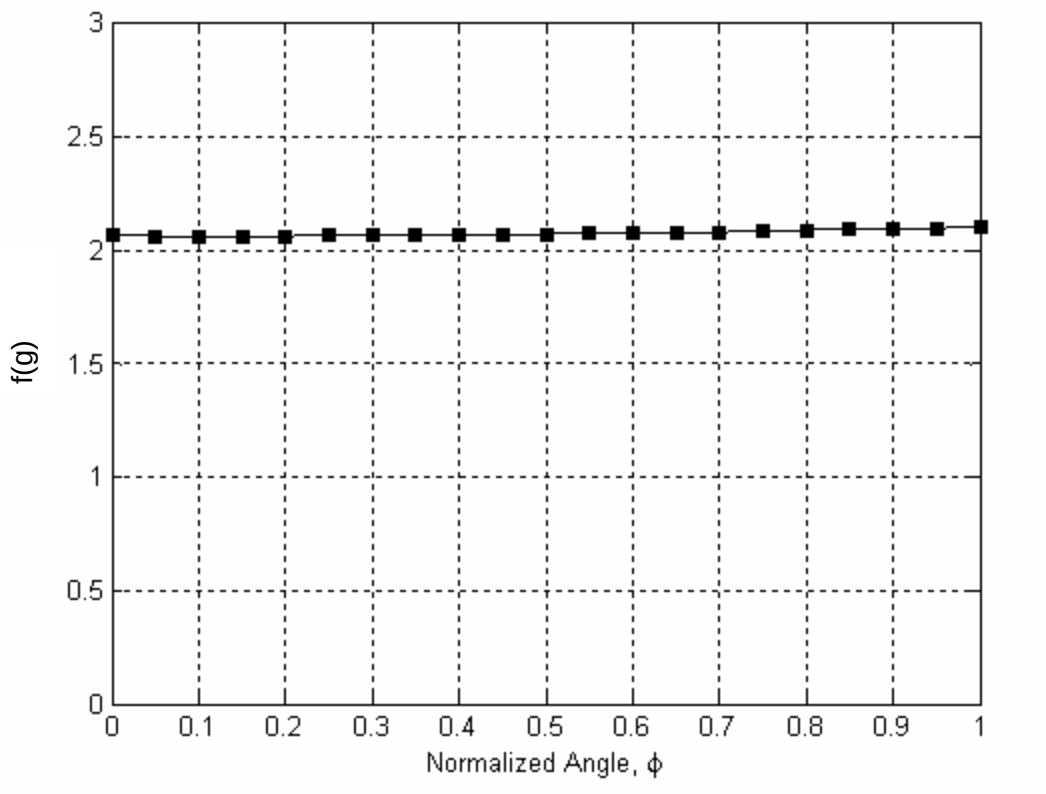

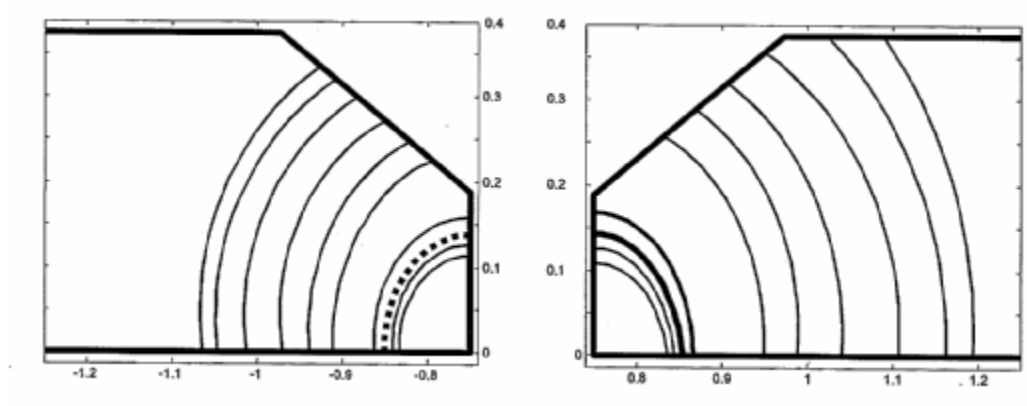

Figure A-90. Geometric Factors for FAA-22 (See table A-90)

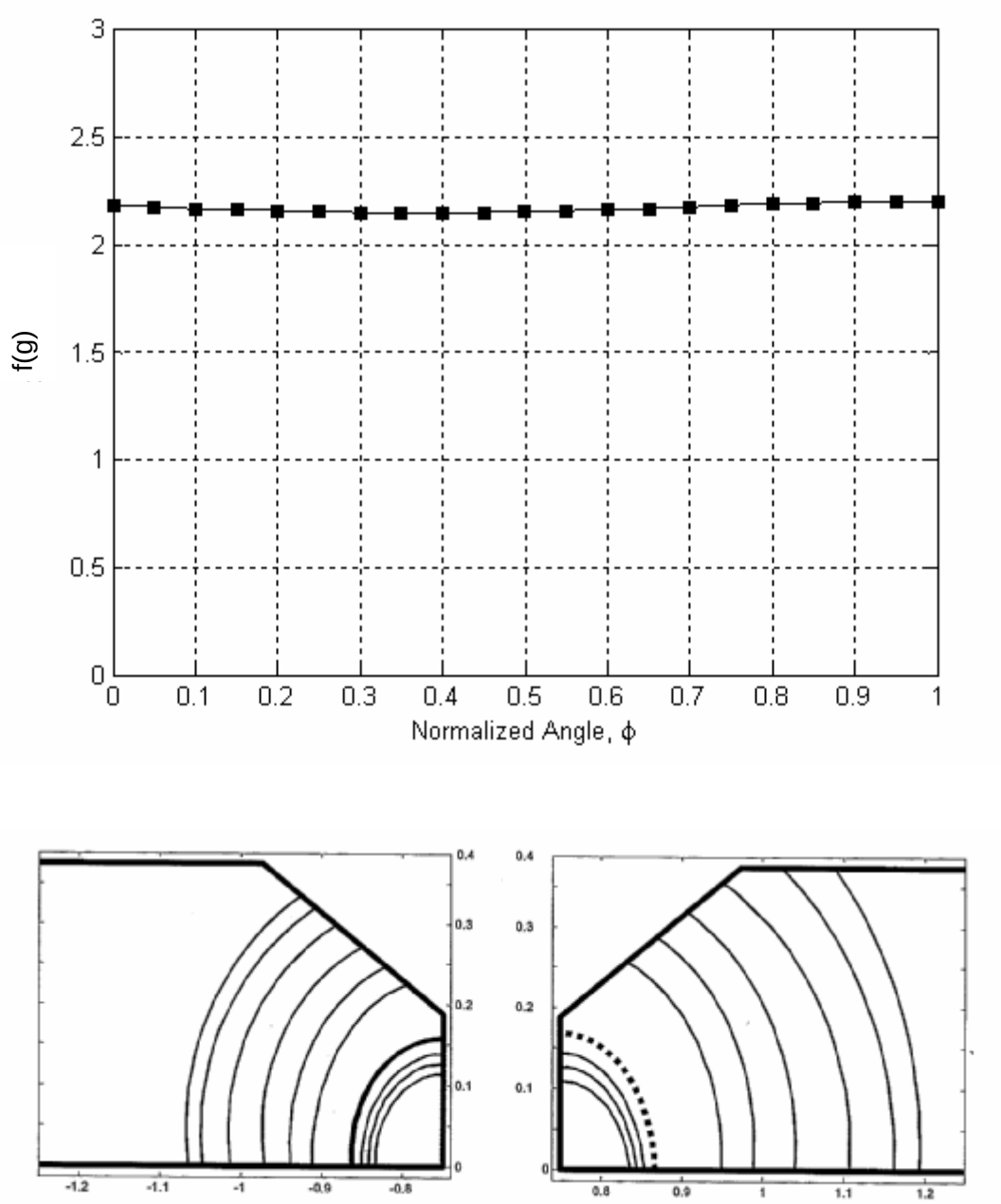

Figure A-91. Geometric Factors for FAA-22 (See table A-91)

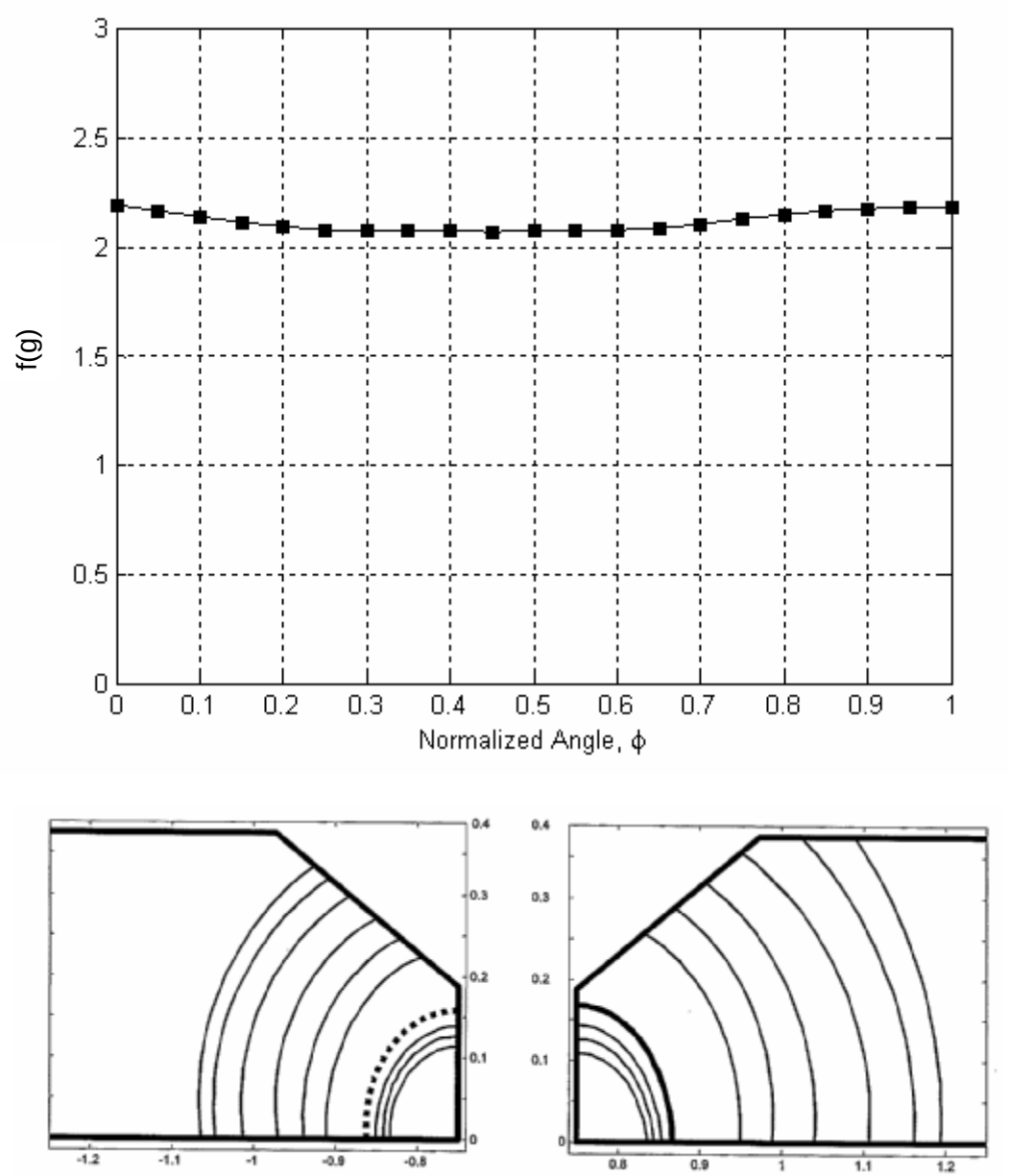

Figure A-92. Geometric Factors for FAA-22 (See table A-92)

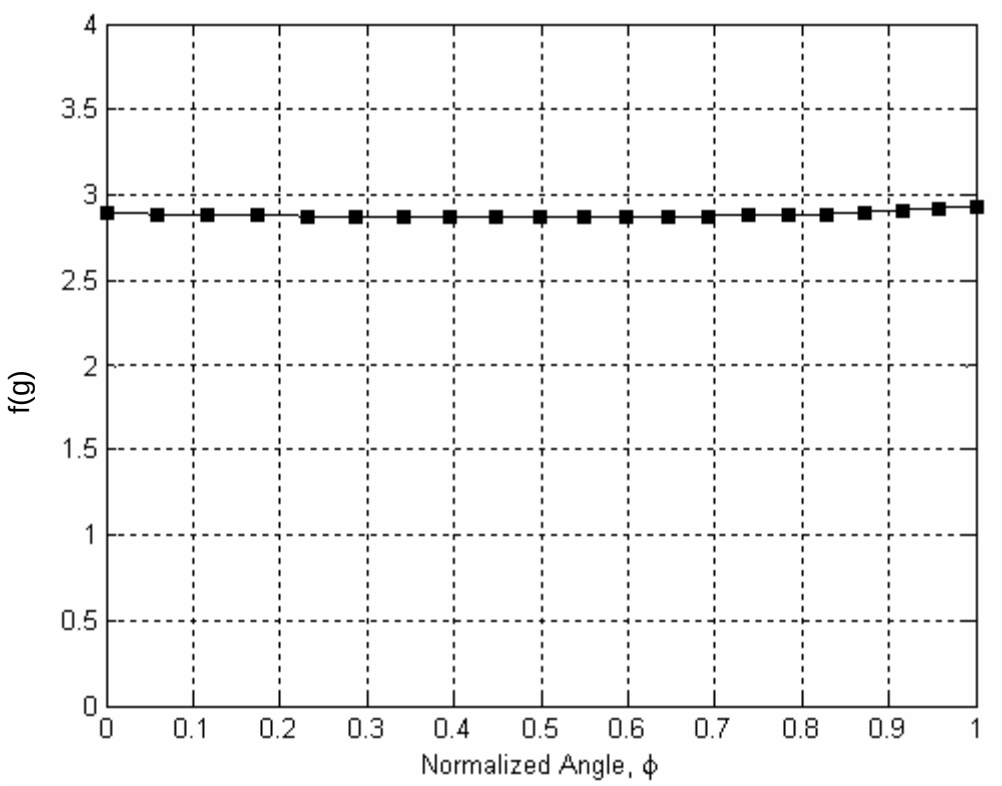

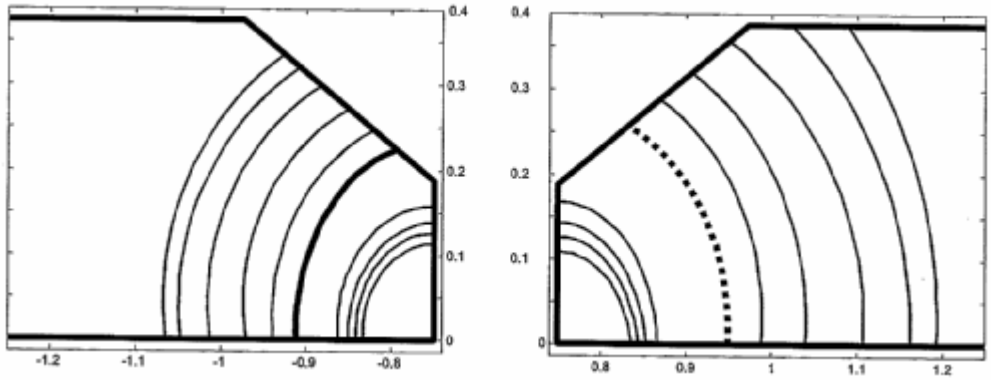

Figure A-93. Geometric Factors for FAA-22 (See table A-93)

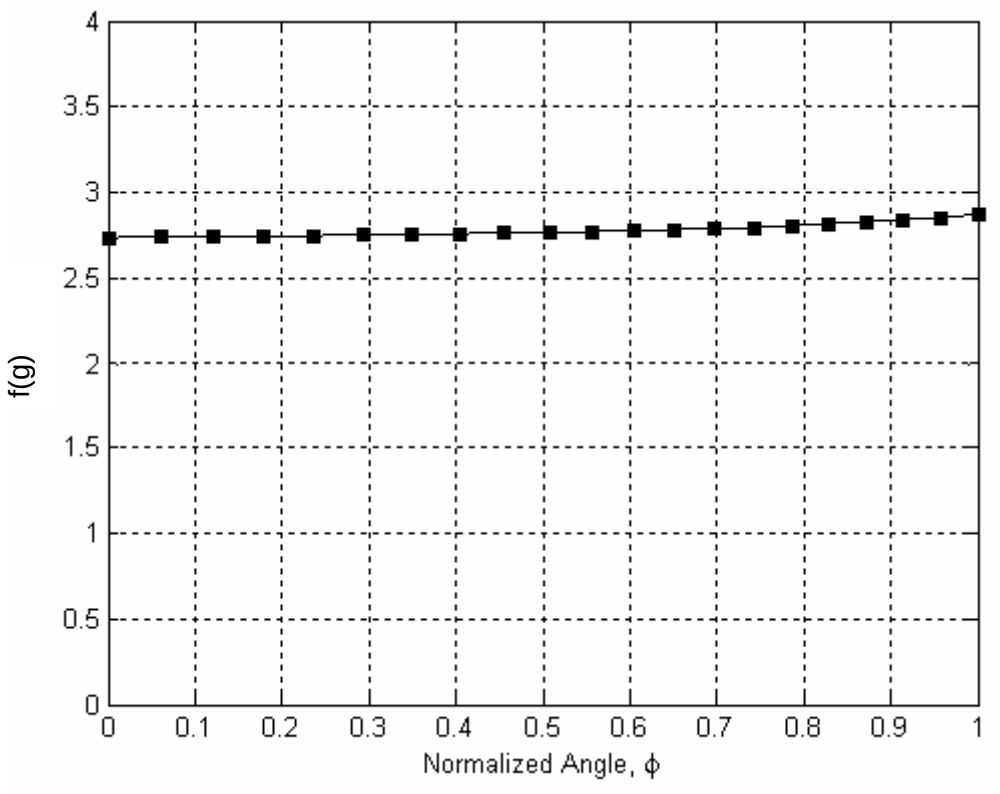

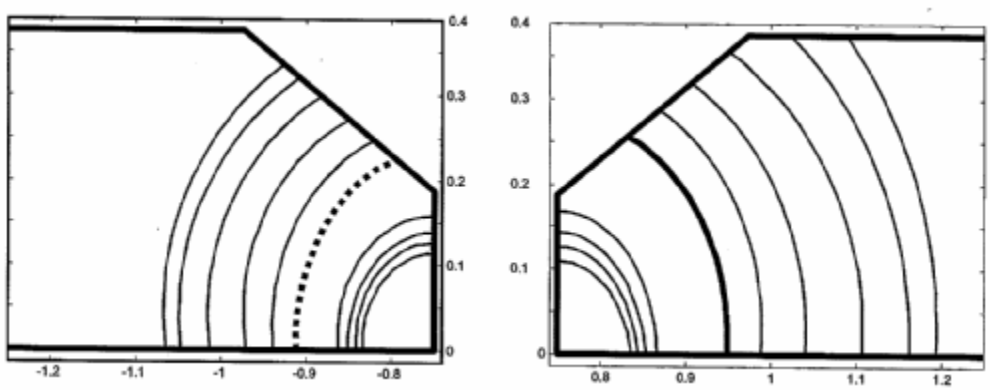

Figure A-94. Geometric Factors for FAA-22 (See table A-94)

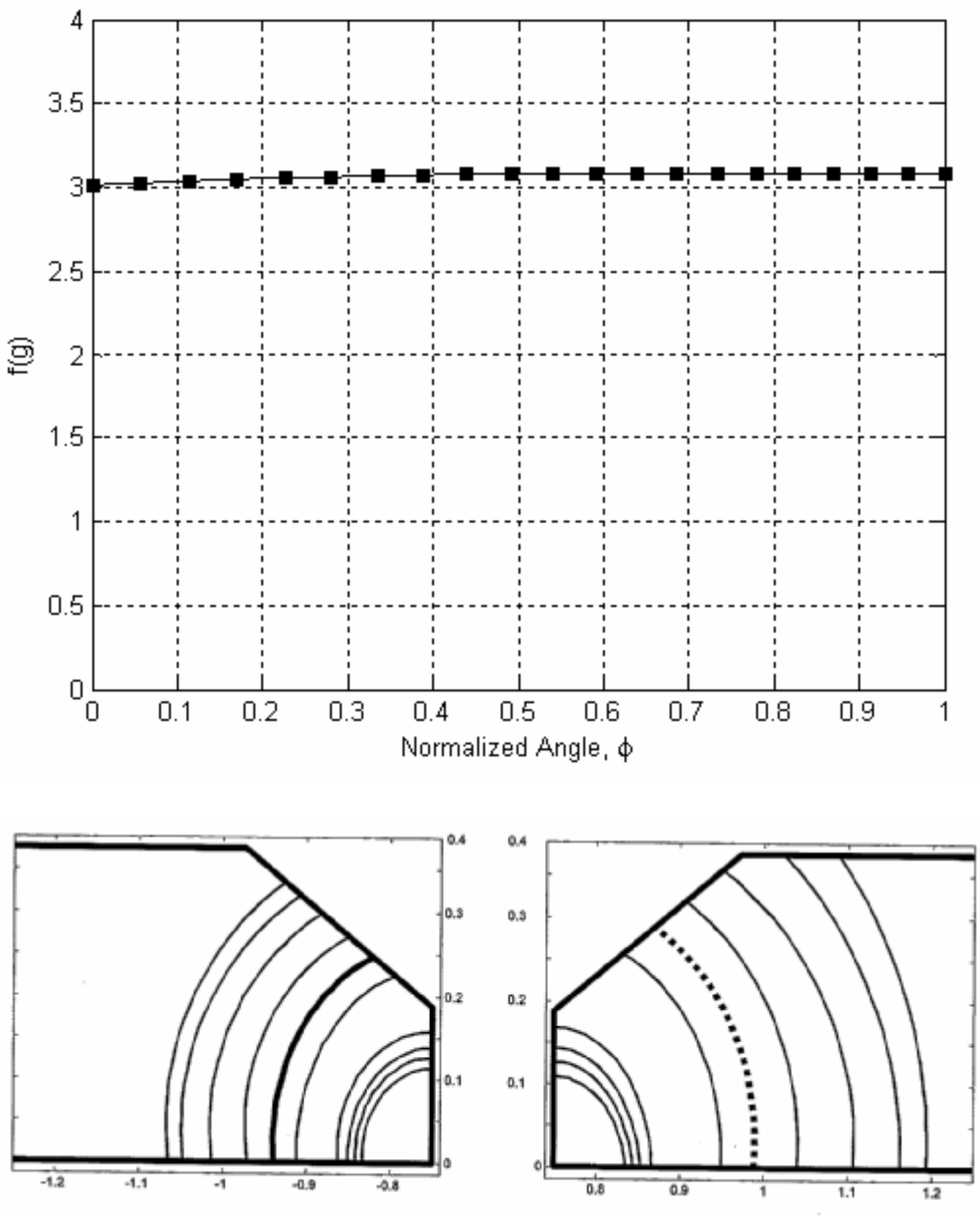

Figure A-95. Geometric Factors for FAA-22 (See table A-95)

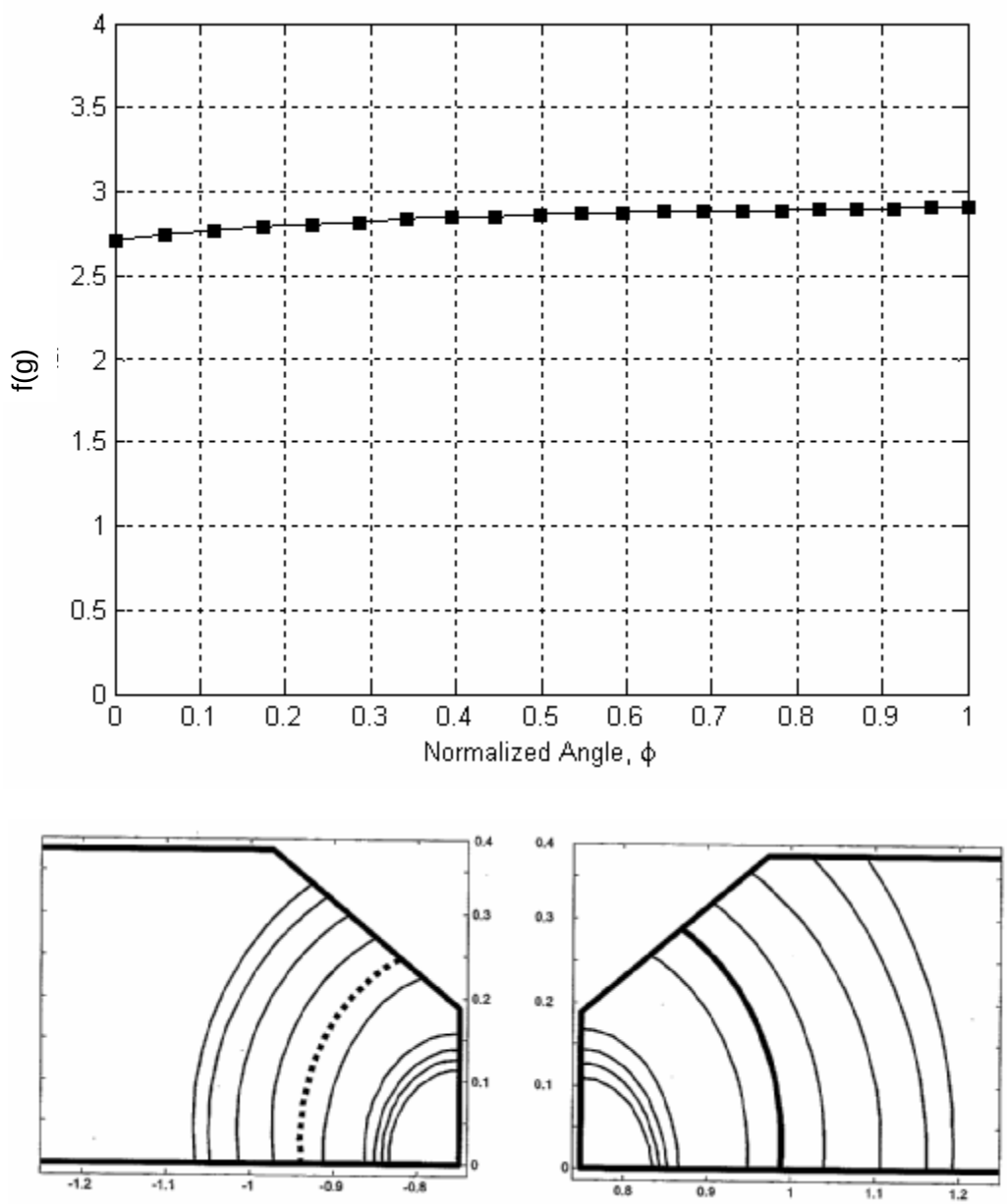

Figure A-96. Geometric Factors for FAA-22 (See table A-96)

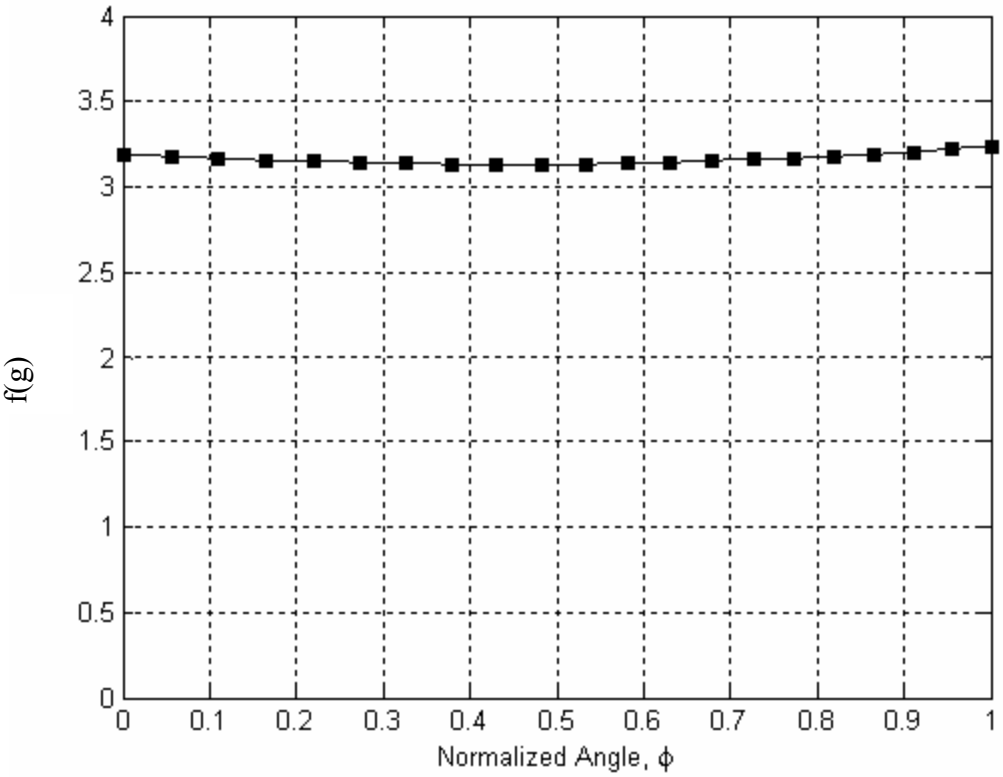

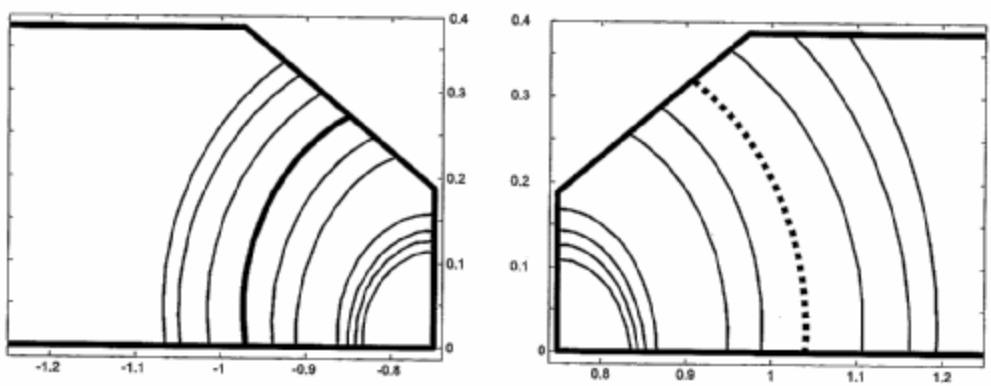

Figure A-97. Geometric Factors for FAA-22 (See table A-97)

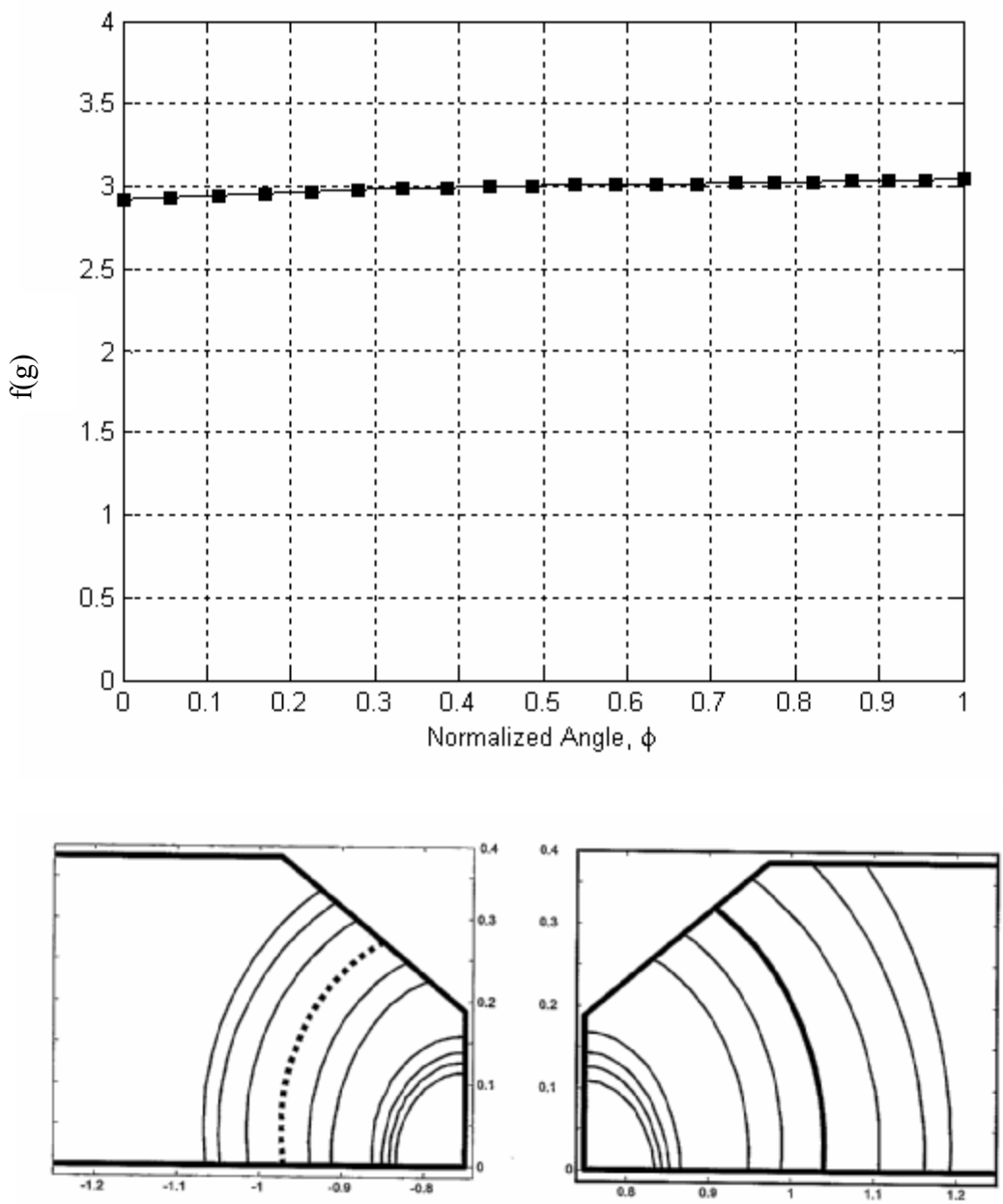

Figure A-98. Geometric Factors for FAA-22 (See table A-98)

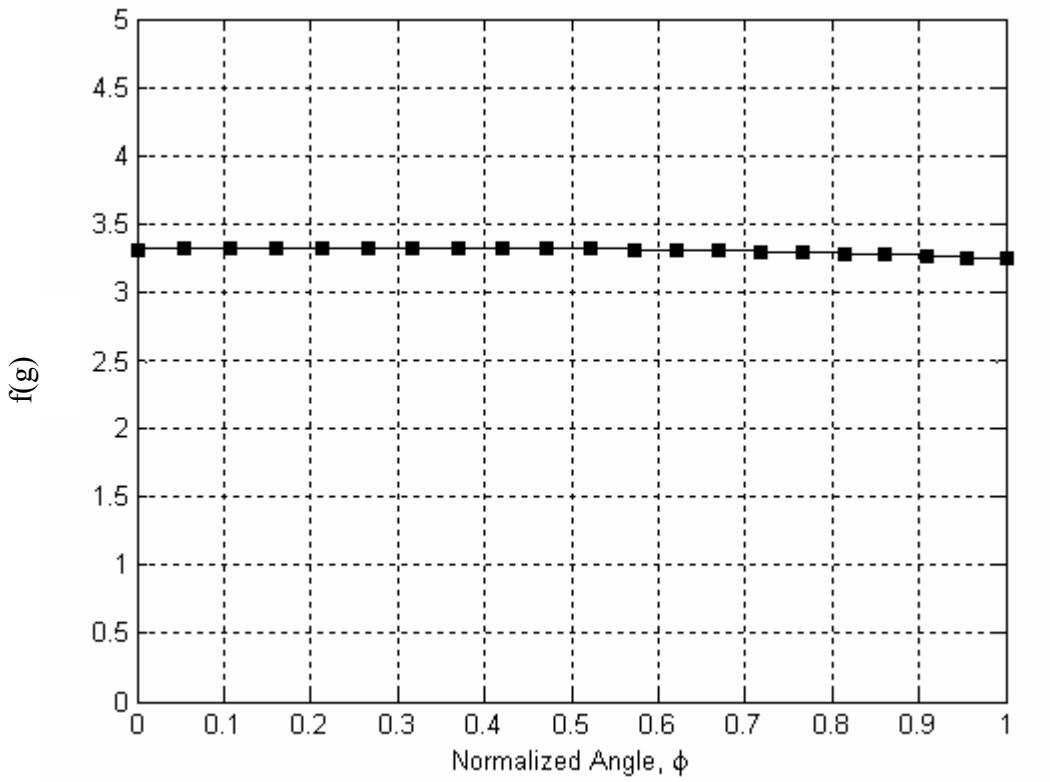

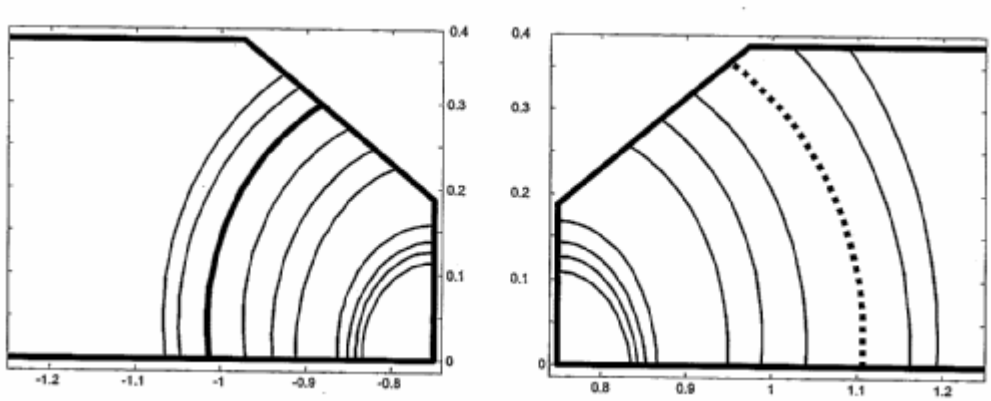

Figure A-99. Geometric Factors for FAA-22 (See table A-99)

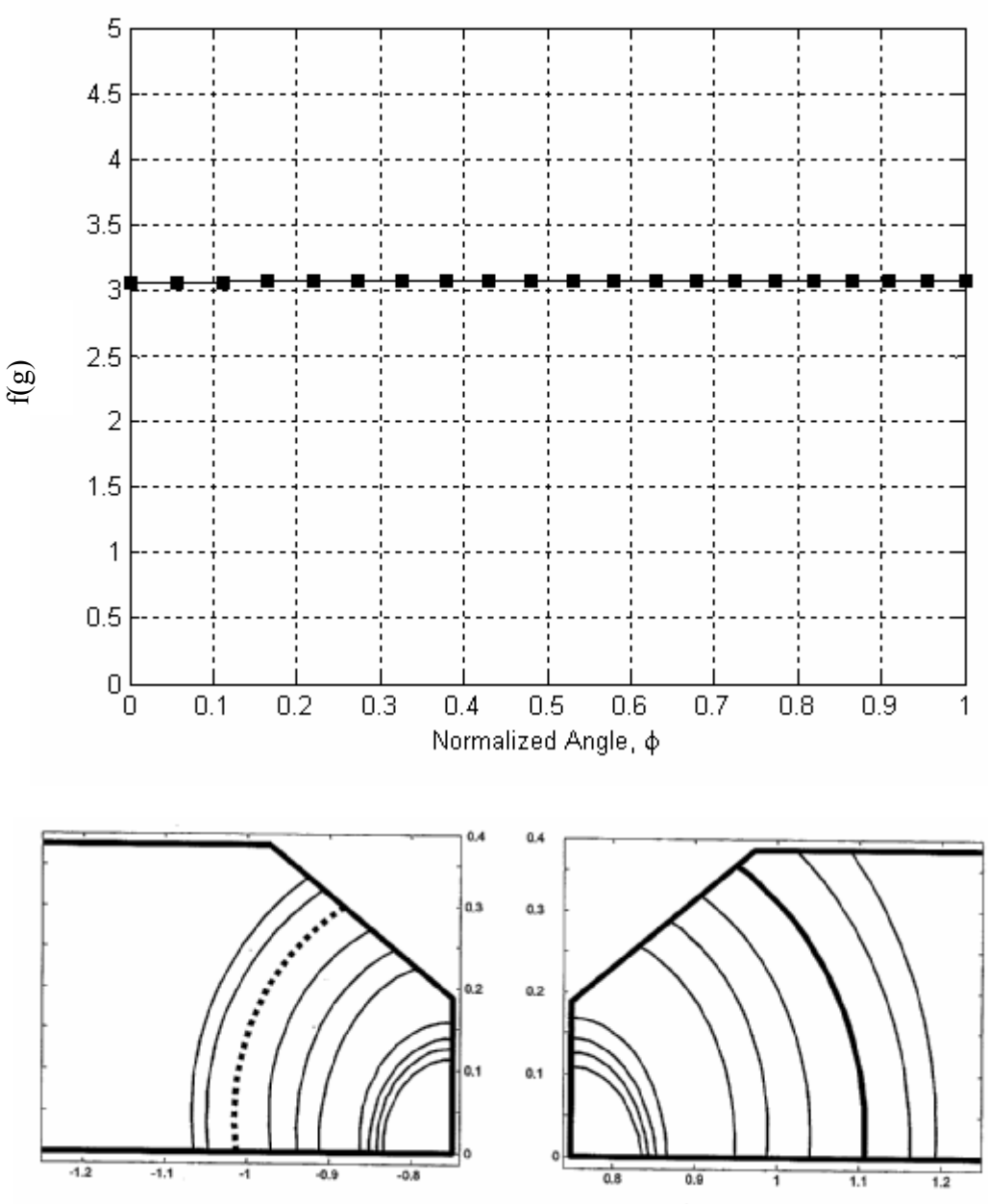

Figure A-100. Geometric Factors for FAA-22 (See table A-100)

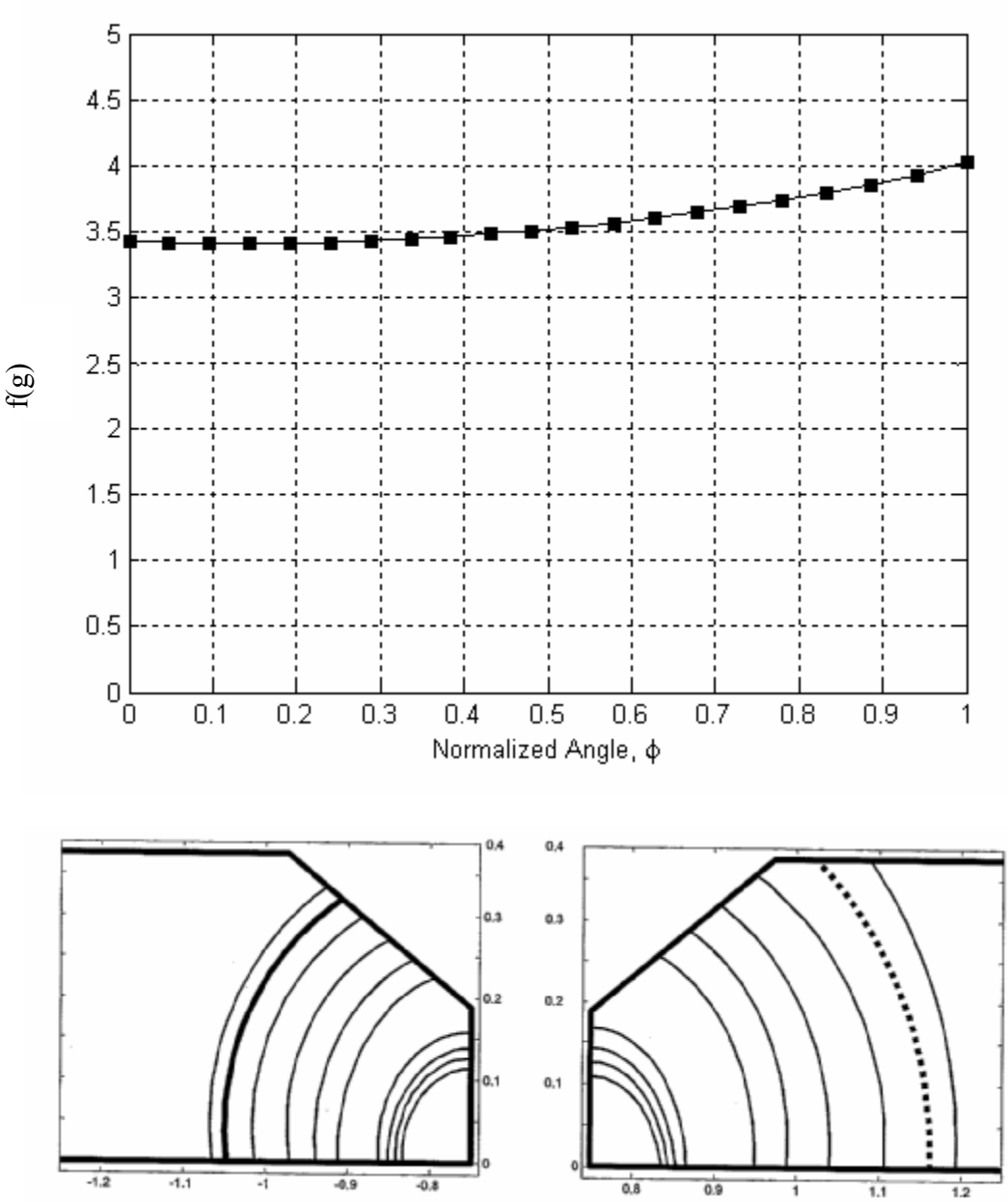

Figure A-101. Geometric Factors for FAA-22 (See table A-101)

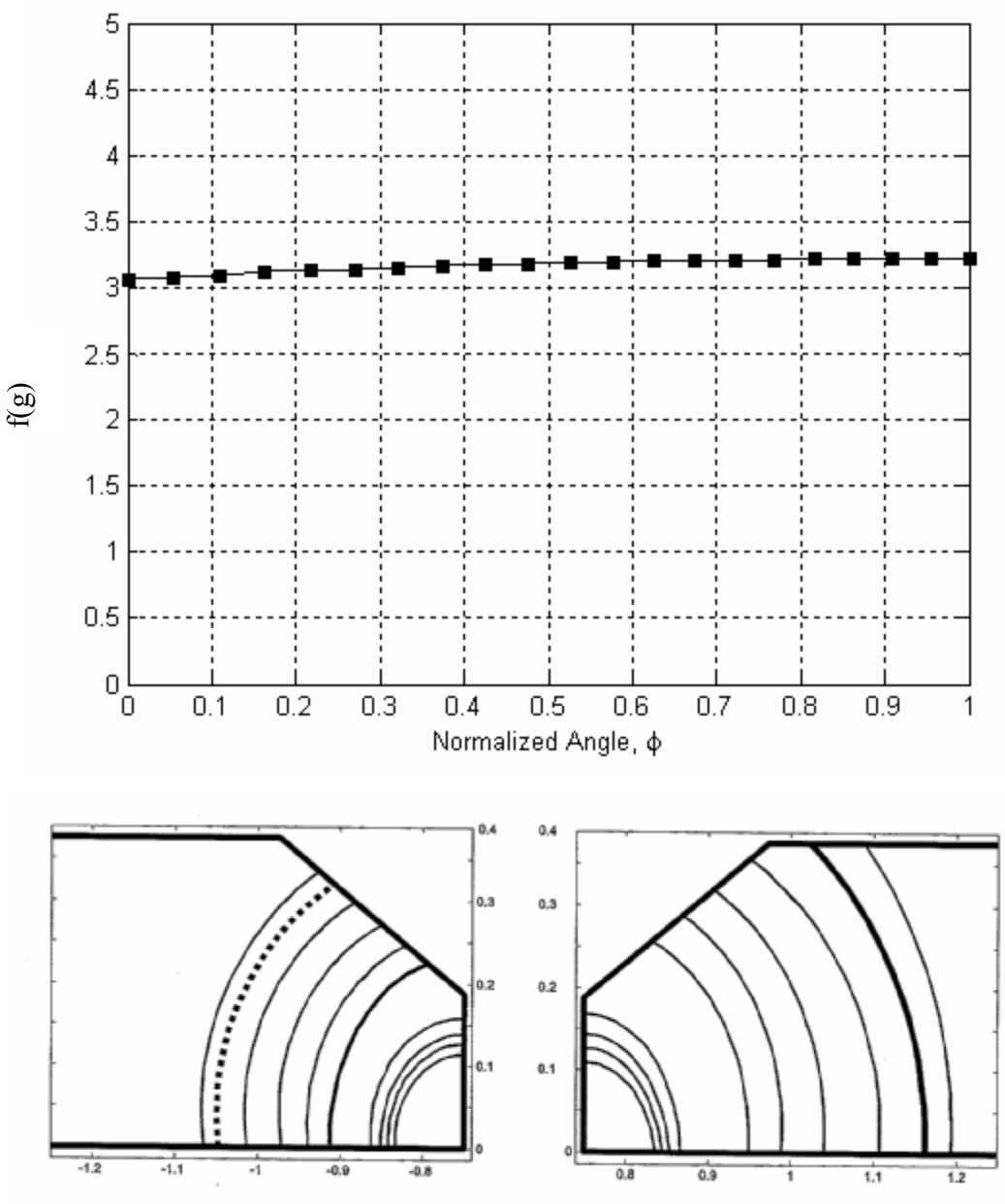

Figure A-102. Geometric Factors for FAA-22 (See table A-102)

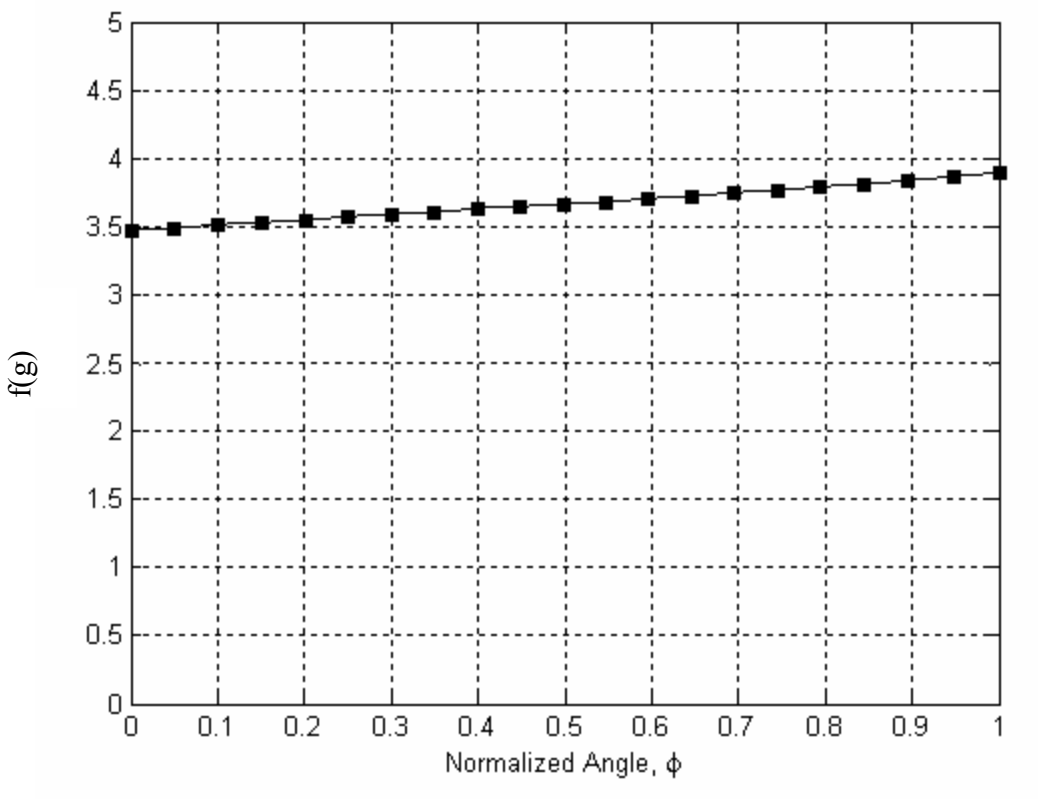

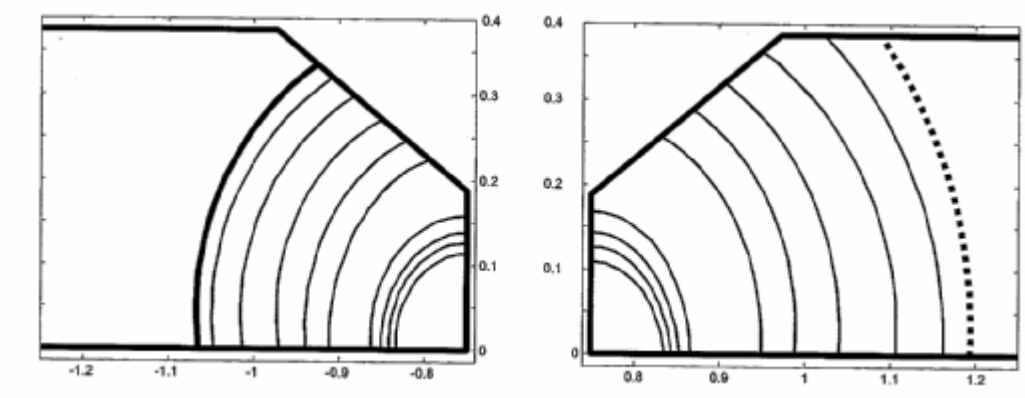

Figure A-103. Geometric Factors for FAA-22 (See table A-103)

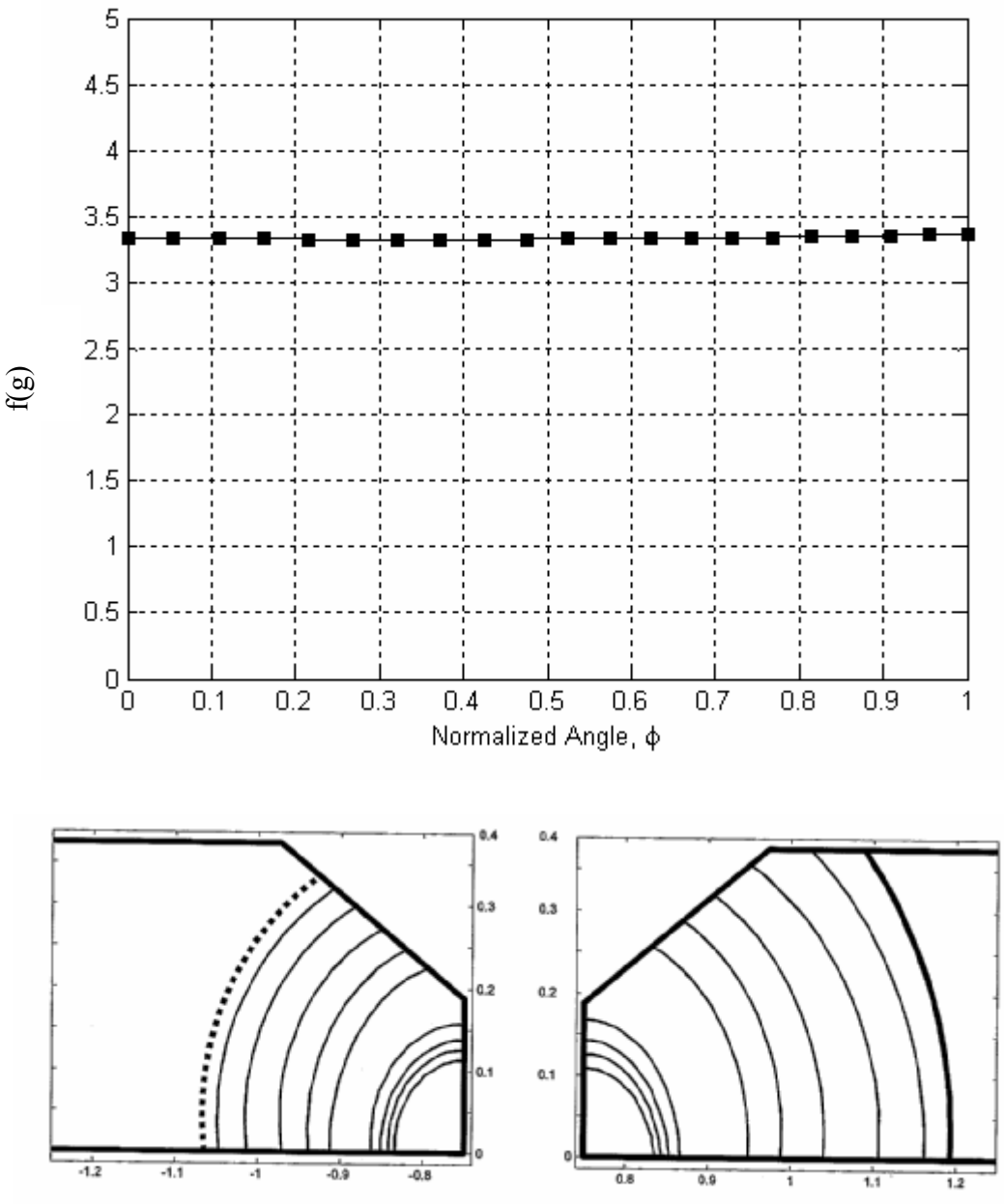

Figure A-104. Geometric Factors for FAA-22 (See table A-104)

Geometric Factors for FAA-17A

Table A-105. Geometric Factors for FAA-17a (See figure A-105)

ϕ	x [in.]	z [in.]	f(g)
0.00	0.9502	0.0000	2.0440
0.06	0.9511	0.0141	2.0584
0.12	0.9515	0.0283	2.0719
0.17	0.9512	0.0424	2.0846
0.23	0.9502	0.0566	2.0966
0.28	0.9485	0.0707	2.1079
0.34	0.9462	0.0848	2.1187
0.39	0.9433	0.0987	2.1289
0.44	0.9396	0.1125	2.1387
0.49	0.9353	0.1260	2.1480
0.54	0.9303	0.1394	2.1571
0.59	0.9247	0.1524	2.1658
0.64	0.9183	0.1652	2.1743
0.69	0.9113	0.1775	2.1827
0.73	0.9036	0.1894	2.1910
0.78	0.8953	0.2008	2.1994
0.83	0.8862	0.2117	2.2078
0.87	0.8766	0.2220	2.2164
0.91	0.8662	0.2316	2.2252
0.96	0.8553	0.2405	2.2345
1.00	0.8437	0.2486	2.2443

Initial Crack Location	Knee
Center of Ellipse	(0.75, 0.0282)
Crack Length	0.2016
Crack Depth	0.2493
Average Crack Front	250,001 and 261,000 cycles

Table A-106. Geometric Factors for FAA-17a (See figure A-106)

ϕ	x [in.]	z [in.]	f(g)
0.00	0.9701	0.0000	2.0195
0.06	0.9718	0.0148	2.0297
0.11	0.9727	0.0297	2.0387
0.17	0.9729	0.0447	2.0466
0.23	0.9724	0.0597	2.0535
0.28	0.9712	0.0747	2.0594
0.33	0.9693	0.0897	2.0643
0.39	0.9666	0.1045	2.0683
0.44	0.9632	0.1192	2.0714
0.49	0.9590	0.1337	2.0738
0.54	0.9541	0.1480	2.0754
0.59	0.9485	0.1621	2.0763
0.64	0.9421	0.1758	2.0765
0.69	0.9351	0.1891	2.0762
0.73	0.9272	0.2020	2.0755
0.78	0.9187	0.2144	2.0743
0.82	0.9095	0.2263	2.0729
0.87	0.8996	0.2376	2.0714
0.91	0.8890	0.2482	2.0699
0.96	0.8778	0.2581	2.0686
1.00	0.8659	0.2673	2.0677

Initial Crack Location	Knee
Center of Ellipse	(0.75, 0.0418)
Crack Length	0.2230
Crack Depth	0.2639
Average Crack Front	261,001 and 267,000 cycles

Table A-107. Geometric Factors for FAA-17a (See figure A-107)

ϕ	x [in.]	z [in.]	f(g)
0.00	1.0035	0.0000	2.0195
0.06	1.0051	0.0160	2.0157
0.11	1.0059	0.0321	2.0116
0.17	1.0059	0.0482	2.0075
0.22	1.0052	0.0643	2.0033
0.27	1.0036	0.0804	1.9989
0.33	1.0013	0.0965	1.9945
0.38	0.9982	0.1124	1.9899
0.43	0.9942	0.1281	1.9852
0.48	0.9895	0.1437	1.9804
0.53	0.9840	0.1589	1.9755
0.58	0.9777	0.1739	1.9706
0.63	0.9707	0.1885	1.9657
0.68	0.9629	0.2026	1.9608
0.73	0.9543	0.2163	1.9560
0.77	0.9450	0.2295	1.9513
0.82	0.9350	0.2422	1.9468
0.87	0.9242	0.2542	1.9426
0.91	0.9129	0.2655	1.9387
0.96	0.9008	0.2761	1.9352
1.00	0.8882	0.2860	1.9323

Initial Crack Location	Knee
Center of Ellipse	(0.75, 0.0406)
Crack Length	0.2561
Crack Depth	0.2914
Average Crack Front	267,001 and 280,000 cycles

Table A-108. Geometric Factors for FAA-17a (See figure A-108)

ϕ	x [in.]	z [in.]	f(g)
0.00	1.0468	0.0000	1.8365
0.05	1.0488	0.0175	1.8492
0.11	1.0499	0.0351	1.8599
0.16	1.0500	0.0528	1.8688
0.21	1.0492	0.0705	1.8761
0.27	1.0474	0.0882	1.8817
0.32	1.0447	0.1057	1.8858
0.37	1.0411	0.1231	1.8885
0.42	1.0366	0.1403	1.8898
0.47	1.0311	0.1572	1.8897
0.52	1.0248	0.1738	1.8885
0.57	1.0175	0.1899	1.8860
0.62	1.0094	0.2057	1.8825
0.67	1.0005	0.2210	1.8780
0.72	0.9907	0.2357	1.8726
0.77	0.9802	0.2499	1.8664
0.81	0.9688	0.2633	1.8595
0.86	0.9568	0.2762	1.8520
0.91	0.9441	0.2882	1.8441
0.95	0.9308	0.2995	1.8360
1.00	0.9168	0.3100	1.8278

Initial Crack Location	Knee
Center of Ellipse	(0.75, 0.0457)
Crack Length	0.3002
Crack Depth	0.3179
Average Crack Front	280,001 and 290,000 cycles

Table A-109. Geometric Factors for FAA-17a (See figure A-109)

ϕ	x [in.]	z [in.]	f(g)
0.00	1.1937	0.0000	1.6310
0.04	1.1956	0.0188	1.6140
0.09	1.1965	0.0375	1.5979
0.13	1.1965	0.0563	1.5826
0.18	1.1956	0.0750	1.5682
0.22	1.1937	0.0938	1.5547
0.26	1.1909	0.1125	1.5422
0.31	1.1872	0.1313	1.5308
0.35	1.1824	0.1500	1.5206
0.40	1.1766	0.1688	1.5117
0.44	1.1697	0.1875	1.5043
0.49	1.1618	0.2063	1.4985
0.54	1.1526	0.2250	1.4945
0.59	1.1421	0.2438	1.4925
0.64	1.1303	0.2625	1.4928
0.69	1.1170	0.2813	1.4957
0.74	1.1020	0.3000	1.5015
0.80	1.0850	0.3188	1.5109
0.86	1.0659	0.3375	1.5246
0.93	1.0441	0.3563	1.5434
1.00	1.0190	0.3750	1.5692

Initial Crack Location	Knee
Center of Ellipse	(0.75, 0.0459)
Crack Length	0.4470
Crack Depth	0.4123
Average Crack Front	312,001 and 318,000 cycles

Table A-110. Geometric Factors for FAA-17a (See figure A-110)

ϕ	x [in.]	z [in.]	f(g)
0.00	1.2250	0.0000	1.5438
0.04	1.2257	0.0188	1.5372
0.09	1.2255	0.0375	1.5313
0.13	1.2245	0.0563	1.5262
0.18	1.2226	0.0750	1.5218
0.22	1.2200	0.0938	1.5181
0.26	1.2165	0.1125	1.5153
0.31	1.2121	0.1313	1.5132
0.35	1.2069	0.1500	1.5120
0.40	1.2007	0.1688	1.5118
0.45	1.1936	0.1875	1.5125
0.49	1.1855	0.2063	1.5143
0.54	1.1763	0.2250	1.5172
0.59	1.1660	0.2438	1.5214
0.64	1.1544	0.2625	1.5269
0.70	1.1416	0.2813	1.5341
0.75	1.1272	0.3000	1.5431
0.81	1.1113	0.3188	1.5543
0.87	1.0934	0.3375	1.5681
0.93	1.0734	0.3563	1.5852
1.00	1.0508	0.3750	1.6066

Initial Crack Location	Knee
Center of Ellipse	(0.75, 0.0233)
Crack Length	0.4758
Crack Depth	0.4543
Average Crack Front	318,001 and 324,000 cycles

Table A-111. Geometric Factors for FAA-17a (See figure A-111)

ϕ	x [in.]	z [in.]	f(g)
0.00	1.2542	0.0000	1.4958
0.04	1.2544	0.0188	1.4950
0.09	1.2539	0.0375	1.4945
0.13	1.2526	0.0563	1.4943
0.18	1.2506	0.0750	1.4942
0.22	1.2478	0.0938	1.4944
0.27	1.2442	0.1125	1.4948
0.31	1.2397	0.1313	1.4955
0.36	1.2345	0.1500	1.4965
0.40	1.2284	0.1688	1.4978
0.45	1.2214	0.1875	1.4995
0.50	1.2134	0.2063	1.5015
0.55	1.2045	0.2250	1.5040
0.60	1.1946	0.2438	1.5070
0.65	1.1835	0.2625	1.5106
0.70	1.1713	0.2813	1.5150
0.76	1.1577	0.3000	1.5202
0.81	1.1427	0.3188	1.5265
0.87	1.1260	0.3375	1.5341
0.93	1.1076	0.3563	1.5435
1.00	1.0869	0.3750	1.5552

Initial Crack Location	Knee
Center of Ellipse	(0.75, 0.0153)
Crack Length	0.5045
Crack Depth	0.4834
Average Crack Front	324,001 and 330,000 cycles

Table A-112. Geometric Factors for FAA-17a (See figure A-112)

ϕ	x [in.]	z [in.]	f(g)
0.00	1.2805	0.0000	1.4516
0.04	1.2809	0.0188	1.4563
0.09	1.2805	0.0375	1.4606
0.13	1.2794	0.0563	1.4645
0.18	1.2775	0.0750	1.4679
0.22	1.2749	0.0938	1.4710
0.27	1.2714	0.1125	1.4738
0.31	1.2671	0.1313	1.4763
0.36	1.2620	0.1500	1.4785
0.41	1.2561	0.1688	1.4804
0.45	1.2493	0.1875	1.4821
0.50	1.2415	0.2063	1.4836
0.55	1.2328	0.2250	1.4848
0.60	1.2231	0.2438	1.4859
0.65	1.2122	0.2625	1.4869
0.70	1.2003	0.2813	1.4878
0.76	1.1870	0.3000	1.4887
0.81	1.1724	0.3188	1.4896
0.87	1.1563	0.3375	1.4907
0.93	1.1385	0.3563	1.4922
1.00	1.1187	0.3750	1.4943

Initial Crack Location	Knee
Center of Ellipse	(0.75, 0.0195)
Crack Length	0.5309
Crack Depth	0.4940
Average Crack Front	330,001 and 335,000 cycles

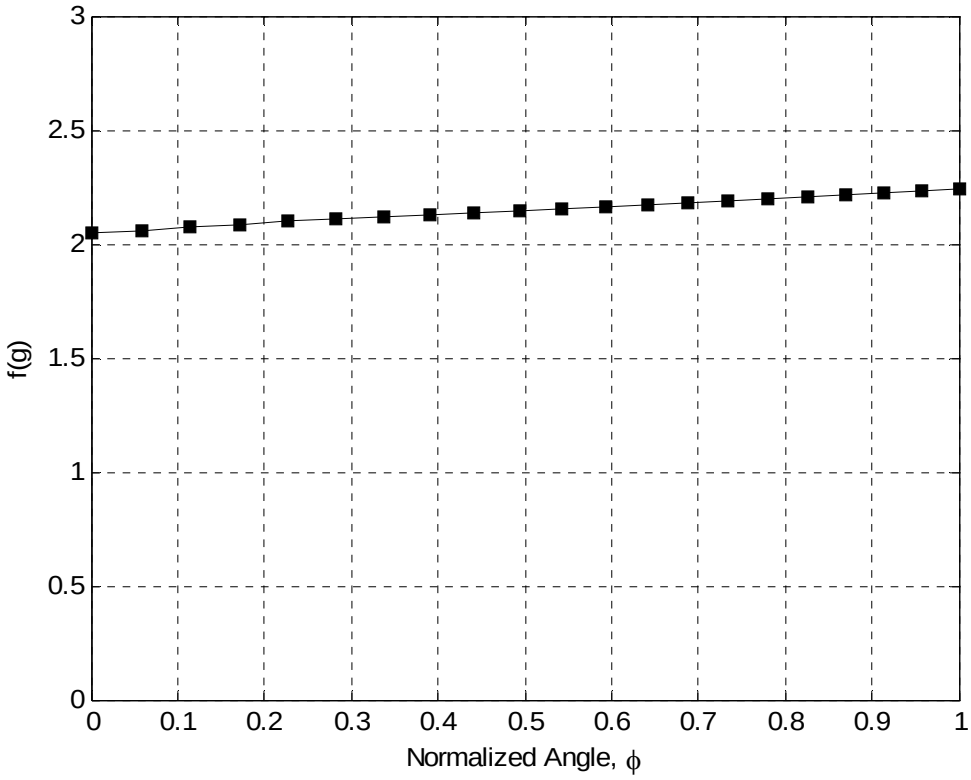

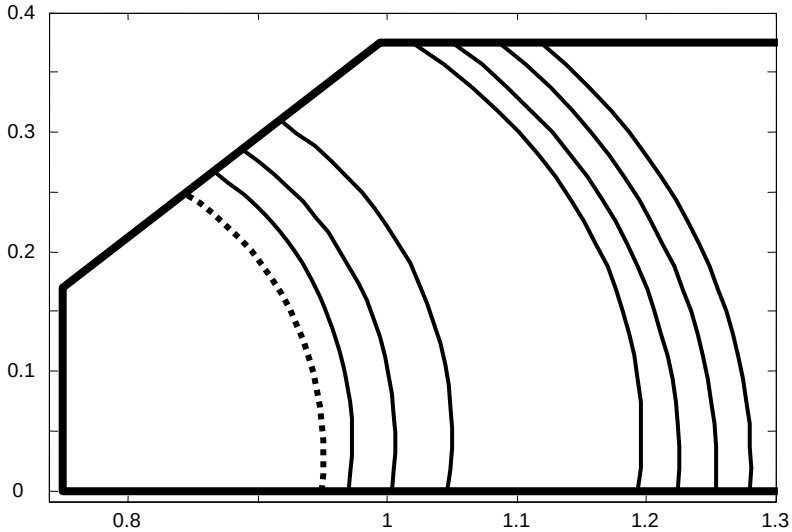

Figure A-105. Geometric Factors for FAA-17a (See table A-105)

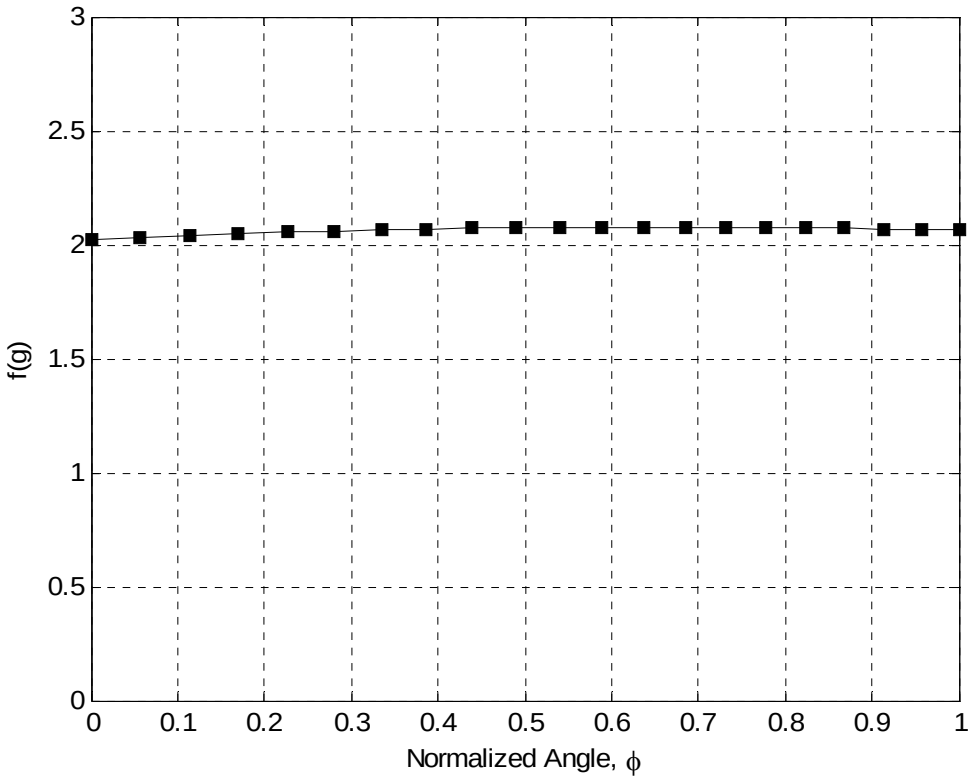

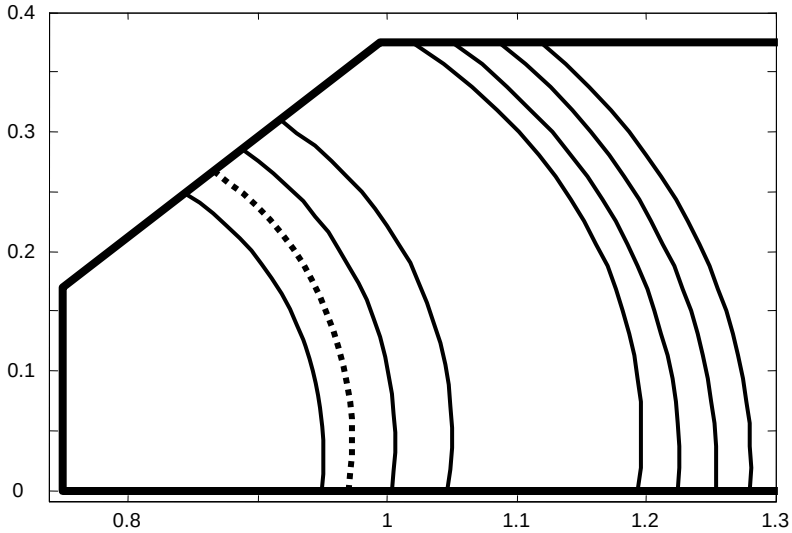

Figure A-106. Geometric Factors for FAA-17a (See table A-106)

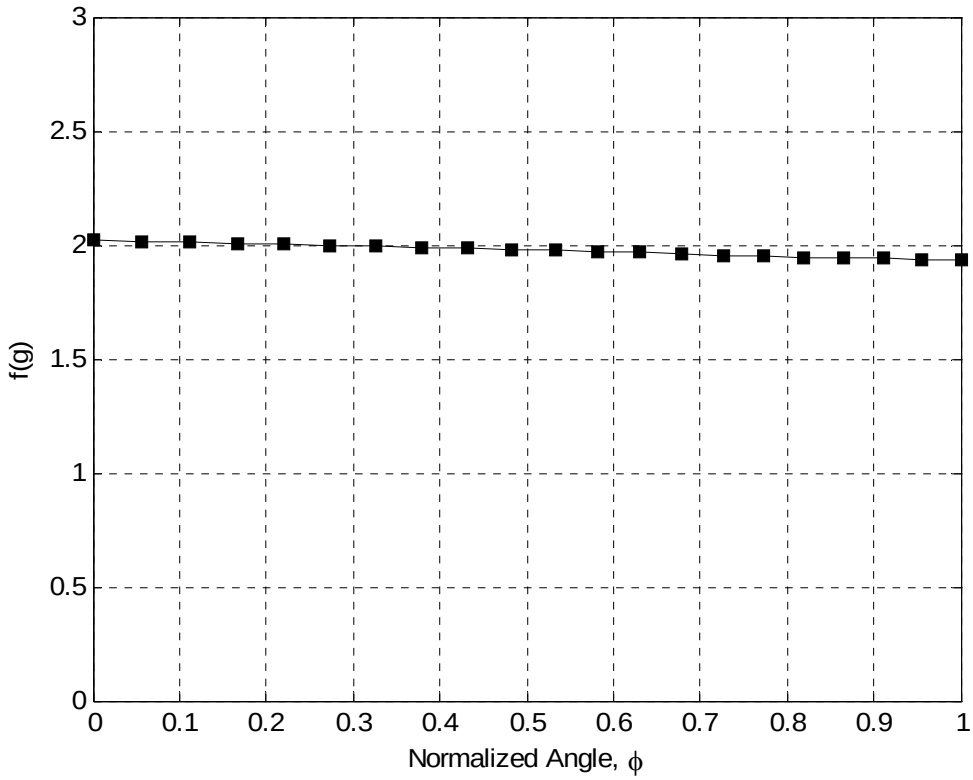

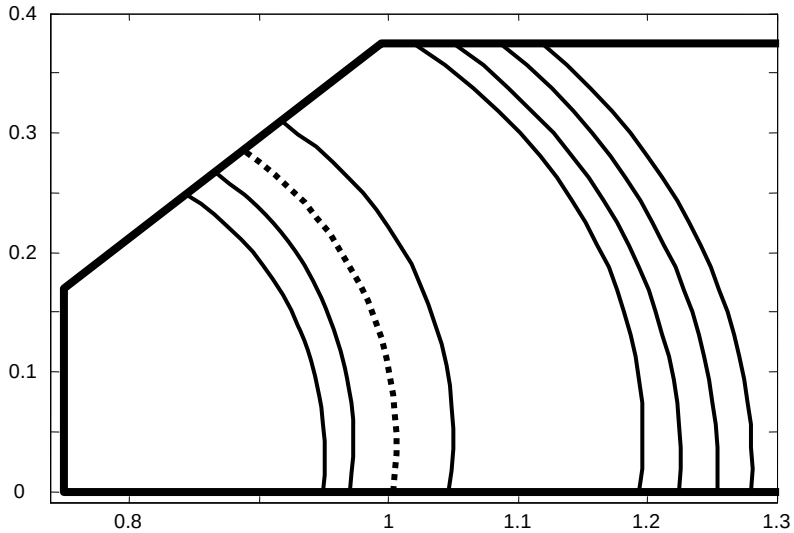

Figure A-107. Geometric Factors for FAA-17a (See table A-107)

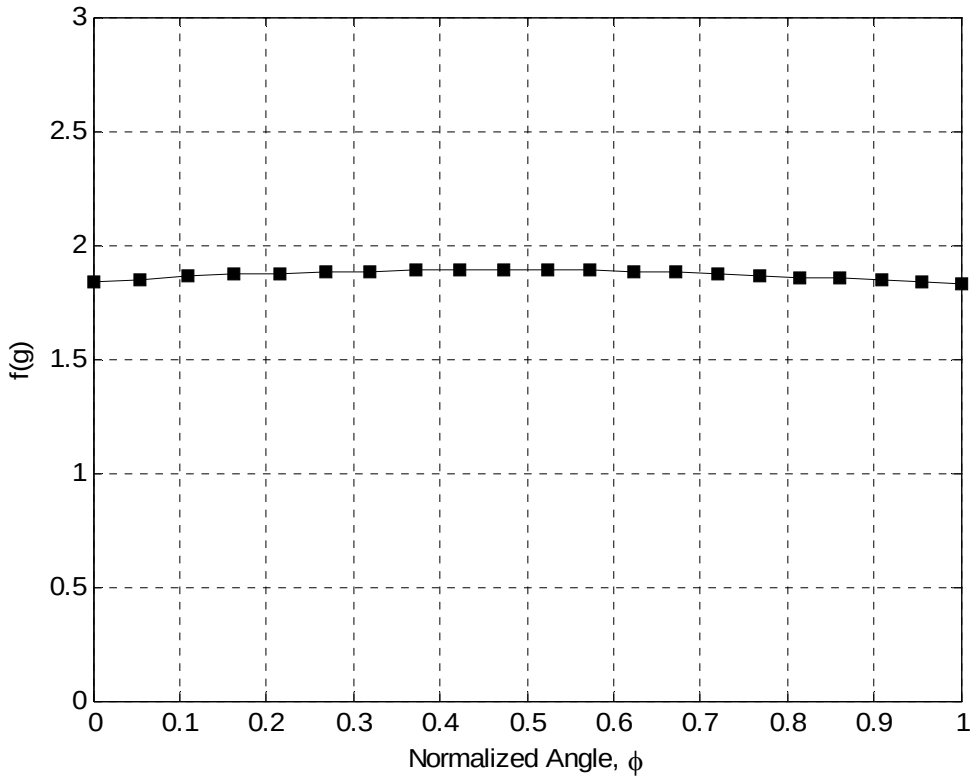

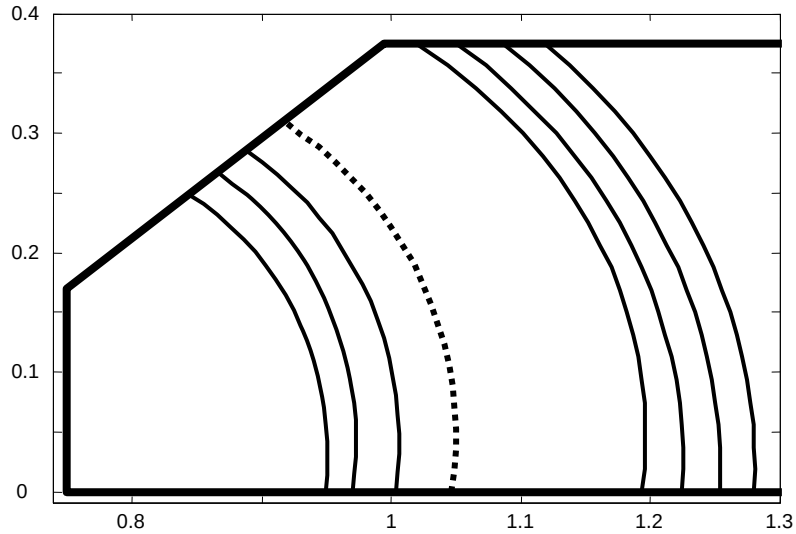

Figure A-108. Geometric Factors for FAA-17a (See table A-108)

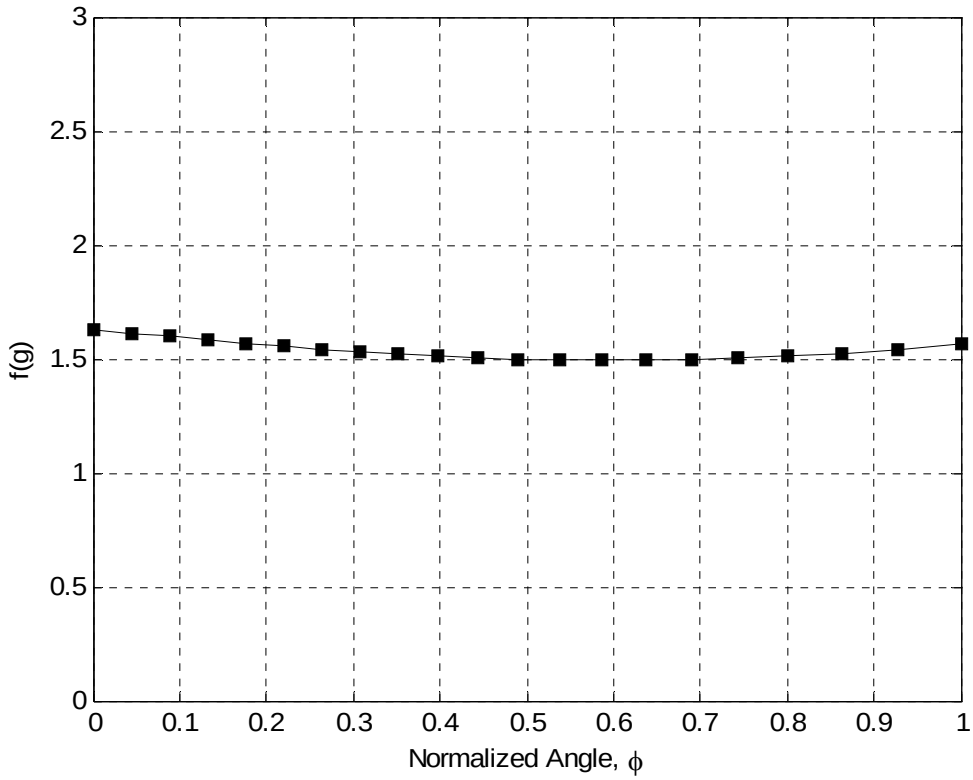

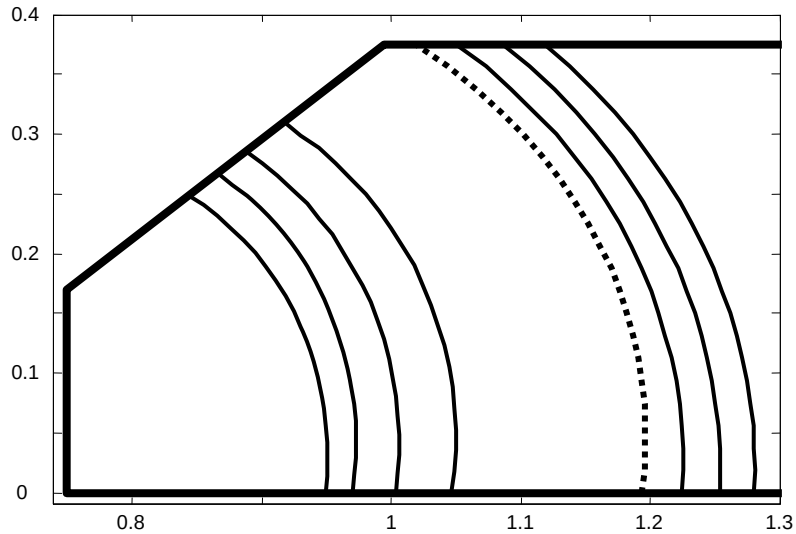

Figure A-109. Geometric Factors for FAA-17a (See table A-109)

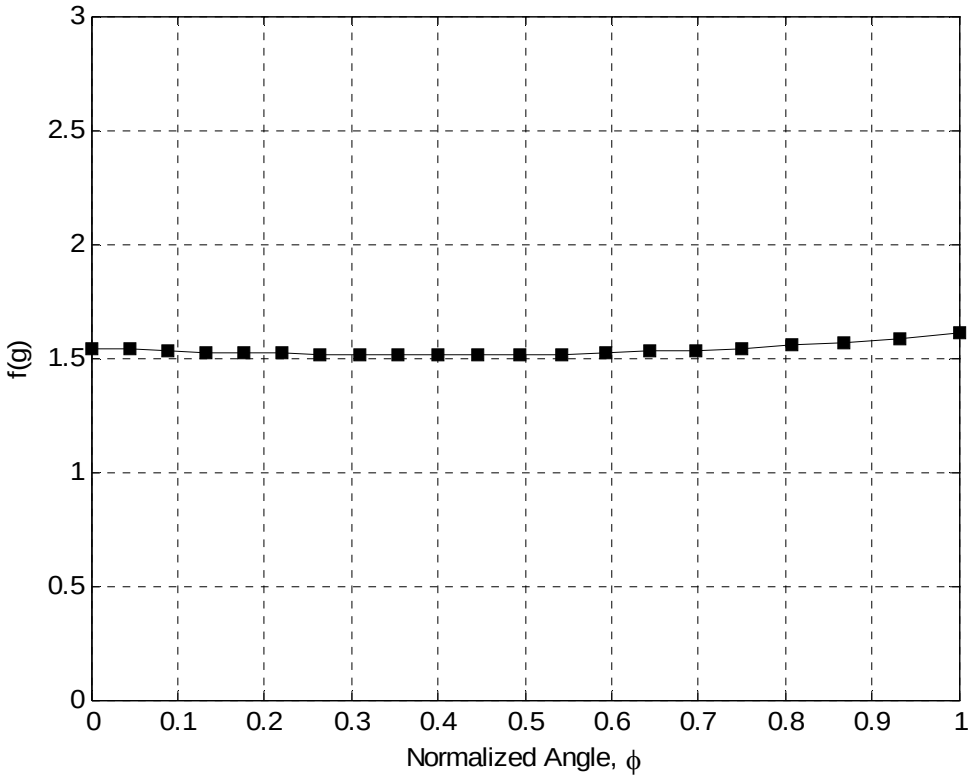

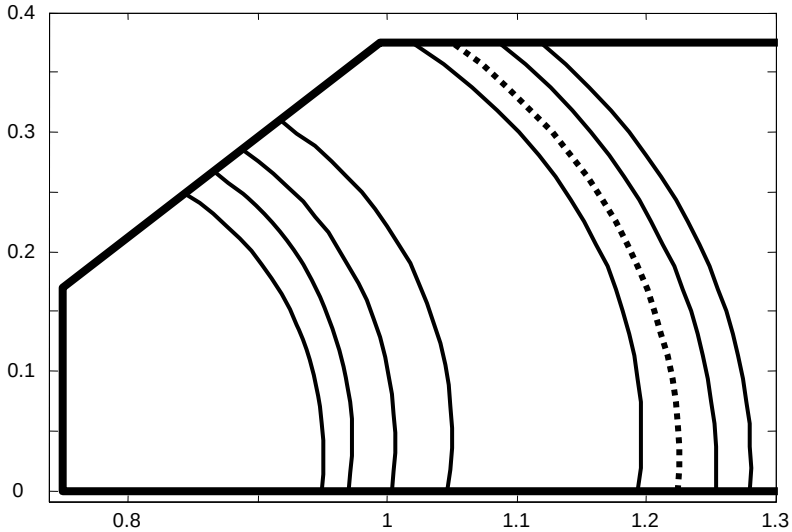

Figure A-110. Geometric Factors for FAA-17a (See table A-110)

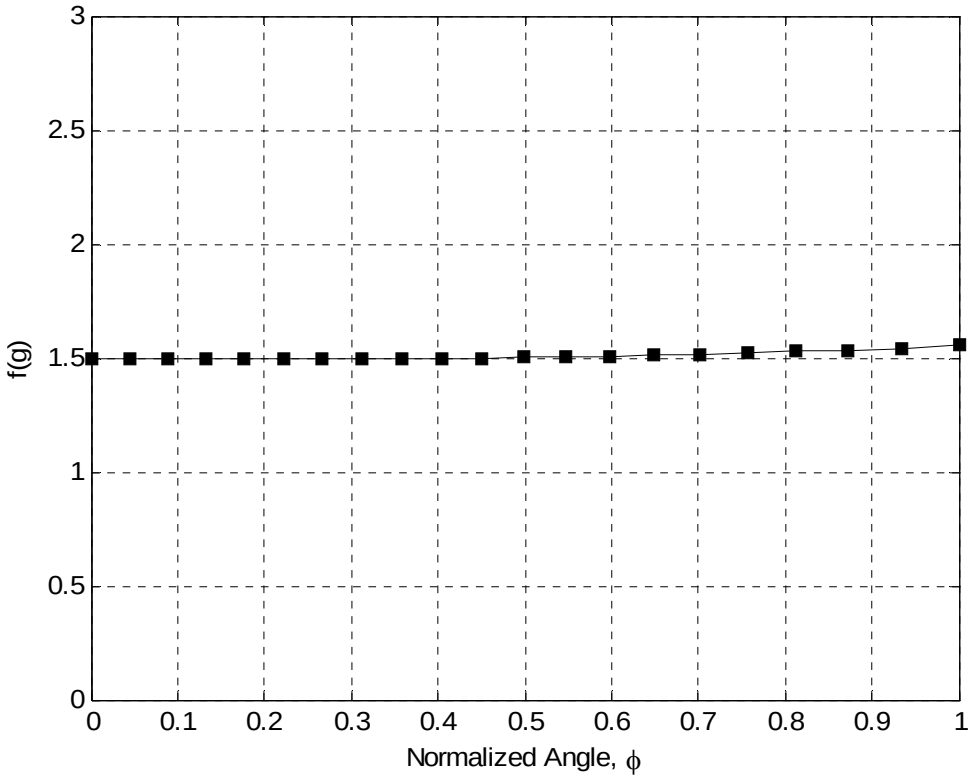

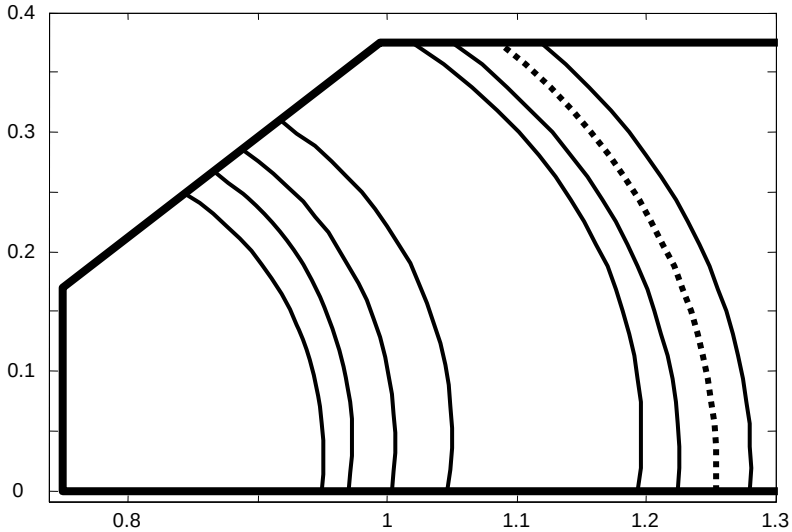

Figure A-111. Geometric Factors for FAA-17a (See table A-111)

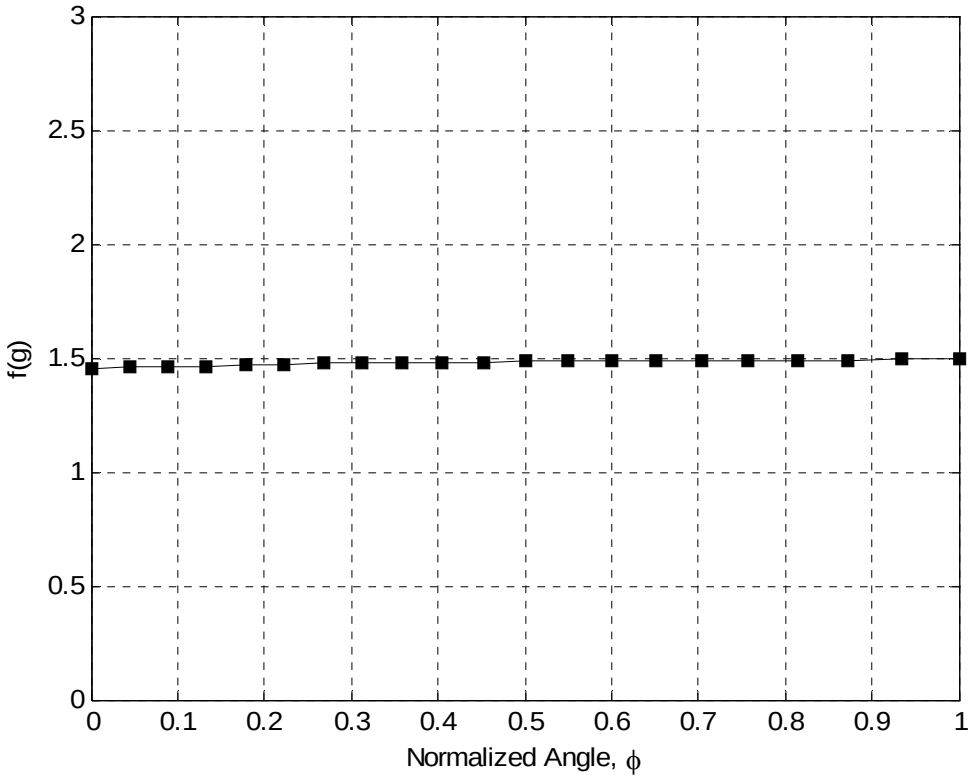

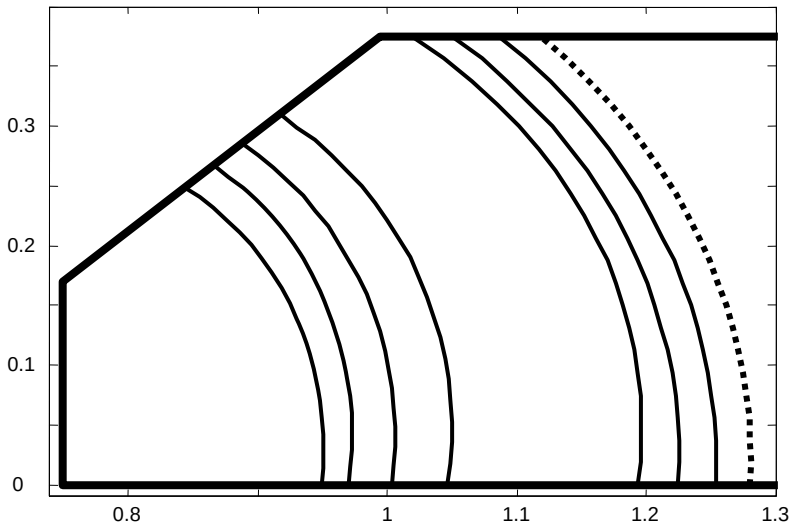

Figure A-112. Geometric Factors for FAA-17a (See table A-112)

APPENDIX B—OPEN-HOLE BENDING DATA

Table B-1. Test Summary of Specimen FAA-17

Specimen ID	FAA-17
Material	PMMA
Gross Width of Test Section (in.)	7.46
Gross Thickness of Test Section (in.)	0.375
Gross Test Sectional Area (in.^{2})	2.7975
Straight Shank Length of Hole (in.)	0.1875
Notch Type	Single Notch at Knee
Precrack Method	Tension
Stress Ratio, R	0.3
Frequency (Hz)	3
Test Environment	Room Temperature, Laboratory Air
Maximum Gross Stress for Precrack (psi)	No. of Cycles
300	1 ~ 4000
400	4001 ~ 9000
500	9001 ~ 15000
600	15001 ~ 20000
700	20001 ~ 23000
600	23001 ~ 27000
570	27001 ~ 30000
540	30001 ~ 33000
Maximum Gross Stress for Test (psi)	No. of Cycles
490	1 ~ 18000
410	18001 ~ 78000

Table B-2. Test Summary of Specimen FAA-18

Specimen ID	FAA-18
Material	PMMA
Gross Width of Test Section (in.)	7.47
Gross Thickness of Test Section (in.)	0.375
Gross Test Sectional Area (in.^{2})	2.80125
Straight Shank Length of Hole (in.)	0.1875
Notch Type	Single Notch at Corner
Precrack Method	Tension
Stress Ratio, R	0.3
Frequency (Hz)	3
Test Environment	Room Temperature, Laboratory Air
Maximum Gross Stress for Precrack (psi)	No. of Cycles
300	1 ~ 5000
400	5001 ~ 10000
500	10001 ~ 15000
600	15001 ~ 30000
700	35001 ~ 45000
600	45001 ~ 60000
570	60001 ~ 70000
540	70001 ~ 80000
Maximum Gross Stress for Test (psi)	No. of Cycles
540	1~ 32000
480	32001 ~ 40000
410	42001 ~ 106159

Table B-3. Test Summary of Specimen FAA-19

Specimen ID	FAA-19
Material	PMMA
Gross Width of Test Section (in.)	7.48
Gross Thickness of Test Section (in.)	0.369
Gross Test Sectional Area (in.^{2})	2.76012
Straight Shank Length of Hole (in.)	0.1845
Notch Type	Double Notch at Knee
Precrack Method	Tension
Stress Ratio, R	0.3
Frequency (Hz)	3
Test Environment	Room Temperature, Laboratory Air
Maximum Gross Stress for Precrack (psi)	No. of Cycles
300	1 ~ 3000
800	3001 ~ 8000
900	8001 ~ 12000
1000	12001 ~ 17000
1100	17001 ~ 20000
1000	20001 ~ 23000
900	23001 ~ 29000
800	29001 ~ 32000
700	32001 ~ 35000
600	35001 ~ 38000
500	38001 ~ 41000
450	41001 ~ 45000
Maximum Gross Stress for Test (psi)	No. of Cycles
450	1 ~ 12000
420	12001 ~ 20000
400	20001 ~ 25000
380	25001 ~ 46000
400	46001 ~ 67000
370	67001 ~ 103909

Table B-4. Test Summary of Specimen FAA-20

Specimen ID	FAA-20
Material	PMMA
Gross Width of Test Section (in.)	7.450
Gross Thickness of Test Section (in.)	0.355
Gross Test Sectional Area (in.^{2})	2.64475
Straight Shank Length of Hole (in.)	0.1775
Notch Type	Double Notch at Knee
Precrack Method	Tension
Stress Ratio, R	0.3
Frequency (Hz)	3
Test Environment	Room Temperature, Laboratory Air
Maximum Gross Stress for Precrack (psi)	No. of Cycles
300	1 ~ 5000
400	5001 ~ 10000
500	10001 ~ 15000
600	15001 ~ 20000
700	20001 ~ 22000
600	22001 ~ 30000
500	30001 ~ 39000
480	39001 ~ 43000
Maximum Gross Stress for Test (psi)	No. of Cycles
480	1 ~ 11000
410	11001 ~ 35000
370	35001 ~ 75000

Table B-5. Test Summary of Specimen FAA-21

Specimen ID	FAA- 21
Material	PMMA
Gross Width of Test Section (in.)	7.465
Gross Thickness of Test Section (in.)	0.360
Gross Test Sectional Area (in.^{2})	2.6874
Straight Shank Length of Hole (in.)	0.1800
Notch Type	Double Notch at Corner
Precrack Method	Tension
Stress Ratio, R	0.3
Frequency (Hz)	3
Test Environment	Room Temperature, Laboratory Air
Maximum Gross Stress for Precrack (psi)	No. of Cycles
300	1 ~ 5000
400	5001 ~ 10000
500	10001 ~ 20000
600	20001 ~ 30000
700	50001 ~ 65000
800	65001 ~ 70000
700	70001 ~ 75000
600	75001 ~ 90000
550	90001 ~ 96000
500	96001 ~ 105000
Maximum Gross Stress for Test (psi)	No. of Cycles
500	1 ~ 39000
430	39001 ~ 57000
390	57001 ~ 107216

Table B-6. Test Summary of Specimen FAA-22

Specimen ID	FAA-22
Material	PMMA
Gross Width of Test Section (in.)	7.48
Gross Thickness of Test Section (in.)	0.375
Gross Test Sectional Area (in.^{2})	2.805
Straight Shank Length of Hole (in.)	0.1875
Notch Type	Double Notch at Corner
Precrack Method	Tension
Stress Ratio, R	0.3
Frequency (Hz)	3
Test Environment	Room Temperature, Laboratory Air
Maximum Gross Stress for Precrack (psi)	No. of Cycles
300	1 ~ 5000
400	5001 ~ 10000
500	10001 ~ 20000
600	20001 ~ 50000
700	50001 ~ 65000
600	65001 ~ 70000
560	70001 ~ 75000
530	750001 ~ 81000
480	81001 ~ 95000
Maximum Gross Stress for Test (psi)	No. of Cycles
480	1 ~ 42000
430	42001 ~ 54000
390	54001 ~ 114709

Table B-7. Test Summary of Specimen FAA-17a

Specimen ID	FAA-17A
Material	PMMA
Gross Width of Test Section (in.)	7.47
Gross Thickness of Test Section (in.)	0.375
Gross Test Sectional Area (in.^{2})	2.80125
Straight Shank Length of Hole (in.)	0.175
Notch Type	Single Notch at Corner
Precrack Method	Tension
Stress Ratio, R	0.3
Frequency (Hz)	3
Test Environment	Room Temperature, Laboratory Air
Maximum Gross Stress for Precrack (psi)	No. of Cycles
300	1 ~ 3000
700	3001 ~ 7000
800	7001 ~ 12000
900	12001 ~ 15000
800	15001 ~ 17000
700	17001 ~ 20000
600	20001 ~ 24000
500	24001 ~ 30000
420	30001 ~ 33541
Maximum Gross Stress for Test (psi)	No. of Cycles
420	1 ~ 193000
380	193001 ~ 393000

APPENDIX C—PIN-LOADED HOLE DATA

C.1 SUMMARY.

This appendix summarizes the dimensionless stress-intensity factors found for pin-loaded countersunk holes. As described in section 4 of this report, these results were obtained from fatigue crack growth rate experiments with transparent polymer Polymethylmethacrylate (PMMA) specimens. Results are reported here for two specimens—corner crack test FAA-009 and knee crack test FAA-012.

The initial corner crack geometry is shown in figure 2-3 and the knee crack geometry is given in figure 2-4 in section 2. Those figures also define the Type I, Type II, and Type III crack configurations used to characterize the growth and transition of the small part-through cracks into a through-the-thickness crack. Other dimensions used to define the crack configurations are given in figures 4-19 and 4-20.

The stress-intensity factors for the pin-loaded geometry is presented in the dimensionless factor *f(g)* defined below.

$$\textit{Boundary correction factor},\ f(g) = \frac{\Delta K}{\Delta\sigma\sqrt{\pi\,\alpha}} \tag{C-1}$$

Here ΔK is the cyclic stress-intensity factor at the crack perimeter position of interest that is computed from the fatigue crack growth rate, $\Delta\sigma$ is the stress, and a is the reference crack length shown in figure 4-20. The parametric angle, ϕ, used to represent the different points of a crack front is defined in figure 4-20. The parametric definitions in figure 4-20(a) were used for Type I, II, and III crack shapes for initial corner crack and Type II and II crack shapes for initial knee crack. The parametric definition in figure 4-20(b) was used for Type I crack shapes for initial knee crack.

The initial corner crack in specimen FAA-009 transitioned from a Type I to a Type II crack at approximately 34,250 cycles into the test. At 57,300 cycles, the crack front has taken a through-the-thickness Type III profile. Fracture of specimen FAA-009 occurred at 245,839 cycles. The initial knee crack specimen FAA-012 transitioned from Type I to Type II at approximately 37,600 cycles into the test. There was a period of fast crack growth between 41,340 and 41,400 cycles, which was the period of transition from Type II to Type III crack profile. Fracture of the specimen occurred at 220,856 cycles.

C.1.1 CORNER CRACK SPECIMEN FAA-09.

Results are presented below for a total of 38 average crack fronts from 41 digitally processed crack fronts for corner crack specimen FAA-009. Tables C-1 through C-38 tabulate the *f*(*g*)'s for each crack front and provide information such as the cycle life and the ellipses used to fit the crack shapes. Figures C-1 through C-38 show the plots of *f*(*g*) as a function of the parametric angle for each crack front. The test load information and dimensions for this specimen are summarized below in tables C-77 and C-78.

C.1.2 KNEE CRACK SPECIMEN FAA-012.

A total of 38 average crack fronts were obtained from 42 digitally processed crack fronts for knee crack specimen FAA-012. Tables C-39 through C-76 tabulate the *f*(*g*)'s for each crack front and provides information such as cycle life and the ellipses used to fit the crack shapes. Figures C-39 through C-76 show the plots of *f*(*g*) as a function of the parametric angle for each crack front. The test load information and dimension for this specimen are given in figures C-78 and C-79.

Table C-1. Corrected Boundary Correction Factors for FAA-009 (See figure C-1)

Initial Crack Location	Corner
Type	I
Center of Ellipse	(0.75, 0)
Horizontal Axis	0.09800
Vertical Axis	0.11595
Cycle	15000-23000

ϕ [degree]	x [inch]	y [inch]	f(g)
0	0.848	0	1.5037
2.14	0.84793	0.00431	1.5038
4.32	0.84772	0.00869	1.5041
6.47	0.84738	0.01301	1.5046
8.63	0.84689	0.01732	1.5059
10.83	0.84625	0.0217	1.5090
13.02	0.84548	0.02602	1.5132
15.26	0.84454	0.0304	1.5182
17.52	0.84345	0.03477	1.5237
19.82	0.8422	0.03915	1.5302
24.58	0.83912	0.04804	1.5458
27.02	0.8373	0.05249	1.5551
29.52	0.83528	0.05693	1.5652
34.84	0.83044	0.06601	1.5891
37.64	0.8276	0.07058	1.6029
40.6	0.82441	0.07522	1.6180
43.73	0.82081	0.07993	1.6350
47.04	0.81678	0.08463	1.6536
50.71	0.81206	0.08952	1.6752
52.66	0.80944	0.09197	1.6866
56.9	0.80353	0.09693	1.7126
61.87	0.79621	0.10209	1.7435
68.06	0.78662	0.10744	1.7599
77.25	0.77163	0.11305	1.7791
90	0.75	0.11595	1.8030

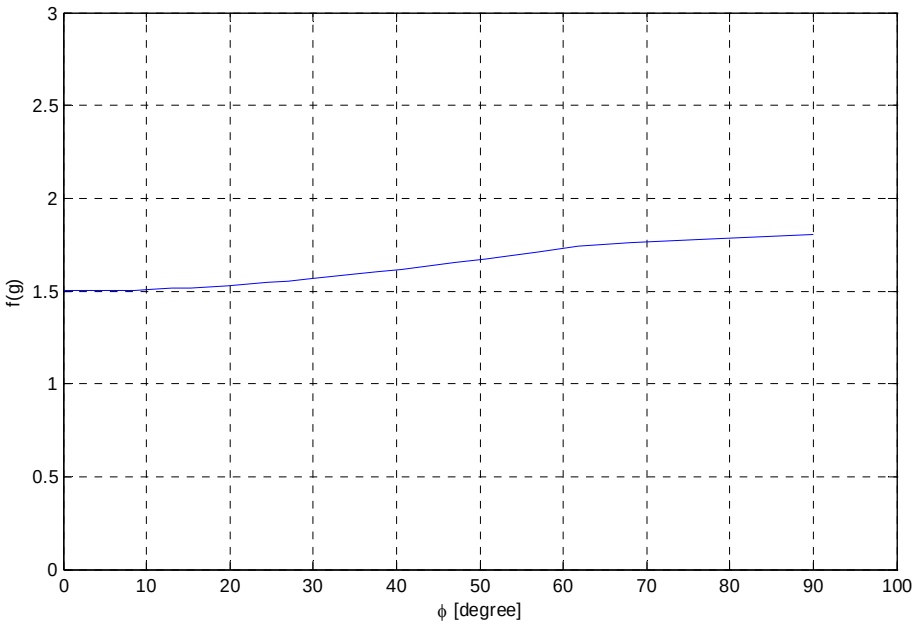

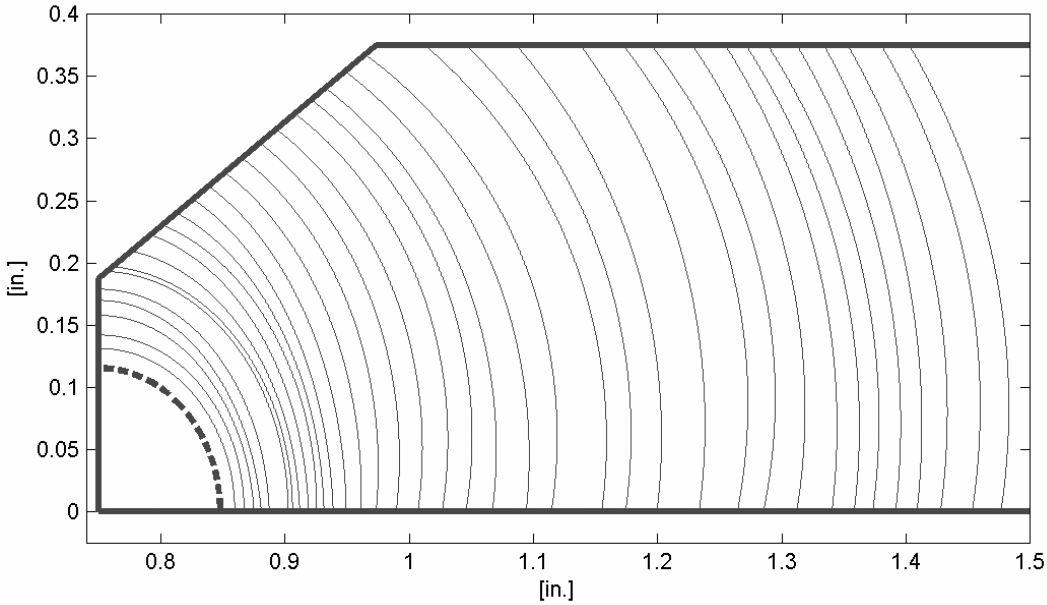

Figure C-1. Corrected BCF for FAA-009 at 15,000-23,000 Cycle, Initial Corner Crack, Type I

Table C-2. Corrected Boundary Correction Factors for FAA-009 (See figure C-2)

Initial Crack Location	Corner
Type	I
Center of Ellipse	(0.75, 0)
Horizontal Axis	0.10950
Vertical Axis	0.13145
Cycle	23000-25500

ϕ [degree]	x [inch]	y [inch]	f(g)
0	0.8595	0	1.5838
3.08	0.85934	0.00706	1.5837
4.63	0.85914	0.01061	1.5835
7.72	0.85851	0.01766	1.5829
10.84	0.85755	0.02472	1.5819
15.57	0.85548	0.03528	1.5799
18.79	0.85367	0.04233	1.5781
20.43	0.85261	0.04588	1.5771
23.75	0.85023	0.05294	1.5748
28.87	0.84589	0.06345	1.5705
30.65	0.8442	0.067	1.5688
34.27	0.84049	0.07401	1.5652
38.06	0.83622	0.08102	1.561
40.02	0.83385	0.08453	1.5588
44.14	0.82858	0.09154	1.5538
46.31	0.82564	0.09504	1.5511
50.9	0.81905	0.10201	1.5453
53.39	0.81529	0.10552	1.5422
56	0.81122	0.10898	1.5389
61.85	0.80166	0.1159	1.5439
65.24	0.79587	0.11936	1.547
69.13	0.78902	0.12282	1.551
73.88	0.7804	0.12628	1.5566
80.76	0.76759	0.12974	1.5664
90	0.75	0.13145	1.5829

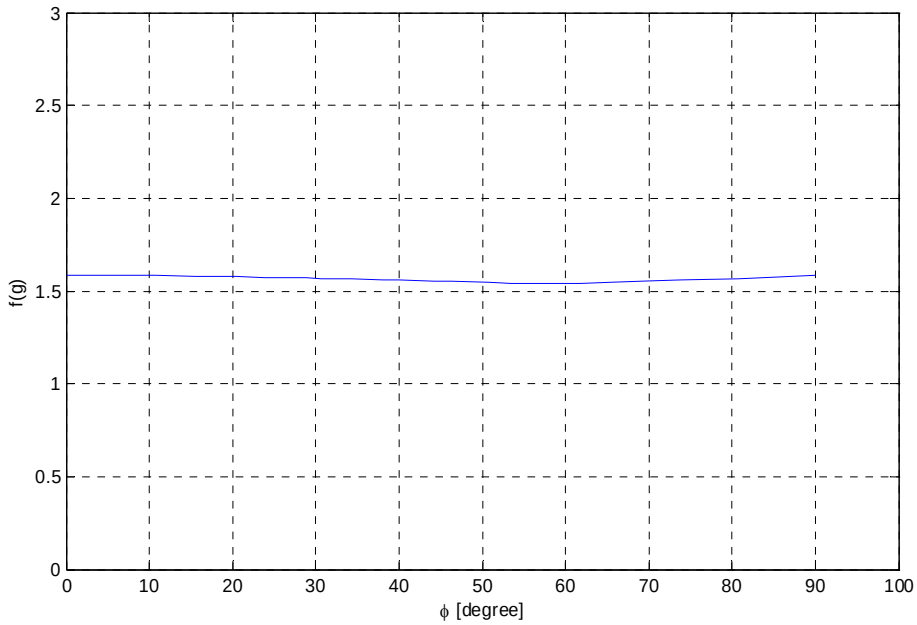

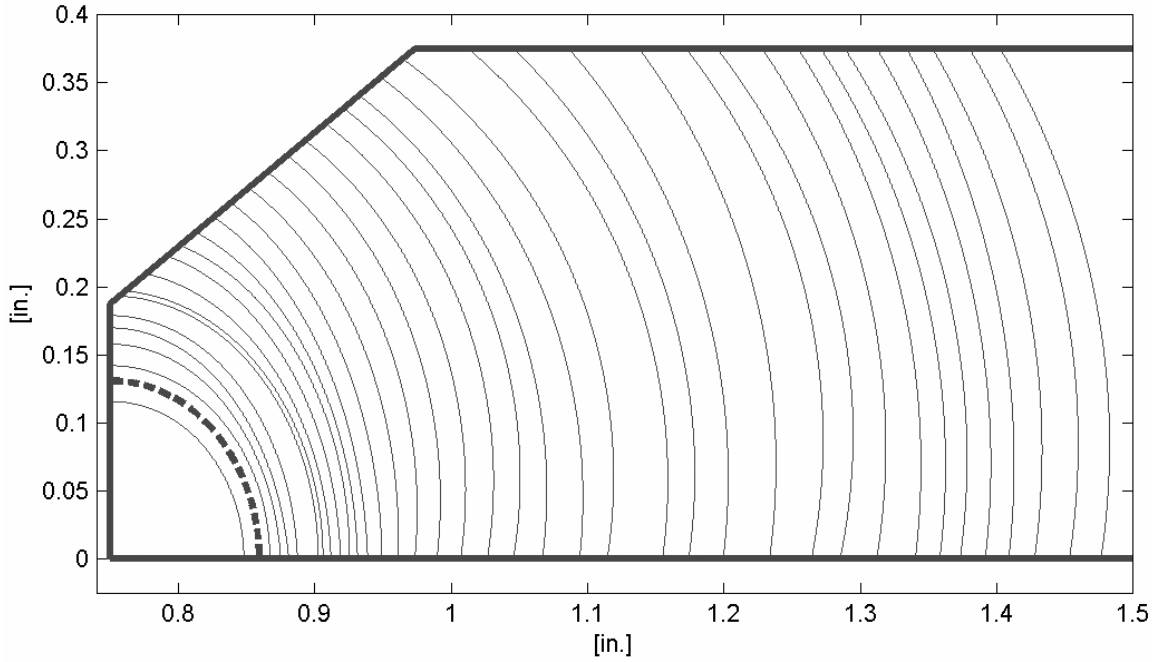

Figure C-2. Corrected BCF for FAA-009 at 23,000-25,500 Cycle, Initial Corner Crack, Type I

Table C-3. Corrected Boundary Correction Factors for FAA-009 (See figure C-3)

Initial Crack Location	Corner
Type	I
Center of Ellipse	(0.75, 0)
Horizontal Axis	0.11700
Vertical Axis	0.14225
Cycle	25500-28500

ϕ [degree]	x [inch]	y [inch]	f(g)
0	0.867	0	1.5635
4.54	0.86663	0.01123	1.5659
6.5	0.86625	0.01607	1.5686
10.43	0.86507	0.02571	1.5767
14.43	0.86331	0.0354	1.5883
18.51	0.86095	0.04508	1.6040
22.71	0.85793	0.05481	1.6234
28.54	0.85278	0.06785	1.6560
31.6	0.84966	0.07441	1.6752
36.44	0.84413	0.08436	1.7081
39.84	0.83983	0.09101	1.7304
43.48	0.8349	0.09775	1.7400
47.37	0.82924	0.10453	1.7508
49.45	0.82606	0.10797	1.7566
53.94	0.81887	0.11488	1.7693
56.42	0.81471	0.11841	1.7798
59.08	0.81012	0.12193	1.7938
61.99	0.80494	0.1255	1.8088
65.3	0.7989	0.12916	1.8252
69.08	0.79178	0.13282	1.8431
71.27	0.78757	0.13467	1.8529
73.74	0.78277	0.13652	1.8634
76.71	0.77689	0.13841	1.8752
80.56	0.76918	0.14031	1.8892
90	0.75	0.14225	1.9155

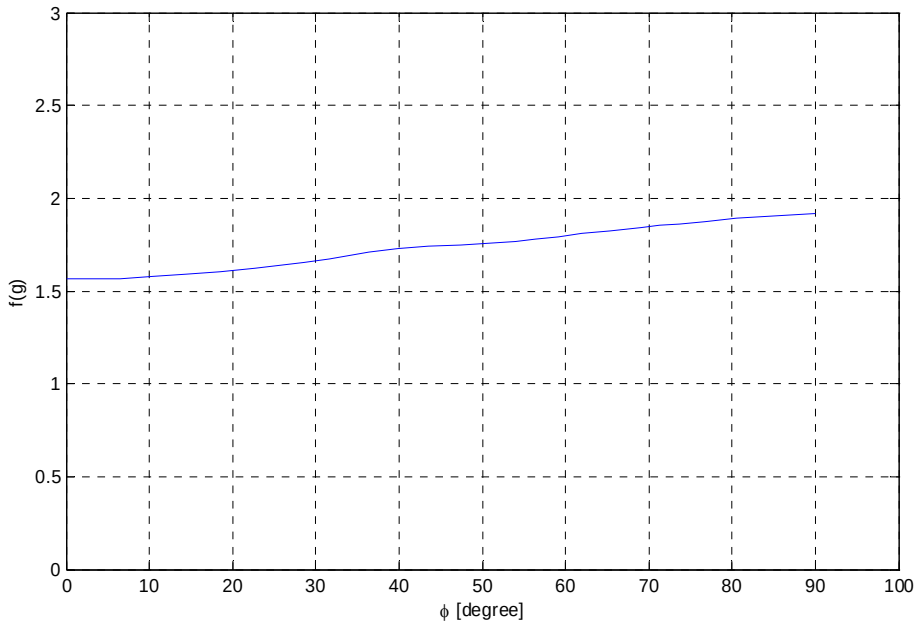

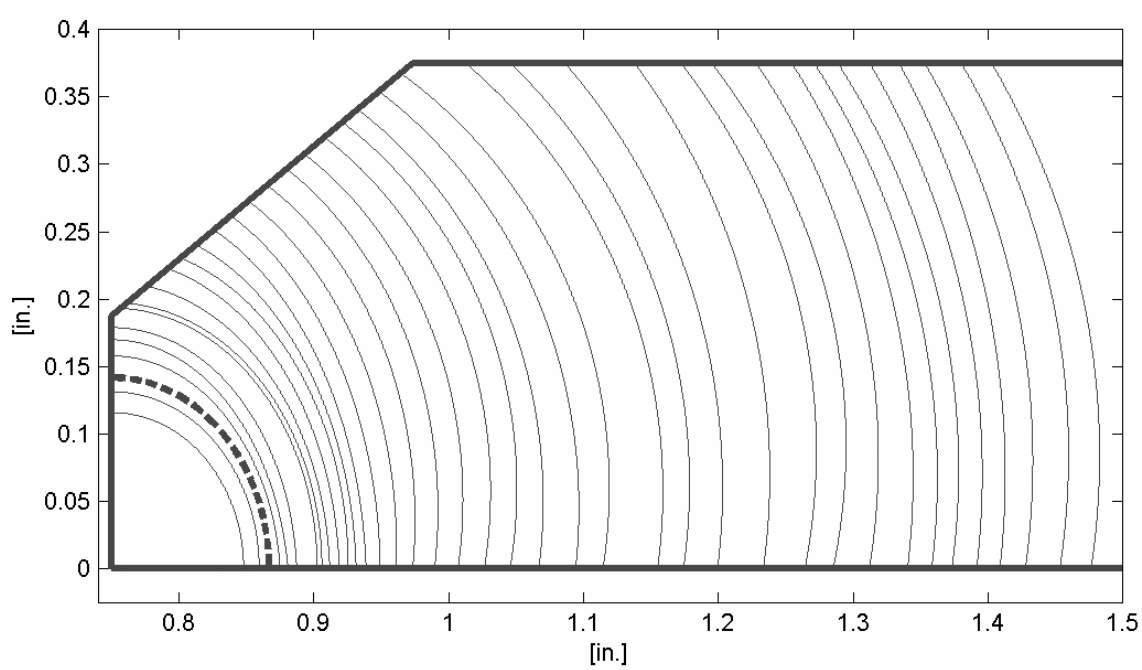

Figure C-3. Corrected BCF for FAA-009 at 25,500-28,500 Cycle, Initial Corner Crack, Type I

Table C-4. Corrected Boundary Correction Factors for FAA-009 (See figure C-4)

Initial Crack Location	Corner
Type	I
Center of Ellipse	(0.75, -0.015)
Horizontal Axis	0.12550
Vertical Axis	0.17300
Cycle	28500-30250

ϕ [degree]	x [inch]	y [inch]	f(g)
6.37	0.87473	0	1.6965
8.01	0.87428	0.00649	1.6696
10.15	0.87354	0.01406	1.6395
14.42	0.87155	0.0277	1.5929
17.44	0.86973	0.03681	1.5685
20.03	0.86791	0.04438	1.5534
25.44	0.86333	0.05956	1.5419
28.84	0.85994	0.06871	1.5491
31.76	0.8567	0.07632	1.5642
34.2	0.8538	0.08247	1.5820
37.36	0.84976	0.09017	1.6114
40	0.84614	0.09636	1.6406
44.22	0.83994	0.10576	1.6940
48.82	0.83264	0.11524	1.7333
53.99	0.82378	0.12493	1.7591
56.87	0.81859	0.12983	1.7805
60.04	0.81268	0.13482	1.8149
62.36	0.80822	0.13819	1.8394
64.94	0.80317	0.14164	1.8652
67.79	0.79745	0.14508	1.8927
71.15	0.79054	0.14866	1.9222
75.33	0.78178	0.15231	1.9550
77.99	0.7761	0.15418	1.9733
81.44	0.76869	0.15605	1.9939
90	0.75	0.158	2.0276

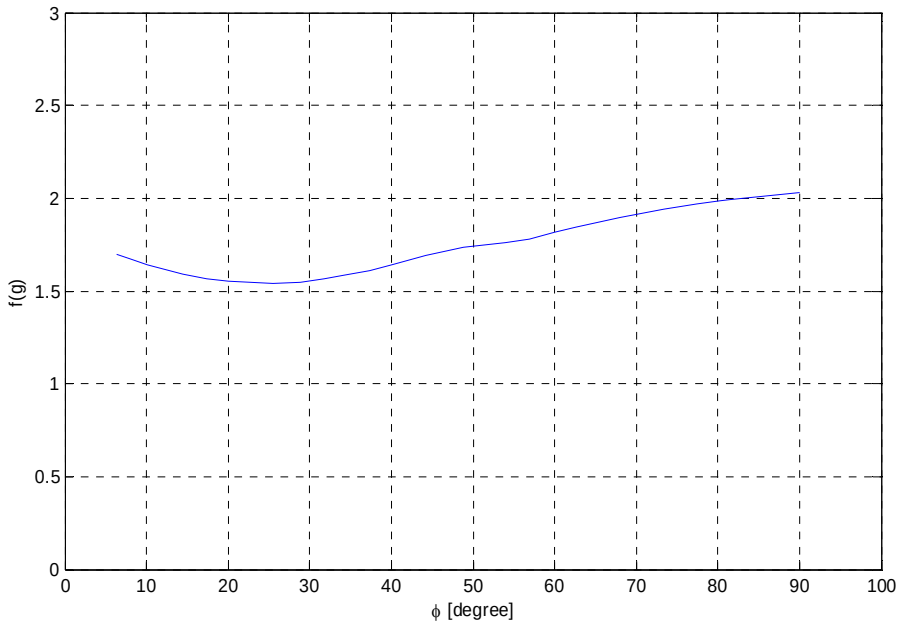

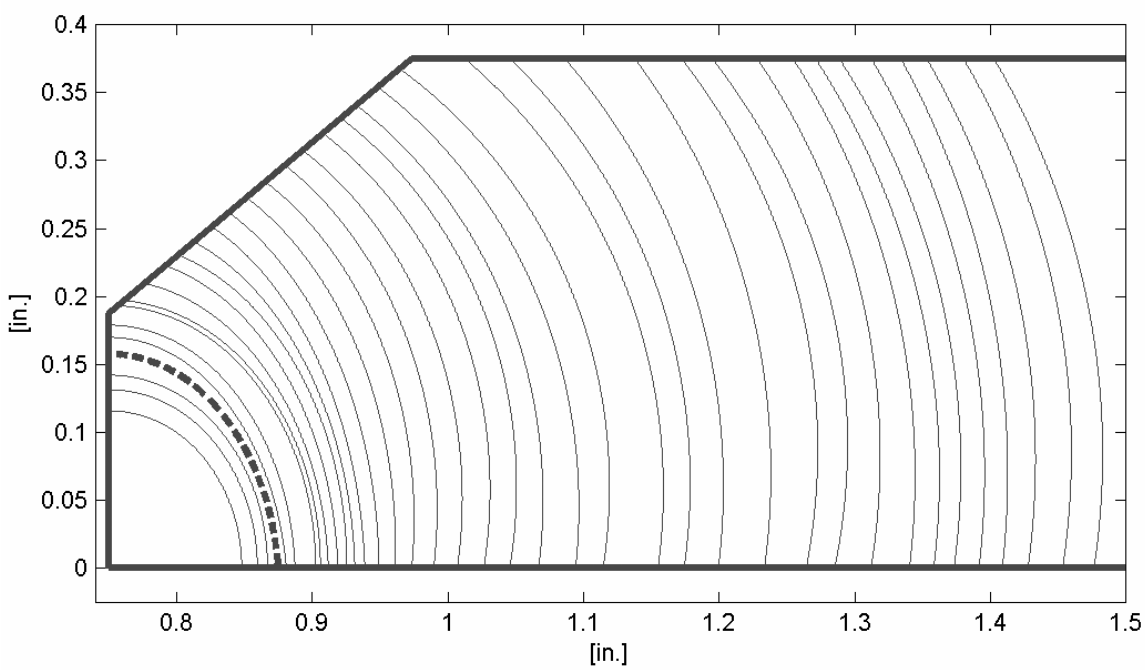

Figure C-4. Corrected BCF for FAA-009 at 28,500-30,250 Cycle, Initial Corner Crack, Type I

Table C-5. Corrected Boundary Correction Factors for FAA-009 (See figure C-5)

Initial Crack Location	Corner
Type	I
Center of Ellipse	(0.75, -0.025)
Horizontal Axis	0.13200
Vertical Axis	0.19500
Cycle	30250-32250

ϕ [degree]	x [inch]	y [inch]	f(g)
7.49	0.88087	0	1.5253
10.2	0.87991	0.00927	1.5424
12	0.87912	0.01534	1.5539
16.12	0.87681	0.02901	1.5796
18.45	0.87521	0.03661	1.5937
21.29	0.87299	0.04573	1.6107
24.2	0.8704	0.05488	1.6283
27.18	0.86742	0.06403	1.6461
32.9	0.86083	0.08088	1.6810
35.07	0.85803	0.08702	1.6945
38.46	0.85337	0.09625	1.7158
42.01	0.84808	0.10548	1.7228
45.14	0.84311	0.11321	1.7300
48.46	0.83754	0.12094	1.7378
51.29	0.83254	0.12716	1.7446
54.32	0.827	0.13338	1.7520
57.62	0.82068	0.13968	1.7603
62.23	0.81151	0.14753	1.7720
66.54	0.80256	0.15387	1.7832
69.03	0.79724	0.15708	1.7928
70.37	0.79434	0.15866	1.7978
75.17	0.78379	0.1635	1.8152
79.53	0.77399	0.16675	1.8299
82.6	0.767	0.16838	1.8396
90	0.75	0.17	1.8597

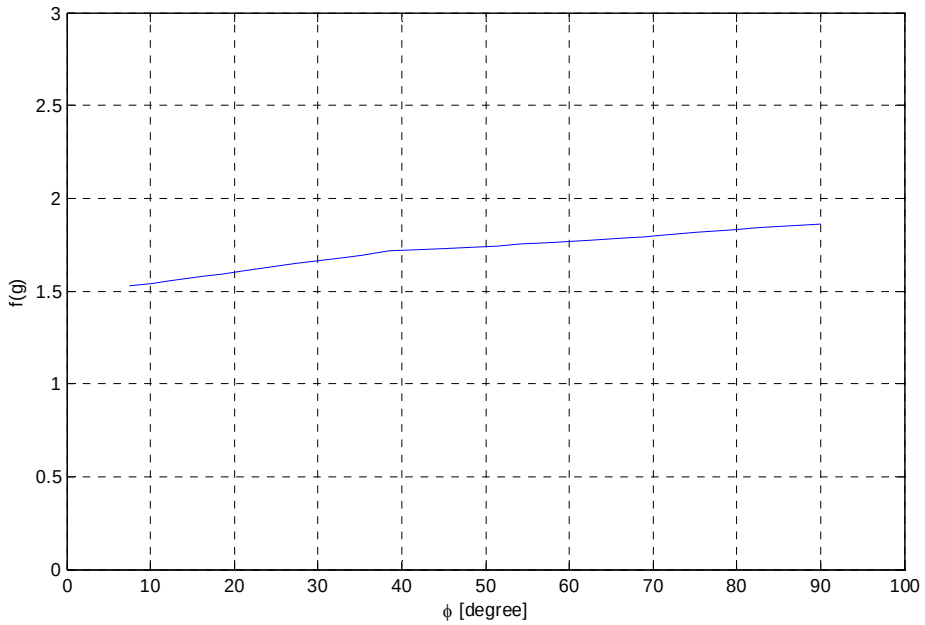

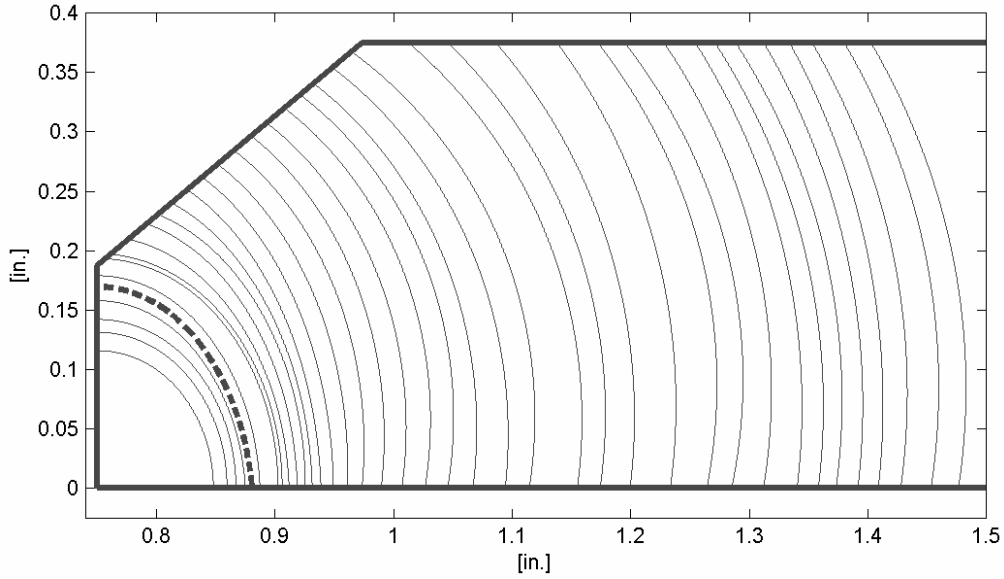

Figure C-5. Corrected BCF for FAA-009 at 30,250-32,250 Cycle, Initial Crack, Type I

Table C-6. Corrected Boundary Correction Factors for FAA-009 (See figure C-6)

Initial Crack Location	Corner
Type	I
Center of Ellipse	(0.75, -0.01)
Horizontal Axis	0.13750
Vertical Axis	0.18900
Cycle	32250-34250

ϕ [degree]	x [inch]	y [inch]	f(g)
4.11	0.88715	0	1.6535
7.07	0.88646	0.0119	1.6844
10.05	0.88539	0.0223	1.7076
13.18	0.88388	0.03278	1.7225
16.4	0.88191	0.04322	1.7383
20.19	0.87905	0.05523	1.7534
24.1	0.87551	0.06724	1.7657
28.14	0.87124	0.07925	1.7754
31.29	0.8675	0.08828	1.7811
34.53	0.86327	0.09726	1.7855
37.93	0.85846	0.10629	1.7887
41.47	0.85302	0.11528	1.7904
44.59	0.84793	0.12277	1.7909
48.56	0.84101	0.13176	1.7902
52.11	0.83445	0.13922	1.7885
56.76	0.82537	0.14813	1.7850
60.21	0.81832	0.15406	1.7819
63.04	0.81233	0.1585	1.7791
66.19	0.80552	0.16293	1.7784
71.06	0.79462	0.16879	1.7836
75.74	0.78387	0.17319	1.7894
77.66	0.77939	0.17464	1.7922
79.93	0.77404	0.17609	1.7958
82.88	0.76703	0.17755	1.8009
90	0.75	0.179	1.8161

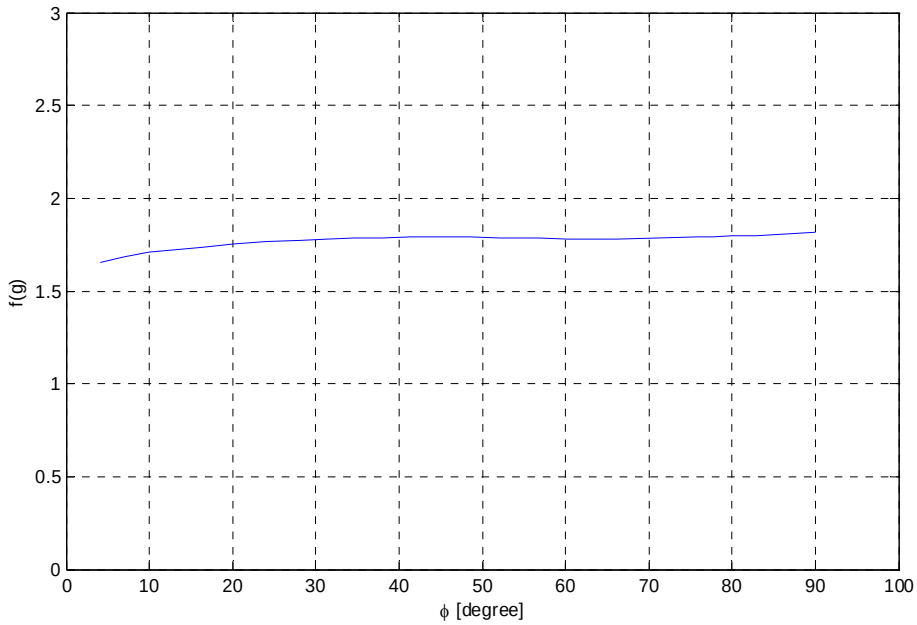

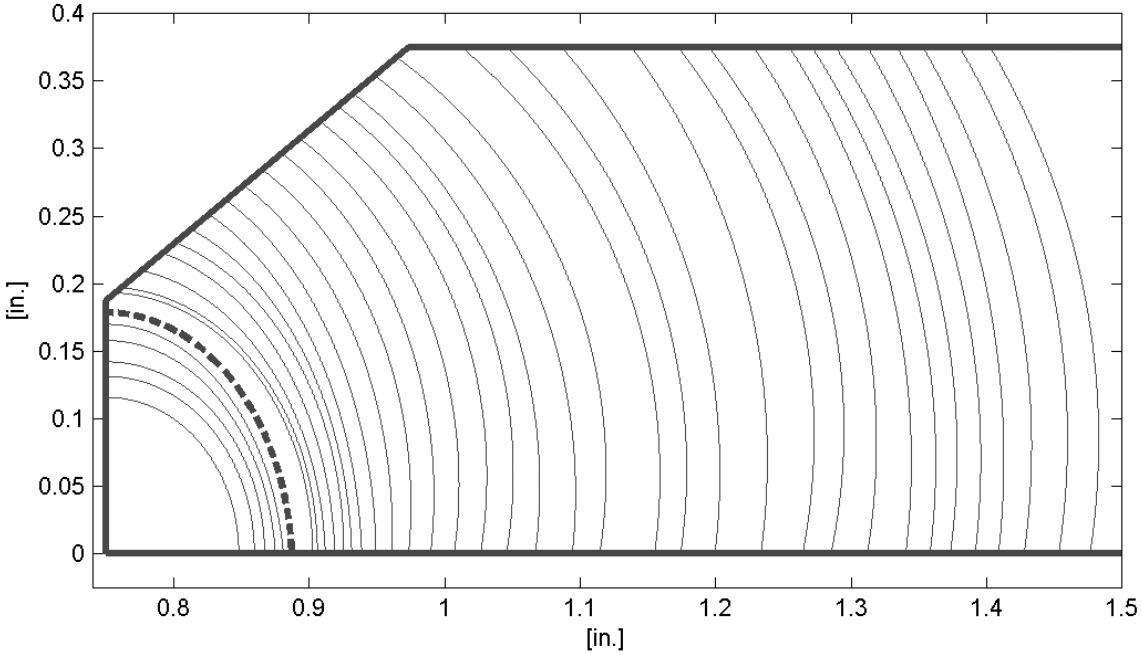

Figure C-6. Corrected BCF for FAA-009 at 32,250-34,250 Cycle, Initial Corner Crack, Type I

Table C-7. Corrected Boundary Correction Factors for FAA-009 (See figure C-7)

Initial Crack Location	Corner
Type	II
Center of Ellipse	(0.75, 0)
Horizontal Axis	0.15250
Vertical Axis	0.19350
Cycle	36250-37000

ϕ [degree]	x [inch]	y [inch]	f(g)
0	0.9025	0	1.6502
3.08	0.90228	0.01041	1.6507
5.28	0.90185	0.0178	1.6516
9.72	0.90031	0.03267	1.6547
12.41	0.89894	0.04159	1.6577
17.41	0.89551	0.05791	1.6651
22.57	0.89082	0.07427	1.6752
28.43	0.88411	0.09211	1.6900
31.47	0.88006	0.10103	1.6961
34.09	0.87629	0.10847	1.6991
40.17	0.86653	0.12482	1.7069
43.12	0.86132	0.13226	1.7112
46.21	0.85553	0.13969	1.7159
48.82	0.85041	0.14564	1.7203
53.77	0.84014	0.15608	1.7291
56.07	0.83513	0.16054	1.7334
58.51	0.82966	0.165	1.7382
62.09	0.82139	0.17099	1.7455
67.26	0.80895	0.17846	1.7568
70.97	0.79973	0.18292	1.7654
73.88	0.79234	0.18589	1.7723
77.49	0.78303	0.18891	1.7812
79.72	0.77722	0.19039	1.7868
82.58	0.7697	0.19188	1.7941
87.41	0.7569	0.19329	1.9018

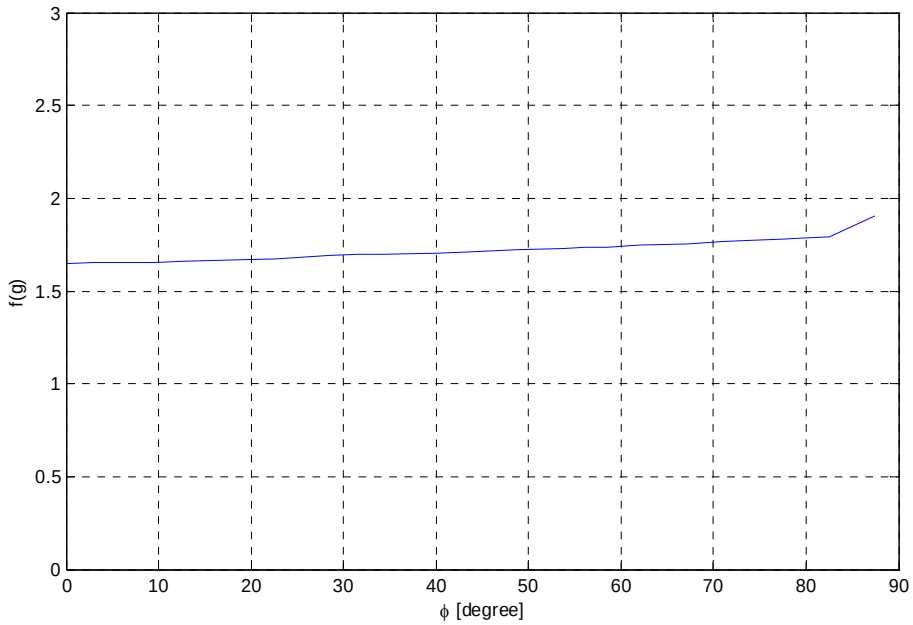

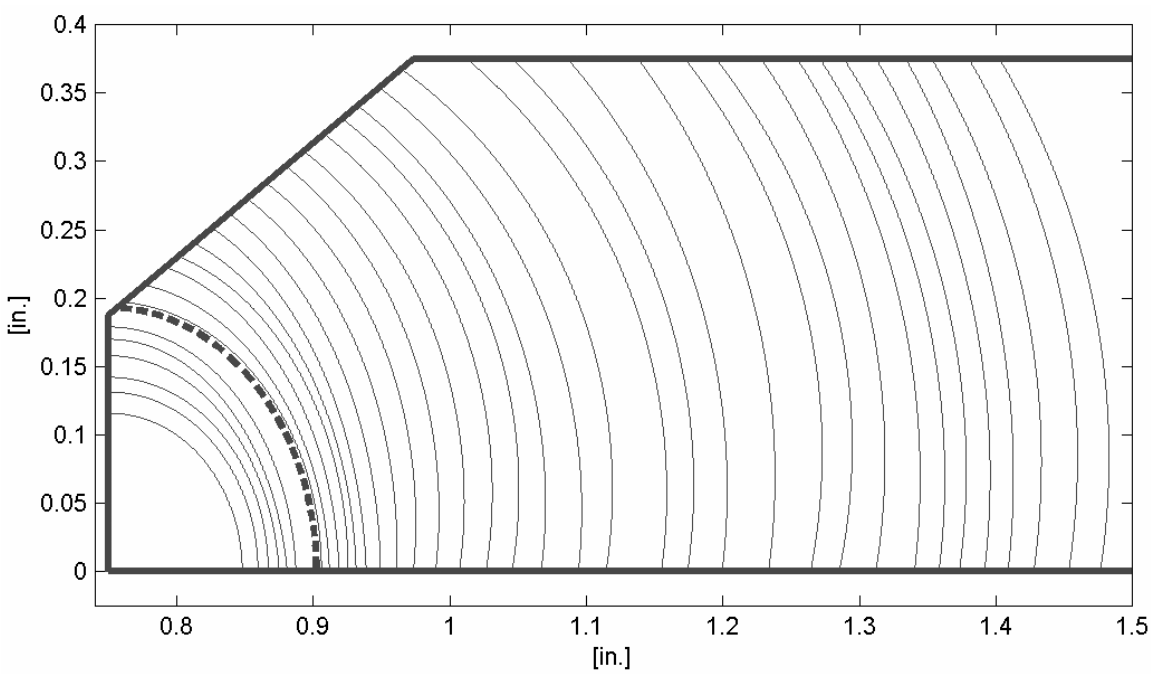

Figure C-7. Corrected BCF for FAA-009 at 36,250-37,000 Cycle, Initial Corner Crack, Type II

Table C-8. Corrected Boundary Correction Factors for FAA-009 (See figure C-8)

Initial Crack Location	Corner
Type	II
Center of Ellipse	(0.75, 0)
Horizontal Axis	0.15600
Vertical Axis	0.19750
Cycle	37000-37750

ϕ [degree]	x [inch]	y [inch]	f(g)
0	0.906	0	1.7353
3.26	0.90575	0.01122	1.7357
6.11	0.90511	0.02103	1.7367
9.4	0.90391	0.03225	1.7385
12.72	0.90217	0.04347	1.7411
16.08	0.8999	0.05469	1.7446
19.93	0.89666	0.06731	1.7495
23.43	0.89314	0.07853	1.7549
27.04	0.88895	0.08979	1.7613
30.29	0.88471	0.0996	1.7677
34.15	0.87911	0.11086	1.7763
40.3	0.86898	0.12774	1.7919
44.17	0.86189	0.13762	1.8027
48.32	0.85374	0.1475	1.8151
52.17	0.84569	0.15598	1.8273
56.38	0.83638	0.16446	1.8413
60.31	0.82728	0.17156	1.8549
65.75	0.81407	0.18008	1.8741
67.85	0.80882	0.18292	1.8815
71.4	0.79976	0.18718	1.8942
75.81	0.78825	0.19147	1.9095
77.63	0.78342	0.19291	1.9159
79.71	0.77787	0.19432	1.9230
82.4	0.77064	0.19576	1.9319
85.86	0.76127	0.19696	2.0685

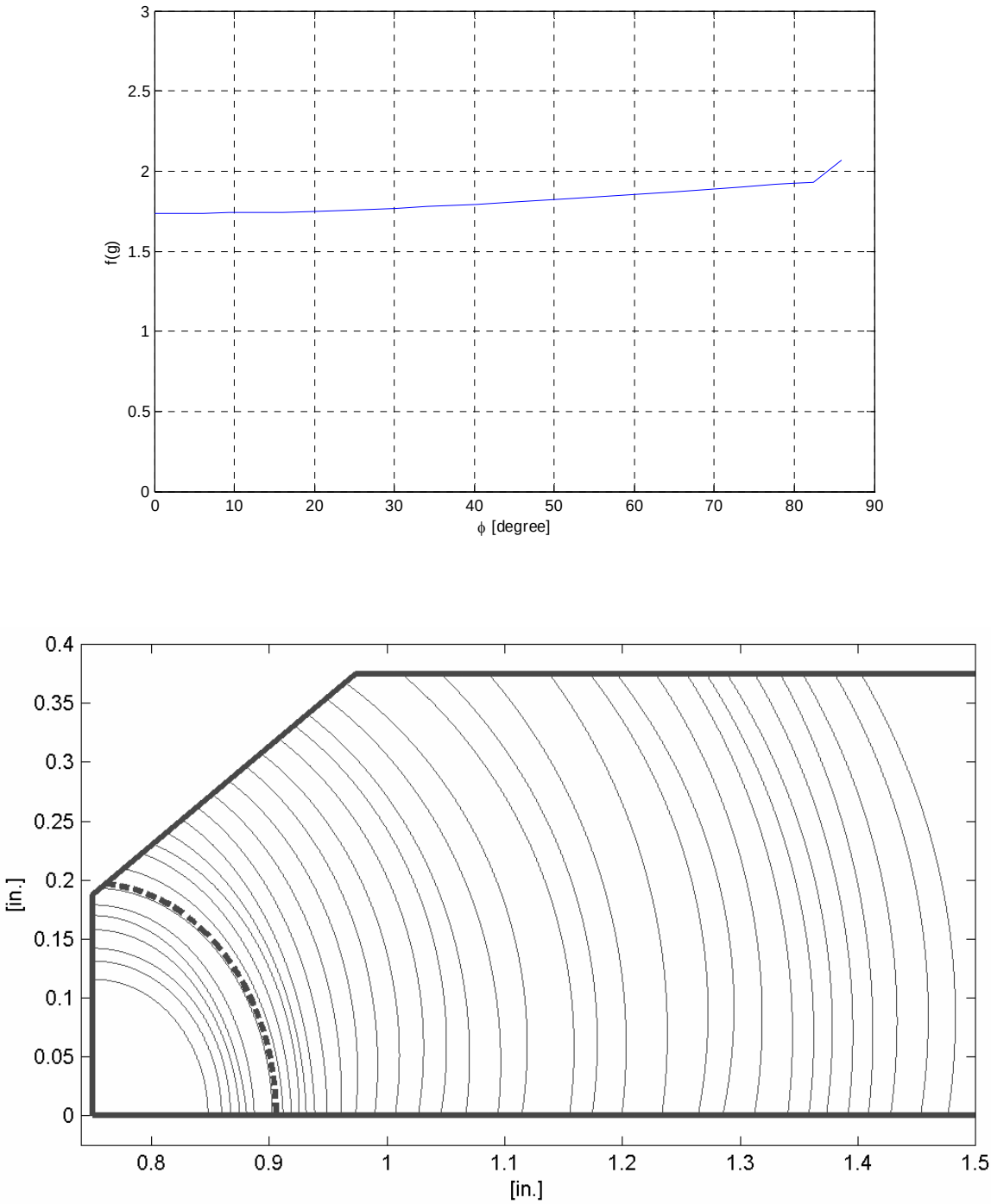

Figure C-8. Corrected BCF for FAA-009 at 37,000-37,750 Cycle, Initial Corner Crack, Type II

Table C-9. Corrected Boundary Correction Factors for FAA-009 (See figure C-9)

Initial Crack Location	Corner
Type	II
Center of Ellipse	(0.75, -0.01)
Horizontal Axis	0.16200
Vertical Axis	0.22250
Cycle	37750-39500

ϕ [degree]	x [inch]	y [inch]	f(g)
3.35	0.91172	0	1.6609
5.04	0.91137	0.00825	1.6437
8.25	0.91032	0.02164	1.6222
11.31	0.90885	0.03366	1.6103
14.11	0.90711	0.04437	1.6067
17.33	0.90465	0.05644	1.6108
20.25	0.90198	0.06718	1.6219
23.24	0.89885	0.07793	1.6406
26.32	0.8952	0.08875	1.6665
29.51	0.89099	0.0996	1.6904
32.39	0.8868	0.10913	1.7022
37.59	0.87836	0.1256	1.7517
39.9	0.87429	0.13253	1.7782
45.34	0.86387	0.148	1.8427
51.48	0.85089	0.16376	1.9164
54.64	0.84375	0.17113	1.9536
57.4	0.83729	0.1771	1.9853
60.43	0.82995	0.18319	2.0190
64.8	0.81898	0.19103	2.0653
67.88	0.81101	0.19586	2.1678
70.23	0.8048	0.19916	2.2773
74.5	0.79328	0.20425	2.3433
78.17	0.78321	0.20766	2.3949
79.3	0.78007	0.20832	2.4451
80.91	0.77561	0.20899	2.5140

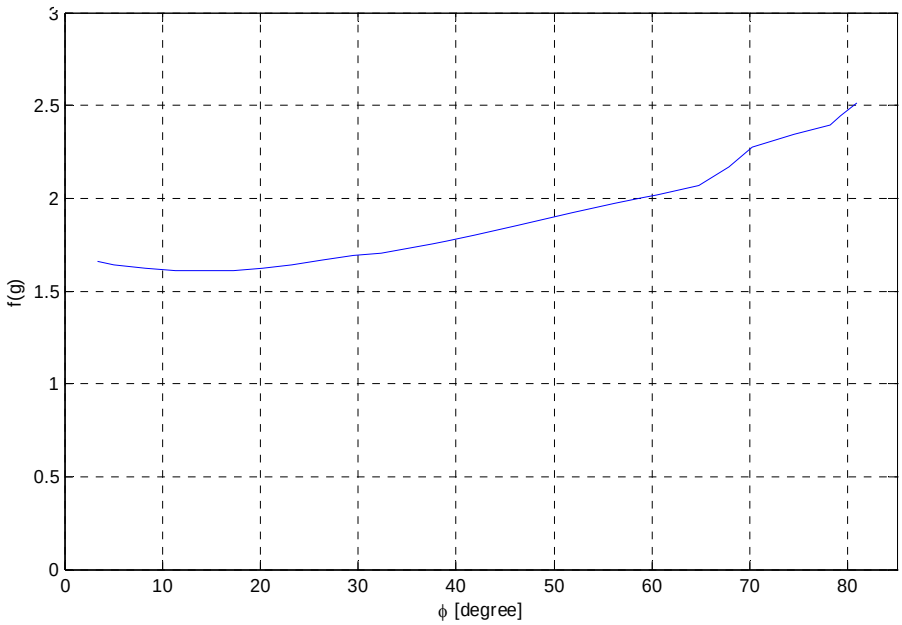

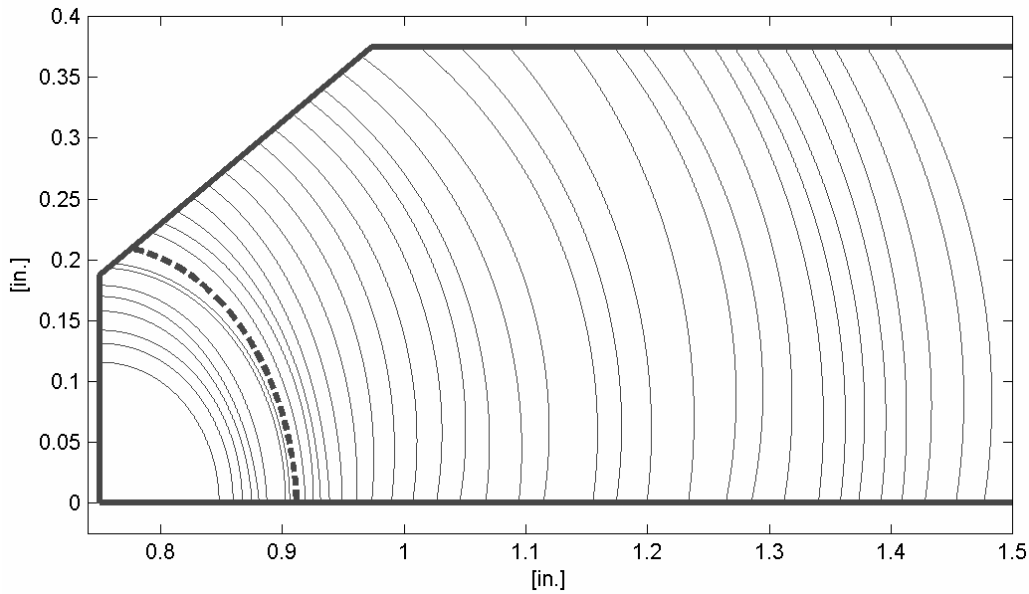

Figure C-9. Corrected BCF for FAA-009 at 37,750-39,500 Cycle, Initial Corner Crack, Type II

Table C-10. Corrected Boundary Correction Factors for FAA-009 (See figure C-10)

Initial Crack Location	Corner
Type	II
Center of Ellipse	(0.75, -0.01)
Horizontal Axis	0.16900
Vertical Axis	0.24000
Cycle	39500-40750

ϕ [degree]	x [inch]	y [inch]	f(g)
3.28	0.91872	0	1.7179
7.29	0.91763	0.01937	1.7636
11.18	0.9158	0.03602	1.7956
14.19	0.91385	0.04854	1.8163
18.3	0.91045	0.06523	1.8404
20.05	0.90875	0.07222	1.8495
24.36	0.90396	0.08898	1.8692
28.06	0.89913	0.10293	1.8836
32.31	0.89283	0.11833	1.8978
36.36	0.8861	0.13235	1.9094
40.63	0.87825	0.14636	1.9200
45.21	0.86907	0.16038	1.9297
49.15	0.86053	0.17161	1.9372
51.26	0.85576	0.17724	1.9408
56.37	0.8436	0.18987	1.9491
58.88	0.83734	0.1955	1.9529
60.89	0.83223	0.19971	1.9560
62.3	0.82855	0.20253	1.9582
64.55	0.82262	0.20674	1.9617
66.14	0.81835	0.20952	1.9643
68.79	0.81114	0.21376	1.9686
70.71	0.80583	0.21654	1.9719
72.87	0.79979	0.21936	1.9759
74.06	0.7964	0.22079	1.9783
75.69	0.79176	0.22254	2.0347

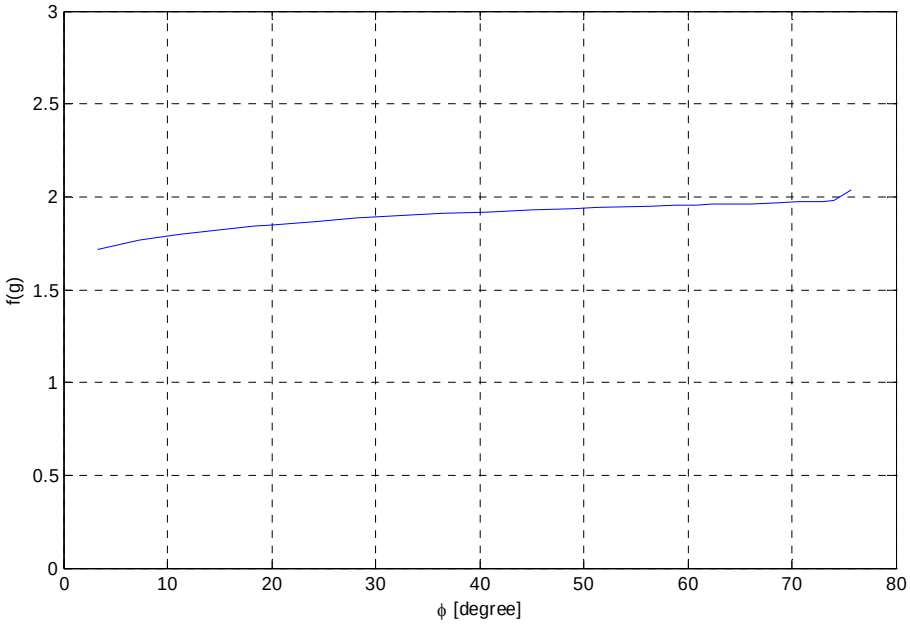

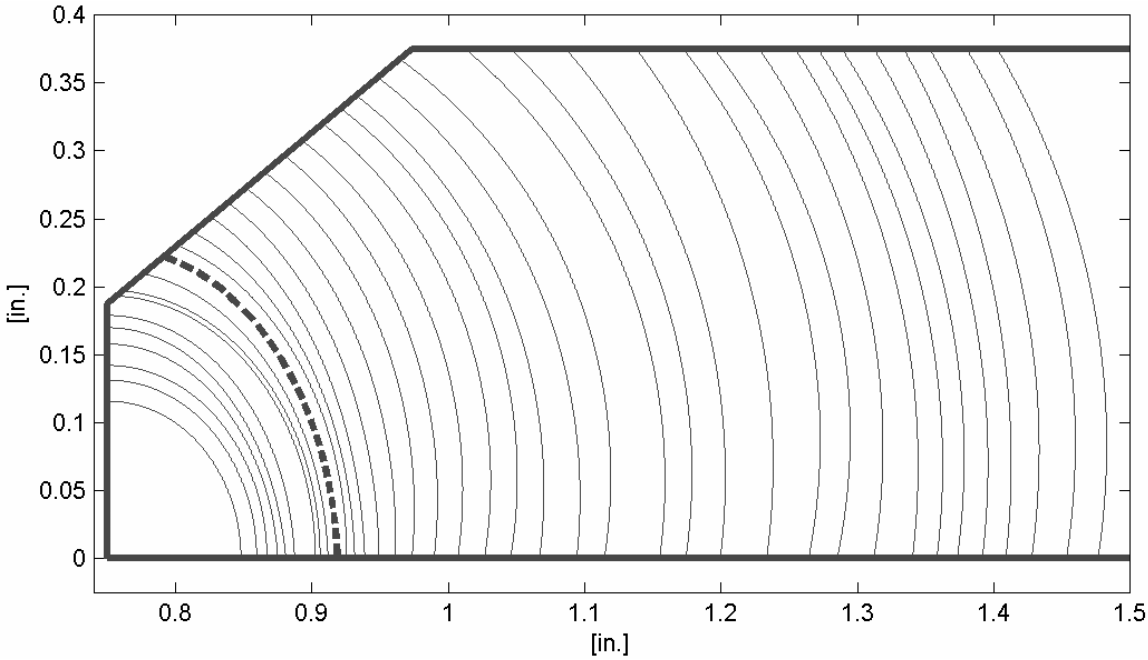

Figure C-10. Corrected BCF for FAA-009 at 39,500-40,750 Cycle, Initial Corner Crack, Type II

Table C-11. Corrected Boundary Correction Factors for FAA-009 (See figure C-11)

Initial Crack Location	Corner
Type	II
Center of Ellipse	(0.75, 0)
Horizontal Axis	0.17550
Vertical Axis	0.24100
Cycle	40750-41500

ϕ [degree]	x [inch]	y [inch]	f(g)
0	0.9255	0	1.9017
2.24	0.92537	0.00942	1.9021
8.03	0.92378	0.03365	1.9064
10.3	0.92267	0.04307	1.9095
12.25	0.9215	0.05113	1.9128
16.22	0.91852	0.0673	1.9210
18.23	0.91669	0.07539	1.9260
20.27	0.91463	0.08349	1.9316
22.34	0.91233	0.09159	1.9379
24.09	0.91022	0.09834	1.9436
26.22	0.90744	0.10647	1.9512
30.24	0.90162	0.12135	1.9668
32.12	0.89863	0.12812	1.9748
34.44	0.89475	0.13626	1.9851
38.04	0.88822	0.14849	2.0023
41.42	0.88161	0.15941	2.0196
47.34	0.86893	0.1772	2.0521
51.36	0.85959	0.18822	2.1326
54.64	0.85156	0.19652	2.2074
58.23	0.84241	0.20486	2.2866
61.54	0.83364	0.21185	2.3232
64.47	0.82565	0.21744	2.3558
68.7	0.81374	0.22453	2.3852
72.47	0.80286	0.22978	2.4157
73.04	0.80118	0.23045	2.4403

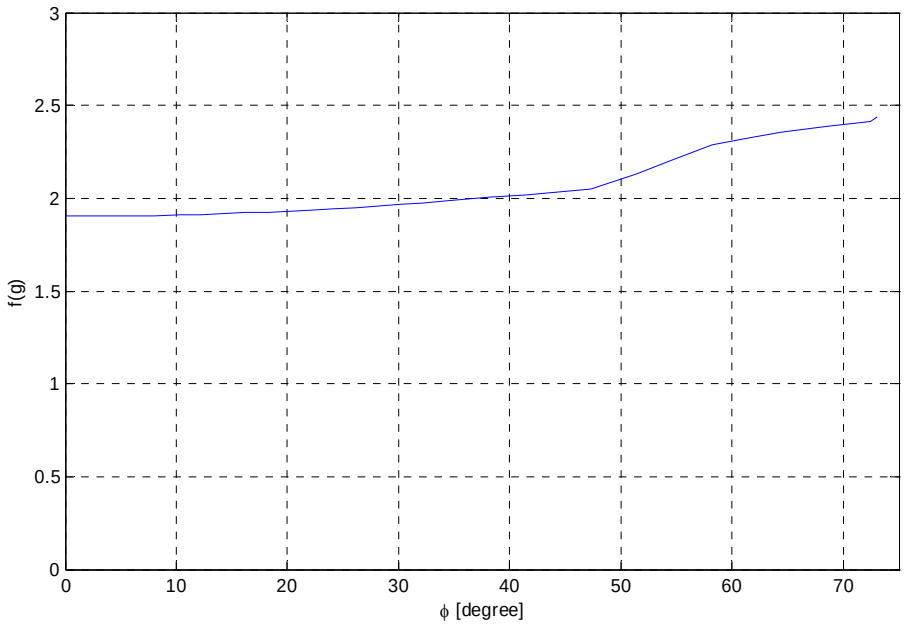

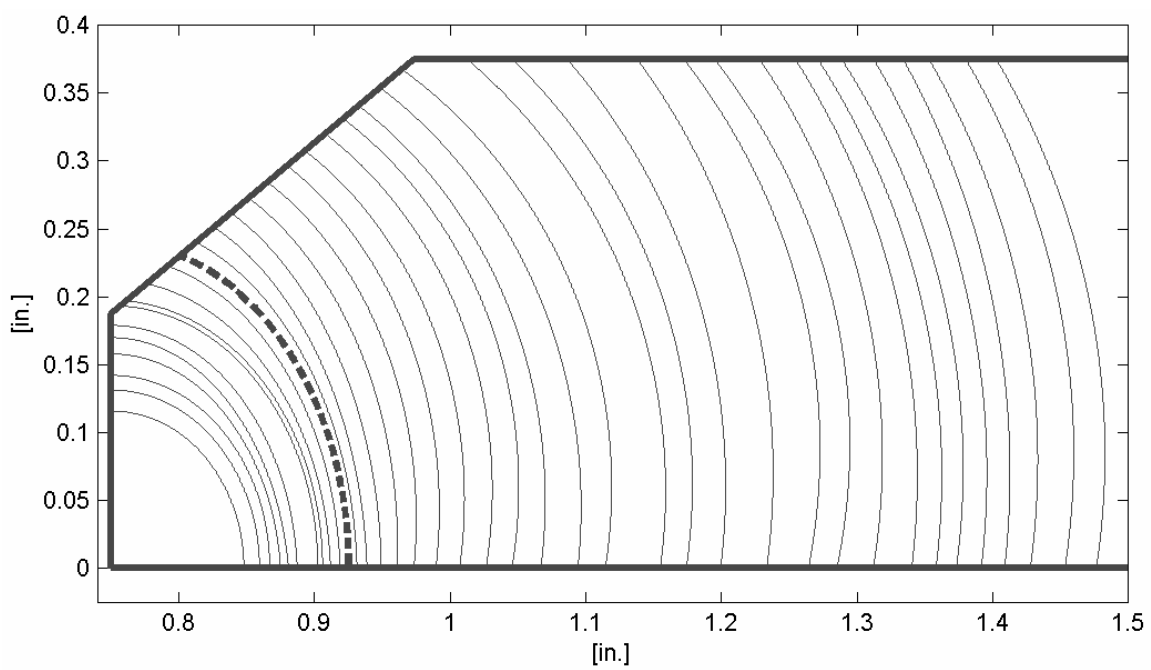

Figure C-11. Corrected BCF for FAA-009 at 40,750-41,500 Cycle, Initial Corner Crack, Type II

Table C-12. Corrected Boundary Correction Factors for FAA-009 (See figure C-12)

Initial Crack Location	Corner
Type	II
Center of Ellipse	(0.75, -0.01)
Horizontal Axis	0.18150
Vertical Axis	0.26650
Cycle	41500-42800

ϕ [degree]	x [inch]	y [inch]	f(g)
2.85	0.93127	0	1.5854
5.22	0.93075	0.01319	1.5503
7.35	0.93001	0.02365	1.5259
10.12	0.92868	0.03671	1.5011
12.38	0.92728	0.04716	1.4872
14.68	0.92558	0.05762	1.4790
17.3	0.92329	0.06938	1.4779
19.37	0.92122	0.07854	1.4833
21.48	0.9189	0.0877	1.4942
26.11	0.91298	0.10738	1.5362
28.34	0.90975	0.11658	1.5637
30.63	0.90618	0.1258	1.5959
32.98	0.90226	0.13506	1.6322
37.54	0.89392	0.15232	1.6824
39.74	0.88956	0.16032	1.6960
42.05	0.88478	0.16838	1.7217
49.16	0.86869	0.19145	1.8270
51.48	0.86304	0.19832	1.8607
56.59	0.84994	0.21226	1.9326
59.46	0.84223	0.21933	1.9713
62.66	0.83336	0.22654	2.0126
65.53	0.82518	0.23238	2.0480
68.81	0.8156	0.23833	2.1913
69.41	0.81384	0.23925	2.2590
69.87	0.81245	0.2399	2.3065

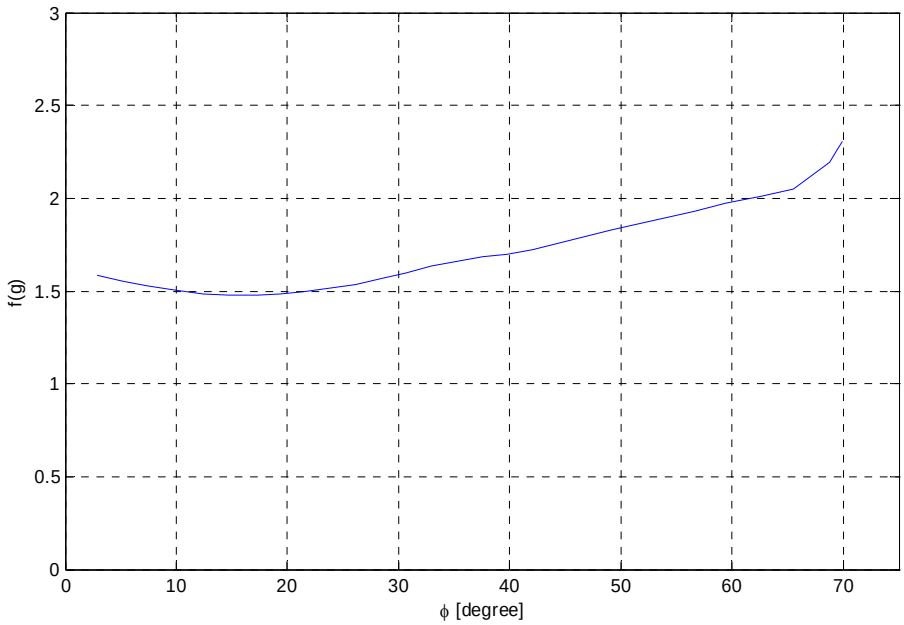

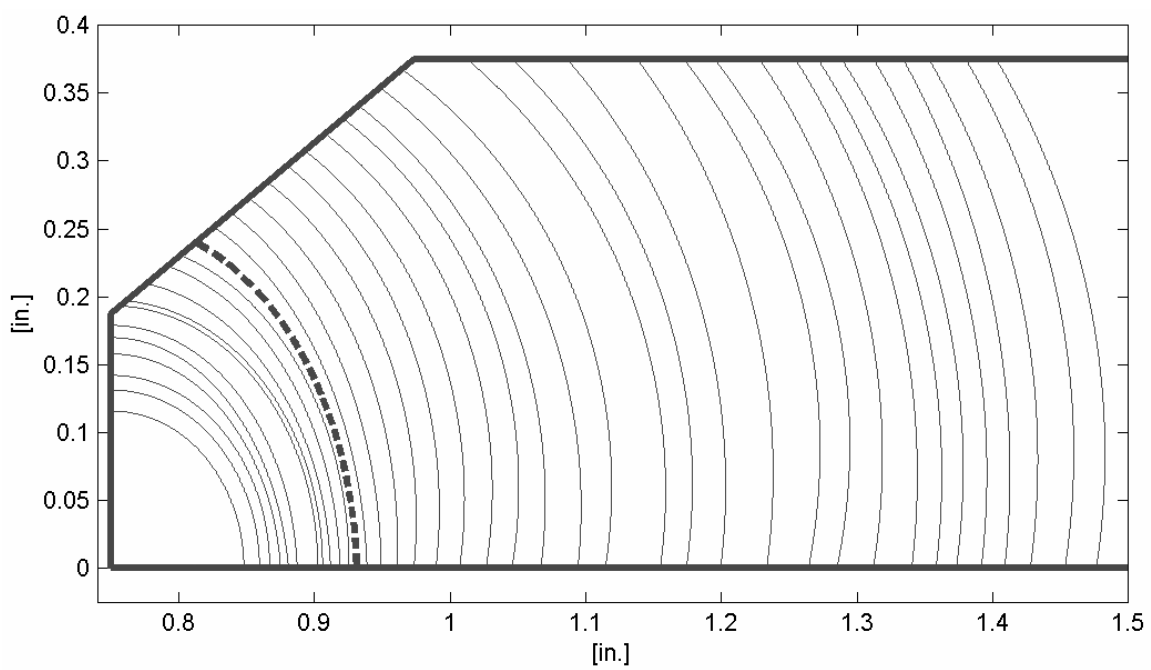

Figure C-12. Corrected BCF for FAA-009 at 41,500-42,800 Cycle, Initial Corner Crack, Type II

Table C-13. Corrected Boundary Correction Factors for FAA-009 (See figure C-13)

Initial Crack Location	Corner
Type	II
Center of Ellipse	(0.75, -0.015)
Horizontal Axis	0.18900
Vertical Axis	0.29050
Cycle	42800-43700

ϕ [degree]	x [inch]	y [inch]	f(g)
3.12	0.93872	0	1.9613
5.14	0.93824	0.01057	1.9695
9	0.93667	0.03019	1.9850
11.09	0.93547	0.04066	1.9934
15.05	0.93251	0.06031	2.0097
17.21	0.93054	0.07081	2.0185
19.11	0.92859	0.07999	2.0264
21.04	0.9264	0.08921	2.0346
25.27	0.92092	0.10893	2.0887
29.07	0.9152	0.12607	2.1307
33.02	0.90847	0.14325	2.1675
37.18	0.90059	0.1605	2.2395
39.17	0.89652	0.16846	2.2494
41.24	0.89212	0.17645	2.2601
43.01	0.8882	0.18313	2.2695
47.13	0.87859	0.19787	2.2927
49.52	0.87269	0.20593	2.3068
51.61	0.86736	0.21267	2.3197
55.21	0.85783	0.22355	2.3427
57.14	0.85254	0.229	2.3555
59.72	0.84529	0.23584	2.3731
61.38	0.84053	0.23998	2.3848
65.01	0.82985	0.24828	2.4110
66.04	0.82676	0.25041	2.4205
66.37	0.82575	0.25106	2.4291

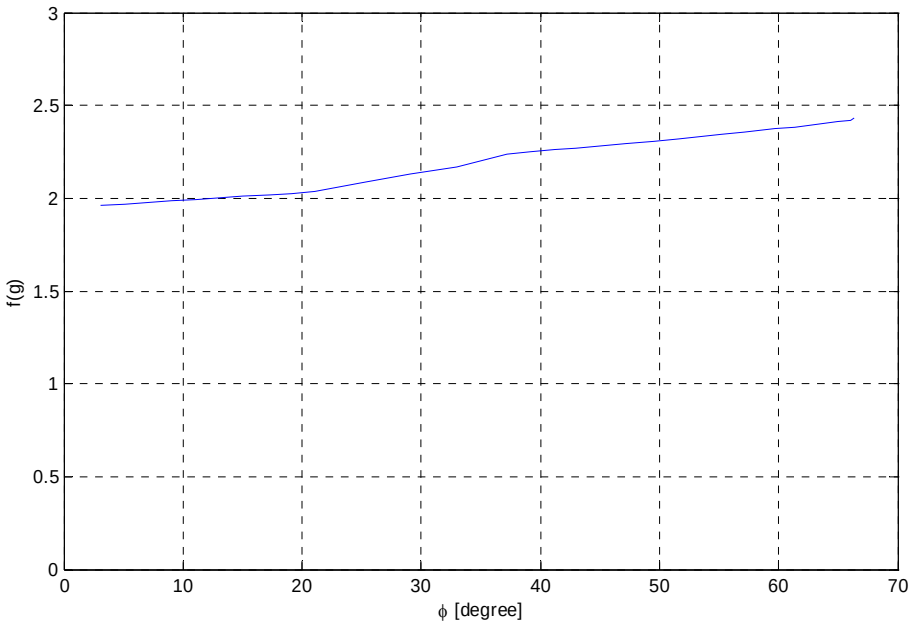

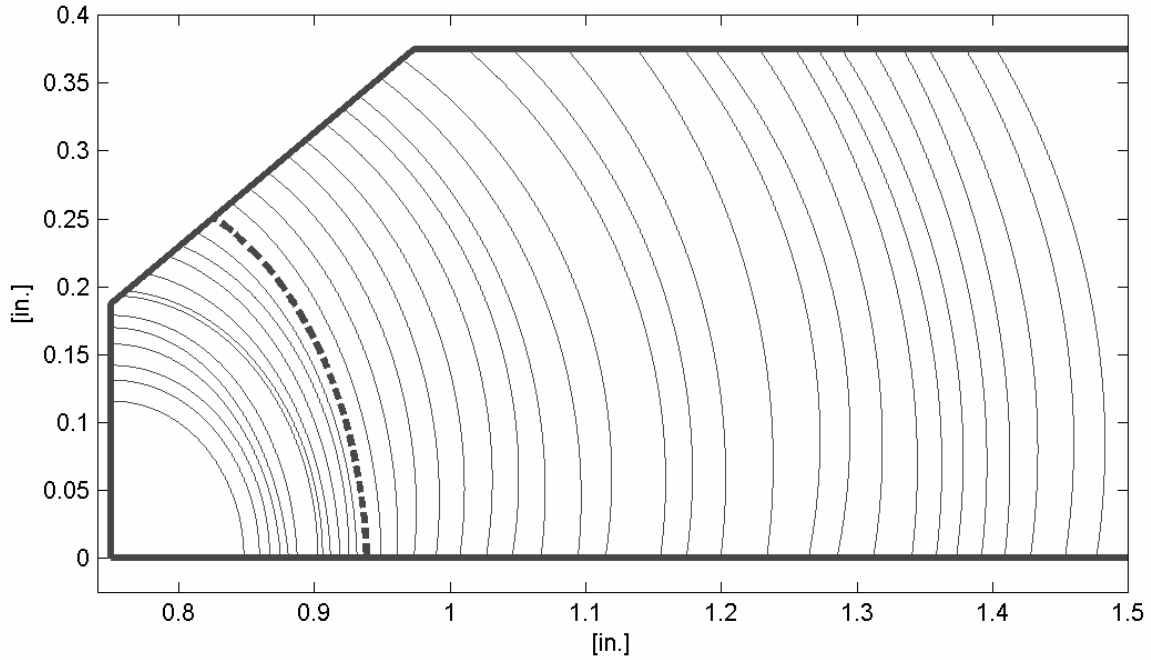

Figure C-13. Corrected BCF for FAA-009 at 42,800-43,700 Cycle, Initial Corner Crack, Type II

Table C-14. Corrected Boundary Correction Factors for FAA-009 (See figure C-14)

Initial Crack Location	Corner
Type	II
Center of Ellipse	(0.75, -0.005)
Horizontal Axis	0.19925
Vertical Axis	0.29750
Cycle	43700-45300

ϕ [degree]	x [inch]	y [inch]	f(g)
1.36	0.94919	0	1.7642
3.1	0.94896	0.0104	1.7712
7.04	0.94775	0.03123	1.7844
9.06	0.94677	0.04166	1.7909
13.14	0.94404	0.06253	1.8034
17.03	0.94051	0.08208	1.8150
19.15	0.93823	0.09255	1.8212
21.02	0.93599	0.10167	1.8266
23.19	0.93315	0.11214	1.8329
25.4	0.92999	0.1226	1.8392
27.09	0.92739	0.13049	1.8440
29.67	0.92313	0.14226	1.8515
32.02	0.91893	0.15276	1.8583
36.31	0.91056	0.17117	1.8710
40.51	0.90148	0.18828	1.8838
42.89	0.89597	0.1975	1.8913
45.01	0.89086	0.20542	1.8981
49.92	0.87828	0.22266	1.9144
51.95	0.87279	0.2293	1.9214
54.08	0.86689	0.23594	1.9289
58.23	0.85489	0.24795	1.9440
60.77	0.8473	0.25462	1.9536
62.41	0.84228	0.25868	1.9599
63.39	0.83924	0.261	1.9650
63.68	0.83835	0.26164	1.9750

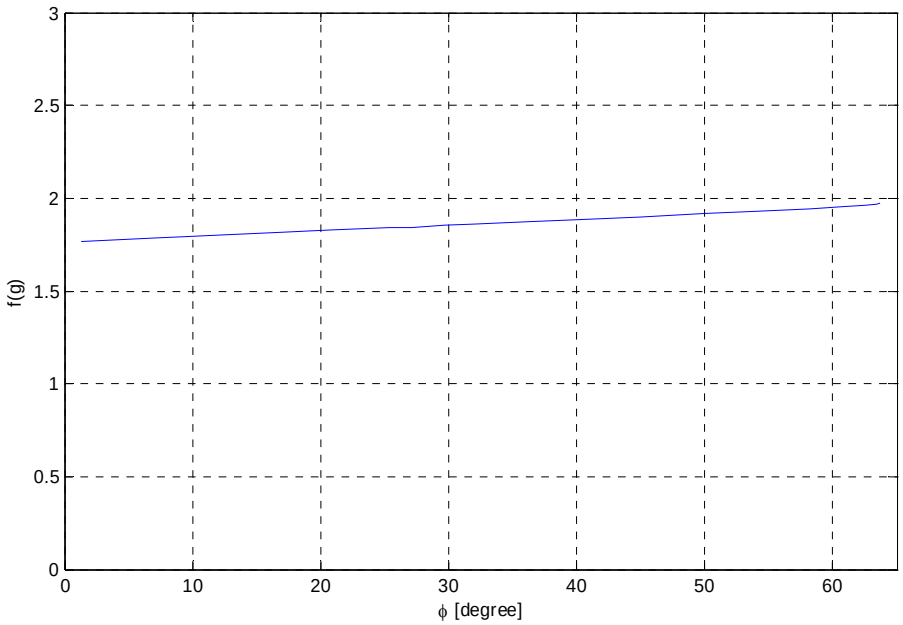

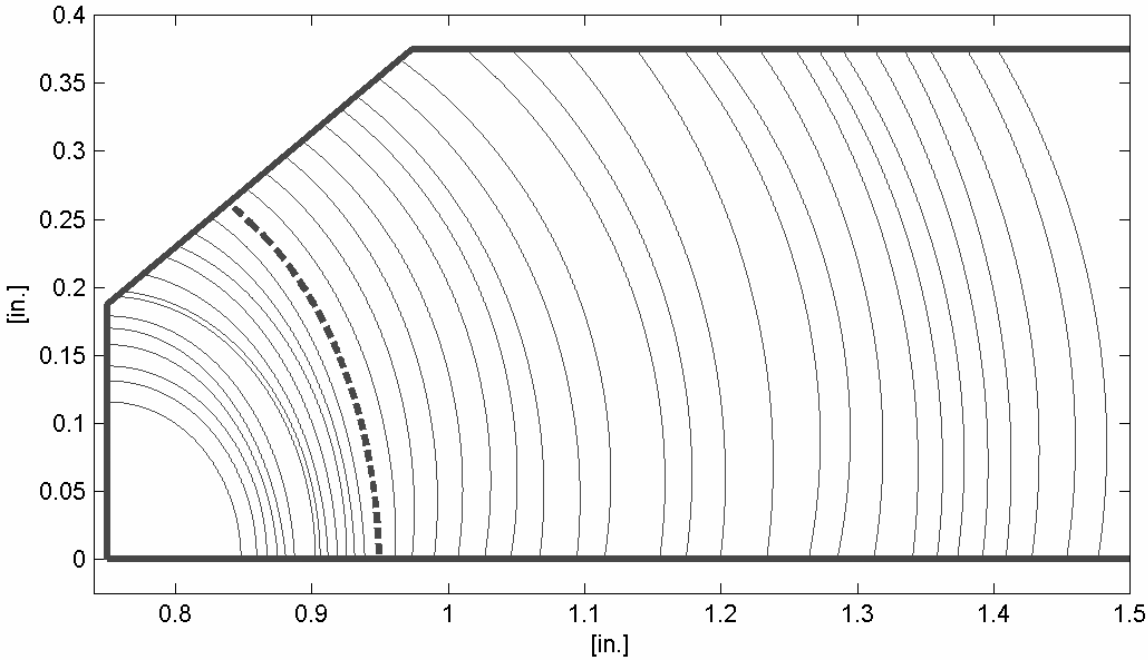

Figure C-14. Corrected BCF for FAA-009 at 43,700-45,300 Cycle, Initial Corner Crack, Type II

Table C-15. Corrected Boundary Correction Factors for FAA-009 (See figure C-15)

Initial Crack Location	Corner
Type	II
Center of Ellipse	(0.75, 0.016)
Horizontal Axis	0.21125
Vertical Axis	0.29250
Cycle	45300-46600

ϕ [degree]	x [inch]	y [inch]	f(g)
-4.63	0.96056	0	1.8662
-3.93	0.96075	0.00589	1.8801
-3.35	0.96089	0.01232	1.8943
-3.19	0.96092	0.01621	1.9024
-3.19	0.96092	0.01748	1.9050
3.22	0.96092	0.02008	1.9102
5.15	0.9604	0.03819	1.9429
7.11	0.95963	0.04987	1.9612
9	0.95865	0.06026	1.9762
11.47	0.95703	0.07331	1.9932
13.5	0.95541	0.08373	2.0056
15.31	0.95375	0.09288	2.0156
19.29	0.94939	0.11252	2.0643
21.18	0.94698	0.12168	2.0785
25.36	0.94089	0.14138	2.1099
29.11	0.93456	0.15846	2.1381
31.49	0.93013	0.16898	2.1566
35.5	0.92197	0.18606	2.2156
40.08	0.91164	0.2045	2.2328
46.08	0.89655	0.22684	2.2568
50.74	0.88369	0.24261	2.2765
53.26	0.87638	0.2505	2.2877
57.79	0.86259	0.26359	2.3088
60.3	0.85468	0.27014	2.3211
61.29	0.85147	0.27264	2.3310

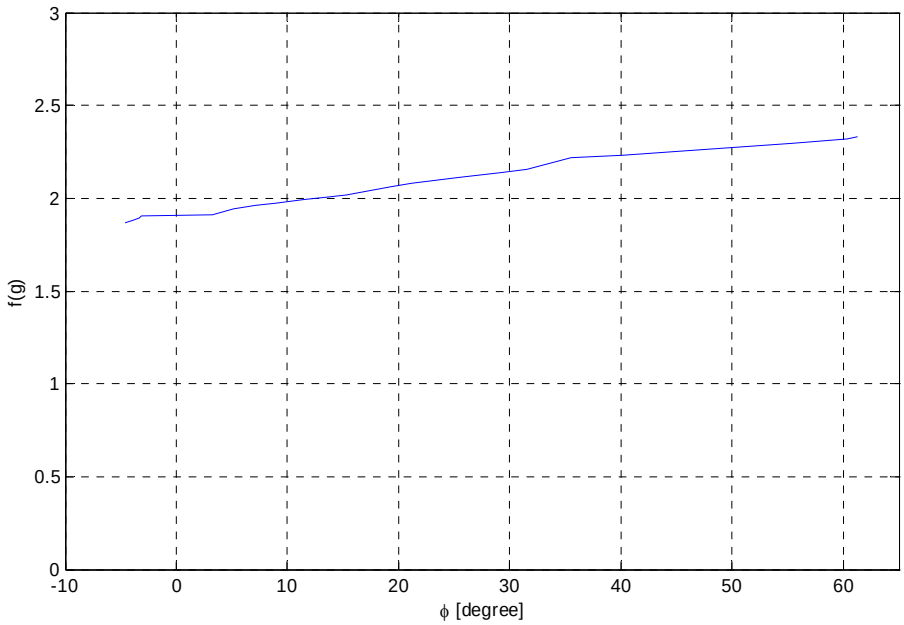

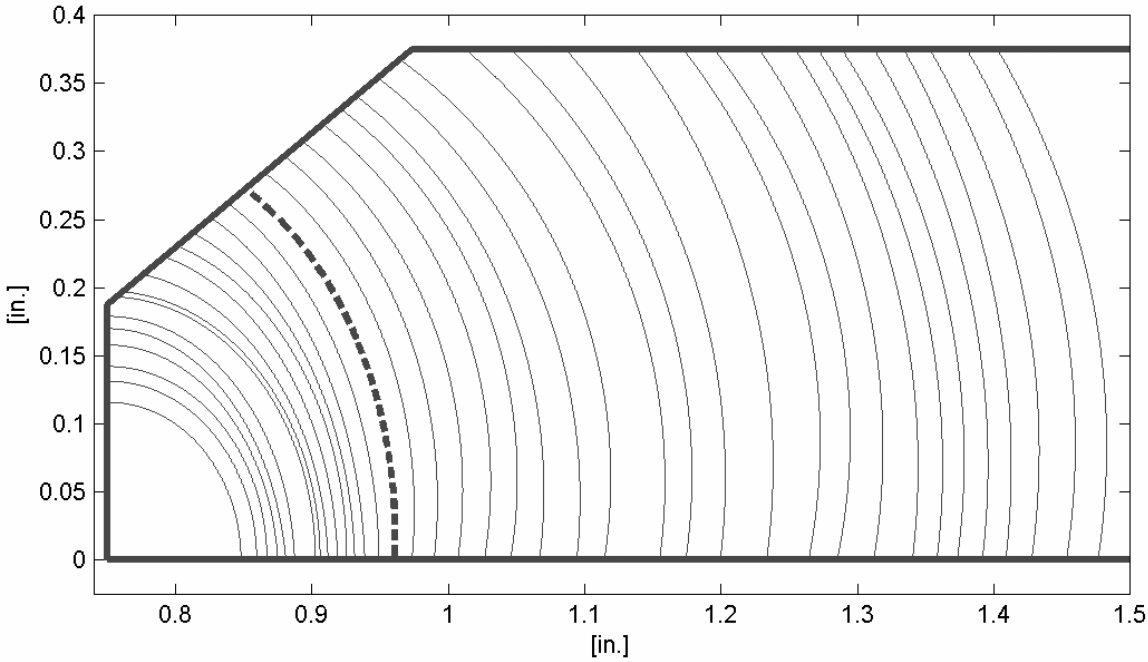

Figure C-15. Corrected BCF for FAA-009 at 45,300-46,600 Cycle, Initial Corner Crack, Type II

Table C-16. Corrected Boundary Correction Factors for FAA-009 (See figure C-16)

Initial Crack Location	Corner
Type	II
Center of Ellipse	(0.75, 0.036)
Horizontal Axis	0.22500
Vertical Axis	0.28900
Cycle	46600-47800

ϕ [degree]	x [inch]	y [inch]	f(g)
-7.2	0.97322	0	1.9109
-5.84	0.97383	0.00699	1.9135
-4.82	0.9742	0.01216	1.9165
-3.81	0.9745	0.01733	1.9195
-2.81	0.97473	0.0225	1.9225
-1.63	0.97491	0.02896	1.9261
-0.9	0.97497	0.03412	1.9289
-0.82	0.97498	0.03671	1.9303
0.89	0.97497	0.038	1.9310
2.08	0.97485	0.04575	1.9352
5.07	0.97412	0.06129	1.9432
8.14	0.97273	0.07682	1.9511
14.15	0.96817	0.10663	1.9658
17.36	0.96475	0.1222	1.9734
20.07	0.96133	0.13518	1.9798
26.24	0.95181	0.1638	1.9943
31.86	0.94111	0.18855	2.0233
36.87	0.93	0.20941	2.0689
39.17	0.92444	0.21855	2.0907
42.25	0.91656	0.23031	2.1206
45.12	0.90878	0.24078	2.1497
51.35	0.89053	0.26171	2.2202
54.36	0.8811	0.27089	2.2361
58.94	0.86608	0.28357	2.2645
59.19	0.86525	0.28421	2.2799

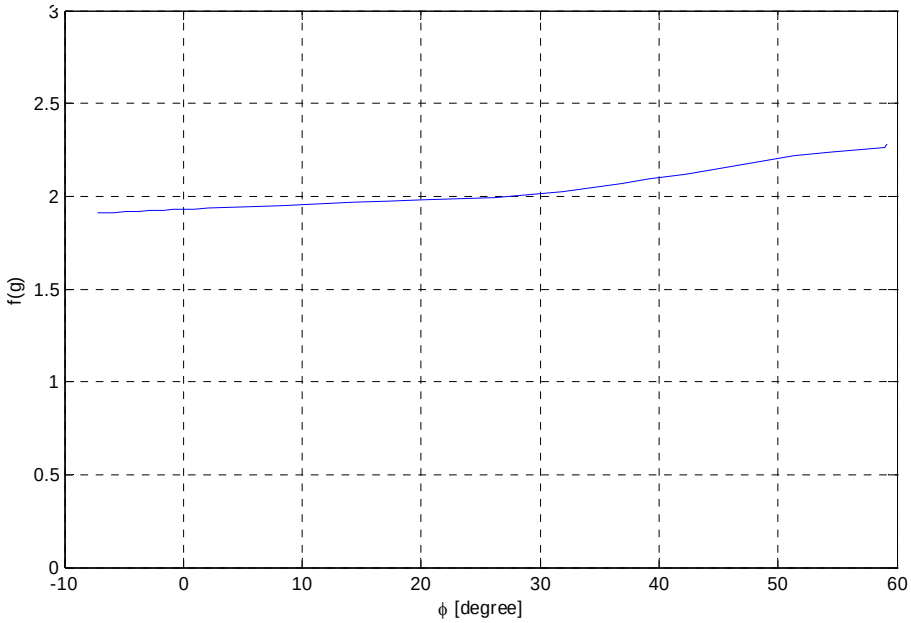

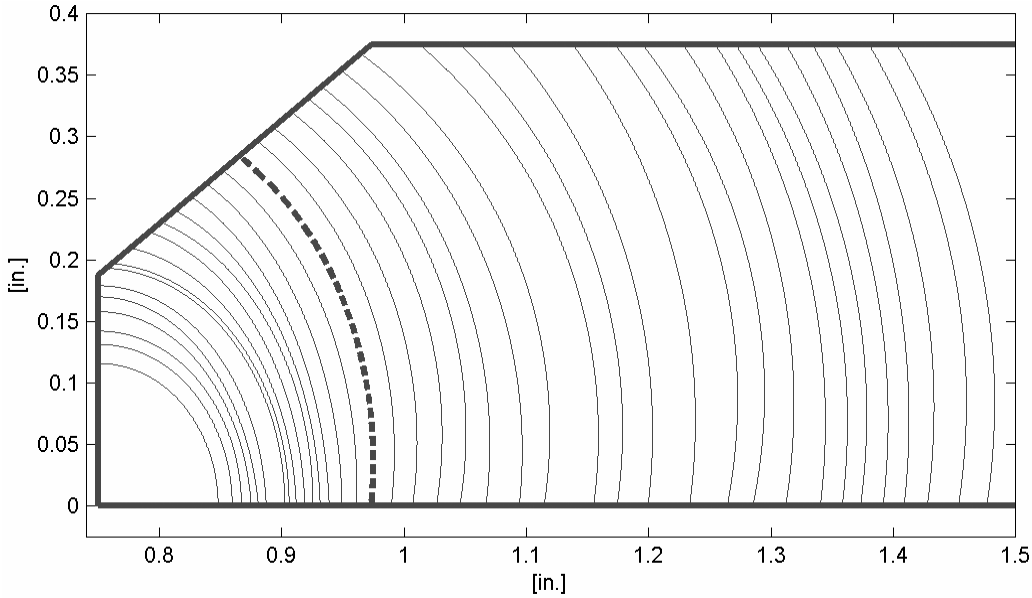

Figure C-16. Corrected BCF for FAA-009 at 46,600-47,800 Cycle, Initial Corner Crack, Type II

Table C-17. Corrected Boundary Correction Factors for FAA-009 (See figure C-17)

Initial Crack Location	Corner
Type	II
Center of Ellipse	(0.75, 0.0435)
Horizontal Axis	0.24200
Vertical Axis	0.29950
Cycle	47800-49100

ϕ [degree]	x [inch]	y [inch]	f(g)
-8.38	0.98942	0	1.9999
-6.91	0.99024	0.00777	2.0001
-4.93	0.9911	0.01811	2.0038
-2.74	0.99172	0.02974	2.0078
-0.96	0.99197	0.04008	2.0114
-0.69	0.99198	0.04398	2.0128
0.76	0.99198	0.04526	2.0132
3.12	0.99164	0.0595	2.0182
6.07	0.99064	0.07506	2.0236
8.31	0.98946	0.08673	2.0277
11.08	0.98749	0.10103	2.0329
13.11	0.9857	0.1114	2.0367
18.01	0.98015	0.13608	2.0463
20.64	0.97646	0.1491	2.0516
24.14	0.97083	0.16601	2.0589
30.31	0.95893	0.19466	2.0725
33.83	0.95102	0.21028	2.0808
37.21	0.94275	0.22462	2.0892
40.09	0.93515	0.23638	2.0967
46.61	0.91625	0.26116	2.1152
49.61	0.90681	0.27163	2.1245
52.8	0.89632	0.28207	2.1349
54.92	0.88908	0.28861	2.1421
55.8	0.88602	0.29122	2.1452
56.7	0.88287	0.29383	2.1484

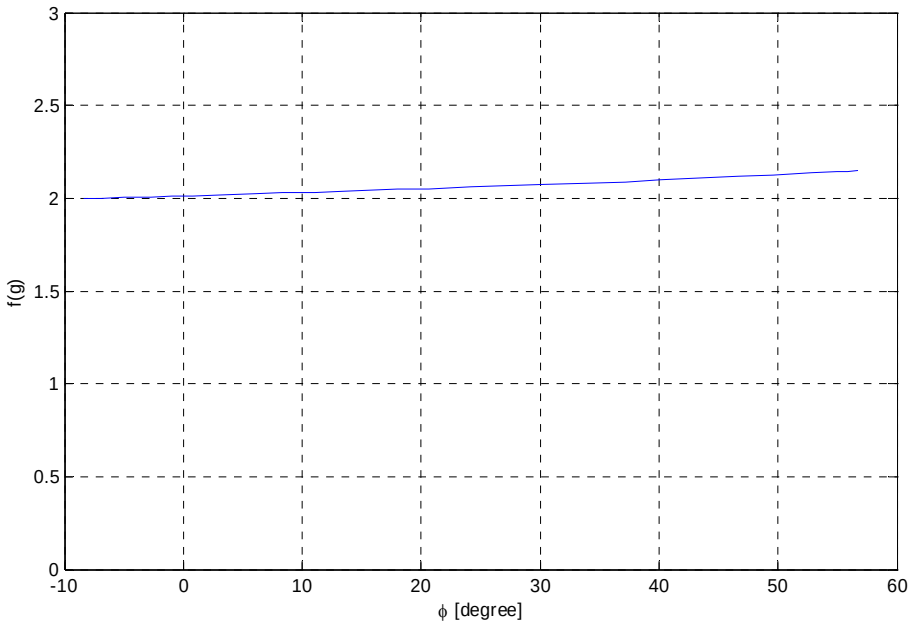

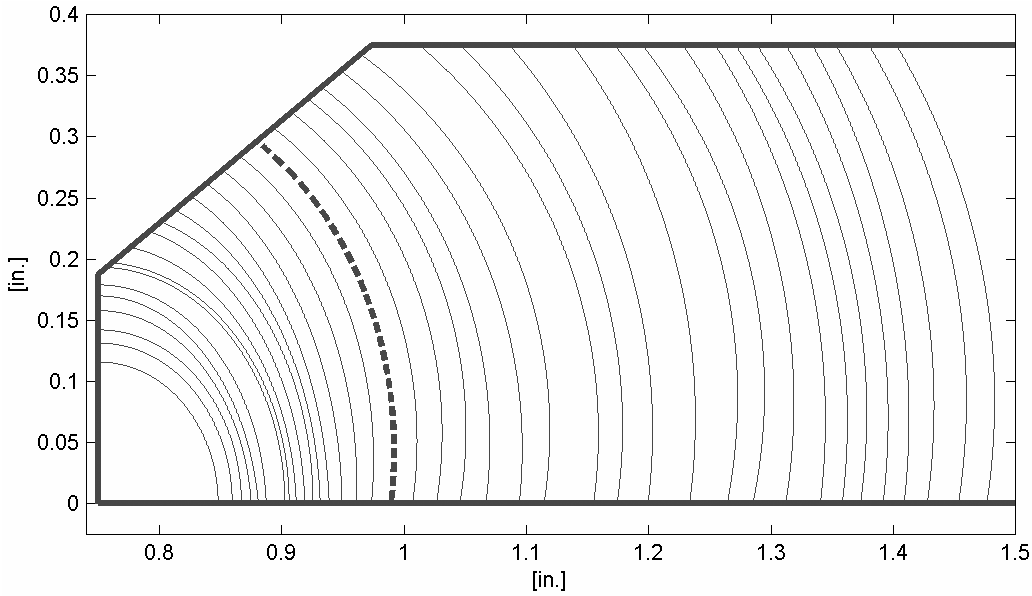

Figure C-17. Corrected BCF for FAA-009 at 47,400-49,100 Cycle, Initial Corner Crack, Type II

Table C-18. Corrected Boundary Correction Factors for FAA-009 (See figure C-18)

Initial Crack Location	Corner
Type	II
Center of Ellipse	(0.75, 0.051)
Horizontal Axis	0.26050
Vertical Axis	0.30650
Cycle	49100-50500

ϕ [degree]	x [inch]	y [inch]	f(g)
-9.63	1.00683	0	1.8836
-7.95	1.00799	0.00904	1.8863
-3.63	1.00998	0.03229	1.9003
-1.56	1.0104	0.04394	1.9064
-0.77	1.01048	0.05169	1.9100
0.83	1.01047	0.05301	1.9106
3.1	1.01012	0.06725	1.9165
6.22	1.00897	0.08413	1.9225
8.4	1.0077	0.09578	1.9260
10.12	1.00645	0.10488	1.9284
12.84	1.00398	0.11916	1.9317
14.59	1.0021	0.12825	1.9334
18.39	0.9972	0.14772	1.9361
20.44	0.99409	0.1581	1.9371
25.71	0.98471	0.184	1.9380
28.15	0.97969	0.19562	1.9376
31.21	0.9728	0.20984	1.9365
36.43	0.95959	0.23302	1.9331
39.17	0.95197	0.24458	1.9306
42.01	0.94354	0.25613	1.9276
45.32	0.93318	0.26891	1.9235
48.1	0.92396	0.27912	1.9196
50.66	0.91514	0.28802	1.9158
53.35	0.90549	0.29688	1.9116
56.75	0.89282	0.30734	1.9143

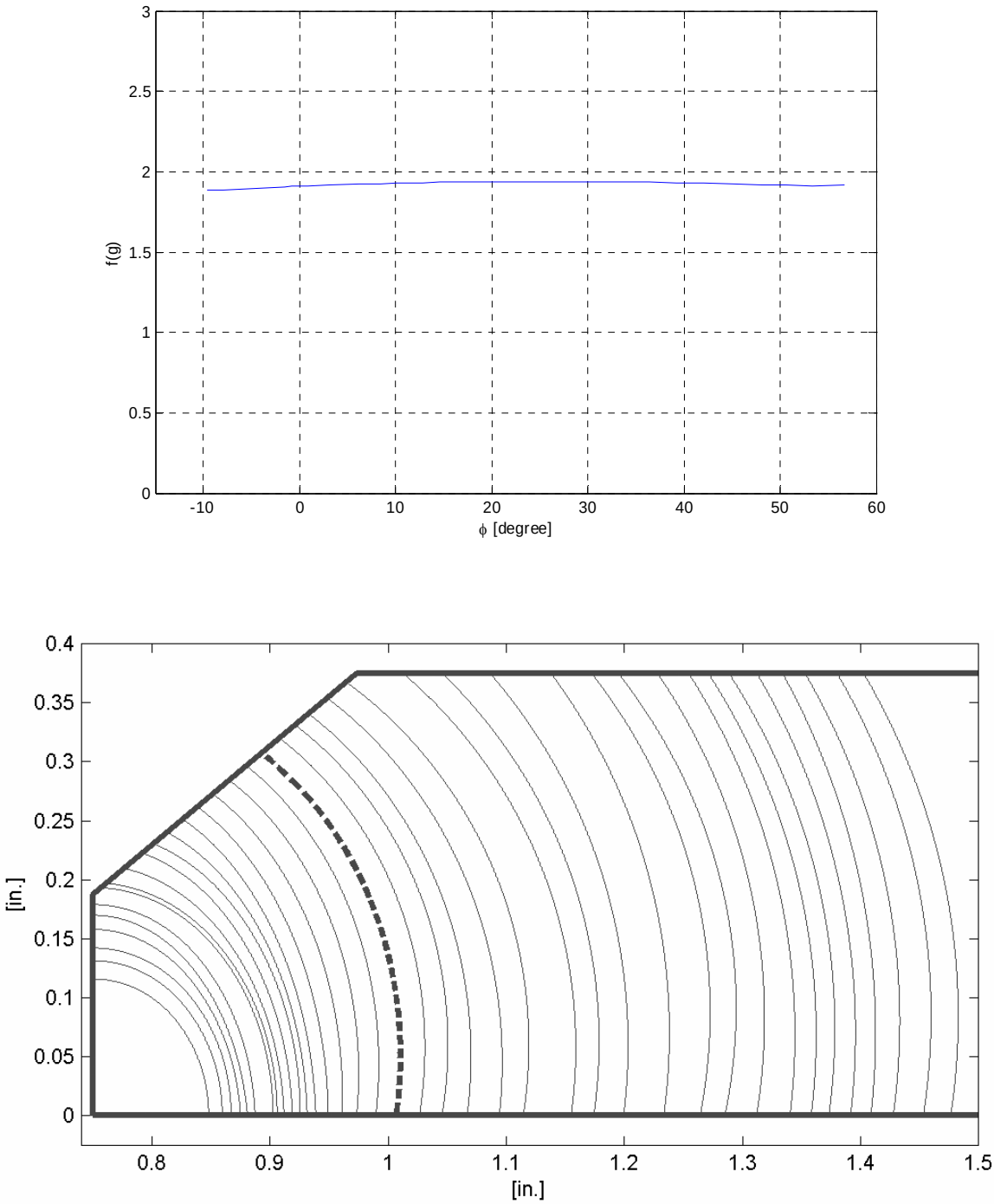

Figure C-18. Corrected BCF for FAA-009 at 49,100-50,500 Cycle, Initial Corner Crack, Type II

Table C-19. Corrected Boundary Correction Factors for FAA-009 (See figure C-19)

Initial Crack Location	Corner
Type	II
Center of Ellipse	(0.75, 0.0575)
Horizontal Axis	0.28100
Vertical Axis	0.31700
Cycle	50500-52000

ϕ [degree]	x [inch]	y [inch]	f(g)
-10.45	1.02634	0	1.9934
-8.95	1.02758	0.00827	1.9874
-6.84	1.029	0.01985	1.9863
-4.98	1.02994	0.03015	1.9860
-2.89	1.03064	0.04176	1.9867
-0.89	1.03097	0.05334	1.9885
-0.5	1.03099	0.05852	1.9895
0.62	1.03098	0.0598	1.9895
2.33	1.03077	0.07014	1.9923
8.15	1.02816	0.10242	2.0058
10.04	1.0267	0.11275	2.0119
15.8	1.02039	0.14378	2.0351
17.99	1.01725	0.15543	2.0459
20.23	1.01367	0.16711	2.0581
24.53	1.00564	0.18912	2.0854
28.72	0.99642	0.20985	2.1407
31.16	0.99046	0.22153	2.1498
34.23	0.98232	0.23583	2.1623
36.53	0.9758	0.2462	2.1725
39.21	0.96772	0.25791	2.1850
42.31	0.9578	0.2709	2.2006
45.24	0.94785	0.28261	2.2164
48.33	0.93683	0.29429	2.2343
51.25	0.92589	0.30472	2.2522
55.85	0.90772	0.31985	2.2875

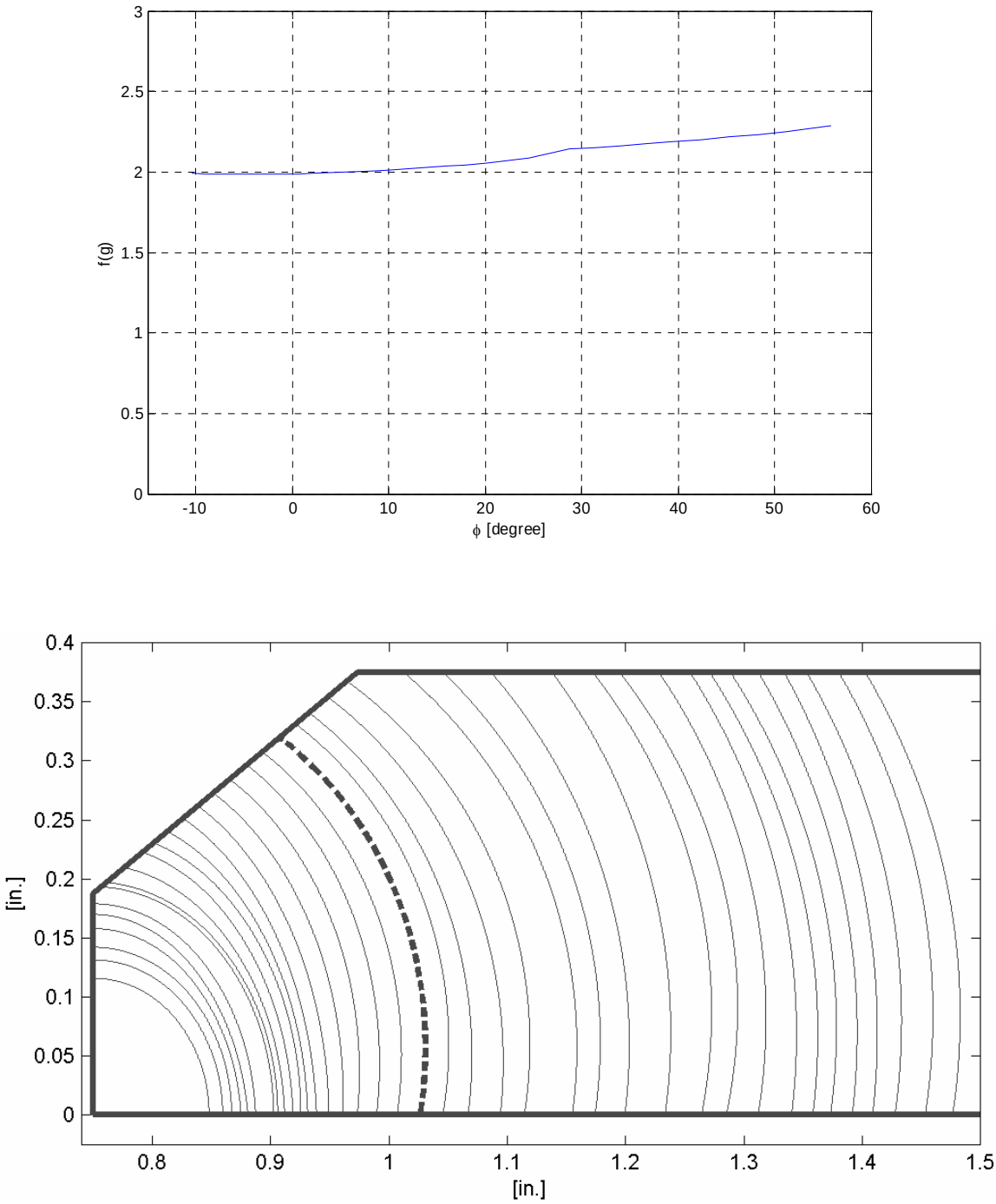

Figure C-19. Corrected BCF for FAA-009 at 50,500-52,000 Cycle, Initial Corner Crack, Type II

Table C-20. Corrected Boundary Correction Factors for FAA-009 (See figure C-20)

Initial Crack Location	Corner
Type	II
Center of Ellipse	(0.75, 0.06)
Horizontal Axis	0.30050
Vertical Axis	0.32950
Cycle	52000-53000

ϕ [degree]	x [inch]	y [inch]	f(g)
-10.49	1.04548	0	1.9595
-8	1.04758	0.01418	1.9514
-6.19	1.04875	0.0245	1.9500
-4.16	1.04971	0.03608	1.9486
-2.14	1.05029	0.0477	1.9479
-0.79	1.05047	0.05543	1.9475
-0.1	1.0505	0.06059	1.9475
3.02	1.05008	0.07736	1.9482
7.08	1.04821	0.10059	1.9507
10.02	1.04591	0.11733	1.9538
13	1.0428	0.13407	1.9580
15.3	1.03985	0.14693	1.9623
17.17	1.03711	0.15724	1.9619
20	1.03238	0.17265	1.9496
26.06	1.01994	0.20473	1.9253
28.82	1.01328	0.21879	1.9205
31.91	1.00508	0.23413	1.9145
34.56	0.99748	0.24686	1.9089
37.85	0.98728	0.26214	1.9012
40.7	0.97781	0.27483	1.8940
43.98	0.96623	0.28877	1.8852
46.47	0.95696	0.29886	1.8782
49.76	0.94411	0.31149	1.8684
52.19	0.93423	0.32027	1.8609
55.32	0.92097	0.33096	1.8596

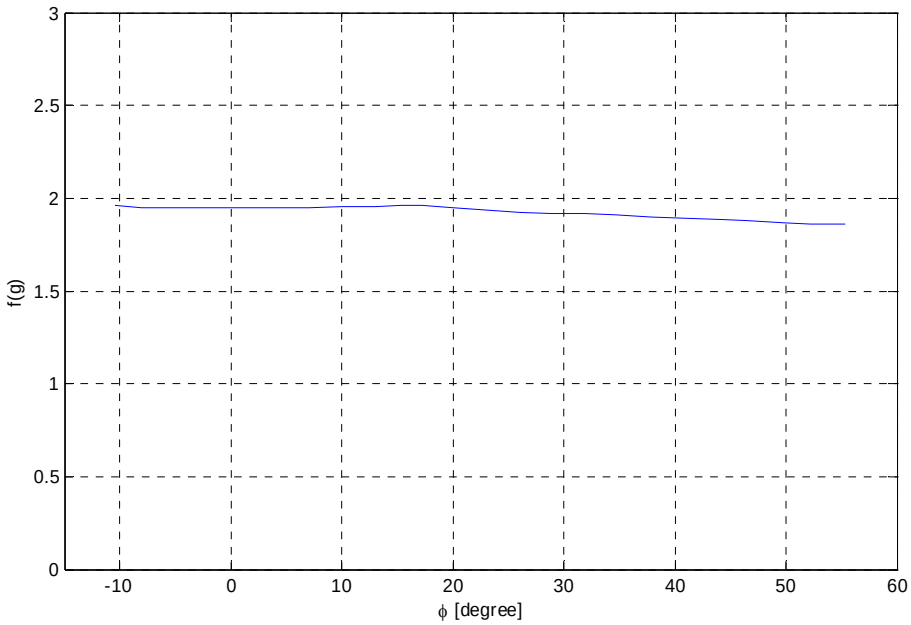

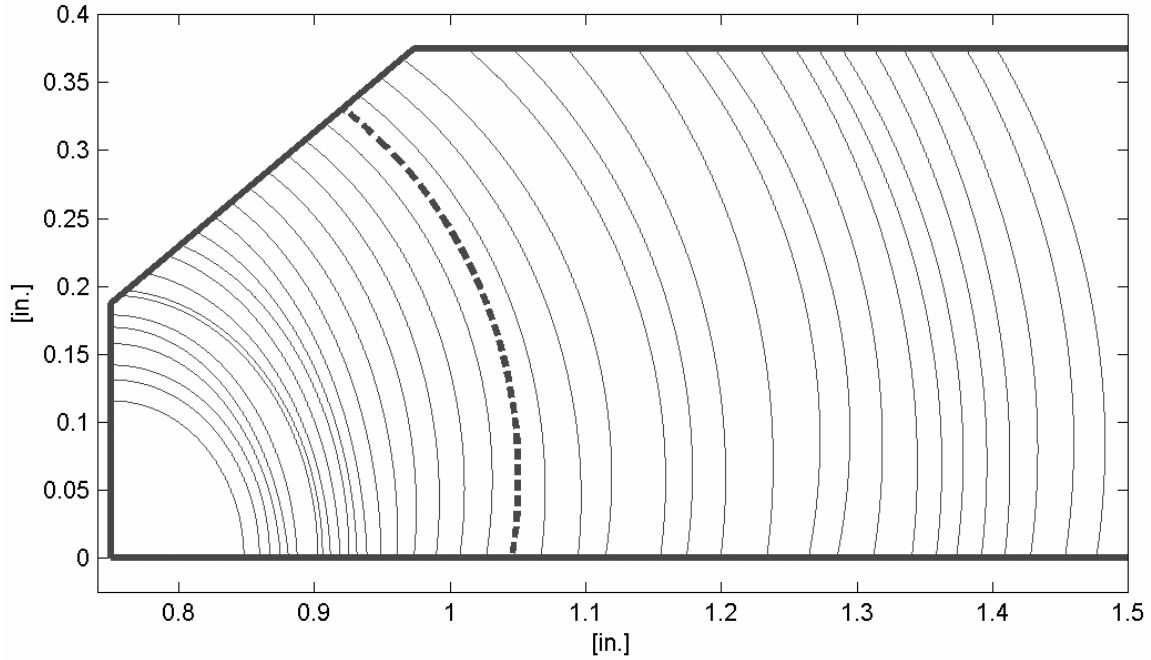

Figure C-20. Corrected BCF for FAA-009 at 52,000-53,000 Cycle, Initial Corner Crack, Type II

Table C-21. Corrected Boundary Correction Factors for FAA-009 (See figure C-21)

Initial Crack Location	Corner
Type	II
Center of Ellipse	(0.75, 0.05)
Horizontal Axis	0.32000
Vertical Axis	0.35350
Cycle	53000-54500

ϕ [degree]	x [inch]	y [inch]	f(g)
-8.46	1.06652	0	2.0072
-6.98	1.06763	0.0089	1.9932
-4.98	1.06879	0.02167	1.9793
-2.93	1.06958	0.0357	1.9654
-1.93	1.06982	0.04463	1.9576
-1.67	1.06986	0.051	1.9527
1.69	1.06986	0.05226	1.9516
2.88	1.0696	0.065	1.9428
4.9	1.06883	0.07893	1.9354
7.09	1.06756	0.0929	1.9295
10.14	1.065	0.11188	1.9239
12.62	1.06226	0.12705	1.9081
15.35	1.05858	0.14347	1.9029
18.13	1.05412	0.15993	1.8994
20.72	1.0493	0.17506	1.8978
23.6	1.04324	0.19152	1.8977
26.08	1.03742	0.20542	1.8992
31.46	1.02296	0.23452	1.9072
36.17	1.00834	0.25865	1.9421
39.03	0.99858	0.27265	1.9775
42.02	0.98772	0.28668	2.0213
48.2	0.96329	0.31355	2.1266
51.1	0.95095	0.32512	2.1541
54.19	0.93722	0.3367	2.1859
55.27	0.93232	0.34049	2.2135

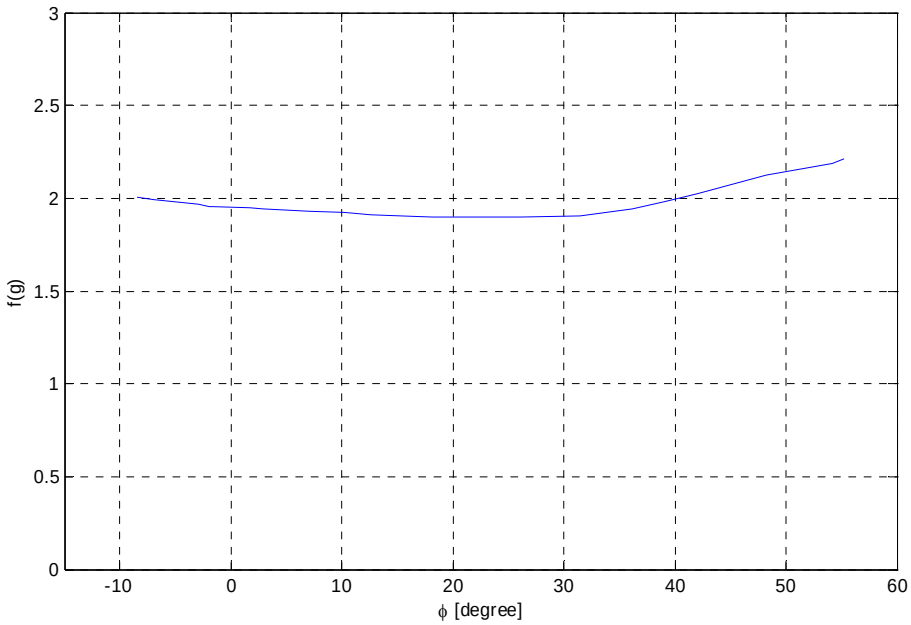

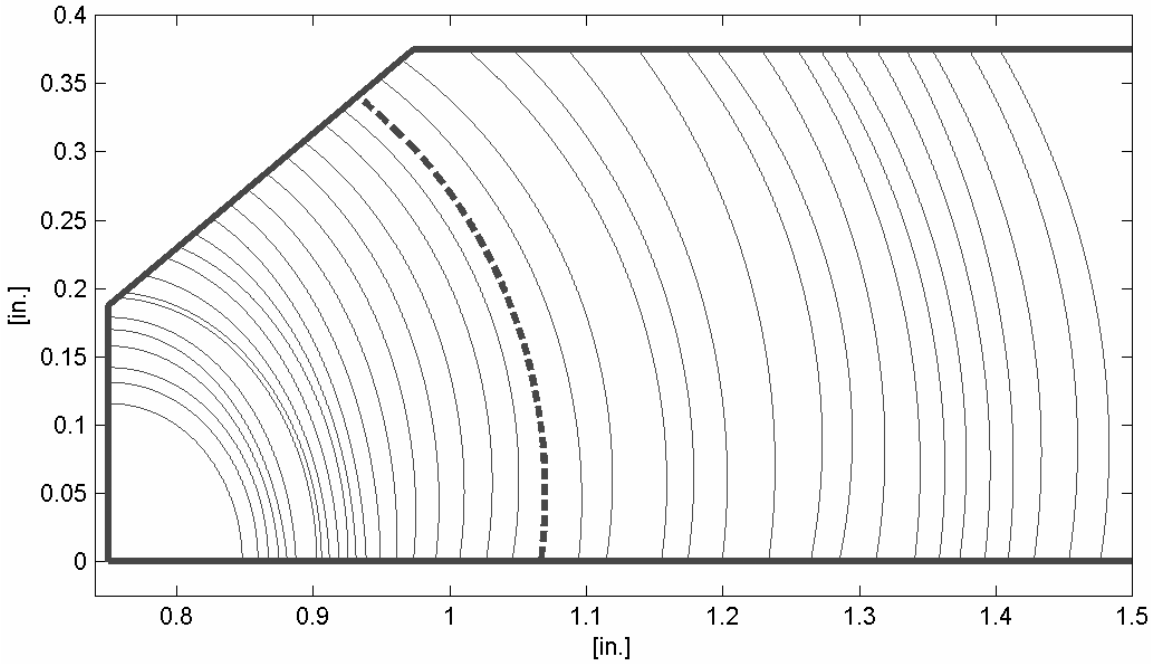

Figure C-21. Corrected BCF for FAA-009 at 53,000-54,500 Cycle, Initial Corner Crack, Type II

Table C-22. Corrected Boundary Correction Factors for FAA-009 (See figure C-22)

Initial Crack Location	Corner
Type	II
Center of Ellipse	(0.75, 0.045)
Horizontal Axis	0.34650
Vertical Axis	0.37650
Cycle	54500-56300

ϕ [degree]	x [inch]	y [inch]	f(g)
-6.93	1.09397	0	1.9223
-4.92	1.09522	0.01355	1.9230
-2.81	1.09608	0.02768	1.9266
-1.07	1.09644	0.04057	1.9301
-0.79	1.09647	0.04572	1.9315
0.83	1.09646	0.04702	1.9319
2.17	1.09625	0.05862	1.9357
5.04	1.09516	0.07799	1.9425
10.17	1.09105	0.11155	1.9567
12.38	1.08845	0.12574	1.9639
15.21	1.08436	0.14382	1.9739
17.66	1.08017	0.15927	1.9832
20.15	1.07529	0.17472	1.9937
22.67	1.06972	0.19014	2.0053
25.02	1.06398	0.20424	2.0169
27.63	1.05698	0.21959	2.0308
30.08	1.04984	0.23365	2.0725
33.03	1.04049	0.25018	2.0807
36.08	1.03003	0.26667	2.0900
38.99	1.0193	0.28183	2.0908
44.64	0.99656	0.30944	2.0775
47.93	0.98215	0.32441	2.0366
50.84	0.96883	0.33682	2.0191
53.28	0.95717	0.3467	2.0038
55.11	0.9482	0.35381	2.0260

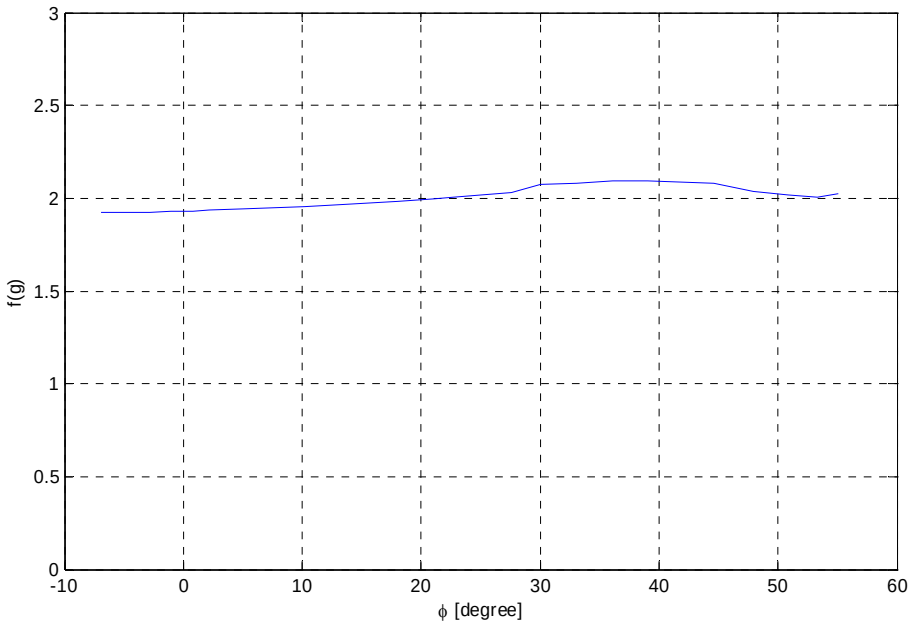

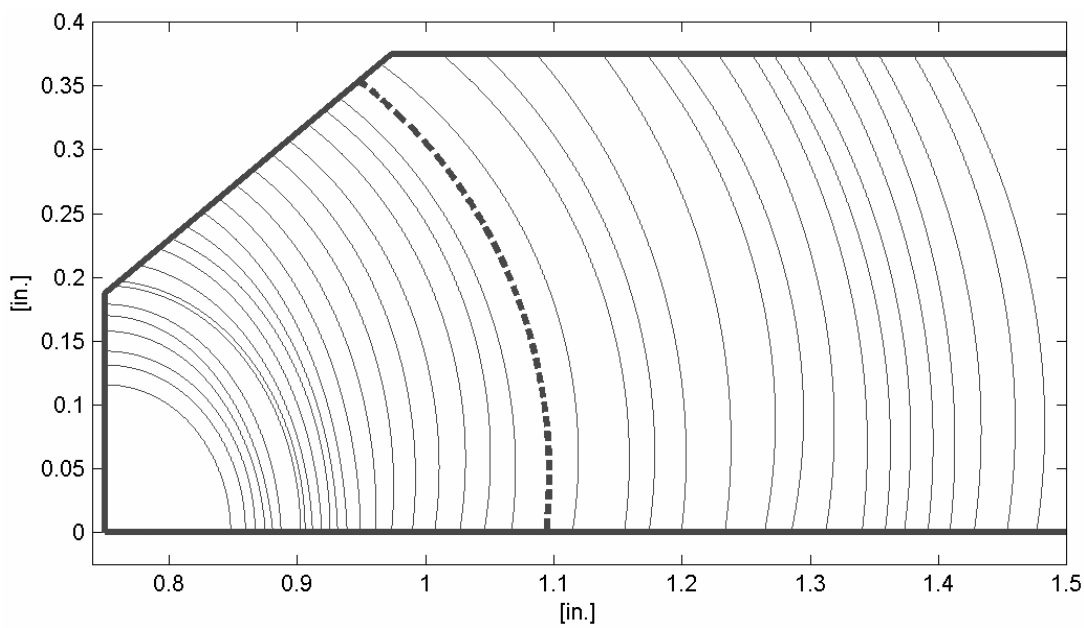

Figure C-22. Corrected BCF for FAA-009 at 54,500-56,300 Cycle, Initial Corner Crack, Type II

Table C-23. Corrected Boundary Correction Factors for FAA-009 (See figure C-23)

Initial Crack Location	Corner
Type	II
Center of Ellipse	(0.75, 0.06)
Horizontal Axis	0.36900
Vertical Axis	0.37750
Cycle	56300-57300

ϕ [degree]	x [inch]	y [inch]	f(g)
-9.31	1.11414	0	1.8307
-7.82	1.11556	0.01011	1.8430
-5.95	1.11701	0.02271	1.8616
-3.94	1.11813	0.03661	1.8826
-1.91	1.11879	0.05308	1.9019
-1.55	1.11886	0.06068	1.9104
1.57	1.11886	0.06195	1.9118
5.11	1.11753	0.09251	1.9460
7.95	1.11545	0.11164	1.9675
10.08	1.11331	0.1257	1.9838
12.44	1.11034	0.14106	2.0020
14.42	1.10737	0.15389	2.0177
17.04	1.1028	0.17055	2.0586
19.91	1.09695	0.18851	2.0697
22.62	1.09061	0.2052	2.0807
25.18	1.08394	0.22062	2.0917
30.01	1.06953	0.24885	2.1137
32.29	1.06195	0.26167	2.1248
35.09	1.05192	0.27707	2.1391
40	1.03267	0.30269	2.1664
45	1.01094	0.32695	2.1969
47.8	0.99787	0.33968	2.2154
50.46	0.98491	0.35115	2.2342
52	0.97716	0.35751	2.2454
54.49	0.96431	0.36733	2.3698

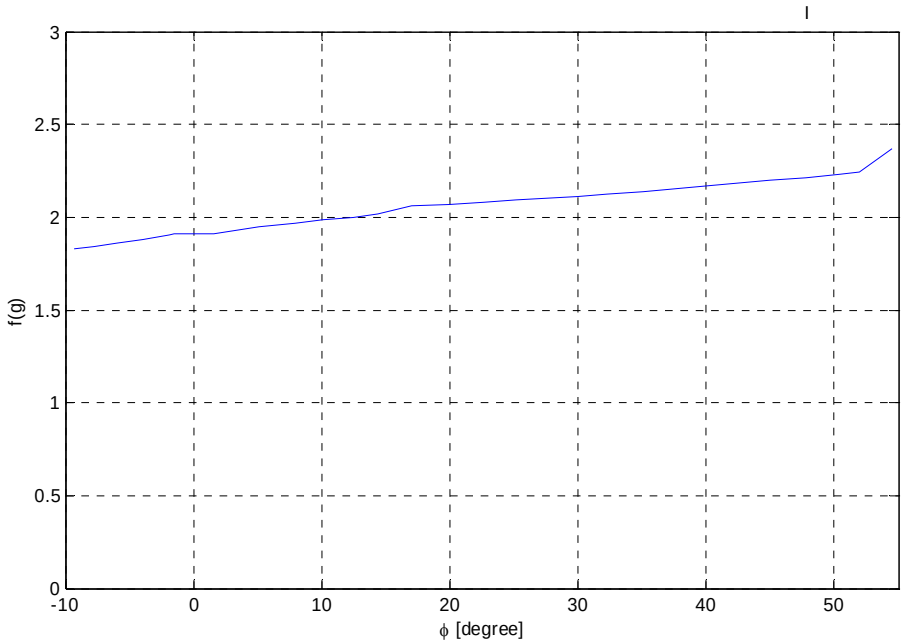

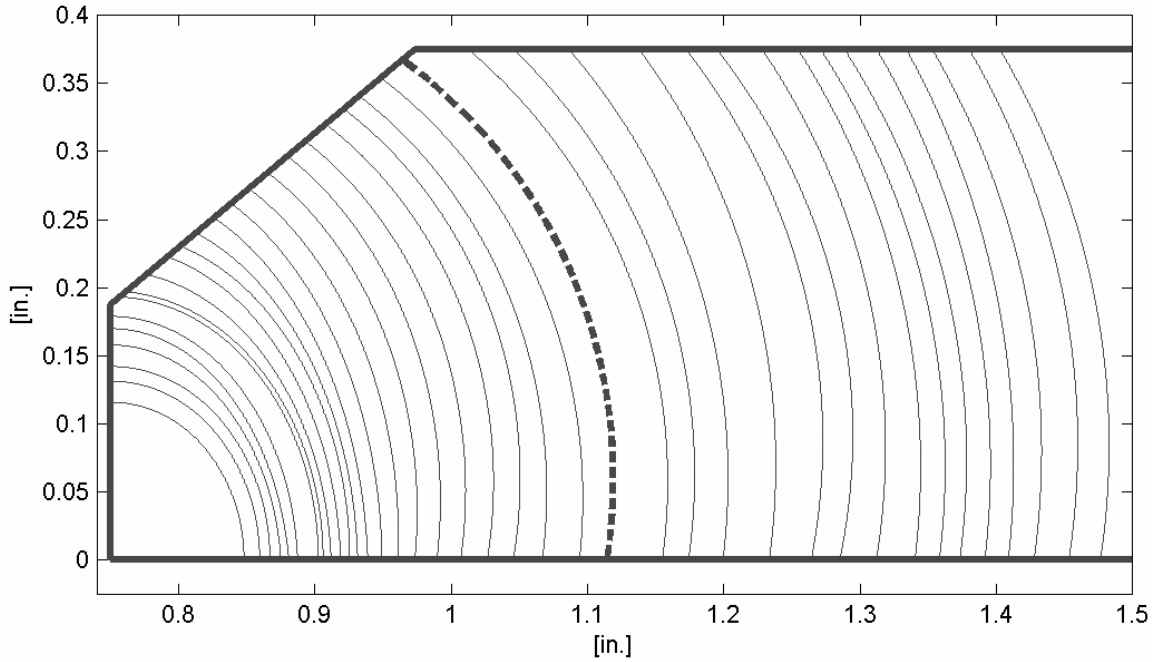

Figure C-23. Corrected BCF for FAA-009 at 56,300-57,300 Cycle, Initial Corner Crack, Type II

Table C-24. Corrected Boundary Correction Factors for FAA-009 (See figure C-24)

Initial Crack Location	Corner
Type	II
Center of Ellipse	(0.75, 0.0575)
Horizontal Axis	0.40875
Vertical Axis	0.41350
Cycle	57800-60300

ϕ [degree]	x [inch]	y [inch]	f(g)
-8.05	1.15473	0	1.6321
-6.14	1.1564	0.014	1.6369
-4.04	1.15774	0.02949	1.6452
-2.04	1.15849	0.04503	1.6534
-1.07	1.15868	0.05743	1.6599
1.08	1.15868	0.059	1.6608
3.19	1.15812	0.07925	1.6715
5.06	1.15715	0.09325	1.6790
8.07	1.1547	0.11511	1.6909
10.25	1.15223	0.13073	1.6995
12.89	1.14844	0.14953	1.7099
15.13	1.14458	0.16523	1.7189
18.07	1.13858	0.18564	1.7309
20.14	1.13375	0.19977	1.7395
23.19	1.12573	0.22022	1.7522
25.1	1.12015	0.23282	1.7604
28.04	1.11078	0.25178	1.7732
30.29	1.10295	0.26599	1.7832
33.12	1.09234	0.28339	1.7961
36.05	1.08049	0.30078	1.8098
40.81	1.05938	0.32771	1.8329
43.18	1.04806	0.34043	1.8684
46.27	1.03253	0.3563	1.9286
48.36	1.02157	0.36646	2.0268
50.26	1.0113	0.3748	2.1822

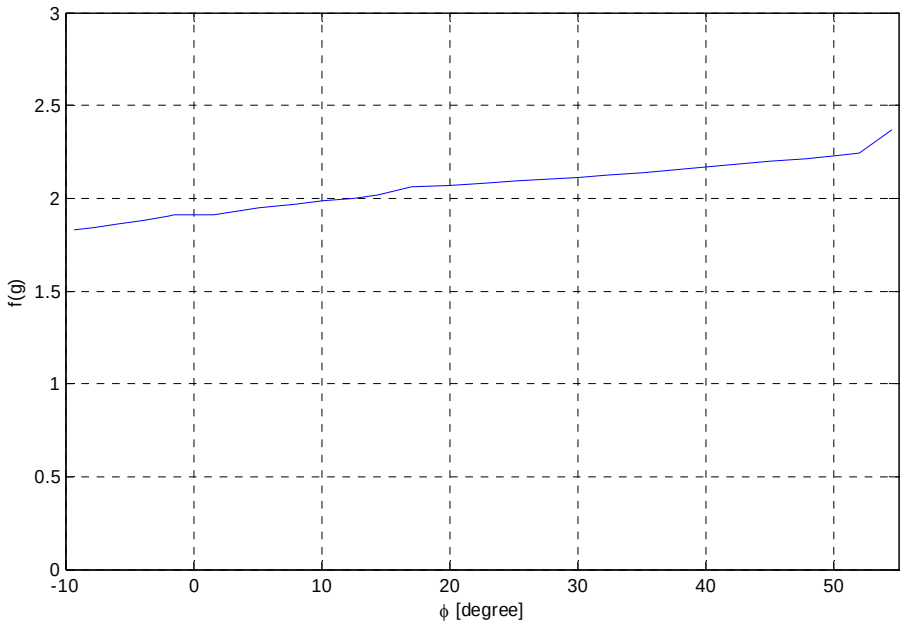

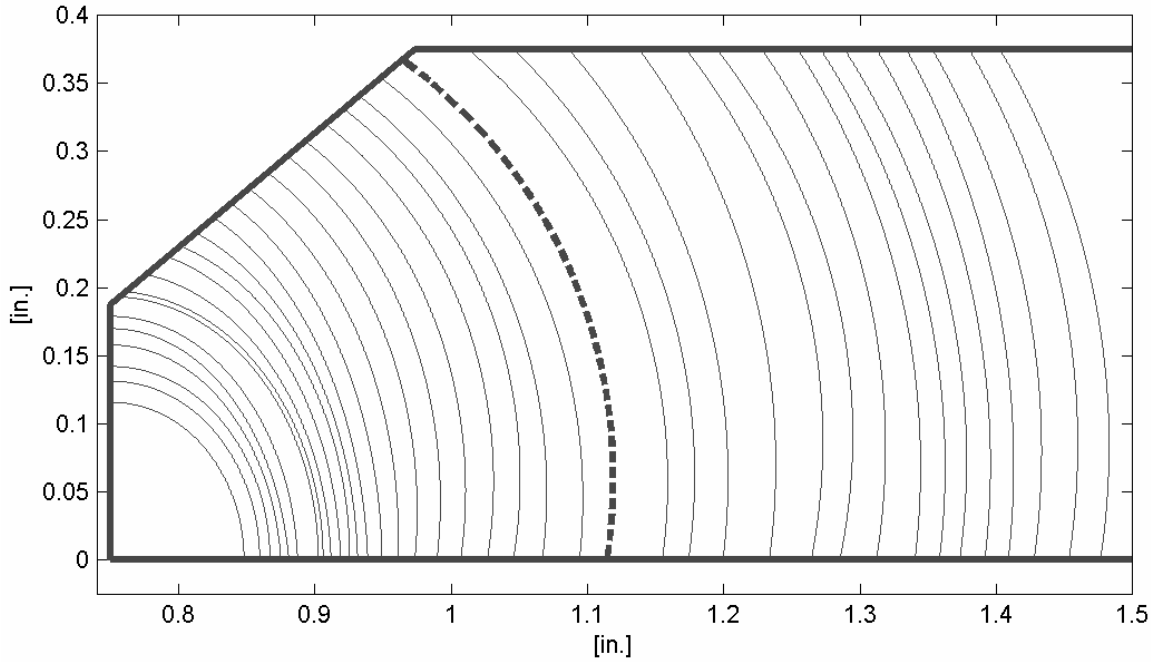

Figure C-24. Corrected BCF for FAA-009 at 56,300-57,300 Cycle, Initial Corner Crack, Type II

Table C-25. Corrected Boundary Correction Factors for FAA-009 (See figure C-25)

Initial Crack Location	Corner
Type	III
Center of Ellipse	(0.75, 0.0625)
Horizontal Axis	0.42850
Vertical Axis	0.43100
Cycle	60300-61500

ϕ [degree]	x [inch]	y [inch]	f(g)
-8.35	1.17395	0	1.8840
-6.08	1.17609	0.01689	1.8719
-4.1	1.17741	0.03182	1.8659
-2.12	1.17821	0.04679	1.8609
-0.84	1.17845	0.05674	1.8581
-0.35	1.17849	0.06172	1.8570
0.36	1.17849	0.06341	1.8567
2.13	1.1782	0.07834	1.8542
4.55	1.17715	0.09656	1.8532
7.2	1.17512	0.11646	1.8535
10.09	1.17187	0.13797	1.8563
12.78	1.16788	0.15784	1.8616
15.28	1.16335	0.17606	1.8680
18.04	1.15744	0.19592	1.8776
21.07	1.14986	0.21739	1.8893
23.43	1.14316	0.23388	1.8900
26.09	1.13482	0.25206	1.8925
28.31	1.12724	0.26691	1.8965
31.09	1.11695	0.28504	1.9033
33.42	1.10766	0.29985	1.9112
35.81	1.09748	0.3147	1.9209
38	1.08765	0.32786	1.9318
43.19	1.06242	0.35746	1.9649
45.32	1.05131	0.36894	2.0033
46.48	1.04506	0.375	2.1354

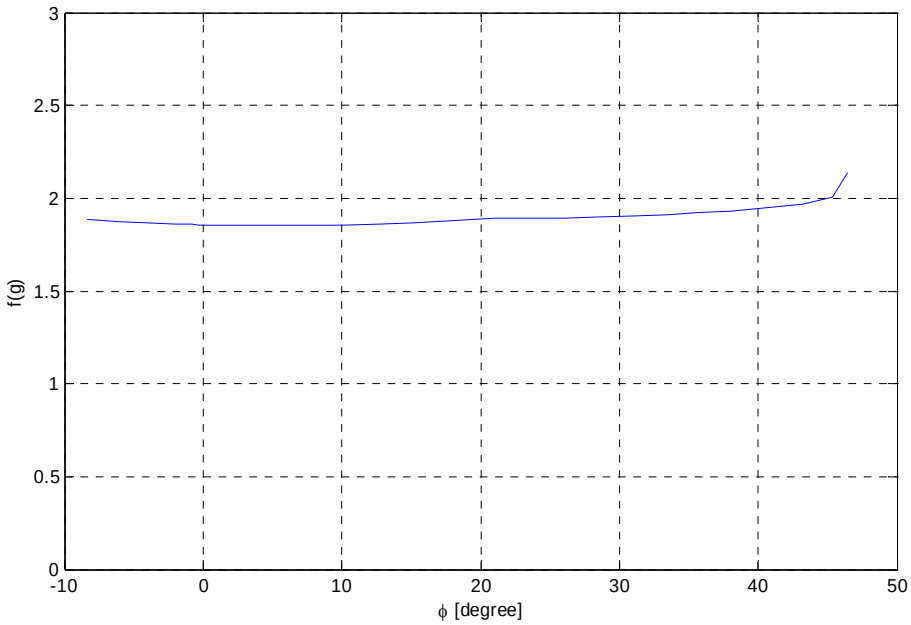

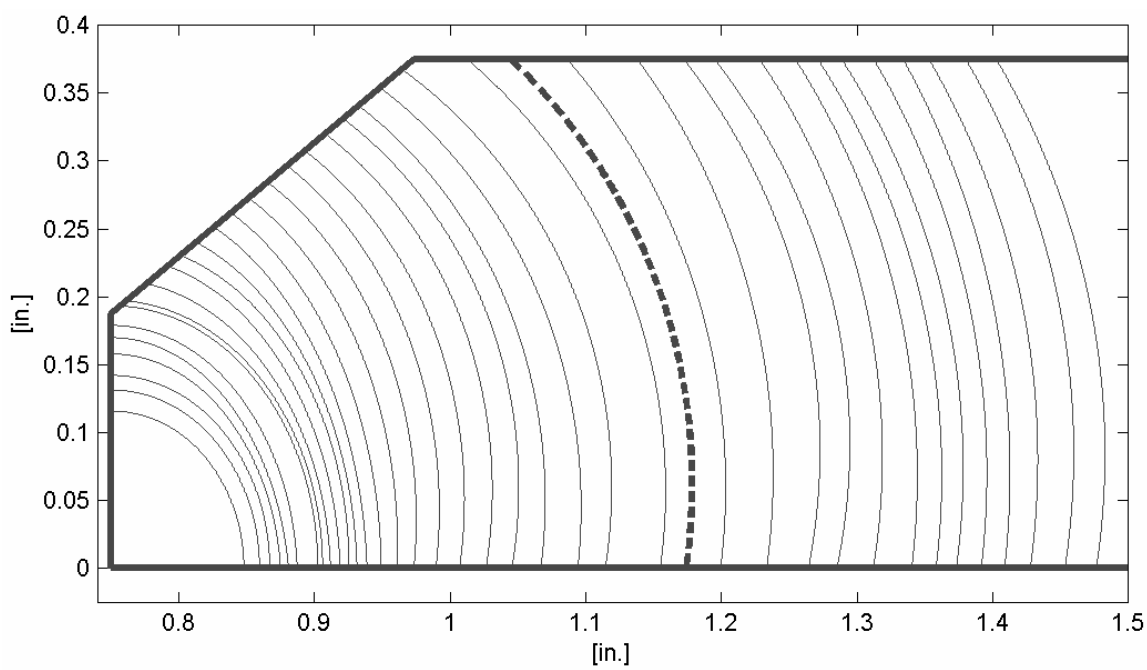

Figure C-25. Corrected BCF for FAA-009 at 60,300-61,500 Cycle, Initial Corner Crack, Type III

Table C-26. Corrected Boundary Correction Factors for FAA-009 (See figure C-26)

Initial Crack Location	Corner
Type	III
Center of Ellipse	(0.75, 0.06)
Horizontal Axis	0.45300
Vertical Axis	0.46950
Cycle	61500-64500

ϕ [degree]	x [inch]	y [inch]	f(g)
-7.37	1.19926	0	1.699
-5.89	1.20061	0.01193	1.694
-4.83	1.20139	0.02052	1.6924
-3.15	1.20232	0.03427	1.6906
-1.89	1.20275	0.04453	1.6897
-0.84	1.20295	0.05313	1.6893
-0.21	1.203	0.05828	1.6893
0	1.203	0.06	1.6892
2.1	1.2027	0.07718	1.6898
4.62	1.20153	0.09776	1.6922
7.15	1.19947	0.11838	1.6962
9.71	1.19651	0.13905	1.702
12.06	1.193	0.15795	1.7088
14.01	1.18952	0.17351	1.7155
16.42	1.18453	0.1925	1.725
18.41	1.17981	0.20806	1.7339
20.43	1.1745	0.22367	1.7438
24.34	1.16273	0.25325	1.7654
26.47	1.15551	0.269	1.7784
29.13	1.1457	0.28827	1.7959
31.12	1.13781	0.30235	1.8097
33.15	1.12925	0.31647	1.8246
35.51	1.11875	0.3324	1.8426
38.51	1.1045	0.352	1.8666
40.31	1.09546	0.36333	1.8831

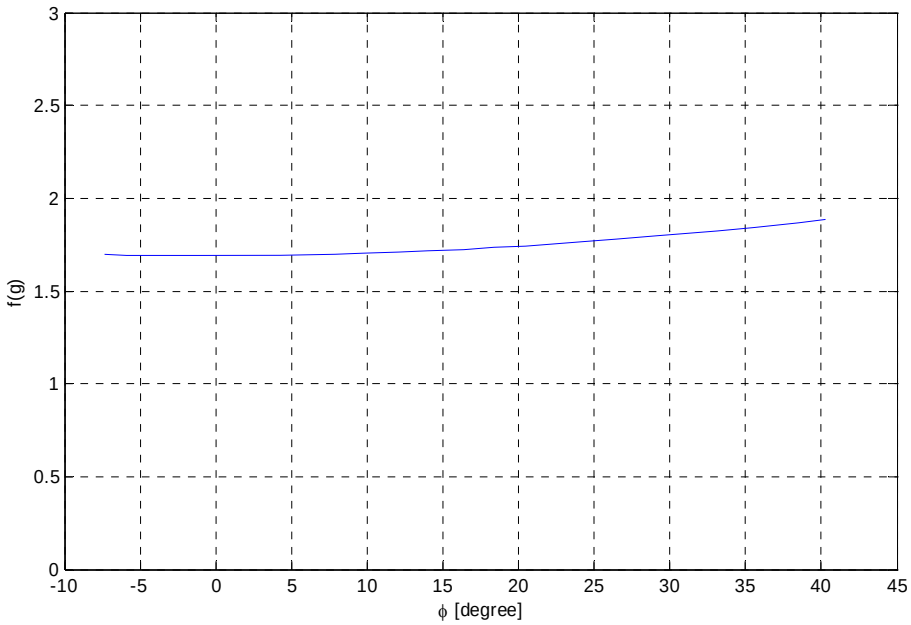

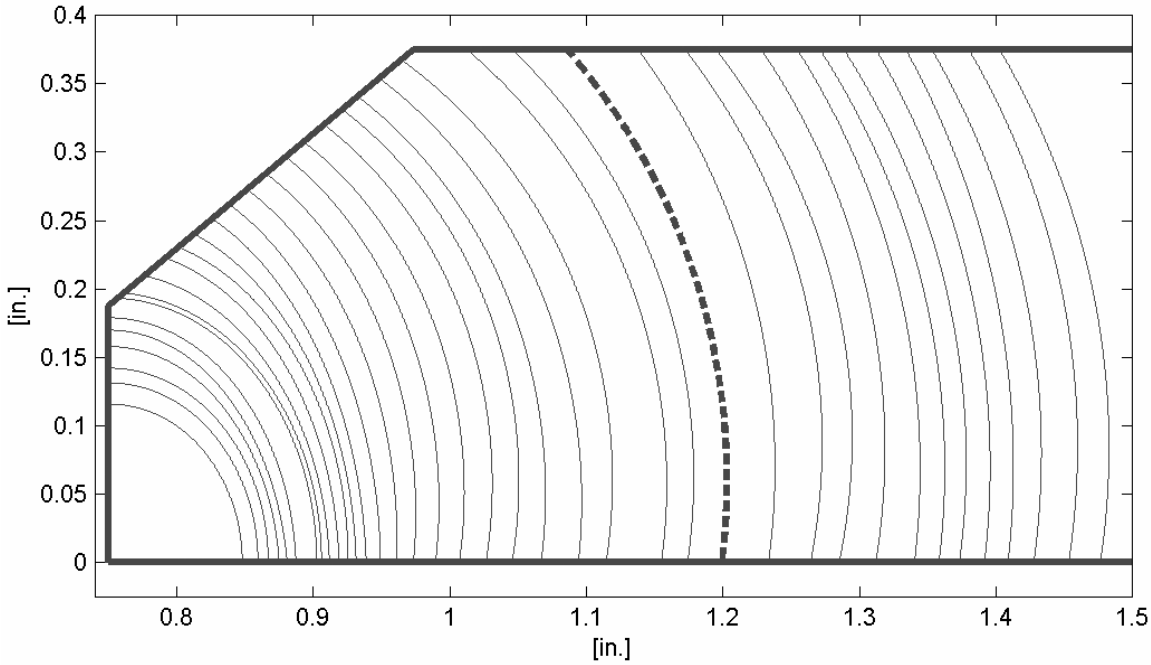

Figure C-26. Corrected BCF for FAA-009 at 61,500-64,500 Cycle, Initial Corner Crack, Type III

Table C-27. Corrected Boundary Correction Factors for FAA-009 (See figure C-27)

Initial Crack Location	Corner
Type	III
Center of Ellipse	(0.75, 0.07)
Horizontal Axis	0.48800
Vertical Axis	0.50200
Cycle	64500-66300

ϕ [degree]	x [inch]	y [inch]	f(g)
-8.13	1.23309	0	1.9118
-6.8	1.23457	0.01228	1.9114
-5.06	1.2361	0.02773	1.9154
-3.99	1.23682	0.03741	1.9180
-1.98	1.23771	0.05682	1.9501
-1.5	1.23783	0.06263	1.9509
-1.19	1.2379	0.07041	1.9521
1.2	1.23789	0.07236	1.9524
3.09	1.23729	0.09568	1.9563
5.01	1.23614	0.11323	1.9597
7.21	1.23414	0.13274	1.9637
9.21	1.2317	0.15029	1.9678
11.69	1.22787	0.17175	1.9732
14.21	1.22308	0.19326	1.9793
16.28	1.21843	0.21081	1.9848
18.38	1.21311	0.22836	1.9908
20.97	1.20567	0.24977	1.9987
23.13	1.19877	0.26727	2.0060
25.32	1.19111	0.28477	2.0138
27.79	1.1817	0.30413	2.0234
30.07	1.17231	0.32158	2.0327
32.39	1.16207	0.33894	2.0430
35.04	1.14957	0.3582	2.0556
36.96	1.13992	0.37196	2.0875
37.37	1.13782	0.37476	2.1041

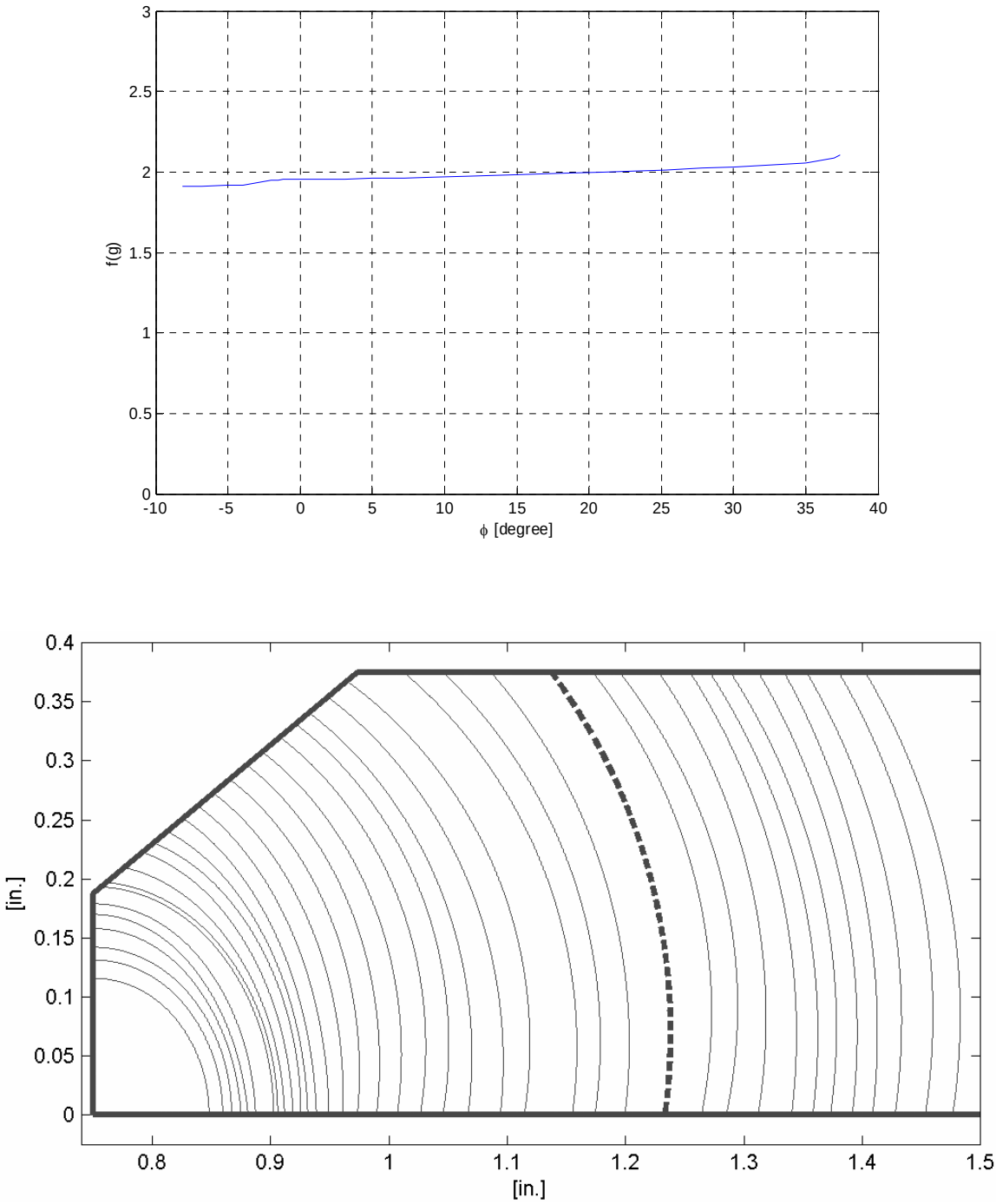

Figure C-27. Corrected BCF for FAA-009 at 64,500-66,300 Cycle, Initial Corner Crack, Type III

Table C-28. Corrected Boundary Correction Factors for FAA-009 (See figure C-28)

Initial Crack Location	Corner
Type	III
Center of Ellipse	(0.75, 0.0875)
Horizontal Axis	0.52250
Vertical Axis	0.48750
Cycle	66300-68000

ϕ [degree]	x [inch]	y [inch]	f(g)
-10.5	1.26375	0	1.7759
-9.01	1.26606	0.01307	1.7759
-7.83	1.26763	0.02303	1.7819
-6.17	1.26947	0.03706	1.7896
-4.52	1.27087	0.05114	1.7964
-3.13	1.27172	0.06325	1.8017
-1.8	1.27224	0.07536	1.8070
-0.92	1.27243	0.08949	1.8123
0.97	1.27242	0.09154	1.8131
2.9	1.27183	0.11179	1.8202
4.76	1.2707	0.12797	1.8252
7.15	1.26844	0.14827	1.8309
9.8	1.26488	0.17053	1.8367
12.47	1.26018	0.19274	1.8417
15.4	1.25373	0.21687	1.8464
17.87	1.24729	0.23689	1.8496
19.86	1.24143	0.25283	1.8514
22.37	1.23318	0.27266	1.8529
24.9	1.22391	0.29234	1.8327
27.22	1.21464	0.30997	1.7717
29.82	1.20331	0.32937	1.7354
32.48	1.19077	0.34868	1.7084
34.37	1.1813	0.36205	1.6858
35.74	1.17412	0.37176	1.6757
36.13	1.17204	0.37469	1.7277

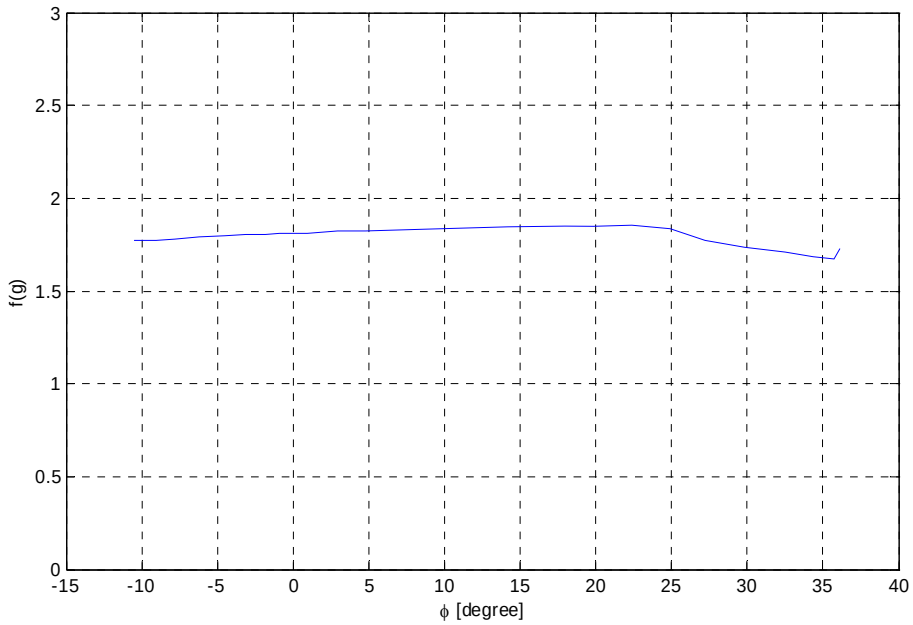

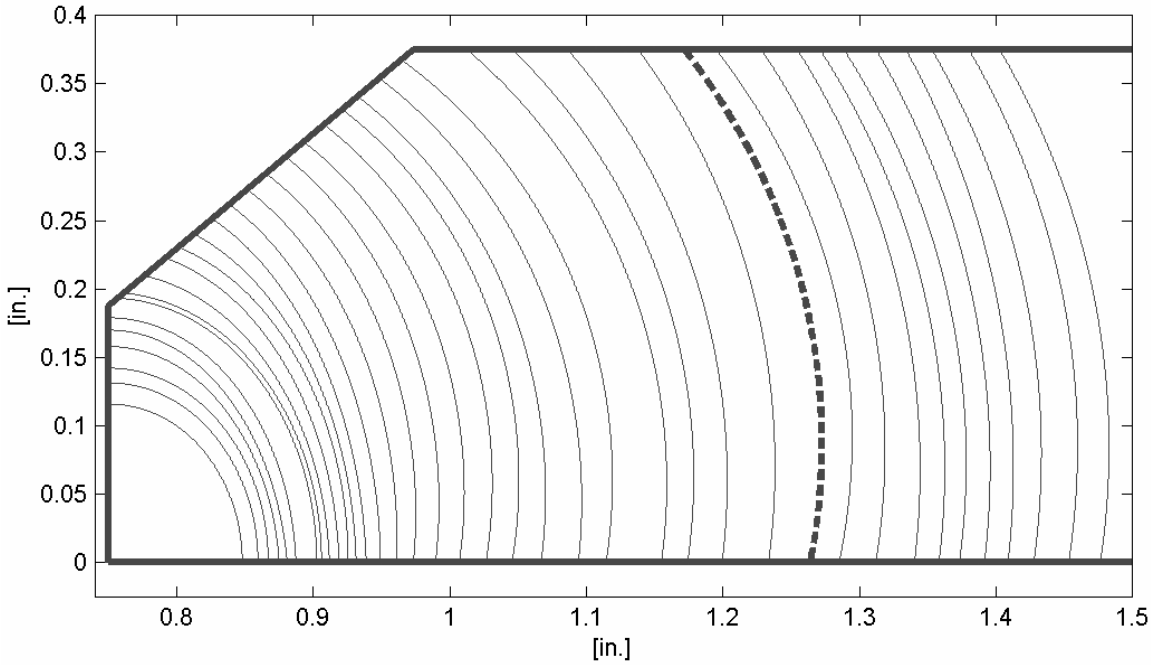

Figure C-28. Corrected BCF for FAA-009 at 66,300-68,000 Cycle, Initial Corner Crack, Type III

Table C-29. Corrected Boundary Correction Factors for FAA-009 (See figure C-29)

Initial Crack Location	Corner
Type	III
Center of Ellipse	(0.75, 0.0915)
Horizontal Axis	0.54450
Vertical Axis	0.49100
Cycle	68000-69500

ϕ [degree]	x [inch]	y [inch]	f(g)
-10.8	1.28485	0	1.6866
-9.16	1.28756	0.01373	1.6695
-7.8	1.28946	0.02523	1.6615
-6.44	1.29106	0.03678	1.6540
-5.1	1.29235	0.04828	1.6473
-3.97	1.29319	0.05789	1.6423
-2.42	1.29401	0.07128	1.6360
-1.33	1.29435	0.08089	1.6321
-0.42	1.29449	0.09234	1.6282
0.51	1.29448	0.09428	1.6276
2.13	1.29412	0.10957	1.6237
4.79	1.2926	0.13252	1.6205
7.03	1.2904	0.15163	1.6205
9.74	1.28664	0.17463	1.6233
12.25	1.2821	0.19569	1.6289
15.01	1.27591	0.21869	1.6381
18.05	1.2677	0.24363	1.6517
21.15	1.25782	0.26863	1.6690
24.08	1.24712	0.29178	1.6880
27.08	1.2348	0.31498	1.7100
29.91	1.22196	0.33628	1.7325
32.3	1.21023	0.35381	1.7953
33.38	1.20467	0.36157	1.8312
34.46	1.19894	0.36924	1.8689
35.31	1.19431	0.37489	1.9747

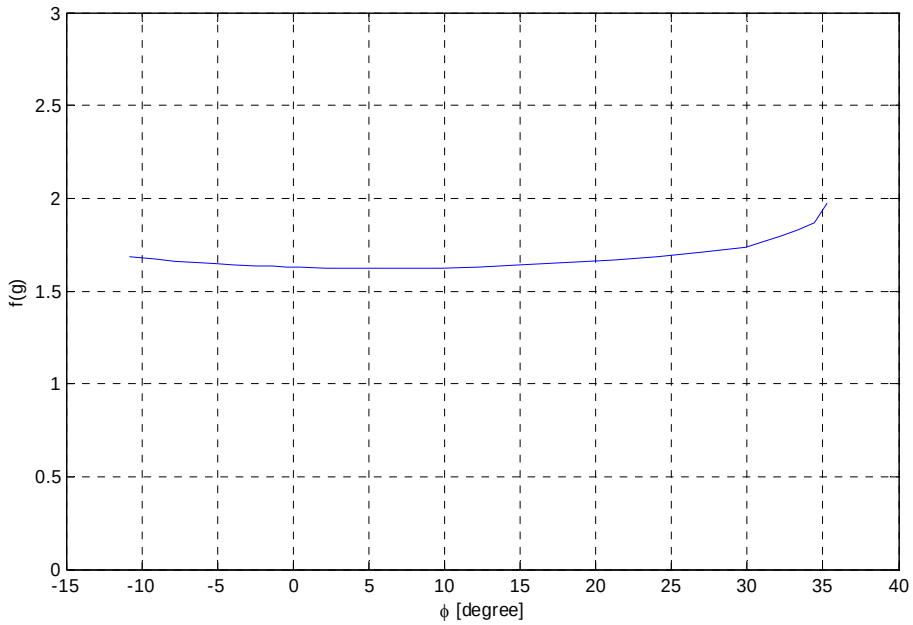

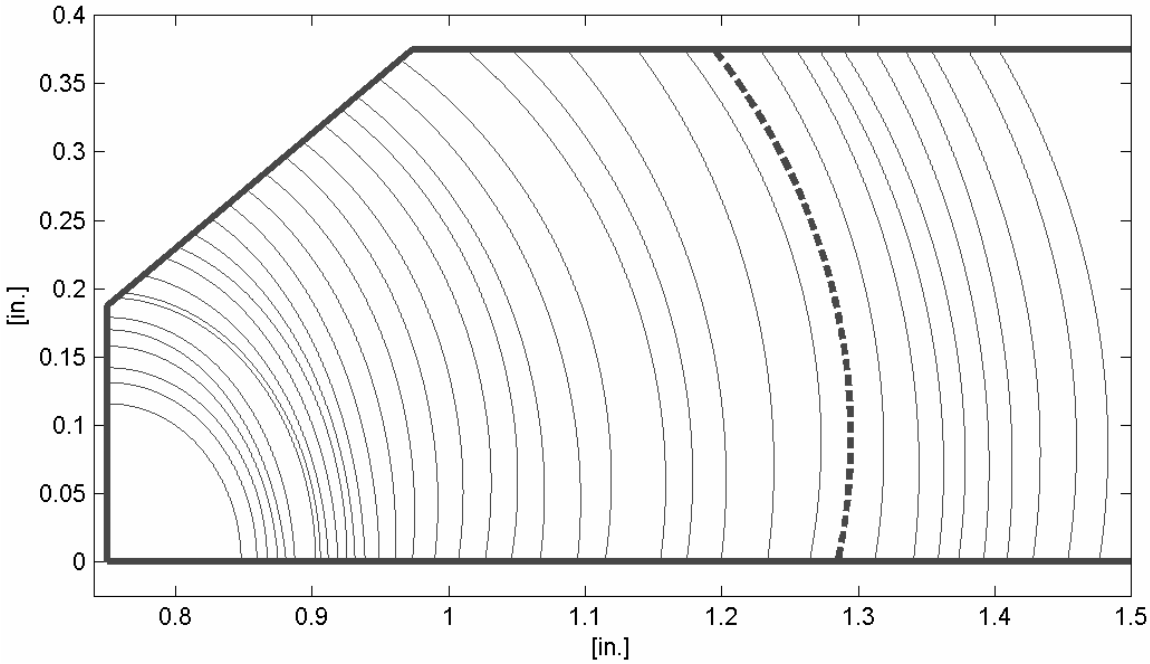

Figure C-29. Corrected BCF for FAA-009 at 68,000-69,500 Cycle, Initial Corner Crack, Type III

Table C-30. Corrected Boundary Correction Factors for FAA-009 (See figure C-30)

Initial Crack Location	Corner
Type	III
Center of Ellipse	(0.75, 0.0825)
Horizontal Axis	0.56850
Vertical Axis	0.54000
Cycle	69500-72000

ϕ [degree]	x [inch]	y [inch]	f(g)
-8.88	1.31169	0	1.7375
-7.79	1.31325	0.00982	1.7188
-6.25	1.31512	0.02429	1.7135
-5.15	1.31621	0.03466	1.7100
-4.06	1.31707	0.04498	1.7069
-3.19	1.31762	0.05323	1.7045
-2.12	1.31811	0.06361	1.7018
-1.12	1.31839	0.07393	1.6994
-0.61	1.31847	0.08217	1.6976
0.63	1.31847	0.08425	1.6972
2	1.31815	0.10074	1.6942
4.14	1.31701	0.12133	1.6915
6.11	1.31527	0.1399	1.6901
8.3	1.31254	0.16049	1.6895
10.29	1.30935	0.179	1.6900
12.3	1.30545	0.19757	1.6914
16.59	1.29483	0.23672	1.6976
18.66	1.28862	0.25529	1.7019
20.75	1.28162	0.27386	1.7075
22.64	1.27471	0.29035	1.7132
24.31	1.26809	0.30482	1.7189
26.01	1.26091	0.31935	1.7358
28.23	1.25086	0.33797	1.7703
30.77	1.2385	0.35872	1.8143
32.78	1.22795	0.37448	1.9342

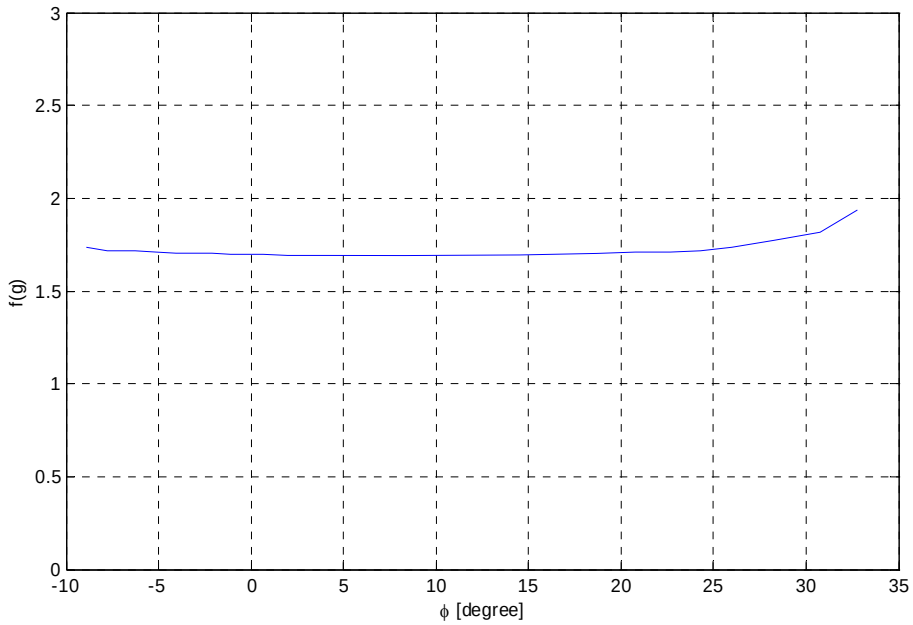

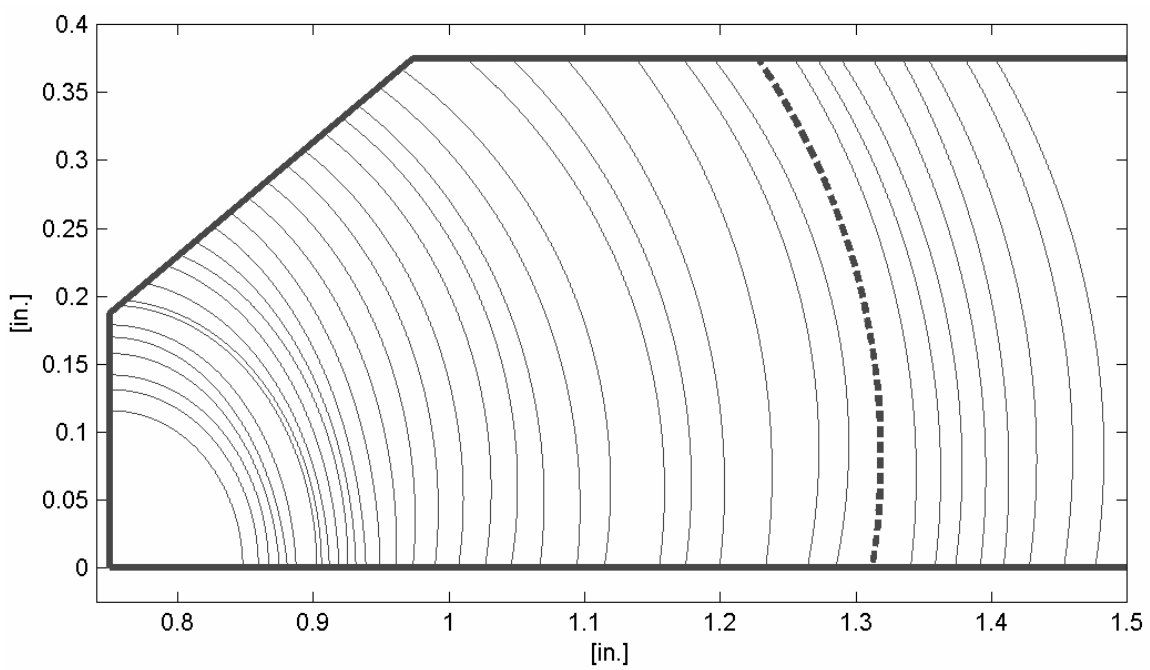

Figure C-30. Corrected BCF for FAA-009 at 69,500-72,000 Cycle, Initial Corner Crack, Type III

Table C-31. Corrected Boundary Correction Factors for FAA-009 (See figure C-31)

Initial Crack Location	Corner
Type	III
Center of Ellipse	(0.75, 0.0685)
Horizontal Axis	0.59425
Vertical Axis	0.57900
Cycle	72000-73500

ϕ [degree]	x [inch]	y [inch]	f(g)
-6.87	1.33999	0	1.6982
-5.67	1.34135	0.01203	1.6894
-4.38	1.34252	0.0252	1.6825
-3.32	1.34325	0.03615	1.6768
-2.09	1.34385	0.04926	1.6701
-1.05	1.34415	0.06238	1.6636
-0.86	1.34418	0.06896	1.6603
0.89	1.34418	0.07112	1.6592
2.16	1.34383	0.0886	1.6507
4.02	1.34279	0.10824	1.6414
6.37	1.34058	0.1322	1.6303
8.52	1.33769	0.15395	1.6204
10.48	1.33434	0.17353	1.6117
12.45	1.33028	0.19307	1.6034
14.66	1.32491	0.21481	1.5943
16.43	1.31998	0.23213	1.5873
18.23	1.31444	0.24945	1.5803
20.5	1.30662	0.27115	1.5720
22.56	1.29876	0.29057	1.5648
24.43	1.29104	0.30789	1.5586
26.32	1.28264	0.32516	1.5526
28	1.27469	0.34027	1.5475
29.22	1.26865	0.35106	1.5440
30.7	1.26099	0.36401	1.5399
31.91	1.25446	0.37452	1.5733

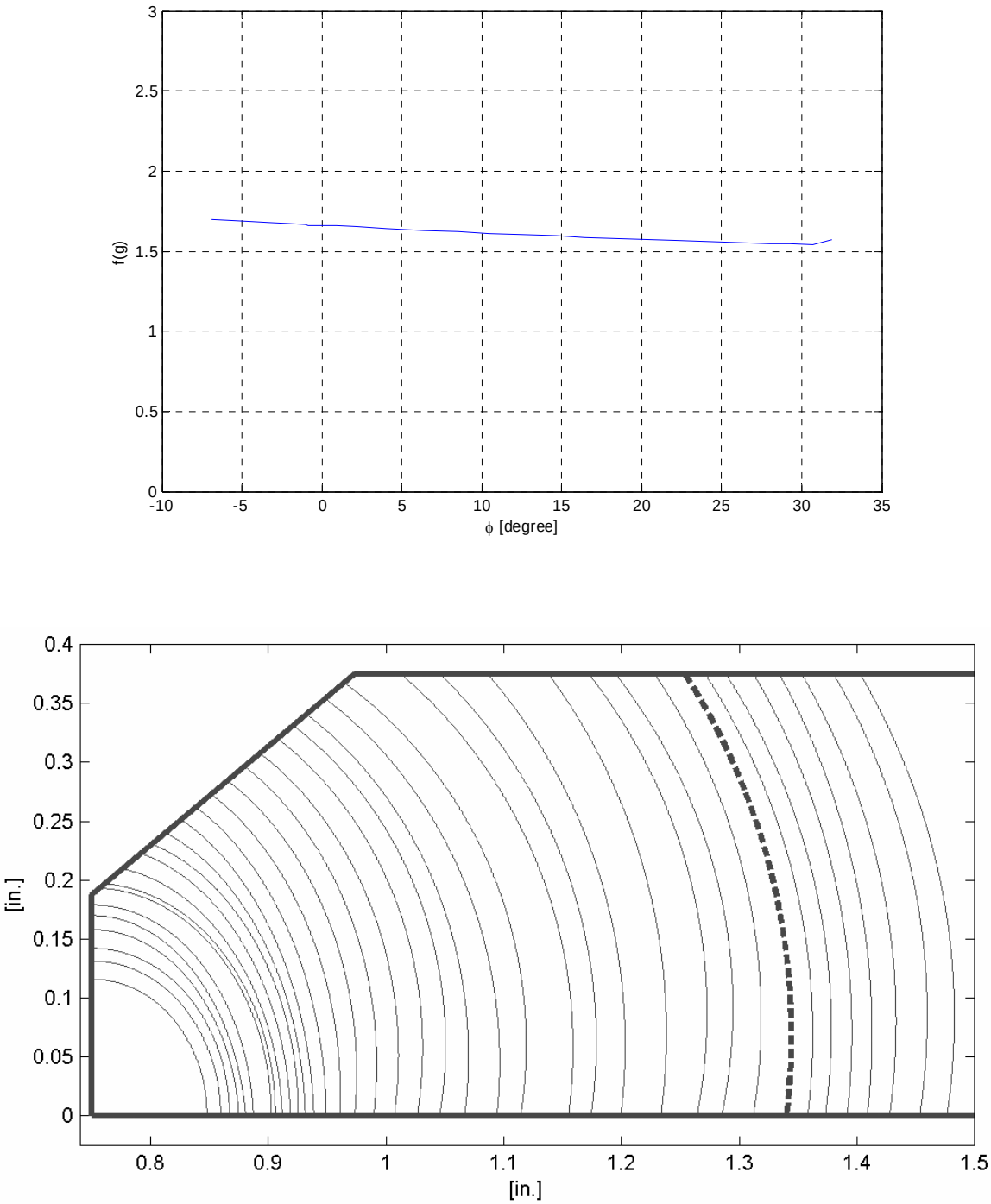

Figure C-31. Corrected BCF for FAA-009 at 72,000-73,500 Cycle, Initial Corner Crack, Type III

Table C-32. Corrected Boundary Correction Factors for FAA-009 (See figure C-32)

Initial Crack Location	Corner
Type	III
Center of Ellipse	(0.75, 0.06875)
Horizontal Axis	0.61225
Vertical Axis	0.58250
Cycle	73500-74750

ϕ [degree]	x [inch]	y [inch]	f(g)
-6.87	1.35785	0	1.6426
-5.5	1.35943	0.01422	1.6520
-4.22	1.36059	0.02741	1.6618
-3.17	1.36132	0.03837	1.6694
-2.14	1.36182	0.04939	1.6766
-1.09	1.36214	0.06257	1.6845
-0.87	1.36218	0.06919	1.6883
0.9	1.36217	0.07142	1.6894
2.14	1.36182	0.08906	1.7000
4.22	1.36059	0.11109	1.7119
6.59	1.35821	0.13541	1.7246
8.55	1.35545	0.15527	1.7352
10.31	1.35237	0.17296	1.7448
12.3	1.34821	0.19283	1.7558
14.31	1.34326	0.21275	1.7672
16.33	1.33754	0.23261	1.7787
18.38	1.33102	0.25247	1.7910
20.45	1.32368	0.27228	1.8037
22.31	1.31642	0.28992	1.8157
24.43	1.30742	0.30973	1.8296
26.34	1.29867	0.32726	1.8632
28.29	1.28915	0.34479	1.8694
31.01	1.27472	0.36889	1.8787
31.21	1.27366	0.37057	1.8806
31.7	1.27092	0.3749	1.9078

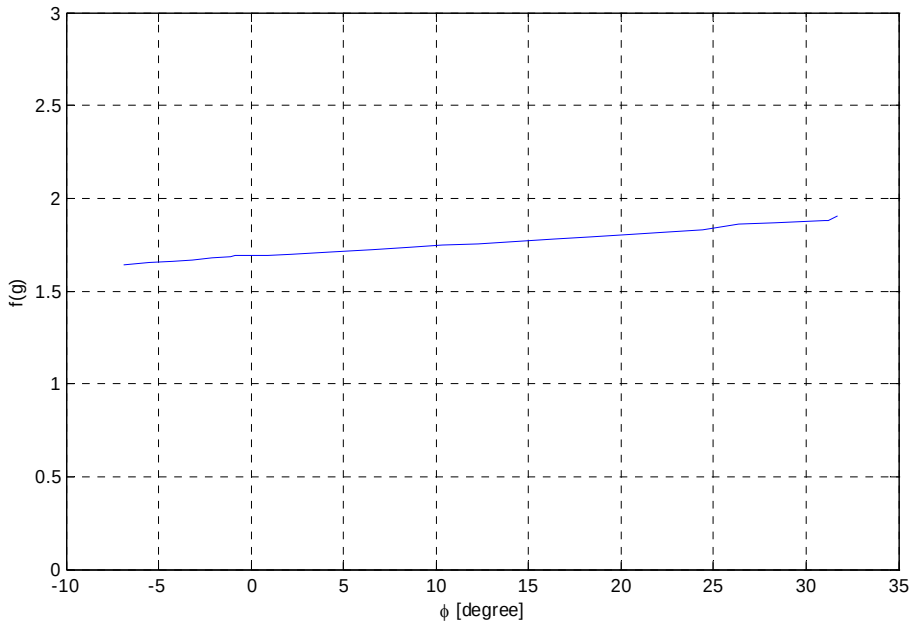

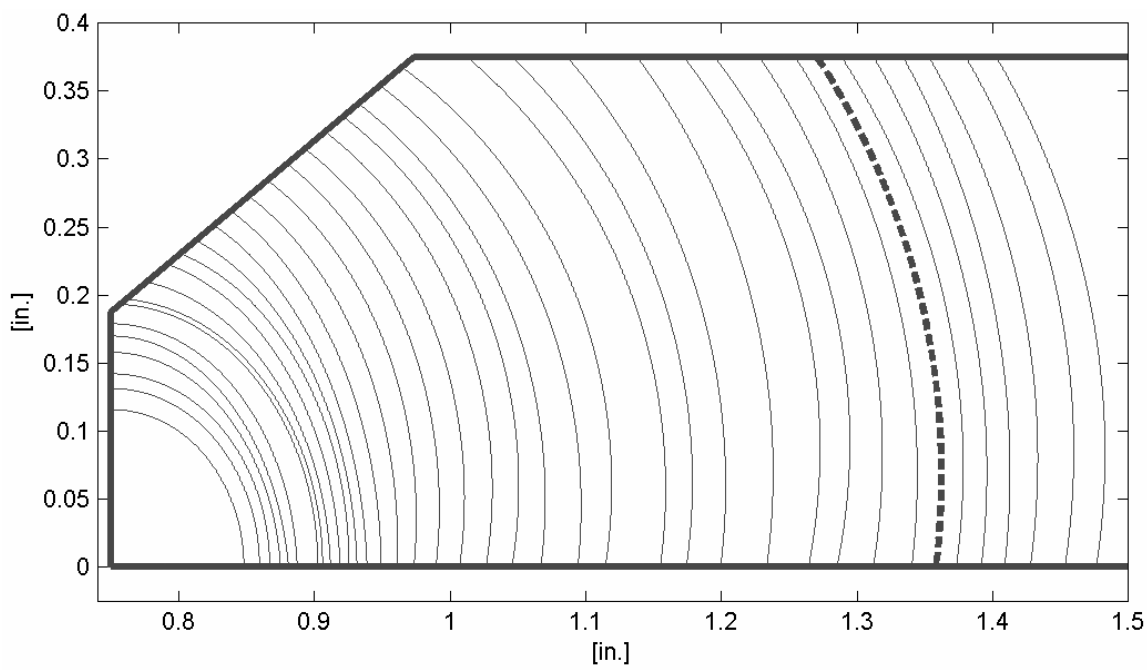

Figure C-32. Corrected BCF for FAA-009 at 73,500-74,750 Cycle, Initial Corner Crack, Type III

Table C-33. Corrected Boundary Correction Factors for FAA-009 (See figure C-33)

Initial Crack Location	Corner
Type	III
Center of Ellipse	(0.75, 0.07375)
Horizontal Axis	0.62800
Vertical Axis	0.58500
Cycle	74750-76000

ϕ [degree]	x [inch]	y [inch]	f(g)
-7.26	1.37296	0	1.6393
-6.05	1.37451	0.01229	1.6319
-5.18	1.37543	0.02107	1.6285
-3.89	1.37655	0.0343	1.6238
-2.6	1.37735	0.04753	1.6194
-1.33	1.37783	0.06076	1.6152
-0.73	1.37795	0.06741	1.6132
-0.37	1.37799	0.07399	1.6113
0.44	1.37798	0.07619	1.6106
1.79	1.3777	0.09162	1.6064
3.07	1.3771	0.10485	1.6030
5	1.37561	0.12466	1.5985
7.16	1.3731	0.14662	1.5942
9.12	1.37006	0.16644	1.5909
11.09	1.36628	0.1862	1.5883
13.06	1.36175	0.20597	1.5864
15.06	1.35642	0.22578	1.5852
17.3	1.34958	0.24774	1.5847
19.34	1.34255	0.2675	1.5850
21.41	1.33468	0.28727	1.5860
23.27	1.32693	0.30483	1.5877
25.63	1.31621	0.32679	1.5906
27.31	1.308	0.34216	1.5934
29.26	1.29785	0.35973	1.5973
30.94	1.28863	0.37452	1.6411

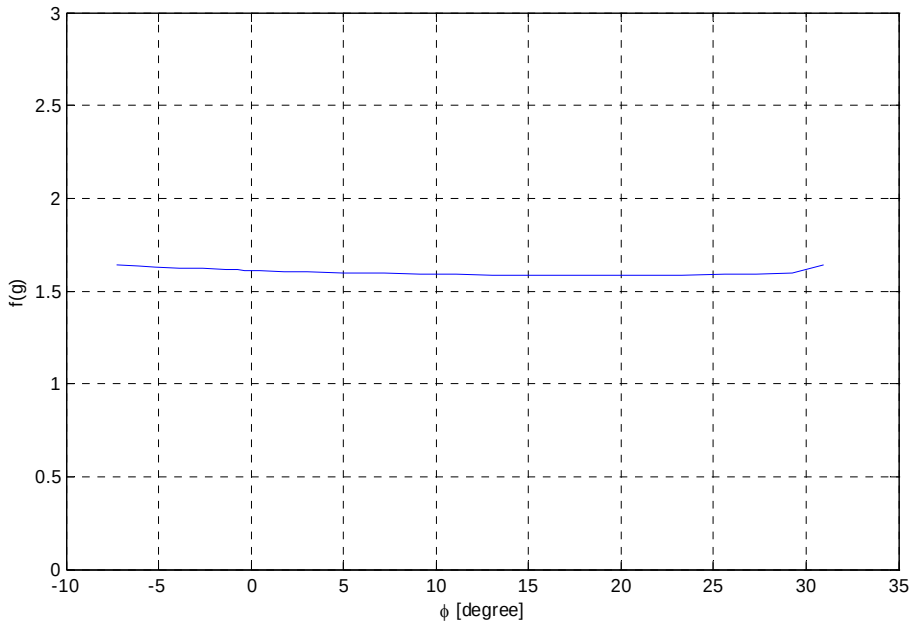

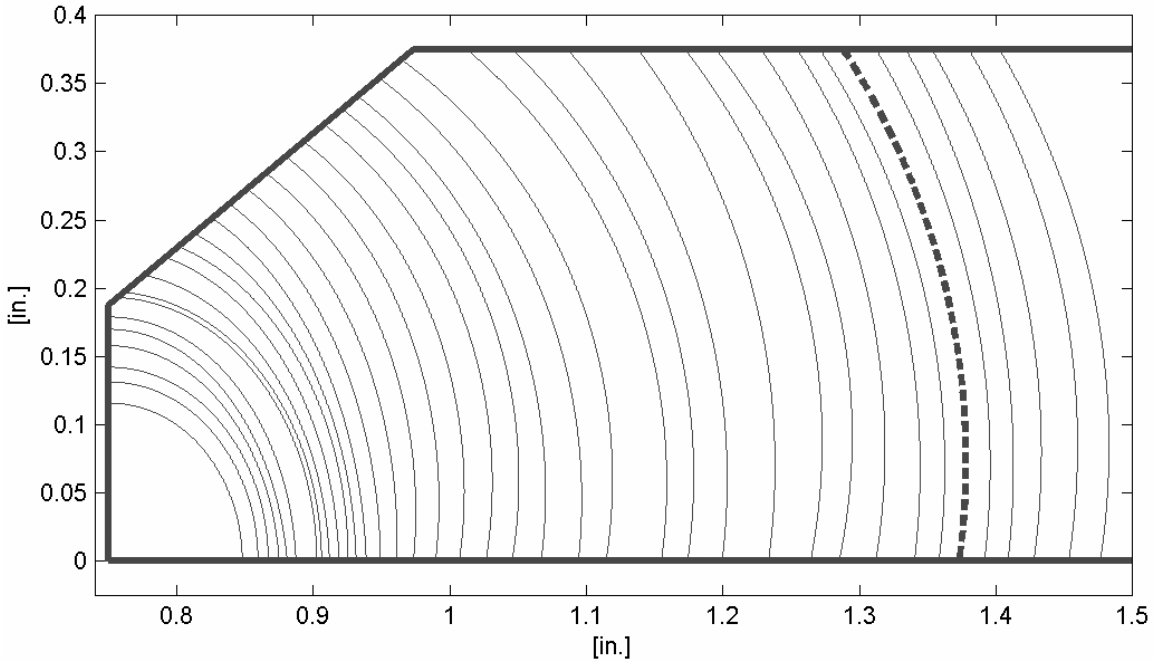

Figure C-33. Corrected BCF for FAA-009 at 74,750-76,000 Cycle, Initial Corner Crack, Type III

Table C-34. Corrected Boundary Correction Factors for FAA-009 (See figure C-34)

Initial Crack Location	Corner
Type	III
Center of Ellipse	(0.75, 0.07)
Horizontal Axis	0.64550
Vertical Axis	0.62000
Cycle	76000-77500

ϕ [degree]	x [inch]	y [inch]	f(g)
-6.49	1.39136	0	1.6839
-5.34	1.39269	0.01231	1.6729
-4.08	1.39386	0.02587	1.6709
-3.04	1.39459	0.03713	1.6694
-2	1.39511	0.0484	1.6685
-1.16	1.39537	0.05742	1.6680
-0.54	1.39547	0.0642	1.6678
-0.09	1.3955	0.07098	1.6678
0.3	1.39549	0.07322	1.6678
2.17	1.39504	0.0935	1.6687
4.05	1.39389	0.11378	1.6708
6.36	1.39153	0.13861	1.6751
8.46	1.38847	0.16119	1.6909
10.37	1.38495	0.18153	1.7022
12.5	1.38019	0.20412	1.7170
14.22	1.37571	0.22222	1.7312
16.4	1.36924	0.24492	1.7520
18.38	1.36258	0.26532	1.7733
20.38	1.35508	0.28578	1.7969
22.42	1.3467	0.30631	1.8422
24.49	1.33743	0.32683	1.8557
26.6	1.32719	0.34741	1.8704
28.5	1.31725	0.36569	1.8848
29.13	1.31386	0.37143	1.8962
29.51	1.31177	0.37476	1.9153

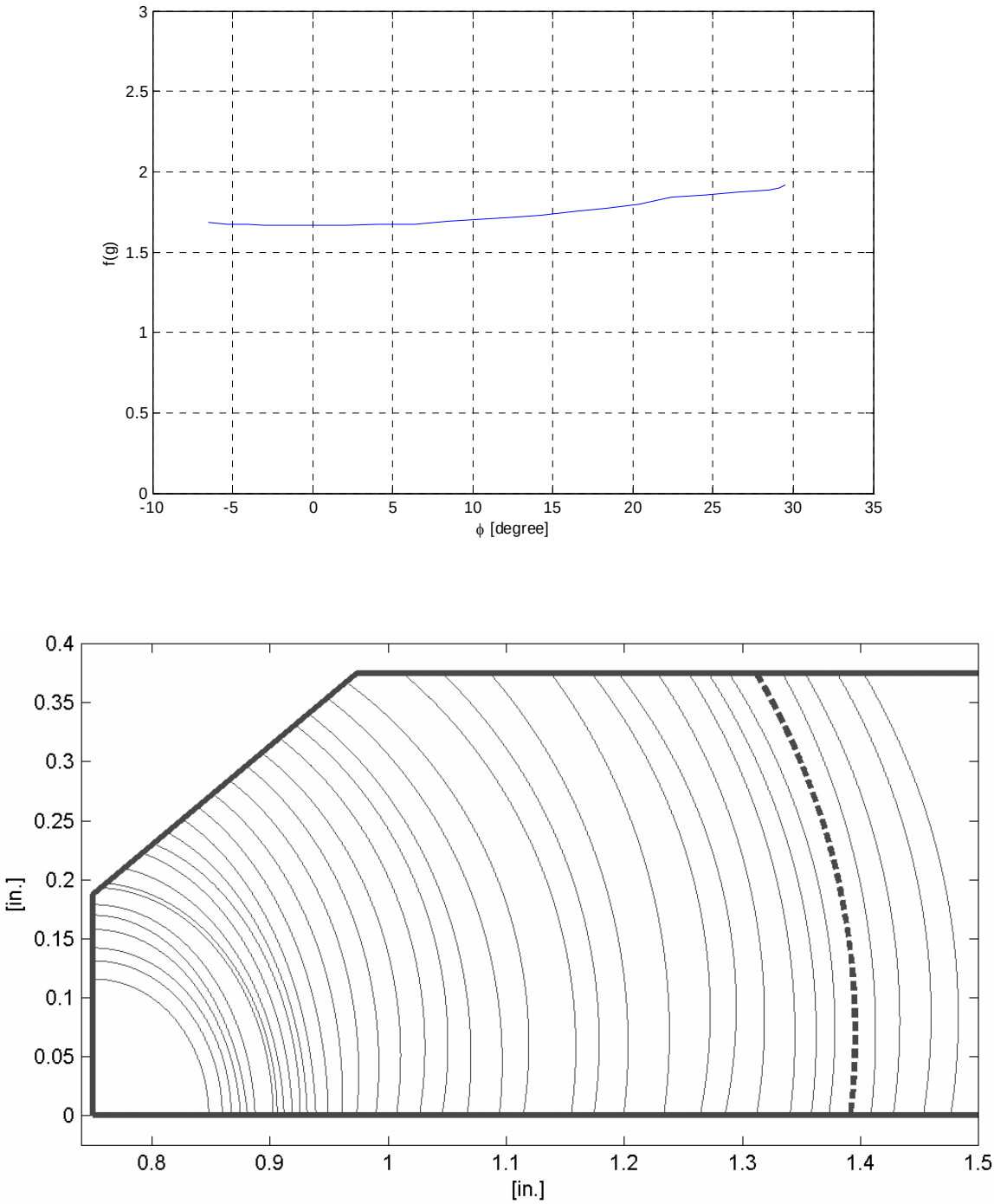

Figure C-34. Corrected BCF for FAA-009 at 76,000-77,500 Cycle, Initial Corner Crack, Type III

Table C-35. Corrected Boundary Correction Factors for FAA-009 (See figure C-35)

Initial Crack Location	Corner
Type	III
Center of Ellipse	(0.75, 0.07)
Horizontal Axis	0.66250
Vertical Axis	0.64500
Cycle	77500-79000

ϕ [degree]	x [inch]	y [inch]	f(g)
-6.23	1.40859	0	1.5188
-5.22	1.40975	0.01132	1.5175
-4.15	1.41076	0.02336	1.5180
-3.08	1.41155	0.03539	1.5183
-2.01	1.41209	0.04743	1.5185
-0.94	1.41241	0.05946	1.5187
-0.51	1.41247	0.06429	1.5187
-0.08	1.4125	0.06912	1.5187
0.13	1.4125	0.0715	1.5187
1.2	1.41235	0.08354	1.5186
2.49	1.41187	0.09801	1.5184
4.2	1.41072	0.11726	1.5179
6.14	1.4087	0.13895	1.5171
8.29	1.40557	0.16302	1.5158
10.25	1.40194	0.18471	1.5143
12.42	1.39699	0.20872	1.5122
14.4	1.39168	0.23041	1.5100
16.4	1.38556	0.25204	1.5073
18.4	1.37862	0.27361	1.5042
20.44	1.37078	0.29524	1.5008
22.5	1.36207	0.3168	1.4968
24.36	1.35353	0.33599	1.4929
26.24	1.34424	0.35512	1.4885
27.19	1.33928	0.36471	1.4862
28.17	1.334	0.37454	1.5108

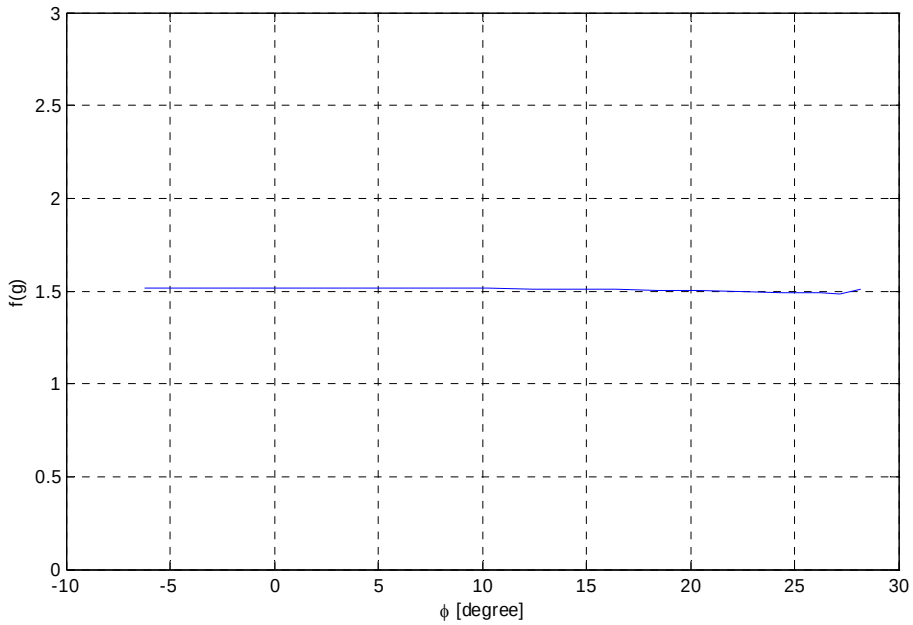

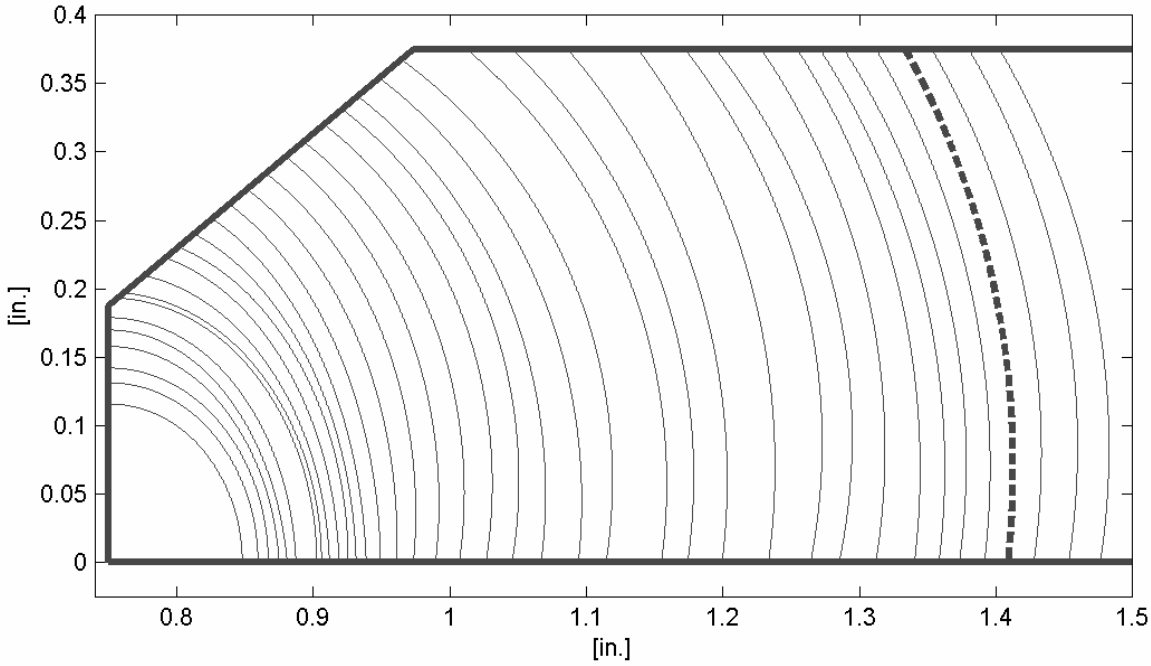

Figure C-35. Corrected BCF for FAA-009 at 77,500-79,000 Cycle, Initial Corner Crack, Type III

Table C-36. Corrected Boundary Correction Factors for FAA-009 (See figure C-36)

Initial Crack Location	Corner
Type	III
Center of Ellipse	(0.75, 0.08)
Horizontal Axis	0.68300
Vertical Axis	0.62750
Cycle	79000-80500

ϕ [degree]	x [inch]	y [inch]	f(g)
-7.47	1.42721	0	1.7018
-6.81	1.42818	0.00763	1.7029
-5.7	1.42962	0.01977	1.7093
-4.6	1.4308	0.03191	1.7150
-3.73	1.43155	0.04169	1.7197
-2.66	1.43226	0.05389	1.7247
-1.66	1.43271	0.06609	1.7301
-1.16	1.43286	0.07346	1.7330
-0.94	1.43291	0.08077	1.7358
0.96	1.43291	0.08324	1.7369
2	1.43258	0.10039	1.7434
3.91	1.43141	0.12243	1.7514
5.02	1.43038	0.13475	1.7553
7.25	1.42754	0.15927	1.7641
9.06	1.42448	0.17889	1.7706
11.11	1.42021	0.20099	1.7776
12.94	1.41567	0.22056	1.7842
15.01	1.4097	0.24254	1.8141
17.1	1.4028	0.26453	1.8173
19.21	1.39498	0.28639	1.8205
21.1	1.38722	0.30578	1.8232
23.01	1.37867	0.32512	1.8259
25.18	1.36812	0.34675	1.8286
26.65	1.36046	0.36119	1.8304
27.99	1.3531	0.37458	1.8512

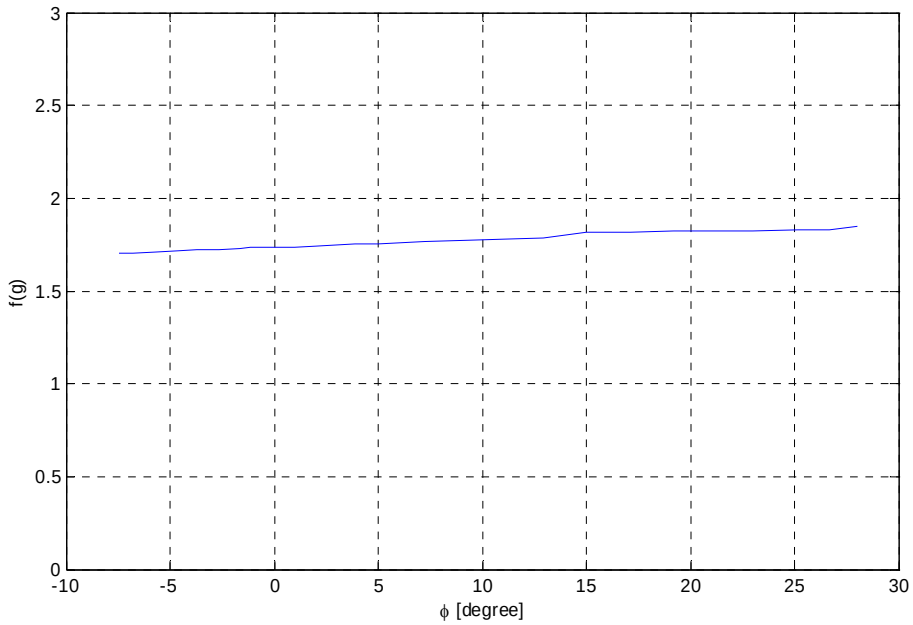

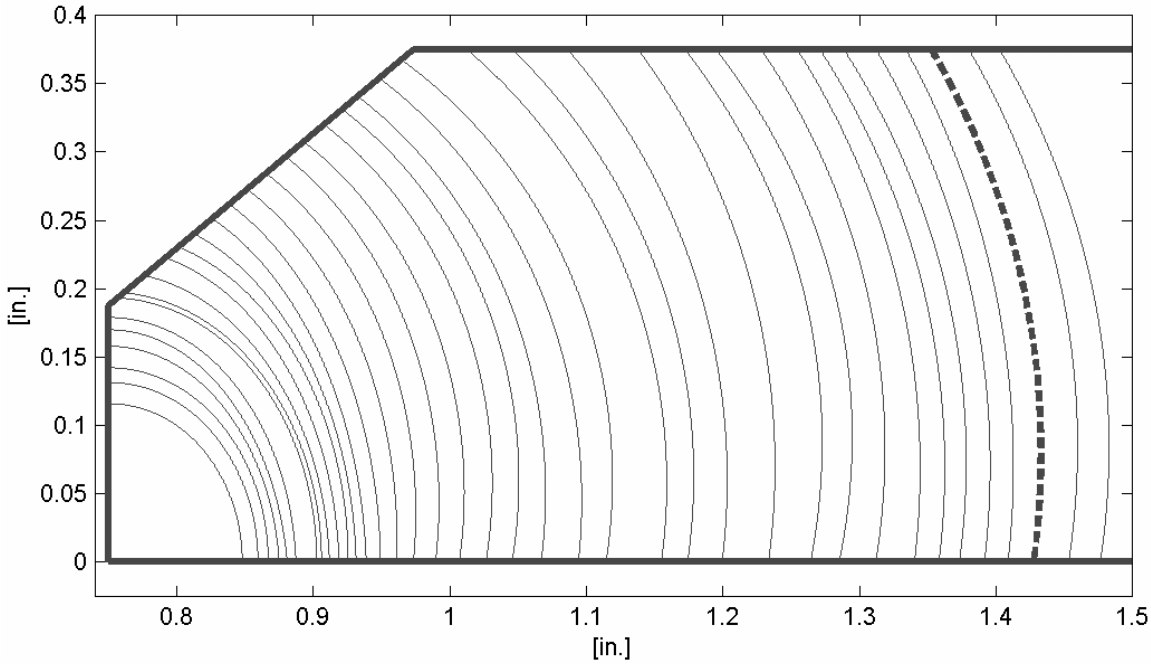

Figure C-36. Corrected BCF for FAA-009 at 79,000-80,500 Cycle, Initial Corner Crack, Type III

Table C-37. Corrected Boundary Correction Factors for FAA-009 (See figure C-37)

Initial Crack Location	Corner
Type	III
Center of Ellipse	(0.75, 0.085)
Horizontal Axis	0.70950
Vertical Axis	0.63000
Cycle	80500-82500

ϕ [degree]	x [inch]	y [inch]	f(g)
-7.8	1.45294	0	1.6246
-6.64	1.45473	0.01241	1.6170
-5.12	1.45667	0.02916	1.6117
-4.03	1.45774	0.04114	1.6082
-3.17	1.45841	0.05067	1.6056
-2.1	1.45902	0.06259	1.6026
-1.07	1.45938	0.07456	1.5997
-0.7	1.45945	0.07933	1.5986
-0.47	1.45948	0.0841	1.5976
0.48	1.45947	0.08648	1.5971
1.29	1.45932	0.0984	1.5948
2.98	1.45854	0.11746	1.5916
4.49	1.45732	0.13415	1.5892
7.52	1.45339	0.16745	1.5860
9.49	1.44978	0.1889	1.5851
11.47	1.44533	0.21029	1.5850
13.02	1.44125	0.22698	1.5856
15.25	1.43451	0.25075	1.5873
17.28	1.42746	0.2722	1.5898
19.33	1.41949	0.29359	1.5932
21.64	1.40949	0.31736	1.5983
23.52	1.40056	0.33643	1.6031
25.42	1.39079	0.35549	1.6089
26.96	1.38238	0.37066	1.6172
27.33	1.38031	0.37416	1.6829

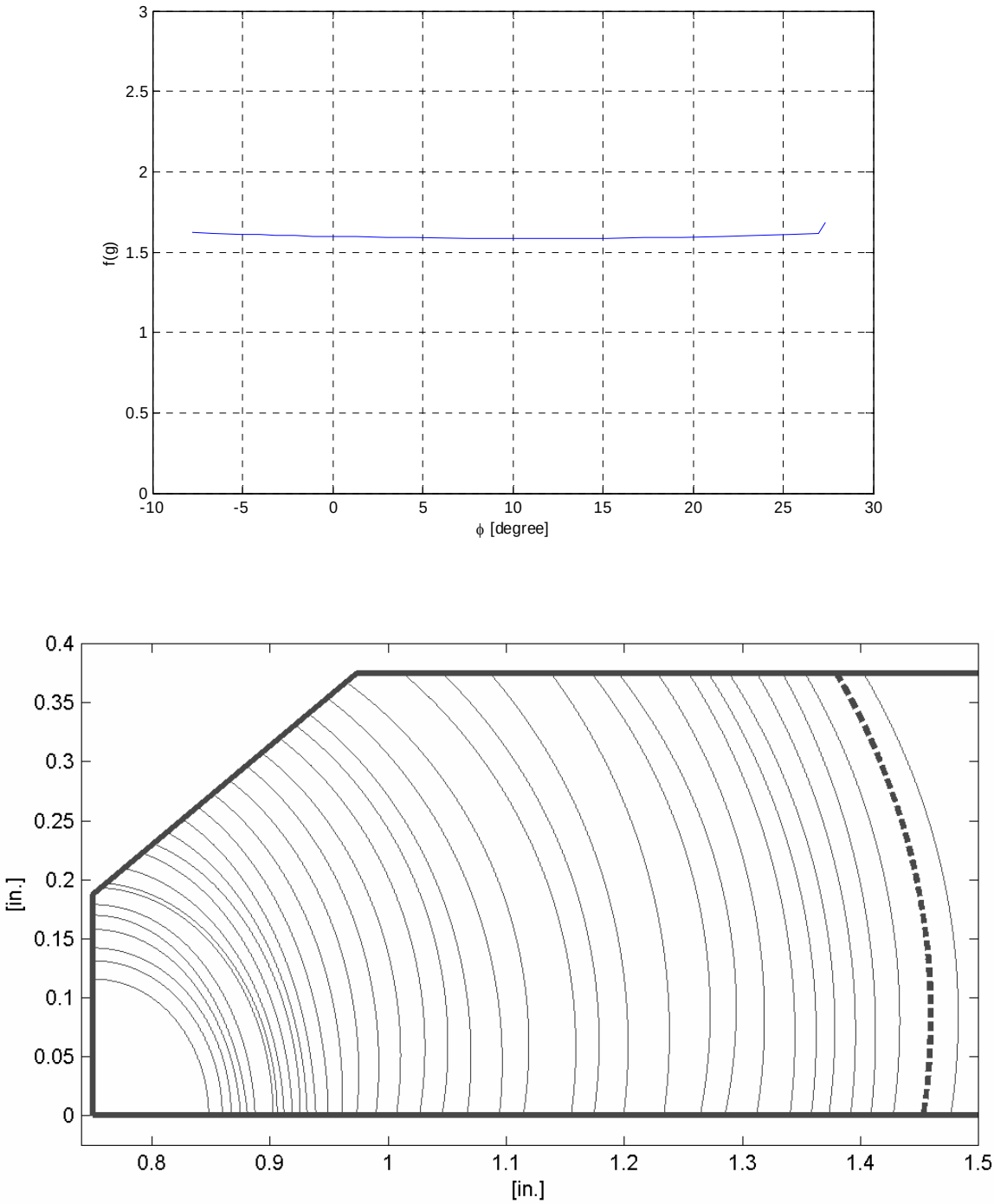

Figure C-37. Corrected BCF for FAA-009 at 80,500-82,500 Cycle, Initial Corner Crack, Type III

Table C-38. Corrected Boundary Correction Factors for FAA-009 (See figure C-38)

Initial Crack Location	Corner
Type	III
Center of Ellipse	(0.75, 0.084)
Horizontal Axis	0.73250
Vertical Axis	0.64000
Cycle	82500-84500

ϕ [degree]	x [inch]	y [inch]	f(g)
-7.57	1.47611	0	1.5132
-6.17	1.47826	0.0157	1.5162
-5.06	1.47965	0.02806	1.5207
-4.17	1.48056	0.03796	1.5239
-3.06	1.48145	0.05038	1.5274
-2.18	1.48197	0.06027	1.5300
-0.7	1.48245	0.07765	1.5341
-0.37	1.48248	0.08512	1.5355
0.47	1.48248	0.0876	1.5360
1.89	1.4821	0.10497	1.5388
3.22	1.48135	0.11987	1.5406
5	1.47972	0.13977	1.5423
6.78	1.47737	0.15962	1.5431
8.81	1.47386	0.182	1.5430
10.61	1.46999	0.20178	1.5419
12.19	1.46597	0.21915	1.5402
14.24	1.45998	0.24141	1.5370
16.31	1.45302	0.26367	1.5326
18.39	1.44509	0.28581	1.5269
20.26	1.43719	0.30548	1.5208
22.38	1.42732	0.32756	1.5123
24.29	1.41766	0.3471	1.5034
25.74	1.40982	0.36176	1.4958
26.68	1.40452	0.37117	1.4905
27.03	1.40249	0.37482	1.5270

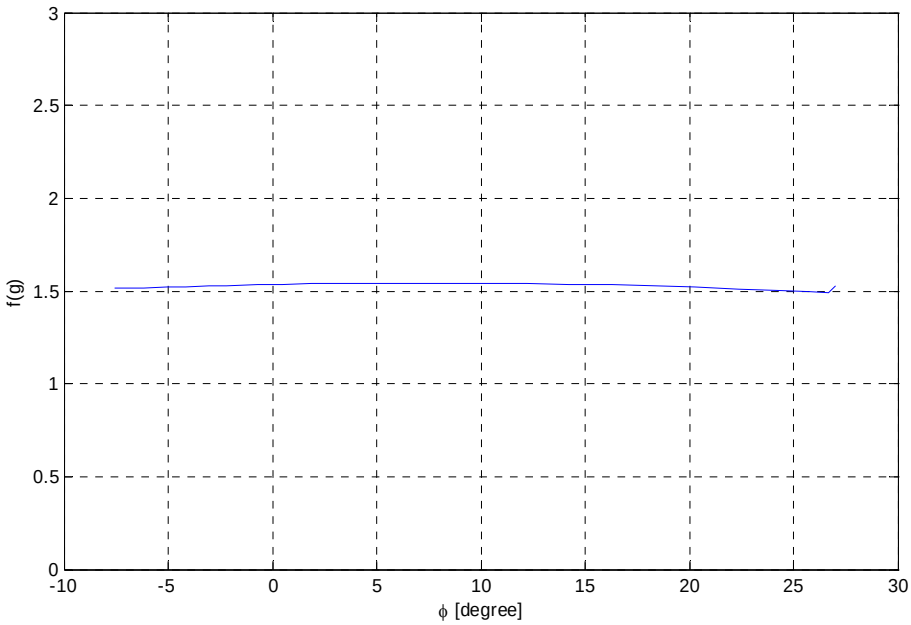

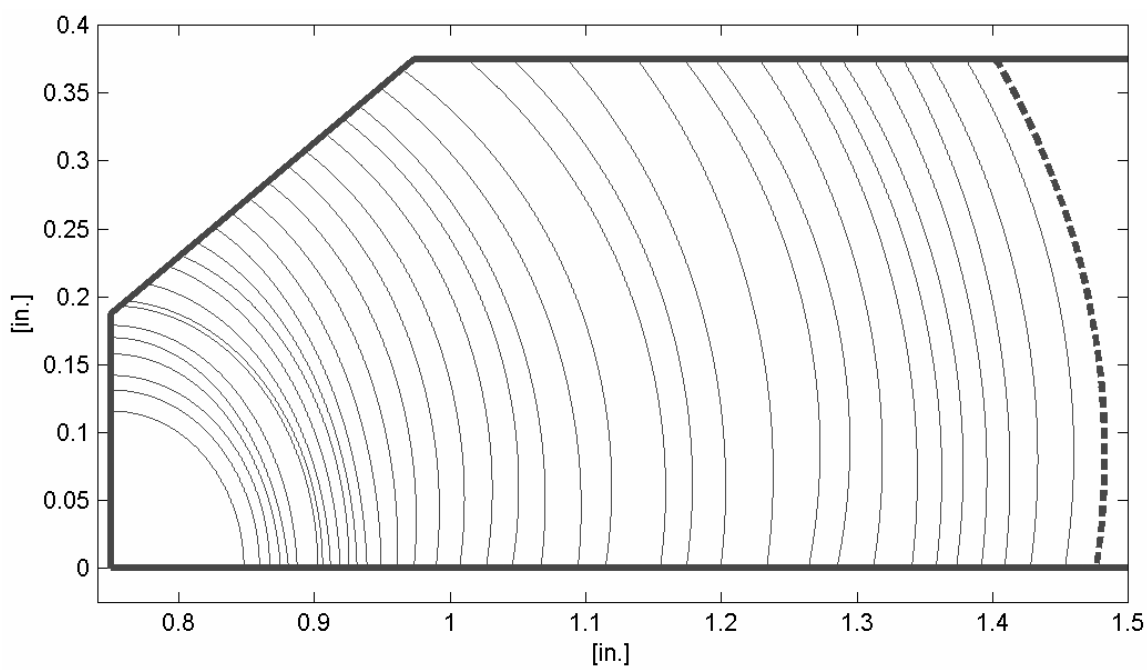

Figure C-38. Corrected BCF for FAA-009 at 82,500-84,500 Cycle, Initial Corner Crack, Type III

Table C-39. Corrected Boundary Correction Factors for FAA-012 (See figure C-39)

Initial Crack Location	Knee
Type	I
Center of Ellipse	(0.75, 0.15075)
Horizontal Axis	0.06750
Vertical Axis	0.06950
Cycle	15000-17500

ϕ [degree]	x [inch]	y [inch]	f(g)
0	0.75	0.08125	1.1909
15.57	0.768	0.0838	1.1694
26.96	0.78042	0.0888	1.1508
31.04	0.78462	0.0912	1.1448
34.69	0.78822	0.09361	1.1393
37.96	0.79132	0.09596	1.1341
43.82	0.79653	0.10061	1.1078
49.01	0.80075	0.10516	1.0816
53.71	0.80421	0.10961	1.0569
58.04	0.80709	0.11396	1.0330
64.12	0.81058	0.12041	0.9983
69.81	0.81322	0.12676	0.9725
75.26	0.81517	0.13307	0.9630
80.45	0.81648	0.13922	0.9535
85.56	0.81723	0.14537	0.9436
90.59	0.81744	0.15147	0.9336
95.59	0.81714	0.15752	0.9232
100.59	0.81633	0.16352	0.9129
105.67	0.81498	0.16952	0.9028
110.88	0.81306	0.17552	0.8936
114.46	0.81145	0.17952	0.8885
120.02	0.80845	0.18552	0.8835
125.92	0.80467	0.19152	0.8830
130.16	0.8016	0.19557	0.8856
134.63	0.79805	0.19957	0.8902

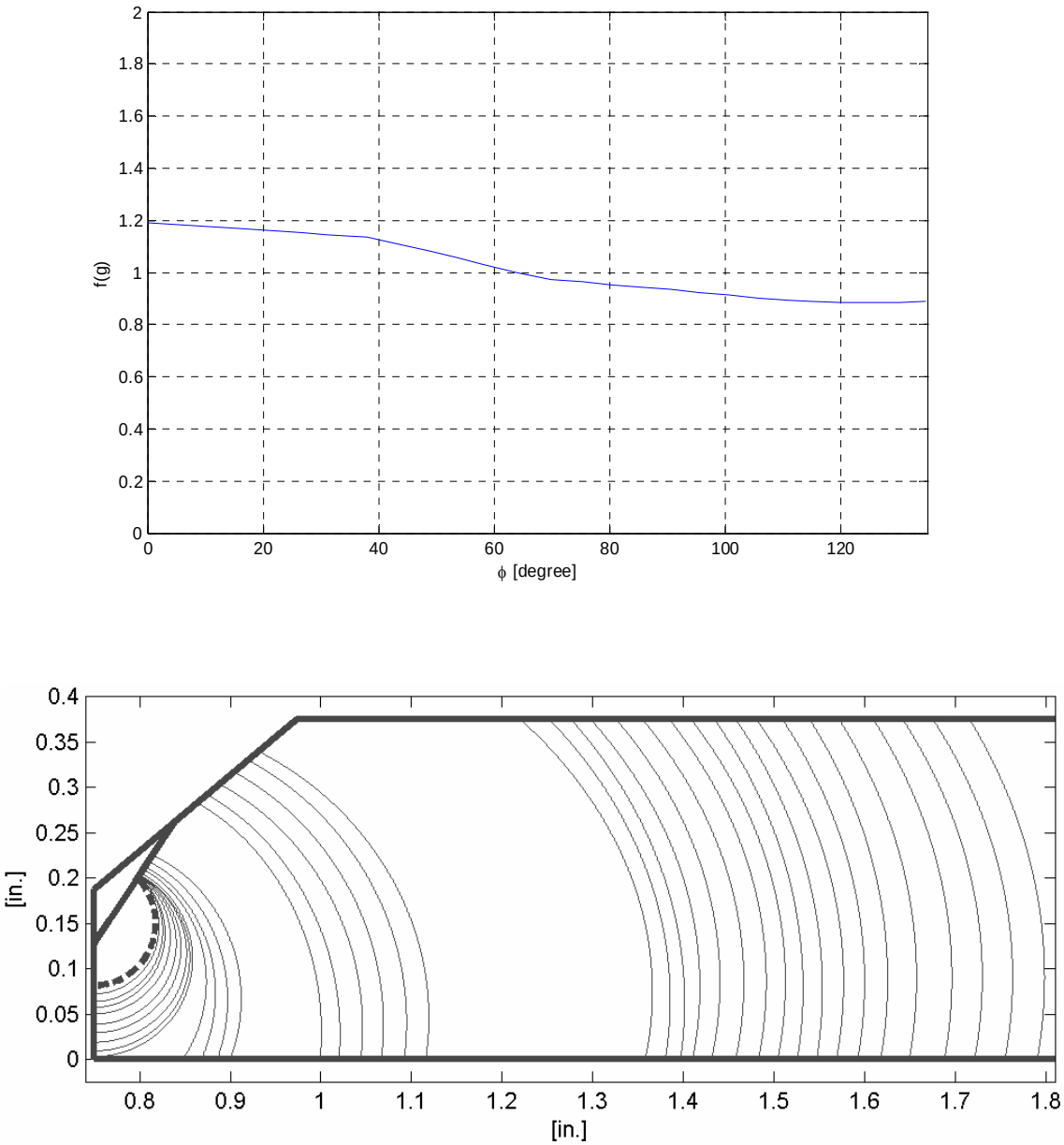

Figure C-39. Corrected BCF for FAA-012 at 15,000-17,500 Cycle, Initial Knee Crack, Type I

Table C-40. Corrected Boundary Correction Factors for FAA-012 (See figure C-40)

Initial Crack Location	Knee
Type	I
Center of Ellipse	(0.75, 0.14625)
Horizontal Axis	0.07130
Vertical Axis	0.07400
Cycle	17500-22000

ϕ [degree]	x [inch]	y [inch]	f(g)
0	0.75	0.07225	0.9883
12.91	0.76593	0.07412	0.9713
18.19	0.77225	0.07595	0.9693
25.91	0.78116	0.07969	0.9668
29.05	0.78462	0.08156	0.9659
34.55	0.79044	0.0853	0.9644
39.43	0.79529	0.08909	0.9632
45.9	0.8012	0.09475	0.9617
49.85	0.8045	0.09854	0.9608
55.41	0.8087	0.10424	0.9594
60.62	0.81213	0.10994	0.9581
65.57	0.81492	0.11565	0.9568
70.34	0.81714	0.12135	0.9553
75.01	0.81887	0.1271	0.9538
79.53	0.82011	0.13281	0.9521
84	0.8209	0.13851	0.9502
89.88	0.82128	0.14609	0.9473
95.71	0.82092	0.15362	0.9440
100.1	0.82016	0.15923	0.9410
104.55	0.81897	0.16484	0.9377
110.56	0.8167	0.17224	0.9322
115.2	0.81445	0.17776	0.9271
119.95	0.81172	0.18319	0.9208
124.93	0.80838	0.18862	0.9128
135.79	0.79963	0.1993	0.8857

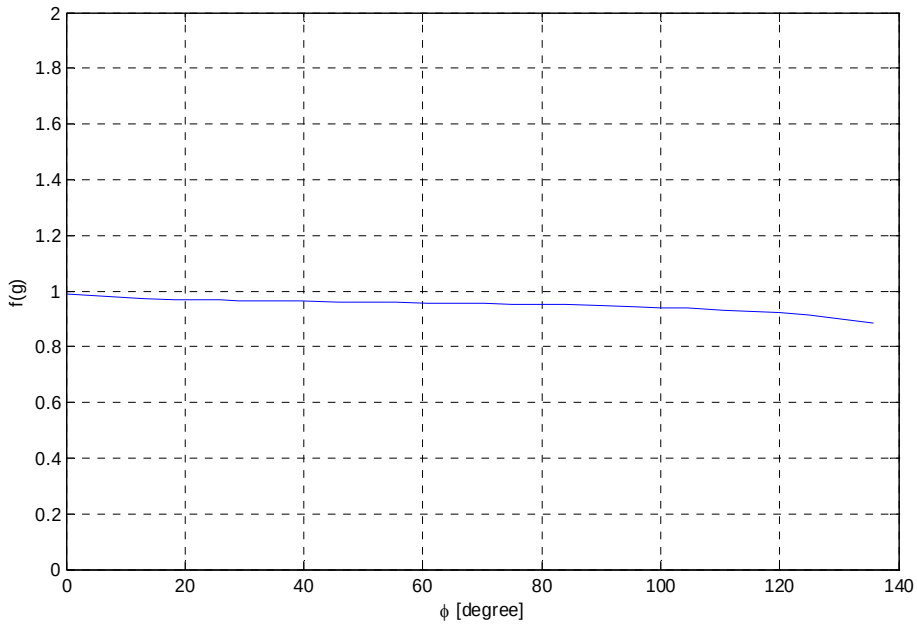

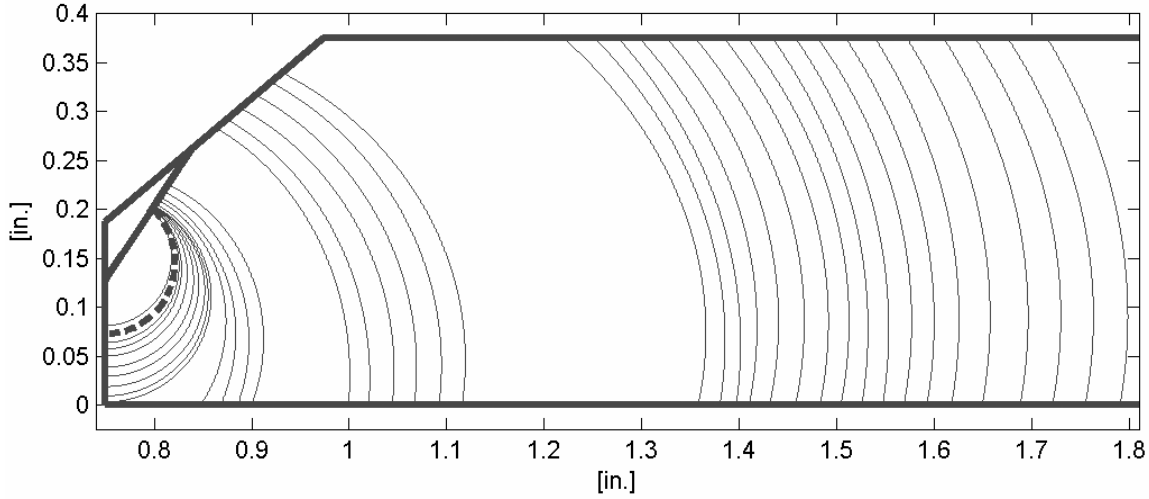

Figure C-40. Corrected BCF for FAA-012 at 17,500-22,000 Cycle, Initial Knee Crack, Type I

Table C-41. Corrected Boundary Correction Factors for FAA-012 (See figure C-41)

Initial Crack Location	Knee
Type	I
Center of Ellipse	(0.75, 0.14175)
Horizontal Axis	0.07535
Vertical Axis	0.07800
Cycle	22000-26000

ϕ [degree]	x [inch]	y [inch]	f(g)
0	0.75	0.06375	1.1386
13.05	0.76695	0.06576	1.1229
18.5	0.77382	0.06778	1.1054
22.62	0.77889	0.06975	1.0911
26.13	0.78308	0.07172	1.0783
29.19	0.78664	0.07365	1.0670
34.56	0.79262	0.07752	1.0461
39.23	0.79753	0.08133	1.0274
45.38	0.8035	0.08696	1.0017
50.84	0.8083	0.0925	0.9783
55.84	0.81223	0.09795	0.9667
60.52	0.81548	0.10337	0.9607
64.96	0.81816	0.10874	0.9548
69.18	0.82033	0.11403	0.9490
73.25	0.82207	0.11927	0.9432
77.2	0.8234	0.12447	0.9375
81.1	0.82437	0.12968	0.9317
82.37	0.82462	0.1314	0.9296
87.42	0.82522	0.13824	0.9218
92.7	0.82503	0.14843	0.9096
96.82	0.82355	0.15859	0.8968
101.64	0.82009	0.17034	0.8812
105.81	0.81546	0.18037	0.8676
110.09	0.80887	0.19044	0.8554
114.47	0.79961	0.20047	0.8474

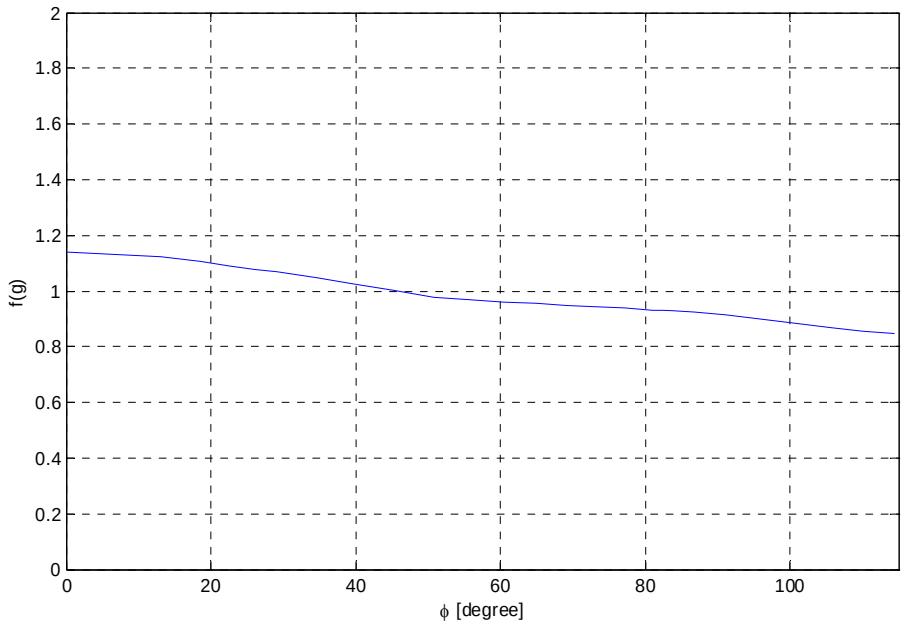

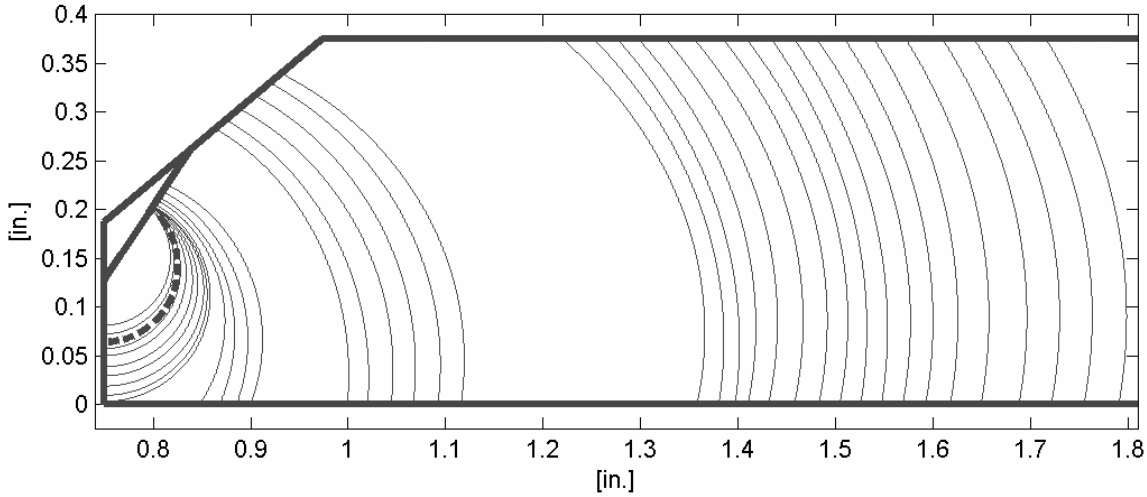

Figure C-41. Corrected BCF for FAA-012 at 22,000-26,000 Cycle, Initial Knee Crack, Type I

Table C-42. Corrected Boundary Correction Factors for FAA-012 (See figure C-42)

Initial Crack Location	Knee
Type	Knee
Center of Ellipse	I
Horizontal Axis	(0.75, 0.1385)
Vertical Axis	0.07785
Cycle	26000-29500

ϕ [degree]	x [inch]	y [inch]	f(g)
0	0.75	0.05726	0.9249
11.22	0.76515	0.05881	0.9204
15.79	0.77118	0.06032	0.9195
22.47	0.77976	0.06343	0.9186
29.92	0.78883	0.06808	0.9186
35.96	0.79572	0.07274	0.9188
42.86	0.80296	0.07895	0.9192
49	0.80875	0.0852	0.9195
54.64	0.81349	0.09148	0.9197
59.88	0.81734	0.09773	0.9197
66.12	0.82119	0.10561	0.9195
72.07	0.82407	0.11349	0.9189
78.94	0.8264	0.12292	0.9178
84.56	0.8275	0.1308	0.9165
89	0.82784	0.13708	0.9152
94.53	0.8276	0.14492	0.9132
99	0.82689	0.15121	0.9111
104.65	0.82531	0.15905	0.9080
109.26	0.82349	0.1653	0.9049
114	0.82111	0.17154	0.9010
118.89	0.81815	0.17775	0.8962
124.03	0.81451	0.18396	0.8900
129.46	0.8101	0.19013	0.8817
135.32	0.80473	0.19626	0.8696
140.16	0.79986	0.20088	0.8560

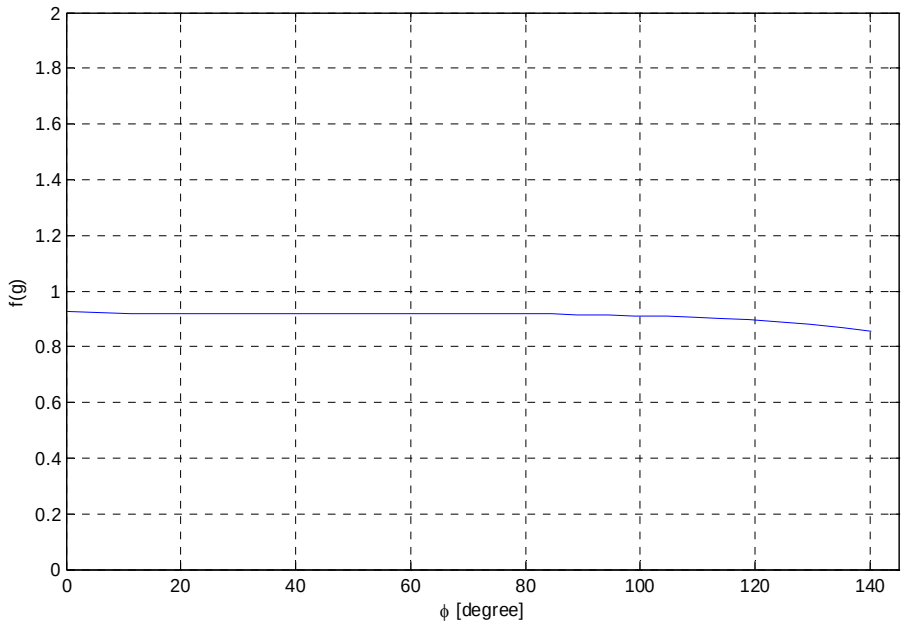

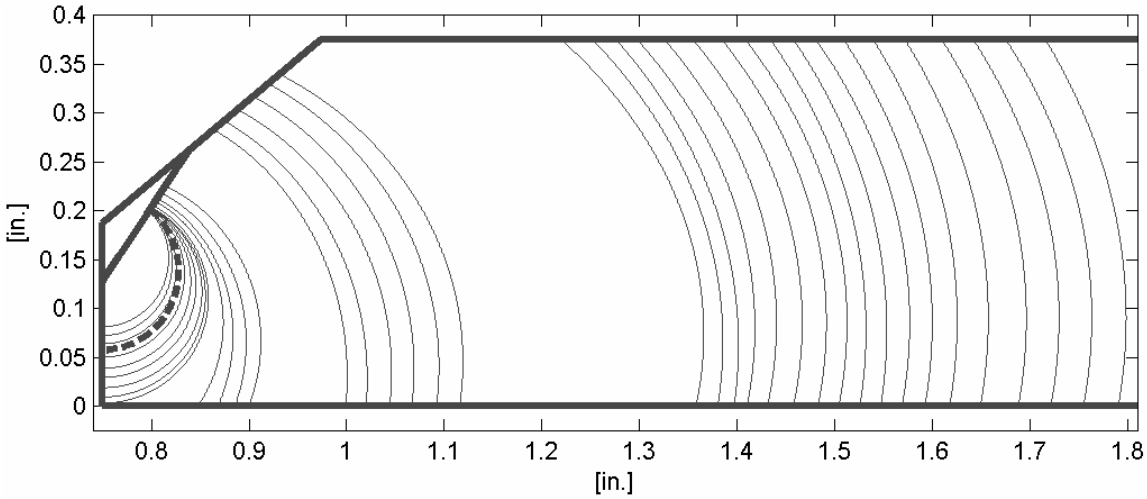

Figure C-42. Corrected BCF for FAA-012 at 26,000-29,500 Cycle, Initial Knee Crack, Type I

Table C-43. Corrected Boundary Correction Factors for FAA-012 (See figure C-43)

Initial Crack Location	Knee
Type	I
Center of Ellipse	(0.75, 0.134)
Horizontal Axis	0.08375
Vertical Axis	0.083995
Cycle	29500-33000

ϕ [degree]	x [inch]	y [inch]	f(g)
0	0.75	0.05001	1.1564
11.03	0.76603	0.05156	1.1462
19.16	0.7775	0.05466	1.1393
24.88	0.78524	0.0578	1.1347
29.56	0.79132	0.06094	1.1310
35.55	0.79871	0.06566	1.1265
40.77	0.8047	0.07039	1.1227
46.99	0.81124	0.0767	1.1115
51.25	0.81532	0.08143	1.1030
56.61	0.81992	0.08778	1.0924
61.66	0.8237	0.09413	1.0823
67.63	0.82742	0.10203	1.0701
73.32	0.83018	0.10989	1.0582
78.82	0.8321	0.11772	1.0459
84.18	0.83323	0.12548	1.0334
89.43	0.83364	0.13316	1.0199
94.62	0.83335	0.14077	1.0051
99.81	0.83238	0.14831	0.9889
105	0.83073	0.15574	0.9705
110.27	0.82838	0.1631	0.9612
116.72	0.82461	0.17176	0.9522
121.16	0.82146	0.17746	0.9446
128.13	0.81566	0.18587	0.9287
135.71	0.80827	0.19413	0.9006
142.81	0.80043	0.20091	0.8305

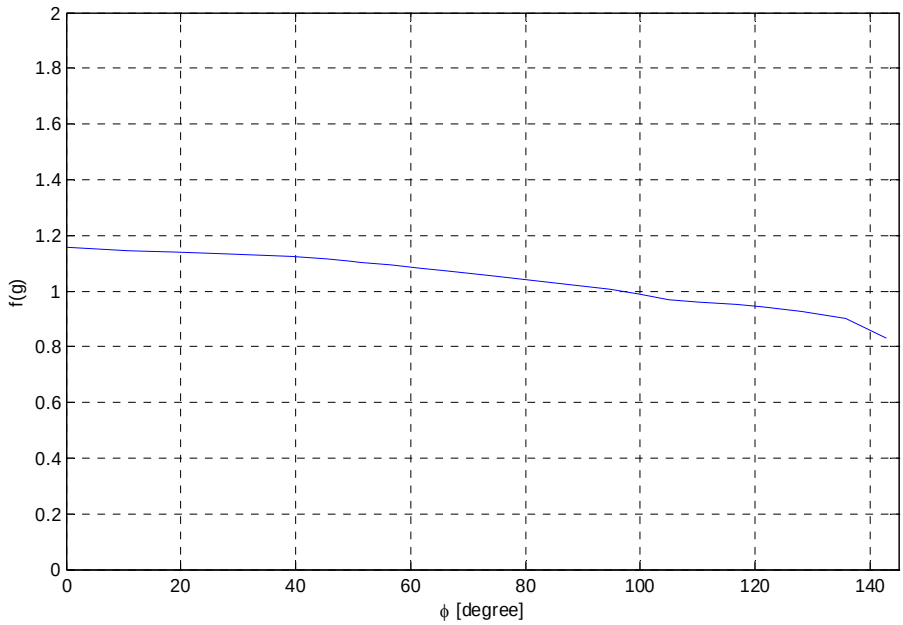

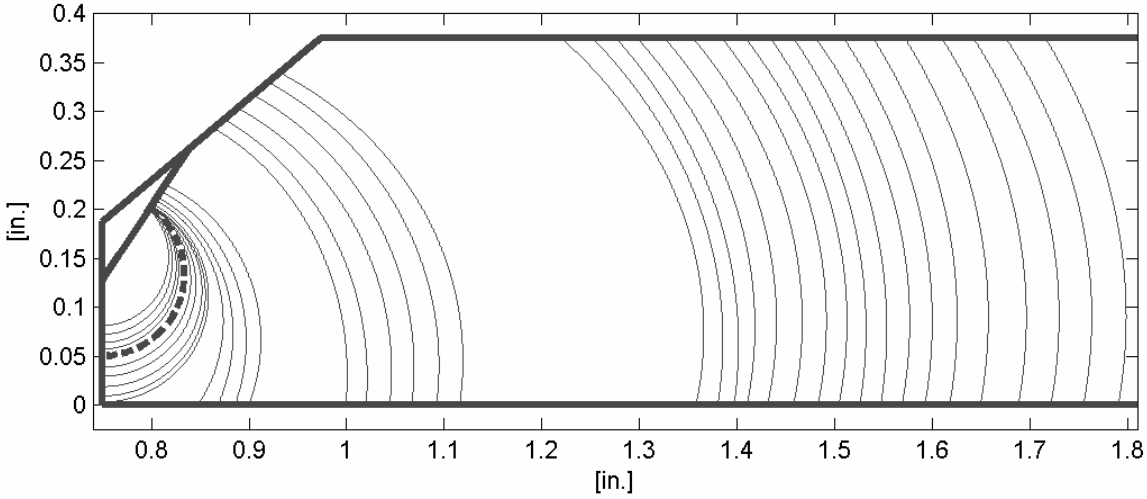

Figure C-43. Corrected BCF for FAA-012 at 29,500-33,000 Cycle, Initial Knee Crack, Type I

Table C-44. Corrected Boundary Correction Factors for FAA-012 (See figure C-44)

Initial Crack Location	Knee
Type	I
Center of Ellipse	(0.75, 0.1275)
Horizontal Axis	0.09025
Vertical Axis	0.08890
Cycle	33000-34750

ϕ [degree]	x [inch]	y [inch]	f(g)
0	0.75	0.0386	1.2246
10.48	0.7664	0.04008	1.2087
18.27	0.77827	0.04308	1.1938
23.62	0.78612	0.04605	1.1822
29.98	0.79506	0.05049	1.167
35.26	0.80205	0.05491	1.1533
41.32	0.80954	0.06074	1.1364
46.73	0.81566	0.06656	1.1204
53.95	0.82292	0.07519	1.0974
59.49	0.8277	0.08237	1.0789
65.66	0.83218	0.09086	1.0569
71.51	0.83554	0.09931	1.0351
76.22	0.8376	0.10632	1.0168
82.58	0.83945	0.11602	0.9908
88.83	0.84019	0.12569	0.964
94.14	0.83998	0.13391	0.9563
99.45	0.83899	0.1421	0.9495
104.83	0.83722	0.15025	0.9424
110.3	0.83462	0.15834	0.935
116.94	0.83044	0.16777	0.9253
122.93	0.82574	0.17582	0.9158
128.24	0.82087	0.18253	0.9063
133.95	0.81497	0.1892	0.8945
140.27	0.80768	0.19587	0.8781
145.99	0.80048	0.20119	0.8581

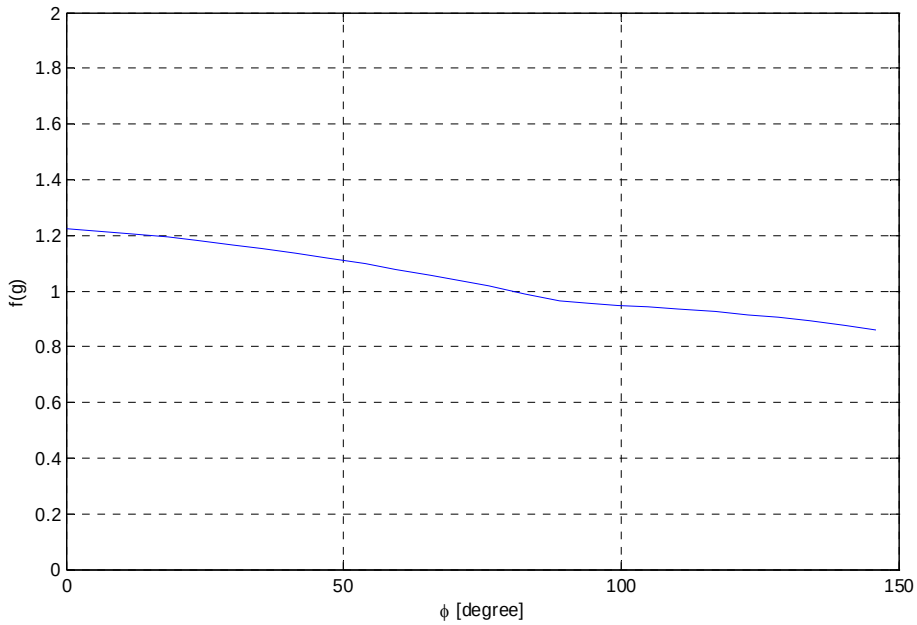

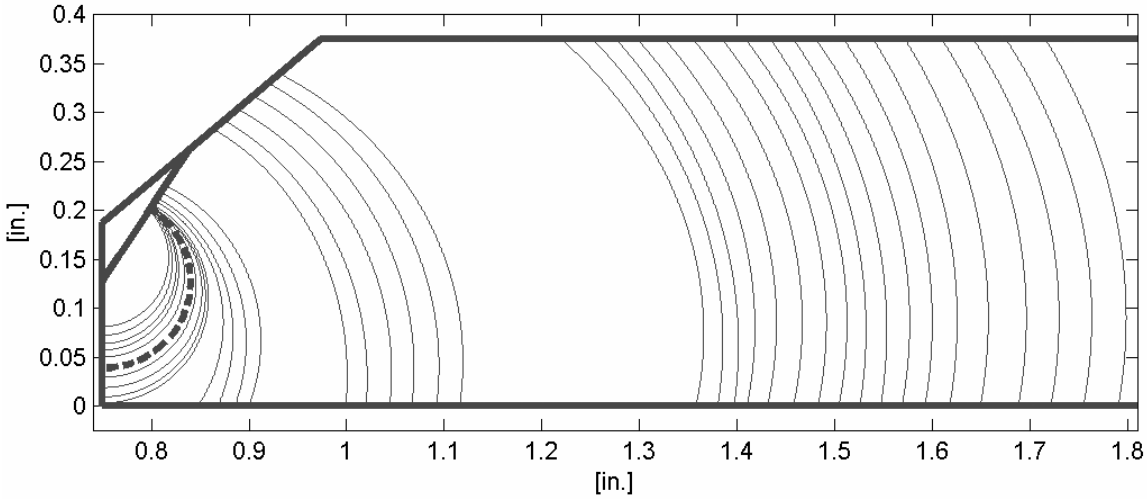

Figure C-44. Corrected BCF for FAA-012 at 33,000-34,750 Cycle, Initial Knee Crack, Type I

Table C-45. Corrected Boundary Correction Factors for FAA-012 (See figure C-45)

Initial Crack Location	Knee
Type	I
Center of Ellipse	(0.75, 0.1225)
Horizontal Axis	0.09550
Vertical Axis	0.09315
Cycle	34750-36250

ϕ [degree]	x [inch]	y [inch]	f(g)
0	0.75	0.02935	1.2202
9.57	0.76588	0.03065	1.2102
16.68	0.77742	0.03327	1.2038
21.66	0.78525	0.03593	1.1997
27.46	0.79404	0.03985	1.1952
33.87	0.80323	0.04516	1.1905
40.59	0.81214	0.05176	1.1856
46.52	0.8193	0.0584	1.1810
52.97	0.82624	0.0664	1.1754
58.91	0.83178	0.0744	1.1695
65.42	0.83684	0.08376	1.1618
71.59	0.8406	0.09309	1.1531
77.55	0.84323	0.10241	1.1430
83.35	0.84483	0.11171	1.1315
89.86	0.84546	0.12227	1.1149
95.5	0.84501	0.13143	1.1011
101.98	0.84336	0.14184	1.0814
106.9	0.84131	0.14958	1.0644
112.75	0.83799	0.15853	1.0413
118.83	0.83359	0.16741	1.0134
124.26	0.82885	0.17494	0.9835
131.01	0.82197	0.18363	0.9529
136.23	0.81598	0.18976	0.9392
141.96	0.80877	0.19586	0.9175
148.51	0.79981	0.20193	0.8667

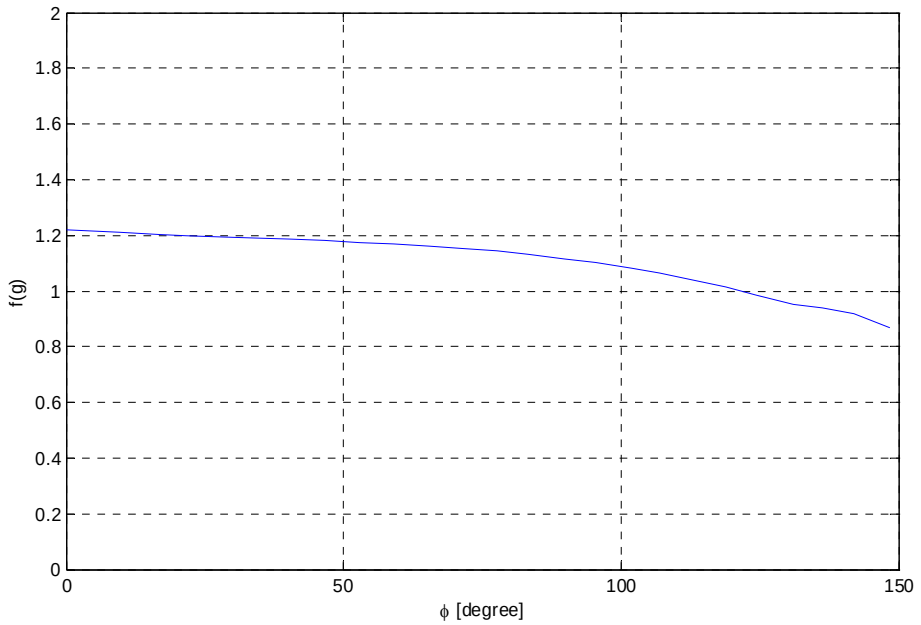

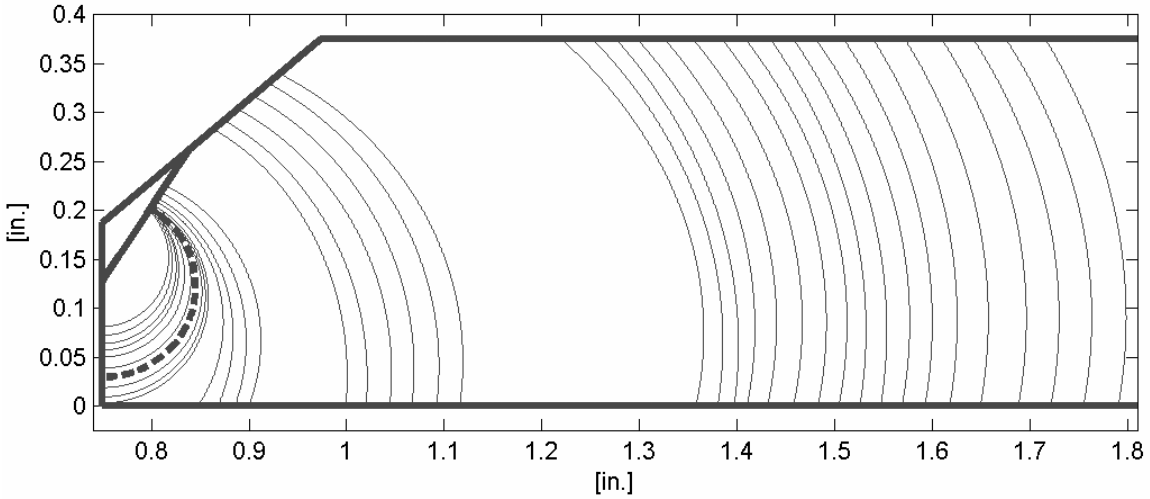

Figure C-45. Corrected BCF for FAA-012 at 34,750-36,250 Cycle, Initial Knee Crack, Type I

Table C-46. Corrected Boundary Correction Factors for FAA-012 (See figure C-46)

Initial Crack Location	Knee
Type	I
Center of Ellipse	(0.75, 0.11675)
Horizontal Axis	0.10175
Vertical Axis	0.09800
Cycle	36250-37100

ϕ [degree]	x [inch]	y [inch]	f(g)
0	0.75	0.01875	1.5802
9.38	0.76657	0.02006	1.5556
18.88	0.7829	0.02402	1.5303
25.07	0.79308	0.02798	1.5059
30.04	0.8009	0.03191	1.4514
36.95	0.81112	0.03843	1.3845
42.9	0.81921	0.04496	1.3524
48.19	0.82579	0.05142	1.3368
54.91	0.8332	0.06041	1.3159
60.23	0.83826	0.06809	1.2984
66.85	0.84349	0.07822	1.2750
72.35	0.8469	0.08703	1.2545
78.4	0.84961	0.09704	1.2306
84.98	0.8513	0.10818	1.2028
90.73	0.85168	0.118	1.1768
96.46	0.85105	0.12777	1.1493
102.91	0.84913	0.13864	1.1159
108.76	0.8463	0.14826	1.0890
114.78	0.84234	0.15782	1.0561
120.25	0.83785	0.16613	1.0235
126.88	0.83135	0.17557	0.9792
132.24	0.8253	0.18262	0.9507
138.06	0.81797	0.18965	0.9350
144.65	0.80885	0.19668	0.9098
151.03	0.79927	0.20249	0.8620

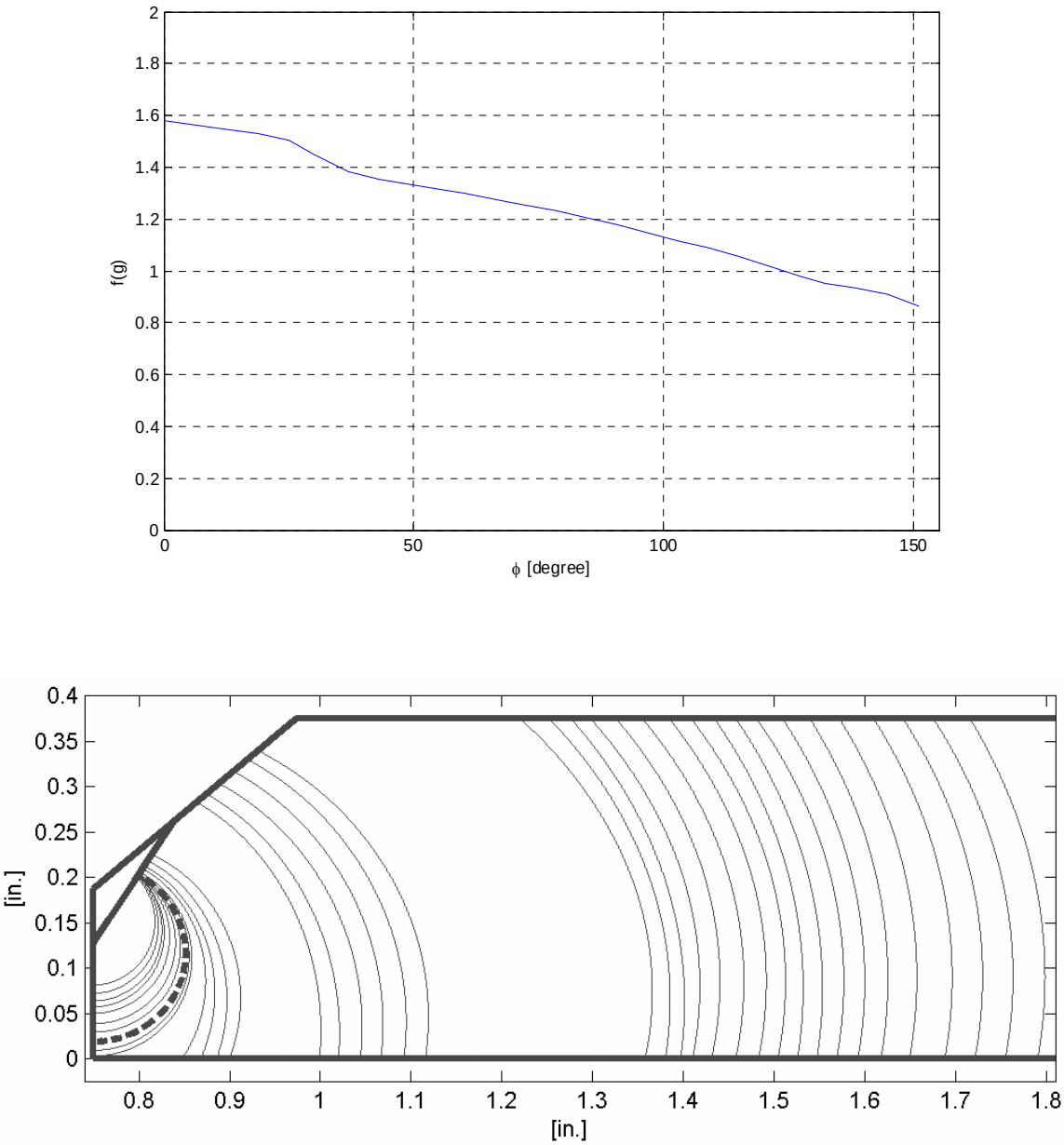

Figure C-46. Corrected BCF for FAA-012 at 36,250-37,100 Cycle, Initial Knee Crack, Type I

Table C-47. Corrected Boundary Correction Factors for FAA-012 (See figure C-47)

Initial Crack Location	Knee
Type	I
Center of Ellipse	(0.75, 0.11225)
Horizontal Axis	0.10525
Vertical Axis	0.10300
Cycle	37100-37400

ϕ [degree]	x [inch]	y [inch]	f(g)
0	0.75	0.00925	1.6330
8.8	0.76609	0.01046	1.6075
15.22	0.77761	0.01286	1.5874
24.96	0.79439	0.01887	1.5555
30.65	0.80362	0.02364	1.5361
36.63	0.81276	0.02959	1.5152
42.79	0.82147	0.03667	1.4933
48.29	0.82855	0.04372	1.4300
54.92	0.83611	0.05306	1.3435
60.28	0.84138	0.06118	1.3123
66.75	0.84668	0.07159	1.2727
72.87	0.85056	0.08191	1.2335
78.78	0.85322	0.09221	1.1950
84.54	0.85476	0.10245	1.1577
90.85	0.85523	0.11379	1.1182
96.55	0.85456	0.124	1.0867
102.92	0.85258	0.13528	1.0580
108.79	0.84964	0.14543	1.0406
114.9	0.84547	0.15561	1.0335
120.57	0.84062	0.16464	1.0373
126.62	0.83447	0.17369	1.0519
132.34	0.8278	0.18162	1.0736
138.65	0.81953	0.18957	1.1037
144.78	0.81069	0.1964	1.1176
150.73	0.80147	0.2021	1.1288

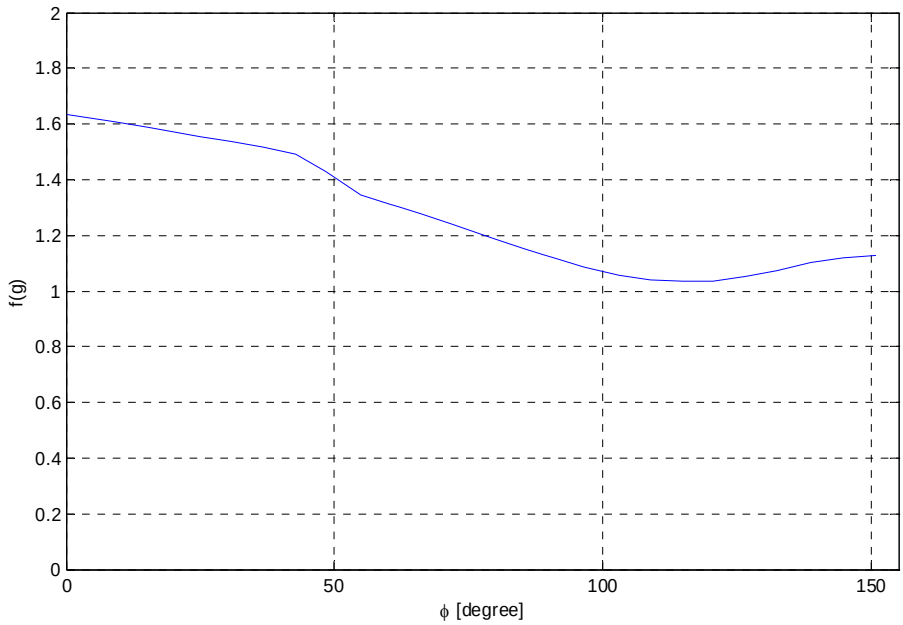

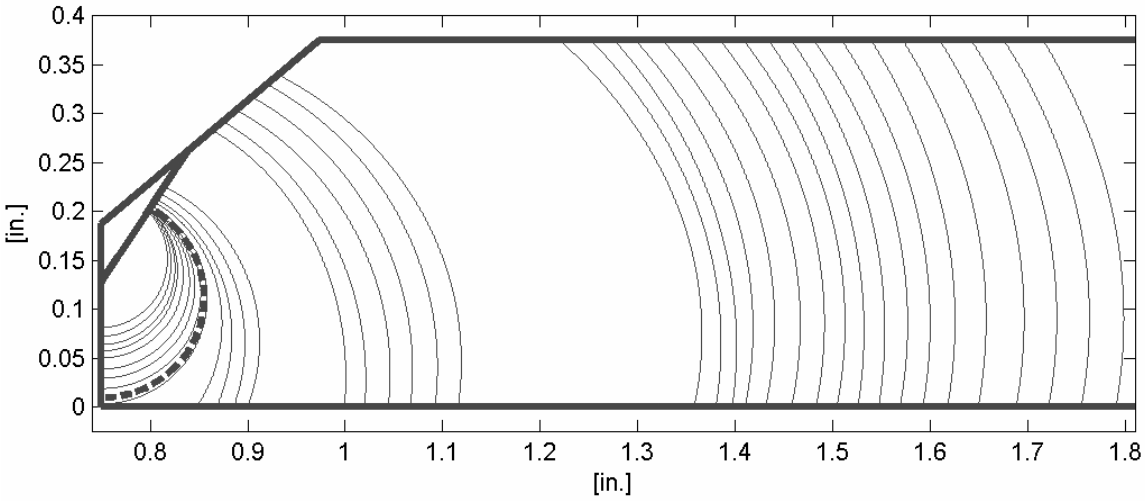

Figure C-47. Corrected BCF for FAA-012 at 37,100-37,400 Cycle, Initial Knee Crack, Type I

Table C-48. Corrected Boundary Correction Factors for FAA-012 (See figure C-48)

Initial Crack Location	Knee
Type	I
Center of Ellipse	(0.75, 0.1105)
Horizontal Axis	0.10825
Vertical Axis	0.10750
Cycle	37400-37600

ϕ [degree]	x [inch]	y [inch]	f(g)
0	0.75	0.003	1.8744
8.23	0.7655	0.00411	1.7477
11.65	0.77186	0.00522	1.6976
18.52	0.78438	0.00857	1.6251
24.9	0.79558	0.013	1.6075
30.05	0.80421	0.01745	1.5938
36.51	0.81441	0.0241	1.5773
42.11	0.82258	0.03074	1.5640
48.72	0.83135	0.03958	1.5493
54.72	0.83837	0.04841	1.5371
60.98	0.84466	0.05835	1.5257
66.85	0.84953	0.06824	1.5164
72.49	0.85323	0.07815	1.5086
84.44	0.85774	0.10009	1.4968
90.87	0.85824	0.11214	1.4929
96.72	0.85751	0.12308	1.4912
102.62	0.85563	0.13399	1.4911
108.68	0.85255	0.14493	1.4926
114.95	0.84815	0.15584	1.4960
120.86	0.84292	0.16565	1.5010
126.45	0.83707	0.17437	1.5071
132.48	0.82984	0.1831	1.5152
138.28	0.82204	0.19074	1.5245
144.84	0.81234	0.19839	1.5366
151.44	0.80175	0.20492	1.5504

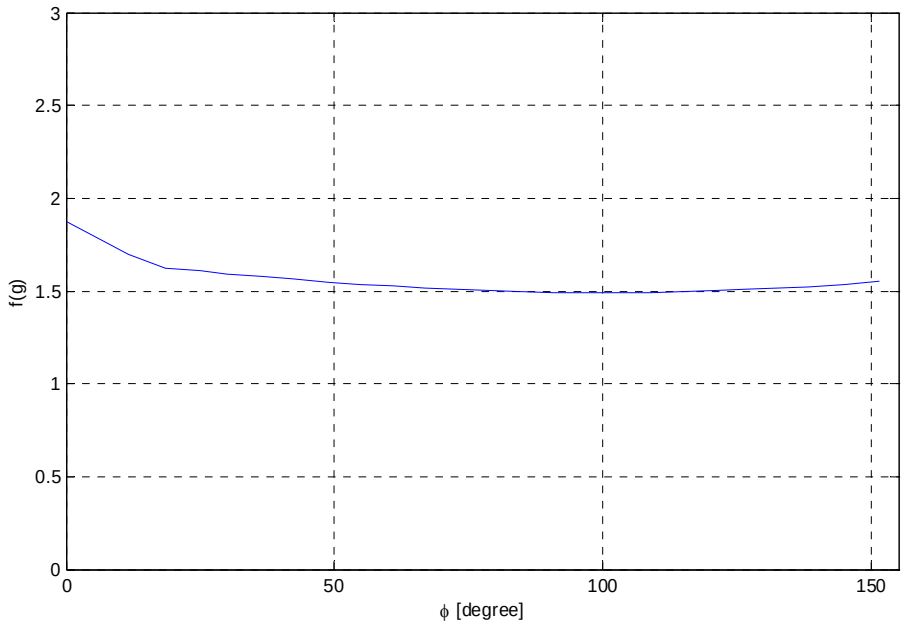

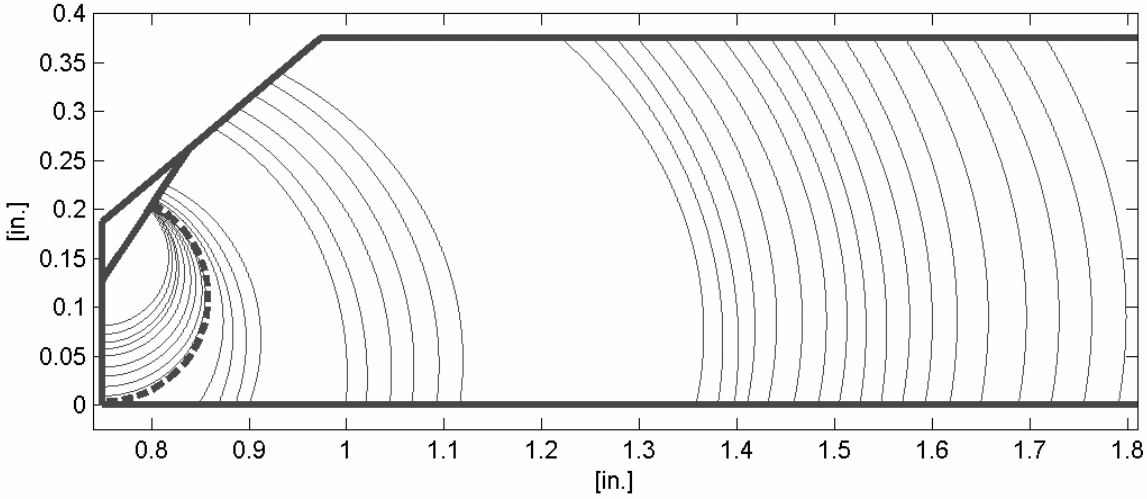

Figure C-48. Corrected BCF for FAA-012 at 37,400-37,600 Cycle, Initial Knee Crack, Type I

Table C-49. Corrected Boundary Correction Factors for FAA-012 (See figure C-49)

Initial Crack Location	Knee
Type	II
Center of Ellipse	(0.75, 0.085)
Horizontal Axis	0.12350
Vertical Axis	0.13800
Cycle	38100-38300

ϕ [degree]	x [inch]	y [inch]	f(g)
-38.35	0.84686	0	1.7394
-34.92	0.85127	0.00618	1.9586
-30.38	0.85655	0.01541	1.9108
-26.67	0.86036	0.02329	1.8754
-22.51	0.86409	0.03243	1.8164
-18.53	0.8671	0.04148	1.7742
-14.11	0.86977	0.05179	1.7612
-10.89	0.87128	0.05948	1.7523
-6.74	0.87265	0.0697	1.7408
-2.14	0.87341	0.0849	1.7247
2.18	0.87341	0.08616	1.7233
10.15	0.87157	0.10881	1.7008
14.31	0.86967	0.11878	1.6910
18.04	0.86743	0.12749	1.6824
22.41	0.86417	0.13743	1.6723
26.34	0.86068	0.14607	1.6630
30.39	0.85653	0.15469	1.6532
34.61	0.85165	0.16327	1.6425
38.38	0.84681	0.1706	1.6321
42.35	0.84128	0.17789	1.5925
50.37	0.82877	0.19124	1.4453
54.47	0.82176	0.19727	1.3978
58.06	0.81534	0.20207	1.3520
61	0.80987	0.20567	1.3111
64.22	0.80372	0.20924	1.2632

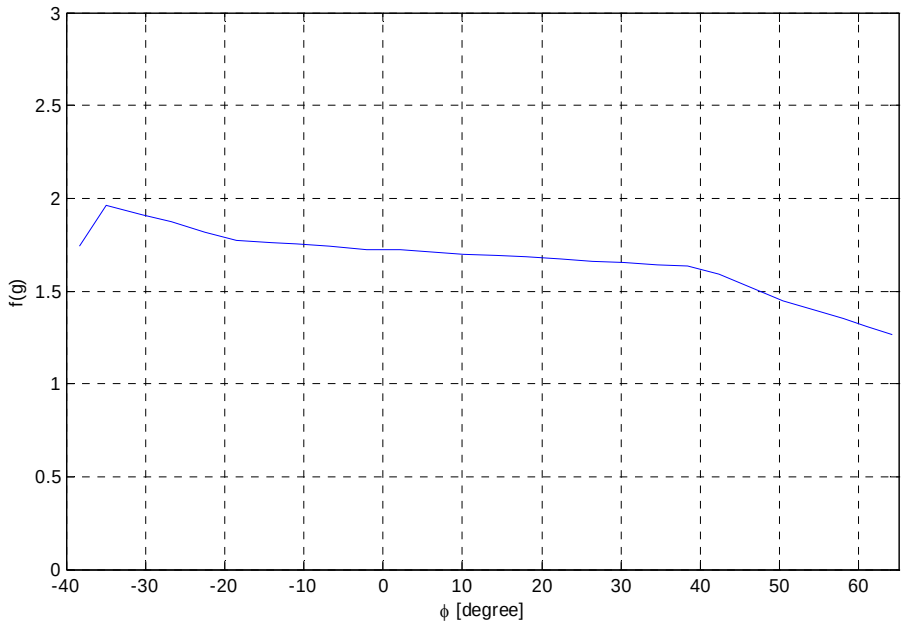

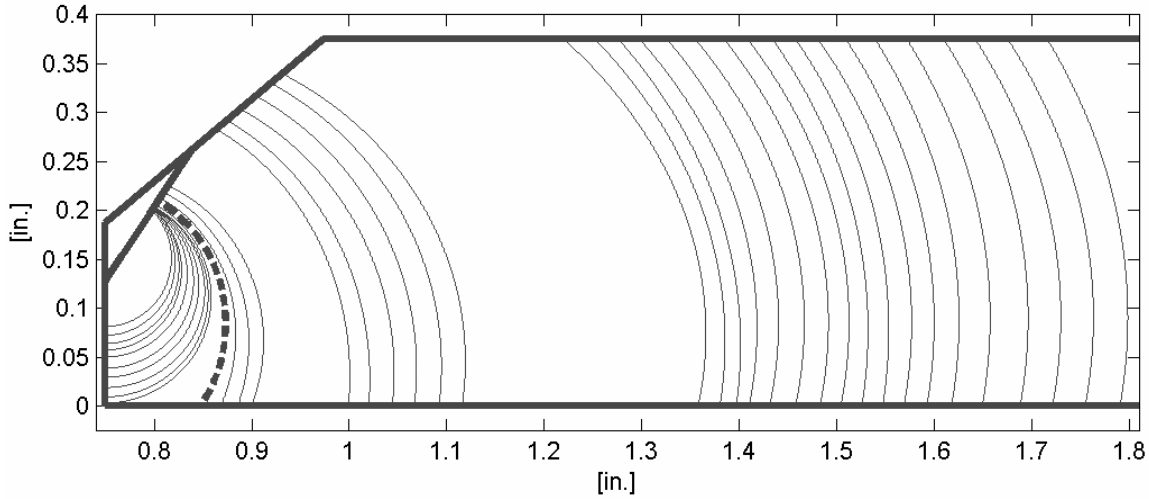

Figure C-49. Corrected BCF for FAA-012 at 38,100-38,300 Cycle, Initial Knee Crack, Type II

Table C-50. Corrected Boundary Correction Factors for FAA-012 (See figure C-50)

Initial Crack Location	Knee
Type	II
Center of Ellipse	(0.75, 0.0725)
Horizontal Axis	0.13350
Vertical Axis	0.15400
Cycle	38300-38525

ϕ [degree]	x [inch]	y [inch]	f(g)
-28.85	0.86693	0	1.7678
-24.86	0.87113	0.00884	1.8898
-20.86	0.87475	0.01885	1.8510
-16.53	0.87798	0.03001	1.8147
-12.83	0.88017	0.03981	1.7685
-8.84	0.88192	0.05076	1.7535
-4.79	0.88303	0.06282	1.7382
-2.88	0.88333	0.07362	1.7258
2.96	0.88332	0.07483	1.7245
6.27	0.8827	0.08796	1.7113
10.01	0.88147	0.09864	1.7019
14.4	0.87931	0.1105	1.6932
18.01	0.87696	0.11994	1.6877
22.19	0.87361	0.13059	1.6833
26.02	0.86997	0.14003	1.6812
30.5	0.86503	0.15065	1.6812
34.13	0.86051	0.15891	1.6833
38.5	0.85448	0.16838	1.6881
42.55	0.84834	0.17667	1.6947
46.26	0.8423	0.18378	1.7024
50.27	0.83533	0.19095	1.7125
54.65	0.82724	0.19812	1.7253
58.71	0.81934	0.20411	1.7387
62.35	0.81196	0.20892	1.7516
65.29	0.80581	0.2124	1.7634

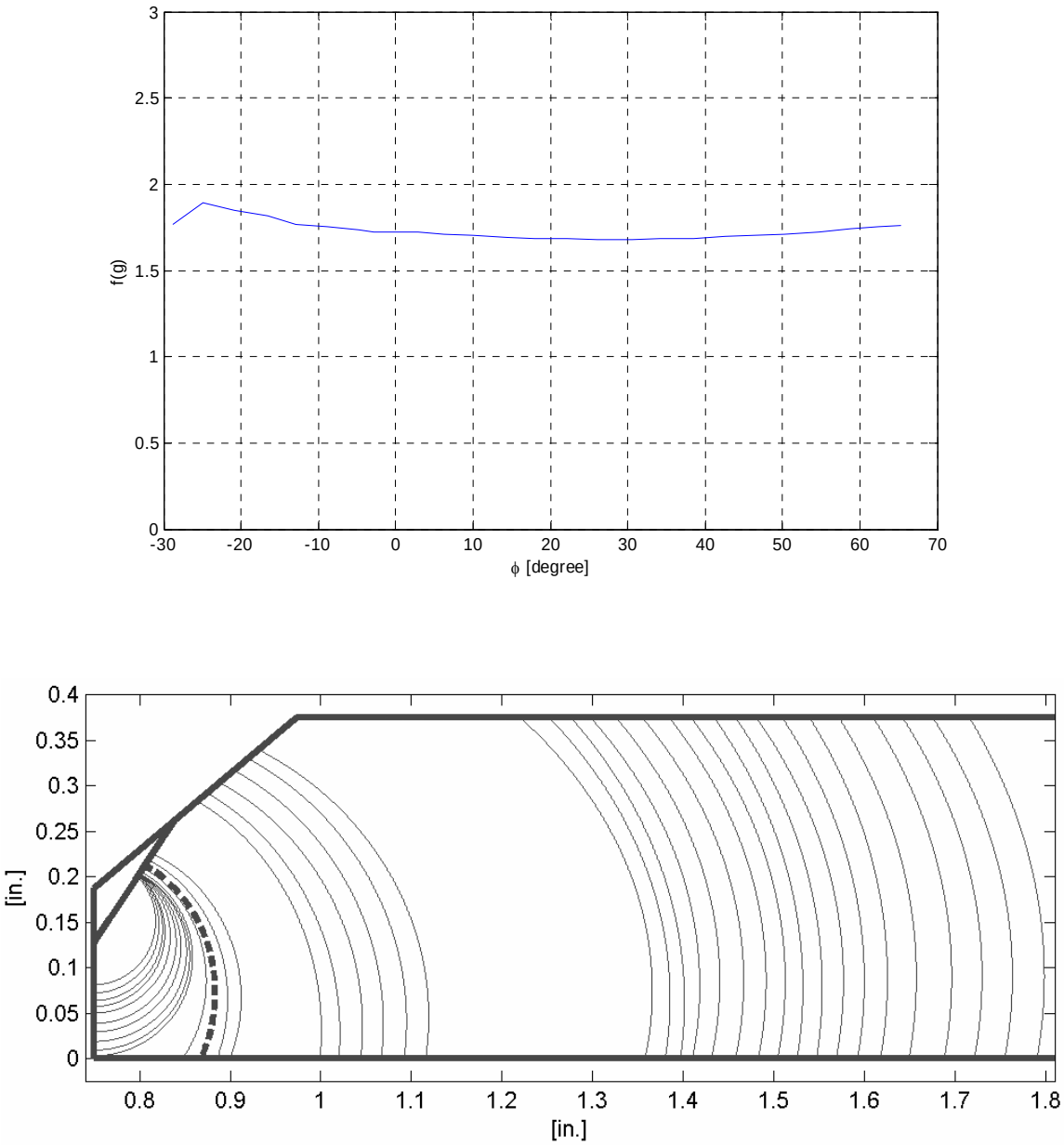

Figure C-50. Corrected BCF for FAA-012 at 38,300-38,525 Cycle, Initial Knee Crack, Type II

Table C-51. Corrected Boundary Correction Factors for FAA-012 (See figure C-51)

Initial Crack Location	Knee
Type	II
Center of Ellipse	(0.75, 0.065)
Horizontal Axis	0.14700
Vertical Axis	0.167500
Cycle	38525-38750

ϕ [degree]	x [inch]	y [inch]	f(g)
-22.82	0.88549	0	1.7493
-19.14	0.88887	0.01015	1.8133
-15.76	0.89147	0.01957	1.7995
-12.43	0.89356	0.02901	1.7875
-9.13	0.89514	0.03846	1.7790
-5.86	0.89623	0.04793	1.7731
-2.6	0.89685	0.05741	1.7697
-0.16	0.897	0.06453	1.7688
0.24	0.897	0.0657	1.7688
3.5	0.89673	0.07521	1.7705
10.45	0.89456	0.09533	1.7824
14.17	0.89253	0.10595	1.7935
17.54	0.89017	0.1154	1.8064
21.37	0.88689	0.12596	1.8211
24.43	0.88384	0.13417	1.8228
31.66	0.87513	0.1528	1.8271
34.97	0.87046	0.16089	1.8280
38.4	0.86521	0.16892	1.8297
45.77	0.85254	0.18491	1.8315
49.19	0.84607	0.19168	1.8315
52.85	0.83877	0.19842	1.8315
56.12	0.83194	0.20398	1.8315
59.68	0.82421	0.20952	1.8323
63.64	0.81527	0.21503	1.8350
66.09	0.80958	0.21809	1.8428

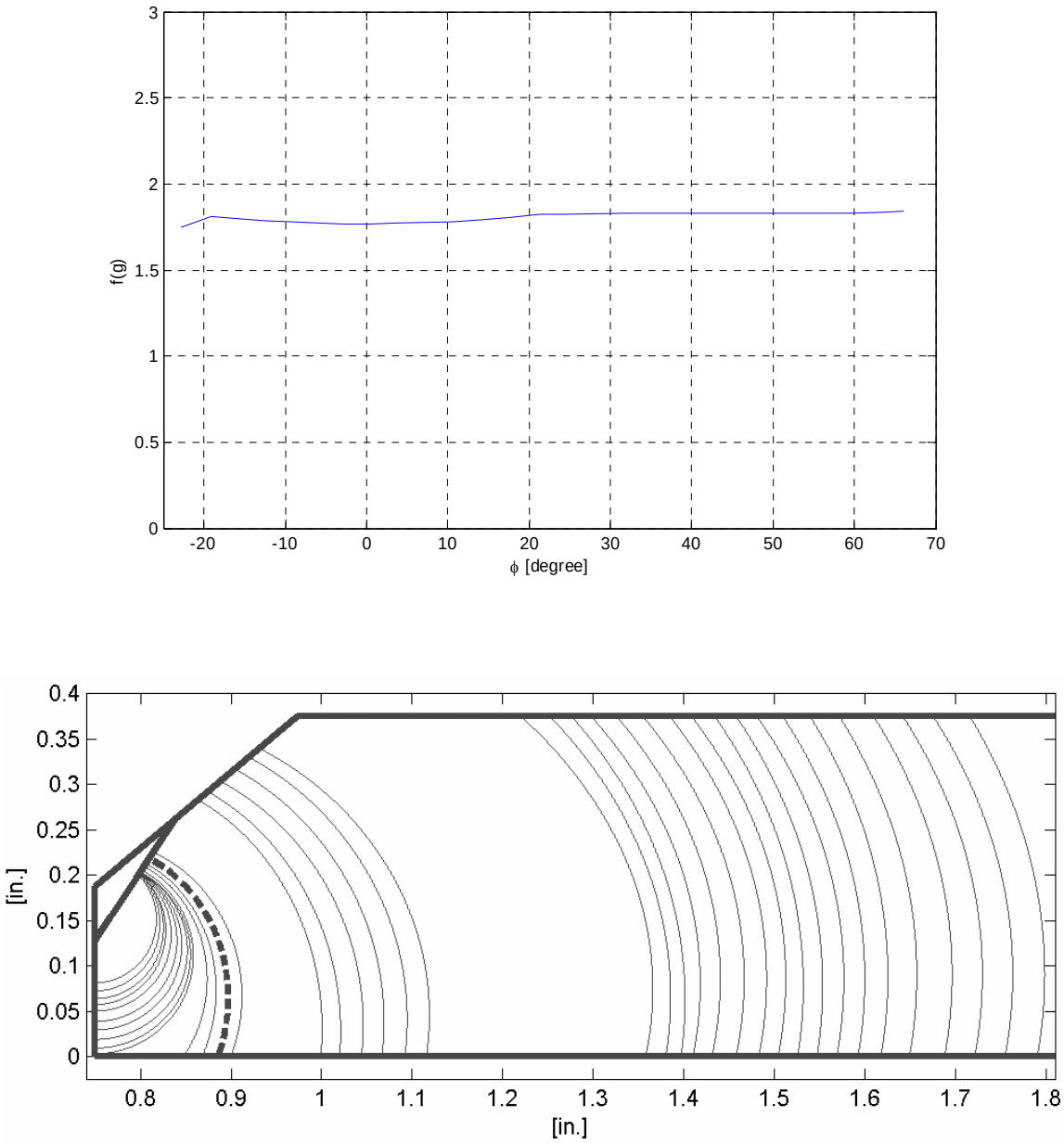

Figure C-51. Corrected BCF for FAA-012 at 38,525-38,750 Cycle, Initial Knee Crack, Type II

Table C-52. Corrected Boundary Correction Factors for FAA-012 (See figure C-52)

Initial Crack Location	Knee
Type	II
Center of Ellipse	(0.75, 0.066)
Horizontal Axis	0.162000
Vertical Axis	0.173000
Cycle	38750-38975

ϕ [degree]	x [inch]	y [inch]	f(g)
-22.43	0.89975	0	1.7394
-19.28	0.90292	0.00899	1.7298
-15.71	0.90595	0.01925	1.7299
-12.2	0.90834	0.02954	1.7305
-8.72	0.91013	0.03986	1.7310
-5.28	0.91131	0.05018	1.7318
-1.86	0.91191	0.06053	1.7327
-0.35	0.912	0.06629	1.7332
0.57	0.91199	0.06742	1.7334
2.39	0.91186	0.07318	1.7341
9.67	0.9097	0.09506	1.7374
13.17	0.90774	0.10541	1.7393
20.32	0.90191	0.12608	1.7568
23.6	0.89845	0.13525	1.7696
26.95	0.89441	0.14439	1.7832
30.4	0.88973	0.15352	1.7987
33.96	0.88437	0.16261	1.8169
37.67	0.87824	0.17169	1.8380
41.05	0.87217	0.17959	1.8583
47.82	0.85877	0.19418	1.9059
51.25	0.8514	0.20089	1.9342
54.92	0.8431	0.20755	1.9675
58.25	0.83524	0.21309	2.0003
61.93	0.82624	0.21863	2.0423
66.7	0.81408	0.22489	2.1136

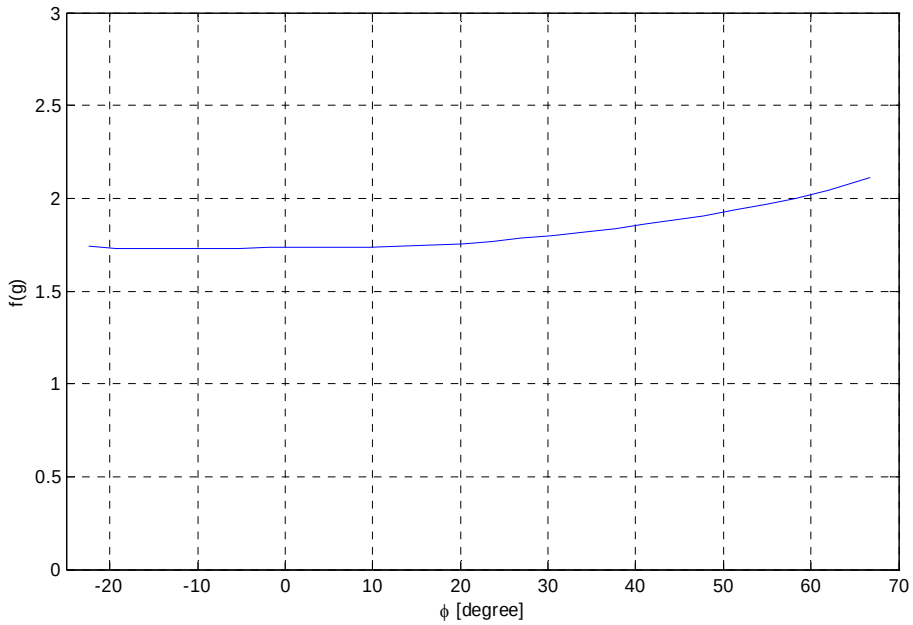

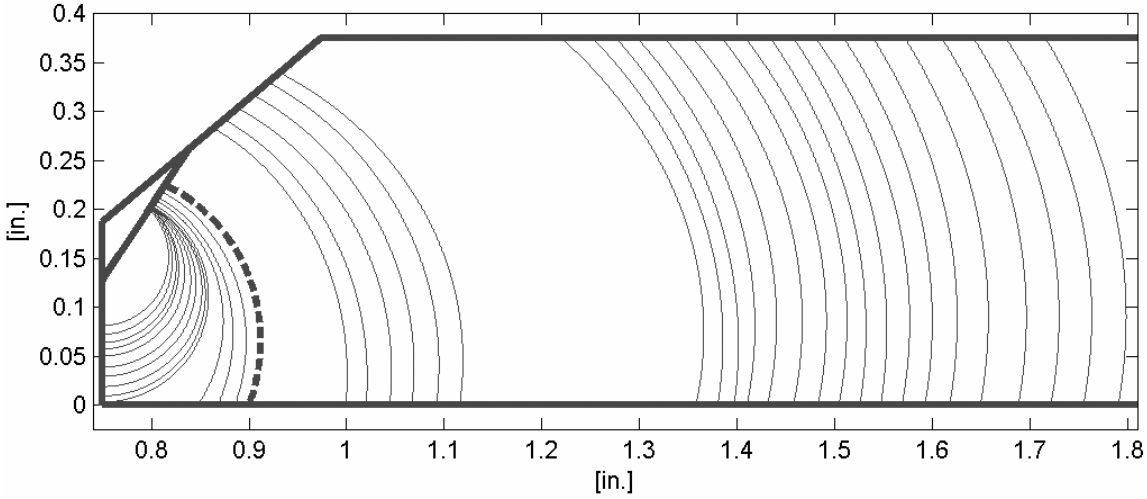

Figure C-52. Corrected BCF for FAA-012 at 38,750-38,975 Cycle, Initial Knee Crack, Type II

Table C-53. Corrected Boundary Correction Factors for FAA-012 (See figure C-53)

Initial Crack Location	Knee
Type	II
Center of Ellipse	(0.75, 0.03)
Horizontal Axis	0.25050
Vertical Axis	0.28350
Cycle	40125-40275

ϕ [degree]	x [inch]	y [inch]	f(g)
-6.56	0.99886	0	1.7491
-5.14	0.99949	0.00732	1.8347
-4.19	0.99983	0.01253	1.8286
-3.11	1.00013	0.01905	1.8234
-2.07	1.00034	0.03078	1.8147
2.09	1.00033	0.03206	1.8138
3.81	0.99995	0.04633	1.8069
6.19	0.99904	0.05928	1.8043
9.49	0.99707	0.07608	1.8069
12.1	0.99494	0.089	1.8121
14.74	0.99226	0.10185	1.8216
19.88	0.98557	0.1263	1.8505
22.94	0.98068	0.14044	1.8771
28.11	0.97094	0.16357	1.8896
30.79	0.96518	0.17514	1.9058
34.8	0.9557	0.19181	1.9423
37.04	0.94994	0.20081	1.9700
40.04	0.94178	0.21241	2.0150
46.48	0.92249	0.2356	2.1434
49.6	0.91235	0.24592	2.2225
52.94	0.90095	0.25626	2.3200
59.03	0.8789	0.2731	2.5341
61.14	0.8709	0.27831	2.6193
62.77	0.86461	0.2821	2.6912
63.06	0.86349	0.28273	2.7710

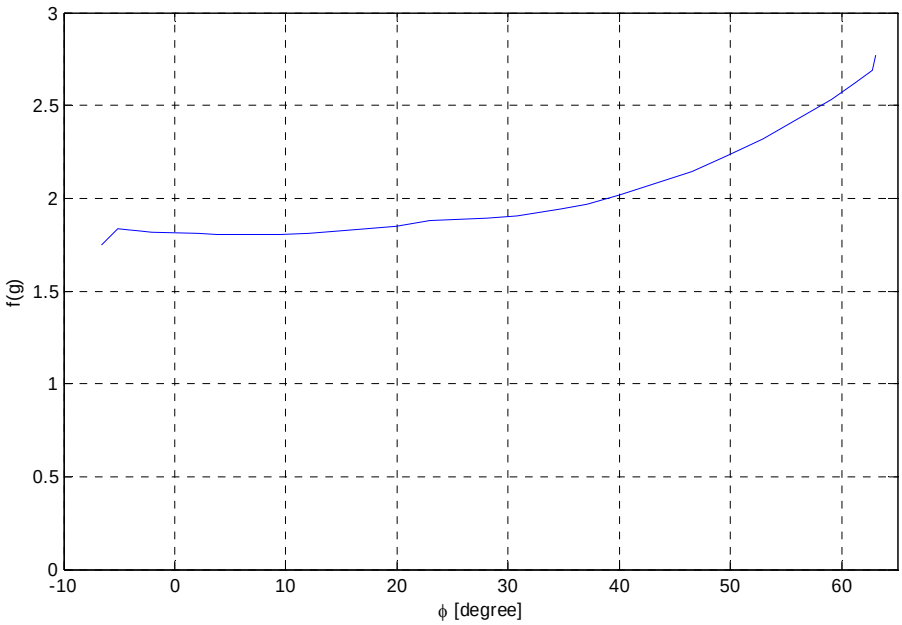

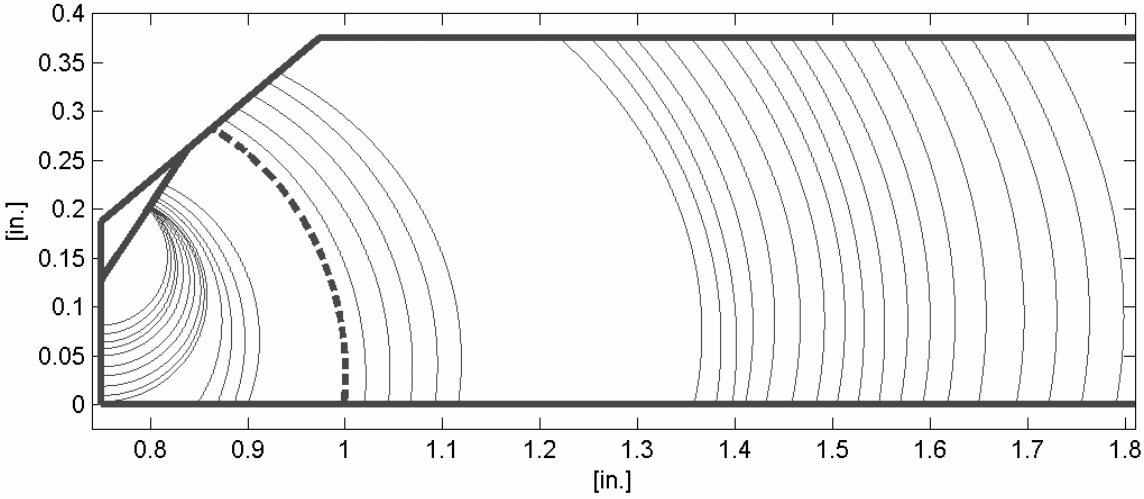

Figure C-53. Corrected BCF for FAA-012 at 40,125-40,275 Cycle, Initial Knee Crack, Type II

Table C-54. Corrected Boundary Correction Factors for FAA-012 (See figure C-54)

Initial Crack Location	Knee
Type	II
Center of Ellipse	(0.75, 0.027)
Horizontal Axis	0.27100
Vertical Axis	0.29800
Cycle	40275-40500

ϕ [degree]	x [inch]	y [inch]	f(g)
-5.43	1.01978	0	1.7791
-4.36	1.02022	0.00628	1.8155
-3.2	1.02058	0.01276	1.8155
-2.15	1.02081	0.01923	1.8155
-1.79	1.02087	0.02183	1.8164
-1.41	1.02092	0.02831	1.8173
1.45	1.02091	0.02961	1.8181
3.21	1.02058	0.04262	1.8225
5.58	1.01972	0.05563	1.8304
8.05	1.01833	0.06864	1.8401
10.57	1.0164	0.08169	1.8534
12.86	1.0142	0.0934	1.8677
17.79	1.00804	0.11815	1.9066
20.18	1.00437	0.12986	1.9295
24.78	0.99605	0.15195	1.9816
27.27	0.99087	0.1636	2.0149
32.42	0.97875	0.18679	2.0935
38.48	0.96215	0.2124	2.2086
41.67	0.95243	0.22508	2.2788
47.46	0.93321	0.24652	2.4270
50.4	0.92275	0.25654	2.5122
53.51	0.91118	0.2665	2.6119
59.53	0.88743	0.28378	2.8340
61.93	0.87751	0.28989	2.9351
62.69	0.87433	0.29182	2.9842

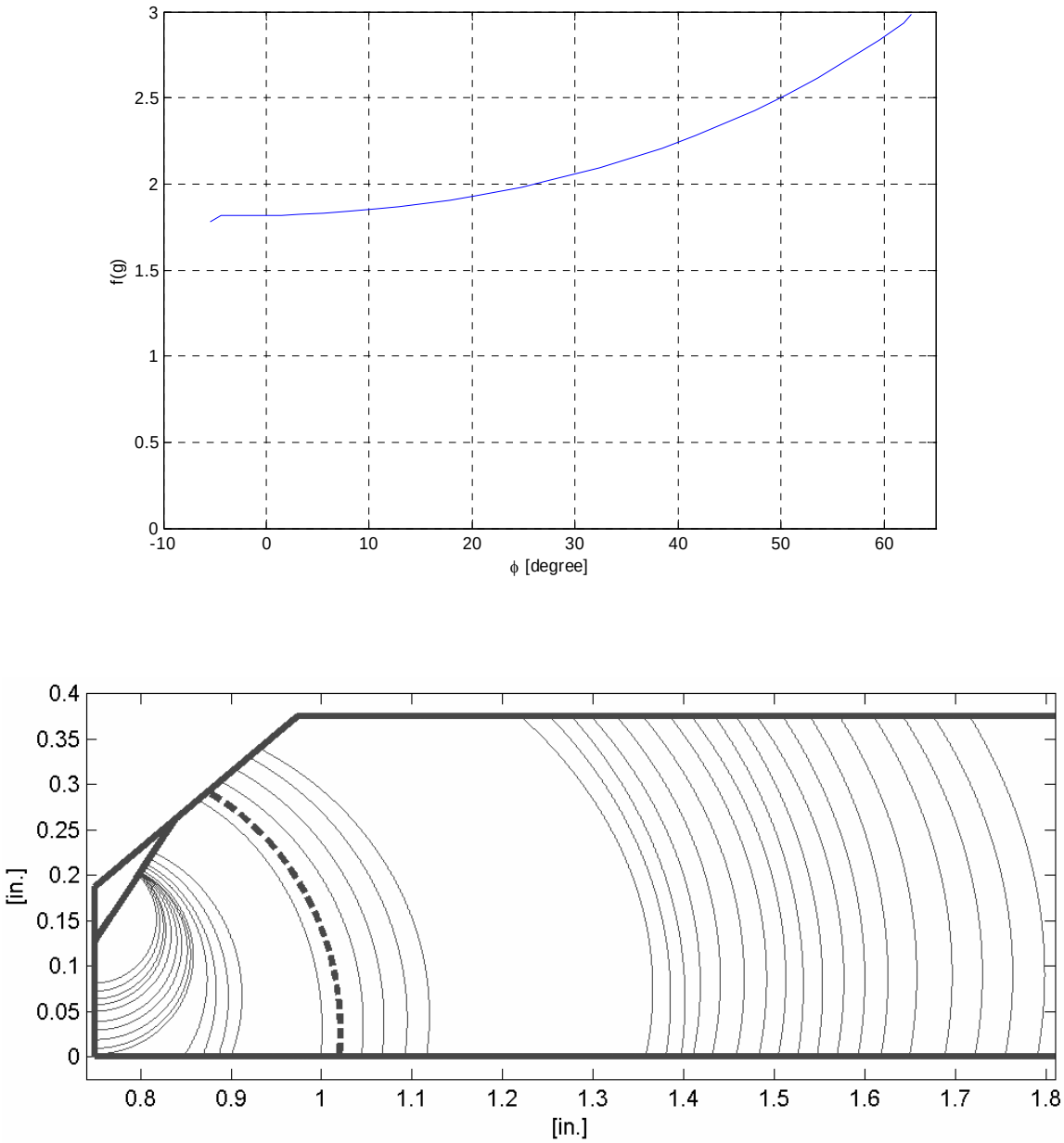

Figure C-54. Corrected BCF for FAA-012 at 40,275-40,500 Cycle, Initial Knee Crack, Type II

Table C-55. Corrected Boundary Correction Factors for FAA-012 (See figure C-55)

Initial Crack Location	Knee
Type	II
Center of Ellipse	(0.75, 0.0345)
Horizontal Axis	0.29590
Vertical Axis	0.30400
Cycle	40500-40725

ϕ [degree]	x [inch]	y [inch]	f(g)
-6.52	1.04399	0	1.7412
-5.57	1.0445	0.00503	1.7886
-3.37	1.04539	0.01667	1.7842
-1.18	1.04584	0.0283	1.7825
-0.69	1.04588	0.03089	1.7816
-0.11	1.0459	0.03475	1.7816
0.3	1.0459	0.03605	1.7816
2	1.04572	0.04509	1.7834
4.44	1.04501	0.05802	1.7869
8.85	1.04237	0.08129	1.8017
13.08	1.03823	0.10326	1.8247
16.09	1.03431	0.11871	1.8461
19.15	1.02953	0.13417	1.8731
25.15	1.01784	0.16366	1.9403
28.13	1.01096	0.17776	1.9818
31.17	1.00318	0.19179	2.0309
37.55	0.98458	0.21973	2.1524
40.94	0.97353	0.23364	2.2302
43.83	0.96345	0.24498	2.3038
46.87	0.95231	0.25629	2.3895
49.71	0.94134	0.26634	2.4779
52.72	0.92925	0.27633	2.5810
58.52	0.9045	0.29373	2.8109
61.33	0.89197	0.30119	2.9389
62.18	0.88809	0.30337	2.9980

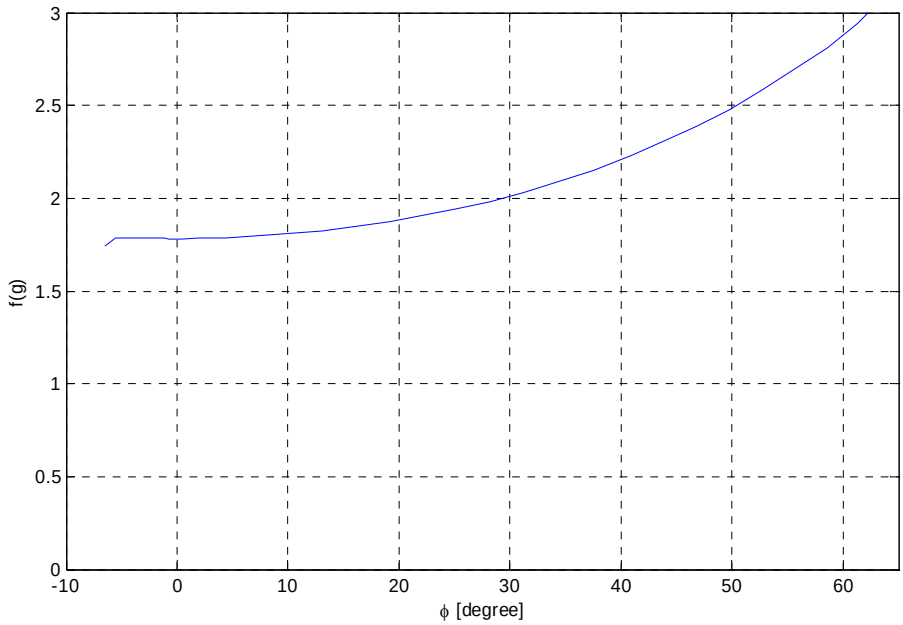

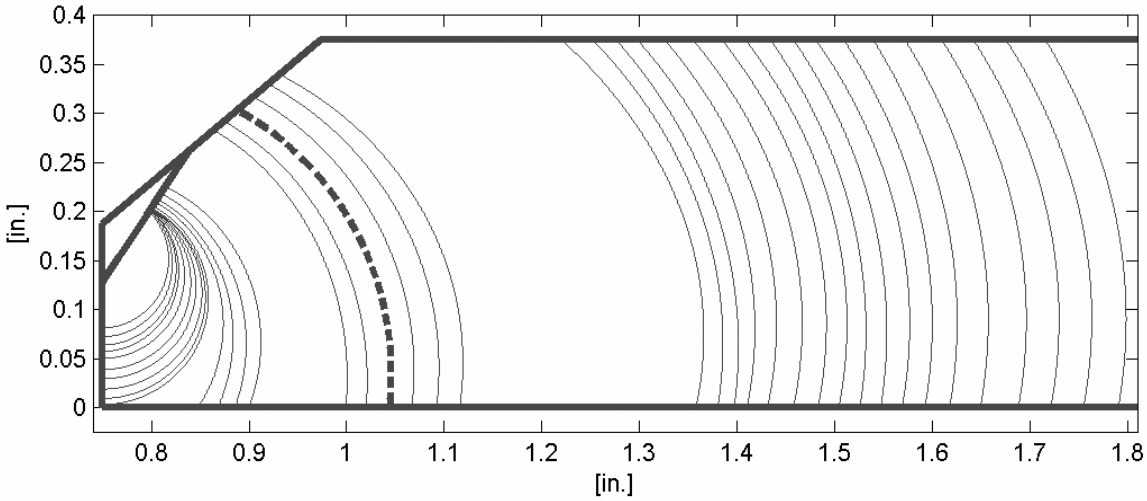

Figure C-55. Corrected BCF for FAA-012 at 40,500-40,725 Cycle, Initial Knee Crack, Type II

Table C-56. Corrected Boundary Correction Factors for FAA-012 (See figure C-56)

Initial Crack Location	Knee
Type	II
Center of Ellipse	(0.75, 0.0375)
Horizontal Axis	0.31890
Vertical Axis	0.31900
Cycle	40725-40950

ϕ [degree]	x [inch]	y [inch]	f(g)
-6.76	1.06668	0	2.3391
-4.96	1.06771	0.01007	2.3383
-2.91	1.06849	0.02157	2.3392
-1.13	1.06884	0.03181	2.3403
-0.92	1.06886	0.03311	2.3404
-0.48	1.06889	0.03694	2.3409
0.48	1.06889	0.03821	2.3411
2.69	1.06855	0.05231	2.3433
5.21	1.06758	0.06641	2.346
8.22	1.06562	0.08308	2.35
14.09	1.05931	0.11514	2.3598
17.2	1.05463	0.13184	2.3663
20.12	1.04943	0.14724	2.3731
23.1	1.04334	0.16264	2.3807
29	1.0289	0.19218	2.3984
32.22	1.0198	0.20758	2.4094
35.56	1.00943	0.22301	2.4219
38.44	0.99979	0.23581	2.4335
40.53	0.99238	0.24481	2.4425
44.6	0.97708	0.26148	2.4612
47.92	0.9637	0.27428	2.4779
50.74	0.95179	0.28451	2.4929
53.36	0.9403	0.29348	2.5077
56.98	0.92377	0.30498	2.5295
59.6	0.91136	0.31265	2.5462

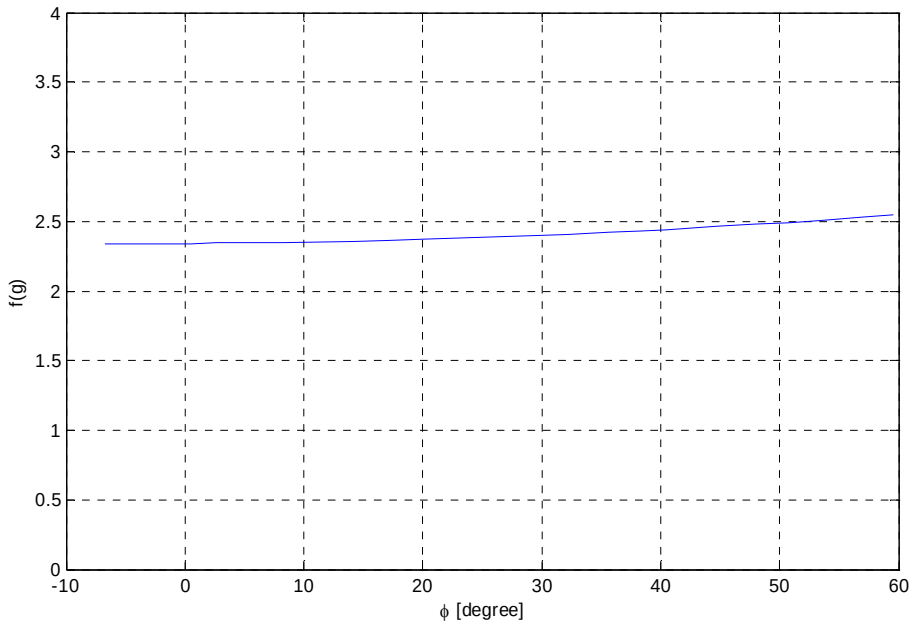

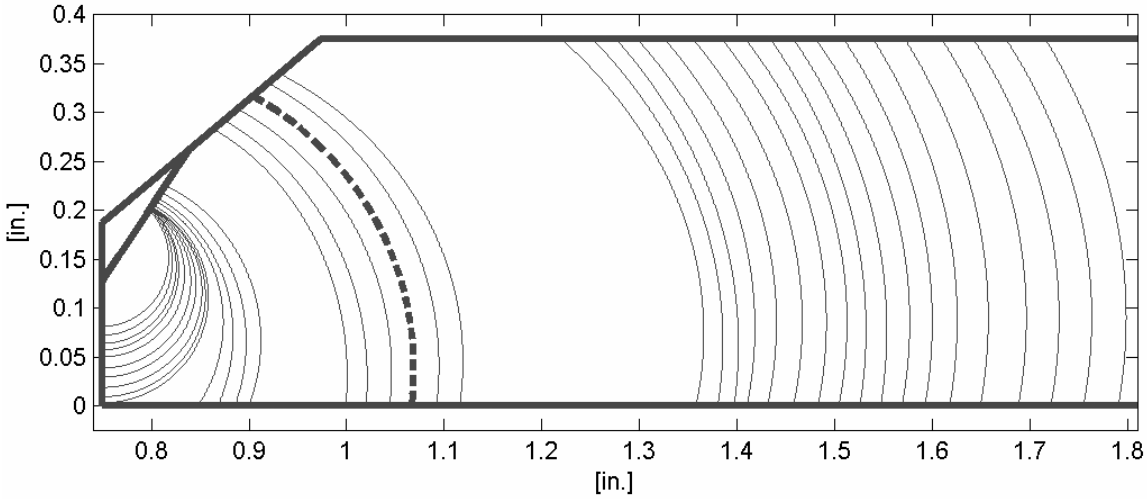

Figure C-56. Corrected BCF for FAA-012 at 40,725-40,950 Cycle, Initial Knee Crack, Type II

Table C-57. Corrected Boundary Correction Factors for FAA-012 (See figure C-57)

Initial Crack Location	Knee
Type	II
Center of Ellipse	(0.75, 0.04)
Horizontal Axis	0.34450
Vertical Axis	0.33300
Cycle	40950-41160

ϕ [degree]	x [inch]	y [inch]	f(g)
-6.9	1.09201	0	1.7047
-4.98	1.0932	0.01111	1.7875
-3.17	1.09397	0.02161	1.7831
-1.59	1.09437	0.03078	1.7813
-0.68	1.09448	0.03605	1.7813
-0.23	1.0945	0.03868	1.7804
0	1.0945	0.03998	1.7804
3.16	1.09397	0.05835	1.7831
6.11	1.09254	0.07539	1.7902
9.07	1.0902	0.0924	1.8018
12.05	1.08691	0.1094	1.8179
15.05	1.08269	0.12635	1.8397
18.08	1.07749	0.14322	1.8663
21.16	1.07127	0.16007	1.8997
27	1.05696	0.191	1.9778
30.26	1.04757	0.20762	2.0317
36.81	1.02581	0.23936	2.1640
39.85	1.01448	0.25322	2.2383
43.61	0.99945	0.26952	2.3415
46.02	0.98922	0.27947	2.4151
49.19	0.97515	0.2919	2.5227
52.21	0.9611	0.30303	2.6369
55.06	0.94732	0.31285	2.7554
58.12	0.93193	0.32268	2.8971
60.51	0.91961	0.32982	3.0353

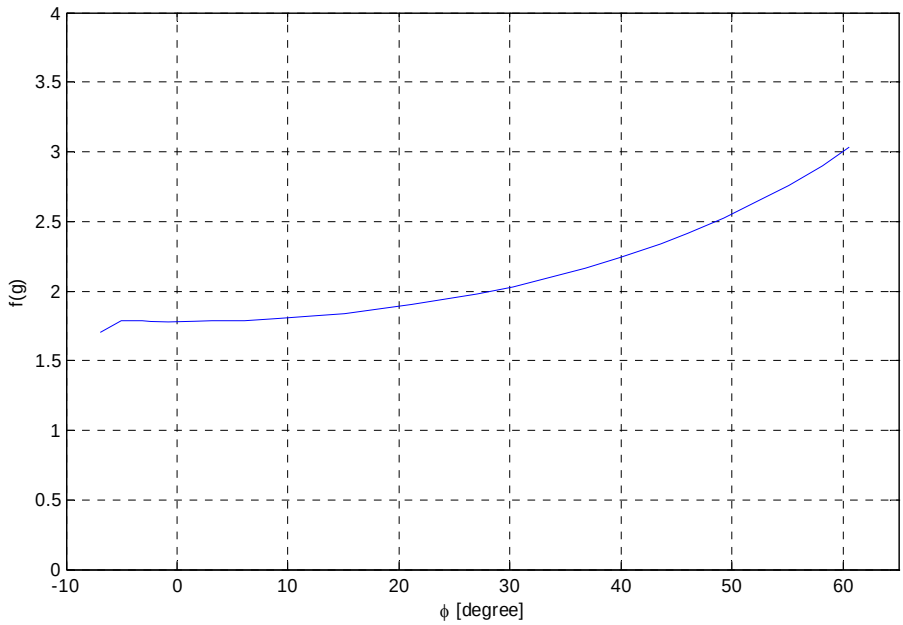

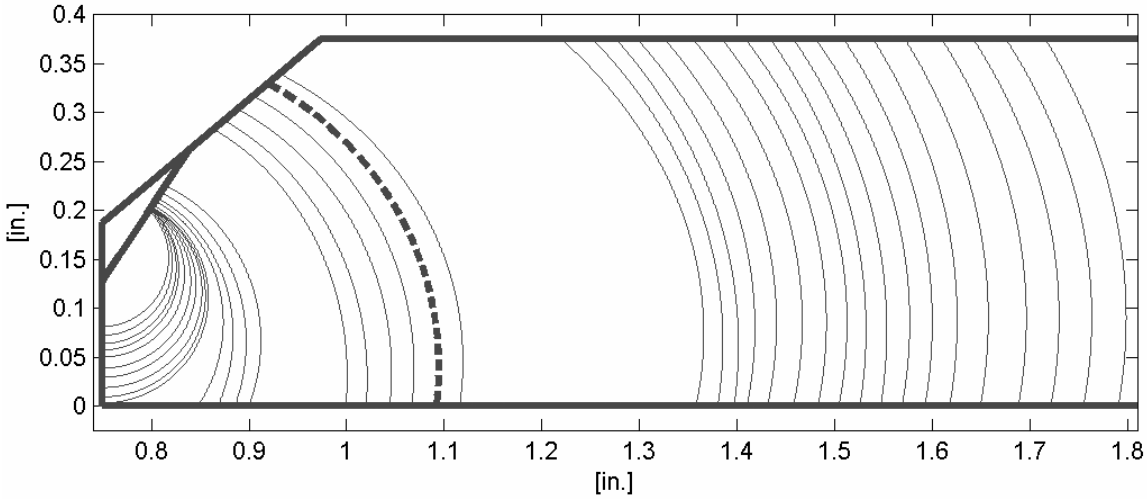

Figure C-57. Corrected BCF for FAA-012 at 40,950-41,160 Cycle, Initial Knee Crack, Type II

Table C-58. Corrected Boundary Correction Factors for FAA-012 (See figure C-58)

Initial Crack Location	Knee
Type	II
Center of Ellipse	(0.75, 0.045)
Horizontal Axis	0.36900
Vertical Axis	0.33800
Cycle	41160-41340

ϕ [degree]	x [inch]	y [inch]	f(g)
-7.72	1.11565	0	1.7020
-5.66	1.1172	0.01243	1.7297
-3.74	1.11822	0.02394	1.7280
-1.89	1.1188	0.03548	1.7289
-1.19	1.11892	0.0406	1.7289
-0.88	1.11896	0.04573	1.7306
0.92	1.11895	0.04701	1.7306
3.04	1.11848	0.06245	1.7359
6.04	1.11695	0.08047	1.7473
9.11	1.11435	0.09849	1.7623
12.21	1.11065	0.11651	1.7837
15.13	1.10621	0.13323	1.8080
18.08	1.10078	0.14993	1.8372
21.08	1.0943	0.16659	1.8723
24.14	1.08674	0.18323	1.9147
27.02	1.07873	0.19854	1.9599
30.21	1.0689	0.21504	2.0169
33.24	1.05864	0.23023	2.0793
39.33	1.03543	0.25918	2.2275
42.41	1.02245	0.27291	2.3166
45.34	1.00938	0.28536	2.4111
48.42	0.99491	0.29777	2.5220
54.46	0.96449	0.31999	2.7790
57.43	0.94866	0.32979	2.9259
60.6	0.93113	0.33949	3.1238

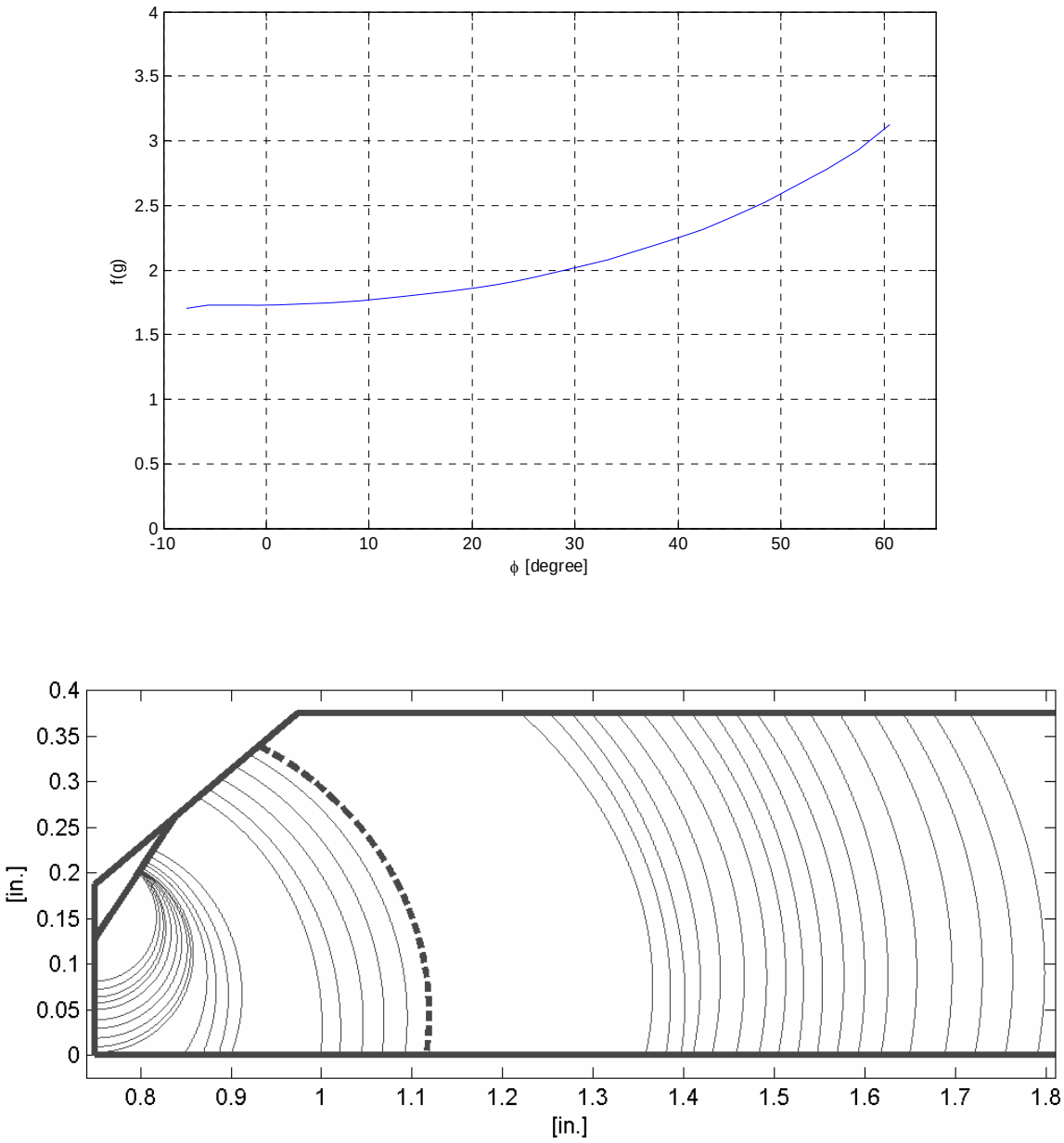

Figure C-58. Corrected BCF for FAA-012 at 41,160-41,340 Cycle, Initial Knee Crack, Type II

Table C-59. Corrected Boundary Correction Factors for FAA-012 (See figure C-59)

Initial Crack Location	Knee
Type	III
Center of Ellipse	(0.75, 0.074)
Horizontal Axis	0.61575
Vertical Axis	0.46500
Cycle	42300-44000

ϕ [degree]	x [inch]	y [inch]	f(g)
-9.22	1.35779	0	1.6110
-7.71	1.36018	0.01244	1.6154
-5.9	1.36249	0.02713	1.6268
-3.87	1.36434	0.0437	1.6381
-1.9	1.36541	0.06032	1.6479
-1.49	1.36554	0.06405	1.6498
-0.77	1.36569	0.07515	1.6555
0.82	1.36569	0.07703	1.6563
2.07	1.36535	0.09001	1.6619
5.2	1.36322	0.11602	1.6711
8.18	1.35948	0.14019	1.6770
11.19	1.35403	0.16431	1.6807
14	1.34745	0.18655	1.6823
17.08	1.33859	0.21058	1.6820
20.19	1.32791	0.23447	1.6799
23.11	1.31635	0.25644	1.6760
26.31	1.30195	0.28007	1.6701
29.35	1.28674	0.30181	1.6630
32.19	1.27111	0.32161	1.6550
34.3	1.25867	0.33594	1.6481
37.29	1.23988	0.35561	1.6374
38.12	1.2344	0.36096	1.6342
39.24	1.22688	0.36806	1.6296
39.75	1.22344	0.37129	1.6486
40.03	1.22151	0.37308	1.6982

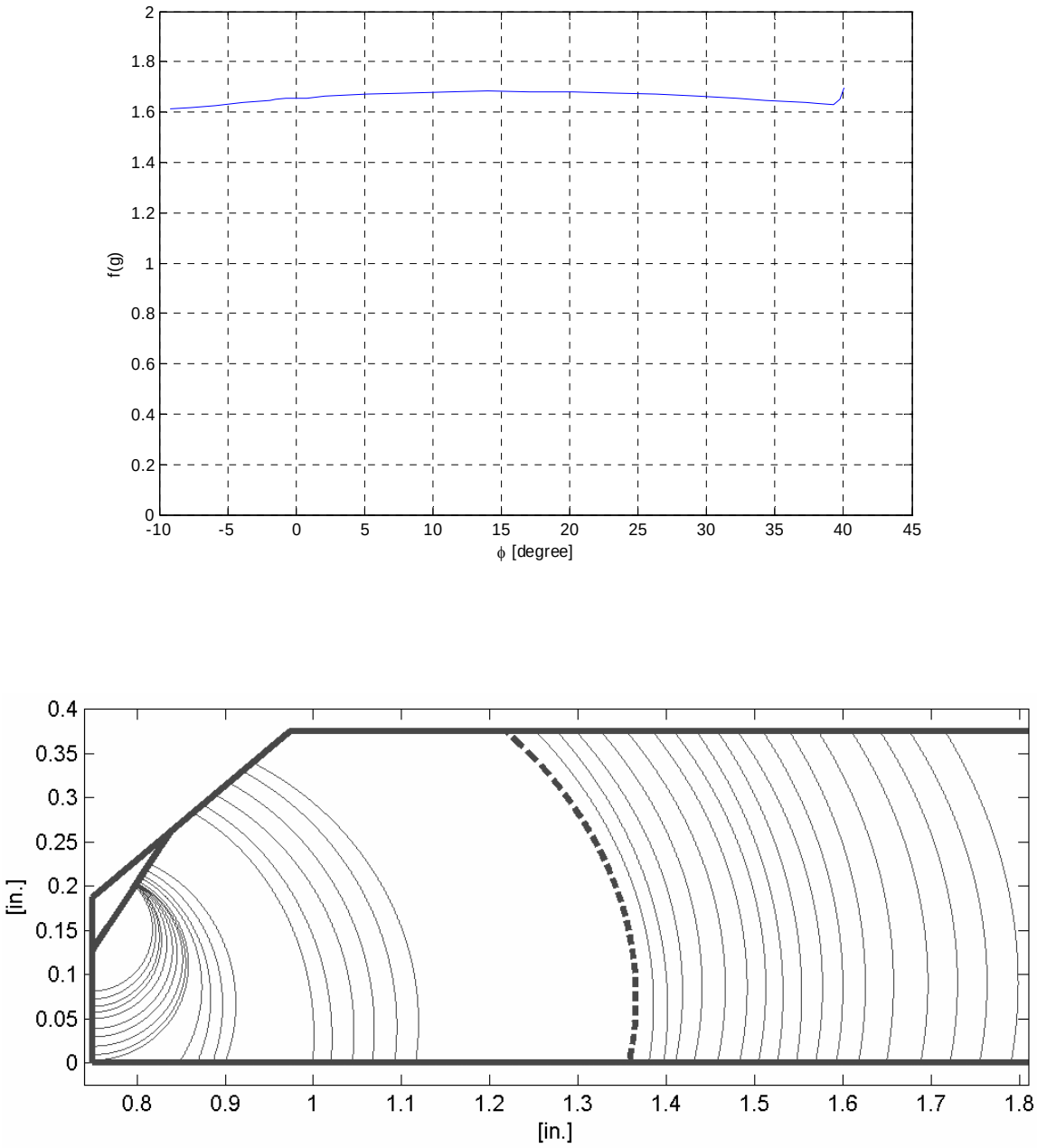

Figure C-59. Corrected BCF for FAA-012 at 42,300-44,000 Cycle, Initial Knee Crack, Type III

Table C-60. Corrected Boundary Correction Factors for FAA-012 (See figure C-60)

Initial Crack Location	Knee
Type	III
Center of Ellipse	(0.75, 0.065)
Horizontal Axis	0.63540
Vertical Axis	0.50500
Cycle	44000-45500

ϕ [degree]	x [inch]	y [inch]	f(g)
-7.95	1.37929	0	1.7365
-5.98	1.38194	0.0172	1.7004
-4	1.38385	0.0357	1.6666
-2.59	1.38475	0.0504	1.6454
-1.86	1.38507	0.06145	1.6306
-1.74	1.38511	0.06875	1.6213
1.78	1.38509	0.0706	1.6190
3.03	1.38451	0.0889	1.5984
5.08	1.3829	0.10895	1.5799
7.3	1.38025	0.12905	1.5668
9.36	1.37695	0.14725	1.5601
11.66	1.37228	0.16735	1.5586
13.36	1.36822	0.18195	1.5615
15.29	1.36291	0.19845	1.5690
17.46	1.35611	0.2168	1.5820
19.46	1.34912	0.2334	1.5978
21.7	1.34037	0.25185	1.6196
23.3	1.33357	0.26485	1.6372
25.4	1.32396	0.28165	1.6623
28.03	1.31087	0.30225	1.7425
30.74	1.29611	0.323	1.8658
33.55	1.27953	0.3439	1.8975
36.48	1.26088	0.365	1.9324
37.57	1.2536	0.372	1.9750
38.02	1.25058	0.3747	2.0037

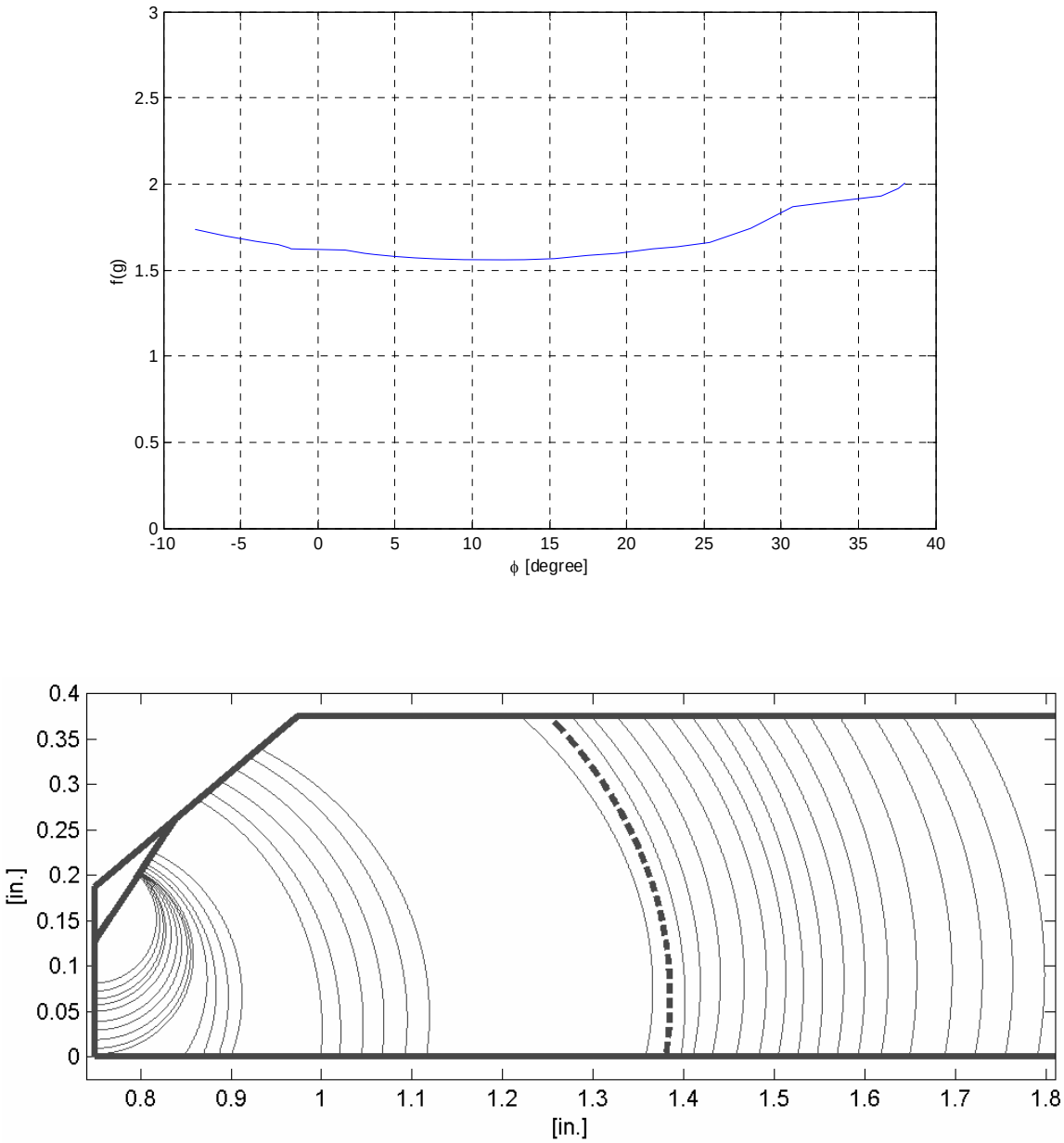

Figure C-60. Corrected BCF for FAA-012 at 44,000-45,500 Cycle, Initial Knee Crack, Type III

Table C-61. Corrected Boundary Correction Factors for FAA-012 (See figure C-61)

Initial Crack Location	Knee
Type	III
Center of Ellipse	(0.75, 0.062)
Horizontal Axis	0.65130
Vertical Axis	0.53000
Cycle	45500-47000

ϕ [degree]	x [inch]	y [inch]	f(g)
-6.97	1.39648	0	1.4474
-5.17	1.39865	0.01722	1.4800
-3.91	1.39978	0.02931	1.5009
-2.33	1.40076	0.04553	1.5247
-1.32	1.40113	0.06383	1.5471
1.35	1.40112	0.06585	1.5494
3.02	1.4004	0.08829	1.5708
5.11	1.39871	0.1087	1.5861
7.73	1.39537	0.13326	1.5997
10.18	1.39104	0.15579	1.6080
12.44	1.38602	0.17625	1.6124
14.93	1.37931	0.19869	1.6139
17.45	1.37131	0.22108	1.6120
19.54	1.36378	0.23937	1.6079
21.65	1.35536	0.25757	1.6012
23.3	1.34817	0.27168	1.5942
25.69	1.33691	0.29175	1.5812
28.12	1.32443	0.31173	1.5643
30.84	1.30919	0.33363	1.5402
33.11	1.29554	0.35139	1.5152
34.14	1.28908	0.35928	1.5022
35.17	1.28241	0.36713	1.4879
35.43	1.28069	0.3691	1.4841
35.87	1.27775	0.37246	1.4800
36	1.27691	0.37346	1.4998

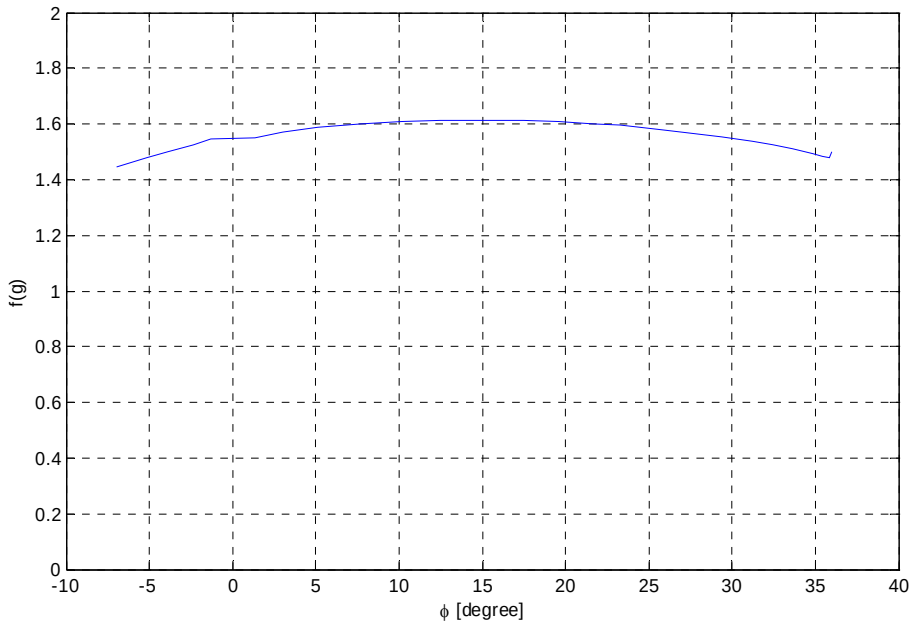

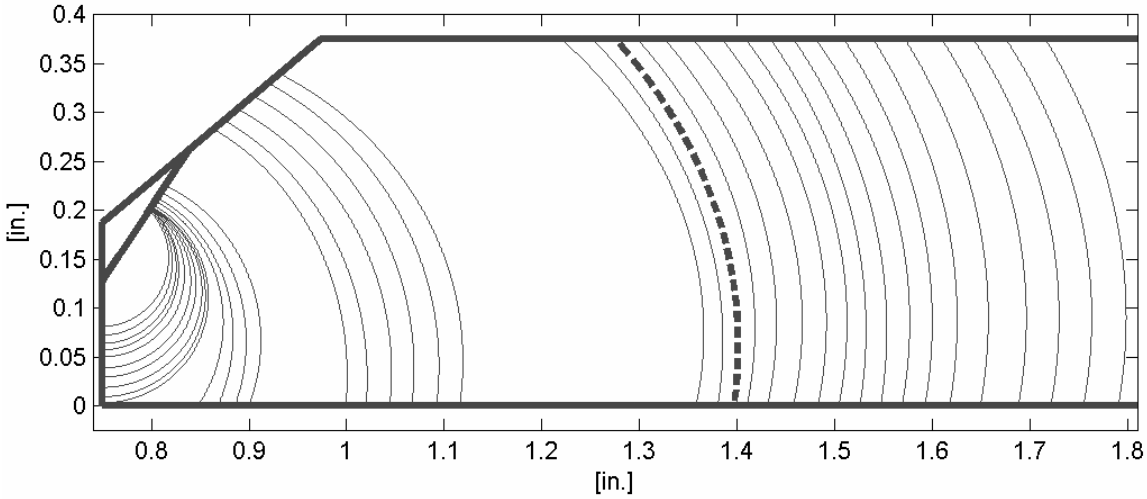

Figure C-61. Corrected BCF for FAA-012 at 45,500-47,000 Cycle, Initial Knee Crack, Type III

Table C-62. Corrected Boundary Correction Factors for FAA-012 (See figure C-62)

Initial Crack Location	Knee
Type	III
Center of Ellipse	(0.75, 0.0795)
Horizontal Axis	0.66815
Vertical Axis	0.51500
Cycle	47000-48750

ϕ [degree]	x [inch]	y [inch]	f(g)
-8.9	1.41011	0	1.5602
-7.35	1.41266	0.01399	1.5612
-6.02	1.41446	0.02588	1.5668
-4.26	1.4163	0.04178	1.5739
-3.17	1.41713	0.05174	1.5782
-2.09	1.41771	0.0617	1.5824
-1.08	1.41803	0.07171	1.5867
-0.63	1.41811	0.07969	1.5899
0.67	1.4181	0.08167	1.5908
2.75	1.41738	0.10367	1.5995
4.72	1.41588	0.12165	1.6064
7.18	1.41291	0.1437	1.6146
10.1	1.40779	0.16977	1.6241
13.06	1.40087	0.19583	1.6332
16.05	1.39209	0.2219	1.6422
19.09	1.38139	0.24796	1.6512
22.19	1.36868	0.27397	1.6603
25.11	1.35503	0.29801	1.6936
28.34	1.33807	0.32397	1.7302
30.12	1.32793	0.33794	1.7511
31.93	1.31707	0.35186	1.7728
33.24	1.30881	0.36182	1.7892
34.14	1.303	0.36854	1.8288
34.67	1.29949	0.37243	1.8801
34.95	1.29768	0.37438	1.8990

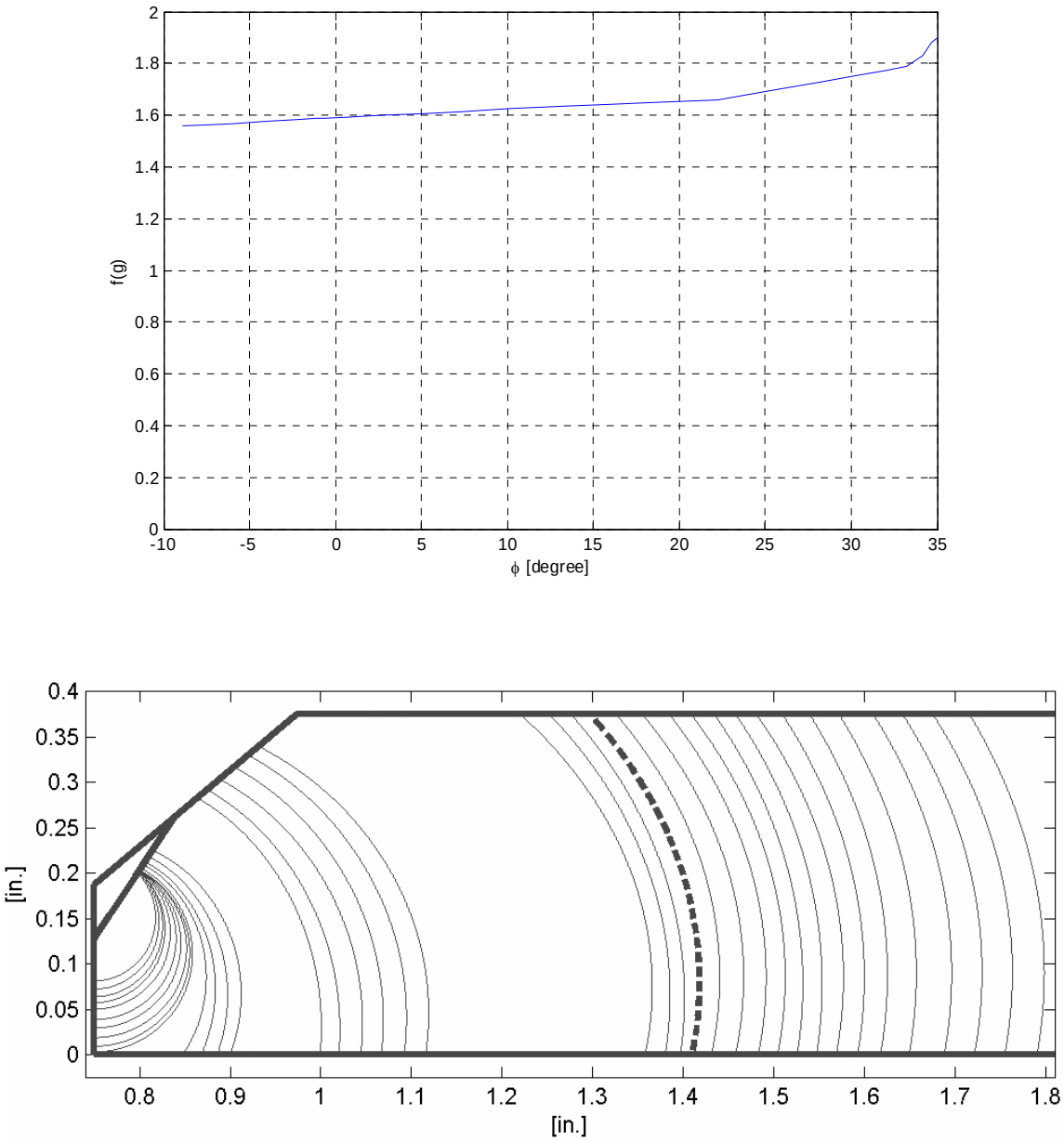

Figure C-62. Corrected BCF for FAA-012 at 47,000-48,750 Cycle, Initial Knee Crack, Type III

Table C-63. Corrected Boundary Correction Factors for FAA-012 (See figure C-63)

Initial Crack Location	Knee
Type	III
Center of Ellipse	(0.75, 0.085)
Horizontal Axis	0.69025
Vertical Axis	0.52500
Cycle	48750-51000

ϕ [degree]	x [inch]	y [inch]	f(g)
-9.32	1.43114	0	1.5724
-8.24	1.43312	0.00979	1.5664
-6.18	1.43624	0.0285	1.5671
-4.13	1.43846	0.04721	1.5676
-1.4	1.44004	0.07218	1.5679
-0.72	1.4402	0.07843	1.5680
-0.03	1.44025	0.08468	1.5680
0.19	1.44025	0.08677	1.5680
2.01	1.43982	0.10344	1.5679
4.06	1.43852	0.12215	1.5677
8.17	1.43325	0.15957	1.5664
10.01	1.42975	0.1762	1.5656
12.08	1.42496	0.19486	1.5647
14.18	1.41923	0.21352	1.5634
16.04	1.41337	0.23004	1.5623
18.16	1.40586	0.2486	1.5608
20.07	1.39835	0.26507	1.5595
22.23	1.38894	0.28357	1.5580
24.43	1.37847	0.30203	1.5563
26.65	1.36691	0.32043	1.5547
28.91	1.3542	0.33878	1.5530
31.23	1.34023	0.35713	1.5515
33.01	1.32883	0.37099	1.5634
33.14	1.32798	0.372	1.5769
33.4	1.32625	0.37401	1.6128

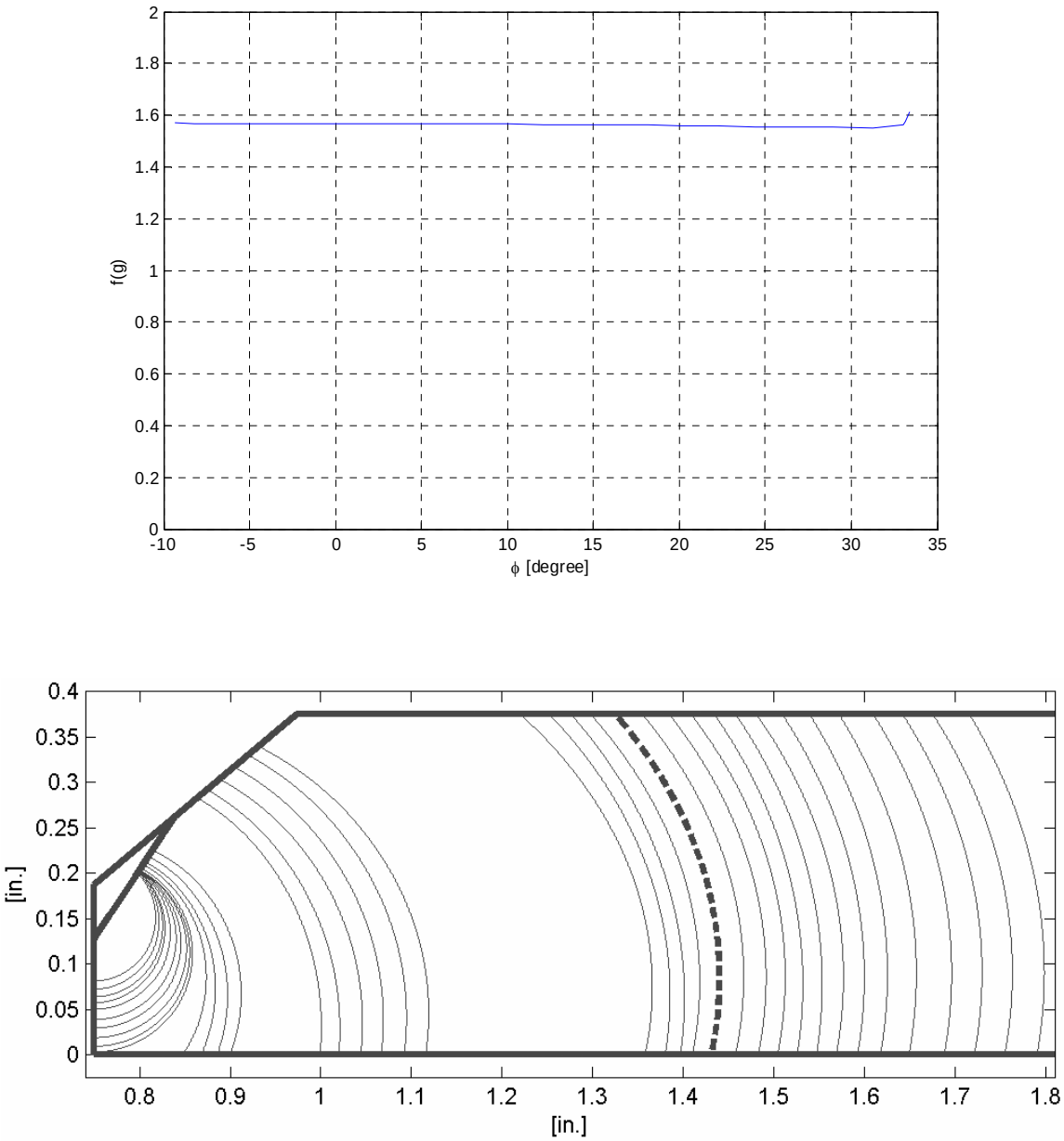

Figure C-63. Corrected BCF for FAA-012 at 48,750-51,000 Cycle, Initial Knee Crack, Type III

Table C-64. Corrected Boundary Correction Factors for FAA-012 (See figure C-64)

Initial Crack Location	Knee
Type	III
Center of Ellipse	(0.75, 0.085)
Horizontal Axis	0.71665
Vertical Axis	0.54000
Cycle	51000-53400

ϕ [degree]	x [inch]	y [inch]	f(g)
-9.06	1.45771	0	1.5839
-7.79	1.46003	0.01178	1.5773
-5.75	1.46304	0.0309	1.5770
-3.94	1.46495	0.04788	1.5768
-2.14	1.46615	0.06487	1.5767
-1.01	1.46654	0.0755	1.5766
-0.1	1.46665	0.08404	1.5766
0.12	1.46665	0.08612	1.5766
2.15	1.46615	0.10524	1.5767
4.18	1.46474	0.12437	1.5768
6	1.46273	0.1414	1.5770
8.04	1.45961	0.16047	1.5773
10.08	1.45558	0.17954	1.5777
12.38	1.44999	0.20074	1.5783
14.45	1.44397	0.21976	1.5791
16.32	1.43779	0.23669	1.5798
18.42	1.42992	0.25565	1.5810
20.32	1.42204	0.27253	1.5821
22.24	1.41334	0.28935	1.5835
24.18	1.4038	0.30612	1.5851
26.64	1.3906	0.32706	1.5875
28.9	1.37742	0.34592	1.5902
30.94	1.36465	0.36264	1.5929
32.23	1.35619	0.37301	1.6793
32.37	1.35532	0.37403	1.7389

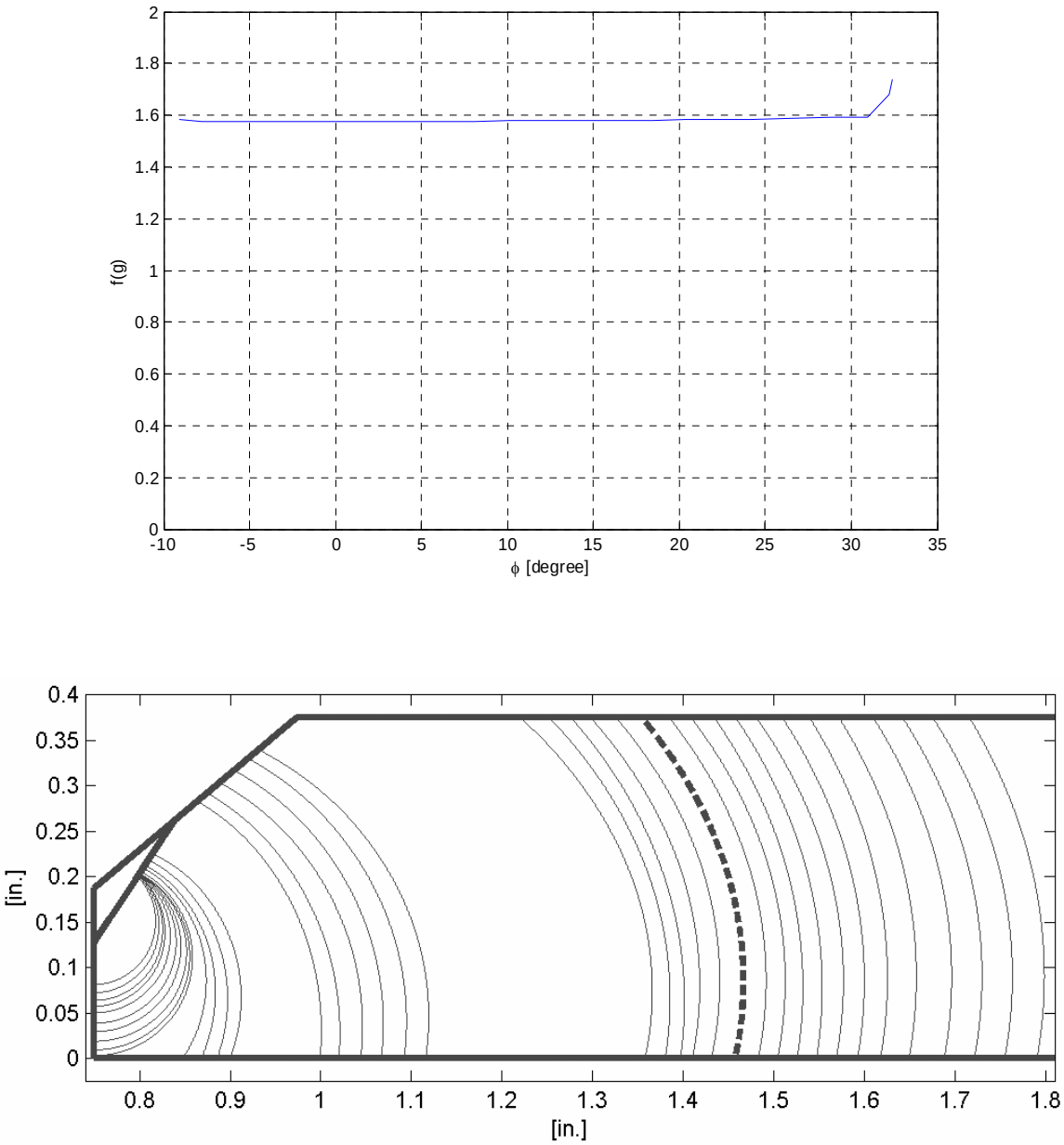

Figure C-64. Corrected BCF for FAA-012 at 51,000-53,400 Cycle, Initial Knee Crack, Type III

Table C-65. Corrected Boundary Correction Factors for FAA-012 (See figure C-65)

Initial Crack Location	Knee
Type	III
Center of Ellipse	(0.75, 0.085)
Horizontal Axis	0.74140
Vertical Axis	0.56000
Cycle	53400-55200

ϕ [degree]	x [inch]	y [inch]	f(g)
-8.73	1.48281	0	1.5719
-6.93	1.48598	0.01739	1.5650
-4.93	1.48866	0.0369	1.5641
-2.93	1.49043	0.05641	1.5635
-1.37	1.49119	0.07163	1.5632
-0.7	1.49134	0.07813	1.5631
-0.04	1.4914	0.08464	1.5631
0.19	1.4914	0.08684	1.5631
2.63	1.49062	0.11071	1.5634
4.64	1.48897	0.13028	1.5640
6.64	1.48642	0.14979	1.5648
8.66	1.48295	0.1693	1.5661
10.68	1.47855	0.18882	1.5676
12.72	1.4732	0.20833	1.5694
14.55	1.46762	0.2257	1.5714
16.62	1.46043	0.24515	1.5741
18.95	1.45124	0.26682	1.5775
20.59	1.44405	0.28192	1.5802
22.73	1.43382	0.30138	1.5841
24.91	1.42245	0.32084	1.5886
26.87	1.41136	0.3381	1.5931
28.87	1.39928	0.35535	1.5981
29.88	1.39283	0.36401	1.6008
30.79	1.3869	0.37164	1.6344
31.18	1.38433	0.37482	1.8078

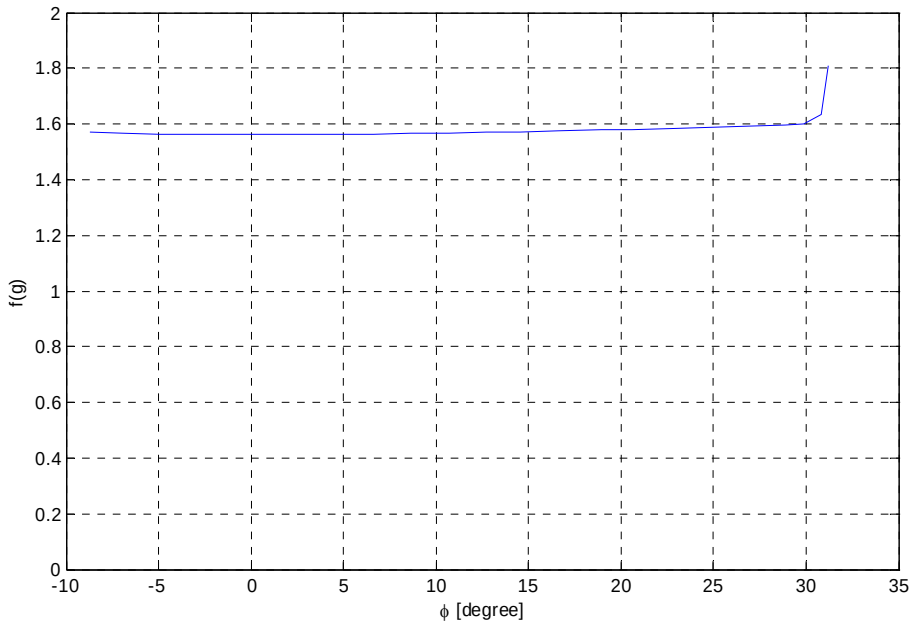

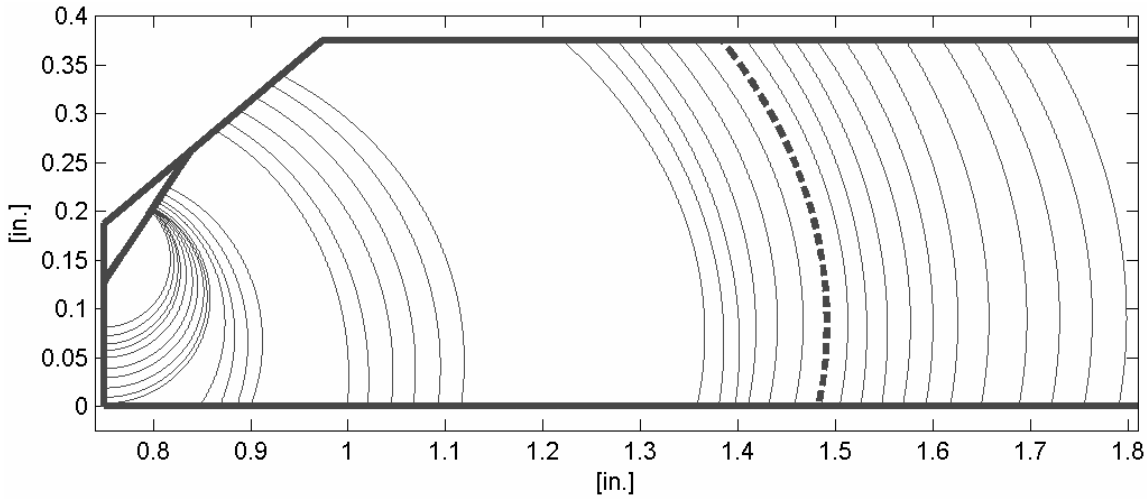

Figure C-65. Corrected BCF for FAA-012 at 53,400-55,200 Cycle, Initial Knee Crack, Type III

Table C-66. Corrected Boundary Correction Factors for FAA-012 (See figure C-66)

Initial Crack Location	Knee
Type	III
Center of Ellipse	(0.75, 0.085)
Horizontal Axis	0.76250
Vertical Axis	0.57500
Cycle	55200-57000

ϕ [degree]	x [inch]	y [inch]	f(g)
-8.27	1.50458	0.00235	1.5493
-7.14	1.50659	0.01357	1.5493
-5.57	1.5089	0.02919	1.5494
-4	1.51064	0.04487	1.5495
-2.66	1.51168	0.05829	1.5495
-1.55	1.51222	0.06946	1.5496
-0.66	1.51245	0.07842	1.5496
-0.01	1.5125	0.08514	1.5496
0.24	1.51249	0.08739	1.5496
1.8	1.51212	0.10307	1.5495
2.47	1.51179	0.10978	1.5495
3.58	1.51101	0.12094	1.5495
5.15	1.50942	0.13662	1.5494
7.62	1.50577	0.16121	1.5493
9.42	1.50222	0.17909	1.5492
11.46	1.4973	0.19922	1.5491
13.73	1.4907	0.2215	1.549
15.11	1.48614	0.23486	1.5489
17.19	1.47845	0.25488	1.5489
19.52	1.46867	0.27711	1.549
21.65	1.45873	0.29707	1.5492
23.56	1.44895	0.31478	1.5495
25.74	1.43683	0.33469	1.55
27.96	1.4235	0.35455	1.5508
29.69	1.41239	0.36978	1.5517

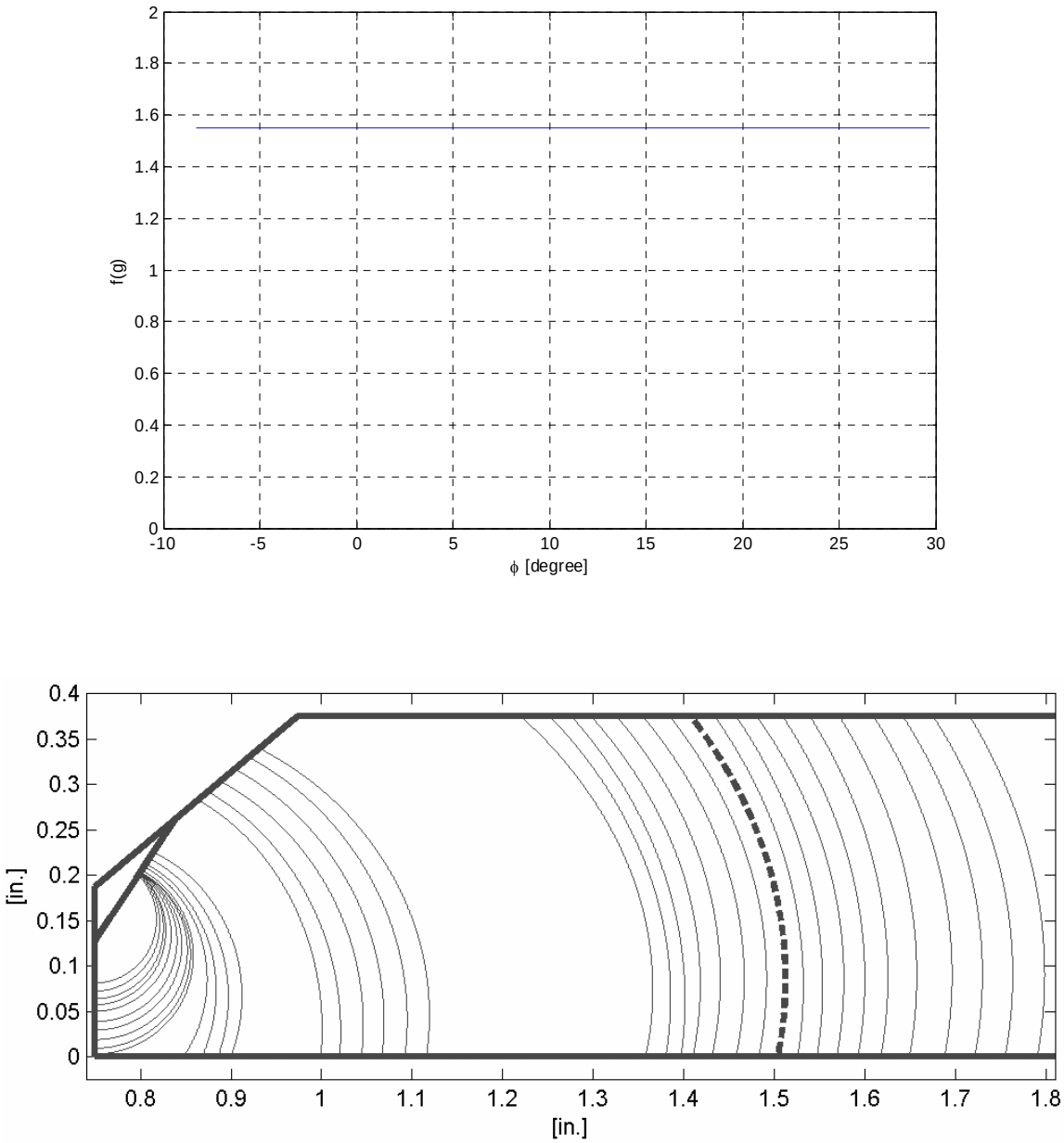

Figure C-66. Corrected BCF for FAA-012 at 55,200-57,000 Cycle, Initial Knee Crack, Type III

Table C-67. Corrected Boundary Correction Factors for FAA-012 (See figure C-67)

Initial Crack Location	Knee
Type	III
Center of Ellipse	(0.75, 0.0775)
Horizontal Axis	0.78200
Vertical Axis	0.61400
Cycle	57000-58800

ϕ [degree]	x [inch]	y [inch]	f(g)
-7.39	1.52551	0	1.5518
-6.01	1.5277	0.0144	1.5368
-4.96	1.52908	0.02575	1.5283
-3.49	1.53055	0.04158	1.5175
-2.06	1.53149	0.05742	1.5077
-1.13	1.53185	0.0687	1.5015
-0.72	1.53194	0.07774	1.4970
0.73	1.53194	0.07999	1.4960
1.99	1.53153	0.09801	1.4884
4.03	1.53006	0.12052	1.4817
6.12	1.52754	0.14303	1.4780
8.03	1.52434	0.1633	1.4774
10.15	1.51976	0.18581	1.4799
12.08	1.51468	0.20608	1.4848
14.03	1.50868	0.2264	1.4923
15.99	1.50173	0.24673	1.5022
17.99	1.49378	0.26712	1.5145
20.01	1.48481	0.28756	1.5290
22.05	1.47478	0.30801	1.5455
24.14	1.46359	0.32857	1.5640
26.03	1.45269	0.34683	1.5819
28.2	1.43919	0.36752	1.6224
28.76	1.43553	0.37255	1.7615
28.89	1.43469	0.37366	1.7755
29.02	1.43385	0.37477	1.7846

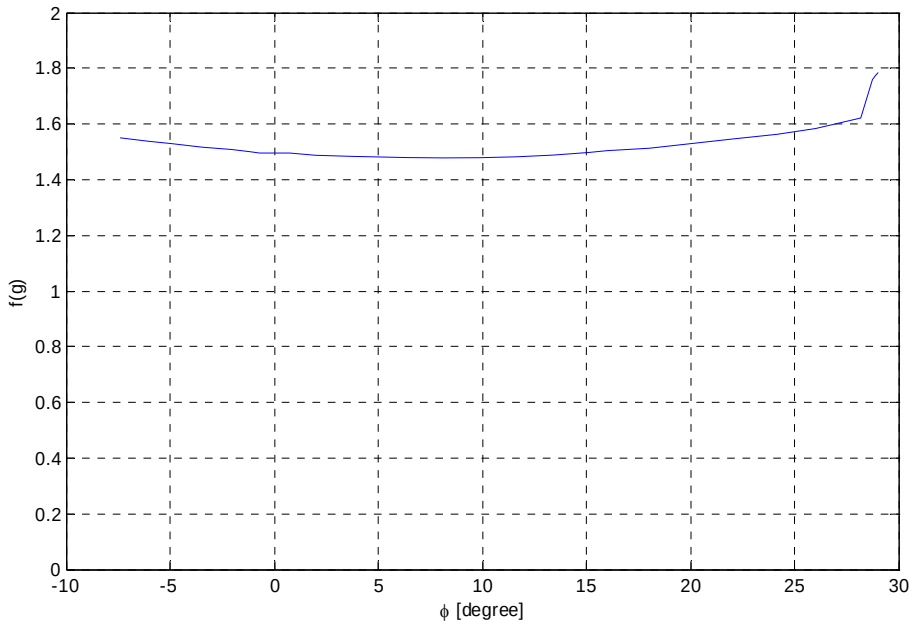

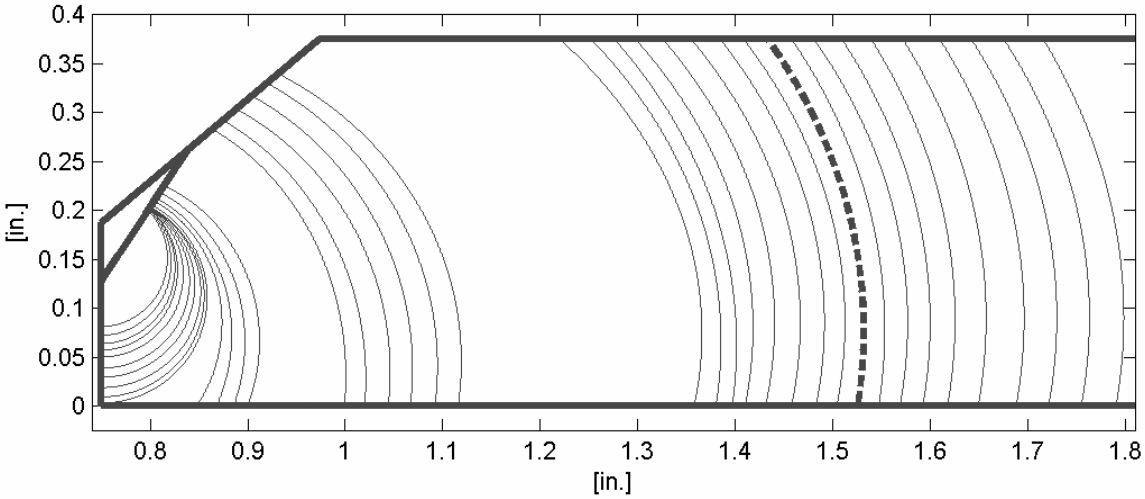

Figure C-67. Corrected BCF for FAA-012 at 57,000-58,800 Cycle, Initial Knee Crack, Type III

Table C-68. Corrected Boundary Correction Factors for FAA-012 (See figure C-68)

Initial Crack Location	Knee
Type	III
Center of Ellipse	(0.75, 0.0775)
Horizontal Axis	0.80325
Vertical Axis	0.62900
Cycle	58800-61100

ϕ [degree]	x [inch]	y [inch]	f(g)
-7.18	1.54696	0	1.4668
-6.05	1.54877	0.01262	1.4722
-4.95	1.55026	0.0248	1.4797
-3.62	1.55165	0.03951	1.4877
-2.1	1.55271	0.05669	1.4958
-1.1	1.5531	0.06899	1.5008
-0.7	1.55319	0.07882	1.5042
0.75	1.55318	0.08129	1.5051
2.19	1.55266	0.101	1.5108
4.17	1.55112	0.12317	1.5153
5.96	1.54891	0.14288	1.5179
7.99	1.54544	0.16506	1.5191
10.04	1.54095	0.18718	1.5185
12.09	1.53543	0.20925	1.5163
14.16	1.52885	0.23131	1.5123
16	1.52213	0.25079	1.5071
18.09	1.51353	0.27268	1.4995
20.2	1.50385	0.29445	1.4898
22.08	1.49433	0.3137	1.4793
23.99	1.48389	0.33289	1.4668
25.91	1.4725	0.35202	1.4520
27.61	1.4618	0.36862	1.4369
27.8	1.46051	0.37057	1.4350
28.04	1.45899	0.37296	1.4506
28.15	1.45822	0.37416	1.4679

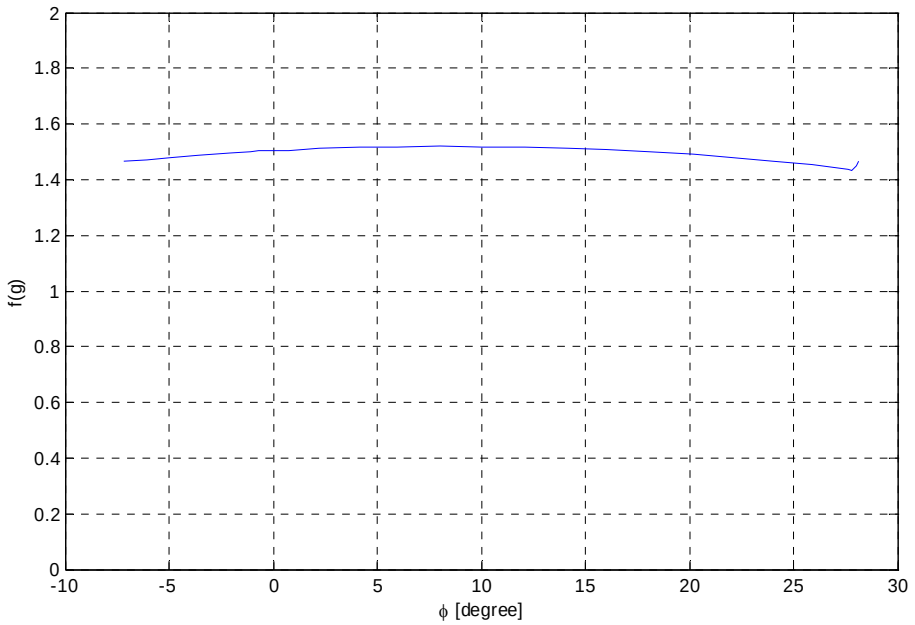

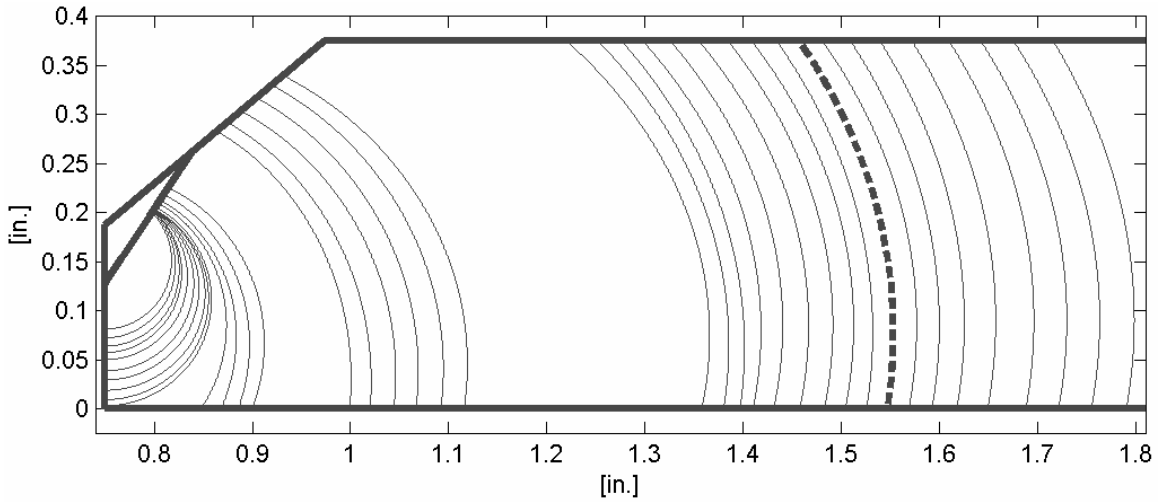

Figure C-68. Corrected BCF for FAA-012 at 58,800-61,100 Cycle, Initial Knee Crack, Type III

Table C-69. Corrected Boundary Correction Factors for FAA-012 (See figure C-69)

Initial Crack Location	Knee
Type	III
Center of Ellipse	(0.75, 0.085)
Horizontal Axis	0.82675
Vertical Axis	0.62000
Cycle	61100-63400

ϕ [degree]	x [inch]	y [inch]	f(g)
-7.88	1.56894	0	1.4761
-6.09	1.57209	0.01924	1.4707
-4.99	1.57362	0.03111	1.4703
-3.45	1.57526	0.04774	1.4700
-2.12	1.57618	0.06202	1.4697
-1.03	1.57662	0.07389	1.4696
-0.81	1.57667	0.07624	1.4696
-0.37	1.57673	0.081	1.4696
-0.07	1.57675	0.08576	1.4696
0.29	1.57674	0.08811	1.4696
1.82	1.57633	0.10474	1.4697
3.14	1.57551	0.11896	1.4699
4.9	1.57372	0.13799	1.4703
7.1	1.5704	0.16167	1.4712
9.1	1.56634	0.18306	1.4723
13.12	1.55517	0.22572	1.4753
15.15	1.54801	0.24705	1.4773
16.97	1.54075	0.26597	1.4793
19.04	1.53153	0.28724	1.4820
21.13	1.52116	0.30851	1.4851
23.02	1.51093	0.32742	1.4882
25.17	1.49825	0.34869	1.4922
27.11	1.4859	0.36755	1.4962
27.54	1.48309	0.37162	1.5111
27.78	1.48145	0.37394	1.5396

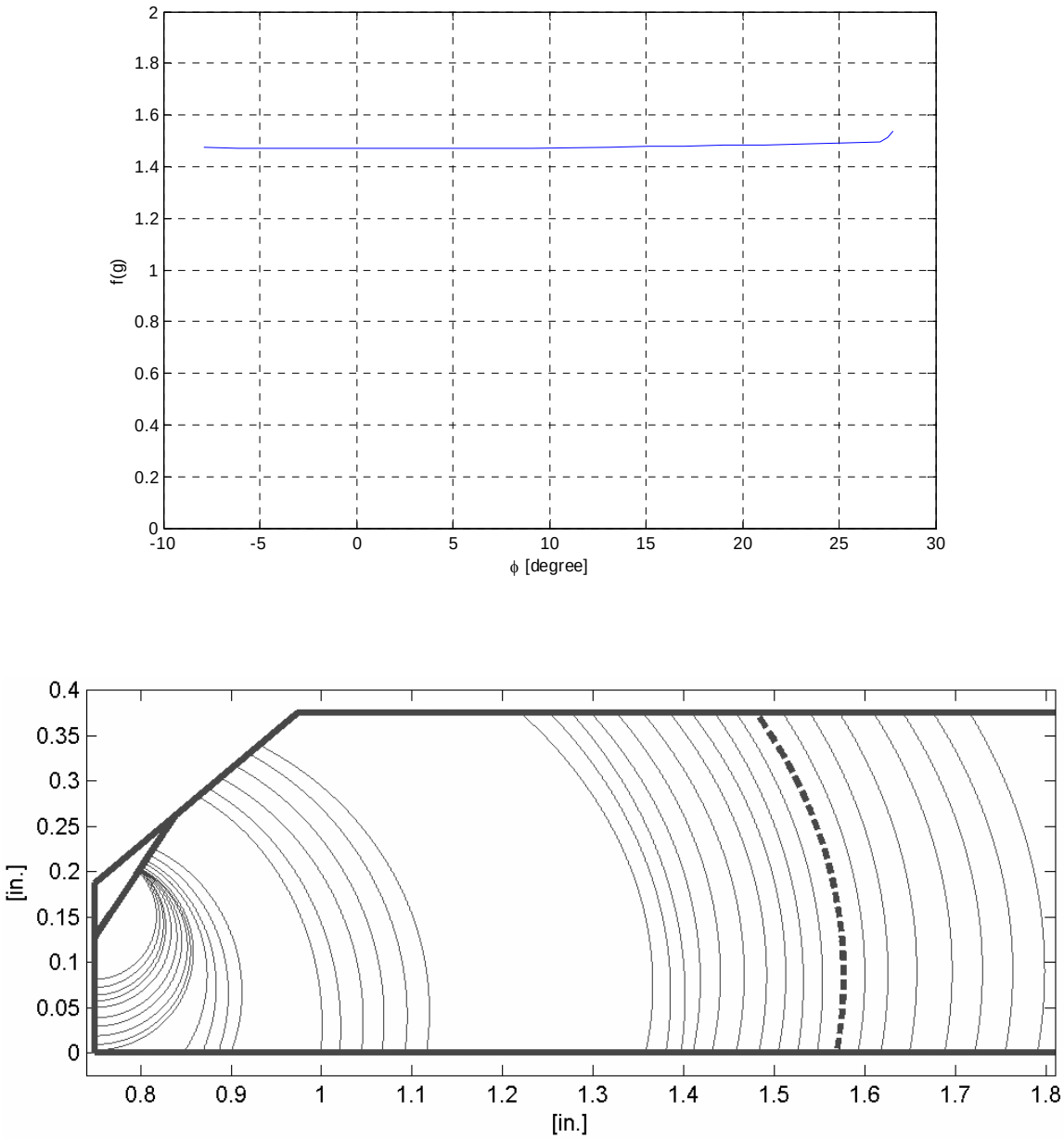

Figure C-69. Corrected BCF for FAA-012 at 61,100-63,400 Cycle, Initial Knee Crack, Type III

Table C-70. Corrected Boundary Correction Factors for FAA-012 (See figure C-70)

Initial Crack Location	Knee
Type	III
Center of Ellipse	(0.75, 0.085)
Horizontal Axis	0.84985
Vertical Axis	0.64500
Cycle	63400-65800

ϕ [degree]	x [inch]	y [inch]	f(g)
-7.58	1.59243	0	1.4697
-6.45	1.59447	0.01255	1.4644
-4.92	1.59671	0.02965	1.4632
-3.62	1.59816	0.04431	1.4624
-2.1	1.59928	0.0614	1.4617
-0.79	1.59977	0.07607	1.4614
-0.36	1.59983	0.08093	1.4614
-0.07	1.59985	0.0858	1.4614
0.29	1.59984	0.08823	1.4614
1.37	1.59961	0.10046	1.4615
3.11	1.5986	0.11999	1.4621
5.07	1.59652	0.14201	1.4633
7.03	1.59346	0.16398	1.4650
9	1.58938	0.18594	1.4674
11.2	1.58365	0.21033	1.4706
13.2	1.57739	0.2323	1.4742
15	1.57091	0.25189	1.4779
17.02	1.56261	0.27385	1.4826
19.08	1.55318	0.29581	1.4880
21.15	1.54258	0.31777	1.4940
23.03	1.53213	0.3373	1.5000
24.21	1.52513	0.34947	1.5040
25.88	1.5146	0.36656	1.5100
26.09	1.51327	0.36863	1.5110
26.69	1.50929	0.37458	1.5592

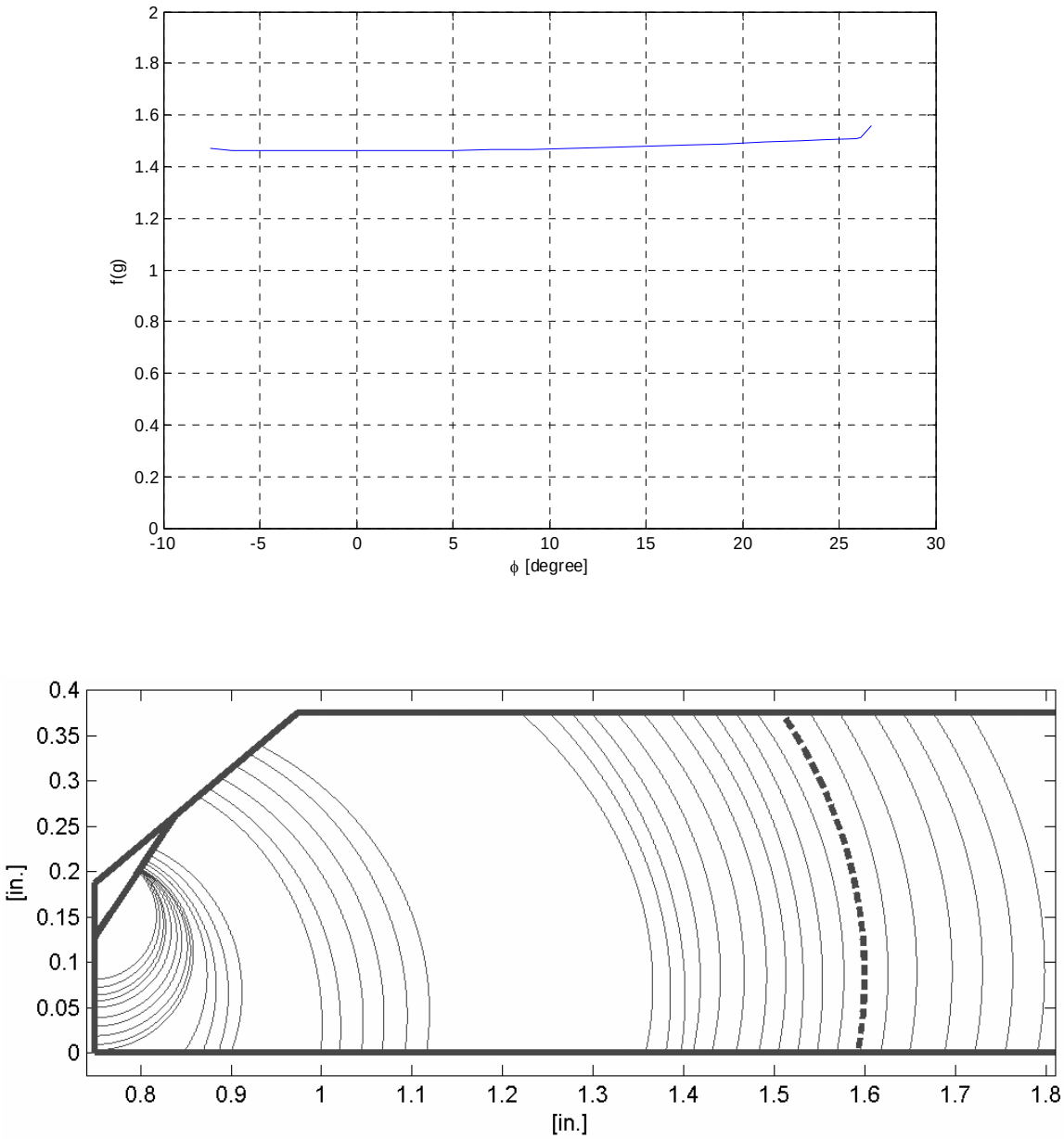

Figure C-70. Corrected BCF for FAA-012 at 63,400-65,800 Cycle, Initial Knee Crack, Type III

Table C-71. Corrected Boundary Correction Factors for FAA-012 (See figure C-71)

Initial Crack Location	Knee
Type	III
Center of Ellipse	(0.75, 0.0875)
Horizontal Axis	0.87535
Vertical Axis	0.66500
Cycle	65800-68800

ϕ [degree]	x [inch]	y [inch]	f(g)
-7.56	1.61773	0	1.4227
-6.01	1.62053	0.01798	1.4209
-4.7	1.62241	0.03322	1.4228
-3.15	1.62402	0.05109	1.4247
-2.06	1.62478	0.06382	1.4261
-0.76	1.62527	0.07919	1.4276
-0.36	1.62533	0.08427	1.4281
0.23	1.62534	0.08684	1.4284
1.49	1.62505	0.10472	1.4300
3.03	1.62413	0.12259	1.4316
5.01	1.622	0.14561	1.4333
7	1.61882	0.16857	1.4351
9	1.61456	0.19158	1.4365
11.01	1.60923	0.21454	1.4379
13.04	1.60279	0.23749	1.4392
15.07	1.59525	0.26039	1.4405
17.12	1.58655	0.28328	1.4415
19.2	1.57666	0.30617	1.4427
21.06	1.56689	0.32643	1.4436
22.94	1.55611	0.34668	1.4446
24.61	1.54586	0.36437	1.4456
25.26	1.54168	0.37123	1.4562
25.37	1.54091	0.37248	1.4657
25.49	1.54013	0.37372	1.4776
25.61	1.53934	0.37496	1.4913

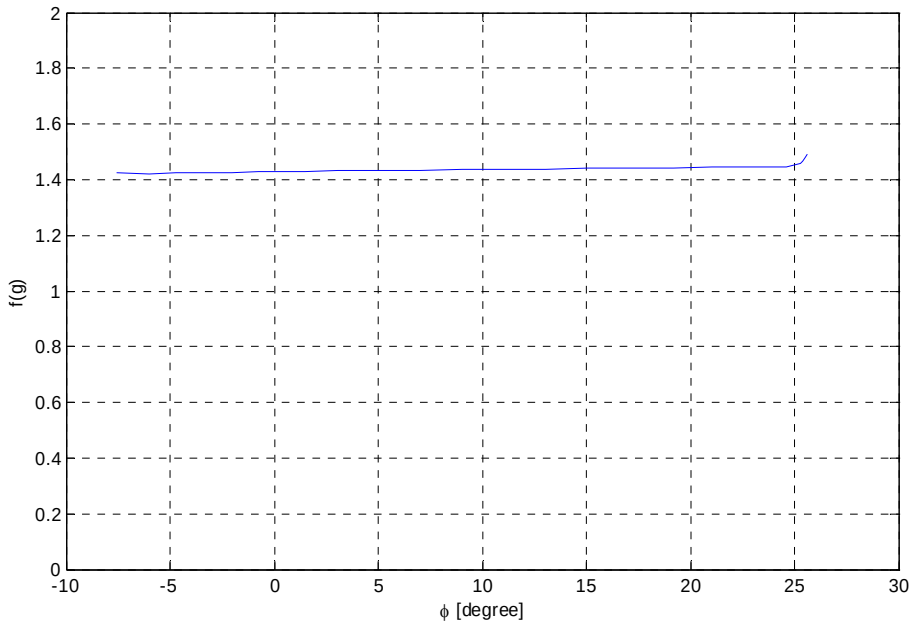

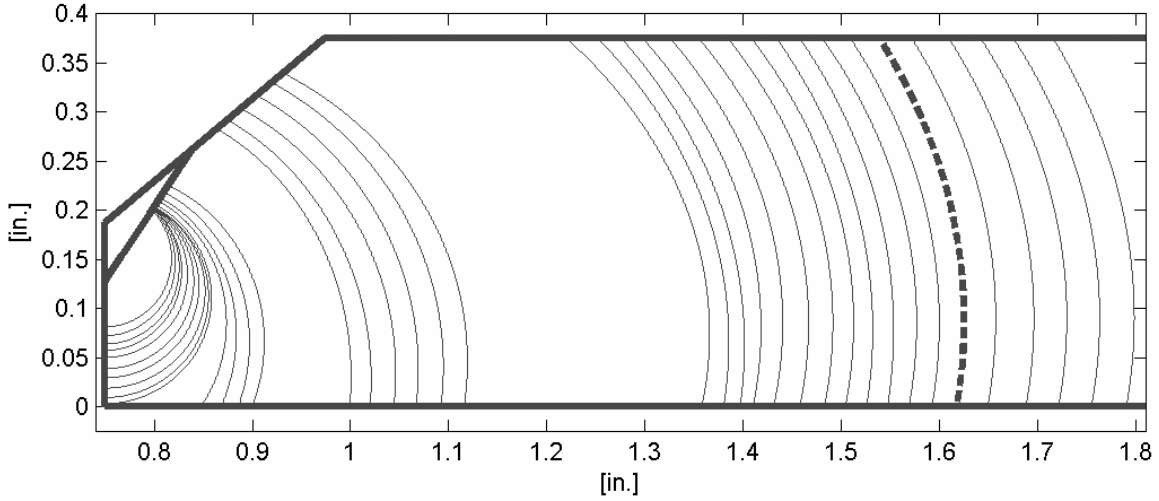

Figure C-71. Corrected BCF for FAA-012 at 65,800-68,800 Cycle, Initial Knee Crack, Type III

Table C-72. Corrected Boundary Correction Factors for FAA-012 (See figure C-72)

Initial Crack Location	Knee
Type	III
Center of Ellipse	(0.75, 0.08945)
Horizontal Axis	0.90725
Vertical Axis	0.67400
Cycle	68800-72300

ϕ [degree]	x [inch]	y [inch]	f(g)
-7.63	1.64923	0	1.4537
-6.35	1.65168	0.01494	1.4499
-5	1.6538	0.03072	1.4503
-3.88	1.65517	0.04389	1.4504
-2.31	1.65652	0.06234	1.4504
-0.96	1.65712	0.07812	1.4504
-0.51	1.65721	0.0834	1.4503
-0.08	1.65725	0.08869	1.4503
0.17	1.65725	0.09129	1.4503
1.06	1.65709	0.10186	1.4501
4.2	1.65482	0.1387	1.4488
5.54	1.65301	0.15448	1.4480
8.47	1.64736	0.18858	1.4459
10.05	1.64334	0.20691	1.4445
11.64	1.63861	0.22524	1.4429
13.23	1.63319	0.2435	1.4411
16.2	1.62121	0.27735	1.4375
17.58	1.61487	0.29287	1.4355
19.21	1.60675	0.311	1.4331
21.08	1.59653	0.33168	1.4302
23.21	1.58384	0.35484	1.4268
24.48	1.57571	0.36858	1.4261
24.59	1.57496	0.36984	1.4300
24.82	1.57343	0.37238	1.4452
25.06	1.57187	0.37491	1.4676

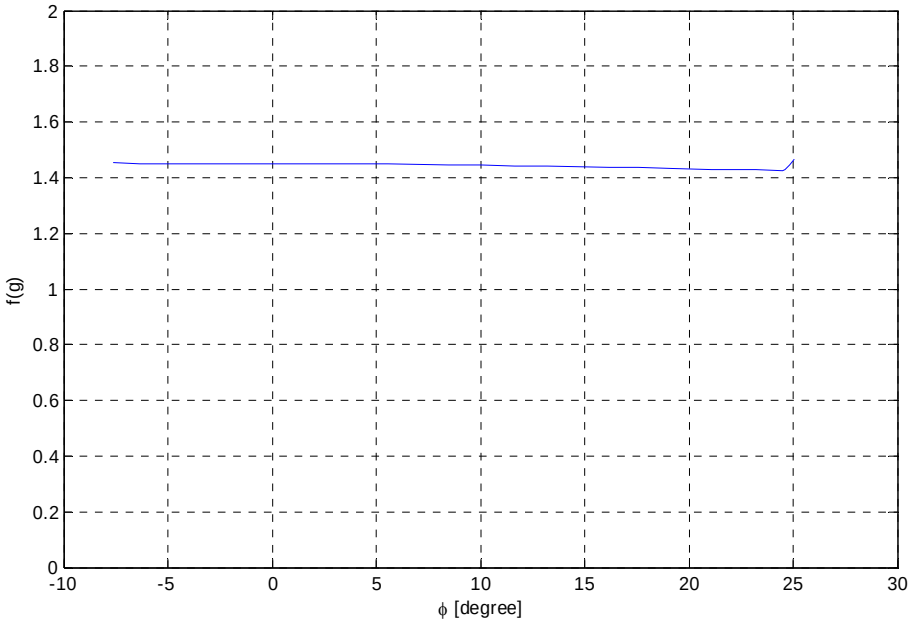

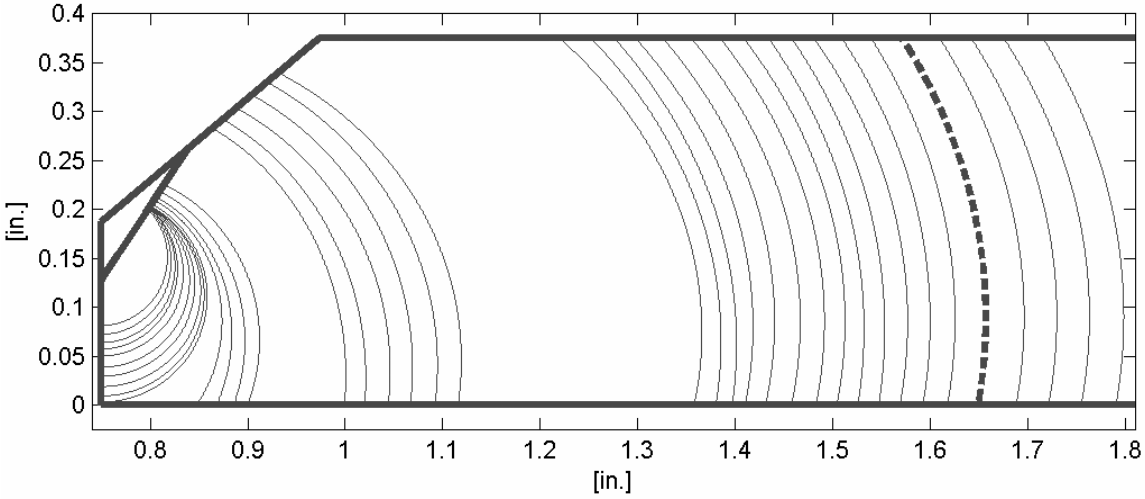

Figure C-72. Corrected BCF for FAA-012 at 68,800-72,300 Cycle, Initial Knee Crack, Type III

Table C-73. Corrected Boundary Correction Factors for FAA-012 (See figure C-73)

Initial Crack Location	Knee
Type	III
Center of Ellipse	(0.75, 0.08945)
Horizontal Axis	0.94625
Vertical Axis	0.68300
Cycle	72300-76500

ϕ [degree]	x [inch]	y [inch]	f(g)
-7.53	1.6881	0	1.4202
-6.07	1.69094	0.01729	1.4171
-4.05	1.69389	0.04131	1.4181
-2.7	1.6952	0.05734	1.4187
-1.35	1.69599	0.07337	1.4192
-0.68	1.69618	0.08142	1.4193
-0.45	1.69622	0.08413	1.4194
-0.05	1.69625	0.08947	1.4195
0.23	1.69624	0.09211	1.4195
1.35	1.69599	0.1055	1.4196
2.92	1.69502	0.12424	1.4196
4.94	1.69273	0.14826	1.4193
6.97	1.68926	0.17227	1.4188
9.01	1.68458	0.19629	1.4179
11.04	1.67872	0.22018	1.4168
13.1	1.67164	0.24406	1.4153
15.15	1.66335	0.26782	1.4137
17	1.65492	0.28894	1.4121
19.08	1.64425	0.31256	1.4100
21.19	1.63227	0.33613	1.4078
22.6	1.62356	0.35177	1.4062
23.55	1.61744	0.36213	1.4051
23.79	1.61584	0.36477	1.4048
24.17	1.61331	0.369	1.4102
24.63	1.61016	0.37411	1.4407

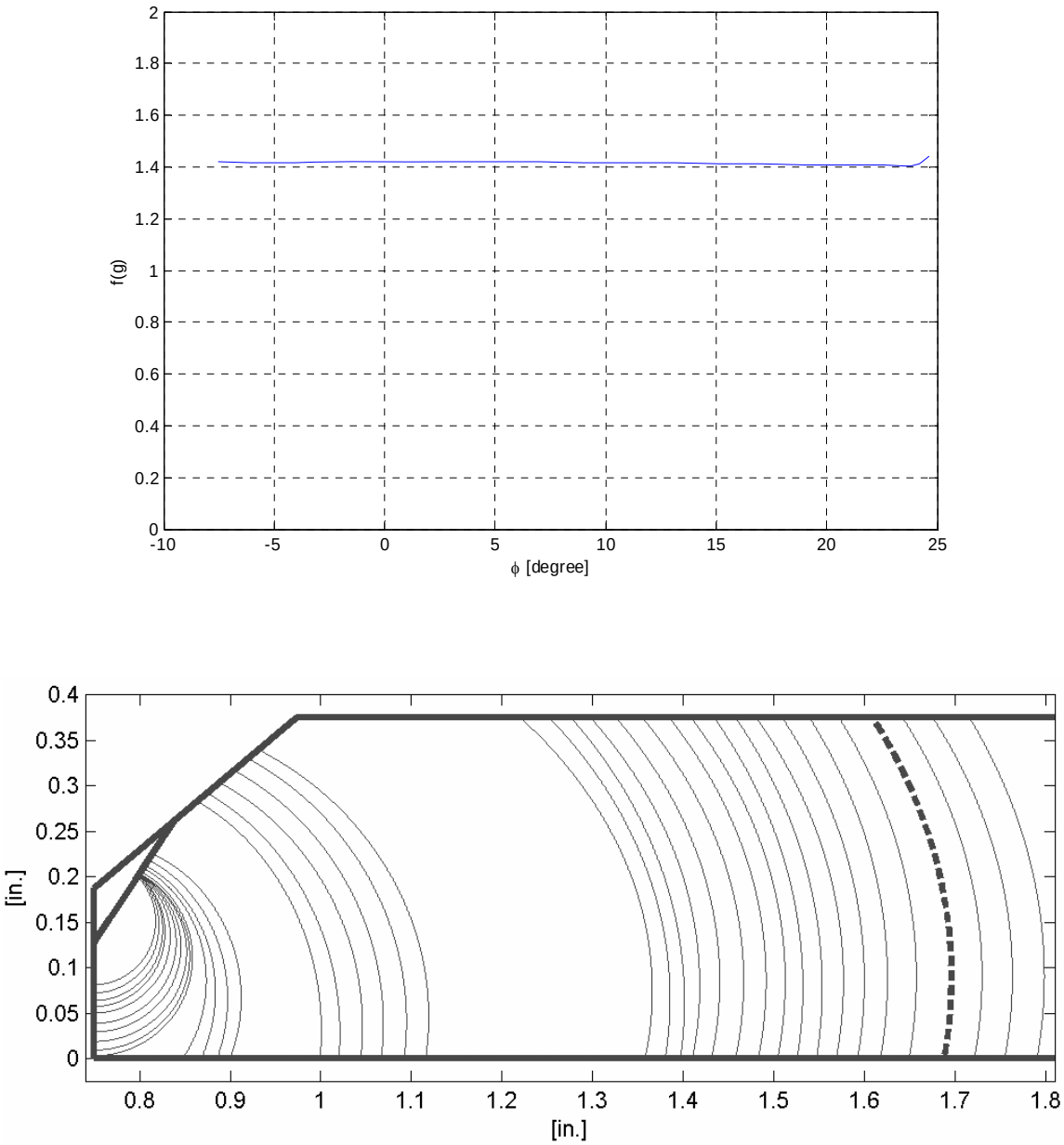

Figure C-73. Corrected BCF for FAA-012 at 72,300-76,500 Cycle, Initial Knee Crack, Type III

Table C-74. Corrected Boundary Correction Factors for FAA-012 (See figure C-74)

Initial Crack Location	Knee
Type	III
Center of Ellipse	(0.75, 0.09)
Horizontal Axis	0.97975
Vertical Axis	0.68900
Cycle	76500-79300

ϕ [degree]	x [inch]	y [inch]	f(g)
-7.51	1.72136	0	1.3859
-5.93	1.7245	0.01882	1.3829
-4.6	1.7266	0.03479	1.3836
-3.04	1.72837	0.05349	1.3843
-1.49	1.72942	0.07212	1.3847
-0.6	1.7297	0.08277	1.3848
-0.07	1.72975	0.09082	1.3849
1.4	1.72946	0.10679	1.3847
2.95	1.72845	0.12542	1.3843
4.51	1.72672	0.14412	1.3836
6.06	1.72427	0.16275	1.3828
7.63	1.72108	0.18138	1.3815
9.41	1.71656	0.20261	1.3798
11.21	1.71107	0.22384	1.3777
13.01	1.70461	0.245	1.3753
15.27	1.69514	0.27142	1.3718
17.1	1.68643	0.29252	1.3687
19.18	1.67538	0.31621	1.3648
21.03	1.66447	0.33718	1.3609
22.91	1.65248	0.35809	1.3568
23.15	1.65087	0.36075	1.3562
23.38	1.64928	0.36334	1.3557
23.62	1.64767	0.36594	1.3552
24.13	1.64416	0.37159	1.3610
24.36	1.64253	0.37418	1.3870

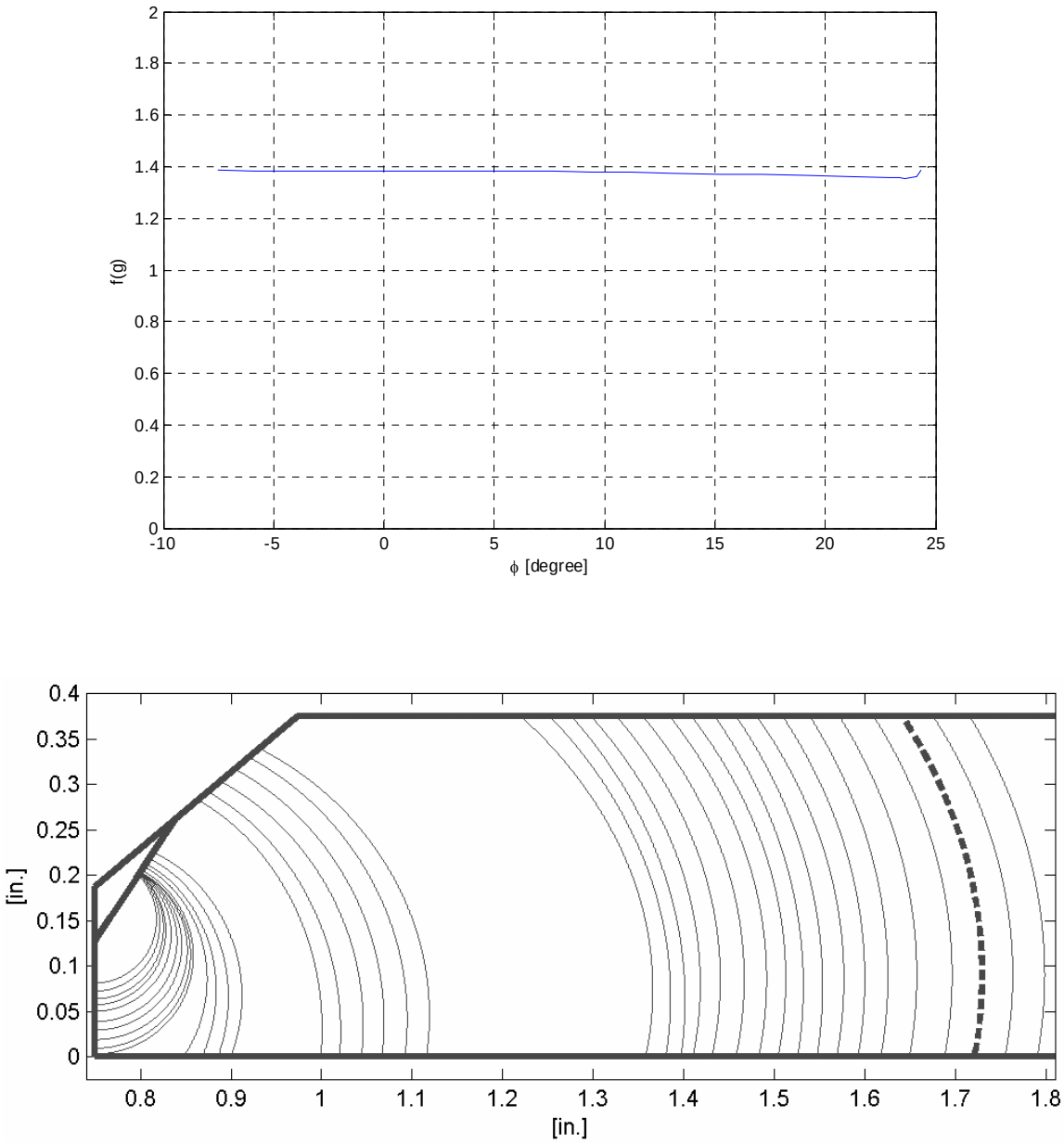

Figure C-74. Corrected BCF for FAA-012 at 76,500-79,300 Cycle, Initial Knee Crack, Type III

Table C-75. Corrected Boundary Correction Factors for FAA-012 (See figure C-75)

Initial Crack Location	Knee
Type	III
Center of Ellipse	(0.75, 0.09)
Horizontal Axis	1.01325
Vertical Axis	0.70000
Cycle	79300-82800

ϕ [degree]	x [inch]	y [inch]	f(g)
-7.39	1.75484	0	1.4431
-6.16	1.75739	0.0149	1.4388
-5.05	1.75932	0.02847	1.4390
-3.7	1.76113	0.0448	1.4392
-2.36	1.76239	0.06113	1.4393
-1.03	1.76309	0.07747	1.4394
-0.36	1.76323	0.08563	1.4394
-0.08	1.76325	0.09103	1.4394
0.31	1.76324	0.0938	1.4394
1.64	1.76283	0.11007	1.4394
3.2	1.76167	0.1291	1.4392
4.99	1.7594	0.1509	1.4390
6.56	1.75663	0.16987	1.4387
8.35	1.75251	0.1916	1.4384
10.14	1.74741	0.2132	1.4379
11.95	1.74129	0.23487	1.4374
13.76	1.73417	0.2564	1.4370
15.81	1.72491	0.28063	1.4364
17.18	1.71802	0.2967	1.4360
19.03	1.70789	0.3181	1.4355
21.12	1.69518	0.34213	1.4350
23	1.6827	0.3634	1.4348
23.53	1.67899	0.36947	1.4442
23.88	1.67652	0.37337	1.4683
24	1.67568	0.37467	1.4787

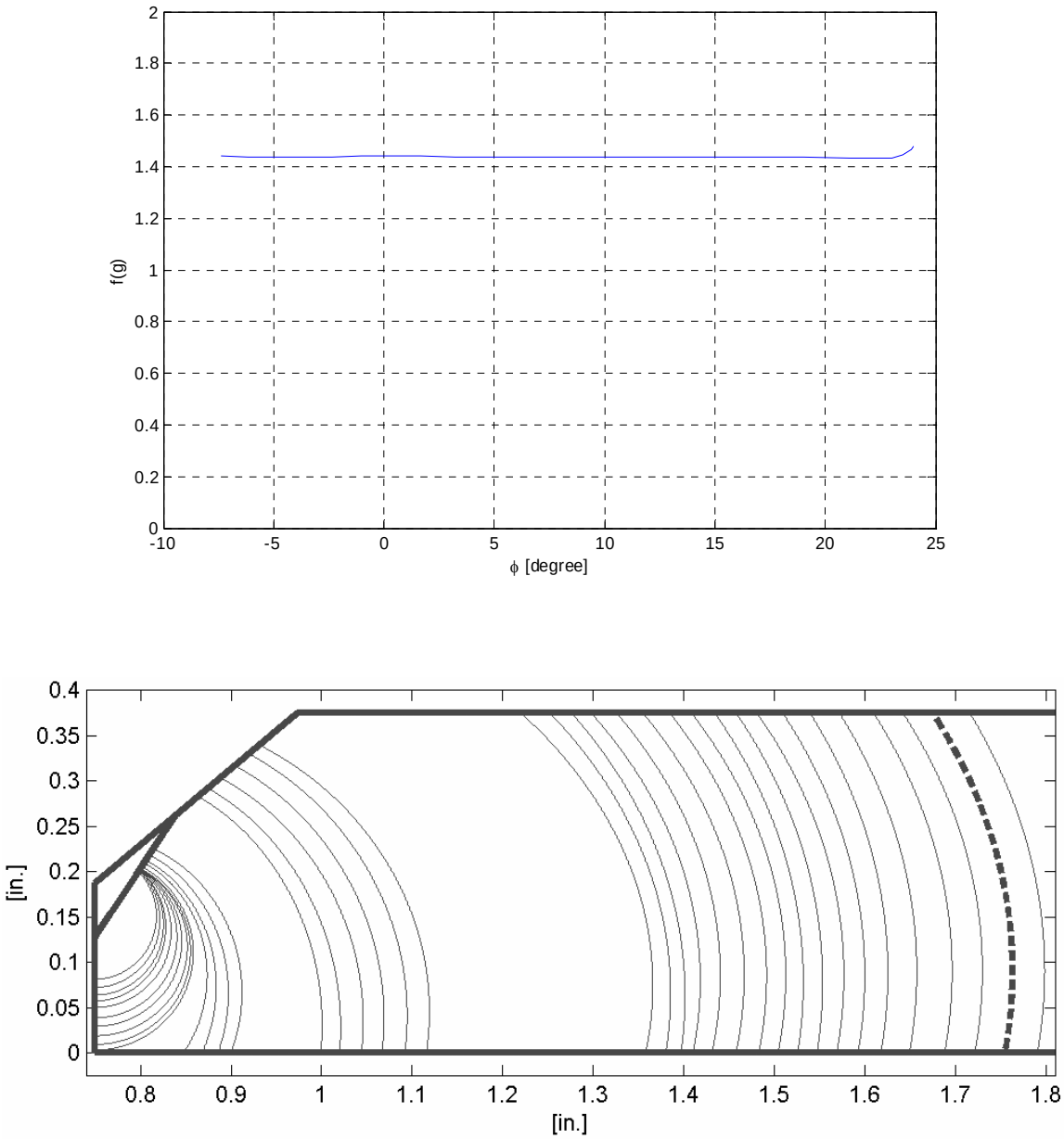

Figure C-75. Corrected BCF for FAA-012 at 79,300-82,800 Cycle, Initial Knee Crack, Type III

Table C-76. Corrected Boundary Correction Factors for FAA-012 (See figure C-76)

Initial Crack Location	Knee
Type	III
Center of Ellipse	(0.75, 0.09)
Horizontal Axis	1.04850
Vertical Axis	0.73250
Cycle	82800-86300

ϕ [degree]	x [inch]	y [inch]	f(g)
-7.06	1.79054	0	1.3437
-5.97	1.79282	0.01384	1.3385
-4.24	1.79563	0.03585	1.3366
-2.52	1.79749	0.05778	1.3355
-1.02	1.79833	0.07697	1.3350
-0.59	1.79844	0.08246	1.3349
-0.05	1.7985	0.09068	1.3349
0.27	1.79849	0.09342	1.3349
1.34	1.79821	0.10713	1.3351
2.84	1.79721	0.12632	1.3357
4.56	1.79518	0.14826	1.3369
6.08	1.79261	0.16752	1.3386
7.59	1.78932	0.18671	1.3406
9.1	1.78529	0.2059	1.3431
10.63	1.78051	0.22509	1.3461
12.17	1.77495	0.24436	1.3496
13.49	1.76959	0.26081	1.3529
15.03	1.76261	0.28	1.3573
16.6	1.7548	0.29926	1.3620
18.17	1.7462	0.31845	1.3672
19.54	1.73812	0.33497	1.3721
21.14	1.72794	0.35416	1.3782
22.49	1.71875	0.37012	1.3910
22.61	1.71793	0.37145	1.3984
22.84	1.71626	0.37412	1.4185

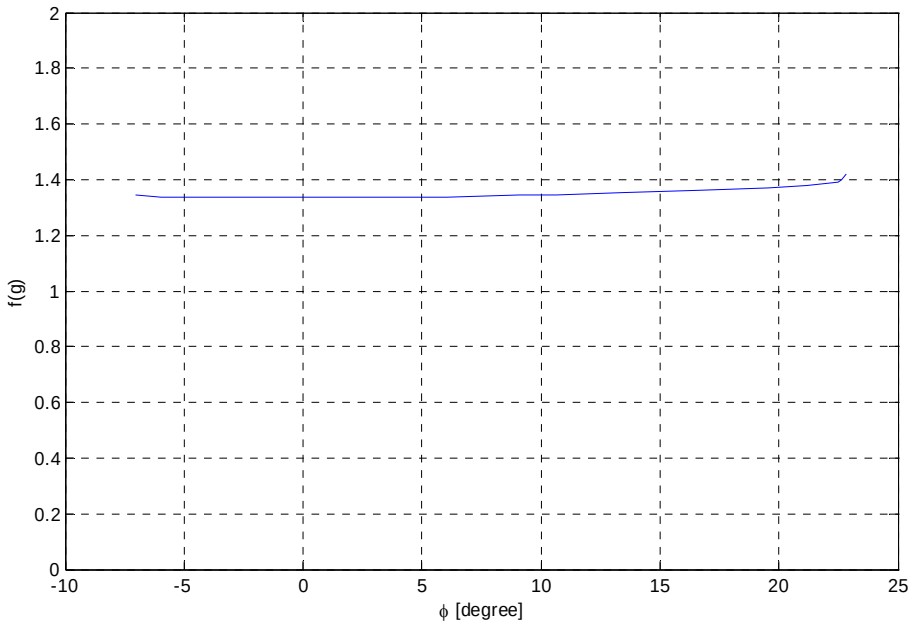

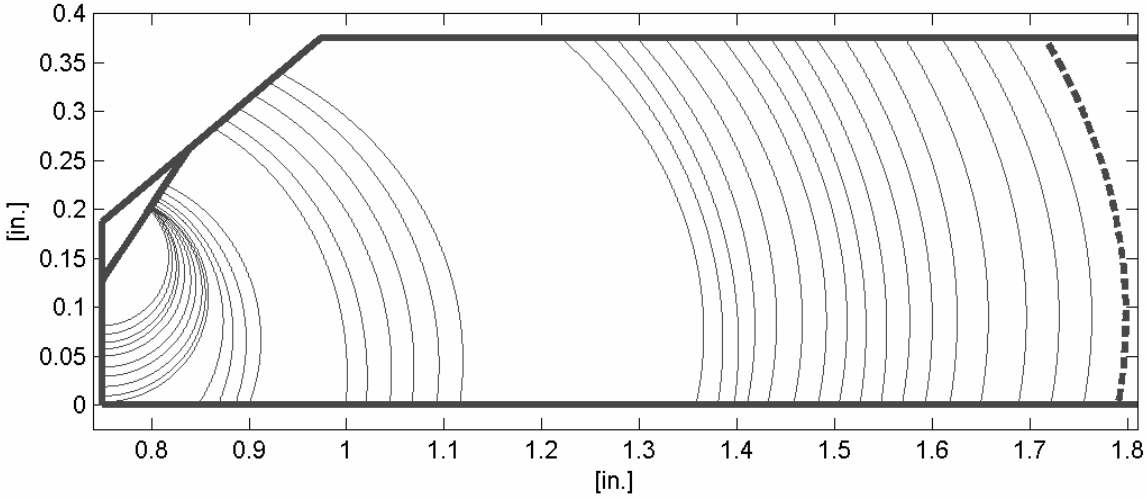

Figure C-76. Corrected BCF for FAA-012 at 82,800-86,300 Cycle, Initial Knee Crack, Type III

Table C-77. Test Load Information for FAA-009

Maximum [lb_f]	Minimum [lb_f]	Max stress (psi)	Minimum stress (psi)	Cycles
600	180	213	64	0-4500
650	195	231	69	4501-15000
700	210	250	75	15001-245839

Table C-78. Dimensions Specimens FAA-009 and FAA-012

Thickness, t (inch)	Width, W (inch)	Gross Area, A (square inches)
0.375	7.5	2.183

Table C-79. Test Load Information for FAA-012

Maximum [lb_f]	Minimum [lb_f]	Maximum stress (psi)	Minimum stress (psi)	Cycles
1100	330	391	117	15001-37800
1000	300	356	107	37801-39200
950	285	338	120	39201-41400
700	210	250	75	41401-220856